Temporal Deregulation of Genes and MicroRNAs in Neurons during Prion-Induced Neurodegeneration

By

ANNA MAJER

A Thesis
Submitted to the Faculty of Graduate Studies
In Partial Fulfillment of the Requirements for the Degree of

DOCTOR OF PHILOSOPHY

Department of Medical Microbiology
College of Medicine, Faculty of Health Sciences
University of Manitoba
Winnipeg, Manitoba

TABLE OF CONTENTS

ABSTRACT

Prion diseases are fatal and incurable neurodegenerative diseases that share many pathological similarities to other neurodegenerative diseases such as Alzheimer's or Parkinson's disease. One of the earliest pathological signs commonly detected in all of these diseases is the dysfunction followed by loss of neuronal synapses, spines and eventually dendrites that collectively contribute to disruption of normal brain function. These pathologies tend to progressively accumulate within the brain tissue such that extensive damage typically precedes clinical symptom manifestation and ultimate death of neurons. Clearly, understanding the molecular processes responsible for these pathologies could uncover critical pathway(s) that are responsible for propagating this brain damage and could therefore be exploited for therapy development. However, molecular mechanisms implicated in this early pathology remain unidentified. To address this gap in knowledge, this thesis describes a transcriptional approach coupled with specific isolation of neuronal-enriched tissue which was used to help delineate cellular pathways involved in prion-induced neurodegeneration. Profiling cell bodies of CA1 hippocampal neurons known to be affected during early prion disease revealed temporal alteration in both gene and microRNA (gene regulators) expression throughout disease. On a gene expression level, changes in transcript expression during preclinical disease were reminiscent of an activity-dependent neuroprotective gene signature previously described in the literature. These neuroprotective genes were induced during preclinical disease, diminished as disease progressed and were abolished at clinical disease. In support of this process, upregulation of the phosphorylated form of the neuroprotective transcription factor CREB was detected during preclinical disease in these neurons. Furthermore, several genes known to be induced by CREB were also upregulated at preclinical disease in prion-infected mice. Interestingly, expression of numerous deregulated

microRNAs paralleled the neuroprotective gene signature of which several are known to remodel neuronal spines and dendrites. To determine whether other preclinically induced microRNAs were also capable of remodeling neuronal structures, gain-of-function studies were performed in primary mouse hippocampal neurons for the uncharacterized miR-26a-5p. Neurons over-expressing miR-26a-5p had enhanced spine density and dendrite arborization, similar to other preclinically-induced microRNAs. Together, these data suggests that CA1 hippocampal neurons induce a neuroprotective transcriptional signature that is evident early in the course of disease within CA1 hippocampal neurons and is abolished by clinical disease. Reestablishment of key molecules that can induce this neuroprotective signature at a time when these genes begin to dissipate could prolong prion disease onset and delay clinical symptom manifestation.

ACKNOWLEDGMENTS

I would like to extend my genuine gratitude to my supervisor, Dr. Stephanie Booth (Adjunct Professor, Department of Medical Microbiology, University of Manitoba), for her continued support, steadfast guid ance and inspiration throughout my PhD studies. Her expertise and kind mentorship allowed me to complete the work presented here and grow as a scientist. I am grateful for all her insightful suggestions, the opportunities that she provided me with and the experience that I gained throughout my degree.

I also wish to extend my heartfelt appreciation to my PhD committee members, Dr. Kevin Coombs (Professor, Department of Medical Microbiology, University of Manitoba), Dr. Mike Drebot (Adjunct Professor, Department of Medical Microbiology, University of Manitoba) and Dr. Yvonne Myal (Professor, Department of Pathology, University of Manitoba) for their valuable insights and suggestions throughout my studies. Their assistance and encouragement allowed me to become a better scientist. I would also like to thank Dr. Andrew Hill (Professor and Head, Department of Biochemistry and Genetics, La Trobe Unversity) for serving as the external examiner and providing me with good comments to improve the quality of the thesis.

Many thanks to all members in Dr. Booth's laboratory that I had a privilege to work with, in particular Yulian Niu for her brilliant technical expertise in histology and the time for kindly performing pathological staining for all *in vivo* tissues presented in this thesis. I thank Kathy Manguiat and Sarah Medina for helping me to execute several experiments including collection of LCM material and subsequent profiling studies presented herein. I would also like to thank my fellow graduate students, especially Amrit Boese, for her continued support and encouragements throughout my degree; thank you for the many pleasant memories to cherish and treasure. Furthermore, Amrit kindly provided me with the total RNA samples from her NMDAR

stimulated primary mouse hippocampal neurons from which I performed my miRNA profiling assays. With the excellent help from Dr. Reuben Saba and Dr. Jyothi Arikkath (Assistant Professor, Developmental Neuroscience in the Munroe-Meyer Institute, University of Nebraska Medical Center) I was successful in establishing the primary mouse hippocampal cultures in the lab that were critical to the success of my final thesis chapter. I would like to thank Dr. Kirk McManus (Associate Professor, Department of Biochemistry and Medical Genetics, University of Manitoba) for allowing me to use Imaris, the software for my Sholl analysis of primary mouse hippocampal neurons. My sincere gratitude to personnel at the National Microbiology Laboratory, especially the animal technical services who were an intricate part in all the animal work presented herein. I would also like to thank all of the support staff at the Medical Microbiology Department for the "behind-the-scene" role and support that allowed me to complete my studies.

I gratefully acknowledge the financial support provided to me by the Natural Sciences and Engineering Research Council (NSERC), Research Manitoba, McCrorie-West Family Fellowship for Alzheimer's Research (U of M), PrioNet and Public Health Agency of Canada.

I would also like to convey my heartfelt gratitude to my fiancé, Sajesh, for the support, scientific discussions and assistance with many aspects of my research, especially the single-cell image analysis using Imaris software that is presented herein. Most importantly, I send all of my love and respect to my parents, brother and friends for their boundless love, support and encouragement during my studies.

ABBREVIATIONS

3'UTR	3'- untranslated region
4-AP	4-Aminopyridine
aa	amino acids
AD	Alzheimer's disease
AID	activity-regulated inhibitor of death
AMPAR	α-amino-3-hydroxy-5-methyl-4-isoxazolepropionic acid receptor
AP	alkaline-phosphatase
APP	amyloid protein precursor
ATCC	American Type Culture Collection
AUD	animal use document
BSC	BioSafety Cabinet
BSE	Bovine spongiform encephalopathy
CaN	calcineurin
CJD	Creutzfeldt-Jakob disease
CNS	central nervous system
CREB	cyclicAMP response element binding protein
CSF	cerebral spinal fluid
C-terminus	Carboxy (COOH) terminus
DAPI	4', 6-diamidino-2-phenylindole
DIV	days *in vitro*
DM	dissection medium
DMEM	Dulbecco's Modified Eagle's Medium
DNA	Deoxy-ribose nucleic acid
DPI	days post infection
E18-20	embryonic day 18-20
EDTA	ethylenediamine-tetraacetic acid
EEG	electroencephalography
eIF2	eukaryotic initiation factor 2
EMEM	Eagle's Minimum Essential Medium
EP	end point
ER	endoplasmic reticulum
FBS	Fetal Bovine Serum
fCJD	familial Creutzfeldt-Jakob disease
FDA	Food and Drug Administration
FDR	false discovery rate
FFI	fatal familial insomnia
GABA	γ-aminobutyric acid
GFAP	glial fibrillary acidic protein
GFP	green fluorescent protein
GPI	glycophosphoinositol

GSS	Gerstmann-Sträussler-Scheinker
HD	Huntington's disease
HEK	human embryonic kidney
IBA1	ionized calcium-binding adapter molecule 1
iCJD	iatrogenic Creutzfeldt-Jakob disease
IP	intraperitoneally
ISH	*in situ* hybridization
kDa	kilo Dalton
LCM	Laser Capture Microdissection
LDH	lactate dehydrogenase
LTD	long-term depression
LTP	long-term potentiation
M cells	microfold cells
MAP2	microtubule-associated protein 2
MeCP2	methyl CpG binding protein 2
miRISC	microRNA-induced silencing complex
miRNA/miR	microRNA
MOI	multiplicity of infection
MRI	magnetic Resonance Imaging
mRNA	messenger RNA
NMDAR	N-methyl-D-aspartate receptor
N-terminus	Amino (NH_2) terminus
OCT	optimal cutting temperature
P-bodies	processing bodies
PBS	phosphate buffer saline
PCR	polymerase chain reaction
pCREB	phospho-CREB
PD	Parkinson's disease
PEN	polyethylene-napthalate
PMCA	protein misfolding cyclic amplification
PrP	prion protein
PrP^{C}	cellular prion protein (normal)
PrP^{Sc}	scrapie prion protein (infectious)
PSD-95	post-synaptic density 95
QC	quality control
qRT-PCR	quantitative real time
RIN	RNA integrity Number
RML	Rocky Mountain Laboratory scrapie strain of prion
RNA	Ribose nucleic acid
RT	reverse transcriptase
RT-QuIC	Real-time quaking induced conversion
SBI	System Biosciences Inc.

sCJD	sporadic Creutzfeldt-Jakob disease
SD	Standard Deviation
SDS	Sequence Detection System
shRNA	short hairpin RNA
siRNA	short interfereing RNA
SLM	*stratum locunosum-moleculare*
SP	*stratum pyramidale*
SR	*stratum radiatum*
SSC	saline-sodium citrate
TBS/T	Tris Buffered Saline with Tween 20
TLDA	TaqMan® Low Density Array
TSE	Transmissible spongiform encephalopathies
UPR	unfolded protein response
UV	Ultra Violet
vCJD	variant Creutzfeldt-Jakob disease

A list of abbreviations is not provided for the genes as they have been defined following annotations described in Entrez.

LIST OF FIGURES

LIST OF TABLES

1.0 INTRODUCTION

Prion and Alzheimer's diseases (AD) are fatal neurodegenerative diseases that are distinct in many pathological and phenotypic traits; however, they share several key features on a subcellular level. The main risk factor associated with neurodegenerative disease is advancing age because clinical signs are detected at mid to late life. On a molecular level, both diseases are caused by misfolding of normal cellular proteins that result in the physical decay and eventual loss of neurons. One of the earliest changes detected within the brain in both diseases is synaptic dysfunction followed by neuronal spine loss. These changes occur well before the onset of clinical signs and the ultimate death of neurons. Although these neuropathological alterations occur in many other neurodegenerative diseases, the molecular process that underlies these pathologies remains largely unknown. The current lack of treatment and the continual rise in incidence worldwide for AD (Dartigues, 2009) necessitates further study of neurodegeneration to fully understand the disease process and thereby aid in the design of effective therapies.

1.1 Common Elements of Neurodegenerative Diseases

Neurodegenerative diseases are a phenotypically heterogenous group of diseases that have unique characteristics. Diseases including AD, Parkinson's disease (PD), Huntington's disease (HD) and prion diseases generally target different subsets of neurons and therefore represent a range of pathological and molecular features. For example, cholinergic neurons of the cerebral cortex and hippocampus are targeted in AD and lead to progressive dementia (Francis *et al*., 1999). Dopaminergic neurons of the substantia nigra are targeted in PD and cause abbarent function in movement (Sulzer and Surmeier, 2013) while GABAergic medium-sized spiny neurons of the striatum are targeted in HD which leads to the development of dementia, motor and psychiatric problems (Graveland *et al*., 1985). In turn, prion diseases can initially target

neurons of the cortex, cerebellum and/or thalamus (Reder *et al*., 1995; Farlow *et al*., 1989) which highlights the phenotypic and pathologic heterogeneity of these diseases. As a result, initial symptoms can vary from dementia, ataxia and psychological problems or insomnia, depending on the specific brain region affected. The specific anatomical region of the brain that is targeted in prion disease is dependent on several factors including the etiology (see *Section 1.3.1*) and the prion strain (see *Section 1.7*), however, the exact mechanism for such disparaty remains unknown.

Although these neurodegenerative diseases affect different regions of the brain, they are all caused by the misfolding of specific cellular proteins which results in the formation of intracellular and/or extracellular aggregates as disease progresses (**Figure 1.1**). This misfolding typically leads to stimulation of neuropathology followed by the eventual death of neurons. Remarkably, disruption of synapses followed by spine loss and dendrite retraction is the earliest pathological alteration observed in all of these diseases (reviewed in Martin, 1999). As these structures are critical for proper neuron function, their progressive removal precedes the onset of symptoms. A similar molecular mechanism may therefore be responsible for driving neurodegeneration downstream of protein misfolding in these diseases. Consequently, identifying cellular processes involved in neurodegeneration in one of these diseases may prove helpful for understanding degeneration in others.

1.2 Rodent Models for Neurodegeneration

Rodent models are excellent tools to study human diseases and have been readily used to study neurodegeneration. They do not naturally acquire neurodegenerative diseases because of their short life span. Therefore, either transgenic mice are produced or misfolded

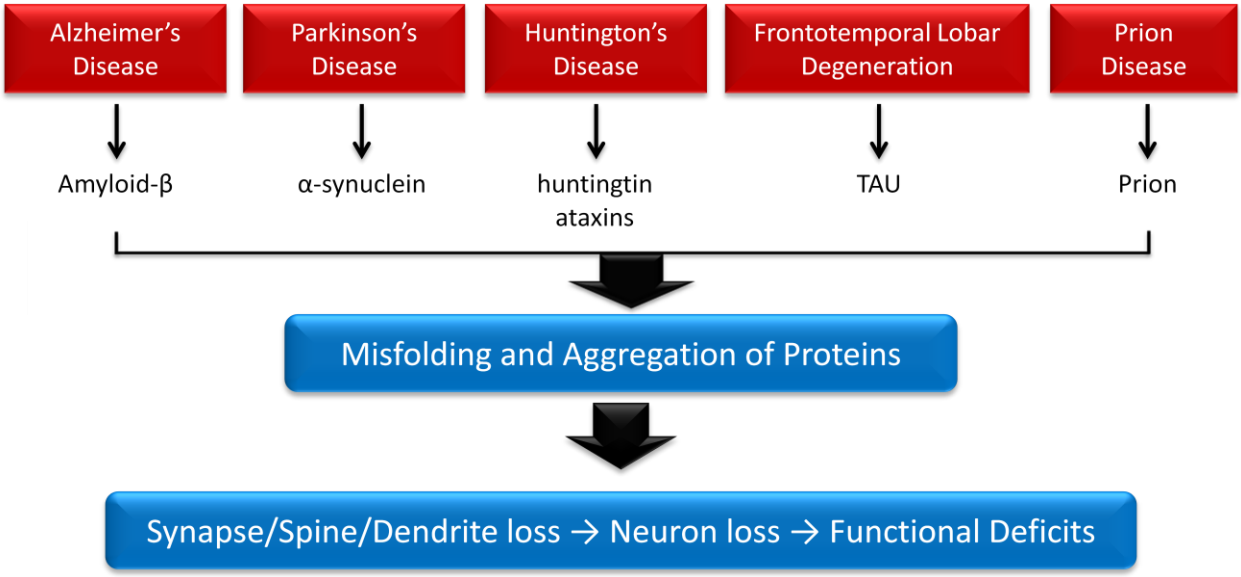

Figure 1.1. Common features among major neurodegenerative diseases. Each of the diseases listed are caused by the misfolding of the normal form of protein or proteins. Upon misfolding, they accumulate and aggregate intracellularly and/or extracellularly. As a consequence, the central nervous system begins to experience neuronal degeneration where in many cases synaptic dysfunction and loss as well as dendrite varicosities occur in neurons.

proteins/peptides are injected into the animals to cause disease. Transgenic animals are useful when studying the etiology of genetic diseases. However, a majority of neurodegenerative diseases are sporadic and are very difficult to model.

Conclusions drawn from animal models are restricted by how accurately the model mimics human disease. A perfect animal model needs to reflect symptoms, lesions and cause of the disease as observed in patients. Unfortunately, most animal models of neurodegenerative diseases fail to completely recapitulate human disease. For example, the most commonly used transgenic mouse model of AD (Tg2576) over-expresses human amyloid precursos protein causing the development of senile plaques and cognitive deficits but not neurofibrillary tangles and neuronal loss which are observed in AD patients (Morrissette *et al.*, 2009; Adlard *et al*., 2014). Similarly, genetic mouse models of PD (autosomal-dominant and autosomal-recessive) have resulted in mice showing only a part of the motor deficits and cellular abnormalities observed in PD patients (reviewed in Dawson *et al.*, 2010; Lee *et al*., 2012) where some mouse models recapitulate motor dysfunction but lack the accumulation of the characteristic Lewy bodies that are detected in PD patients (Richfield *et al*., 2002).

Animal models of prion disease however recapitulate the majority of the neuropathological and biochemical hallmarks of human disease. Animals inoculated with infectious brain homogenates from terminally ill mice develop progressive clinical signs of neurological illness such as ataxia (uncoordinated movement), kyphosis (hunched back) and tail rigidity. Neuropathological assessment of prion-infected mouse brain further exemplifies the characteristic hallmarks of prion disease observed in patients, including spongiform degeneration (vacuolation of the brain), deposition of misfolded prion protein, prominent astrocytic gliosis and detection of proteinase K resistant infectious prion protein (biochemical signature of prion

disease). Clearly, studying molecular changes in prion-infected animals would best represent the process of neurodegeneration that occurs in human prion disease. The work presented in this dissertation is therefore focused on identifying molecular alterations in a prion-infected mouse model.

1.3 Prion Diseases

Prion diseases, also known as transmissible spongiform encephalopathies (TSEs), are invariably fatal neurodegenerative diseases that affect both humans and animals (**Table 1.1**). Although quite rare in the human population, prion diseases have affected industrial (*i.e.* cattle) and wild-life (*i.e.* deer and elk) animal populations at a much larger scale. In fact, it was prion-infected cattle that brought the disease to light for the general public as a potentially serious public health concern.

During the 1990s the most devastating animal epidemic occurred in bovines, crippling the cattle industry in the UK and around the world. More than 180,000 cattle were diagnosed with bovine spongiform encephalopathy (BSE), otherwise known as "mad cow disease", and it was estimated that ~2 million were infected. This resulted in the slaughter of more than 4.4 million cattle in the hope of eradicating the disease (Ghani *et al.,* 2002). It was later identified that BSE originated from cattle feed that contained meat and bone meal from other cattle infected with BSE which was not properly decontaminated to neutralize the infectious agent. Once the cattle feed was banned, the epidemic slowly declined and only individual cases of BSE are currently identified worldwide. Unfortunately, ~480,000 BSE-infected animals entered the human food chain (Valleron *et al.,* 2001) and after ingestion of this prion-contaminated beef a new form of human prion disease emerged (Will *et al.,* 1996).

Table 1.1. The list of prion diseases observed within human and animal populations.

Prion Diseases	Affected Species
Kuru	Human*
Creutzfeldt-Jakob Disease (CJD)	Human*
Gerstmann-Sträussler-Scheinker (GSS)	Human*
Fatal Familial Insomnia (FFI)	Human*
Scrapie	Sheep
Bovine Spongiform Encephalopathy (BSE)	Cattle
Chronic Wasting Disease (CWD)	Deer and Elk
Transmissible Mink Encephalopathy (TME)	Mink
Feline Spongiform Encephalopathy (FSE)	Cats

* more detail pertaining to the human prion disease can be found in **Table 1.2**

1.3.1 Human Prion Diseases

Human prion diseases can be further categorized into three distinct etiologies that reflect the mode of transmission: sporadic, inherited and acquired (**Table 1.2**). These include Kuru, the various phenotypes of Creutzfeldt-Jakob disease (CJD), Gerstmann-Sträussler-Scheinker (GSS) and fatal familial insomnia (FFI).

Kuru was first described in the late 1950s within the Fore linguistic group and their neighbors of Papua New Guinea (Gajdusek and Zigas, 1957; Gajdusek and Reid, 1961). The cause of Kuru was later identified to be related to cannibalistic mourning rituals performed by the Fore people. Once this ritualistic practice was halted, the incidence of disease was effectively abolished.

Currently, CJD is the most common prion disease found within the human population, affecting approximately 1-2 people per million per year (Ladogana *et al.*, 2005). There are 4 major forms of CJD that reflect the unique route of transmission: sporadic (sCJD), familial (fCJD) or otherwise known as genetic or inherited, iatrogenic (iCJD) and variant (vCJD). The most common is sCJD, which accounts for approximately 85% of the total incidence of CJD and arises from a spontaneous somatic mutation within the prion protein gene (*PRNP*) or through a random structural change of the prion protein itself (Colby and Prusiner, 2011). However, the sporadic form of CJD comprises a broad spectrum of clinicopathological variants that are heterogeneous in disease duration, symptomatology and the type or regional distribution of brain lesions (reviewed in Parchi *et al*., 2011). This heterogeneity is believed to be primarily caused by prion strains (see *Section 1.7*). Approximately 2 out of 3 sCJD patients die within six months of symptom onset. One risk factor for sCJD is the presence of the methionine homozygosity at

Table 1.2. Brief description of human prion diseases. Adapted from Mallucci and Collinge, 2005.

Classification	Etiology	Disease Nomenclature	Frequency
Sporadic	Random distribution affecting 1-2 people per million worldwide per year	Sporadic Creutzfeldt-Jakob disease (sCJD)	~85%
Inherited	Autosomal dominant mutations in *PRNP*	Familial Creutzfeldt-Jakob disease (fCJD)	~10-15%
		Gerstmann-Sträussler-Scheinker Disease (GSS)	~1/100 million
		Fatal familial insomnia (FFI)	~100
Acquired	Exposure to prions from human pituitary hormones, tissue grafts or contaminated surgical instruments	Iatrogenic Creutzfeldt-Jakob disease (iCJD)	<5%
	Exposure to BSE prion via diet	Variant Creutzfeldt-Jakob disease (vCJD)	~ 200 cases
	Endocannibalism	Kuru	Epidemic in 1950s in Fore people of Papua New Guinea

codon 129 within *PRNP* which was detected in approximately 80% of sCJD cases (Palmer *et al.*, 1991).

Genetic causes comprise the remaining 15% of CJD cases where an inherited autosomal dominant mutation within *PRNP* mediates the disease with very high penetrance (Owen *et al.*, 1989; Goldgaber *et al.*, 1989). The abnormalities within the *PRNP* sequence arise from deletions/insertions or point mutations that result in amino acid substitutions within the protein. To date, over 40 different pathogenic variants and numerous insertions have been identified within *PRNP* of which the majority have been associated with CJD patients (reviewed in Colby and Prusiner, 2011). In addition, two other forms of prion disease, namely GSS and FFI, are also caused by an autosomal-dominant mutation within *PRNP* (Goldgaber *et al.*, 1989; Medori *et al.*, 1992). The wide array of mutations categorized within *PRNP* dictates different presentations of disease onset, symptom manifestation and neuropathology (Imran and Mahmood, 2011; Puoti *et al.*, 2012).

The remaining two forms of CJD occur at very low incidence and represent prion disease transmission through medical means, iCJD, or through ingestion of prion-contaminated beef, vCJD. Over the past 40 years, approximately 300 cases of iCJD arose due to contaminated human material such as human pituitary hormones and transplantation of corneal or dura mater grafts (Duffy *et al.*, 1974; Heckmann *et al.*, 1997; CDC, 2008; reviewed by Will, 2003). Some cases were due to medical equipment not being properly decontaminated (Bernoulli *et al.*, 1997; Nevin *et al.*, 1960: reviewed by Will, 2003). Current decontamination practices circumvent this form of CJD.

The most recent emergence of prion disease in humans is vCJD where ~200 cases were reportedly caused by ingestion of prion-contaminated beef (Will *et al.*, 1996; Aguzzi and

Weissmann 1996; Bruce *et al.,* 1997; Hill *et al.,* 1997). Most patients were in their late 20-30s and were all methionine homozygous at codon 129 (129M/M) and had deposits of florid plaques (reviewed in Will, 2003). Due to a potentially long incubation period that can span more than 30 years, it is possible that people who are heterozygous at codon 129 and have been exposed to BSE may develop the disease in the upcoming years; similar to what was observed with Kuru (Collinge *et al.,* 2006). Furthermore, vCJD can also be transmitted via blood transfusion, which is of additional public health concern.

1.3.2 Diagnosis of Human Prion Diseases

The most reliable method for diagnosis of prion diseases is to analyze a brain biopsy for the presence of infectious prion proteins using immunohistochemistry and western blot techniques. This procedure is highly invasive which sparked development of alternative diagnostic approaches. Currently, electroencephalography (EEG) is the most reliable non-invasive diagnostic test available for prion disease. However, this method has relatively low sensitivity (65%) and specificity (80%) and cannot differentiate between CJD and other neurodegenerative diseases such as AD (Steinhoff *et al.,* 1996; Tschampa *et al.,* 2001). A more accurate method that can successfully distinguish the subtypes of CJD is based on Magnetic Resonance Imaging (MRI) (Zerr *et al.,* 2009). This type of analysis includes evaluating up to 13 regions of the brain for abnormalities. In cases where a genetic cause of prion disease is suspected, a DNA sample is collected from the patient and the entire prion gene is sequenced and analyzed for mutations.

At a molecular level, several protein biomarkers detected within the cerebral spinal fluid (CSF) are used as a diagnostic tool for prion diseases. Some of these include 14-3-3 (Harrington

et al., 1986; Will *et al.,* 2000; Matsui *et al.,* 2010), total and/or phosphorylated TAU (Blennow *et al.,* 2005), brain specific markers such as calcium-binding protein B (S100B) and neuron-specific enolase (Ladogana *et al.,* 2009). Using these protein biomarkers in combination provides a more reliable diagnosis for prion disease where detection of 14-3-3 in combination with elevated total TAU showed 96% specificity and 84% sensitivity (Bahl *et al.,* 2009).

A relatively novel diagnostic strategy is by detecting infectious prion particles within a patient's CSF sample. This detection strategy was made possible using the real-time quaking induced conversion (RT-QuIC) assay that amplifies infectious prions from a single molecule into readily detectable abundances (Atarashi *et al.,* 2011). The assay is able to detect misfolded prion protein from CSF and shows great promise with 91% sensitivity and 98% specificity (McGuire *et al.,* 2012). Unfortunately, identification of a prion positive patient is almost impossible during preclinical stages of disease. Unless the disease is hereditary, prion disease patients remain undiagnosed until well into the clinical phase. Further research is therefore necessary to discover a preclinical biomarker for prion disease. Temporal transcriptomic analysis, such as that performed in this study, may be useful to identify alternative disease-specific candidates as preclinical biomarkers for early diagnosis.

1.3.3 A Treatment Strategy for Human Prion Diseases

There is currently no treatment available to combat prion diseases. Three major approaches have been undertaken to devise a therapeutic which, to date, have lead to no avail. Recent developments into the understanding of prion disease have provided alternative targets to use for therapeutic applicability.

One of the first strategies was to administer drugs that could prevent the propagation of PrP^{Sc} and therefore inhibit the spread of the infectious prion particle. Several drugs that are already FDA approved have been found to have this property along with an affinity for the PrP^{Sc} structure (Janka and Maldarelli, 2004). One of these drugs is quinacrine, which is often used as an anti-malaria drug. Due to its ability to pass the blood brain barrier and effectively clear PrP^{Sc} from cells *in vitro* (Korth *et al*., 2001), quinacrine was believed to be an excellent drug candidate to combat prion disease. However, a recent clinical trial using quinacrine did not improve survival in sCJD cases (Geschwind *et al*., 2013). Other drugs have been tested in animal models with varying degrees of therapeutic efficacy (Riemer *et al*., 2007). However, these treatments were not effective when animals were injected with higher dosage of infectious material. In humans, diagnosis occurs very late in the disease course, a time period when high dosage of infectious prion material is expected in the CNS. Therefore, these drugs will likely not be efficacious in humans unless a good preclinical biomarker can be discovered and treatment commenced at the earliest possible time, ideally before clinical symptoms are observed. In addition to drug-based approaches, antibodies designed to target regions of prion protein after it misfolds have been developed. Using these antibodies as a vaccine in highly susceptible Tga20 mice revealed that animals remained disease free (clinically and pathologically) even when only 3 vaccine doses were administered (Maattanen *et al*., 2013). It would be most interesting to determine whether this vaccine strategy works once clinical disease has commenced.

Another therapeutic avenue was to develop compounds that could interfere with the conversion process from normal form of the prion protein, PrP^{C}, to the infectious form, PrP^{Sc} by modulating the expression of PrP^{C} or making it inaccessible for conversion. Several different molecules have been used for this purpose including drugs, antibodies and small RNA

molecules. Several drugs that proved effective in animal models failed in clinical trials showing no or modest treatment efficacies (reviewed in Sim and Caughey, 2009). A recent drug screening targeted to identify compounds which decreased PrP^{C} expression among drugs already approved for human use revealed a promising candidate, astemizole. This drug is used to treat seasonal allergic rhinitis and was found to slightly prolong survival of prion-infected mice (Karapetyan *et al*., 2013). Another approach was to render PrP^{C} inaccessible to conversion using antibodies that specifically targeted certain epitopes of PrP^{C}. These antibodies effectively blocked available regions on the protein required for propagation of PrP^{Sc} (Enari *et al*., 2001; Peretz *et al*., 2001; Gilch *et al*., 2003). Lastly, small RNA molecules have been used to specifically deplete the expression of the prion protein gene, *Prnp*, and therefore limit the number of PrP^{C} molecules on the cell surface. By using short hairpin RNAs (shRNAs) or short interfering RNAs (siRNAs), successful knockdown of PrP^{C} was observed *in vitro* (Tilly *et al*., 2003; Daude *et al*., 2003) and *in vivo* (White *et al*., 2008). Although depletion of PrP^{C} is well tolerated in animals (Manson *et al*., 1994; Bueler et al., 1992; Yu *et al*., 2009; Zhu *et al*., 2009; Richt *et al*., 2007), the potential side effects of decreasing PrP^{C} expression in humans has yet to be determined. Therefore, caution needs to be taken when designing these types of targeted therapeutics for human use.

One promising approach for therapy development is by modulating key molecules that are central to the process of neurodegeneration. One such recently identified candidate is the α–subunit of eukaryotic initiation factor 2 (eIF2α) which is part of the unfolded protein response (UPR). This protein becomes phosphorylated during prion disease and causes a shutdown of global protein synthesis (Moreno *et al.,* 2012). A total shutdown of protein synthesis impedes the production of proteins critical for normal function of neurons, causing eventual cellular degeneration and death. Over-expression of GADD34, a specific eIF2α phosphatase, effectively

reversed the shutdown of protein synthesis and helped prion-infected animals survive significantly longer (Moreno *et al.,* 2012). A similar effect was observed when another component of the UPR system upstream of eIF2α was targeted (Moreno *et al.,* 2013). These data provide evidence that molecules outside the PrP^{Sc} conversion process can be beneficial targets for therapy development. Clearly, further research is required to glean a better understanding of the disrupted molecular processes involved in degeneration. Unraveling the molecular basis of neurodegeneration holds promise to ignite the development of a universal treatment against these conditions.

1.4 Two Major Prion Protein Isoforms

During the 1960s, it was proposed by two researchers that TSEs are caused by an infectious agent devoid of nucleic acids; namely a protein (Alper *et al.,* 1967; Griffith, 1967). Several decades later, this protein was isolated and termed "prion" due to its properties as a "proteinaceous infection particle" (Prusiner, 1982). The prion protein exists in two major conformational isoforms, the normal form of the prion protein (PrP) termed cellular PrP (PrP^{C}) and the infectious, misfolded form termed Scrapie PrP (PrP^{Sc}). This led to the formulation of the protein-only hypothesis which proposes that the infectious agent is a protein that self-propagates by misfolding PrP^{C} in the absence of nucleic acids. Additional evidence in support of this revolutionary idea began to accumulate within the past 10 years once the infectious prion particles were successfully formed *in vitro* without the presence of nucleic acids (Castilla et al., 2005; reviewed in Diaz-Espinoza and Soto, 2010). In fact, full-length recombinant PrP that was converted into cross-β-sheet amyloid fibrils in the presence of normal brain homogenate or albumin resulted in the production of infectious PrP when inoculated into wild-type hamsters

(Makarava *et al*., 2010). Serial transmission into hamsters gave rise to very slow progressive phenotype after onset of clinical signs (Makarava *et al*., 2010). Recently, infectious PrP was generated by using a bacterially expressed PrP as a template for the serial protein misfolding cyclic amplification (PMCA) assay (Zhang *et al*., 2013). Intracerebral inoculation of these generated infectious prions caused disease in wild-type mice (Zhang *et al*., 2013) and intraperitoneal inoculation of these synthetically generated prions were pathogenically and pathologically identical to naturally occurring prion disease (Wang *et al*., 2015). However, many questions pertaining to the physical nature of an infectious "prion" still remains unanswered, including the molecular basis of prion-induced neuronal toxicity that triggers the neurodegenerative process.

1.4.1 The Cellular Prion Protein (PrP^C)

The normal form of the prion protein is encoded by the *PRNP* gene (Basler *et al.,* 1986). The gene has 2 exons that are separated by an intron; exon 2 contains the open reading frame of PrP^C (Puckett *et al.,* 1991). The gene is located on chromosome 20 in humans and chromosome 2 in mice (Sparkes *et al.,* 1986; Puckett *et al.,* 1991) and produces a protein ~ 250 amino acids (aa) in length and 30-35 kDa in size (**Figure 1.2**). The PrP^C protein contains an N-terminal region that is flexible and random coiled followed by a globular C-terminal domain consisting of 3 α-helices and 2 β-sheets (Zahn *et al.,* 2000). At the N-terminus, a signal domain of 22 aa mediates transport of the protein to the Golgi where it is glycosylated and further transported to the cellular membrane. A total of 4 octapeptide domains (PHGGGWGQ) are located within the octapeptide repeat region which allows binding to metal ions at varying affinities, including Zn^{2+}, Cu^{2+}, Ni^{2+} and Mn^{2+} (Jackson *et al.,* 2001). The C-terminus consists of two glycosylation

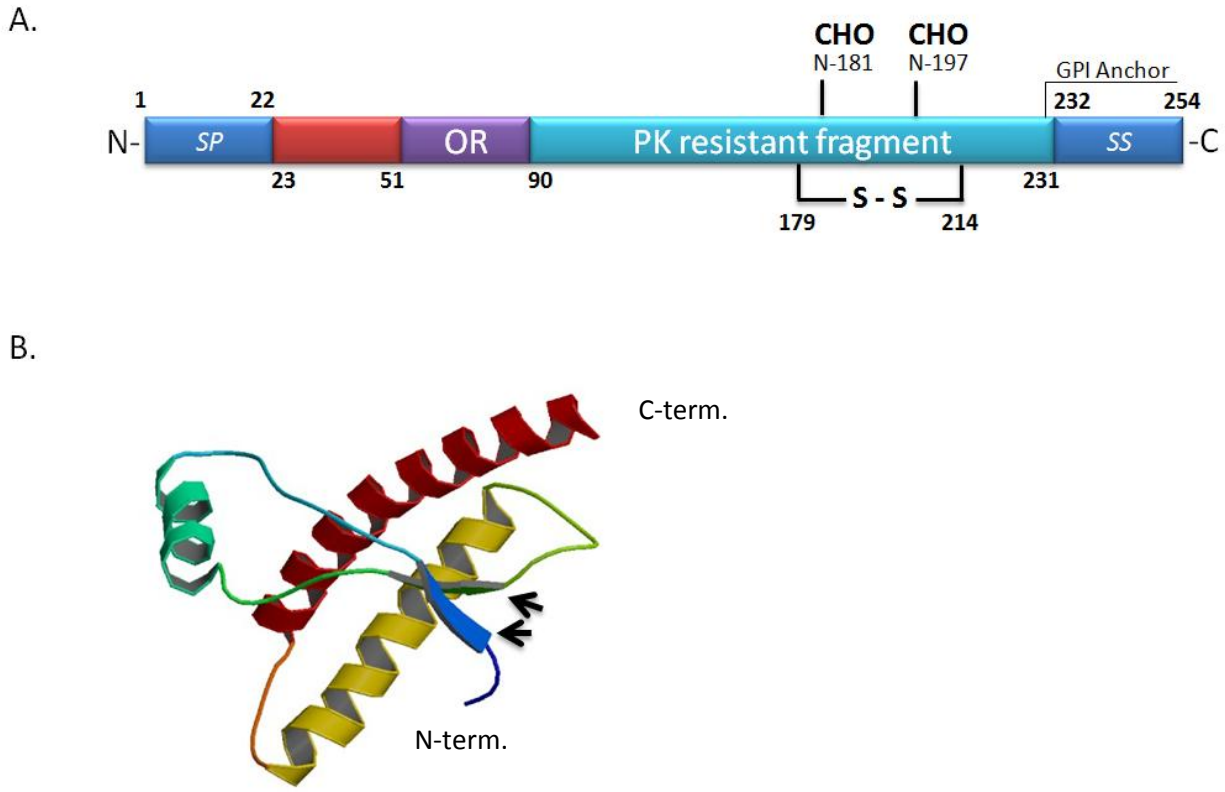

Figure 1.2. The human cellular prion protein (PrP^C). (**A**) Linear form of PrP^C depicting several features of the protein. SP represents signl peptide; OR represents octapeptide region; PK is Proteinase K; SS is signal sequence. S-S indicates the location of the disulphide linkage and CHO are carbohydrate modification sites. (**B**) Three dimensional reconstruction of PrP^C as determined by Zahn *et al.*, 1999. The structure was provided by the protein databank (Berman, 2010). Arrows indicate the 2 β-sheets while the 3 α-helices are identified by different colours. The N- and C-termini of the protein are labeled. Note thast this structure does not contain the unstructured N-terminal domain of PrP^C.

sites (181N and 197N) that can be unglycosylated, monoglycosylated or diglycosylated, two residues involved in intra-molecular disulfide bonding and a signal sequence for a glycophosphoinositol (GPI) anchor. A highly conserved hydrophobic core links the random coil to the globular domain of the protein. Biochemical analysis of PrP^C revealed that it is highly sensitive to digestion by cellular proteases, such as proteinase K, extremely sensitive to chemical treatments and becomes inactivated by heat or UV.

PrP^C is expressed in all mammals and in many vertebrates (Lee *et al.,* 1998; Wopfner *et al.,* 1999). Although the primary sequence is fairly diverse across these species, numerous elements of the protein are highly conserved allowing for these proteins to retain specific tertiary fold (Pastore and Zagari, 2007; Wopfner *et al.,* 1999). It is therefore fair to assume that PrP^C must play an important role in cellular processes fundamental to all of these species.

PrP^C is abundantly expressed in the CNS, specifically within neurons (reviewed in Linden *et al.,* 2008). Particular areas of the brain such as the neocortex, hippocampus, thalamus, medulla oblongata, purkinje cells of the cerebellum and spinal motor neurons express the most PrP^C (McLennan *et al.,* 2001; Bailly *et al.,* 2004; Harris *et al.,* 1993; Ford *et al.,* 2002). Peripheral tissues such as all lymphatic organs plus leukocytes and hematopoietic stem cells also express high levels of PrP^C (reviewed by Isaacs *et al.,* 2006; Zhang *et al.,* 2006; Miele *et al.,* 2003; Tichopad *et al.,* 2003) and may contribute to the propagation of prion disease outside of the central nervous system (see *Section 1.5*).

On a cellular level, PrP^C is typically tethered by its GPI anchor (Stahl *et al.,* 1987) to the cell membrane within lipid microdomains called lipid rafts. In neurons, lipid rafts are crucial for various functions including synaptic transmission and growth-factor signal transduction among others (reviewed in Sebastiao *et al.,* 2013). The location of PrP^C on the

cellular membrane points to a similar functional role as observed for other GPI-anchored proteins such as signal transduction and intracellular trafficking (Kasahara and Sanai, 1999). However, the exact function of PrP^C remains largely unknown (see *Section 1.4.1a*). Once located on the extracellular membrane, PrP^C resides there quite briefly (~ 60 minutes) and becomes internalized via copper stimulated endocytosis (Shyng *et al.,* 1993; Pauly and Harris, 1998) that is mediated by clatherin-coated pits in neurons and glia (Shyng *et al.,* 1994; Shyng *et al.,* 1995).

1.4.1a Potential Physiological Roles of PrP^C in Neurons

Numerous PrP^C knockout animals that were generated did not reveal a distinct functional role for PrP^C within neurons (Bueler *et al.,* 1992; Manson *et al.,* 1992). These mice develop normally and only minor abnormalities are observed, such as changes in circadian rhythm and sleep patterns (Tobler *et al.,* 1996), alterations in hippocampal-dependent spatial learning (Craido *et al.,* 2005), deficits in synaptic transmission of hippocampal neurons (Collinge *et al.,* 1994) but not of cerebellar Purkinje cells (Herms *et al.,* 1995), increased sensitivity to oxidative stress (Brown *et al.,* 2002), increased susceptibility to glutamate excitotoxicity (Khosravani *et al.,* 2008; Rangel *et al.,* 2007; Walz *et al.,* 1999), depressive-like behaviour (Gadotti *et al.,* 2012), reduced threshold for pain (Gadotti and Zamponi, 2012) and decreased amount of membrane-associated copper (Singh *et al.,* 2009). However, further studies performed on these mice concurrently with additional *in vitro* work provided glimpses into the cellular processes in which PrP^C may play a role. These include anti-apoptotic function, protection against oxidative stress, synapse function, cell signalling, receptor for amyloid oligomers of AD, involved in microRNA (miRNA or miR) activity, neuronal development and neurite outgrowth, copper and/or zinc ion transport or metabolism and the maintenance of white matter (**Table 1.3**). In

Table 1.3. Physiological roles proposed for PrP^C.

Physiological Role of PrP^C	References
Synaptic transmission and membrane excitability	Collinge *et al.*, 1994; Mallucci *et al.*, 2002; Khosravani *et al.*, 2008
Cell signaling	Reviewed in Linden *et al.*, 2008; Chiarini *et al.*, 2002; Spudich *et al.*, 2005
Neuritogenesis	Graner *et al.*, 2000
Binding and metabolism of divalent metals	Kramer *et al.*, 2001; Chattopadhyay *et al.*, 2005; Thackray *et al.*, 2002; Choi *et al.*, 2006
Anti-apoptotic activity	Bounhar *et al.*, 2001; Gains *et al.*, 2006; Roucou *et al.*, 2003; Lin *et al.*, 2008; Laroche-Pierre *et al.*, 2009
Anti-oxidant activity	Brown *et al.*, 1997a; Brown *et al.*, 1997b; Brown *et al.*, 2002; White *et al.*, 1999; Choi *et al.*, 2007; Oh *et al.*, 2012; Klamt *et al.*, 2001
Uptake and transport of cellular iron	Singh *et al.*, 2009
Potential receptor for amyloid oligomers	Strittmatter *et al*., 2009
Involved in miRNA activity	Gibbings *et al*., 2012

many instances, PrP^C function could be executed by proteins that interact with PrP^C. Some of these auxiliary proteins are laminin, glial fibrillary acidic protein (GFAP) and Bcl-2 (reviewed in Lee *et al.,* 2003a).

One potential function of PrP^C pertains to the reported disruption of calcium homeostasis. Interruption of Ca^{2+} homeostasis causes fluctuations that can have dire consequences on neurons. PrP^C-deficient mice exhibited alterations of Ca^{2+}-dependent K^+ currents in hippocampal pyramidal neurons, cerebellar Purkinje cells and granular cells of the cerebellum that are likely a result of disrupted intracellular Ca^{2+} homeostasis (Colling *et al.,* 1996; Herms *et al.,* 2001; Herms *et al.,* 2000). This suggests that PrP^C may function to regulate intracellular Ca^{2+} homeostasis in neurons but likely through other mechanisms besides directly modulating voltage gated Ca^{2+} channels (Herms *et al.,* 2000). One possible mechanism is via N-methyl-D-aspartate receptor (NMDAR) signaling. When NMDAR become activated it stimulates a signal transduction pathway that is mediated by an influx of Ca^{2+} into the cell. If NMDAR signaling is disrupted, the effects can be measured using electrophysiology. Indeed, neurons from PrP^C knockout mice had impaired synaptic inhibition that was mediated by a weakened γ–aminobutyric acid A ($GABA_A$) receptor-mediated fast inhibition (Collinge *et al.,* 1994). This suggests that inhibitory effects of GABAergic transmission were diminished, causing those neurons to be more excitable and therefore susceptible to glutamate-dependent toxicity termed excitotoxicity (see *Section 1.9.2*). In support of this proposed mechanism, recent evidence suggests that knockout of PrP^C caused an enhanced activation of NMDARs both *in vitro* and *in vivo* resulting in the eventual over-stimulation of these receptors leading to the ultimate death of neurons (Khosravani *et al.,* 2008).

Recently, a transmembrane form of PrP^{C} (comprising ~1-10% of the produced PrP^{C}) has been found to bind to AGO2 via the octapeptide repeat (Gibbings *et al*., 2012). AGO2 is a protein that is part of the microRNA silencing complex which is involved in inhibiting protein translation of certain target transcripts (see *Section 1.15.1*). As a result, PrP^{C} helps enhance and stabilize AGO2-microRNA complexes which is necessary for efficient miRNA-mediated repression (Gibbings *et al*., 2012). Interestingly, mutations within the octapeptide repeat region cause inherited neurological diseases while accumulation of transmembrane PrP^{C} was detected in Creutzfeldt-Jacob disease animal models (Hedge *et al*., 1999; Emerman *et al*., 2010).

Another possible role of PrP^{C} is its function as a receptor for amyloid-β oligomers. It has been shown that PrP^{C} binds to synthetic amyloid-β oligomers with high affinity and therefore contributed to the oligomer-mediated inhibition of hippocampal long-term potentiation (Strittmatter *et al*., 2009). Therefore, PrP^{C} may have a direct role in the neuropathology of Alzheimer's disease and has been shown to be an accurate measure of memory impairment in AD mouse models and human AD patients (Kostylev et al., 2015).

1.4.2 Infectious Prion Protein (PrP^{Sc})

The infectious prion protein was first discovered to co-purify in brain extracts from rodents infected with prions. Proteinase K digestion produces PrP^{Sc} molecules that are 27-30kDa in size which consist of 142 aa C-terminal segments while PrP^{C} completely degrades (Bolton *et al.,* 1984; McKinley *et al.,* 1991). Biochemical analysis of PrP^{Sc} revealed that it had an identical primary sequence and post-translational modifications as PrP^{C} which include glycosylations and the GPI anchor. Modifications such as the 2 *N*-glycans of PrP^{C} are therefore not required for conversion of PrP^{C} to PrP^{Sc} (Tuzi *et al.,* 2008; Neuendorf *et al.,* 2004). Only the structural

conformation was found to be unique, accounting for their diverse physical and chemical properties (Stahl *et al.,* 1993). The secondary structure of PrP^{Sc} is primarily β-sheet in conformation (**Figure 1.3**) causing insolubility, resistance to heat and UV inactivation plus resistance to treatment by several chemicals including acids, bases and bleach (Stahl *et al.,* 1993; Pan *et al.,* 1993; McKinley *et al.,* 1986; Caughey *et al.,* 1991). Most importantly, this β-sheet conformation exposes parts of the protein normally buried allowing for a higher degree of "stickiness" between these proteins (Nelson *et al.,* 2005). As a result, PrP^{Sc} has the propensity to aggregate into prion fibrils believed to be composed of trimeric left-handed β-helical discs that stack on top of each other (Wille *et al.,* 2002; Govaerts *et al.,* 2004). These can range from various polymeric sizes that include oligomers, protofibrils and fibrils (reviewed in Caughey and Lansbury, 2003). All of these sizes are commonly detected within prion-infected brain tissue, however, only the soluble oligomers (sizes ranging from 17-27nm) have by far the highest infectivity and activity of structural conversion (Silveira *et al.,* 2005). Non-fibril particles that are of equivalent mass to 14-28 PrP molecules, composed solely of PrP^{Sc}, are therefore the most infectious (Silveira *et al.,* 2005) and toxic to neurons (Simoneau *et al.,* 2007).

1.5 Routes of PrP^{Sc} Infection and Spread to the CNS

The most relevant route of acquired prion disease in nature is via oral ingestion of prion contaminated material which enters the stomach and crosses the wall of the digestive tract at the follicle-associated epithelium of the Peyer's patches (Kimberlin and Walker, 1989; Prinz *et al.,* 2003). At these locations, infectious prions can transverse the intestinal wall via microfold cells (M cells) (Heppner *et al.,* 2001; Donaldson *et al.,* 2012) or through enterocyte-mediated transcytosis (Kujala *et al.,* 2011). Experimental evidence has also indicated that prions can be

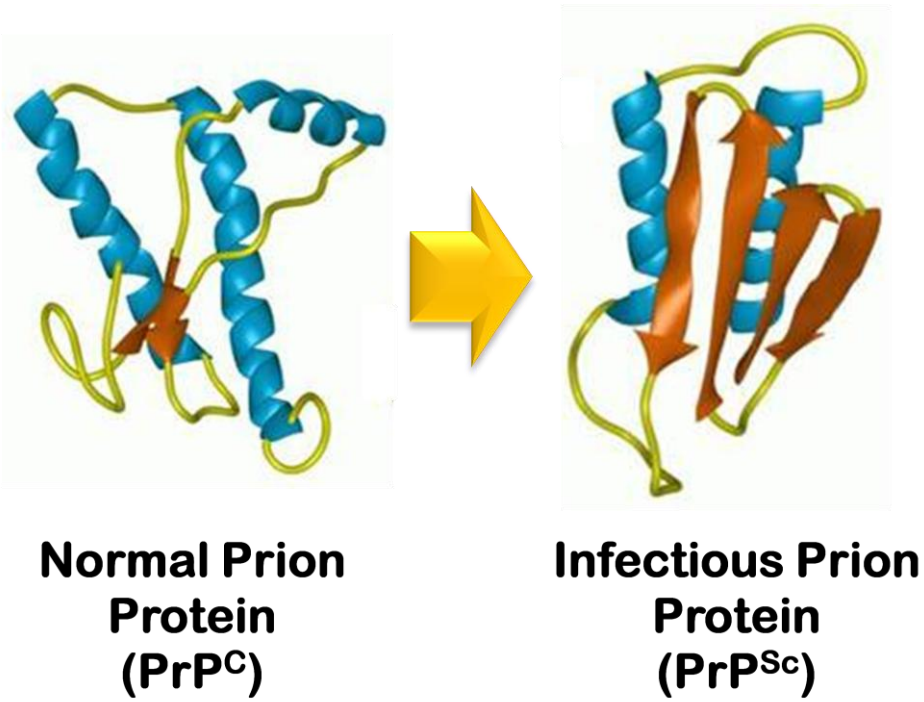

Figure 1.3. Structure of the 2 isoforms of the prion protein. The normal PrP^{C} is primarily composed of α–helices (blue) while a model of the infectious PrP^{Sc} form is primarily β–sheet (orange). Of note, atomic-level structures are not available for PrP^{Sc}. Image adapted from BSEinfo, 2015.

transmitted through the skin (Carp, 1982; Glaysher *et al.,* 2007; Mohan *et al.,* 2004) and via aerosols (Denkers *et al.,* 2013; Haybaeck *et al.,* 2011; Nichols *et al.,* 2013) which allows prions to colonize draining lymph nodes soon after exposure. In these cases, M cells and epithelial cells of the nasal mucosa seem to be involved in prion transport (Kincaid *et al.,* 2012).

Once the infectious prions pass through the intestinal wall, local dendritic cells can aid their entry into the blood and lymphatic fluid (Raymond *et al.,* 2007). Through this peripheral route of exposure, PrP^{Sc} typically invades lymphoid organs where it undergoes first rounds of replication and accumulation. Peripheral replication of PrP^{Sc} is an important determinant of the incubation time of disease (Kimberlin and Walker, 1989) and does not alter the function of the immune system or other peripheral organs before neuroinvasion is observed (Aguzzi *et al.,* 2013). Of note, PrP^{Sc} replication in peripheral organs does not occur in all instances (Mohri *et al.,* 1987) and the degree of lymphotropism is dependent on several factors including the strain of PrP^{Sc}, route of inoculation, host species and the gene sequence encoding PrP^{C} (reviewed in Aguzzi *et al.,* 2013). Depending on the initial site of PrP^{Sc} exposure, different peripheral organs may serve as reservoirs for amplification and/or delivery into the CNS. From these peripheral sites, amplified PrP^{Sc} begins to enter the CNS mainly via peripheral nerves through the sympathetic and parasympathetic nerves (Clarke and Kimberlin, 1984; Cole and Kimberlin, 1985; McBride and Beekes, 1999; Heggebo *et al.,* 2003; Haik *et al.,* 2003). However, PrP^{Sc} can also access the CNS by directly passing through the blood-brain barrier (Banks *et al.,* 2004). Once nerves are invaded by infectious prions, these proteins travel up the spinal cord to the brain. Although this mechanism remains largely unknown, prions may be internalized at the nerve endings and be transported to the cell soma using retrograde transport (Bartz *et al.,* 2002). To date, the original site of PrP^{Sc} misfolding in sCJD, the most common human prion disease

remains unidentified. However, ~1 in 3 patients had detectable levels of PrP^{Sc} within their peripheral tissues (Glatzel *et al.*, 2003).

1.6 PrP^{Sc} Formation and Propagation

Except for acquired prion disease, the initial step in the formation of self-propagating proteinaceous particles within an organism is largely unknown. Once the infectious prion protein is generated it acts as a template to promote conversion of PrP^{C} into PrP^{Sc}, leading to aggregate formation. However, the mechanism of PrP^{Sc} conversion and subsequent aggregation is also unknown. Two distinct standard models have emerged in order to explain this process: 1) the template-assisted model and, 2) the seeding/nucleation model (**Figure 1.4**). These models will be briefly described below.

The template-assisted model proposes that PrP^{Sc} molecules contain refolding blueprints that are applied to PrP^{C} upon interaction of the two isoforms. This conversion is catalyzed by an enzyme or a chaperone (termed protein X) and mediated by the formation of a conformational intermediate (reviewed in Cohen and Prusiner, 1998). This process is kinetically controlled where a high activation energy barrier prevents spontaneous conversion. Once converted, a dimer of PrP^{Sc} molecules is produced which interacts with other dimers forming larger aggregates. However, oligomers composed of less than six units of PrP^{Sc} were non-infectious in Syrian hamsters (Silveira *et al.*, 2005), which challenges the likelihood of this model.

The seeding/nucleation model follows thermodynamic principles and proposes that PrP^{C} and PrP^{Sc} exist in equilibrium with each other where formation of PrP^{C} is strongly favoured. In turn, the monomeric PrP^{Sc} is only stabilized once it aggregates and forms oligomers. These

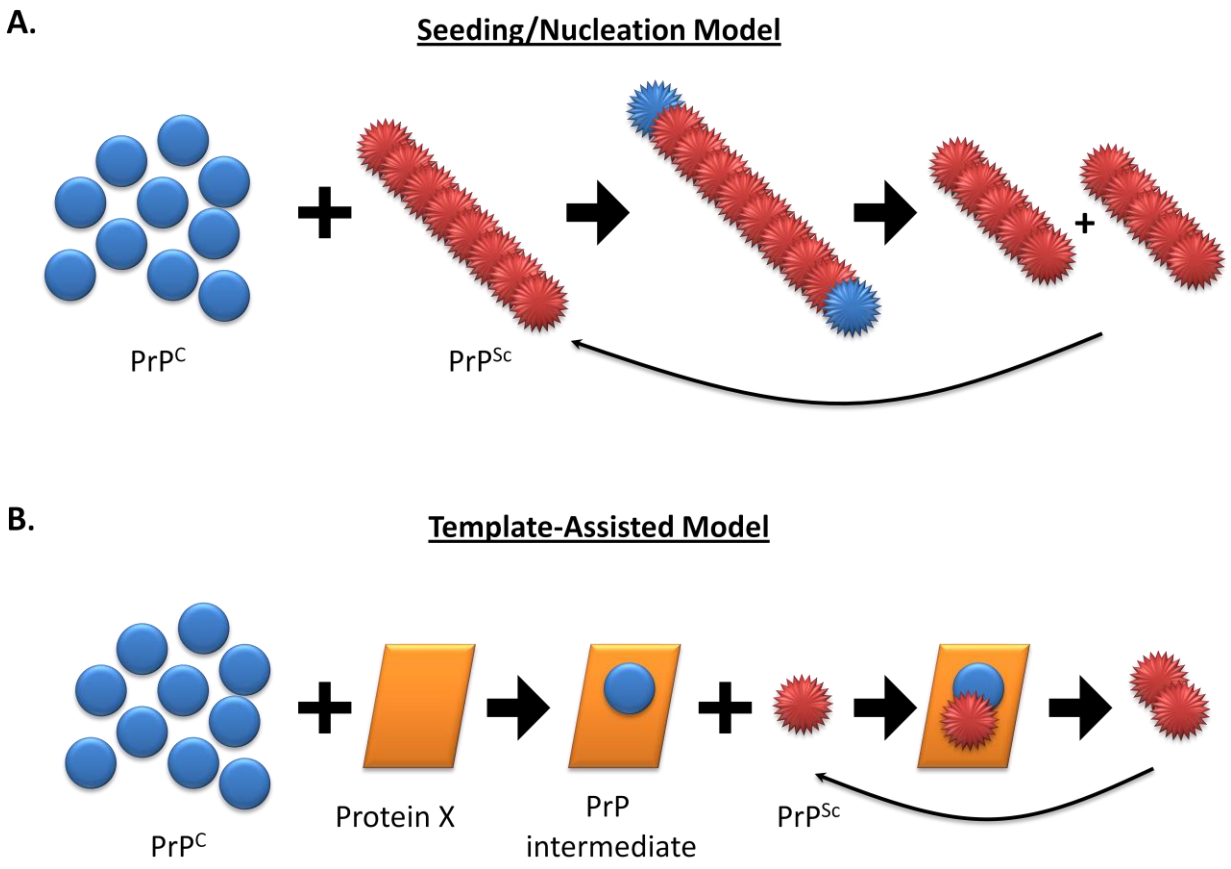

Figure 1.4. Two models proposed to explain PrP^{Sc} propagation. (**A**) Schematic diagram of the seeding/nucleation model proposes that PrP^{C} and PrP^{Sc} exist in equilibrium with each other where formation of PrP^{C} is favoured. PrP^{Sc} oligomers act as seeds that bind and help stabilize PrP^{Sc} monomers. These PrPSc oligomers aggregate and fragment which are then used as seeds for further conversion. (**B**) Schematic diagram of the template assisted model which proposes that protein X (co-factor) catalyzes the conversion of PrP^{C} into a conformational intermediate. The PrP intermediate then interacts with PrP^{Sc} to produce a dimer of PrP^{Sc} molecules. These PrP^{Sc} dimers then serve as a template for further conversion. Adapted from Abid and Soto, 2006.

oligomers act as seeds that bind and further stabilize PrP^{Sc} monomers. Once a seed is generated, recruitment of monomeric PrP^{Sc} occurs at a much faster rate than the initial seed formation. Perhaps the continual fragmentation of large aggregates which increase the surface area for conversion could explain the observed exponential increase of PrP^{Sc} during infection.

In cells, conversion of PrP^{C} to PrP^{Sc} occurs on lipid rafts and/or along the endocytic pathway prior to exposure of the content to the lysosome (Veith *et al.,* 2009). These are either recycled to the cell surface or enter the Golgi through retrograde transport (Goold *et al.,* 2013) and are quickly degraded by lysosomes (Luhr *et al.,* 2004; Goold *et al.,* 2013; Barmada and Harris, 2005; Uchiyama *et al.,* 2013). However, progressive accumulation of PrP^{Sc} in the Golgi delays the recycling of other proteins back to the cell surface, including PrP^{C} (Uchiyama *et al.,* 2013). PrP^{Sc} can spread to nearby cells by cell-to-cell contact (Tanaka *et al.,* 2010; Paquet *et al.,* 2007) and/or released by microvesicles into the extracellular space (Fevrier *et al.,* 2004; Alais *et al.,* 2008). As a result, PrP^{Sc} is detected both intra- and extra-cellularly.

1.7 Prion Strains

Multiple PrP^{Sc} isoforms have been isolated from nature and designated as strains. These different strains of PrP^{Sc} have unique properties of infectivity, species tropism, pathology, neurotropism and biophysical traits including protease sensitivity and glycoform ratio (reviewed in Morales *et al*., 2007; Solforosi *et al*., 2013). Furthermore, these strain properties are often retained on serial transmission (Dickinson and Meikle, 1969; Fraser and Dickinson, 1973). Unlike for viruses, prion strains are not produced by accumulating mutations within the nucleic acids because the prion-only hypothesis dictates that the infectious particles leading to prion disease are only misfolded proteins. Therefore, the specificity of prion strains must arise from

conformational variability. In other words, PrP^{Sc} can assume several different conformations that retain its self-propagating potential and thus enciphers a distinct protein strain (Bessen and Marsh, 1994; Collinge *et al*., 1996; Telling *et al*., 1996; Peretz *et al*., 2001a). The diversity of these conformational states may be a result of various factors including the amino acid sequence of the substrate PrP^{C}, the environment where conversion occurs (Deleault *et al*., 2012; DebBurman *et al*., 1997) and the process leading to the selection of the dominant strain from the initial PrP^{Sc} population (Collinge, 2010; Giles *et al*., 2010). It is speculated that the phenomenon of domain swapping, which has been documented in other proteins (reviewed in Bennett *et al*., 1995) may be responsible, at least in part, for the generation of different prion strains (reviewed in Cohen and Prusiner, 1998). Interestingly, animal work has shown that molecules with the PrP sequence which is most suited to adopt the PrP^{Sc} template within the organism are selected for conversion (Ghaemmaghami *et al*., 2013). This suggests that PrP^{Sc} exist as a conformationally diverse population and when separated, each strain can replicate with high fidelity. However, within an organism, the properties of these strains slowly changes in such a way as to adopt the conformation that is most optimal for *in vivo* propagation (Ghaemmaghami *et al*., 2013). As a consequence, the competition and selection among the pool of strains generated can provide a mechanism for the transformation and adaptation of PrP^{Sc} across different host species (Li *et al*., 2010).

1.8 The Species Barrier

Interspecies and intraspecies transmission of infectious prions has been observed in prion diseases. The efficiency of such a transmission across different species is attributed to a phenomenon called the species barrier. This barrier represents natural mechanisms that prevent

the spread of the disease from one species to another. Occasionally, the species barrier is of sufficient magnitude to completely block transmission or prevent many animals from getting sick from the disease (Hill *et al*., 2000). This barrier however can be negligible depending on the species involved. For example, the scrapie prion identified in sheep is not transmitted to humans based on epidemiological data but the BSE prion identified from diseased cattle is transmitted to humans and is responsible for the emergence of vCJD (Hill *et al*., 1997; Bruce *et al*., 1997). It is believed that the major contribution for the species barrier is the concept of PrP^{Sc} strains, which highlight the ability of certain prion strains to be transmissible to other species (reviewed in Hagiwara *et al*., 2013). Due to the observed adaptability of prion strains within a new host species, it is believed that the species barrier does not block disease entirely but rather prolongs disease onset for an extended period of time. During this time, PrP^{Sc} replicates and slowly adapts to the PrP^{C} template of the new host, resulting in the eventual manifestation of clinical disease (Castilla *et al*., 2008). If this newly generated prion strain is passaged within the same species, the incubation period becomes shortened as the new strain stabilizes within the host environment (reviewed in Hill and Collinge, 2004).

1.9 Neurotoxicity of PrP^{Sc}: Mechanisms of Neuronal Degeneration

1.9.1 Initiation of Degeneration by PrP^{Sc}

Animal studies revealed that PrP^{C} must be expressed on the surface of neurons for prion disease to occur (Brandner *et al.*, 1996; Chesebro *et al.*, 2005; Mallucci *et al.*, 2003). However, the molecular basis for the observed prion-induced neurotoxicity remains unknown. To date, three possible scenarios have been proposed: 1) loss of PrP^{C} function; 2) gain of direct toxic function of PrP^{Sc} and; 3) gain of indirect toxic function by changing the role of PrP^{C}.

Based on the potential roles attributed to PrP^C (**Table 1.3**) it is possible that its loss during prion disease may result in neurodegeneration (reviewed in Hetz *et al.,* 2003). However, compelling counter evidence suggests that loss of PrP^C is not the initiating factor for prion-induced neurodegeneration. For example, PrP^C null mice are fairly healthy (see *Section 1.4.1a*) and do not show any disease phenotype after infection with prions. On the contrary, knockdown of PrP^C in prion-infected animals decreased pathology and increased animal survival (Mallucci *et al.,* 2003; White *et al.,* 2008) further indicating that loss of PrP^C function during prion disease is not the catalyst for neurodegeneration.

The progressive accumulation of PrP^{Sc} in the brain may directly cause a toxic effect on neurons. It is known that PrP^{Sc} aggregates accumulate in areas of the brain that are most damaged during disease (Ettaiche *et al.,* 2000; Hetz *et al.,* 2003; Simoneau *et al.,* 2007) which can stimulate production of significant endoplasmic reticulum (ER) stress (Hetz *et al.,* 2003). In support of these observations, ER stress markers were detected in brain areas containing substantial accumulation of PrP^{Sc} from scrapie-diseased mice and humans suffering from sporadic and variant CJD (Hetz *et al.,* 2003). ER is part of the secretory pathway which functions to synthesize, modify and deliver proteins to other subcellular locations. PrP^C is one of these proteins that pass through the ER before it is delivered to the cell membrane. Once ER stress occurs, it invariably affects PrP^C trafficking which itself can lead to the formation of potentially neurotoxic forms of PrP (Rane *et al.,* 2008; Orsi *et al.,* 2006).

Even though PrP^{Sc} accumulation, neurodegeneration and disease in most cases are well correlated, rare cases exist where disease is observed in the absence of detectable PrP^{Sc} (Lasmezas *et al.,* 1997) and when an abundance of PrP^{Sc} deposits are observed with no neurodegeneration or disease (Piccardo *et al.,* 2007). These observations suggest that other

factors aside from the presence of PrP^{Sc} are required to initiate disease. Perhaps the presence of small toxic oligomers which are not detectable by conventional immunohistochemical assays (*Section 1.4.2*) are responsible for pathology and clinical signs of disease. Another possible explanation is that the replicative and infectious form of PrP^{Sc} is not the same as the neurotoxic form (Harris and True, 2006). Lastly, PrP^{Sc} could modify the normal function of PrP^{C} through direct binding. In CJD patients, PrP^{Sc} accumulates at synaptic terminals (Kitamoto *et al.,* 1992) prior to the detection of neuronal dysfunction. At these sites, PrP^{Sc} binds to PrP^{C} which could activate a signal transduction pathway leading to neurotoxicity rather than neuroprotection. This effect can be produced by PrP^{Sc} cross-linking cell-surface PrP^{C}, which induces neuronal apoptosis *in vivo* (Solforosi *et al.,* 2004).

1.9.2 Mechanisms of Neuronal Death

To date, data suggests that neurons die as a result of chronic overstimulation of NMDARs which makes them susceptible to NMDA-induced excitotoxicity (Khosravani *et al.,* 2008). Autophagy and apoptosis are two main pathways that have also been implicated in prion-induced neurodegeneration. Importantly, many molecules are shared among these pathways (Fimia and Piacentini, 2010) and all could be important contributors to death of neurons in prion disease. However, the exact molecular mechanism causing neuronal death still needs to be elucidated.

Overstimulation of NMDARs can result in cellular damage and death due to excitotoxicity mechanisms. Under physiological conditions, excitatory neurotransmitters including glutamate bind to and activate receptors such as NMDARs and α-amino-3-hydroxy-5-methyl-4-isoxazolepropionic acid receptors (AMPARs) which cause an influx of Ca^{2+} into the

cell and mediates signal transduction. These processes are under strict homeostatic control. When NMDARs become over-stimulated, via a glutamatergic storm or by removal of inhibitory controls, excessive amount of Ca^{2+} enters and overwhelms the cell. This in turn causes activation of numerous cellular processes and enzymes that progressively damage and degrade the neuron. In prion disease, it has been proposed that NMDARs become over-stimulated due to the lack of inhibitory function by PrP^{C} (Collinge *et al.,* 1994; Maglio *et al.,* 2004; Khosravani *et al.,* 2008). This in turn causes disruptions in Ca^{2+} homeostasis and result in a hypersensitive state to excitotoxicity (reviewed in Black *et al.,* 2014). Downstream effects of NMDAR activity, mainly perturbations in Ca^{2+} signaling and homeostasis, were also detected in several studies of prion-infected animals. For example, Ca^{2+}/calmodulin-dependent phosphatase calcineurin (CaN) controls intracellular Ca^{2+} signalling and was induced at late stages of prion disease (Biasini *et al.,* 2006). When CaN was inhibited, prion-infected animals survived longer and had decreased neurodegeneration (Mukherjee *et al.,* 2010). Several additional groups reported a reduced Ca^{2+} response in prion-infected brain and/or cultured neurons that likely lead to the detected electrophysiological and morphological synaptic abnormalities (Chiti *et al.,* 2006; Wong *et al.,* 1996; Florio *et al.,* 1998; Barrow *et al.,* 1999). This type of disruption in Ca^{2+} homeostasis and signaling was also identified in other neurodegenerative diseases including AD, HD and PD (reviewed in Dong *et al.,* 2009). This implies that a common process of neurodegeneration may be involved in all of these diseases, a process that warrants further study.

Intracellular organelles and long-lived proteins are degraded by the catabolic mechanism of autophagy. This cellular degradation process has been implicated in protein and organelle turnover, stress response, cellular differentiation and programmed cell death (reviewed in Lee 2009; Mizushima 2009). Typically, organelles and proteins are sequestered in a vesicle called an

autophagosome. This vesicle fuses with a lysosome to form an autophagolysosome at which point lysosomal hydrolases degrade the contents of the vesicle. In prion-infected cells, stimulation of autophagy significantly reduced PrP^{Sc} in a dose- and time-dependent manner (Aguib *et al.,* 2009; Heiseke *et al.,* 2009) while inhibition of autophagy caused the opposite effect (Aguib *et al.,* 2009). In prion infected patients, these types of vacuoles have been detected (Liberski *et al.,* 2008) and could play an important role in prion-induced neurodegeneration (Liberski *et al.,* 2004; Sikorska *et al.,* 2004; Liberski *et al.,* 2008).

Apoptosis is a form of programmed cell death typically mediated by proteases known as caspases (reviewed in Degterev *et al.,* 2003). However, caspases are rarely detected in prion disease (Nuvolone *et al.,* 2015) and are likely not an important mechanism of cell death. Indeed, no change in disease progression was observed in prion-infected animals after deletion of caspase-12 (Steele *et al.,* 2007) suggesting that caspase-dependent apoptosis may not be involved in prion-induced neurodegeneration.

1.10 Synaptic and Dendritic Alterations during Prion Disease

One of the earliest pathological abnormalities observed in prion-induced neurodegeneration are synaptic and dendrite structural and functional irregularities. Progressive loss of spine structures and therefore functions, have been observed in animal models of prion disease (Jeffrey *et al.,* 2000; Johnston *et al.,* 1997; Hogan *et al.,* 1987; Belichenko *et al.,* 2000; Fuhrmann *et al.,* 2007), prion-infected organotypic slice cultures (Campeau *et al.,* 2013) and brain samples from CJD patients (Ferrer *et al.,* 1981; Landis *et al.,* 1981). The loss of spine structures leads to communication failure between neurons and is associated with early behavioural deficits (Cunnigham *et al.,* 2003; Hilton *et al.,* 2013). In fact, this pathology

precedes the manifestation of severe clinical signs of disease and eventual death of neurons (Fuhrmann *et al.,* 2007; Cunningham *et al.,* 2003). However, our current understanding of this process on a molecular level remains extremely limited. Gene expression studies can therefore be performed to help elucidate the molecular alterations that occur in disease-affected neurons.

1.11 Unraveling the Molecular Processes Involved in Prion-Induced Neurodegeneration: A Transcriptomic Approach

Gene expression profiling technologies provide one of the most comprehensive, global views of studying alterations within the transcriptome. Using microarray or next generation sequencing platforms, one can identify the global transcriptional profile at any given time within the cell. Through this approach, one can measure the activity of thousands of genes at once and obtain a global picture of the cellular functions. Other "–omic" approaches such as proteomics can identify changes in protein expression, although only a fraction of the total proteins can be identified in the cell at one time using proteomic approaches such as mass-spectrometry. Therefore, gene expression profiling provides the most inclusive global picture possible to obtain in a single experiment. Emergence of sophisticated bioinformatics analysis software provides the capability to analyze this high-throughput data and thereby build gene ontology networks in order to identify the pathways that are deregulated. In parallel with the bioinformatics software, the reference databases for gene associations are becoming increasingly encompassing and informative. Furthermore, with the development of improved technologies and reagents, the amount of starting material required for these platforms has significantly decreased over the years, allowing for accurate profiling of transcripts from only a few cells. As a result, numerous

gene expression studies were performed in an effort to identify the molecular processes that were deregulated during prion disease.

1.12 Previous Gene Expression Profiling Studies Performed in Prion Mouse Models Lack Neuronal Representation

Many global transcriptional profiling studies using mouse models of prion disease were performed over the years from which a temporally driven molecular signature emerged (**Figure 1.5)**. Interestingly, deregulation of these biological processes are inoculation route and prion strain-independent because numerous mouse strains were inoculated intracerebrally or intraperitoneally with different prion strains including ME7, RML, 22A, 79A and 139A (refer to **Table 1.4** for details). Furthermore, several of these studies profiled gene expression changes in certain brain regions including the hippocampus (Brown *et al*., 2005), cortex, medulla and pons (Riemer et al., 2004) while others analyzed gene expression of whole brain tissue from varying strains of mice (**Table 1.4**). Several of these molecular processes identified by these transcription studies will be briefly discussed below. However, neuronal-specific transcriptional changes were not well represented and molecular processes that reflect neurodegeneration remain unidentified. Of note, different gene expression profiles have been detected when using different prion strains, different mouse genetic backgrounds as well as different routes of inoculation. These differences in gene expression are most pronounced when analyzing preclinical time points, which likely reflects the difference in incubation period and neuropathology of the mouse model of prion disease used for the studies.

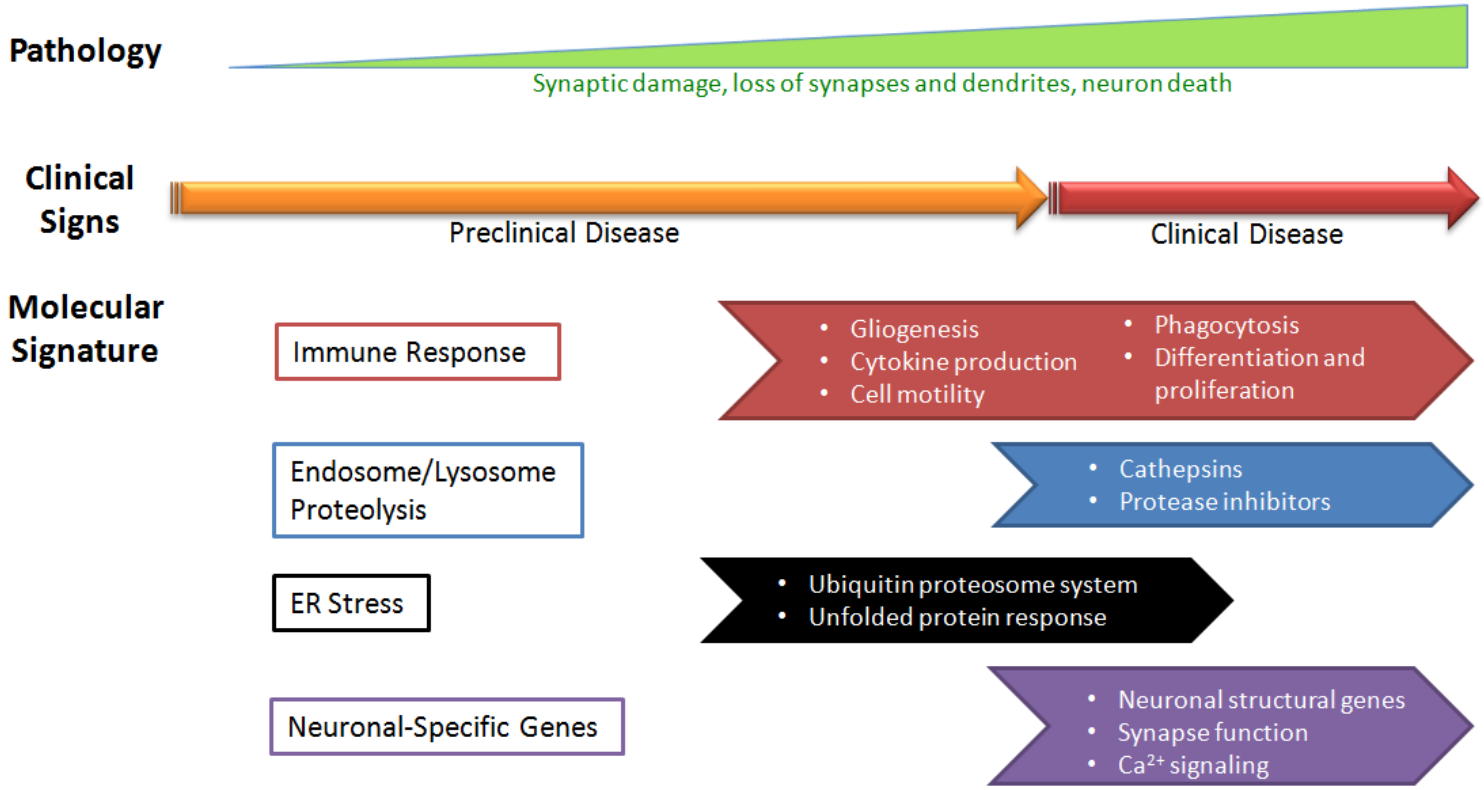

Figure 1.5. Temporal deregulation of transcripts identified during prion disease in whole brain or macrodissected brain regions. As prion disease progresses from preclinical to clinical disease, pathology such as synaptic damage, loss of synapses and dendrites followed by neuronal death accumulate within the brain. Transcriptional profiling approaches revealed a molecular signature that represents genes involved in immune response, endosome/lysosome proteolysis, endoplasmic reticulum (ER) stress and neuronal-specific genes. Genes within these processes are deregulated as indicated by the ribbons. The specific molecular signatures depicted in the figure are explained in more detail within the text. Modified from Majer and Booth, 2014.

Table 1.4. Previous transcriptional studies performed in mouse models of prion disease.

Mouse Genetic Background	Prion Strain	Inoculation Route	Brain Tissue Collected	Reference
C57BL/6	79A, ME7	Intracerebral	Total Brain	Booth *et al*., 2004
CV	ME7	Intracerebral	Total Brain	Brown *et al*., 2004
C57BL/6	139A	Intraperitoneal	Cortex, Medulla, Pons	Riemer *et al*., 2004
C57BL/6	ME7, RML	Intracerebral	Total Brain	Xiang *et al*., 2004
CV	ME7	Intracerebral	Hippocampus	Brown *et al*., 2005
C57BL/10	ME7, 22L, Chandler/RML	Intracerebral	Total Brain	Skinner *et al*., 2006
C57BL/10	ME7, 22L, Chandler/RML	Intracerebral	Total Brain	Kim *et al*., 2008
VM C57BL/6	22A 22A, ME7, 79A	Intracerebral	Total Brain	Sorensen *et al*., 2008
B6, B6.1, FVB, Tg4053, $Prnp^{0/+}$, $Prnp^{0/0}$	RML, 301V	Intracerebral	Total Brain	Hwang *et al*., 2009
CD-1	RML	Intraperitoneal	CA1 Hippocampal Neurons	Majer *et al*., 2012

1.12.1 Immune Response and Related Genes

Immune related genes were found to be one of the largest, most consistently deregulated groups of genes identified from the whole brain of prion-infected animal models, irrespective of the models used. Several of these pathways were found to be induced during preclinical stages of disease coinciding with the detection of PrP^{Sc} deposits (Xiang *et al.,* 2004; Hwang *et al.,* 2009) and activation of microglia (Giese *et al.,* 1998). Majority of genes responsible for complement activation (Xiang *et al.,* 2004; Skinner *et al.,* 2006; Sorensen *et al.,* 2008; Kim *et al.,* 2008; Hwang *et al.,* 2009), reactive microgliosis and astrocytosis (Sorensen *et al.,* 2008; Riemer *et al.,* 2004; Hwang *et al.,* 2009), and other inflammatory response pathways such as cytokines and chemokines (Xiang *et al.,* 2004; Kim *et al.,* 2008; Hwang *et al.,* 2009), cell adhesion/ growth/maintenance (Xiang *et al.,* 2004; Sorensen *et al.,* 2008; Booth *et al.,* 2004; Riemer *et al.,* 2004; Hwang *et al.,* 2009), cell differentiation and proliferation (Xiang *et al.,* 2004; Sorensen *et al.,* 2008; Booth *et al.,* 2004; Riemer *et al.,* 2004; Hwang *et al.,* 2009), pattern recognition receptors and leukocyte extravasation (Hwang *et al.,* 2009) were upregulated in prion-infected animals at clinical disease. However, these genes are known to be of glial origin and are related to immune activation (Sorensen *et al.,* 2008) rather than indicative of neuronal degeneration processes.

1.12.2 Endosome/Lysosome and Proteolysis

Another dominant group of genes deregulated in prion-disease animal models were transcripts involved in the protein degradation pathways, namely the lysosome pathway (Hwang *et al.,* 2009; Kim *et al.,* 2008; Xiang *et al.,* 2004; Brown *et al.,* 2005). Within this pathway, cathepsins were the major group of upregulated genes. Cathepsins are proteases that exert

proteolysis within lysosomal vesicles (reviewed by Nakanishi, 2003) and are likely induced to degrade the accumulating PrP^{Sc}. Cathepsins could also originate from activated microglia and function to degrade extracellular matrix proteins that are on the surface of neuronal cells. This mechanism may contribute to the neurodegeneration process even at an early stage of disease. The detection of protease inhibitors found to be induced concurrently with these lysosomal proteases (Brown *et al.,* 2004; Xiang *et al.,* 2004; Skinner *et al.,* 2006) may indicate that a possible mechanism to circumvent the potential damaging proteolysis is activated within prion-diseased animals.

1.12.3 Oxidative and Endoplasmic Reticulum Stress

Stress-related genes were better represented in hippocampal samples as compared to whole brain tissue (Brown *et al.,* 2005). Specifically, genes involved in oxidative and ER stress were induced at preclinical disease (Brown *et al.,* 2005) which correlated to the time when 50% of the CA1 hippocampal neurons were lost (Jeffrey *et al.,* 2001) and inflammatory responses were not detected.

The ER is an organelle responsible for proper folding of proteins and directing misfolded proteins for degradation. This homeostatic function is mainly governed by the UPR. During prion disease, misfolded proteins accumulate which help perturb Ca^{2+} homeostasis (Torres *et al.,* 2010); both conditions lead to ER stress. As a result, UPR is stimulated which activates multiple strategies to return the ER to homeostasis (reviewed in Sitia and Braakman, 2003). These strategies include the production of chaperones, decreased translation and thus limiting overall protein load within the cell, upregulation of transcription including ER-resident proteins and folding assistants as well as factors that facilitate ER-associated degradation (reviewed in Sitia

and Braakman, 2003). Although various chaperones and lipid synthesis representatives were induced in prion disease (Brown *et al.,* 2004; Sorensen *et al.,* 2008; Hwang *et al.,* 2009; Brown *et al.,* 2005; Reimer *et al.,* 2004), only within the hippocampus was the representation of these molecules abundant enough for accurate network building. Chaperones function to assist with proper protein folding while lipids help enlarge the volume of the ER in order to accommodate the influx of misfolded proteins (Halperin *et al.,* 2014). If the UPR system fails to clear the misfolded protein load, the cell initiates apoptosis.

Recent evidence has revealed that the UPR system is chronically over-activated in prion diseased animals, leading to a long-term translational inhibition causing a decline of critical neuroprotective proteins (Moreno *et al.,* 2012). Preventing the translational inhibition observed in prion infected animals restored normal translation rates and rescued synaptic dysfunction and neuronal loss, positively affecting animal survival (Moreno *et al.,* 2012). Oral administration of a pharmacological drug that targets a different UPR kinase responsible for translational inhibition within prion-infected mice also showed pathological and phenotypic recovery (Moreno *et al.,* 2013). These data clearly point to a major player in prion-induced neuropathogenesis for which gene expression profiling, even when applied to a specific brain region, was able to uncover.

1.12.4 Calcium Signaling and Neuronal-Specific Genes

Ca^{2+} is not only an essential messenger of cell signaling crucial for neuronal activity, but it is also important for the development and maintenance of neuronal circuitry (Carafoli *et al.,* 2001). Disruption of Ca^{2+} homeostasis, especially over long periods, severely impedes neuronal function. Calcium deregulation has been detected very early in prion disease (Colling *et al.,* 1996; Herms *et al.,* 2001; Herms *et al.,* 2000) and may contribute to the perturbation of long-

term potentiation and synapse function. Evidence suggest that PrP^{C} may help regulate Ca^{2+} homeostasis (Lazzari *et al.,* 2011; Herms *et al.,* 2000; Powell *et al.,* 2008; Fuhrmann *et al.,* 2006; Colling *et al.,* 1996) and its progressive depletion from the cell surface during PrP^{Sc} conversion could explain deregulation of this pathway during disease. Upon Ca^{2+} deregulation, numerous physiological alterations occur which can inhibit neuronal activity by slowing afterhyperpolarization events. Deregulation of Ca^{2+} can also contribute directly to ER stress (reviewed in Krebs *et al*., 2015).

On a gene expression level, changes in neuronal-related genes were primarily detected at clinical stages of disease (Skinner *et al.,* 2006; Sorensen *et al.,* 2008; Hwang *et al.,* 2009). Several neuronal-specific structural genes were deregulated in these studies such as S100 proteins (Xiang *et al.,* 2004), neurofilaments (Riemer *et al.,* 2004; Brown *et al.,* 2005) and SNAP-25 (Skinner *et al.,* 2006), validating that microarrays can detect progressive degradation of neuronal cyto-architecture. Down-regulated genes responsible for synapse function, calcium signaling, long-term potentiation, ERK/MAPK signaling and cholesterol metabolism were also detected (Sorensen *et al.,* 2008). However, these molecular changes are typically observed in greater abundance at a time when disease is fairly widespread throughout the whole brain and therefore cannot accurately delineate the potential triggering mechanisms that drives disease (Hwang *et al.,* 2009). Clearly, to better understand the process of neuronal degeneration accurate detection of neuronal-specific changes, especially during early stages of disease, must be achieved.

1.13 Neuronal Conundrum: Necessity for Enrichment Strategies

The brain is a highly heterogeneous tissue of which ~10% is composed of neurons. The proportion of neurons affected during disease, especially at preclinical stages, is even less. As a result, transcriptional analysis of whole brain tissue is primarily representative of non-neuronal cell types. Therefore, to identify transcriptional changes within diseased neurons, especially at preclinical disease, it is necessary to enrich for these neurons in the sample analyzed. This type of enrichment will greatly increase the likelihood of detecting molecular alterations within diseased neurons. One enrichment strategy is to physically isolate neurons from the brain using laser capture microdissection (LCM) (reviewed in Standaert *et al.,* 2005). One major advantage of this technology is that it is able to preserve the morphology of the original tissue and allow to specifically isolate a region of choice while avoiding contamination from surrounding tissue. This technology allowed me to study transcriptional changes within a neuronal-enriched population of cells during prion disease progression.

1.14 Gene Regulators

The progression of neurodegeneration is multifaceted and is driven by proteins and their regulatory mechanisms. Gene expression is regulated by various cellular processes including a recently described post-transcriptional mechanism mediated by short, non-coding RNAs termed microRNAs. The role of these small RNA species has been critical in almost all biological processes including development and function of the central nervous system (see *Sections 1.15.2-1.15.4*). Therefore, identifying which miRNAs are involved and understanding their impact in the disease process will help elucidate the pathways driving neurodegeneration. In conjunction with mRNA profiling, miRNAs can therefore be used as a tool to minimize the

complexity of transcriptomic data by identifying regulatory circuits that are disrupted during neurodegenerative disease.

1.15 MicroRNAs

MicroRNAs are small (~22 nucleotides in length) RNA species that function to regulate gene expression at the post-transcriptional level. The first microRNA was identified in the nematode *Caenorhabditis elegans* in 1993 (Lee *et al.,* 1993) but soon after, others were found expressed in animals, plants and in some viruses. To date, 28645 miRNAs have been identified in various phyla (miRBase release 21, June 2014). The sheer abundance of identified miRNAs highlights their importance in regulating a vast array of biological systems. A large proportion of identified miRNAs are highly conserved across numerous mammalian species (*i.e.* mouse, human, rat) demonstrating their evolutionary selection as gene regulators.

1.15.1 MiRNA Biogenesis and Function

MicroRNAs are produced endogenously by the cell from genomic DNA (**Figure 1.6**). Whether organized in clusters or individually, these RNA species are transcribed from intergenic or intronic regions by RNA Polymerase II or sometimes RNA Polymerase III. The primary transcript containing the miRNA(s) is polyadenylated and capped and is referred to as pri-miRNA. The pri-miRNA is cleaved by the DROSHA/DGCR8 microprocessor into a stem-loop structure that is ~70 nucleotides in length which is called a pre-miRNA. The pre-miRNA is exported to the cytoplasm through exportin-5 where it is cleaved by DICER to produce the double-stranded miRNA duplex (~18-23 nucleotides in length). One of these strands is preferentially loaded into the AGO protein to form the miRNA-induced Silencing Complex

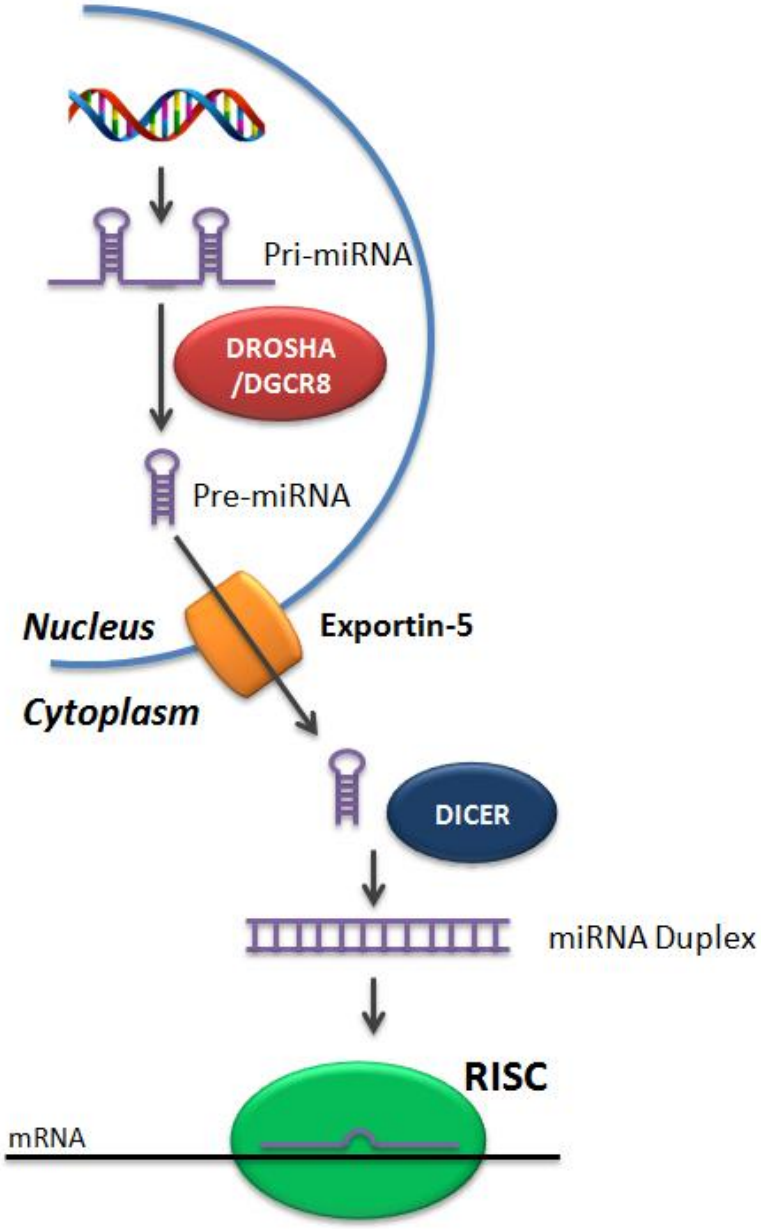

Figure 1.6. The biogenesis of miRNAs. MiRNAs are transcribed from genomic DNA typically by RNA Polymerase II into the primary transcript called pri-miRNA. The pri-miRNA is cleaved by DROSHA/DGCR8 microprocessor into a stem-loop structure called a pre-miRNA. The pre-miRNA is exported by Exportin-5 to the cytoplasm where it is cleaved by DICER to produce a double-stranded miRNA duplex. One of these miRNA strands are preferentially loaded into the miRNA-induced SilencingComplex (miRISC). This complex then binds to the mRNA based on imperfect sequence complementarity between the miRNA and the 3'-untranslated region of mRNA. Adapted from Saumet and Lecellier, 2006.

(miRISC) while the other strand is degraded by as yet an unidentified mechanism. To distinguish the 2 miRNAs, the one closest to the 5'-end is designated as miR-X-5p while the complementary miRNA is referred to as miR-X-3p.

Once the miRISC is formed, the complex subsequently binds to the 3'- untranslated region (3'-UTR) of the target transcript and is transported to specialized RNA centers known as processing bodies (P-bodies). At these non-membranous centers, the miRISC-targeted mRNAs can undergo: 1) translational inhibition by facilitating ribosomes to drop-off their target substrates (reviewed by Huntzinger and Isaurralde, 2011); 2) decrease gene expression by degradation of the mRNA (Guo *et al.,* 2010) or 3) be stored (Brengues *et al.,* 2005) for later de-repression (Bhattacharyya *et al.,* 2006).

A miRNA typically recognizes its target through binding of the seed sequence at nucleotides 2-8 of the 5'-end of the miRNA (otherwise known as the seed sequence). However, the remaining portion of the miRNA can also bind to the mRNA target and thereby modulate gene expression (Martin *et al.,* 2014). Due to the incomplete complementation between miRNAs and their target mRNAs, miRNAs can collectively regulate most of protein-coding genes (Friedman *et al.,* 2009). The efficiency of a miRNA for silencing its target mRNA depends on several factors: 1) concentration of the miRNA; 2) number of miRNA binding sites; 3) concentration of the target mRNA; and 4) turn-over rate in the miRISC (Baccarini *et al.,* 2011). However, the exact biological values for these factors remain unknown.

It is important to consider that miRNAs confer their function on target genes that are co-expressed within the same cell. Therefore, the same miRNA can bestow completely different functions in different cell-types. For example, miR-132-3p is expressed in neurons and is well known to mediate structural changes within these cells by targeting mRNAs such as p250GAP

(Vo *et al.,* 2005; Wayman *et al.,* 2008). Conversely, miR-132-3p expressed in primary lymphatic endothelial cells can negatively regulate antiviral innate immunity by targeting p300 (Lagos *et al.,* 2010). Clearly, to understand the biologically relevant function of a miRNA, it is essential to identify the cell-type that miRNA is expressed from.

1.15.2 Global Disruption of the miRNA Biogenesis Pathway Results in Neurodegeneration

Numerous *Dicer* knock-out animal models revealed the critical importance of miRNA expression for normal development and function of the CNS. In zebrafish, severe deficits in brain morphogenesis were detected when miRNAs were not expressed (Giraldez *et al.,* 2005). These deficits can be prevented by restoring the expression of the miR-430 family in these animals (Giraldez *et al.,* 2005). Although still largely unidentified, such indispensable miRNAs most likely exist in higher mammals as *Dicer* ablation leads to the death of embryos very early in development (Bernstein *et al.,* 2003; Choi *et al.,* 2007; Kim *et al.,* 2007; Schaefer *et al.,* 2007; Kawase-Koga *et al.,* 2009; Davis *et al.,* 2008). Specifically, miRNAs are critical for proper differentiation and survival of newborn neurons (De Pietri Tonelli *et al.,* 2008) as well as normal cellular expansion (Kawase-Koga *et al.,* 2010). Conditional *Dicer* loss in certain cell types such as Purkinje cells in the cerebellum (Schaefer *et al.,* 2007), dopaminergic neurons of the midbrain (Kim *et al.,* 2007), neocortical neurons (De Pietri Tonelli *et al.,* 2008), oligodendrocytes (Shin *et al.,* 2009) and, neuronal stem cells (Kawase-Koga *et al.,* 2010) leads to cell death, indicating that miRNAs regulate the health of differentiated post-mitotic neurons.

The pivotal role miRNAs play in neuronal differentiation, development, function and survival is exemplified by these studies. However, which miRNAs regulate these pathways in the CNS remain to be determined. Identification of these regulatory loops in which miRNAs play

such important roles may shed some light onto the identification of molecular mechanisms that are involved in neuronal degeneration.

1.15.3 Activity-Mediated Dynamics of miRNAs at the Synapse

Selective enrichment of miRNAs has been previously detected within the specialized anatomical compartments called synaptoneurosomes (Kye *et al.,* 2007; Schratt *et al.,* 2006; Pichardo-Casas *et al.,* 2012; Lugli *et al.,* 2008; Ho *et al.,* 2014) suggesting that miRNAs regulate local synaptic protein synthesis and plasticity. In fact, detection of miRISC proteins in both pre- and post-synaptic structures (Hengst *et al.,* 2006; Murashov *et al.,* 2007; Lugli *et al.,* 2008; Pichardo-Casas *et al.,* 2012; Kye *et al.,* 2007) implies that miRNAs are functional at those sites. How miRNAs are delivered from the nucleus to these distal sites is currently a topic of study. Recent evidence suggests that pre-miR-134 contains a specific dendritic localization sequence that allows its transport to dendrite locations which are proximal to synapses (Bicker *et al.,* 2013). More research however is necessary to determine whether other miRNAs are transported by a similar mechanism.

Neuronal spines are extremely dynamic structures that readily exhibit morphological and functional plasticity. The particular size and geometry of spines are coupled to synaptic strength (Matsuzaki *et al.,* 2004; Nagerl *et al.,* 2004; Zito *et al.,* 2004) such that the larger the spine, the stronger the connection; a process readily modulated by synaptic activity. For example, long-term depression (LTD) of synaptic transmission typically reduces the efficacy of neuronal synapses and is usually associated with spine shrinkage and loss. On the contrary, long-term potentiation (LTP) of synaptic transmission typically strengthens synapses and is characterized by spine formation and enlargement (reviewed in Bourne and Harris, 2008). Interestingly,

selective enrichment of certain miRNAs has been observed within these specialized anatomical compartments (Kye *et al.,* 2007; Schratt *et al.,* 2006; Pichardo-Casas *et al.,* 2012; Lugli *et al.,* 2008; Ho *et al.,* 2014) suggesting that miRNAs are locally involved in these structural and functional dynamics. Not surprisingly, miRNA expression was deregulated during both LTP and LTD (Joilin *et al.,* 2014; Pai *et al.,* 2014; van Spronsen *et al.,* 2013; Hu *et al.,* 2014). Exposure to other stimuli that activate synaptic transmission between neurons including cocaine (Chandrasekar and Dreyer, 2009), alcohol (Wang *et al.,* 2009) or kainic acid (Pichardo-Casas *et al.,* 2012) also caused a dynamic change in miRNA expressed, even within synaptoneurosomes. MiRNA expression is clearly changing in response to synaptic stimuli and undoubtedly regulates a function within these structures.

1.15.4 The Function of miRNAs at Synaptic Structures

Several miRNAs are known to modulate morphology and function of spines in an activity-dependent manner (reviewed by McNeill and Vactor, 2012). One such miRNA, miR-132-3p, is induced after stimulation of neuronal activity (Nudelman *et al.,* 2010; Vo *et al.,* 2005). At the synapse, this miRNA increases the number and size of spines by targeting p250GAP (a brain-enriched GTPase-activating proteins) which in turn activates signaling pathways that drive actin dynamics (Impey *et al.,* 2012; Wayman *et al.,* 2008). Additionally, miR-132-3p positively amplifies the activity of a transcriptional factor termed cyclicAMP response element binding protein (CREB) by sensitizing adenylyl cyclases (Wayman *et al.,* 2008). This transcription factor is known to be involved in numerous cellular processes including cell survival (Kolonics *et al.,* 2001) and neuronal plasticity (Sgambato *et al.,* 1998). Interestingly, CREB promotes expression of several plasticity mediating genes such as *Bdnf* and miR-132-3p, thereby forming a positive

feedback loop that enhances the synaptic response. In addition to being involved in this process, miR-132-3p also targets the LTP and memory formation inhibitor MeCP2 (methyl CpG binding protein 2), effectively facilitating synaptogenesis and thus synaptic plasticity (Klein *et al.,* 2007; Li *et al.*, 2011). Clearly, miR-132-3p is an excellent example of an activity-dependent miRNA that mediates structural and functional synaptic plasticity of neurons.

Considering that the majority of activity-dependent stimuli evoke signal transduction that is mediated by intracellular calcium signaling, there is an implication that miRNAs are also modulated in response to events that change synaptic Ca^{2+} concentrations. Other miRNAs have also been described within this context of synaptic plasticity (reviewed by McNeill and Vactor, 2012). However, the majority of synaptically-enriched miRNAs have not been well studied and their roles currently remain unknown.

1.16 Rationale and Statement of Project Goals, Hypotheses and Aims

The number of patients suffering from neurodegenerative diseases continues to rise and the current lack of treatment underpins the necessity for further study of these diseases. It is well known that the earliest neuropathological change is very similar among many neurodegenerative diseases. Specifically, synapse dysfunction and neuronal spine loss precedes neuronal death and clinical disease. However, the molecular mechanisms that represent this neuropathology remain unknown. To address this gap in knowledge, my goal was to study transcriptional changes occurring within a neuronal-enriched sample during prion-induced neurodegeneration. Changes in genes and miRNAs were analyzed at several time points spanning the entire disease course, with special focus on preclinical stages of disease. Identifying the deregulated pathways as well as their regulators, miRNAs, will help pinpoint the biological processes that are disrupted in

neurons during early stages of disease. Better understanding of these mechanisms at a molecular level will undoubtedly aid in the design of therapeutic interventions.

Overall Goal

To identify neuronal-specific molecular mechanisms which initiate or inhibit the neurodegenerative process in an animal model of prion disease. Knowledge gained from this study could aid in the search for potential therapeutic targets.

Overall Hypothesis

Neurons respond to the replicating infectious prion particles by altering molecular mechanisms that potentiate or impede cellular degeneration.

Hypotheses and Aims

1. Hypothesis: The gene and microRNA expression profile of neurons will be temporally altered and represent molecular processes that are changed during disease.

   Aim: Identify aberrant expression of transcripts and microRNAs that are temporally deregulated throughout prion disease in a neuronal-enriched LCM sample using microarrays.

2. Hypothesis: Upregulation of microRNA-26a-5p will promote dendrite and spine formation.

   Aim: Over-express miR-26a-5p in primary mouse hippocampal neurons and measure its effect on neuronal morphology by single-cell microscopic analysis.

2.0 MATERIALS AND METHODS

2.1 Ethics Statement

All procedures involving animals were approved by the Canadian Science Centre for Human and Animal Health - Animal Care Committee or the University of British Columbia Animal Care Committee according to the guidelines set by the Canadian Council on Animal Care. All protocols were designed to minimize animal discomfort. The approval identifications for this work involved animal use document (AUD) #H-08-009, AUD#H-08-012 and AUD #H-11-020 for the prion animal experiments and AUD #H-12-016 for the primary mouse hippocampal cultures.

2.2 Mouse Model of Prion Disease

CD-1 mice, between 4 and 6 weeks of age, were intraperitoneally inoculated with the Rocky Mountain Laboratory (RML) strain of scrapie using 200 μL of 1 % brain homogenate in phosphate buffer saline (PBS; Life Technologies) from either clinically ill or healthy control CD-1 mice. Animals were sacrificed at 6 time points [40, 70, 90, 110, 130 and mean end-point 176.6 ± 11.5 days post infection (DPI) or terminal disease], and brain tissue was collected and processed accordingly for either LCM or pathological analysis. Samples designated for laser capture microdissection were covered in optimal cutting temperature (OCT) medium (Sakura Finetek), flash-frozen in dry ice/methanol mixture and stored at −80 °C until processing. Samples designated for pathology were kept in formalin prior to tissue processing and embedding.

2.3 Cell Culturing

Lentiviral production was performed in human embryonic kidney 293T (HEK293T or 293T) cells and viral titer was determined in HeLa cells as described in *Section 2.16*. Primary mouse hippocampal cultures were used for functional characterization of miR-26a-5p. All work was performed by using the BioSafety Cabinet (BSC) and 70% ethanol following proper aseptic technique.

2.3.1 HEK293T and HeLa Culture Maintenance and Counting

All tissue culture cell lines were purchased from the American Type Culture Collection (ATCC). Human embryonic kidney 293T (CRL-3216) cells were used for lentiviral production and HeLa (CCL-2) cells were utilized for confirmation of lentiviral transduction and viral titering. All tissue culture cells were maintained in 75 cm^2 flasks (Corning) at 37 °C and 5 % CO_2. The maintenance medium for 293T cells was composed of Dulbecco's Modified Eagle's Medium (DMEM) (Life Technologies) supplemented with 10 % heat-inactivated Fetal Bovine Serum (FBS) (Life Technologies) and 1 % penicillin/streptomycin (Life Technologies). HeLa cells were maintained in Eagle's Minimum Essential Medium (EMEM) (Life Technologies) supplemented with 10 % heat-inactivated FBS and 1 % penicillin/streptomycin. Serial passages were carried out twice a week for cell maintenance. Briefly, culture medium was aspirated, cells rinsed in PBS and trypsinized by adding 2 mL of 0.25 x Trypsin-EDTA (Life Technologies) to the cells and incubating the flask at 37 °C and 5 % CO_2 for up to 5 minutes. A total of 4 mL of maintenance medium was added and cells were gently mixed to disrupt cell clumps and 1.5-2 mL further passaged into a new 75 cm^2 flask containing 15 mL fresh maintenance medium.

Cells were counted by trypsinizing an approximately 80 % confluent flask following the protocol described above and a 20 µL aliquot of resuspended cells was added to 80 µL of Trypan Blue stain (Life Technologies). A total of 10 µL of cell suspension was added to one side of the hemocytometer and the clear, non-stained cells were visualized using a brightfield microscope (Olympus) and counted on each of the 4 outer grids. The following equation was used to calculate number of viable cells:

$$viable\ cells\ \left(\frac{cells}{mL}\right) = \frac{sum\ of\ cell\ counts\ in\ all\ grids}{number\ of\ grids} \times dilution\ factor \times 10^4$$

2.3.2 Culturing Primary Mouse Hippocampal Neurons

All solutions described for this protocol are listed in **Appendix 1**. Cultures of dissociated primary hippocampal cells from embryonic day 18-20 (E18-20) CD-1 mice (supplied from University of Manitoba) were prepared using an M60 (Leica) microscope as follows. Brains were collected from embryos, meninges removed and hippocampi structures dissected in 1 x dissection medium (DM) on ice. The DM was prepared by diluting the 10 x DM stock (stored at -20 °C) with Hank's Balanced Salt Solution (Life Technologies). Generally, hippocampal material was pooled from at least 4-5 pups per each culture preparation. Samples were chemically digested by incubating in 5 mL of 0.2 µm filtered papain mixture for 4 minutes at 37 °C. Solution was removed and hippocampi washed 3 times in 5mL trypsin inhibitor mixture by incubating the tissues at 37 °C for 3 minutes per wash. Tissues were then washed once with plating medium which consisted of NbActiv4 (BrainBits) supplemented with 1 % penicillin/streptomycin (Life Technologies). Hippocampi were resuspended in 1 mL of plating

medium and subject to gentle mechanical digestion by triturating for no more than 15 times using a P1000 pipette. Cells were counted and plated at a density of 50,000 cells/well in 24-well plates that were coated with 10 µg of poly-D-lysine (Sigma-Aldrich) in borate buffer. Cultures were maintained for up to 20 days *in vitro* (DIV) and ½ the media (250 µL) was changed every 3-4 days. Cells designated for imaging analysis were plated on 24-well plates containing 13mm high precision glass coverslips (Zeiss) that were previously washed in 1 M hydrochloric acid (HCl) for 20 hours, rinsed in distilled water, autoclaved and wiped with 70 % ethanol prior to use. Coverslips were also coated with poly-D-lysine prior to use.

2.4 Laser Capture Microdissection of Cell Bodies from CA1 Hippocampal Neurons

The OCT embedded brain samples were cryo-sectioned using the Cryostat (Leica) into 8 µm thick coronal sections containing the CA1 hippocampal regions. These sections were placed on polyethylene-napthalate (PEN) membrane slides (Molecular Devices), stored at −80 °C and processed within 4 weeks. Sections were stained for cell nuclei using Cresyl Violet followed by dehydration in increasing concentrations of ethanol as described by the manufacturer for the LCM staining kit (Life Technologies). CA1 hippocampal neurons were microdissected via the Veritas LCM instrument (Arcturus, Molecular Devices). Briefly, the CA1 region was identified under the microscope and magnified to encompass the entire area designated for capture. The cap containing the thermoplastic film was positioned over the CA1 region and the area to be captured was manually selected. The capture laser was initiated by using 50-100 mW laser power with 2 or fewer laser pulses per capture. In total, approximately 700-1500 neuronal CA1 cells were isolated per cap by combining the capture material from multiple serial sections from each animal.

2.5 Extraction of Total RNA

Two methods were used to extract total RNA that depended on the initial abundance of cells within each sample. All RNA work was performed by first decontaminating all surfaces using RNAse-Zap (Life Technologies) to reduce potential RNA degradation.

2.5.1 Total RNA Extraction from LCM Samples

Samples collected after LCM were subjected to the RNAqueous – Micro Kit (Life Technologies) following manufacturer's recommendations. Briefly, the thermoplastic film from the cap containing the pooled CA1 hippocampal regions was peeled off and submerged in 100 μL lysis solution for 30-40 minutes at 42 °C. A total of 3 μL of the LCM additive was added to the solution, mixed by vortexing and followed by adding 130 μL of 100 % ethanol to precipitate and thus collect both large and small RNA species. Samples were passed through a filter column to collect the RNA, impurities were washed using the appropriate wash solution and RNA eluted by passing 10 μL of 95 °C water twice through the column. RNA concentration and quality was assessed by capillary electrophoresis on the 2100 Bioanalyzer RNA 6000 Pico Kit (Agilent Technologies) following the manufacturer's protocol. Only samples with RNA integrity (RIN) value of 5.9 and above were used for all downstream applications. Microdissected CA1 hippocampal neurons from each individual mouse were pooled together to constitute a biological replicate. These samples were utilized for both mRNA and miRNA profiling analyses.

2.5.2 Total RNA Extraction from Cultures

To collect total RNA from *in vitro* cultures, such as primary mouse hippocampal neurons, the *mir*Vana miRNA Isolation Kit (Life Technologies) or the Total RNA Purification Micro Kit (Norgen Biotek Corp.) was utilized following the protocol recommended by the manufacturer. Briefly, for the *mir*Vana miRNA Isolation Kit adherent cells in a 24-well plate were lysed using 600 µL of lysis buffer per well and the lysate was transferred to a 1.5mL microcentrifuge tube. A total of 60 µL of the miRNA homogenate was added to each sample, vortexed and incubated on ice for 10 minutes. This was followed by adding 600 µL of Acid-Phenol:Chloroform to each sample, mixed on a vortex for 30 seconds and centrifuged for 10 minutes at 10, 000 xg. The aqueous layer from the supernatant was removed, 1.25 x volume of 100 % ethanol was added to each sample to precipitate both mRNA and miRNA. Samples were added and passed through a filter column to collect the RNA, impurities were washed using the appropriate wash solution and RNA eluted by passing 100 µL of 95 °C water through the column.

Cells that were lysed using the Total RNA Purification Micro Kit consisted of washing each well with PBS followed by adding 350 µL of the lysis buffer called Buffer RL. Cells were incubated for 5 minutes then scraped and lysate collected into a 1.5mL microcentrifuge tube. A total of 200 µL of 100 % ethanol was added to precipitate RNA. Samples were added and passed through a filter column to collect RNA. Impurities were washed by adding 400 µL of wash solution A three times and RNA eluted by passing 30 µL of elution solution to the filter. RNA concentration and quality of these samples was assessed using the Nanodrop Spectrophotometer (ND-1000) (Thermo Scientific).

2.6 Whole Genome Transcriptional Profiling and Analysis

Total RNA from 4-6 infected and 4-6 control mice were profiled using the Agilent whole mouse genome 4 x 44K arrays (Agilent Technologies Inc.). Due to the limited material collected by the LCM procedure, two rounds of amplification from 2 ng of input total RNA were performed using the Amino Allyl MessageAmp™ II aRNA Amplification Kit (Life Technologies) following the manufacturer's protocol. The amplified RNA samples were labeled using either Alexa-Fluor 555® or 647® (Life Technologies) as described in the Amino Allyl MessageAmp™ II aRNA Amplification Kit. One control and one infected sample from the same time point were randomly mixed and hybridized against the same array in order to perform a two-colour competitive hybridization. Dye swap experiments were carried out to remove potential dye bias. As a result, a total of 8 arrays were preformed per time point. The hybridization, wash and scanning protocols were followed as described for the two-color microarray-based gene expression analysis (Agilent Technologies Inc.) according to the manufacturer's recommendations. Raw image files were converted to data files followed by subsequent quality control (QC) assessment that was performed using Feature Extraction Software versions 9.1 to 10.5.1.1 (Agilent Technologies Inc.). Only arrays that passed the QC were further considered for analysis. Overall, at least 4 array data sets were collected for all time points and can be accessed at Gene Expression Omnibus # GSE34530.

Data from each array was further filtered to only include genes that were detected above a threshold level of 100 units to remove potential background signal. Genes with at least a 2.5-fold change in expression between RML-infected and control mice and having a false discovery rate (FDR) lower than 1 % was considered significant. These data sets were initially analyzed for enriched gene ontologies during prion disease using ToppCluster (Kaimal *et al.*, 2010). All data

sets representing either upregulated or downregulated genes from each time point were analyzed by ToppCluster using a p-value cut-off of 0.05 and the Bonferroni correction method. This analysis revealed the most significantly deregulated "Gene Ontologies" as well as associated "Mouse Phenotypes". Networks to visualize these ontologies were constructed by exporting the data from ToppCluster using the 'Abstract' network option and generating the networks using the Spring Embedded Layout function in Cytoscape (Smoot *et al.,* 2011). Significance of these network graphics was based on edge weights. Hierarchical cluster plots from a subset of genes (1026 genes with $\geq$ 2-fold change and FDR $\leq$ 0.001) were constructed via GeneMathsXT (www.applied-maths.com) by using the cosine corrections and WPGMC (median linkage) measure.

2.7 Detection and Analysis of mRNAs using qRT-PCR

Reverse transcription of the mRNA material followed by quantitative real-time PCR (qRT-PCR) was performed to assess the expression levels of various genes in the *in vivo* samples. Briefly, total RNA was reverse transcribed using the High Capacity cDNA reverse transcription kit (Life Technologies). The generated cDNA was purified using the ChargeSwitch PCR Clean-Up Kit (Life Technologies) as per manufacturer's recommendations. Samples were eluted in 20 µL volume and were assessed for concentration and quality using ND-1000. A total of 50 ng of cDNA was used as input template for qRT-PCR assays via the TaqMan® fast universal PCR master mix (2x), no AmpErase UNG (Life Technologies) following the fast run specifications recommended by the manufacturer. All assayed probes were normalized to the endogenous control, *Gapdh*, and fold changes were calculated by the $2^{-(\Delta\Delta Ct)}$ method (Livak and

Schmittgen, 2001). Standard error was used to assess variation and Student's *t*-test was calculated to determine significance where a p-value ≤ 0.05 was deemed significant.

2.8 TaqMan® Low Density Array (TLDA) miRNA Profiling and Analysis

The TLDA Rodent Card A (Life Technologies) platform was used to profile 335 unique mouse miRNAs from the CA1 hippocampal neurons. Due to the low concentration of total RNA in each sample, a pre-amplification step was performed according to the manufacturer's recommendations. Briefly, 1 ng of total RNA from each sample was reverse transcribed using the megaplex primer pools for Card A. Subsequently, 2.5 µL of the reverse transcriptase (RT) product was preamplified following manufacturer's recommendations. A total of 9 µL of the preamplification product was mixed with the TaqMan® Universal PCR Master Mix (2x), No AmpErase UNG (Life Technologies) and loaded onto the TLDA. Overall, 2 scrapie-infected and 2 mock-infected samples were separately run on each TLDA card using the TaqMan® 7900HT Thermocycler (Life Technologies) with Sequence Detection System (SDS) software version 2.3. Analysis was performed by RQ Manager version 1.2 which automatically calculates the Ct values. Initial inspection of each miRNA amplification curve was performed manually and only profiles with smooth curves were considered for further analysis. Normalization control was considered from all miRNAs detected within the sample using real-time StatMiner software version 4.2 (Intergromics). A total of 3 stability scoring methods from StatMiner (Normfinder, Genorm and minimum variance median) were employed to reveal that snoRNA-135 was the most stable endogenous control within the *in vivo* experiments. In addition, snoRNA-135 was expressed in similar abundance to the majority of the miRNAs detected. Ct values of snoRNA-135 for each card were used to normalize the signal from each probe (ΔCt). Fold changes were

calculated by the $2^{-(\Delta\Delta Ct)}$ method. Student's *t*-test was calculated such that a p-value ≤ 0.1 reflected significance.

MiRNAs resulting in a fold change calculated for at least 6 individual arrays, representing 3 different time points, were included within the list of miRNAs used to construct a one-dimentional hierarchical cluster using GeneMathsXT. The UPGMA method and the Euclidean distance (with variance) measure were employed.

2.9 Detection and Analysis of Mature miRNAs using qRT-PCR

MicroRNA detection was performed by employing a multiplex strategy using the TaqMan® probe system (Life Technologies). For each sample, 1-8 ng of total RNA was subject to RT-PCR following the manufacturer's recommendations. However, each miRNA primer was diluted 1:4 to make a final primer stock of which 4 µL was added to each reaction in place of the 5x TaqMan® miRNA RT primer. This modification allowed the detection of all the miRNAs of interest from the same cDNA mixture. The qRT-PCR reaction was performed using the TaqMan® Universal PCR Master Mix (2x), no AmpErase UNG (Life Technologies) following the manufacturer's recommendations for the standard program.

Samples collected from the LCM material were pooled from 3-4 mice per treatment to standardize the control samples and save on the limited material. From each sample, 1 ng of total RNA was used as template. The qRT-PCR assays were run in triplicate and Ct values for each probe were normalized to snoRNA-135. Standard error was used to assess variation and Student's t-test was used to calculate significance.

For material originating from primary mouse hippocampal cultures, 5-8 ng of total RNA was used to test for miRNAs from duplicate samples collected from 3 independent culture

preparations (n=6). Samples were run in duplicate using the ViiA 7 (Applied Biosystems, Life Technologies) qRT-PCR system and the ViiA 7 software was used to automatically calculate the Ct values. The Ct values for each probe were normalized to snoRNA U6. The $2^{-(\Delta\Delta Ct)}$ method was used for analysis as described in *Section 2.7*. Standard deviation and Student's *t*-test were used to assess variation and significance, respectively.

2.10 MiRNA Target Prediction using Bioinformatics

MiRNA data that originated from LCM samples were subject to mouse specific miRNA targets prediction using TargetScan (Human) versions 5.2 (June 2011) (Lewis *et al.,* 2005) with mouse being the selected species. A list of miRNA targets were compiled for all miRNAs of interest and processed by ToppCluster module from ToppGene Suite software (Chen *et al.,* 2009) to assess gene ontologies potentially regulated by these miRNAs. Gene ontology for features such as molecular function, biological processes and cellular component were determined using the Bonferroni correction and a p-value of 0.05 as a cut-off. Networks to visualize these ontologies were constructed by exporting the data from ToppCluster using the 'Abstract' network option and generating the networks using the Spring Embedded Layout function in Cytoscape. Significance of these network graphics was based on edge weights.

2.11 *In situ* hybridization

Detection of miR-16-5p, miR-26a-5p, miR-132-3p and miR-140-5p was performed separately following the specific conditions outlined for each probe (**Table 2.1**). Paraffin-embedded sections were processed as described (Majer *et al.,* 2012) and pre-hybridized by

Table 2.1. Specifications for *in situ* hybridization analysis.

miRNA	Concentration (nM)	Hybridization Temperature (°C)
miR-16-5p	40	53
miR-26a-5p	20	54
miR-132-3p	50	55
miR-140-5p	80	50

incubating slides for 4 hours at room temperature in pre-hybridization buffer (BioChain Institute Inc.) at 55 °C. Between 20-80 nM of the linearized dual DIG-labeled miRNA specific LNA probes (Exiqon) were used to detect the 4 individual miRNAs. Probes were hybridized overnight at the indicated temperatures (**Table 2.1**) in ready to use hybridization solution (BioChain Institute Inc.). Slides were washed twice in 3 different saline-sodium citrate (SSC) (Ambion) wash buffers with increasing stringencies: 2 x SSC for 10 minutes at 55 °C, 1.5 x SSC for 10 minutes at 55 °C and, 0.2 x SSC for 20 minutes at 37 °C. Slides were washed twice in Tris Buffered Saline with Tween 20 (TBS/T, pH 7.4) (Sigma-Aldrich) followed by 1 hour incubation at room temperature with 1 x blocking solution (BioChain Institute Inc.). To visualize the staining, sections were incubated with 1:500 alkaline-phosphatase (AP) conjugated anti-digoxigenin antibody in blocking solution at 4 °C overnight. Slides were incubated with AP buffer twice for 5 minutes followed by NBT/BCIP colour development solution for 4 hours at room temperature. Slides were rinsed with distilled water, counterstained with Nuclear Fast Red (Vector Laboratories) and mounted with aquatic buffer.

2.12 Immunohistochemistry Staining of Brain Tissue

Brain sections from prion infected animal experiments were processed using immunohistochemistry to detect the presence of microglia, PrP^{Sc} deposits, total CREB and phospho-CREB (pCREB) levels.

2.12.1 Staining for Microglial Cells

Immunohistochemistry was used to stain for microglia cells using the ionized calcium-binding adapter molecule 1 (IBA1) cell marker following a previously described protocol (Majer

et al., 2012). A rabbit anti-IBA1 antibody (Wako Pure Chemical Industries; 019-19741) was used at a 1:1500 dilution in EnVision FLEX antibody diluent (Dako). Briefly, brain samples from control and infected mice were fixed in 10 % neutral buffered formalin and paraffin-embedded. Coronal sections (5 µm thick) containing the hippocampal region were prepared. Sections were baked overnight at 37 °C, deparaffinized and hydrated. Endogenous enzyme activity was blocked by treatment with 2.5 % hydrogen peroxide (Fisher Scientific) diluted in 5 % ethanol for 10 minutes at 37 °C. Antigen retrieval was performed by exposing the slides to 10mM sodium citrate buffer (pH 6.0) at 121 °C for 10 minutes. Once cooled, 100 µL of the diluted primary antibody was incubated on the sections overnight at 4 °C. Signal was detected using Klear Mouse HRP-Polymer DAB Detection System (Golden Bridge International GBI, Inc.) following the manufacturer's recommendations. Sections were counterstained using hematoxylin (Surgipath), dehydrated, cleared in xylene (Surgipath) and mounted using Paramount (Fisher Scientific).

2.12.2 Staining for PrP^{Sc} Deposits

To detect PrP^{Sc} deposits in brain sections the rabbit prion monoclonal antibody (Abcam; EP1802Y) was utilized at a 1:7000 dilution in EnVision FLEX antibody diluent. Sections were processed as described above (*Section 2.12.1*) including the antigen retrieval and blocking endogenous enzyme activity. Staining intensity was enhanced by treating the sections with 80 % formic acid for 10 minutes at room temperature, rinsed and treated with 4 M guanidine thiocyanate for 2 hours at 4 °C and rinsed in TBS/T. Sections were incubated with primary antibody at 4 °C overnight and stain was detected using the Clear Mouse HRP-Polymer DAB

Detection System (Golden Bridge International Inc.). Counterstaining to detect nuclei was performed using hematoxylin, sections were then cleared in xylene and mounted.

As a technical consideration, sequence homology between PrP^{C} and PrP^{Sc} renders primary antibodies unable to discriminate between these two forms of PrP and detects both in the tissue. Therefore, PrP staining can be observed in some regions of mock-infected brain tissue. However, this staining pattern is much more diffuse than PrP^{Sc} in prion-infected brain and does not amass as disease progresses.

2.12.3 Staining for Total CREB and pCREB

Sections were stained for total cyclicAMP response element binding protein (CREB) and pCREB separately. Sections were processed as described above (*Section 2.12.1*) and stained with the following primary antibody dilutions. Total level of CREB was detected by using a rabbit anti-CREB (48H2) antibody (Cell Signaling Technology; 9197) at 1:2000 dilution in SignalStain Antibody Diluent (Cell Signaling Technologies) while pCREB was detected using the rabbit anti-pCREB antibody (Millipore; 06-519) at a 1:800 dilution in EnVision FLEX antibody diluent.

2.13 Immunofluorescence

Immunofluorescence staining was employed to detect the presence of astrocytes and degeneration of neurons in brain samples from prion-infected animals. In addition, immunofluorescence staining was used to determine the proportion of astrocytes and neurons within the cultures of primary mouse hippocampal neurons and to confirm culture maturity.

2.13.1 Staining for Astrocytes within in Brain Tissue

Sections were processed up to and including the antigen retrieval step as previously described (*Section 2.12.1*), followed by blocking in 1:20 normal goat serum (Cedarlane) diluted in EnVision FLEX antibody diluent for 1 hour at room temperature. To detect astrocytes a rabbit GFAP antibody (Abcam; ab7260) at a dilution of 1:500 in EnVision FLEX was added to the sections and incubated at 4 °C overnight. Once rinsed, sections were incubated with Alexa-Fluor 594® goat anti-rabbit IgG secondary antibody (Life Technologies) diluted 1:1000 in EnVision FLEX for 1 hour. To counterstain for nuclei, 4', 6-diamidino-2-phenylindole (DAPI) at 1:1000 dilution was added to the sections for 20 minutes at room temperature. Slides were rinsed, dehydrated, cleared and mounted using DPX containing coverslips (Sigma).

2.13.2 Flouro-Jade® C Staining to Detect Degenerating Neurons within Brain Tissue

To detect degenerating neurons sections were processed as described above up to the antigen retrieval step. Subsequently, sections were incubated in Flouro-Jade® C (Millipore) solution for 30 minutes. These were then rinsed, dehydrated, cleared in xylene and mounted using DPX containing coverslips.

2.13.3 Immunostaining of Primary Mouse Hippocampal Cultures and Image Analysis

The number of neurons and astrocytes within the primary mouse hippocampal cultures was determined by immunofluorescence. Astrocytes were detected by using a 1:500 dilution of anti-GFAP rabbit antibody (Dako; Z0334) and a goat anti-rabbit secondary conjugated to a Cy3 (Abcam; ab6939). Neurons were detected by using a 1:1000 dilution of microtubule-associated protein 2 (MAP2) chicken antibody (Abcam; ab5392) and a 1:200 dilution of goat anti-chicken

secondary conjugated to Alexa-Fluor® 555 (Abcam; ab150174). All antibodies were diluted in PBS at pH 7.4 (Life Technologies). Briefly, cells at indicated times post plating were fixed with 4 % paraformaldehyde (Sigma-Aldrich) for 10 minutes, washed twice with PBS and permeabilized using 0.5 % Triton X-100 (Sigma-Aldrich) in PBS for 10 minutes. Cells were incubated with primary antibodies for 1 hour at room temperature, washed once with 0.1 % Triton X-100 and twice with PBS followed by a 1 hour incubation with secondary antibodies at room temperature. Cells were further washed once with 0.1 % Triton X-100 in PBS and twice with PBS followed by mounting with ProLong Gold (Life Technologies).

MIRAX MIDI scanner (Zeiss) was used to scan each coverslip to determine the proportion of neurons and astrocytes within the culture. An area of interest equal to 3150 x 2150 µm was used to manually count the proportions of each cell type compared to the total number of neurons and astrocytes. The LSM700 laser scanning confocal microscope (Zeiss) was used to capture high resolution representative images.

Detection of post-synaptic densities was obtained by using an antibody against PSD-95 in addition to an antibody against MAP2 for visualization of neurons in the culture. The same immunoflourescence protocol was employed as described above. PSD-95 structures were detected by using a 1:25 dilution of the primary antibody (Thermo Fisher; MA1-046 clone 6G6-1C9) and a 1:100 dilution of goat anti-mouse secondary conjugated to Alexa-Fluor® 660 (Life Technologies; A21055). High resolution images were taken using the LSM700 laser scanning confocal microscope (Zeiss).

2.14 Immunohistochemical Image Acquisition and Analysis of *In Vivo* Material

Slides processed for immunohistochemical detection of CREB and pCREB were scanned using the MIRAX MIDI scanner (Zeiss). Images containing regions of interest within the hippocampus, primarily the CA1 neurons, were exported and analyzed with ImageJ software (Schneider *et al.*, 2012). Briefly, images were colour deconvolved to separate haematoxylin and DAB stains. The haematoxylin-stained nuclei channel was employed to delineate the CA1 hippocampal region. The nuclear region was isolated empirically via the threshold pixel intensity to generate a mask of the region of interest. The area of the masked region was measured and this area was used to segregate the CA1 hippocampal region in the DAB-stained probe channel. Positive signal intensity was thresholded and binned into 3 ranges by increasing the threshold amounts from background to the maximal intensity. The student's *t*-test was used to determine statistical significance. Graphing was performed using GraphPad Prism version 5 (GraphPad Software).

2.15 Stimulating Neuroprotection in Primary Mouse Hippocampal Cultures

Primary mouse hippocampal cultures were grown in 24-well plates for either 9 or 12 DIV prior to stimulating neuroprotective responses. To activate the synaptic NMDARs the growth medium from the primary mouse hippocampal neurons was removed and neurons were exposed to fresh growth medium containing 250 µM 4-Aminopyridine (4-AP) (Sigma-Aldrich) and 250 µM bicuculline (Sigma-Aldrich) for 4 and 16 hours at 37 °C and 5 % CO_2. As a control, dimethyl sulfoxide (DMSO) (Sigma-Aldrich) was added to the wells that did not receive treatment and were considered "media only". After the incubation, medium was removed, cultured neurons washed once with cold PBS and cells lysed using the miRVana miRNA

Isolation kit following the total RNA isolation procedure as per manufacturer's recommendations (*Section 2.5.2*).

2.16 Lentiviral Preparation and Titre Determination

Lentiviral miRNA vector constructs were commercially obtained from System Biosciences Inc. (SBI) and were used to manipulate the expression levels of miRNAs within primary mouse hippocampal cultures. *Escherichia coli* cultures expressing the miRNA vectors were incubated at 37 °C overnight in Luria Broth (prepared in house) supplemented with 50 ng/mL Carbenicillin (Sigma-Aldrich). The miRNA vector was extracted and purified using the EndoFree Plasmid Maxi kit (Qiagen) in accordance with the manufacturer's instructions. DNA concentration and quality were assessed using the Nanodrop ND-1000 Spectrophotometer. Confirmation of the miRNA sequence within the vector was performed in house by sequence analysis of the cloning site in the vector using the EF1 reverse primer sequence (5'-GCACCCGTTCAATTGCCG).

Lentiviral particles were produced by transfecting 293T cells with 24 µg of pPACKH1 HIV packaging vector mix (SBI) and 2 µg miRNA vector (either miR-26a-5p or scrambled sequence) using Lipofectamine 2000 (Life Technologies) following manufacturer's recommendations. Medium was changed 24 hours post transduction. Viral particles were harvested 48 hours post transduction by collecting the medium from the cells. To remove cell debris, harvested medium was centrifuged at 3000 xg for 15 minutes and viral particles were concentrated using PEG-*it*™ buffer (SBI) as described by the manufacturer.

Viral titres for each miRNA vector packaged into lentiviral particles was determined by transducing HeLa cells seeded at 50,000 cells/well with 10 µL of undiluted, 1:10 and 1:100

diluted virus in PBS. After incubating cells for 72 hours, immunofluorescence and bright field images of the same field of interest were taken. The number of GFP positive cells was counted manually within each field of interest for each dilution. Viral titer was calculated by the following equation:

$$viral\ titer\ \left(\frac{TU}{mL}\right) = \frac{\left(\frac{\%\ GFP\ positive\ cells}{100}\right) \times cells\ transduced}{volume\ of\ virus\ (mL)}$$

2.17 Cell Death Assay - Lactate Dehydrogenase

The lactate dehydrogenase (LDH) assay CytoTox 96 Non-Radioactive Cytotoxicity Assay (Promega) was employed to measure the proportion of cell death in the culture after lentiviral treatment. To test the sensitivity of the assay in primary mouse hippocampal cultures, cells that were freshly triturated were counted and a set number of cells were distributed into 1.5 mL microcentrifuge tubes. The range of cells tested for the assay were 0 (background control), 500, 1000, 2500, 5000, 10000, 20000 cells/100 µL. These were compared to the culture that was grown until 16 DIV for which all but 100 µL of media was removed from the culture. Cells were subsequently frozen at -80 °C for at least 30 minutes and thawed at 37 °C for 15 minutes. Samples were centrifuged at 250 xg for 4 minutes to pellet debris. A total of 50 µL of cell lysis was mixed with 50 µL of reconstituted Substrate Mix in each well of a 96-well flat bottom plate. The plate was incubated for 30 minutes to allow for the enzymatic reaction to take place after which 50 µL of the Stop Solution was added to each well to quench the reaction. Plate was read using the GloMax-Multi Detection System (Promega) at an absorbance of 450 nm within 5 minutes of adding the Stop Solution. For testing the cell death post lentiviral treatment, 115 µL of medium was removed at 13, 16 and 17 DIV which represents 24, 72 and 96 hours post

treatment, respectively. These samples were frozen at -80 °C until assay was performed (less than 1 week of time).

Analysis was performed by subtracting the absorbance of the background control well from all of the other wells. Percent of cell death was calculated by dividing the background subtracted wells from the wells that contained maximum cell death, which in the case of the sensitivity test was DIV 16. For the lentivirus treated wells the maximum cell death was established at 13, 16 and 17 DIV for each respective time point sampled.

2.18 Single Cell Image Analysis

Primary mouse hippocampal neurons at 12 days *in vitro* (DIV) were transduced with lentiviral particles. For single cell analysis, primary cultures were transduced at 0.2 multiplicity of infection (MOI). After 24 hrs post transduction, ½ of the media was changed and cultures incubated for an additional 3 days at 37 °C and 5 % CO_2. Coverslips were fixed on DIV 16 using 4 % paraformaldehyde/sucrose reagent preheated to 37 °C for 10 minutes and mounted using ProLong Gold. Images of GFP-positive pyramidal shaped neurons were taken using the LSM700 laser scanning confocal microscope (Zeiss) via the 63 x oil objective. Laser power for imaging was set to 2.0 and master gain was adjusted to range between 750-900 units and digital gain did not surpass 1.9.

For Sholl analysis, low-magnification images of GFP-positive neurons were taken and dendrite complexities analyzed with Imaris® Version 7.7.2 (Bitplane). At least 7 individual neurons for each experimental condition from a total of 2-3 independent experiments were measured. A 3-dimensional reconstruction of each neuron was performed using Imaris® Version 7.7.2 (Bitplane). Briefly, the diameter of each neuron that was proximal (thickest) and distal

(thinnest) to the soma was measured in the slice view using the "measure" tool. Subsequently, images of neurons were opened with the Surpass view and processed using FilamentTracer by employing a combination of automatic, semiautomatic and manual segmentation and filament generation utilities. Using AutoPath and AutoNetwork functions, all filaments originating from the soma (user denoted) of the neuron were automatically computed and traced. The connections of the traced filaments were visualized and erroneous connections were manually rectified. Once the filaments were manually confirmed to be the exact representation of the neuron being analyzed, Scholl intersections were automatically computed with concentric circles of diameter increasing by 1μm.

For spine analysis, high resolution z-stack (1 μm distances with pixel dwell time of 0.71 μs and pinhole 41 μm) images of GFP-positive neurons were taken using LSM 700 where the signal was the average of 4 images. Neurons which displayed pyramidal morphology were chosen from the datasets. Spines were subsequently quantified with ImageJ software. For each condition, spines from 12-13 representative hippocampal neurons (on average ~500 spines per neuron) derived from two to three independent experiments were measured.

3.0 RESULTS

3.1 Gene Expression Profiling of LCM-Isolated CA1 Hippocampal Neurons

Rationale: The molecular processes underlying the earliest neuropathologies in prion disease are very poorly understood. Gene expression profiling studies provide a comprehensive snapshot into the cellular processes that may be deregulated at any given time in disease. However, a neuronal-specific sample needs to be analyzed to obtain a transcriptional signature indicative of this observed neuropathology. This enrichment is especially important when investigating changes that occur during preclinical disease, a time when only a proportion of neurons are affected by replicating PrP^{Sc}. Therefore, it is necessary to specifically isolate neurons from the brain for transcriptomic analysis. For this purpose, LCM was used to physically isolate cell bodies from CA1 hippocampal neurons, a brain region known to be affected during preclinical prion disease. Gene expression profiles were obtained from this neuronal-enriched sample using microarrays at 6 time points post infection. Time points spanned the entire disease course in order to monitor temporal changes within neurons during prion disease. Majority of the time points fell within the pre-clinical stages of disease to perform a more extensive sampling of this time period. Transcripts were initially analyzed for gene markers specific to astrocytes and microglia to assess the temporal proportion of these cells within the neuronal-dense LCM region during disease progression. This transcriptional analysis was then correlated to pathology of the CA1 hippocampal region. Subsequent meta-genomic analyses were performed to identify which functional pathways were deregulated in these neurons during disease.

3.1.1 Mouse Model of Prion-Induced Neurodegeneration

A well-established rodent model for prion-induced neurodegeneration was used for all animal experiments. Neuroinvasion was simulated by inoculating mice intraperitoneally (IP) with brain homogenates from either terminally ill mice infected with RML strain of mouse-adapted scrapie or healthy controls for mock-infected mice. Animals were sacrificed at 6 time points: 40, 70, 90, 110, 130 DPI and terminal disease or end-point (EP). The mean incubation period (± SD) for mice that reached terminal stage of disease was 177 ± 11 days (100%). Brain samples at each time point were collected and processed accordingly for pathological and molecular analyses. Beginning at approximately 130 DPI, infected animals showed symptoms of disease such as kyphosis, dull ruffled fur, more than 20 % weight loss and ataxia. Based on the absence/presence of these symptoms, the time-line of prion disease in this animal model represented two broad stages: asymptomatic or early (0-110 DPI) followed by symptomatic or late stage of disease (130 DPI-EP). Of note, early and late disease that is referred to in this thesis pertains to changes, molecular and pathological, that occurs within the LCM-isolated region and may not represent temporal changes that occur in other regions of the brain. Unless otherwise stated, early changes encompass up to and including 110 DPI while late changes represent 130 DPI to terminal disease.

3.1.2 Laser Capture Microdissection of CA1 Hippocampal Neurons

Anatomically distinct cell bodies of CA1 hippocampal neurons (**Figure 3.1A** and **B**) comprising the pyramidal layer (*stratum pyramidale* or SP) were selected for neuronal-enrichment and subsequent transcriptomic analysis. This region was chosen to study changes in gene expression because many rodent-adapted prion strains show particular tropism to the

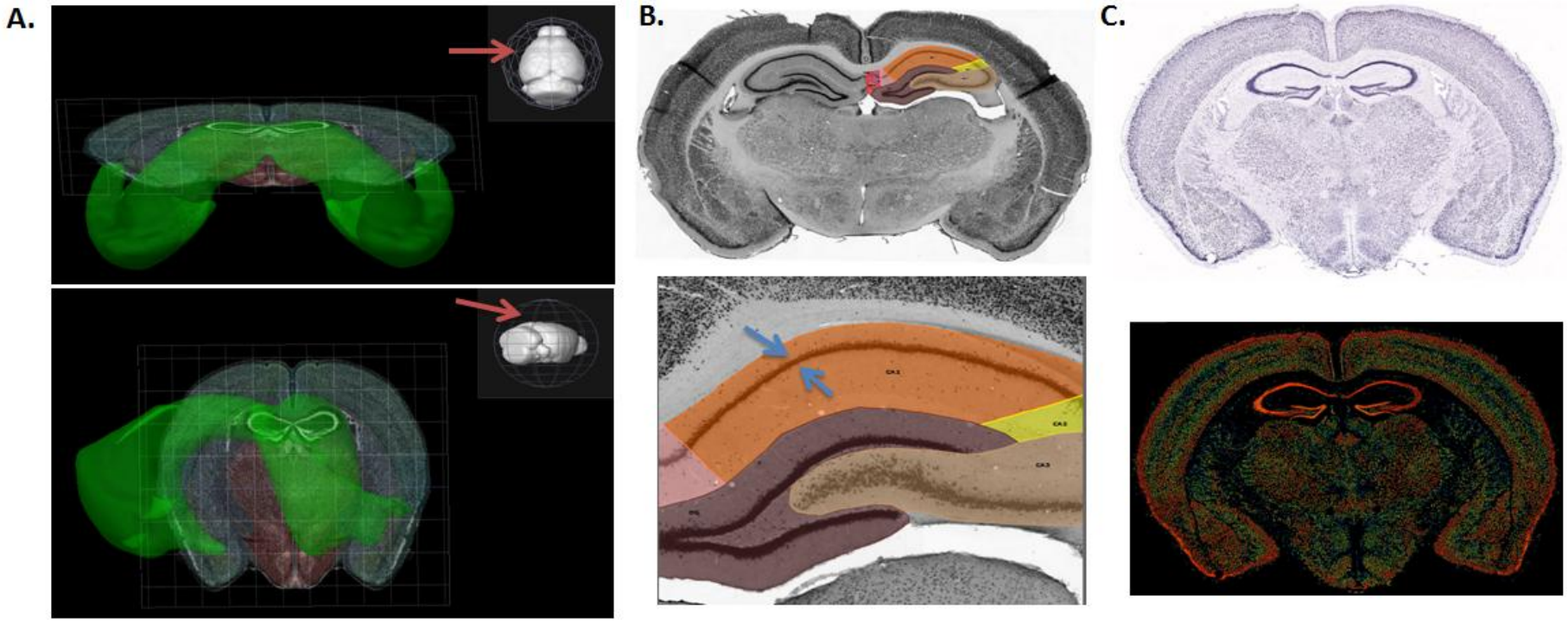

Figure 3.1. The anatomy of the rodent hippocampus. (**A**) The 3-dimensional rendering of the hippocampi (green region) within mouse brain. Red arrow points to the coronal cross section. Image was generated using Brain Explorer 2 (Allen Institute for Brain Science) (**B**) The anatomy of the hippocampus highlighting the CA1 (orange), CA2 (yellow) and CA3 (light brown) regions along with the DG (dark brown) and *fasciola cinereum* (red-pink). The zoomed in panel highlights the CA1 region in which the blue arrows indicate the pyramidal layer of CA1 neurons termed *stratum pyramidale* (SP), an area that is the focus of this work. Images were generated using the Rodent Brain Workbench. DG is *dentate gyrase* and CA is *Cornu ammonis*. (**C**) The expression of *Prnp* in mouse brain where red represents most abundant expression of the gene detected by *in situ* hybridization. Images generated by Allen Brain Atlas (Allen Institute for Brain Science).

hippocampus, including RML (Scott and Fraser, 1984; Bruce *et al.*, 1991). Furthermore, lesions within the hippocampus have been reported in rodent models and CJD patients (Kaneko *et al.*, 2008; Kaneko *et al.*, 1999), which help explain some of the observed early behavioural abnormalities. Also, the abundant expression of *Prnp* within neurons includes the ones residing within the hippocampus structure (**Figure 3.1C**) which suggests that PrP^{C} is present on the surface of these neurons and available for conversion by replicating PrP^{Sc} during early disease. Lastly, the specific CA1 region of the hippocampus consists of a neuronal-dense nuclei region that provides the most homogeneous and accessible biological material to study alteration in the transcriptome. The nuclei-rich SP layer was therefore physically isolated from the brain using LCM (**Figure 3.2**). Total RNA was extracted and only samples with a RIN of more than or equal to 5.9 were used for further analysis (**Figure 3.2**). This cut-off provided a high confidence that the RNA samples used for downstream analysis were not degraded. Of note, both RML and mock-infected samples collected at 40 DPI failed to meet the minimum RIN cut-off value and were therefore not used in the gene expression profiling study.

3.1.3 Expression of Cell-Type Specific Gene Markers in the LCM-Isolated Region

Relative global gene expression levels between infected and control animals were determined at each time point using whole mouse genome microarrays that contain ~ 44, 000 probes. A total of 2,580 genes were deregulated in at least one time point by more than 2.5-fold with an FDR of less than 1 % (**Appendix 2**). To confirm the relative proportion of neurons, astrocytes and microglia detected within the sampled CA1 region, signal intensities for several cell-specific gene markers were analyzed from the microarray data. This provided a gene-specific baseline for detecting different cell-types and also served to

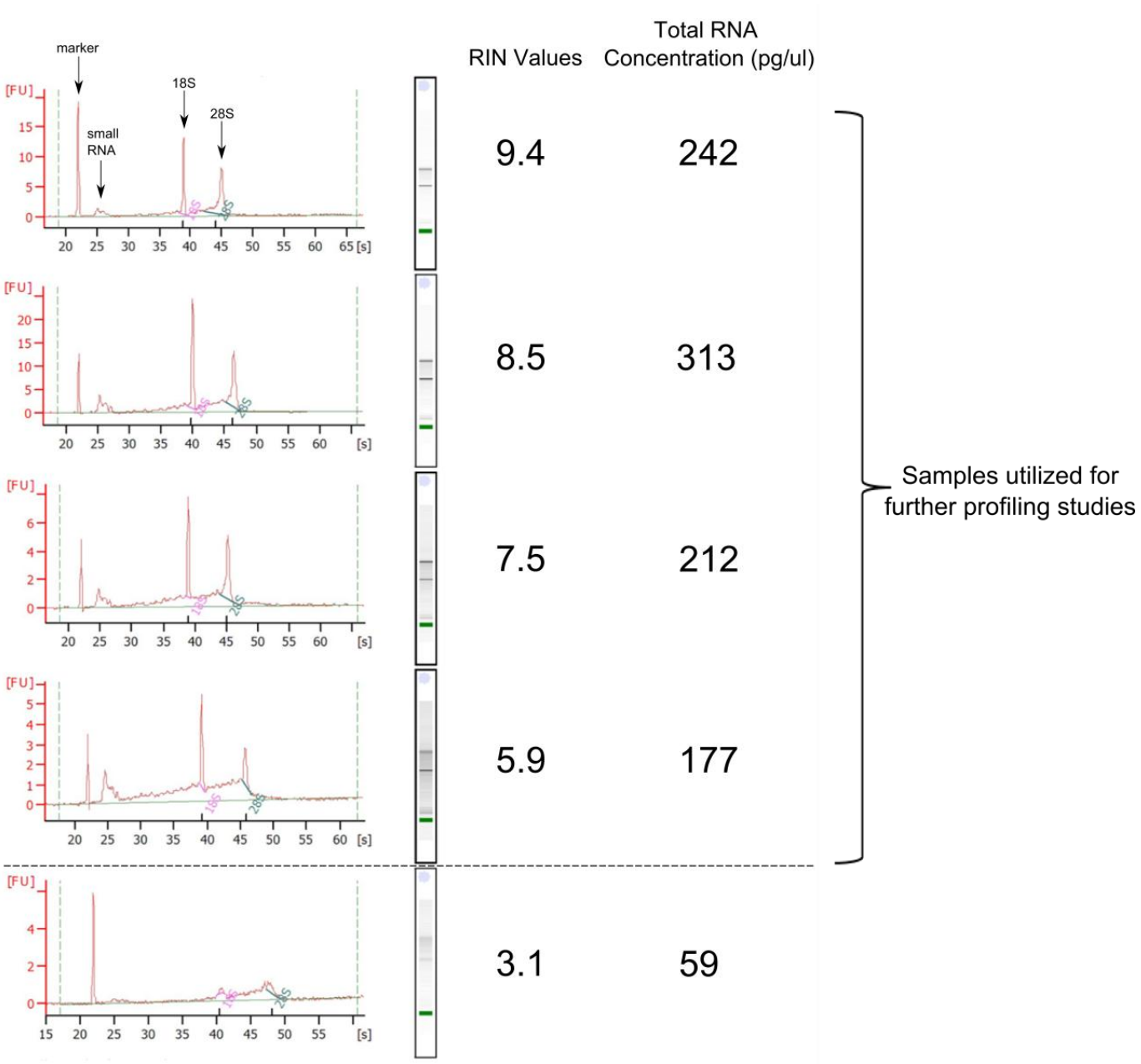

Figure 3.2. Representative bioanalyzer readings for laser capture microdissected RNA samples. The electropherogram recordings for each respective sample followed by the resulting RIN values and total RNA concentrations. The key components of the electropherogram characteristics are annotated as marker, small RNA, 18S and 28S regions. Samples with a RIN (RNA integrity number) of 5.9 and above were used for subsequent profiling analysis. Adapted from Majer *et al.*, 2012.

quantitatively measure the proportion of astrocyte and microglia cells within the LCM region. For these analyses, a house-keeping gene, *glyceraldehyde 3-phosphate dehydrogenase* (*Gapdh*), was used as an internal control for normalization across all datasets because its expression remained stable throughout the time course of disease in both control and infected mice (**Figure 3.3**).

Two cell-type specific gene markers were used to determine proportion of astrocytes and microglia within the LCM region. To monitor the abundance of astrocytes, *Gfap* signal intensities within each sample was assessed. The spot intensities of *Gfap* were below the threshold of detection in all control samples studied. However, a pronounced increase in *Gfap* signal was observed in RML-infected samples at terminal disease (**Figure 3.4**). Temporal analysis of the microglial gene marker *allograft inflammatory factor-1* (*Aif-1*), also known as *Iba1*, was used to monitor the abundance of microglia within the LCM region. *Iba1* showed a low but consistent signal in both control and prion-infected animals up to and including 110 DPI. Signal intensities for the *Iba1* probe were significantly increased at 130 DPI and EP in RML-infected animals (**Figure 3.4**).

The signal intensities of 3 highly-enriched neuronal-specific gene markers were examined by microarrays to determine whether the proportion of neurons was reduced by degeneration as disease progressed. The 3 genes chosen were *neurofilament light* and *medium polypeptides* (*Nefl* and *Nefm*) which are present in axon and/or dendrites and *synaptosomal-associated protein 25* (*Snap25*) that is located in pre-synaptic structures. The expression level within the control mice for all these genes remained consistent throughout the time period studied while the expression levels within prion-infected animals were significantly decreased during later stages of disease. Specifically, *Nefl* levels began to decrease as early as 110 DPI

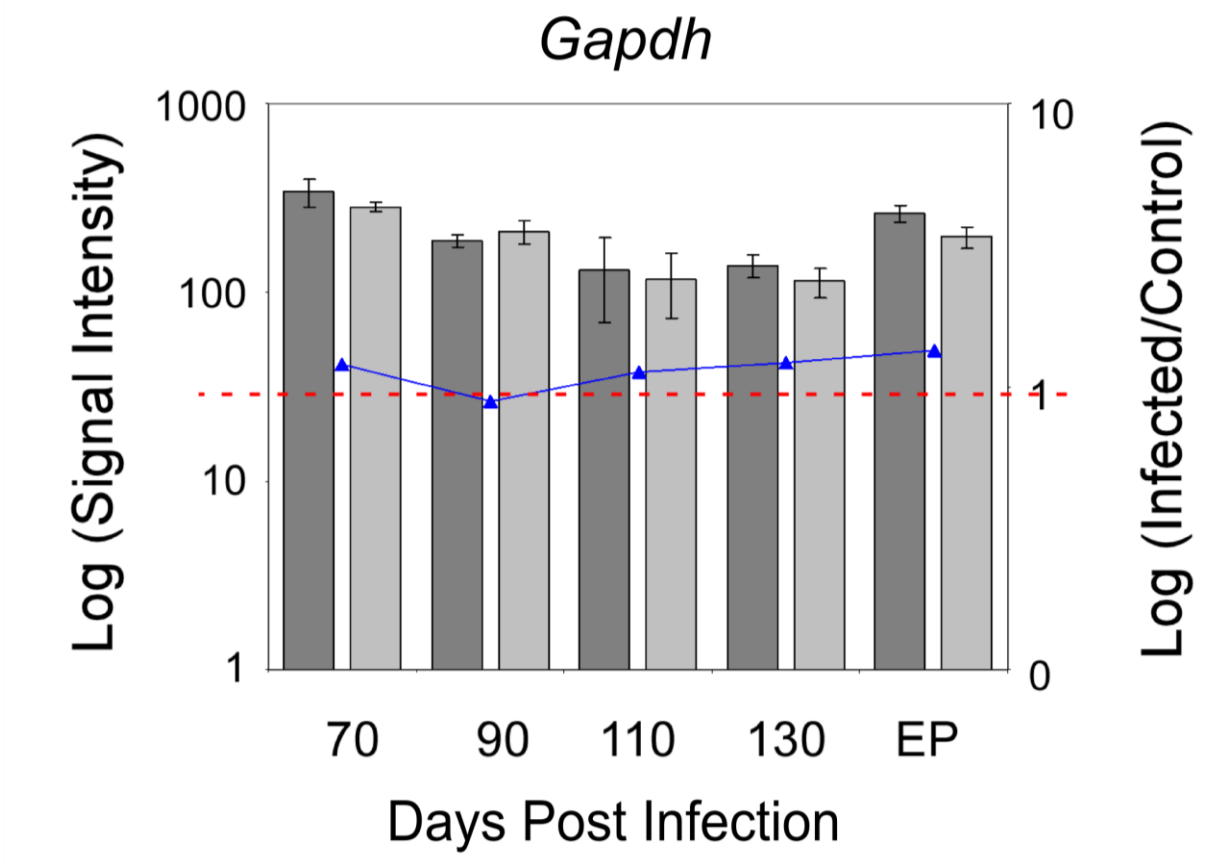

Figure 3.3. Temporal expression of *Gapdh* during prion disease in CA1 hippocampal neurons. Microarray expression levels of *Gapdh* within both infected (dark gray bars) and control (light grey bars) samples are plotted as log signal intensity values over the time course of disease. The relative abundance of *Gapdh* between the two samples (infected/control) at each time point is plotted as a line graph. The red dashed line represents a lack of fold change between the two samples. Student's t-test was performed to assess statistical significance. The `EP` designation represents the end-point of disease. Adapted from Majer *et al.*, 2012.

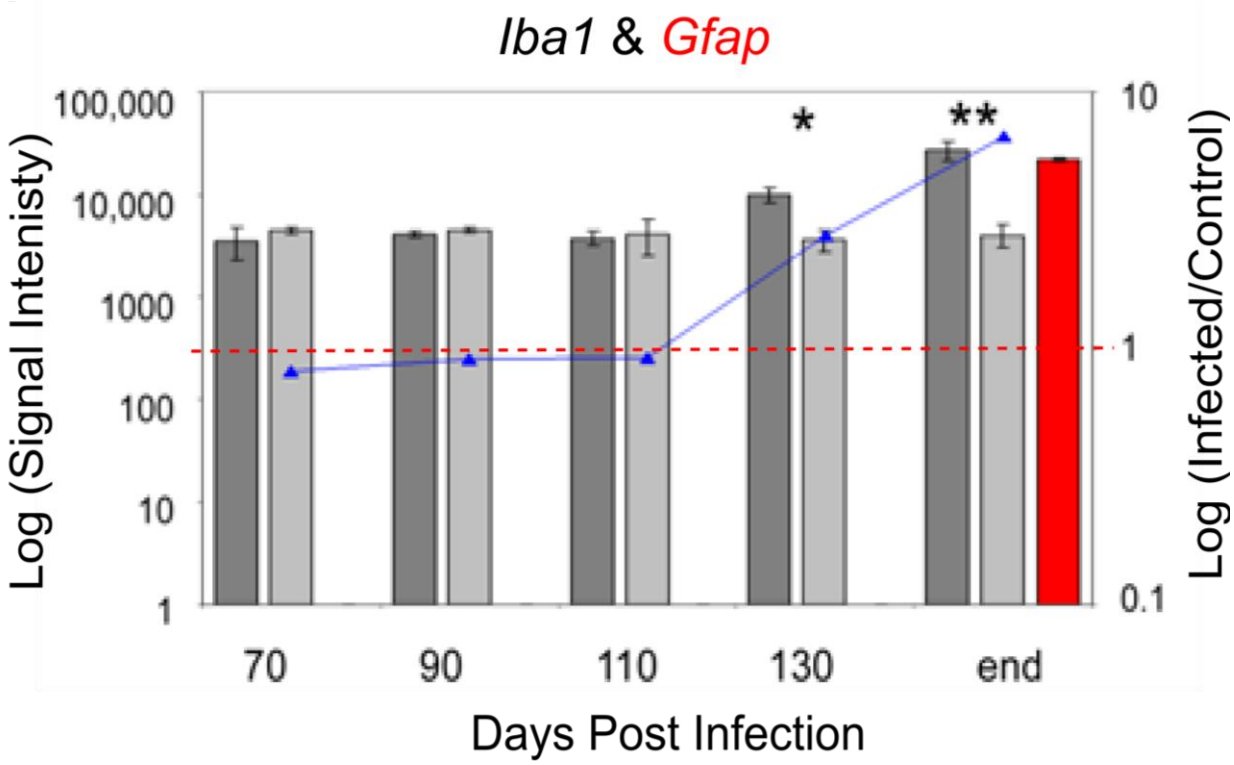

Figure 3.4. Temporal expression of *Iba1* and *Gfap* in CA1 hippocampal neurons during prion disease. The expression levels of microglia (*Iba1*) and astrocyte (*Gfap*) cell markers determined by microarrays. Log signal intensities for prion-infected (dark grey bars) and control (light grey bars) samples are plotted over time for microglia. The relative abundance of *Iba1* between infected and control samples (infected/control) are plotted as a line graph. The red bar reflects *Gfap* signal intensity in prion-infected samples only. The red dashed line represents a lack of fold change between the two samples. Student's t-test was performed to assess statistical significance where * is $p \leq 0.05$ and ** is $p \leq 0.01$. The `end` designation represents the end-point of disease. Adapted from Majer *et al.*, 2012.

while *Nefm* showed stark downregulation at EP. Similarly, *Snap25* was significantly decreased at both 130 DPI and EP (**Figure 3.5**).

3.1.4 Pathological Analysis of the RML Scrapie Model

Prior to performing an in-depth analysis of the transcriptomic data, several key pathological features characteristic of prion disease were assessed. Histology methods (described in the Materials and Methods *Sections 2.12* and *2.13*) were used to detect the presence of PrP^{Sc} deposits, vacuole formation, the degree of astrocytosis and microgliosis and the presence of neurodegeneration throughout disease progression.

3.1.4a Progressive Accumulation of PrP^{Sc} Deposits were Detected within Brain Tissue Beginning at Preclinical Disease

Whole brain sections were initially inspected for areas where PrP^{Sc} deposits were first detected. PrP^{Sc} deposits were observed as early as 70 DPI within the thalamus, fiber tract of the lateral forebrain bundle system and hypothalamus (**Figures 3.6-3.8**). Within these regions, PrP^{Sc} staining progressively accumulated over time until terminal disease. Congruent with the literature, the specific PrP^{Sc} staining pattern in prion-infected animals included the typical "aggregate"-like deposits as well as a fine, granular pattern of immunoreactivity that is recognized as a "synaptic pattern" of staining (Chiti *et al.,* 2006). This pattern of staining was also detected within the hippocampus, specifically the *stratum locunosum-moleculare* (SLM) (**Figure 3.9**), as early as 90 DPI. More extensive PrP^{Sc} staining was evident among the cell bodies of CA1 neurons in the SP and *stratum radiatum* (SR) regions beginning at 110 DPI,

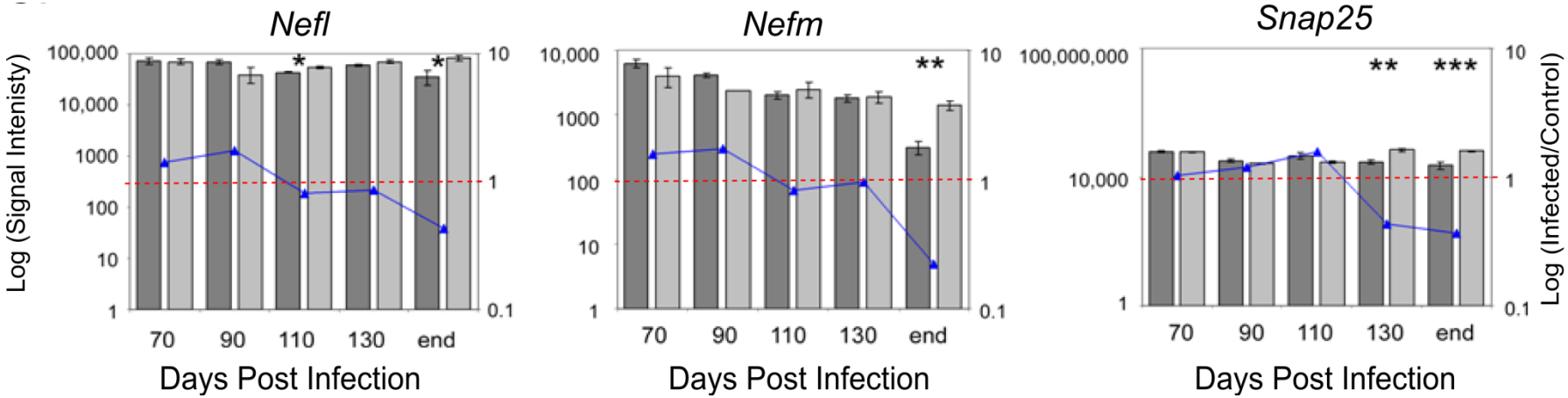

Figure 3.5. Temporal expression of neuronal-specific gene markers in CA1 hippocampal neurons during prion disease. Gene expression levels of 3 neuronal markers (*Nefl*, *Nefm* and *Snap25*) in both prion-infected (dark gray bars) and control (light gray bars) samples plotted as log signal intensity over days post inoculation. The line graph represents the relative abundance of signal detected for infected/control samples for each gene. For all the graphs, the red dashed line represents a lack of fold change between the two samples. Student's t-test was performed to assess statistical significance where * represents a p-value of ≤ 0.05; ** for a p-value of ≤ 0.01 and *** for a p-value of ≤ 0.001. The `end` designation represents the end-point of disease. Adapted from Majer *et al.*, 2012.

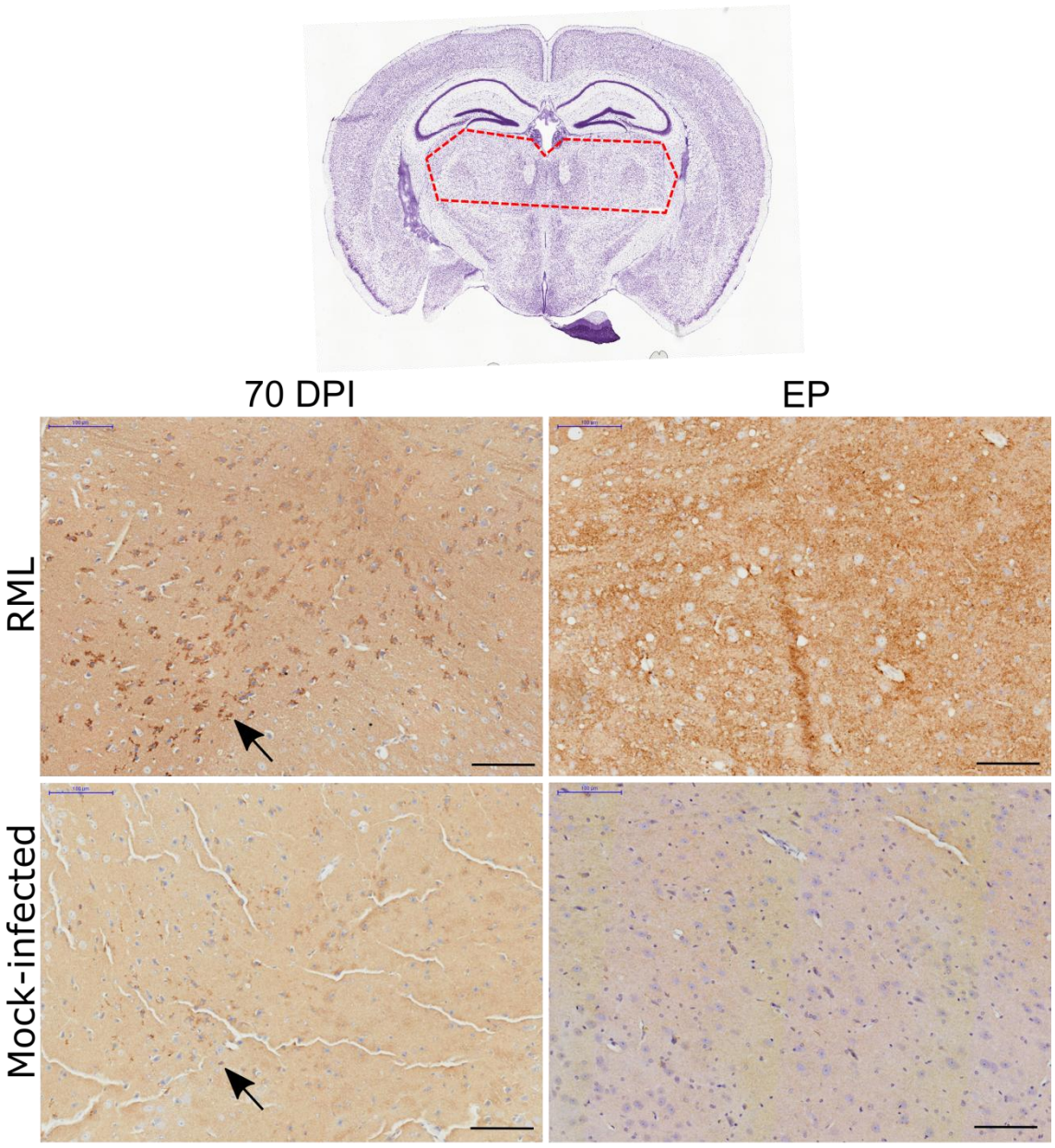

Figure 3.6. Deposition and continued accumulation of PrP^{Sc} within the thalamus of prion-infected brain tissue. A map of the coronal cross section of mouse brain (Allen Brain Atlas) depicting the thalamus region. Images for 70 DPI (pre-clinical) and EP (clinical) reveal extent of PrP^{Sc} deposition (brown staining) while blue represents cell nuclei. Some PrP^{Sc} positive areas are highlighted by arrows. EP represents end point; DPI is days post infection; RML is the Rocky Mountain Laboratory scrapie strain of prion. Scale bar = 100 µm.

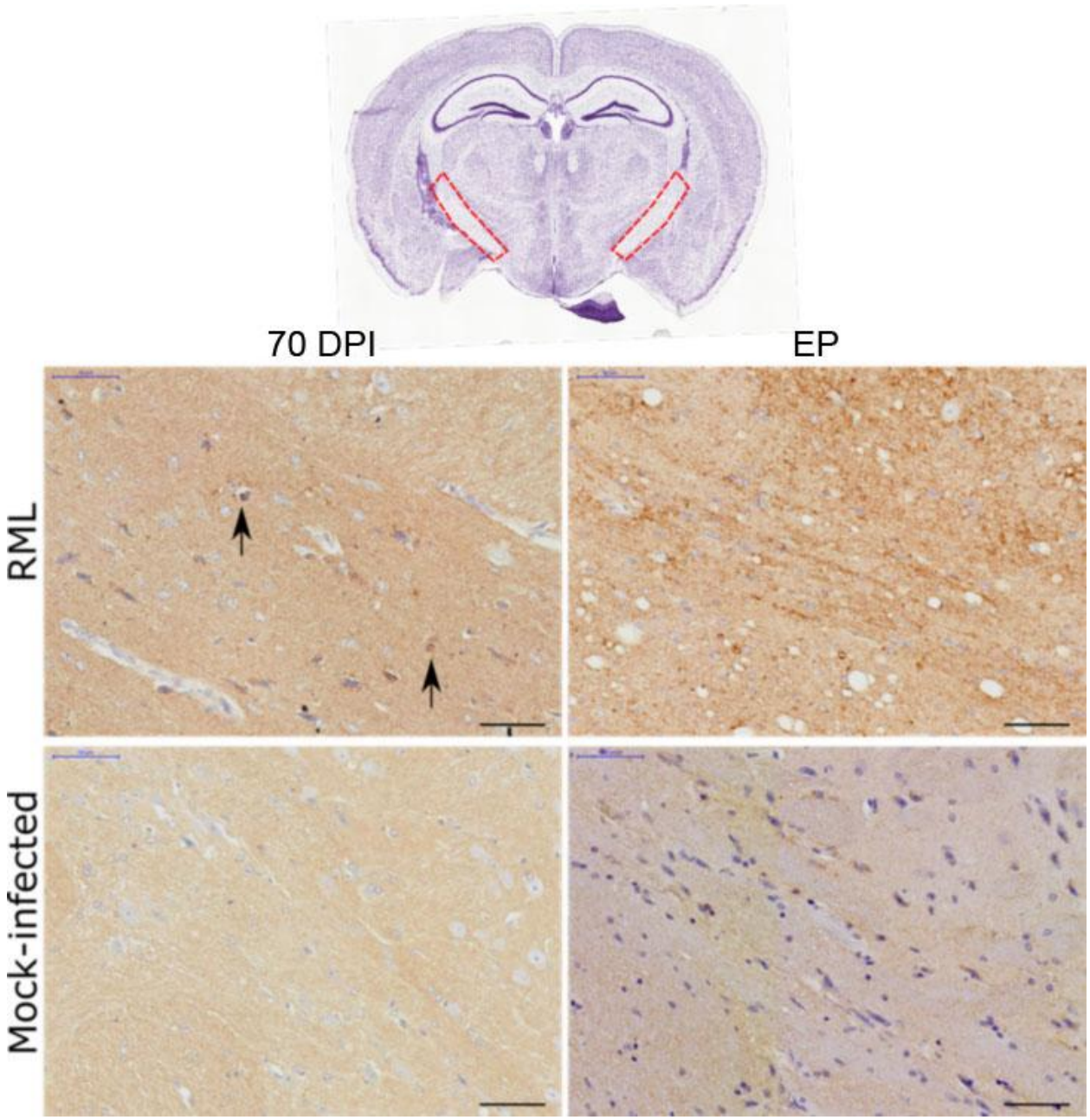

Figure 3.7. Deposition and continued accumulation of PrP^{Sc} within the fiber tract of prion-infected brain tissue. A map of the coronal cross section of mouse brain (Allen Brain Atlas) depicting the fiber tract region. Images for 70 DPI (pre-clinical) and EP (clinical) reveal extent of PrP^{Sc} deposition (brown staining) while blue represents cell nuclei. Some PrP^{Sc} positive areas are highlighted by arrows. EP represents end point; DPI is days post infection; RML is the Rocky Mountain Laboratory scrapie strain of prion. Scale bar = 50 µm.

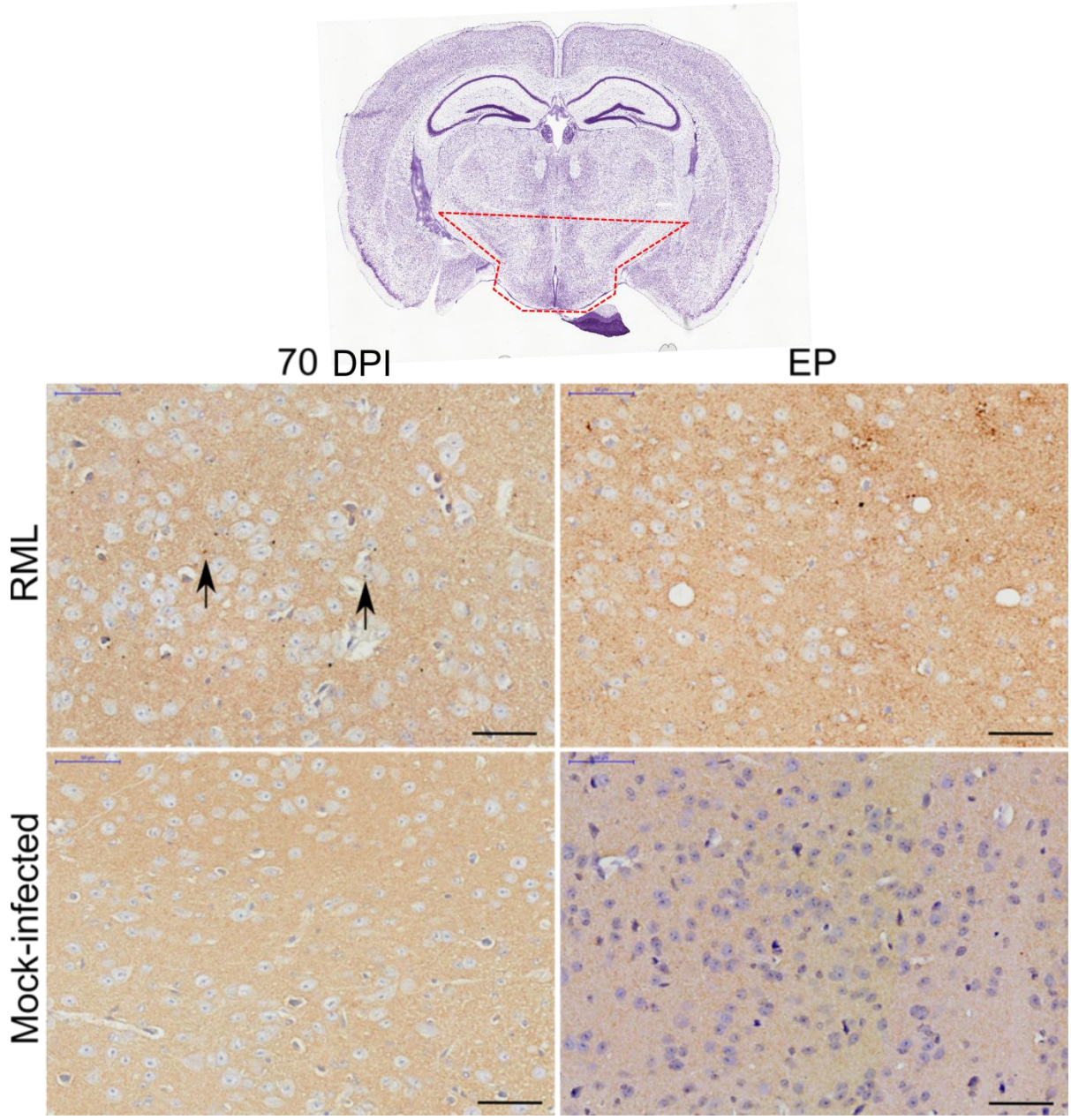

Figure 3.8. Deposition and continued accumulation of PrP^{Sc} within the hypothalamus of prion-infected brain tissue. A map of the coronal cross section of mouse brain (Allen Brain Atlas) depicting the hypothalamus region. Images for 70 DPI (pre-clinical) and EP (clinical) reveal extent of PrP^{Sc} deposition (brown staining) while blue represents cell nuclei. Some PrP^{Sc} positive areas are highlighted by arrows. EP represents end point; DPI is days post infection; RML is the Rocky Mountain Laboratory scrapie strain of prion. Scale bar = 50 µm.

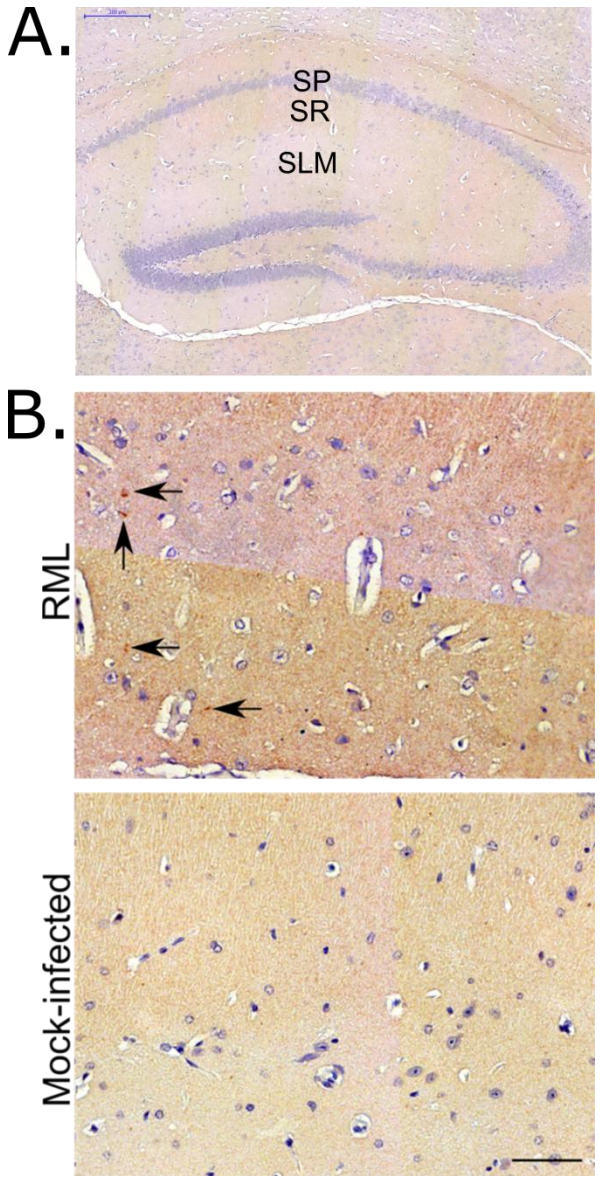

Figure 3.9. Deposition and accumulation of PrP^{Sc} within the *stratum locunosum-moleculare* of the hippocampus of prion-infected brain tissue at 90 DPI. (**A**) A map of the coronal cross section of mouse brain (Allen Brain Atlas) depicting the *stratum pyramidale* (SP), the *stratum radiatum* (SR) and the *stratum locunosum-moleculare* **(**SLM) regions. (**B**) Immunohistochemistry images for PrP^{Sc} deposits within the hippocampus region at 90 DPI in RML and mock-infected mice. Brown staining represents PrP^{Sc} deposition (some areas are highlighted by arrows) while blue represents cell nuclei. EP represents end point; DPI is days post infection; RML is the Rocky Mountain Laboratory scrapie strain of prion. Scale bar = 50 µm. Adapted from Majer *et al.*, 2012.

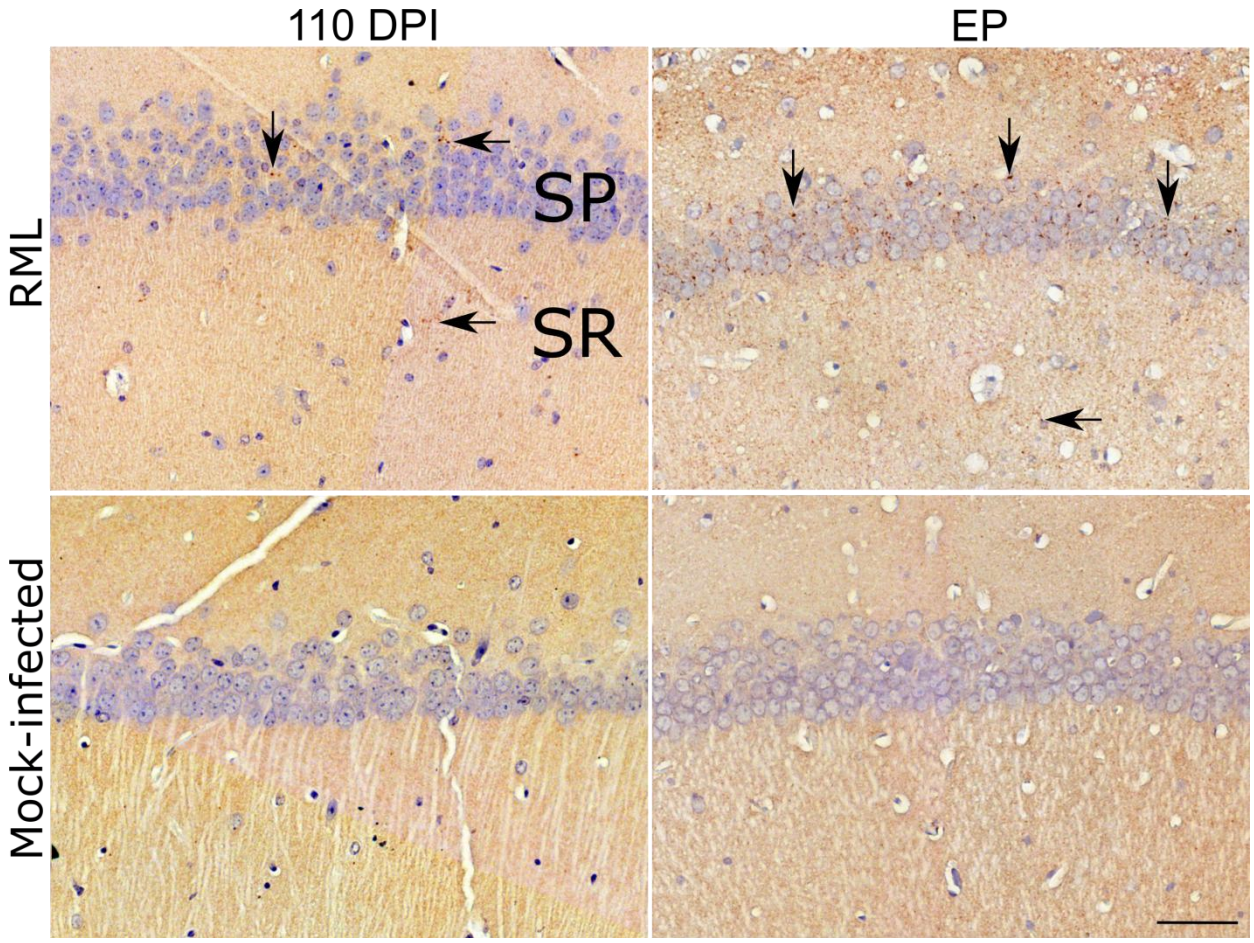

Figure 3.10. Deposition and continued accumulation of PrP^{Sc} within the pyramidal layer of CA1 hippocampal neurons of prion-infected brain tissue. Immunohistochemistry images for PrP^{Sc} deposits within the hippocampus region at 110 DPI and EP in RML and mock-infected mice. Brown staining represents PrP^{Sc} deposition (some areas are highlighted by arrows) while blue represents cell nuclei. EP represents end point; DPI is days post infection; RML is the Rocky Mountain Laboratory scrapie strain of prion. SP is *stratum pyramidale* and SR is *stratum radiatum*. Scale bar = 50 µm. Adapted from Majer *et al.*, 2012.

which continued to accumulate until terminal disease (**Figure 3.10**). Severe spongiform formations within the neuropil were detected only in prion-infected animals at EP.

3.1.4b Astrocyte Numbers Increased within the CA1 Hippocampal Region at Clinical Disease

To determine the proportion of astrocytes within the neuronal-dense CA1 hippocampal region, the GFAP cell marker was used to visualize these cells. A very small number of astrocytic cell bodies were identified within the CA1 region of the hippocampi in healthy control mice. Conversely, more staining of astrocytic cell bodies were detected at EP of disease in prion-infected animals (**Figure 3.11**), coinciding with the microarray data (**Figure 3.4**).

3.1.4c Microglia Numbers Increased within the CA1 Hippocampal Region at Clinical Disease

To determine the proportion of microglia cells within the neuronal-dense CA1 hippocampal region, the IBA1 cell marker was used to visualize these cells. Microglia cell bodies were detected in limited numbers within the CA1 hippocampal region of uninfected animals while the number of these cells significantly increased in prion-infected mice at 130 DPI, an increase that persisted into terminal disease (**Figure 3.12**).

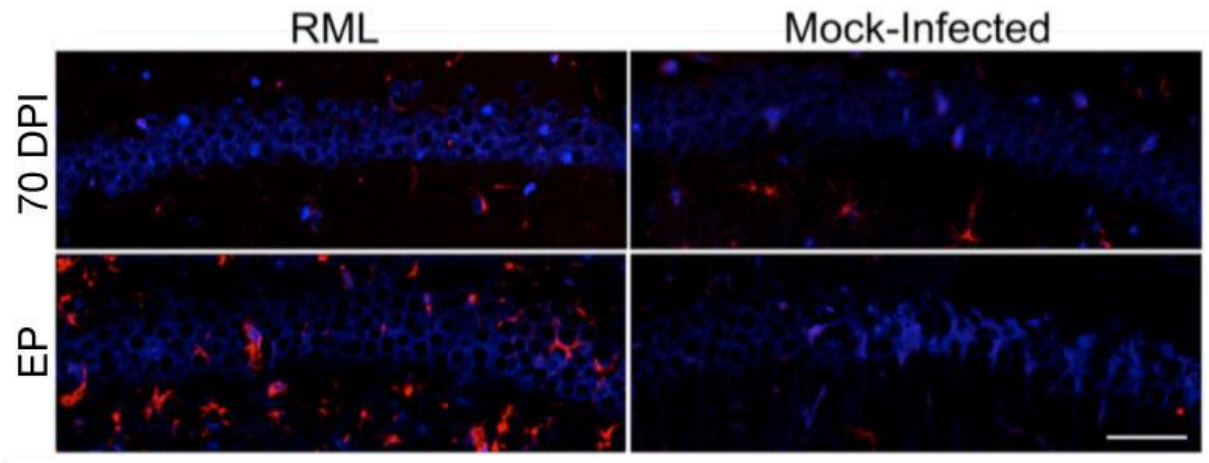

Figure 3.11. Astrocytes infiltrate the cell bodies of CA1 hippocampal neurons at clinical stages of prion disease. Immunofluorescence images representing astrocyte cells (red) among the CA1 hippocampal neurons (blue) in both prion-infected and control samples at preclinical (70 DPI) and clinical (EP) disease. EP represents end point; DPI is days post infection; RML is the Rocky Mountain Laboratory scrapie strain of prion. Scale bar = 50 µm. Adapted from Majer *et al.*, 2012.

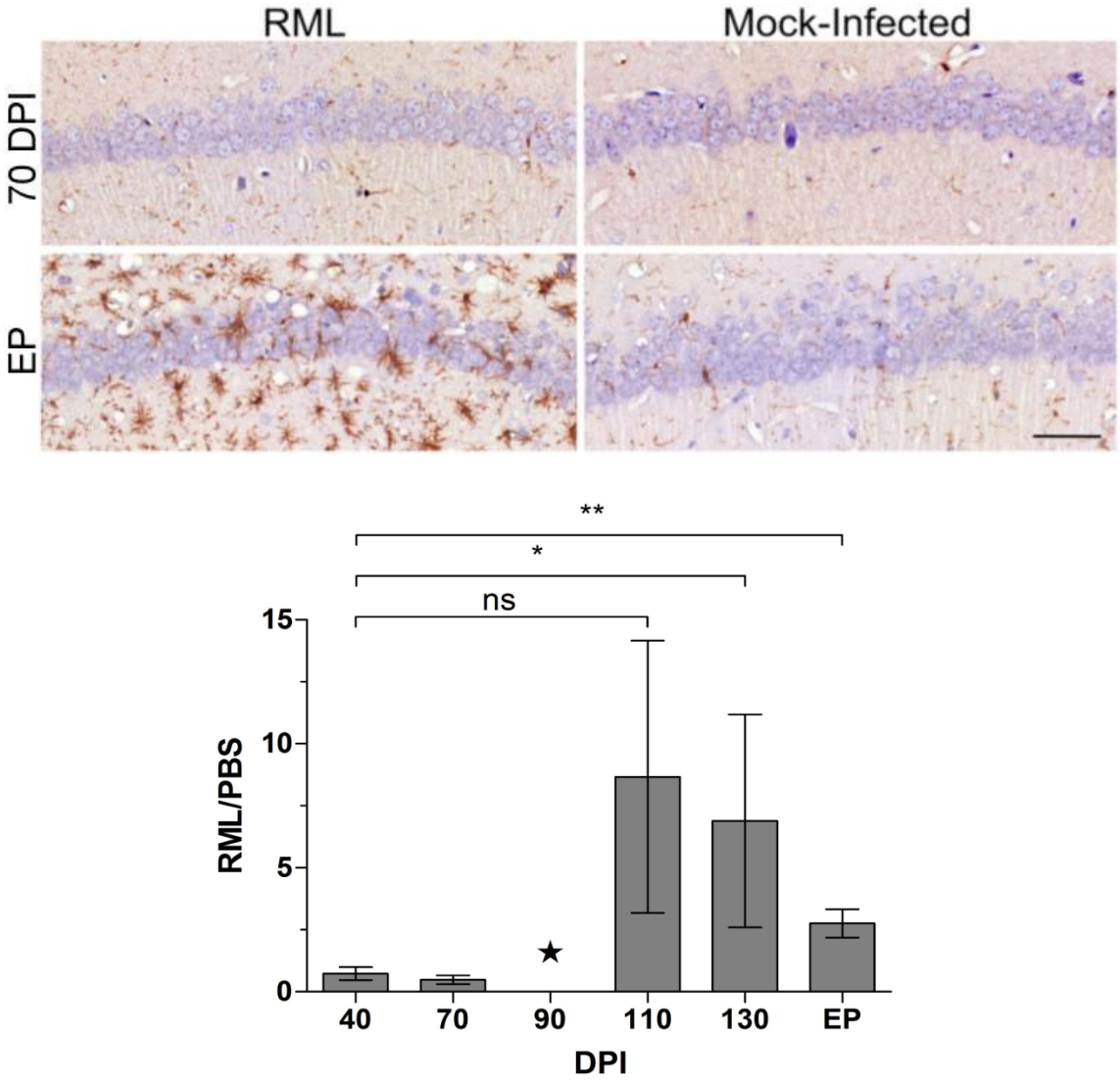

Figure 3.12. Microglia infiltrates cell bodies of CA1 hippocampal neurons at clinical stages of prion disease. Immunohistochemistry images for microglia (brown) detection in the CA1 neuronal layer (blue) in both infected and control samples. The 70 and EP time points are represented. Scale bar = 50 µm. The bar graph represents the relative quantification of the microglial cells detected within the nuclei dense CA1 neuronal layer throughout prion infection (n=3-4). Data is represented as mean ± SEM. The star for 90 DPI indicates insufficient replicates for accurate statistical analysis. Student's t-test was used to assess significance: ns = no significance; * = p-value of ≤ 0.05; ** = p-value of ≤ 0.0005. RML is the Rocky Mountain Laboratory scrapie strain of prion. DPI refers to days post infection. Adapted from Majer *et al.*, 2012.

3.1.4d Degeneration of Hippocampal Neurons was Detected Only at Clinical Stages of Prion Disease

The marker that was used to detect neuronal degeneration was Fluoro-Jade® C (Schmued *et al.*, 2005). This stain has a high affinity for endogenous molecules associated with neurodegeneration, allowing for effective detection of degenerating neurons by a wide range of molecular mechanisms (Schmued *et al.,* 2005). On a cell structural level, Fluoro-Jade® C can detect cell bodies, distal dendrites, axons or terminals of degenerating neurons at an ultra-high resolution making it superior to standard histological stains (*i.e.* Nissl, H&E or silver stains) used for detecting neuronal degeneration (Schmued *et al.,* 2005). Using this staining method, degeneration was not detected in either RML or mock-infected samples at 70 DPI within the entire coronal cross-section of the hippocampi (**Figure 3.13**). Only at terminal disease a small proportion of neurons were stained with Fluoro-Jade® C in the CA1 pyramidal layer. At this time, a much greater number of interneurons belonging to the SR or SLM of the hippocampus were positively stained with Fluoro-Jade® C in prion-infected mice (**Figure 3.14**).

Collectively, the pathological analysis of the hippocampal region exemplified all of the neuropathological hallmarks of prion disease. More importantly, the region that was isolated for neuronal-enrichment was largely made up of neuronal cell bodies. Only at 130 DPI did the proportion of neurons to glial cells change such that more glial cells were detected within this region.

3.1.5 Stable Expression of *Prnp* in CA1 Hippocampal Neurons

PrP^C protein expression on the surface of neurons is essential for the initiation of prion-mediated neurodegeneration processes. Therefore, it was of interest to determine if the

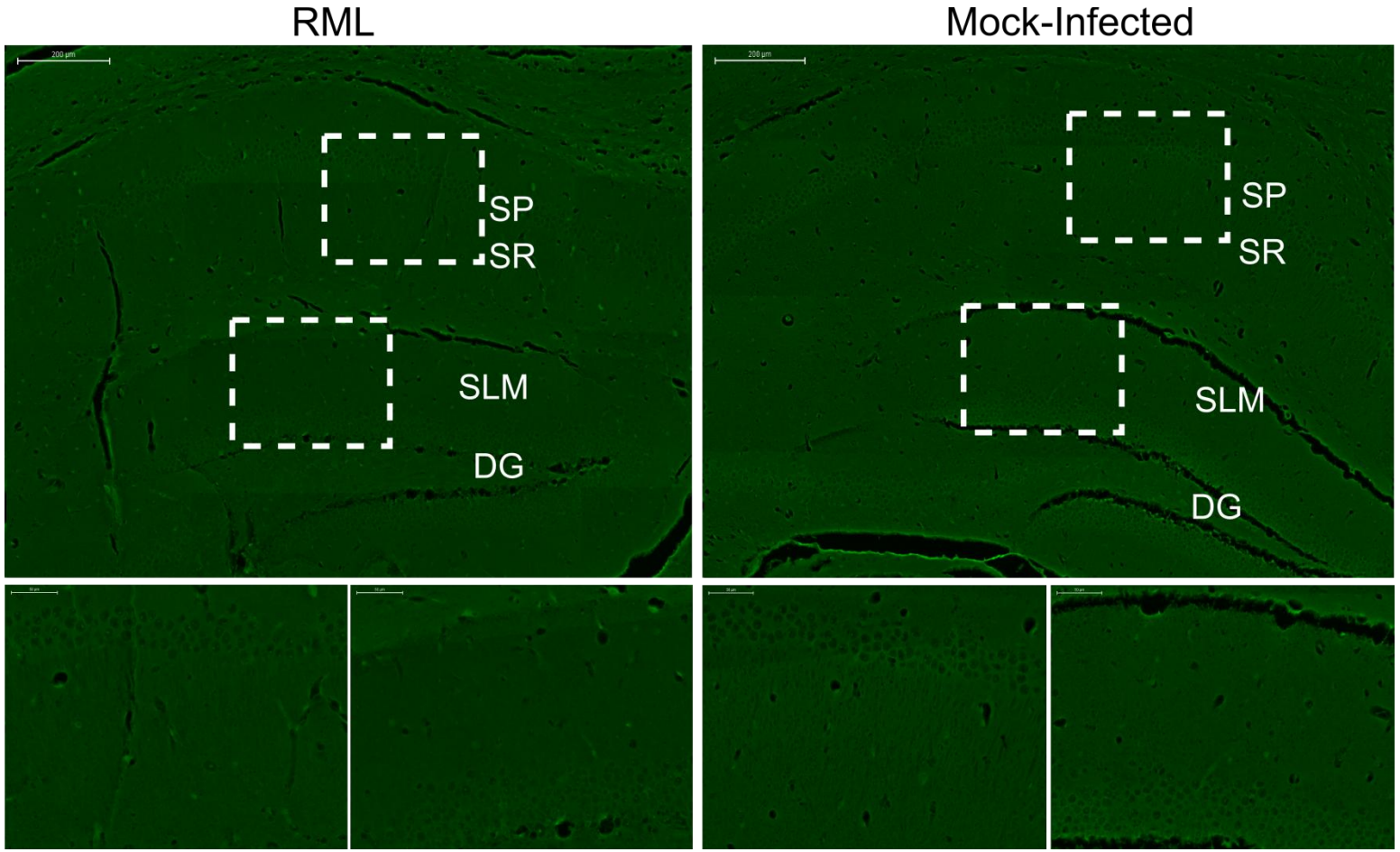

Figure 3.13. Neurodegeneration is undetected within the hippocampus at early stages of prion disease. Immunofluorescent images of coronal cross-sections of the hippocampus in RML and mock-infected samples at 70 DPI. Large images represent hippocampal regions (scale bar = 200 µm) while the outlined rectangles are regions that are further magnified (scale bar = 50 µm). SP is *stratum pyramidale*; SR is *stratum radiatum*; SLM is *stratum lacunosum-moleculare*; DG is dentate gyrase. RML is the Rocky Mountain Laboratory scrapie strain of prion. Adapted from Majer *et al.*, 2012.

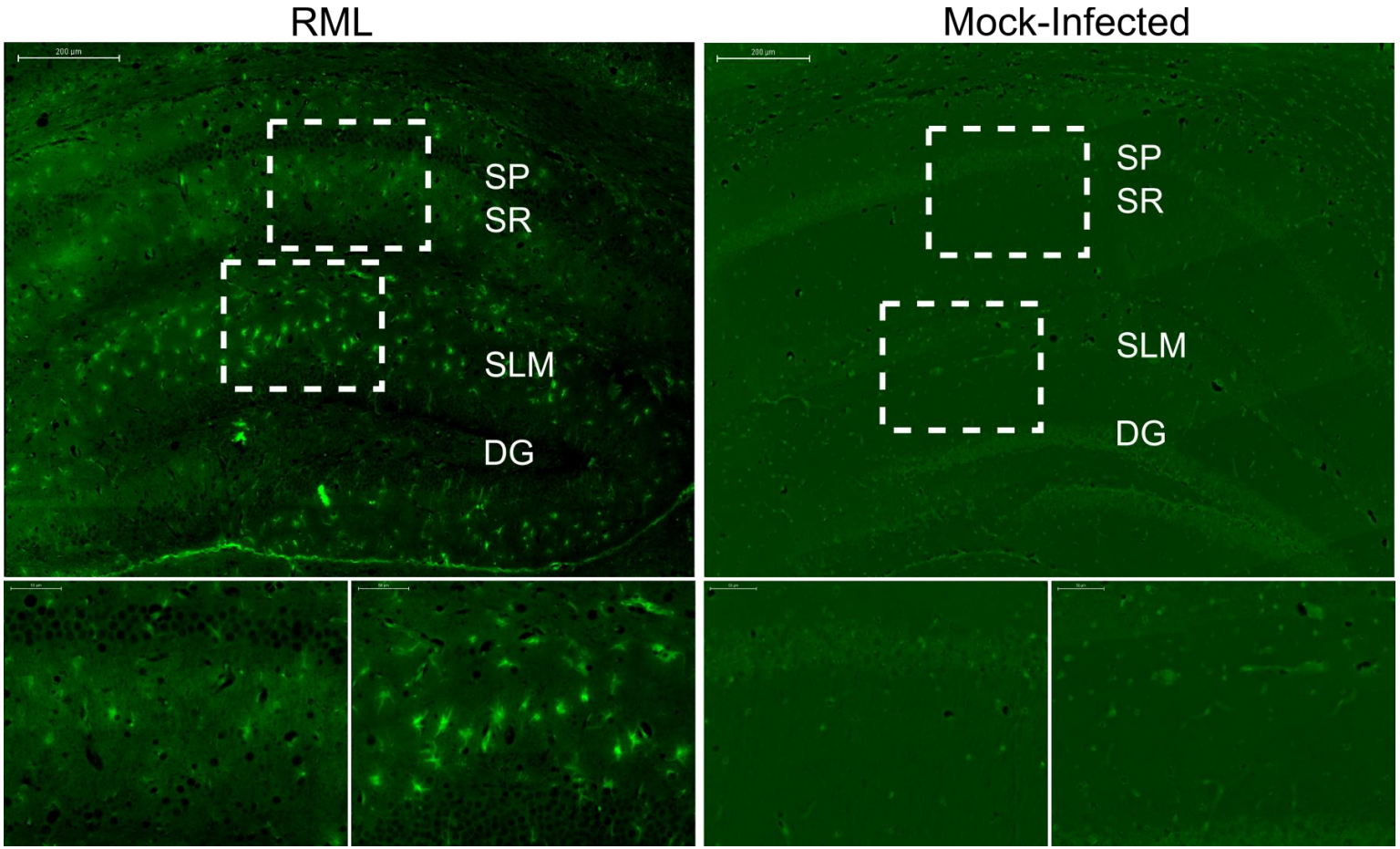

Figure 3.14. Neurodegeneration is detected within the hippocampus at terminal prion disease. Immunofluorescent images of coronal cross-sections of the hippocampus in RML and mock-infected samples at EP. Bright green staining observed only at EP of disease in RML-infected mice indicates degeneration. The large images represent hippocampal regions (scale bar = 200 µm) while the outlined rectangles are regions that are further magnified (scale bar = 50 µm). SP is *stratum pyramidale*; SR is *stratum radiatum*; SLM is *stratum lacunosum-moleculare*; DG is dentate gyrase. RML is the Rocky Mountain Laboratory scrapie strain of prion. Adapted from Majer *et al.*, 2012.

expression of *Prnp* throughout the disease time course was altered within the cell bodies of CA1 hippocampal neurons. Microarray data did not reveal significant differences in *Prnp* signal intensities between prion-infected and control animals at any time point analyzed. In a similar manner, qRT-PCR failed to show any significant difference between control and prion-infected animals ($p < 0.05$). However, *Prnp* expression showed a trend towards downregulation in prion-infected samples at 70 DPI ($p < 0.1$) which returned to basal expression levels with disease progression (**Figure 3.15**).

3.1.6 Temporal Delineation of 2 Major Clusters of Genes

To determine whether the deregulated gene profiles followed a temporal pattern of expression, a hierarchical cluster plot was generated. To do so, the list of 2,580 genes was further filtered to include only genes for which expression changed at least 2-fold between infected and control samples [FDR < 0.001 (0.1 %)]. This resulted in a subset of 1,026 genes that were significantly changed in at least one time point during disease progression. From the hierarchical analysis, a distinct temporal pattern for two major gene clusters emerged (**Figure 3.16A**). Genes that grouped in the first cluster were primarily induced at either 70 and/or 90 DPI in prion-infected samples. As disease progressed, the expression of these genes slowly diminished and was abolished at clinical disease (130 DPI-EP) in prion- as compared to mock-infected animals. The second major hierarchical cluster consisted of genes that were primarily downregulated in prion-infected samples as compared to controls during preclinical disease. Within this cluster, a subset of genes was induced at 130 DPI while a much larger group of genes was upregulated at EP in prion-infected animals.

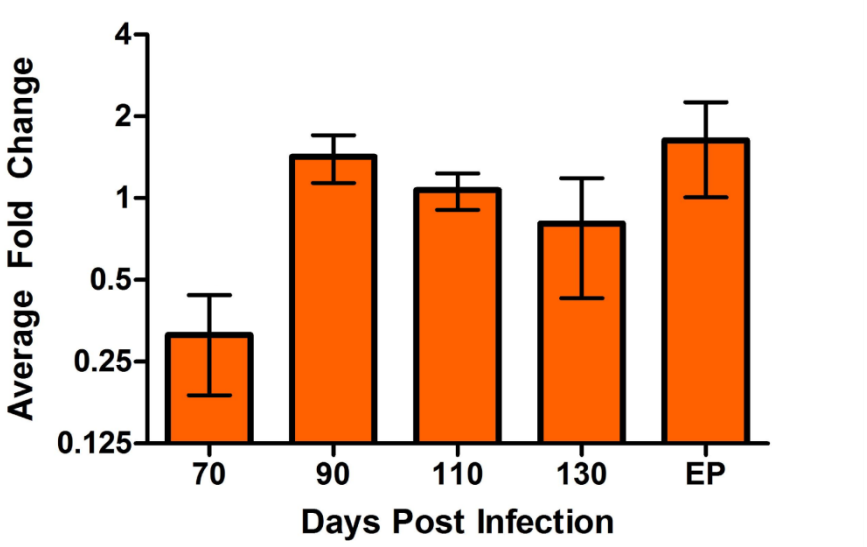

Figure 3.15. The relative fold change of *Prnp* in cell bodies of CA1 hippocampal neurons during prion disease using qRT-PCR. The qRT-PCR values are reported as mean ± SD and student's t-test was used to calculate significance (n=3-4 mice per condition).

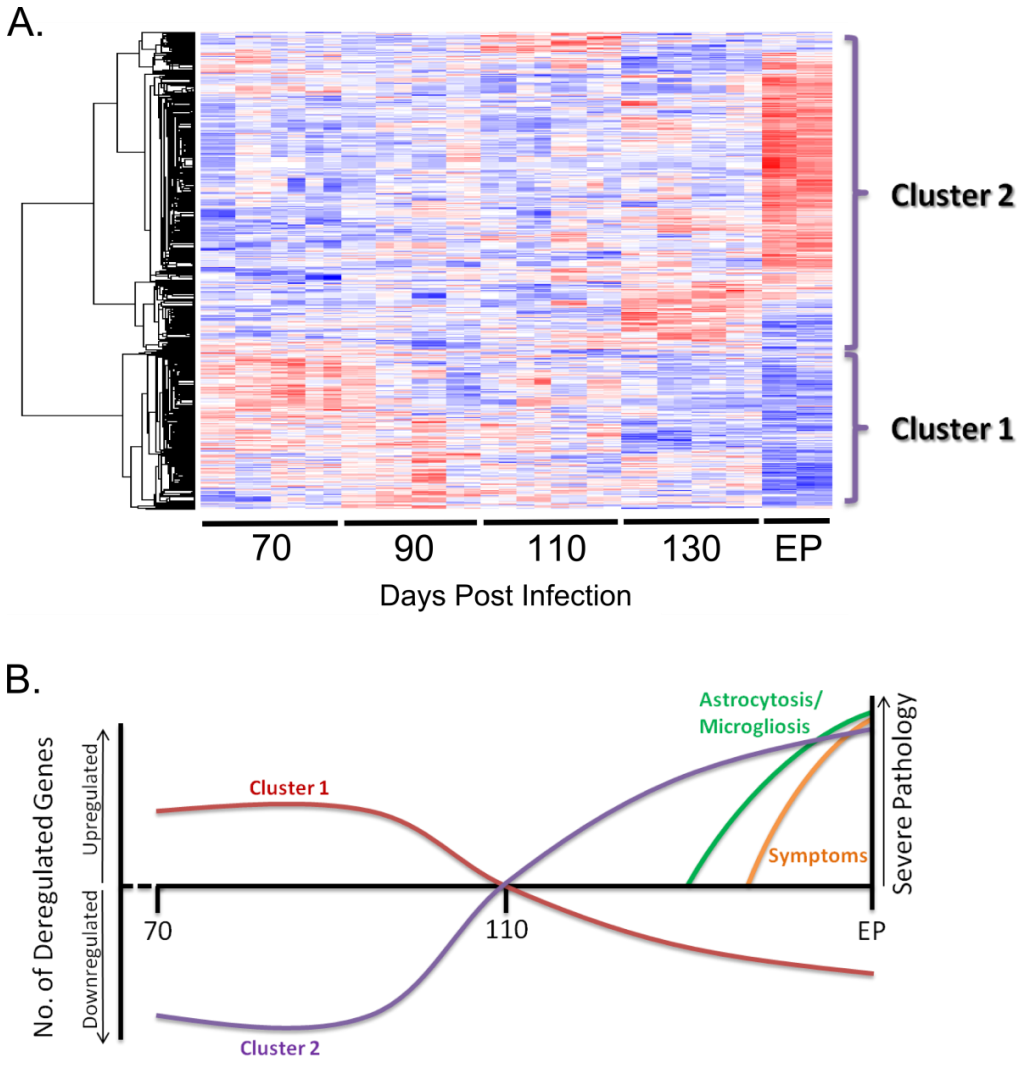

Figure 3.16. Gene expression profiling revealed two temporally defined gene clusters that were deregulated during prion disease. (**A**) Hierarchical cluster analysis of 1026 genes that showed significant differential expression during prion- as compared to mock-infected samples (FDR < 0.001 and at least 2-fold change). Hierarchical cluster analysis was performed using GenMathsXT. Red bars indicate upregulated and blue bars represent downregulated gene expression levels relative to the mean (white). Two clusters are further highlighted. (**B**) Relative schematic representation of the two clusters of genes overlaid onto the prion disease time course. A large proportion of genes within cluster 1 (red line) were induced at preclinical disease, however, the expression of these genes decreased as disease progressed into clinical stages. An inverse relationship was observed for genes belonging to cluster 2 (purple line). Symptom manifestation and detection of astrocyte and microglia cells within the CA1 hippocampal neurons were induced after 130 DPI, when additional severe pathology was observed. The dotted segment on the x-axis represents a time period from 0 up to 70 DPI when gene expression profiling was not assessed in this study. Adapted from Majer *et al.*, 2012.

Several parallels can be drawn when comparing the temporal expression of genes belonging to these two hierarchical clusters to the time when severe pathology was detected. It appears that genes belonging to cluster 1 are inversely correlated to expression of genes belonging to cluster 2 and detection of severe pathology. The induction of genes belonging to cluster 2 coincides with the detection of astrocytosis/microgliosis and symptom onset in prion-infected animals. Conversely, the expression of genes in cluster 1 are induced during preclinical disease and either return to basal levels or become significantly downregulated when severe pathology and symptoms are detected (**Figure 3.16B**).

3.1.7 Ontological Analysis of Gene Expression Data

To glean a better appreciation for the functional relevance of the deregulated gene clusters at different stages of disease, all genes that were deregulated in at least one time point were analyzed using the bioinformatic program ToppCluster. This program facilitates a comparative enrichment and network analysis of multiple gene lists, such as the temporally deregulated genes identified in this study, and provides a functional readout indicating which functional features are shared between the different time points analyzed and which are time point specific. To identify which functional networks were globally upregulated and downregulated throughout disease progression, list of deregulated genes were separated into two major lists: a group that consisted of all upregulated genes and another group that was representative of all downregulated genes curated from the broader analysis that was initially performed (2,580 altered genes). Genes within these 2 major lists were further subdivided based on the time points when they were significantly deregulated. As a result, this approach was more inclusive of the deregulated genes and allowed for an improved discrimination between the

functional ontologies that were either upregulated or downregulated as disease progressed. Functional ontologies for these comparisons were visualized using Cytoscape (Cline *et al.,* 2007; Smoot *et al.,* 2011).

3.1.8a Ontological Analysis of Upregulated Genes

Functional ontologies identified from the upregulated gene list were induced at both preclinical and clinical disease. A smaller group of functionally related transcripts were upregulated only during preclinical disease (70-110 DPI). These genes represented several molecular functions for which one of the earliest biological processes, occurring at 70 DPI, was the cellular response to stress (*i.e. Egr1* and *Fos*) followed closely by the unfolded protein binding process (*i.e. Hspa9, Pfdn2* and *Tcp1*). Several additional biological processes were shared between preclinical time points and terminal disease. For example, cell substrate adhesion (*i.e. Icam1* and *Vcam1*), regulation of cell proliferation (*i.e. Tgm2* and *Adra2a*) and cell-cell signaling (*i.e. S100a4* and *Bmp7*) were induced at 110 DPI and continued to increase at terminal disease. In contrast, other functional processes such as regulators of apoptosis (*i.e. Prkcd*, *Fadd* and *Dub2*) were induced only at clinical disease.

Overall, the largest proportion of functional ontologies identified from the upregulated gene list was induced only at EP. Approximately 85% of the ontologies at this time point reflected the development and function of the immune response (**Figure 3.17**). Many of these biological processes represented activation of inflammation (*i.e. Ccl5*, *Ccl3* and *Cxcl10*) and gliogenesis (*i.e. Gfap* and *S100b*). The representative genes and their relative signal intensities between infected and control samples for each pathway are provided in **Figure 3.18**.

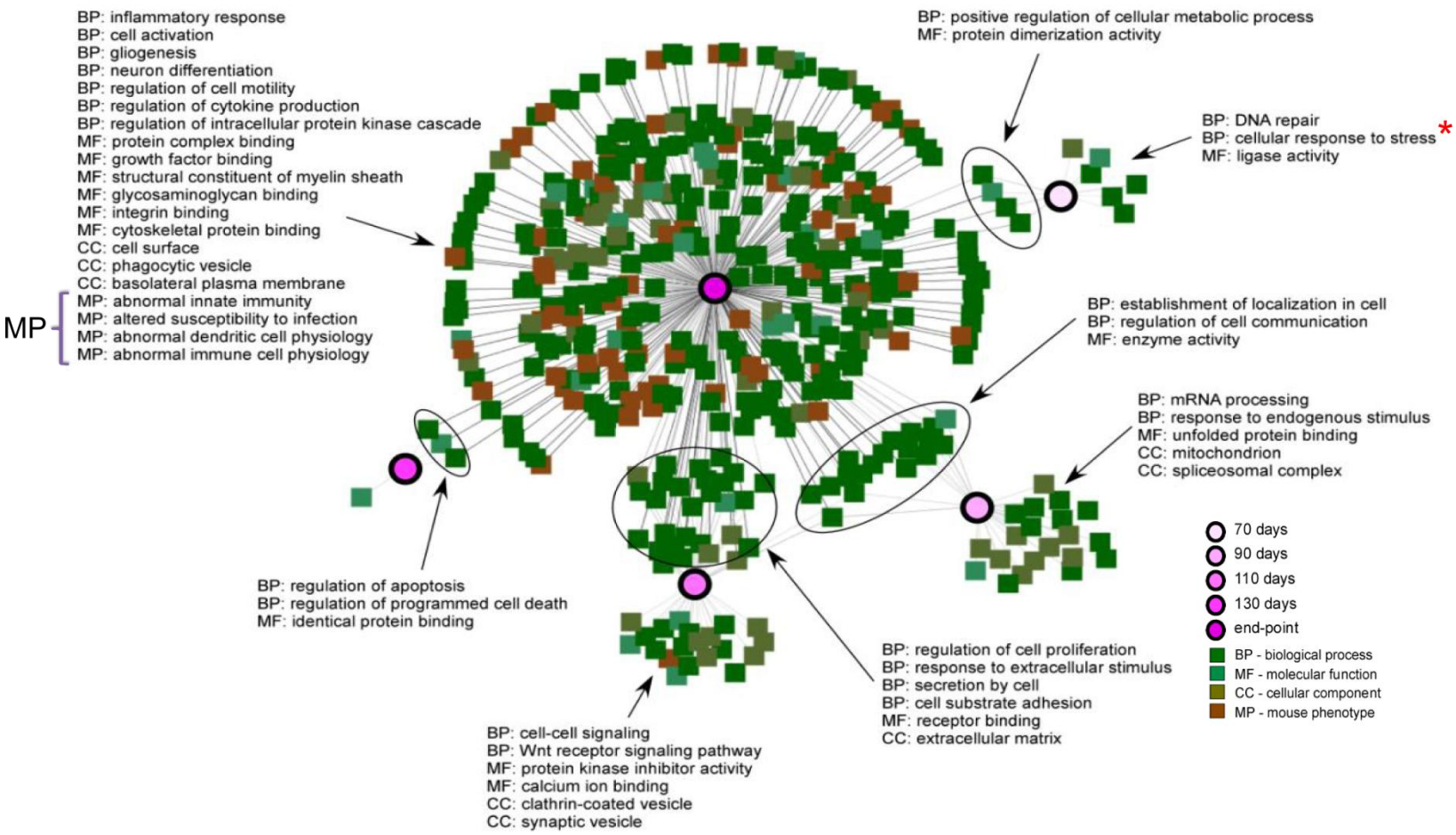

Figure 3.17. Gene ontology networks identified from the upregulated gene list. Gene ontologies were grouped according to the time points analyzed. Select ontologies are highlighted of which majority reflect immune-regulated genes at clinical stage of disease. The cellular response to stress is further indicated by * at 70 DPI while mouse phenotype ontologies are depicted by MP. The gene ontology network was generated using Cytoscape. Adapted from Majer *et al.*, 2012.

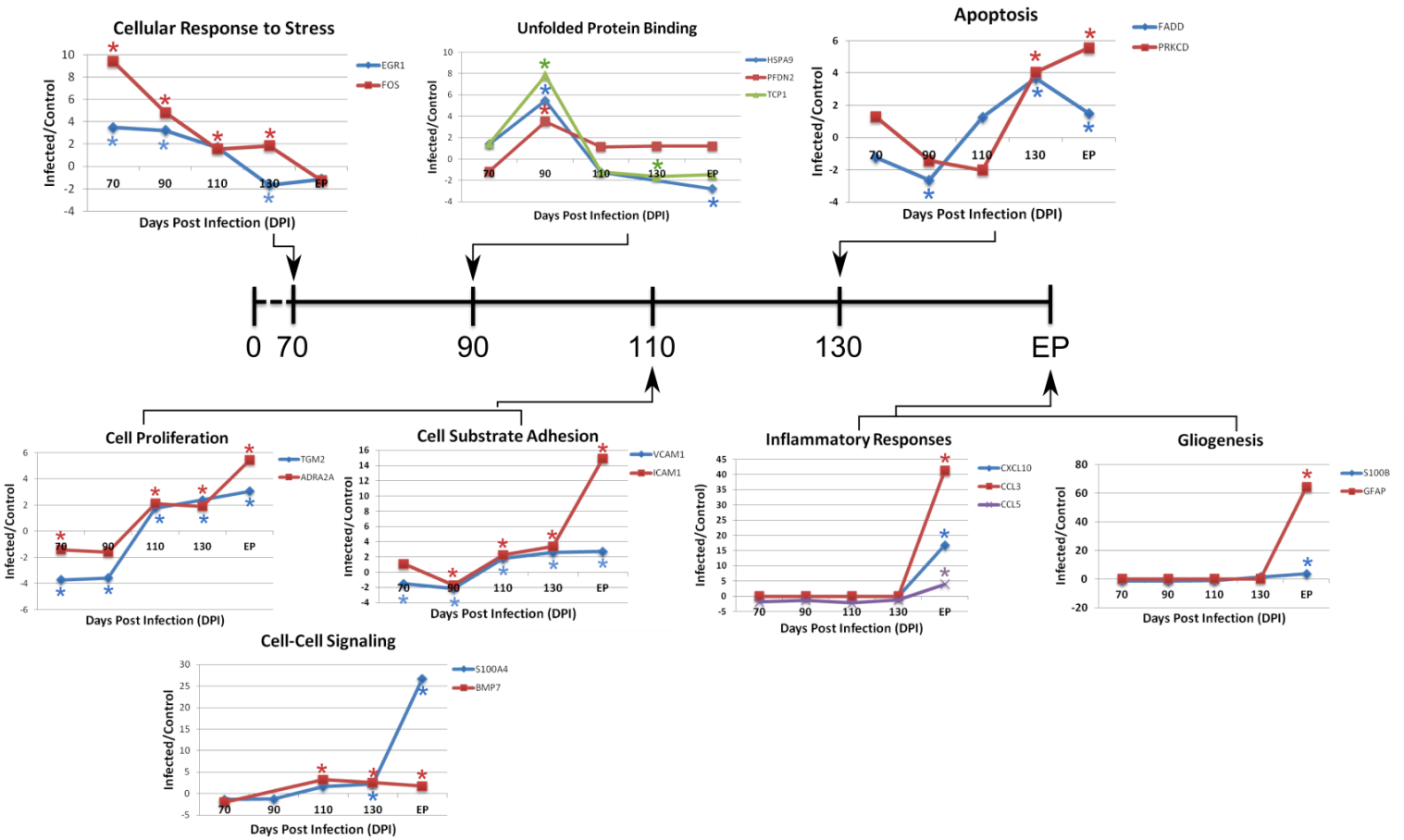

Figure 3.18. Genes representing biological processes that were upregulated during prion disease within cell bodies of CA1 hippocampal neurons. Arrows indicate the time at which the genes were significantly induced for each biological process. Each graph depicts the signal intensity ratio between infected and control samples for the representative genes throughout the time course of disease. Missing data for a particular time point is indicated by the line being connected by the surrounding 2 data points. When more than 2 data points are missing, the infected/control ratio was set to 0. Significance (FDR < 5) is indicated by * which is colour coded for each respective gene. Time preceding 70 DPI was not analyzed for gene expression.

3.1.8b Ontological Analysis of Downregulated Genes

The predominant ontologies obtained from the downregulated gene list are largely representative of neuronal function, regardless of the time point inspected. Strikingly, a group of ontologies involved in neuronal projection and synaptic transmission were consistently downregulated throughout the entire disease process (**Figure 3.19**). Several biological processes that contained downregulated genes at 70 DPI included synapse assembly (*i.e. Nrg1* and *Nrxn1*), dendrite development (*i.e. Chat*) and neurotransmitter transport (*i.e. Cplx2* and *Sypl1*). However, genes specifically involved in synapse formation and/or maintenance were also strongly downregulated at terminal disease. These genes include synaptophysin (*Syp*), α-synuclein (*Snca*) and *Snap25*. Additional functions such as calcium ion binding and receptor activities (*i.e. Gabra1*, *Gabra2, Chrna7*, *Adora2a* and *Thbs2*) were altered during 70-90 DPI while at clinical disease, vesicle formation and transport (*i.e. Vti1a* and *Exoc5*) plus structural proteins related to cytoskeletal physiology (*i.e. Tppp* and *Tubgcp4*) were all decreased. The temporal expression profile for these downregulated genes can be found in **Figure 3.20**.

3.1.8c Phenotypic Changes Detected in Deregulated Genes

In addition to the biological functions identified within the two gene lists, groups of bioinformatically predicted genes that are associated with phenotypic changes in mice were almost exclusively restricted to the LCM samples collected at terminal disease. These phenotypes include abnormal innate immune activation (**Figure 3.17**) as well as synaptic transmission, which inevitably result in abnormalities in learning and memory (**Figure 3.19**). Collectively, these detected phenotypes are representative of the clinical symptoms of

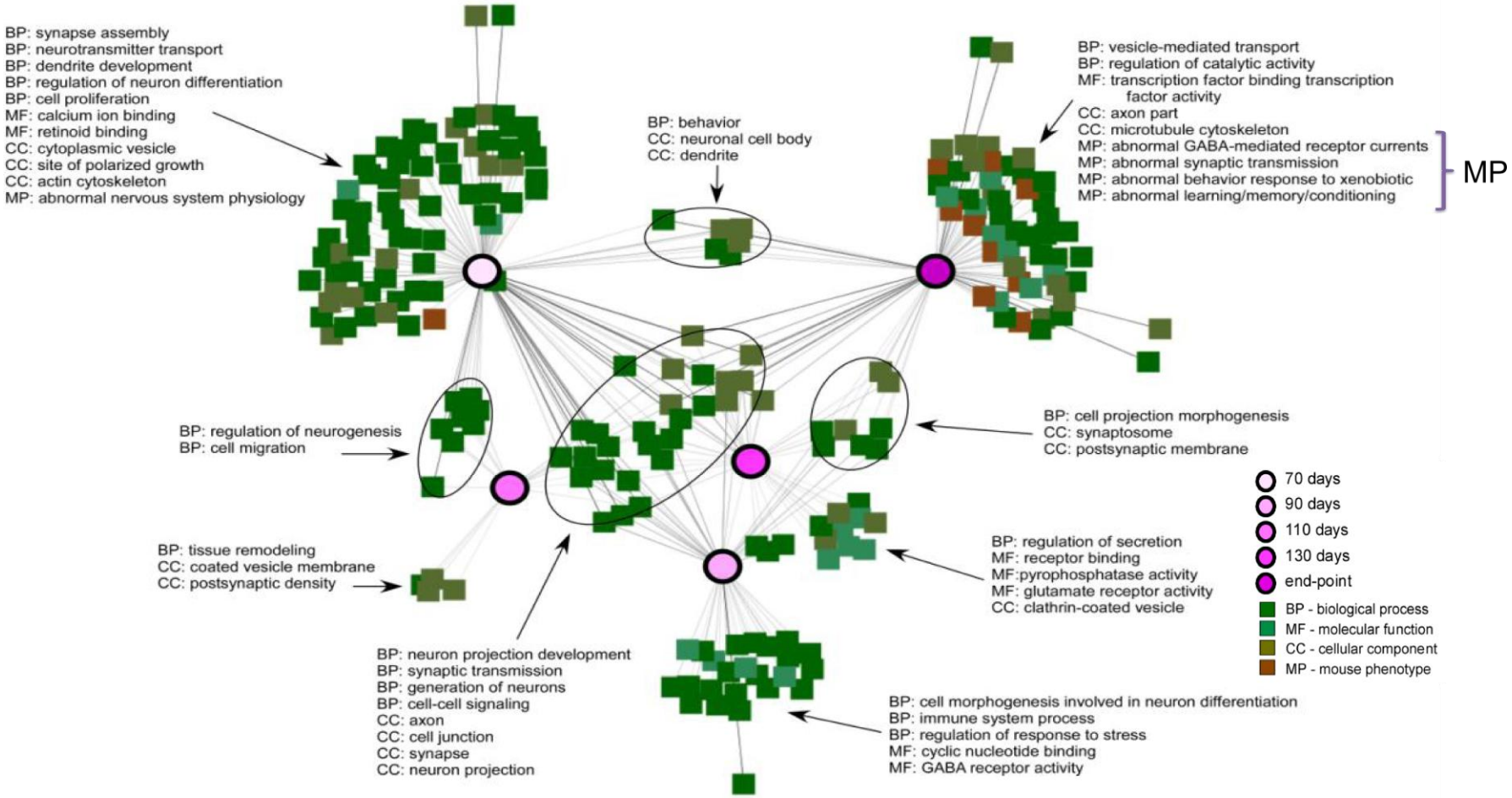

Figure 3.19. **Gene ontology networks identified from the downregulated gene list**. Gene ontologies were grouped according to the time points analyzed. Select ontologies are highlighted for which majority reflect neuronal-specific gene expression. The cellular response to stress is further indicated by * at 70 DPI while mouse phenotype ontologies are depicted by MP. The gene ontology network was generated using Cytoscape. Adapted from Majer *et al.*, 2012.

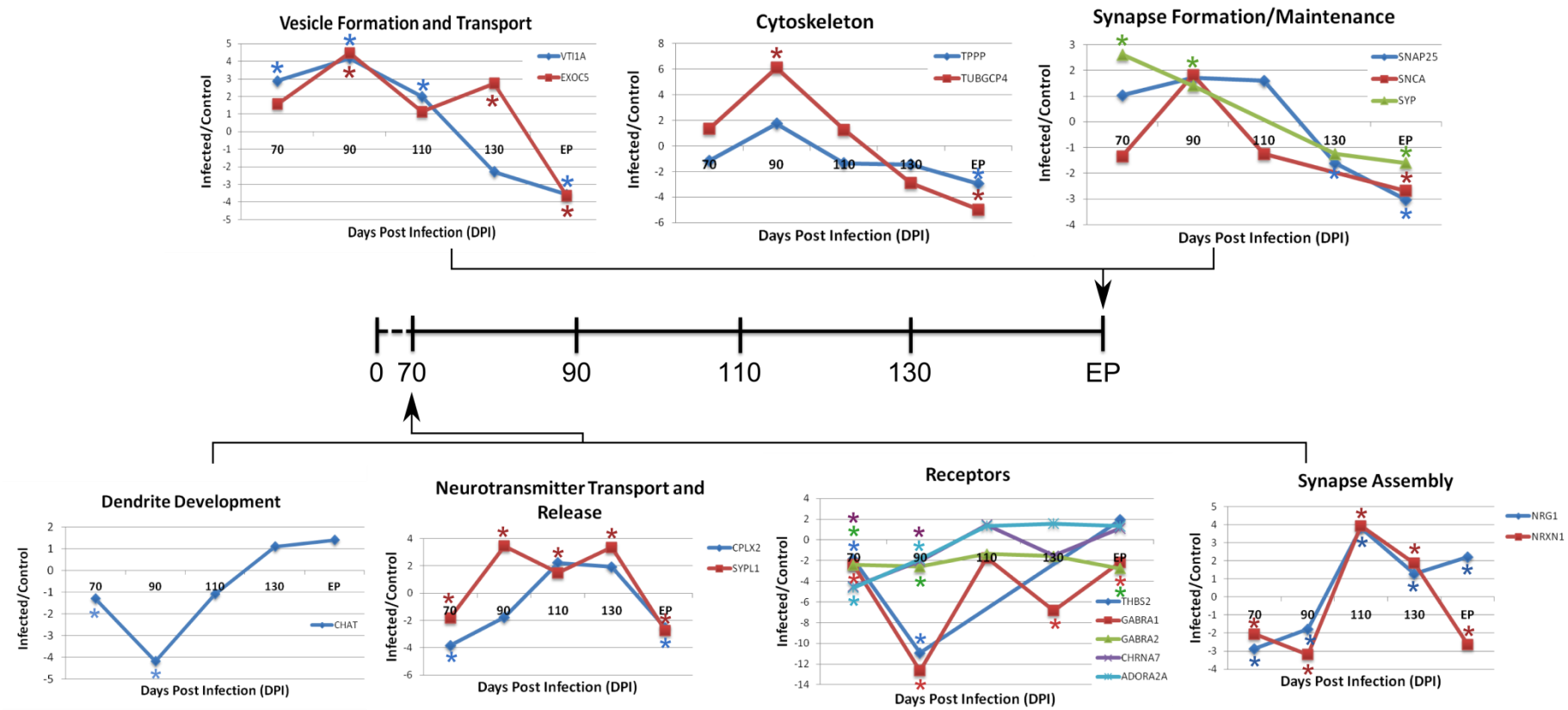

Figure 3.20. Genes representing biological processes that were downregulated during prion disease within cell bodies of CA1 hippocampal neurons. Arrows indicate the time at which the genes were significantly downregulated for each biological process. Each graph depicts the signal intensity ratio between infected and control samples for the representative genes throughout time course of disease. Missing data for a particular time point were connected by the surrounding 2 data points. When more than 2 data points are missing, the infected/control ratio was set to 0. Significance (FDR < 5) is indicated by * which is colour coded for each respective gene. Time preceding 70DPI was not analyzed for gene expression.

neurodegenerative diseases and correlate with the time when glial cells are more represented in the LCM sample.

3.1.9 Transcriptomic Alterations during Preclinical Disease Revealed the Induction of a Neuronal Survival Mechanism

From the global gene expression analysis described above, approximately 400 genes were deregulated within the CA1 pyramidal neurons during preclinical disease (70-110 DPI). Since many of these genes were involved in cellular responses to stress, a meta-genomic analysis was performed comparing this list of genes to published genomic data that was generated from hippocampal neurons undergoing survival/death mechanisms (Zhang *et al.,* 2009). The list of genes referenced for this comparison originated from an experiment where the authors stimulated synaptic NMDARs in primary hippocampal neurons to evoke an activity-induced neuroprotective transcriptional process (Zhang *et al.,* 2009). Comparing this list of 185 activity-induced neuroprotective genes (Zhang *et al.,* 2009) to the genes deregulated during preclinical prion disease revealed a stark overlap. A total of 141 genes (**Figure 3.21**) were found in common between the two gene lists (> 75 %) from which 97 were significantly deregulated during early stages of disease while 22 were not detected, 45 remained unchanged and 21 were not present on the microarray (**Figure 3.22**). Furthermore, a total of 9 out of the 185 genes were considered to be crucial mediators of neuroprotection termed "activity-regulated inhibitor of death" genes or AIDs (Zhang *et al.*, 2009). During preclinical prion disease, 6 out of the 9 genes (*Btg2*, *Gadd45g*, *Gadd45b*, *Npas4*, *Nr4a1*, *Inhba*) were up-regulated in CA1 neurons while the other 3 genes (*Atf3*, *Ifi202b* and *Serpinb2*) were below the level of detection (**Figure 3.22** and **Table 3.1**).

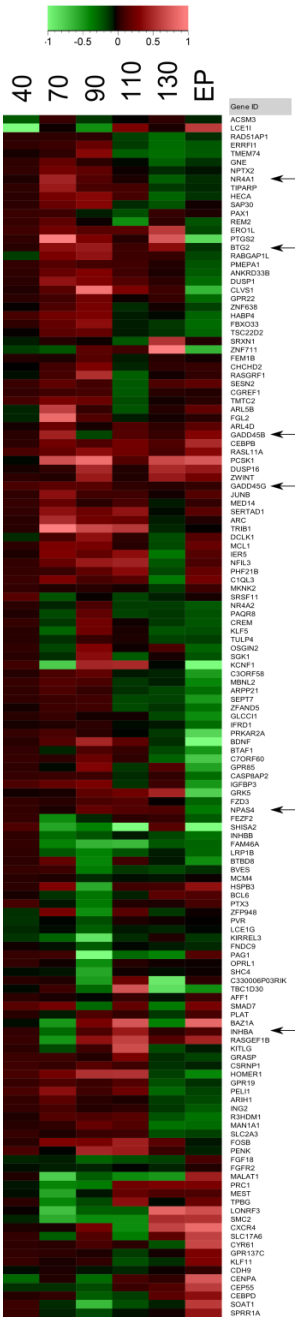

Figure 3.21. A subgroup of genes deregulated during preclinical prion disease is involved in neuroprotection. A hierarchical plot depicting the 141 activity-regulated neuronal genes identified by Zhang *et al*. (2009) that were found to be deregulated during early prion disease within the CA1 hippocampal neurons. The legend depicts the log fold change beween RML and mock-infected sample where red represents upregulation and green bars represent downregulation. Arrows indicate the activity-regulated inhibitor of death (AID) genes that were induced during early prion disease that are described further in the text. Adapted from Majer *et al.*, 2012.

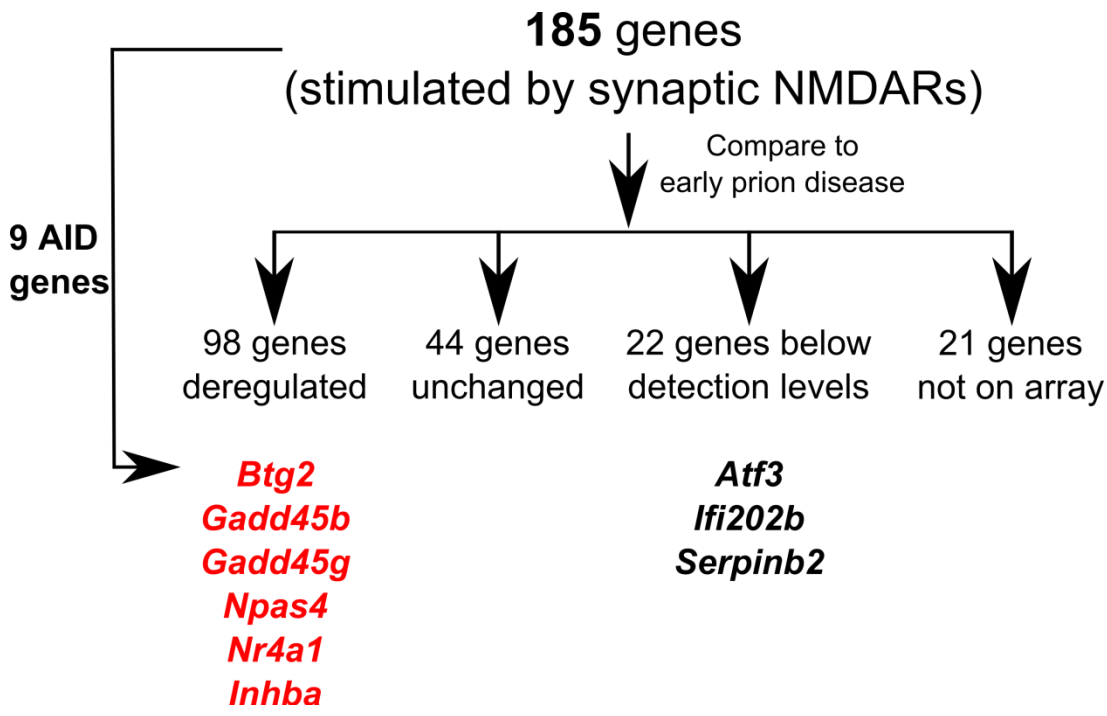

Figure 3.22. Genes deregulated during preclinical prion disease that are involved in neuroprotection. A schematic diagram portrays the 185 neuroprotective genes as compared to the preclinical prion disease profile. The 9 core neuroprotective genes termed activity-regulated inhibitor of death (AID) are further highlighted where genes in red were upregulated in prion disease and black were not detectable. Adapted from Majer *et al.*, 2012.

Table 3.1. Microarray expression data for 6 activity-dependent neuroprotective genes induced at preclinical prion disease.

	Fold Change				
Gene ID	**70 DPI**	**90 DPI**	**110 DPI**	**130 DPI**	**EP DPI**
Btg2	**-4.2**	**3.2**	-2.3	3.6	1.6
Gadd45b	**3.4**	**1.6**	**1.5**	-1.3	**3.4**
Gadd45g	**1.5**	**3.1**	1.2	1.1	1.2
Npas4	**1.2**	**2.5**	2.2	1.2	**-3.1**
Nr4a1	**3.9**	**2.6**	1.1	-1.8	1.3
Inhba	-1.7	1.9	**2.9**	1.2	2.4

Red highlights time when genes significantly induced in prion-infected samples
Bolded values indicate false discovery rate ≤ 5

A sample set of 30 genes that were deregulated during preclinical disease were chosen for validation using qRT-PCR. These genes were chosen because they have high basal expression levels in the brain and are involved in numerous neuronal-specific functions. Additionally, they were identified to be deregulated during early stages of prion disease with respect to calcium regulation, receptors for signal transduction and neurotransmission, neuronal survival and modification of anatomical structures. The majority of these genes were validated, of which almost all were involved in neuronal-specific function (**Table 3.2**). Among this group were 4 genes with a previously annotated neuroprotective function: *Rasgrf2*, *Trib1*, *Mcl1* and *Homer1* (underlined in **Table 3.2**). The expression of all 4 of these genes was significantly induced within the preclinical time period (70-110 DPI) in prion-infected samples (**Figure 3.23**).

3.1.10 CREB1 Phosphorylation Mediates, in Part, the Induction of Neuronal Survival Genes

CyclicAMP response element binding protein 1 (CREB1) is a core component in the synaptic NMDAR signaling cascade that activates transcription of neuroprotective genes (**Figure 3.24**). Due to the central role of CREB in this process, the transcript and protein levels of this transcription factor were monitored by qRT-PCR and immunohistochemistry during disease, respectively. The expression of *Creb1* remained unaltered within CA1 hippocampal neurons during prion disease (**Figure 3.25**). This was further corroborated by detecting no difference in total CREB levels within CA1 neurons throughout disease (**Figure 3.26A** and **B**). However, it is the phosphorylation of CREB (pCREB) at serine 133 that results in its activation and subsequent transcription of a large subset of genes (Bonni *et al.,* 1995). Detection of pCREB using antibody-

Table 3.2. A list of 30 genes further validated using qRT-PCR. Adapted from Majer *et al.*, 2012.

Gene ID	Pre-Clinical	Clinical	Implicated Function	References
Adcy7		+++ (+++)	adenylate cyclase 7 which catalizes the formation of cyclic AMP; upstream signaling molecule for CREB activation	Antoni, 2000; Antoni *et al.*, 2003
Bad	- (+)	+ (+)	pro-apoptotic Bcl-2 family member	Chong *et al.*, 2005
Cacna1c	(+)	(++)	calcium channel that functions in NMDAR-independent synaptic plasticity and memory	Moosmang *et al.*, 2005
Camk1	++ (++)	(++)	Ca^{2+} /calmodulin-dependent protein kinase and is a positive transducer of growth cone mobility and axon outgrowth	Wayman *et al.*, 2004
Camk2d	+++ (++)	++	Ca^{2+} /calmodulin-dependent protein kinase may function in long term potentiation and neurotransmitter release	Moriguchi *et al.*, 2011
Camk4		+/-	Ca^{2+} /calmodulin-dependent protein kinase that stimulates activation of CREB and promotes neuronal survival	Anderson and Kane, 1998; Hansen *et al.*, 2003
Cap1	(-)	(-)	regulates neurite outgrowth by rearranging F-actin	Lu *et al.*, 2011
Creb1		+	transcription factor involved in neuronal pro-survival mechanisms	Riccio *et al.*, 1999; Finkbeiner, 2000; Lonze and Ginty, 2002
Dab2	++ (+)	(++)	negative regulator of neurite outgrowth	Huang *et al.*, 2007
Dock1	+++ (-)	(+++)	promotes spine morphogenesis in hippocampal neurons	Kim *et al.*, 2011
Egr2	++	++	immediate early gene induced by BDNFand are important for terminal dendrite differentiation	Calella *et al.*, 2007
Gpm6b	(-)	(--)	regulates serotonin uptake by modulating the trafficking of seratonin transporters	Fjorback *et al.*, 2009
Grin2b	-- (--)	(---)	NMDAR subunit that promotes neuronal cell death and survival	von Engelhardt *et al.*, 2007; Martel *et al.*, 2009
Hdac9	- (--)	(--)	histone deacetylase 9 enzyme inhibits dendrite growth	Sugo *et al.*, 2010
Homer1	+ (++)	(-)	dendritic scaffold proteins that regulate group 1 metabotrophic glutamate receptor (mGluR) function and have roles in growth cone turning	Gasperini *et al.*, 2009
Mcl1	++(+)		Anti-apoptotic protein that is responsive to excitotoxic insults in the central nervous system	Mori *et al.*, 2004
Mef2d	-		transcription factor positively regulates hippocampal synaptic function	Akhtar *et al.*, 2012;

			and promotes neuronal survival	Wang *et al.*, 2009
Myo5a	+ (+)	- (---)	modulator of synaptic plasticity by helping release neuropeptides via exocytosis recycling of neurotransmitter receptors via endosomes	Rudolf *et al.*, 2011
Myo6	++ (+)	+ (+)	plays a role in clathrin-mediated endocytosis of AMPARs and BDNF-mediated neurotransmission	Osterweil *et al.*, 2005; Yano *et al.*, 2006
Pip5k3	- (-)	+	lipid kinase that regulates endosomal and lysosomal degradation of calcium channels, protecting neurons from excitotoxicity	Tsuruta *et al.*, 2009
Ppp1r15	+++ (++)	(--)	dephosphorylates eIF2α-P	Harding *et al.*, 2009
Ppp3ca	-	+	calcineurin protein mediates neurotoxicity in Alzheimer's disease and decreases synaptic plasticity	Wu *et al.*, 2010; Spires-Jones *et al.*, 2011
Prosapip1	+		postsynaptic scaffolding protein the helps regulate synaptic development and plasticity	Grabrucker *et al.*, 2011; Wendtholt *et al.*, 2006
Rac1	- (++)	+	belongs to the Rho family of GTPases and is required for proliferation and survival of progenitor cells in subventricular zone	Leone *et al.*, 2010; Linseman and Loucks, 2008
Rasgrf2	+++ (++)	--	(calcium sensors) member of calcium/calmodulin-regulated guanine-nucleotide exchange factors that activate the Ras GTPases	Feig, 2011
Rcan1	- (-)		regulator of calcineurin 1 mediates apoptosis via caspase-3 activation	Sun *et al.*, 2011
Rnasen	(+)	-	core nuclease that initiates microRNA processing in the nucleus	Lee *et al.*, 2003b
Slc6a13	++ (+++)	++ (+++)	GABA transport protein (GAT-2) which is primarily localized to extra-synaptic areas and may regulate extra-synaptic GABA levels	Borden *et al.*, 1995
Trib1	++ (+++)		negative regulator of retinoic acid receptors and is involved in modulating signaling of MAP kinase cascades	Imajo and Nishide, 2010; Kiss-Toth *et al.*, 2004: Kiss-Toth, 2011
Wasf2	++ (+)	(++)	regulated dendite spine formation	Ito *et al.*, 2010

+/- represents a 1-2 fold change between infected and control ($p<0.1$)
++/-- represents a 2.1-3.0 fold change between infected and control ($p<0.1$)
+++ represents ≥ 3.1 fold change between infected and control ($p<0.1$)
Blank spaces represent a lack of significant signal within pre-clinical (70-110 DPI) and clinical (130 DPI and terminal disease) range.
Relative microarray fold changes are highlighted in parenthesis.
Underlined genes are further depicted in **Figure 3.23**.

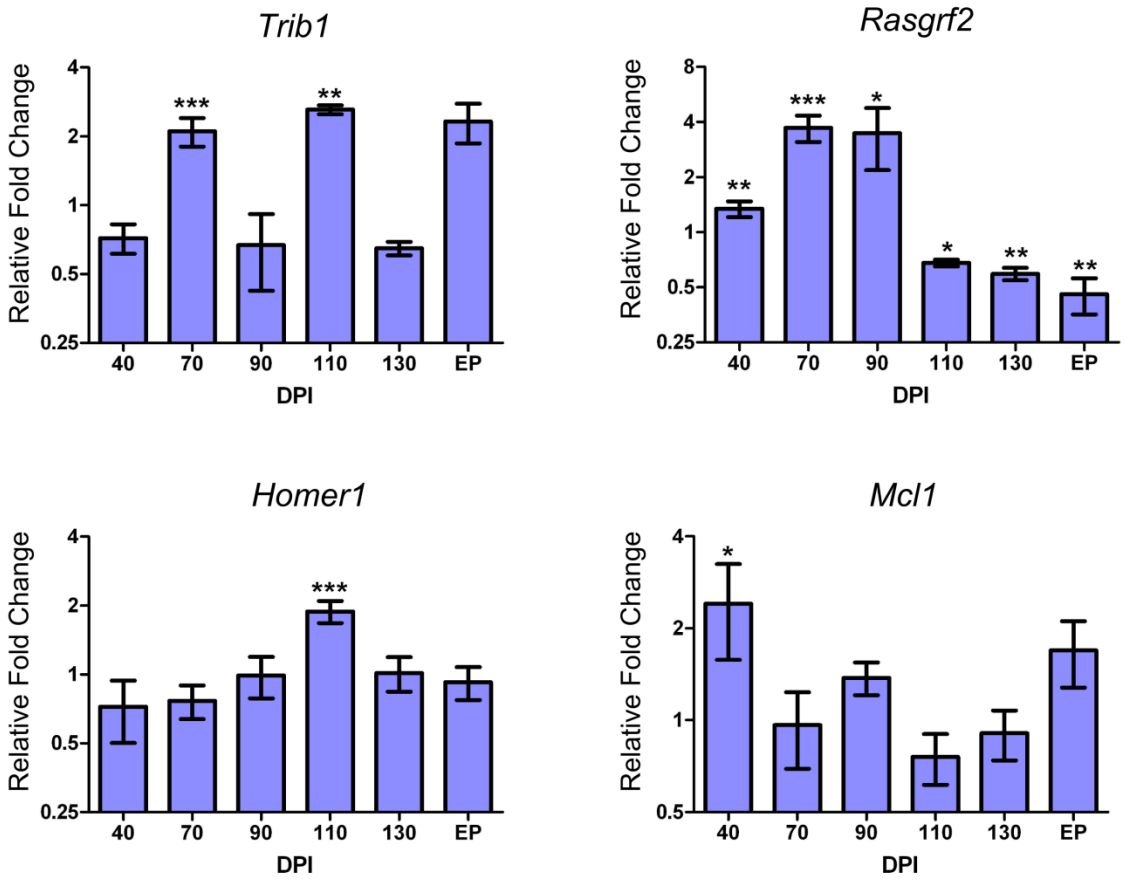

Figure 3.23. Validation of 4 activity-induced neuroprotective genes by qRT-PCR. Graphs represent the relative fold change between prion-infected and control samples over days post infection (DPI). Significance was calculated using Student's t-test where * represents a p-value of ≤ 0.05; ** a p-value of ≤ 0.01 and *** a p-value ≤ 0.001. Data is represented as mean ± SE (n=3-5 mice per treatment per time point). Adapted from Majer *et al.*, 2012.

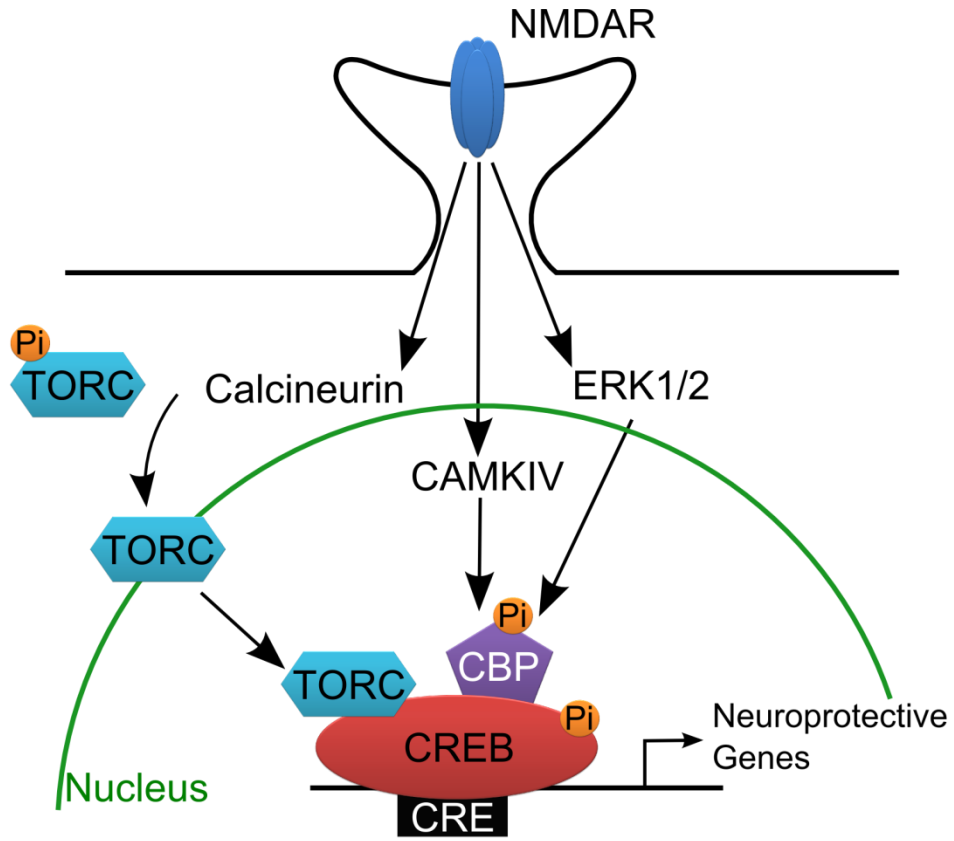

Figure 3.24. Schematic representation of the critical role pCREB plays during the recruitment and activation of an activity-dependent neuroprotective response. Stimulation of N-methyl-D-aspartate receptor (NMDAR) activity leads to the induction of intracellular Ca^{2+} which in turn activates the CaM kinase (CAMKIV) and Ras-ERK1/2 pathways. These pathways phosphorylate the cyclicAMP response element binding protein (CREB) at serine-133 which is required for recruitment of the co-activator CREB binding protein (CBP). CBP also is phosphorylated by CaMKIV at serine 301. Synaptic NMDAR-induced Ca^{2+} signals also promote nuclear translocation of the transducer of regulated CREB activity (TORC) via a Ca^{2+}-dependent dephosphorylation. TORC assists in the recruitment of CBP to CREB. Once pCREB and its co-activator are recruited, transcription of neuroprotective genes are initiated. Adapted from Hardingham and Bading (2010).

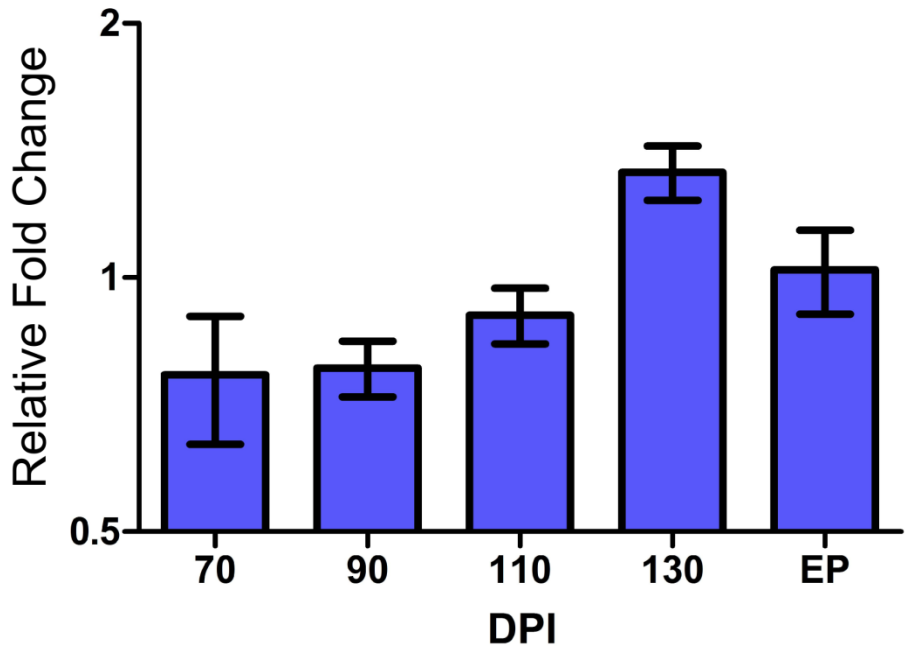

Figure 3.25. The relative fold change of *Creb1* during prion disease detected by qRT-PCR. Significance was assessed using a student's t-test statistic. Data is represented as mean ± SE (n=3-5 mice per treatment per time point).

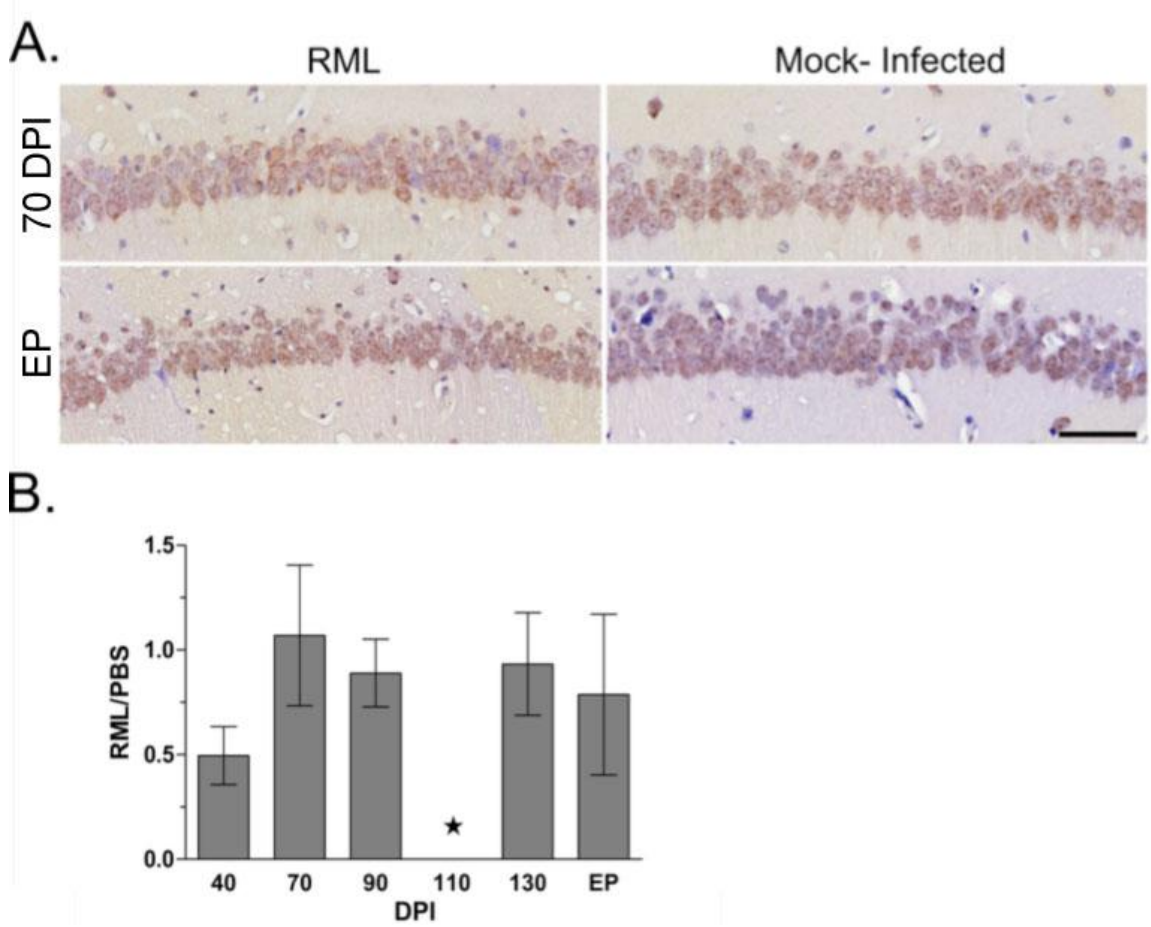

Figure 3.26. Immunohistochemical representation of total CREB levels at 70 and EP DPI in prion- and mock-infected samples. (**A**) Total CREB levels are depicted as brown against the blue stained nuclei. Scale bar = 50 µm. (**B**) Quantitation of total CREB levels between RML infected and control CA1 hippocampal samples throughout disease progression. The star represents insufficient number of replicates for statistical purposes. DPI refers to days post infection. RML is the Rocky Mountain Laboratory scrapie strain of prion. Data is represented as mean ± SE (n=3-5 mice per treatment per time point). Adapted from Majer *et al.*, 2012.

specific immunohistochemistry revealed a significantly higher proportion of pCREB in CA1 hippocampal neurons during preclinical disease in prion-infected mice as compared to controls (**Figure 3.27A** and **B**). In support of this induction, signal intensities from microarray data of several genes known to be activated by pCREB were also induced during preclinical disease (**Table 3.3**). Conversely, no significant difference between infected and control samples was observed at clinical disease.

3.1.11 Transcriptomic Alterations in the LCM Sample during Clinical Disease Highlights Immune Activation

The largest ontological group identified during clinical disease consisted of immune-related transcripts that represented the migration of activated glia into our LCM sample. Exploring the immune-related molecular landscape that was deregulated at clinical disease signifies glia-related gene expression while the primary focus of this work was concentrated on identifying transcriptional signatures of neurons. Nevertheless, it is worth mentioning that many of these genes identified at clinical disease are the same as detected by transcriptomic studies of whole brain tissue in other prion animal models (**Figure 3.28**). The majority of this immune-related group of genes was strongly over-expressed during clinical disease, however, expression of several genes followed a sequential induction as early as 110 DPI (such as *Icam1*, *Vcam1*, *Fyb* and *S100a4*) while others showed a decline in expression (such as *Irak1* and *Cdc42*) as disease progressed. Regardless of the temporal expression profile, these genes were detected prior to the over-expression of immune activation markers such as cytokines and chemokines (*i.e. Cxcl10*, *Cccl9*, *Ccl4* and *Ccl6*), which were upregulated preferentially in the samples taken during

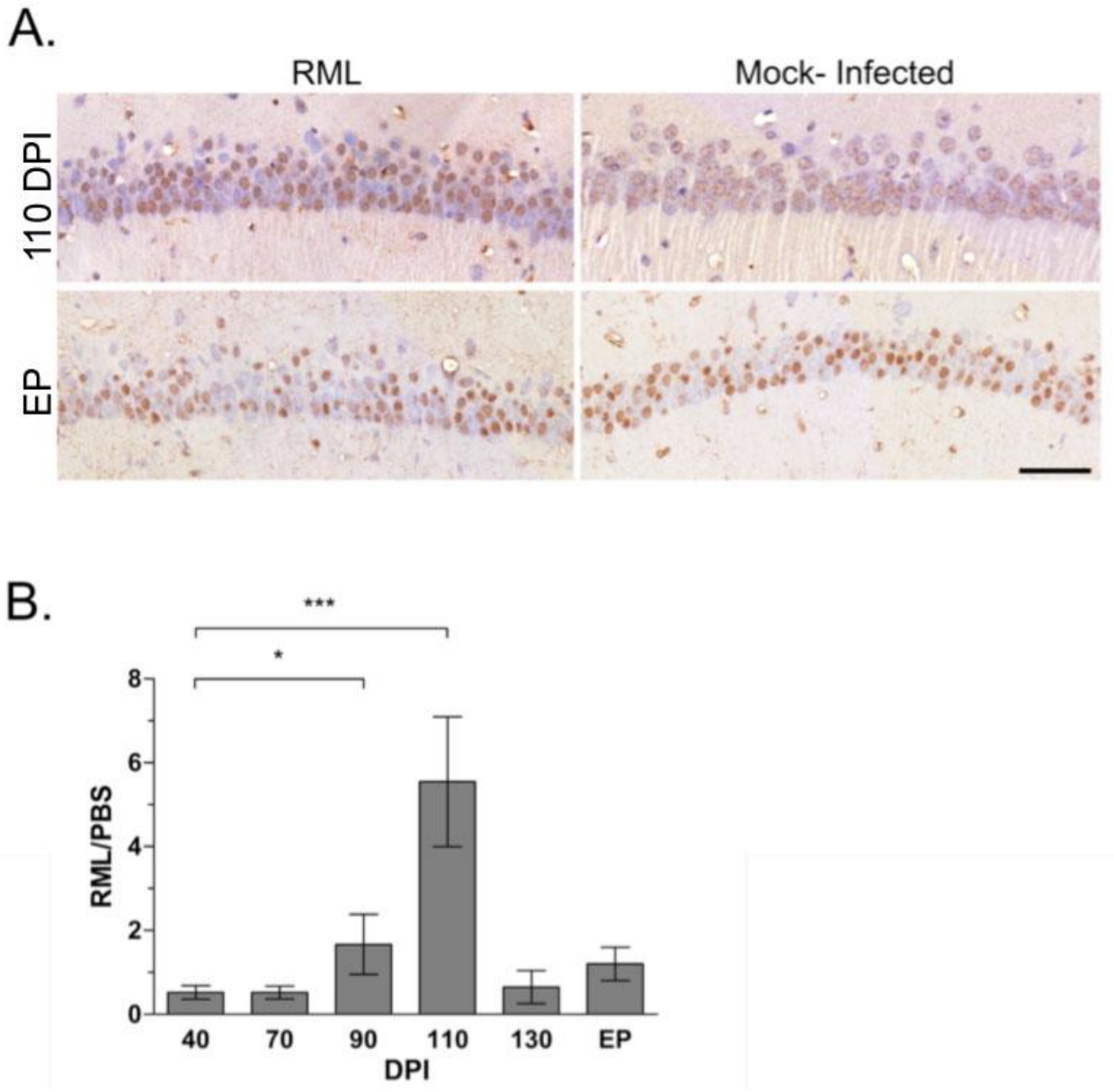

Figure 3.27. Immunohistochemical detection of pCREB throughout prion disease progression. (**A**) Brown staining represents pCREB levels against the blue stained nuclei at preclinical disease (110 DPI) and terminal disease (EP) for prion-infected (RML) and mock-infected samples. Scale bar = 50µm. (**B**) Quantitative assessment of pCREB within cell bodies of CA1 neurons at each time point. Student's t-test statistic; * represents a p-value of ≤ 0.05 and *** a p-value ≤ 0.0001. DPI referes to days post infection. RML is the Rocky Mountain Laboratory scrapie strain of prion. Data is represented as mean ± SE (n=3-5 mice per treatment per time-point). Adapted from Majer *et al.*, 2012.

Table 3.3. Representative list of genes induced during preclinical prion disease that is also activated by pCREB. Blank spaces represent genes that failed to pass the FDR ≤ 4 threshold.

	70 DPI		90 DPI		110 DPI		130 DPI		EP DPI	
Gene ID	**Fold Change**	FDR	**Fold Change**	FDR	**Fold Change**	FDR	**Fold Change**	FDR	**Fold Change**	FDR
Arc	**3.83**	0.05	**2.05**	0.57	**1.87**	1.10				
Camk1			**3.12**	0.83	**1.90**	0.72				
Camk2d	**-2.61**	3.16	**2.33**	3.01	**9.89**	0.09	**1.87**	0.12		
Egr1	**3.48**	0.32	**3.21**	0.60			**-1.67**	1.88		
Fos	**9.40**	0.05	**4.81**	0.11	**1.56**	0.64	**1.84**	0.51		
Fosb					**3.05**	0.09	**1.60**	1.33		
Homer1	**2.05**	0.93	**4.30**	0.99			**-2.49**	0.57	**-2.56**	0.39
Rasgrf2			**2.42**	0.88	**2.06**	0.44	**-1.66**	3.87	**-5.79**	0.02

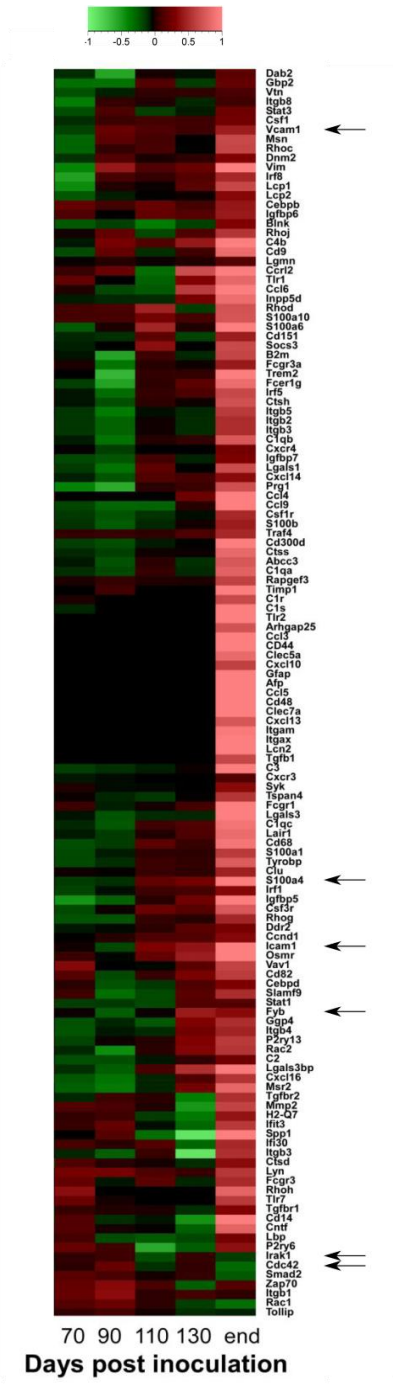

Figure 3.28. Genes strongly induced during clinical prion disease in CA1 neurons are involved in the immune response. A subgroup of genes deregulated within the CA1 hippocampal neurons were also found induced within whole brain tissue in other prion animal models and other neurodegenerative conditions. Red bars represent upregulated while green bars represent downregulated genes. Legend depicts log fold changes. Arrows indicate genes that were further discussed in the text. The 'end' refers to the EP or terminal disease.

clinical disease (**Table 3.4**). Furthermore, the detection of these genes appeared to occur before significant infiltration of activated immune cells such as astrocytes and microglia into the CA1 region (*Sections 3.1.3 and 3.1.4b-c*) and is likely of neuronal origin.

Table 3.4. Select list of immune-related genes that were temporally deregulated during prion disease.

	70 DPI		90 DPI		110 DPI		130 DPI		EP DPI	
Gene ID	**Fold Change**	**FDR***	**Fold Change**	**FDR***	**Fold Change**	**FDR***	**Fold Change**	**FDR***	**Fold Change**	**FDR***
Icam1			**-1.69**	3.21	**2.25**	2.06	**3.40**	0.34	**14.96**	0.02
Vcam1	**-1.53**	1.43	**-2.13**	4.12	**1.82**	1.31	**2.59**	0.95	**2.72**	0.21
Fyb			**-1.85**	3.21			**2.02**	1.62	**2.80**	0.02
S100a4					**1.62**	9.63	**2.24**	0.35	**26.73**	0.02
Irak1			**2.63**	1.77			**-1.33**	6.93	**-3.88**	0.17
Cdc42			**4.40**	0.51					**-2.70**	0.02
Cxcl10									**16.75**	0.12
Ccl9			**-2.22**	2.12	**-2.08**	0.44			**20.75**	0.02
Ccl6					**-1.64**	2.66	**5.01**	0.35	**56.75**	0.02

* FDR is false discovery rate

Genes highlighted in red are upregulated where the FDR < 10 while blank spaces represent genes that failed the FDR cut-off.

3.2 MicroRNA Expression Profiling of CA1 Hippocampal Neurons during Prion Disease

Rationale: MiRNAs are global gene regulators that are critically involved in the development and function of neurons. Several are known to modulate synaptic structure and function. Not surprisingly, deregulation of miRNA expression is well documented in numerous neurodegenerative diseases including prion disease. However, how the deregulation of certain miRNAs contributes to neuronal death has not been well studied. To address this gap in knowledge, my second aim was to identify miRNAs that are aberrantly expressed in hippocampal neurons during prion disease. Based on the transcriptional data, it is anticipated that miRNAs would also be deregulated in these animals and likely modulate several of the deregulated biological processes.

3.2.1 Deregulation of the miRNome During Prion Disease

The same total RNA samples that were used for gene expression studies were also utilized for miRNA profiling. Total RNA from two randomly chosen mice were profiled for miRNAs for each time point and condition using TaqMan low-density arrays (TLDAs), which detected a total of 335 unique miRNAs. The profiled data was inspected for miRNAs that showed the least variation across all of the time points analyzed for use as the normalization control. Using real-time StatMiner software version 4.2 (Intergromics), 2 small RNAs were identified to have the least variability within the entire dataset: snoRNA-135 and snoRNA-202. Comparison of these two RNAs to snoRNA U6, an endogenous control previously used in the study of microRNAs during prion disease (Saba et al., 2008), via 3 stability scoring methods from StatMiner (Normfinder, Genorm and minimum variance median) revealed snoRNA-135 to

be the most stable endogenous control across all samples. In addition, snoRNA-135 was expressed in similar abundance to the majority of the miRNAs detected within each sample (**Figure 3.29**). Therefore, snoRNA-135 served as the endogenous control and was used to normalize the signal of each detected miRNA.

From the 335 miRNAs detected by TLDA, 86 were deregulated in at least 1 time point throughout prion disease progression (**Figure 3.30** and **Appendix 3**). Out of these miRNAs, 17 were found to be significantly deregulated ($p < 0.1$) (2 miRNAs with $p < 0.05$; miR-128-3p and miR-434-3p) during early preclinical prion disease (70-110 DPI), 9 were significantly deregulated at 130 and/or EP while an additional 18 were detected only at EP in both prion-infected animals (**Table 3.5**). Of note, a less stringent p-value was used as a cut-off because only 2 animals per time point per treatment were used for analysis. This was done to limit the amount of RNA material used in the microRNA screen and to preserve this material for subsequent qRT-PCR validation. Also, this approach allowed to monitor the extent of variation between animals because pooling RNA samples across each treatment and time point would represent an average of this variation. Therefore, a slightly higher variation was anticipated across these biological replicates and was accounted for by setting a less stringent p-value. As a result, numerous miRNAs followed a trend in expression profiles when comparing these biological replicates, indicating a possible biologically relevant function. However, additional mice would need to be sampled for qRT-PCR analysis to confirm this consensus profile.

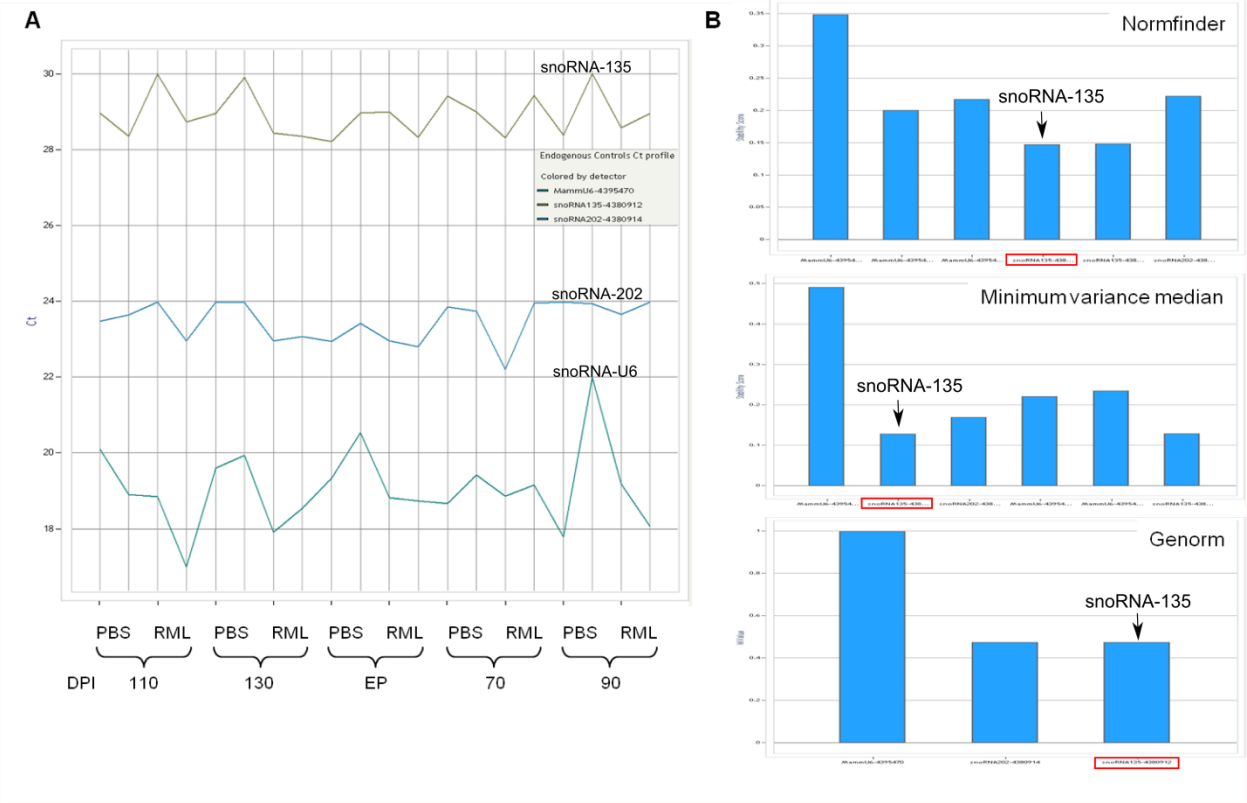

Figure 3.29. SnoRNA-135 was identified as the best normalization control for the TLDA cards. (**A**) Ct values for 3 potential controls, snoRNA-135, snoRNA-202 and U6 were compared across all the samples tested. Both snoRNA-135 and -202 were chosen manually based on the smallest Ct range across all the samples while U6 was chosen based on it being readily used as a control in the literature. (**B**) Graphs representing the stability scores calculated for the 3 RNA species in combination or separately. The lower the stability score or M value, the more stable the RNA throughout the entire system. Highlighted in red and annotated is the most stable control, snoRNA-135. Adapted from Majer *et al.*, 2012.

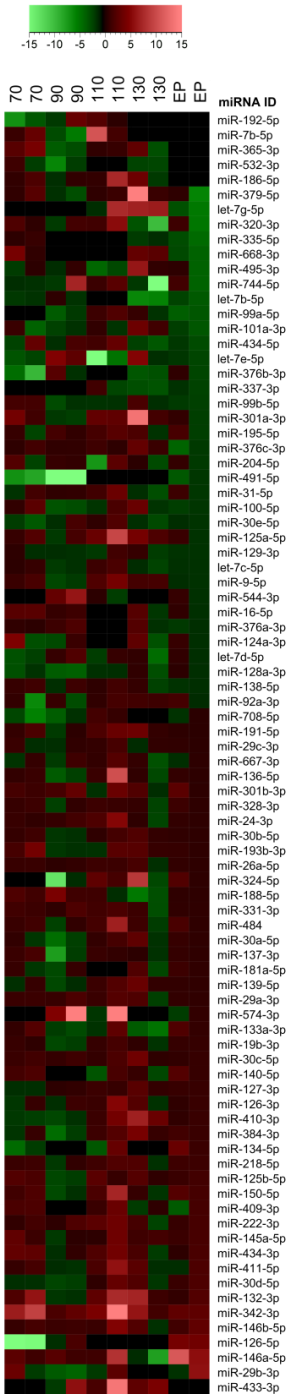

Figure 3.30. Hierarchical plot summarizing deregulation of 86 miRNAs during prion disease progression. Two mice per time point per treatment were assessed by TLDA and fold changes calculated by the ΔΔCt method for each indicated miRNA. Legend represents fold change where the more downregulated miRNAs are represented by a brighter green colour while upregulated miRNAs are bright red. Hierarchical plot generated by GeneMathsXT. Black spots represent no change in expression. Modified from Majer *et al.*, 2012.

Table 3.5. **List of miRNAs expressed in prion-infected samples at either 130 and/or EP of disease**.

	Ct Values			
miRNA ID	**130**	**130**	**EP**	**EP**
miR-103-3p	31.012	33.035		
miR-106a-5p			23.184	22.857
miR-130a-3p	31.248	31.974	32.048	31.411
miR-155-5p	32.517	36.003		
miR-192-5p	35.998	33.613	33.986	34.553
miR-194-5p			31.858	33.025
miR-19a-3p			35.606	36.057
miR-203-3p			32.990	35.937
miR-223-3p	35.966	33.596		
miR-23b-3p			32.965	31.994
miR-340-5p		36.000	33.999	34.261
miR-344-3p	30.682	31.895		
miR-34b-3p	31.974	30.298	30.968	31.124
miR-383-5p			31.801	35.940
miR-451a			33.885	34.992
miR-532-5p	31.993	35.703		
miR-676-3p	34.017	33.642	30.972	30.221
miR-7b-5p	32.486	33.761	31.922	

Blank cells represent samples not detected.
EP = end-point of disease

3.2.1 Temporal Dynamics of MicroRNA Expression was Analogous to the Transcriptomic Data

To determine if miRNA abundance was altered in a way to indicate the observed gliosis in samples collected at 130 DPI and EP, the list of miRNAs that were either significantly deregulated or only detected within prion-infected samples during this time period were compared to the literature. Specifically, 9 significantly deregulated miRNAs and 18 miRNAs detected only in RML samples at 130 DPI and/or EP were compared to a list of 212 miRNAs previously identified in activated primary astrocytes (Mor *et al.*, 2011). This comparison revealed that all 9 significantly deregulated miRNAs and 17/18 miRNAs detected only in RML samples were upregulated in activated primary astrocytes (**Figure 3.31A**). From the list of 9 miRNAs found to be significantly deregulated during clinical disease (130 DPI and/or EP), all but one miRNA, miR-129-3p, followed the same trend as documented for the activated primary astrocytes. From the 17 miRNAs that were detected only in RML samples, 16 were induced while only miR-532-5p was downregulated in activated primary astrocytes. Although significance was not attributed to the majority of miRNAs detected at later stages of prion disease (130 DPI and EP), the expression profile for most of these miRNAs followed a trend toward overexpression in prion-infected samples. From the list of 62 potentially upregulated miRNAs, 59 were also deregulated during stimulation of primary astrocytes (**Figure 3.31B**).

MiR-146a-5p is an immune-related miRNA that was previously shown to be induced during clinical prion disease (Saba *et al.*, 2008; Lukiw *et al.*, 2011) at a time when gliosis was reported. To confirm the induction of this miRNA, the upregulation of miR-146a-5p was therefore analyzed in the LCM samples at clinical disease. Based on TLDA data, miR-146a-5p was induced within prion infected samples at both early (70-110 DPI) and terminal stages of

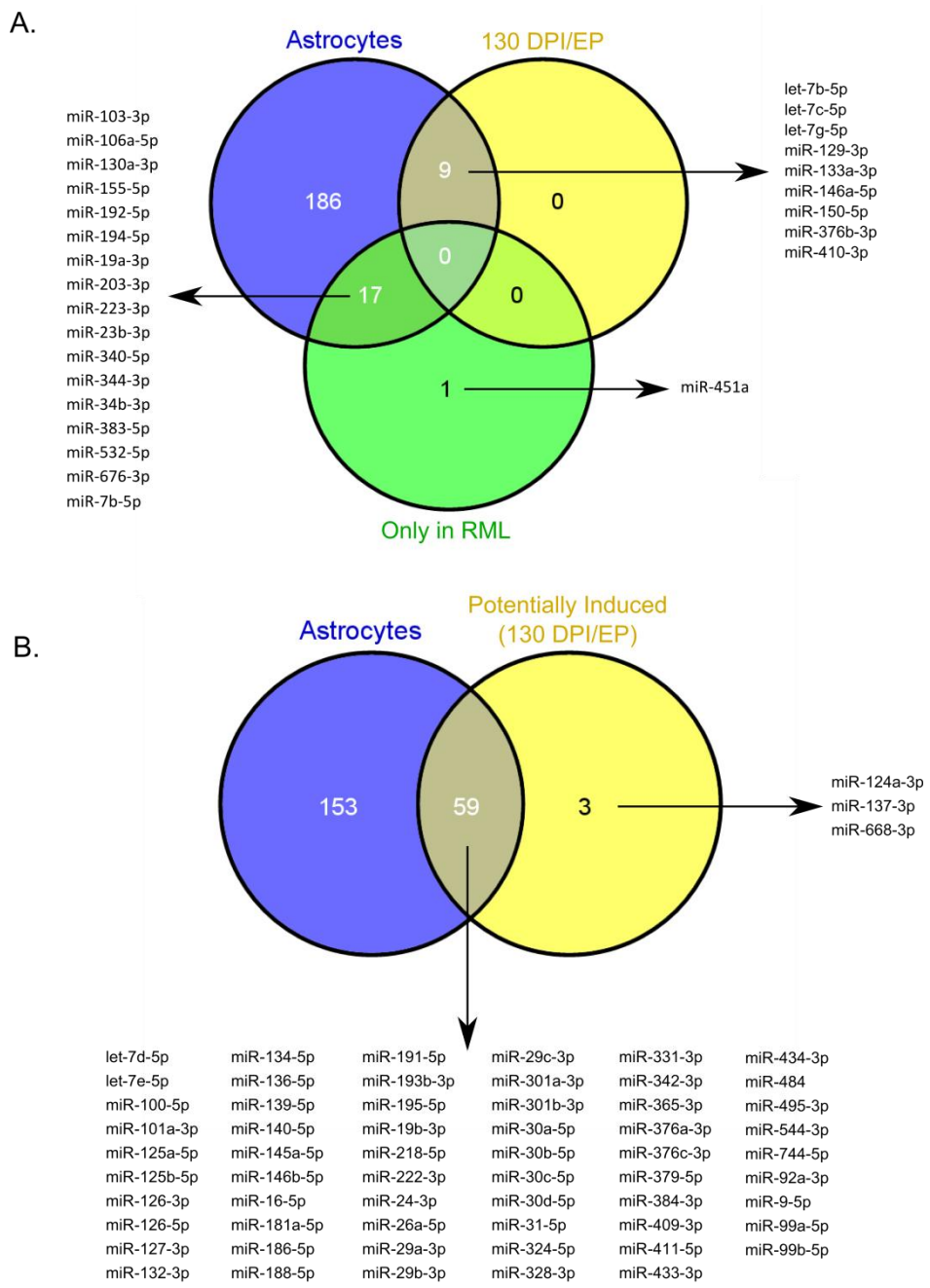

Figure 3.31. MicroRNAs deregulated during late stages of prion disease were upregulated in activated primary astrocytes. (**A**) The list of miRNAs that were significantly deregulated either at 130 DPI or EP in prion disease or were only detected in two of the RML-infected samples at clinical disease. (**B**) A total of 62 miRNAs were found to be potentially upregulated at 130 DPI or EP in prion disease of which 59 were also deregulated in activated astrocytes. Prion data compared to Mor *et al.*, 2011.

disease. Validation of miR-146a-5p using qRT-PCR corroborated these findings. Specifically, miR-146a-5p was upregulated in prion-infected samples at 70 DPI to approximately 8-fold higher than control levels. As disease progressed, the over-expression diminished to 2-fold at 110 DPI and was significantly lower than control levels at 130 DPI. At EP, miR-146a-5p was upregulated by approximately 4-fold in prion- as compared to mock-infected samples (**Figure 3.32A**).

Conversely, miR-124a-3p is highly enriched within neurons (Kye *et al.,* 2007; Zovoilis *et al.,* 2011) and served as a representative miRNA for neuronal tissue. Hence, miR-124a-3p expression levels were assessed to determine if they were comparable to the neuronal-specific gene expression profile. Based on TLDA data, miR-124a-3p was expressed within all samples tested; a signal analogous to the neuronal gene markers detected by the microarray (*Section 3.1.3*). However, the expression profile of miR-124a-3p was not significantly different between prion-infected and control animals. Validation of miR-124a-3p using qRT-PCR revealed a slightly different expression profile as the one detected by the TLDA. Within prion-infected samples, miR-124a-3p was significantly upregulated at 70 and 90 DPI as compared to mock-infected samples. However, as disease progressed, the expression of miR-124a-3p returned to basal levels at 110 DPI and significantly decreased at clinical disease (**Figure 3.32B**). Of note, aside from the EP time point, the expression profile of miR-124a-3p followed a similar pattern to miR-146a-5p.

3.2.2 Upregulated MicroRNAs during Early Preclinical Prion Disease

Identifying miRNAs which are deregulated during preclinical disease (70-110 DPI) can help to pinpoint the molecular pathways that are altered during early prion disease. Initial TLDA screen

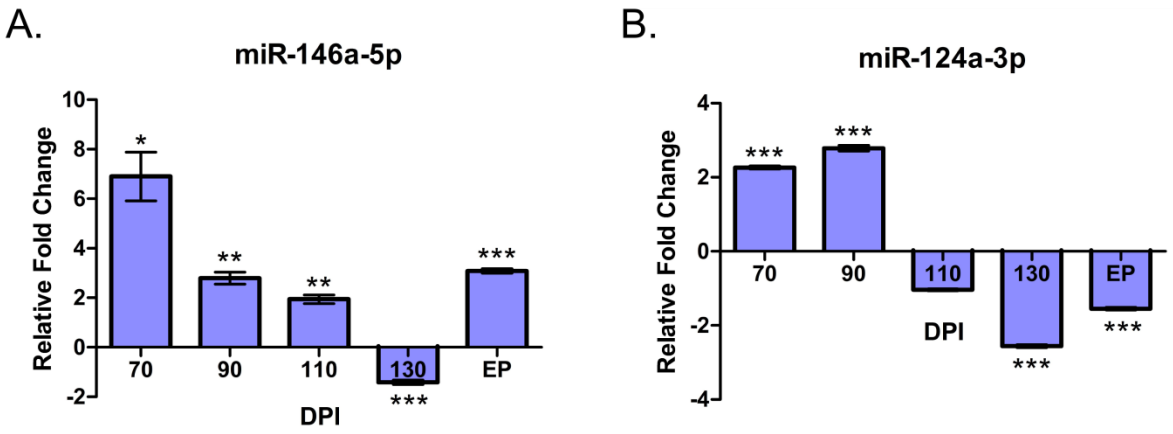

Figure 3.32. Expression profile of miR-146a-5p and miR-124a-3p using qRT-PCR confirmed the TLDA data. The relative fold changes of (**A**) miR-146a-5p and (**B**) miR-124a-3p between prion- and mock-infected samples at each time point throughout prion disease progression. Student's t-test statistic was performed to assess significance where * represent a p-value $\leq$ 0.1, ** represents a p-value $\leq$ 0.05 and *** represents a p-value $\leq$ 0.005. Data is represented as mean ± SE (n=3-5 animals per condition).

identified a total of 17 significantly deregulated miRNAs between 70-110 DPI (**Table 3.6**). From the list of 17 miRNAs, 5 (miR-16-5p, miR-26a-5p, miR-29a-3p, miR-132-3p and miR-140-5p) were chosen for validation by qRT-PCR of which 4 (miR-16-5p, miR-26a-5p, miR-132-3p and miR-140-5p) were further validated by *in situ* hybridization (ISH). The qRT-PCR confirmed the upregulation of all 5 miRNAs during the preclinical prion disease time period in prion- as compared to mock-infected animals (**Figure 3.33A-E**). Specifically, expression of all 5 miRNAs was significantly induced in RML as opposed to mock-infected samples at 70-90 DPI. As disease progressed, the expression of these miRNAs decreased, albeit gradually. Specifically, miR-132-3p remained upregulated at 110 DPI, miR-140-5p was unchanged while the rest of the miRNAs were significantly downregulated in prion-infected samples as compared to controls. This progressive decrease was evident in all 5 miRNAs at 130 DPI when compared to mock-infected controls. Although the expression levels of all 5 miRNAs increased slightly at EP in the prion-infected LCM-isolated regions, it still remained significantly lower than controls. ISH further confirmed the upregulation of the 4 miRNAs (miR-16-5p, miR-26a-5p, miR-132-3p and miR-140-5p) during preclinical disease (**Figure 3.33F-I**). Interestingly, the temporal profile for these miRNAs was comparable to miR-146a-5p and miR-124a-3p, especially during early stages of disease (**Table 3.7**).

To determine if the 7 preclinically induced miRNAs were expressed within neurons under normal conditions, Ct values for each miRNA were compared across the entire time course in control animals (**Figure 3.34**). Expression of all 7 miRNAs and the normalization control snoRNA-135 were stably and abundantly expressed across the entire study. SnoRNA-135, miR-16-5p, miR-26a-5p, miR-29a-3p and miR-132-3p were all detected between 27-29 Cts,

Table 3.6. The list of 17 significantly altered miRNAs at preclinical prion disease. Modified from Majer *et al.*, 2012.

	TLDA Data ($p \leq 0.1$)	Validations*	
miRNA ID	Average Fold Change ± SEM	qRT-PCR	ISH**
miR-132-3p	5.63 ± 2.37	Y	Y
miR-544-3p	5.09 ± 1.49		
miR-434-3p	3.36 ± 0.12		
miR-16-5p	2.91 ± 0.03	Y	Y
miR-324-5p	2.63 ± 0.63		
miR-195-5p	2.45 ± 0.41		
miR-218-5p	2.14 ± 0.41		
miR-140-5p	2.13 ± 0.20	Y	Y
miR-29a-3p	1.53 ± 0.02	Y	
miR-328-3p	1.51 ± 0.12		
miR-26a-5p	1.46 ± 0.01	Y	Y
miR-365-3p	0.37 ± 0.05		
miR-7b-5p	0.32 ± 0.11		
miR-128-3p	0.31 ± 0.01		
let-7e-5p	0.14 ± 0.08		
miR-491-5p	0.14 ± 0.01		
miR-126-5p	0.05 ± 0.02		

* Y highlights the miRNAs for which further validation was performed
** ISH is *in situ* hybridization that was performed for the indicated miRNA on brain sections

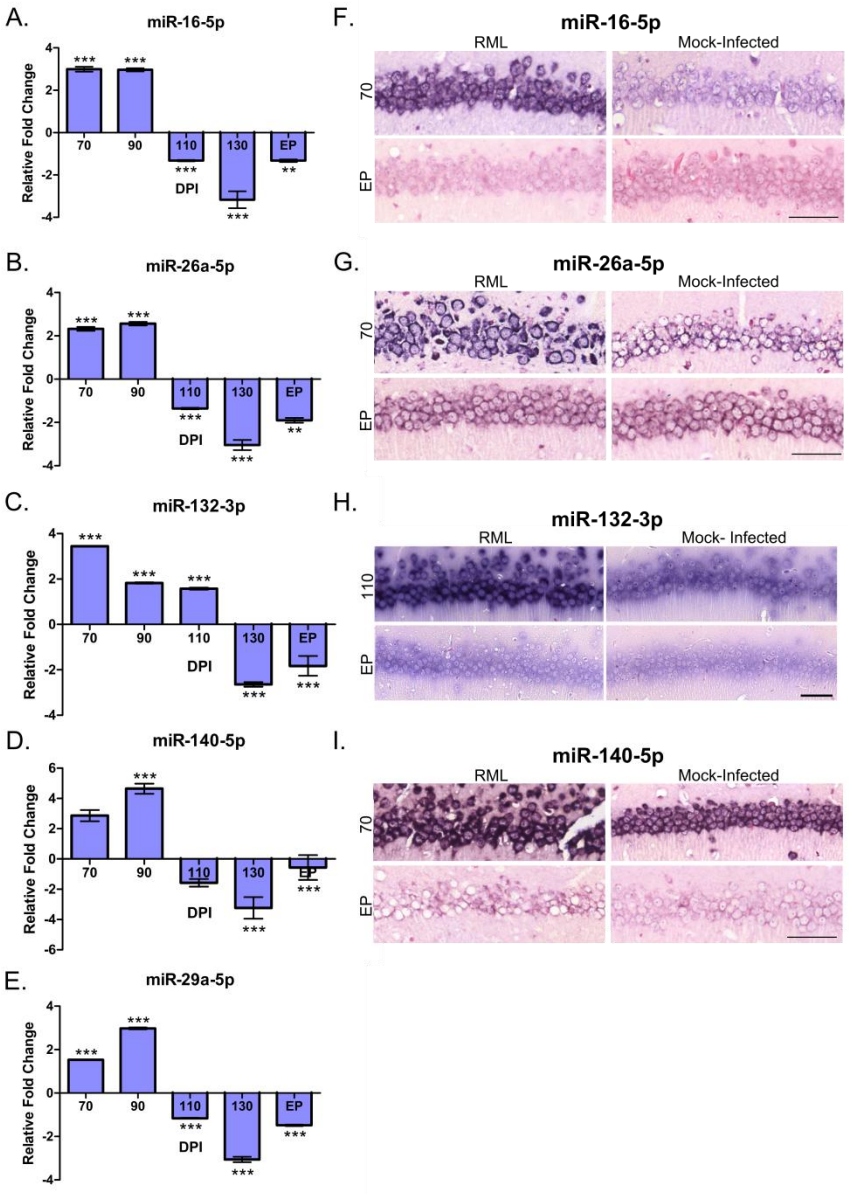

Figure 3.33. Validation studies using qRT-PCR and *in situ* hybridization support the over-expression of 5 miRNAs at early preclinical stages of prion disease. (**A-E**) Expression profiles using qRT-PCR for 5 miRNAs (miR-16-5p, miR-26a-53p, miR-132-3p, miR-140-5p and miR-29a-3p) were graphed with the relative fold change between infected and control samples against the days post infection (DPI). Significance was assessed using the Student's t test statistic where ** indicates p-value ≤ 0.05 and *** represents p-value ≤ 0.005 (n=3-5 animals per time-point per treatment). Data is represented as mean ± SE (**F-I**) Representative *in situ* hybridization images of miR-16-5p, miR-26a-5p, miR-132-3p and miR-140-5p in RML and control CA1 hippocampal samples during preclinical (70-110 DPI) and clinical (EP) prion disease. RML is the Rocky Mountain Laboratory scrapie strain of prion. Scale bar = 50 µm.

Table 3.7. A relative expression profile of the 7 candidate miRNAs induced at preclinical disease within prion-infected CA1 hippocampal neurons.

Mouse	Pre-Clinical			Clinical	
miRNA ID	70	90	110	130	EP
miR-16-5p	+++	++	-	---	-
miR-26a-5p	++	++	-	---	--
miR-29a-3p	+	++	-	---	--
miR-124a-3p	++	++	ns	---	--
miR-132-3p	+++	+	+	---	--
miR-140-5p	ns	+++	ns	---	-
miR-146a-5p	+++	++	+	-	+++

ns indicates no significance
+++ indicates >2.5 fold change; ++ indicates 2-2.5 fold change; + indicates 1.5-2 fold change; --- indicates < -2 fold change; -- represents -1.5 to -2 fold change; - represents -1.15-1.5 fold change.

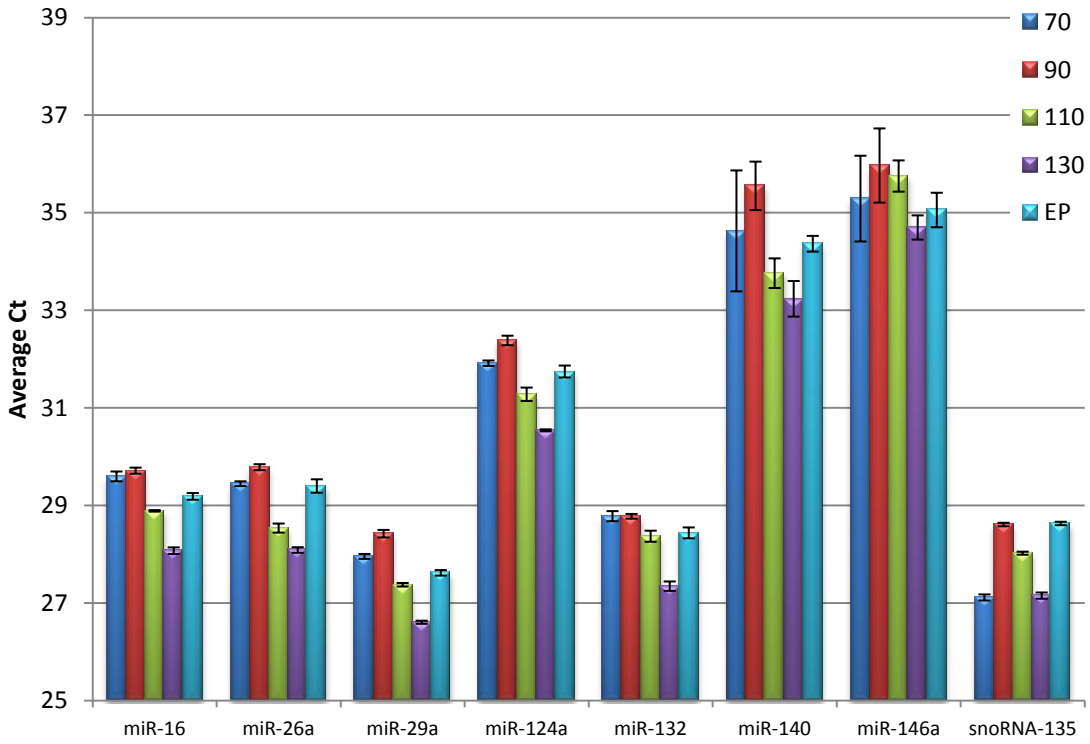

Figure 3.34. Temporal expression leves of 7 miRNA candidates in CA1 hippocampal neurons. The average Ct values for all 7 candidate miRNAs along with snoRNA-135 (normalization control) are plotted for all time points tested (from 70 DPI to EP) within control samples. MiR-16 (miR-16-5p); miR-26a (miR-26a-5p); miR-29a (miR-29a-3p); miR-124a (miR-124a-3p); miR-132 (miR-132-3p); miR-140 (miR-140-5p); miR-146a (miR-146a-5p). Mean Ct ± SD (n = 3-5 animals per time-point per treatment).

miR-124a-3p was detected at approximately 31 Ct while both miR-140-5p and miR-146a-5p were detected between 32-36 Cts (**Table 3.8**).

3.2.3 Bioinformatic Analysis of Preclinically Induced Candidate miRNAs Support Neuronal-Specific Function

A bioinformatic approach was used to discern which biological processes may be regulated by 7 candidate miRNAs identified during preclinical prion disease. Lists of predicted gene targets for each miRNA were curated using TargetScan (version 5.2; June 2011) which identified approximately 100-1200 targets per miRNA (**Table 3.9**). To determine the biological processes potentially regulated by these miRNAs, all the curated targets for each miRNA were analyzed using ToppCluster. The majority of the functions identified were neuronal-specific and potentially regulated by more than one miRNA. For example, genes involved in neurogenesis, neuron projection development and neuron differentiation were targeted by 5 out of the 7 miRNAs (miR-16-5p, miR-26a-5p, miR-29a-3p, miR-132-3p and miR-146a-5p). Neuronal projection morphogenesis and axonogenesis were targeted by miR-29a-3p and miR-16-5p (**Figure 3.35**). Additional processes regulated by these miRNAs were protein phosphorylation, signal transduction, posttranscriptional regulation of gene expression, among others.

To garner a biologically relevant representation of the functions potentially regulated by these miRNAs, the list of predicted gene targets were further filtered to only include genes that were also significantly downregulated during early preclinical prion disease (FDR < 5 % and ≥ 2 fold change). This resulted in filtering out approximately 90 % of genes from the original list of potential miRNA targets (**Table 3.9**). Analysis of these genes through ToppCluster revealed a smaller representation of the biological processes potentially regulated by these miRNAs. This

Table 3.8. The endogenous expression of 7 miRNAs found over-expression at early stages of prion disease.

	CA1 Hippocampal Neurons	Mouse Hippocampus**		
miRNA ID	Control Mice (Average Ct)*	Total Counts (NGS data)	% of Total miRNA counts	% of miR-124 counts
miR-26a-5p	29.05	227704	1.54	571.80
miR-16-5p	29.09	12775	0.09	32.08
miR-132-3p	28.34	62864	0.43	157.86
miR-29a-3p	27.60	388133	2.63	974.67
miR-140-5p	34.31	7898	0.05	19.83
miR-146a-5p	35.35	17814	0.12	44.73
miR-124a-3p	31.57	39822	0.27	100.00

* data represents an average Ct over the entire time course studied
** data collected and reanalyzed from Zovoilis *et al.*, 2011
MiRNA-124a-3p expression levels are highlighted for reference purposes.

Table 3.9. List of predicted miRNA gene targets identified by TargetScan along with the number which is also significantly downregulated during early prion disease.

miRNA ID	No. Predicted Targets	No. Genes Downregulated	% Represented
miR-16-5p	821	70	8.5
miR-26a-5p	552	55	10.0
miR-29a-3p	760	64	8.4
miR-124a-3p	1203	113	9.4
miR-132-3p	235	25	10.6
miR-140-5p	193	25	13.0
miR-146a-5p	109	9	8.3

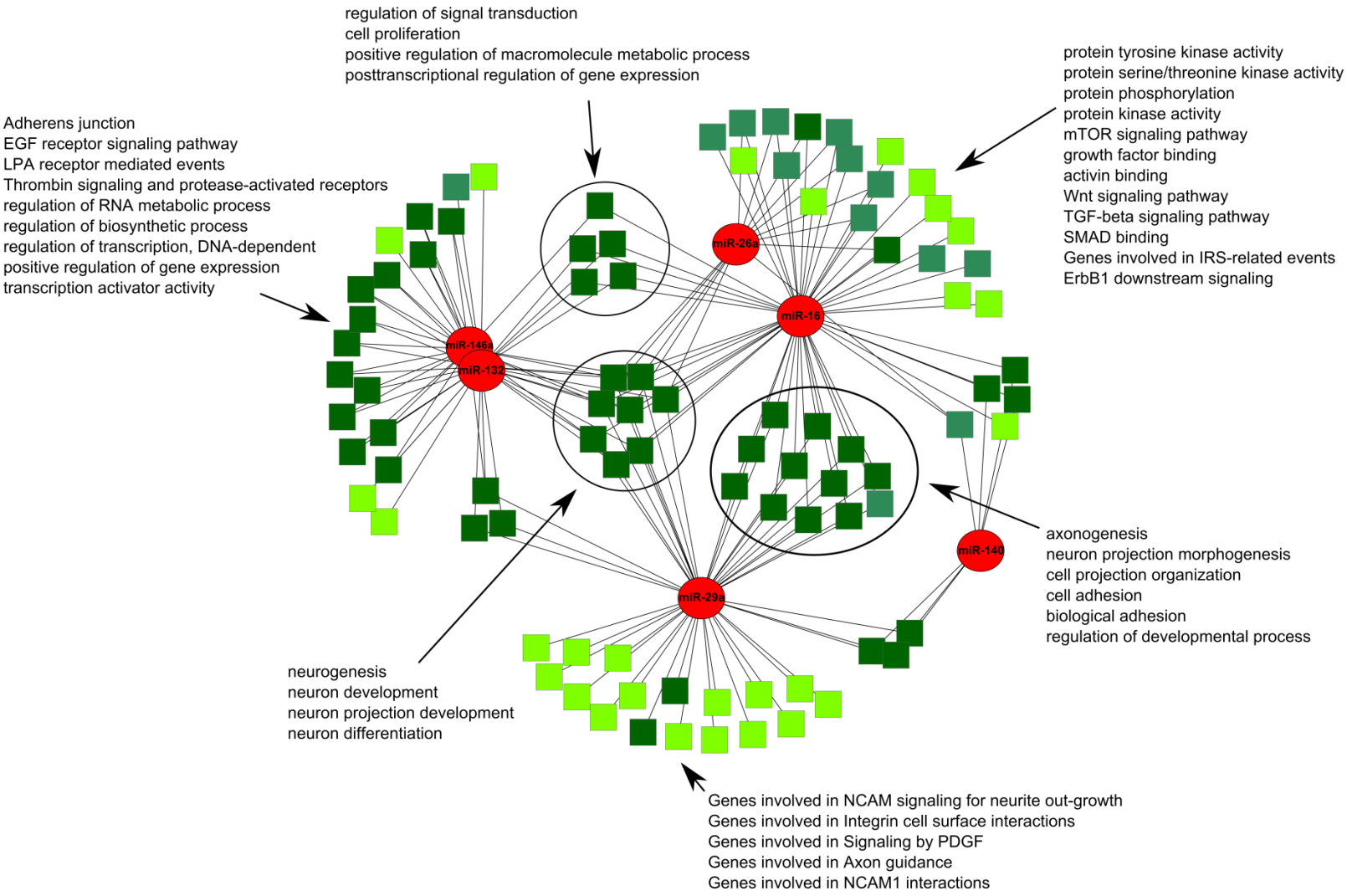

Figure 3.35. Biological processes potentially regulated by all 7 candidate miRNAs. Gene ontologies were grouped according to the miRNAs analyzed. Select ontologies are highlighted of which majority are of neuronal-specific function. Network was generated using Cytoscape.

analysis effectively separated the 7 miRNAs into 3 clusters based on their potential targets (**Figure 3.36**). One of the clusters consisted of a large proportion of neuronal-specific processes including postsynaptic density, neurogenesis, neuronal differentiation and neuron projection. The representative genes amid these processes were regulated by either miR-26a-5p or miR-124a-3p. In turn, miR-132-3p, miR-16-5p and miR-146a-5p were involved in regulating genes associated with forebrain development, miRNA catabolic process and negative regulation of gene expression, among others. Lastly, gene targets of miR-29a-3p composed the third cluster in which genes involved in positive regulation of transcription and proteinaceous extracellular matrix were identified. This analysis revealed that several of the miRNA gene targets were specifically involved in neuronal related functions while others had a broader function not exclusive to neurons. However, the major cellular compartment these genes were found to associate with was intimately reflective of the anatomy of the neuronal cell. In particular, neuronal projection, axon, post-synaptic density and synapse were the top 10 represented (**Figure 3.37**). Overall, genes targeted by several of these miRNAs were directly involved in remodeling neuronal structures such as synapses, spines and/or dendrites.

3.2.4 Stimulation of an Activity-Dependent Neuroprotective Response in Culture Leads to Upregulation of Select Candidate miRNAs

Previous pharmacological stimulation of primary mouse hippocampal cultures induced neuronal activity which led to the expression of genes involved in mediating a neuroprotective state via a nuclear calcium-CREB axis (Zhang *et al.,* 2009). Interestingly, the same axis was detected to play a role in early stages of prion disease within the CA1 hippocampal region. It is therefore possible that miRNAs deregulated at this time could also be involved in this

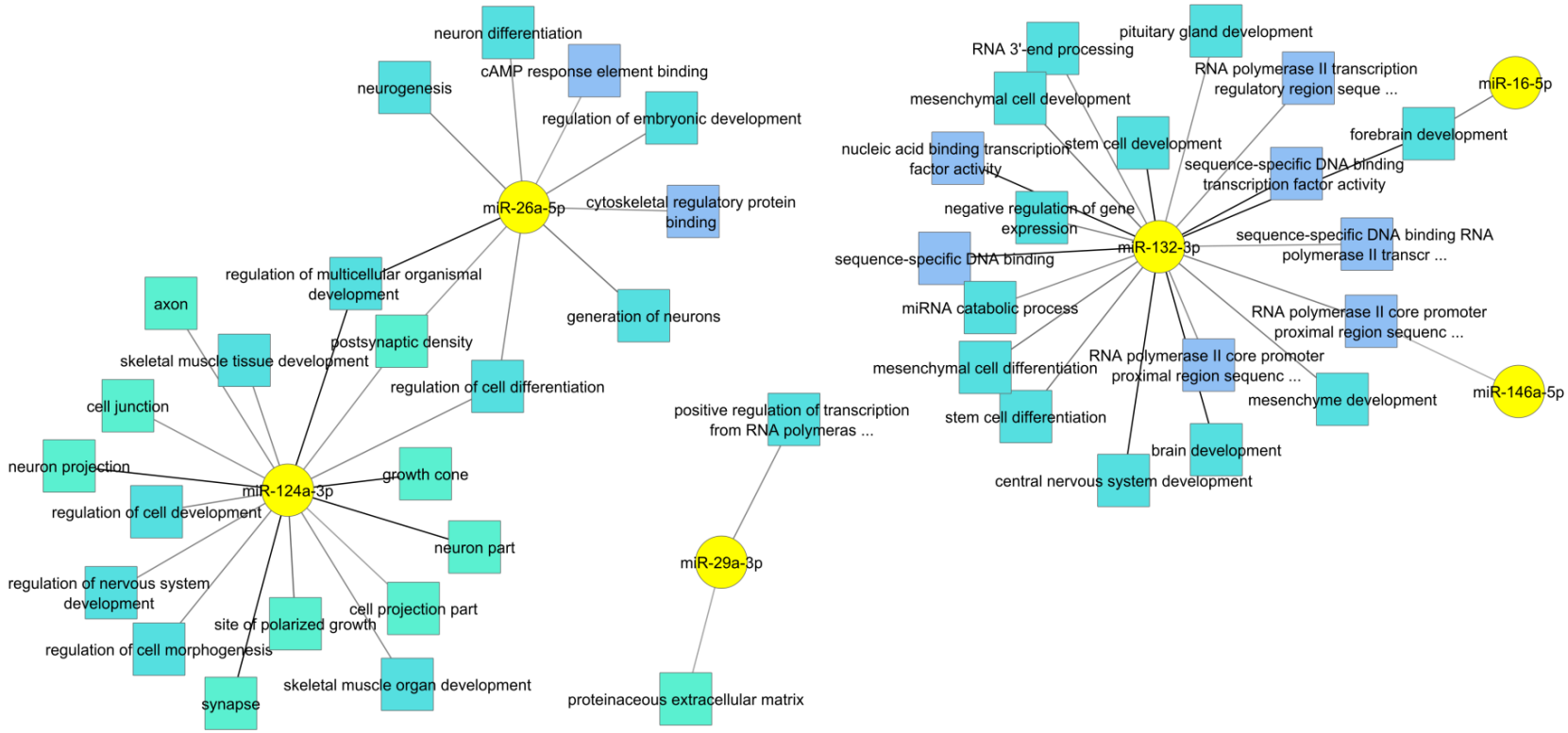

Figure 3.36. Biological processes potentially regulated by all 7 candidate miRNAs enriched by genes that were also downregulated during preclinical prion disease. Gene ontologies were grouped according to the miRNAs analyzed. Network was generated using Cytoscape.

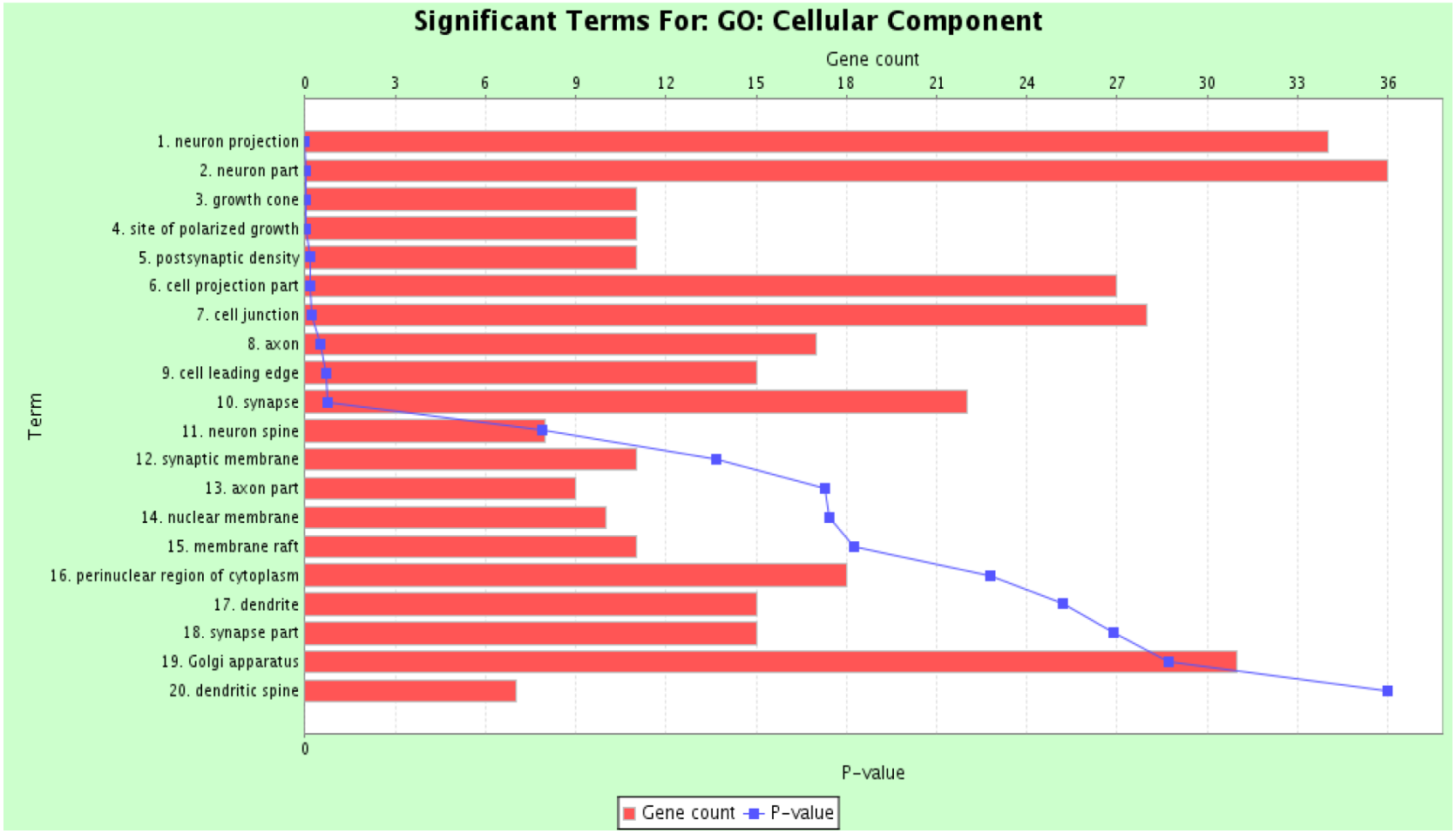

Figure 3.37. Cellular compartments that were highly represented by the genes identified to be potential miRNA targets. Graph depicting the number of genes (red bars) that matched the specific cellular compartment term. The significance is represented by the p-value (blue line). Graph generated from ToppGene Suite.

neuroprotective process. In fact, the temporal expression profiles of these 7 candidate miRNAs (miR-16-5p, miR-26a-5p, miR-29a-3p, miR-124a-3p, miR-132-3p, miR-140-5p and miR-146a-5p) mirrored this activity-induced neuroprotective gene signature in CA1 hippocampal neurons. To determine their association with a protective gene signature, expression of these miRNAs was measured after neurons were stimulated to evoke an activity-induced neuroprotective state.

To activate synaptic NMDARs, media in the primary mouse hippocampal cultures (culture is described in more detail in *Section 3.4.1*) was removed and replenished with media containing 250 µM 4-AP and 250 µM bicuculline for either 4 hours to induce short-term synaptic activity or for 16 hours to stimulate long-term (chronic) synaptic activity. $GABA_A$ receptors are located on neurons and function in the central nervous system to inhibit neuronal activation by diminishing the chance for an action potential to occur within that neuron. Bicuculline is a competitive antagonist of $GABA_A$ receptors which suppresses these inhibitory signals and allows for unabated action potential bursting (Hardingham *et al.,* 2001; Hardingham *et al.,* 2002; Arnold *et al.,* 2005). In turn, 4-AP is an organic compound that blocks voltage-dependent K+ channels which are crucial for returning a depolarized (active neuron) to its resting state. When adding 4-AP to neurons in culture, it prolongs an active state within these neurons. In combination, 4-AP increases the frequency of bicuculline-induced action potential bursts, causing an increase of nuclear calcium which in turn enhances CREB-mediated transcription and activity-induced neuroprotection (Hardingham *et al.,* 2001; Hardingham *et al.,* 2002; Arnold *et al.,* 2005). A schematic diagram of this process in provided in **Figure 3.38**.

The mixture of 4-AP and bicuculline compounds were added to cultures at two different stages of growth, 9 DIV and 12 DIV, to determine the age at which these neurons were most responsive to the treatment. The 9 DIV old neuronal cultures were most responsive to treatment

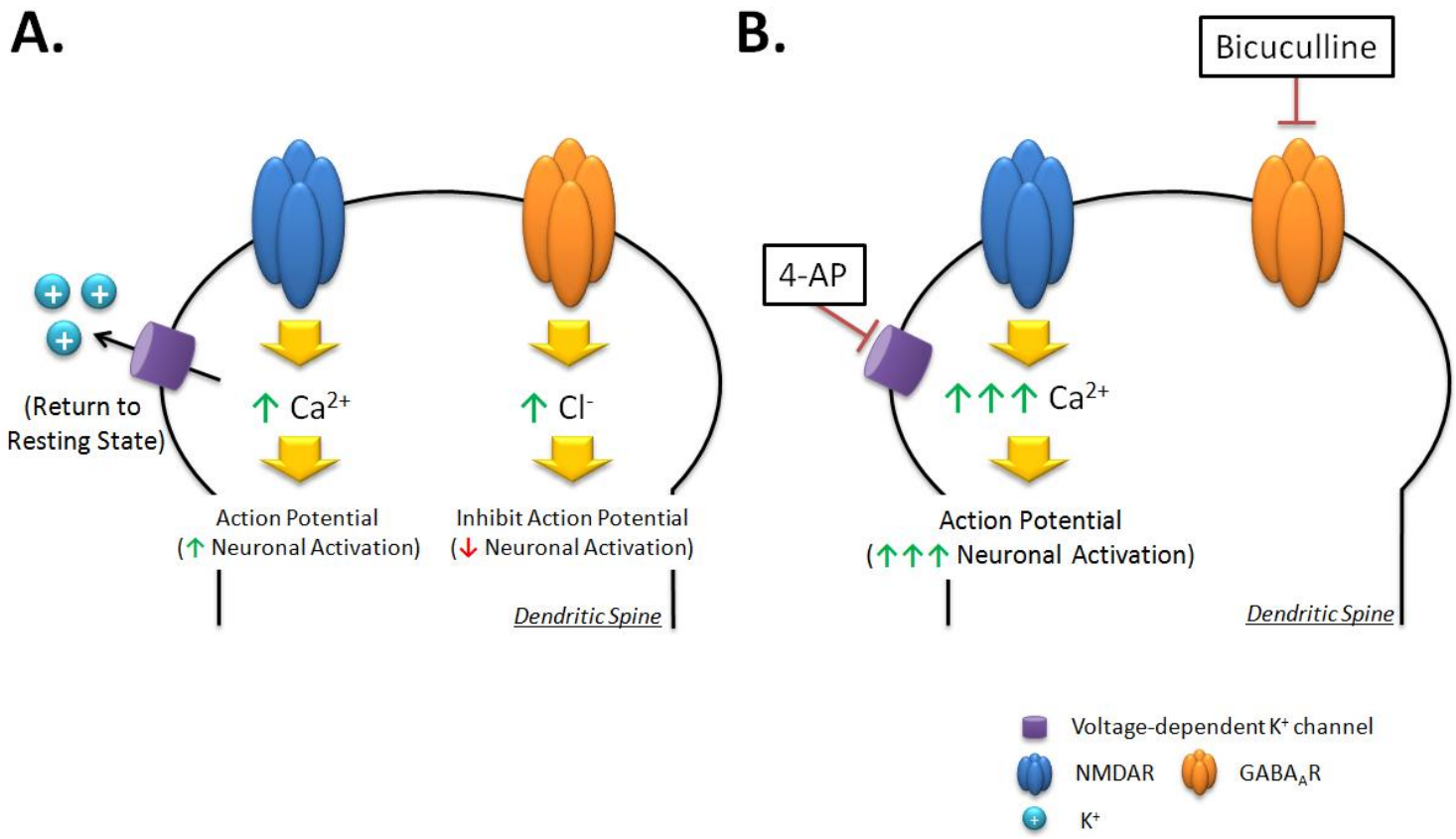

Figure 3.38. Schematic representation of the mechanistic function of bicuculline and 4-AP treatment in neurons. (**A**) Stimultaed NMDARs induce a signaling pathway mediated by increased intracellular calcium concentrations that lead to neuronal activation and induction of an action potential. The enhanced concentration of intracellular calcium activates voltage-dependent K^+ channels which release K^+ ions extracellularly and help return the activated neuron to a resting state. Similarly, signaling through $GABA_AR$ allows Cl^- ions to enter the cell and thereby decreasing the positive charge and inhibiting action potential. (**B**) The $GABA_AR$ antagonist bicuculline blocks the receptor and prevents Cl^- from entering the cell. The voltage-dependent K^+ channel can be blocked by 4-AP which inhibits release of K^+ from the cell. Collectively, this causes an increase in frequency and duration of action potential bursts and allows calcium to stimulate CREB-mediated transcription and activity-induced neuroprotection.

and at 4 hours post stimulation, expression of miR-124a-3p and miR-132-3p were significantly upregulated (**Figure 3.39A**). This upregulation was also observed in miR-132-3p at 16 hours while miR-124a-3p expression returned to basal levels (**Figure 3.39B**). However, stimulating activity-dependent neuroprotection for 16 hours evoked a significant increase in miR-16-5p, miR-26a-5p and miR-29a-3p while expression of miR-140-5p and miR-146a-5p remained unchanged. In 12 DIV cultures, miRNA expression remained at basal levels at 4 hours after treatment (**Figure 3.39C**) while only miR-132-3p was significantly induced at 16 hours post treatment (**Figure 3.39D**). MiR-26a-5p expression showed a slight albeit not significant increase at 16 hours post treatment.

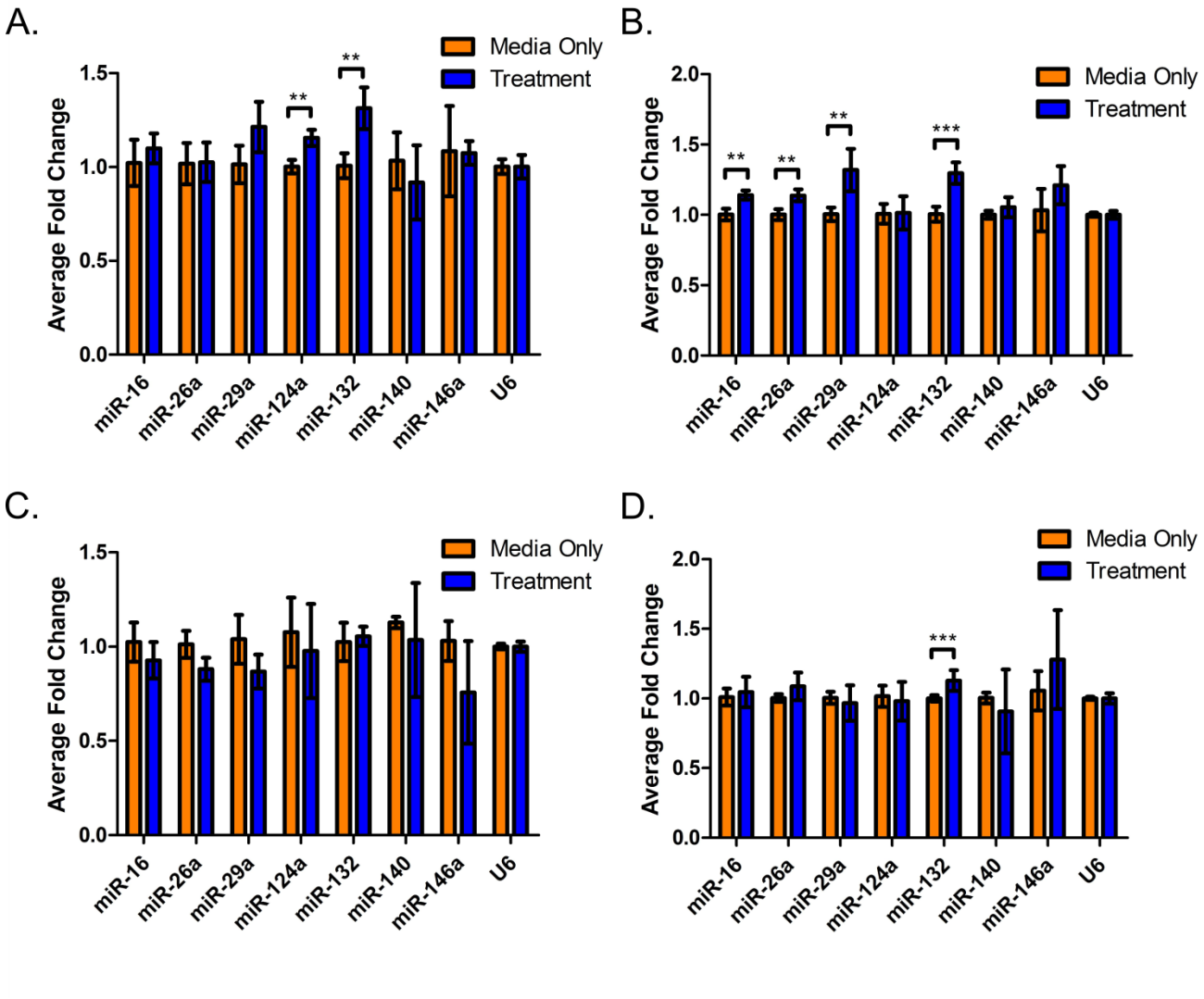

Figure 3.39. Induction of select miRNAs after pharmacological stimulation of a neuroprotective response in primary mouse hippocampal neurons. The expression levels of 7 miRNAs along with the endogenous control snoRNA U6 (U6) were determined for each indicated treatment condition tested. All graphs represent the average fold change for miR-16-5p (miR-16), miR-26a-5p (miR-26a), miR-29a-5p (miR-29a), miR-124a-3p (miR-124a), miR-132-3p (miR-132), miR-140-5p (miR-140) and miR-146a-5p (miR-146a) for either media only (orange bars) or 4-AP+bicuculine (blue bars). Treatment conditions were (**A**) 4 hours on 9 DIV, (**B**) 16 hours on 9 DIV, (**C**) 4 hours on 12 DIV and (**D**) 16 hours on 12 DIV old primary mouse hippocampal cultures. Statistical analysis was performed via the student's t-test where ** reflects a p-value ≤ 0.05 and *** represents a p-value ≤ 0.01. Fold change is reported as a mean ± SD (n=3).

3.3 Functional Characterization of miR-26a-5p

Rationale: A number of miRNAs were induced during early prion disease in CA1 hippocampal neurons. Of these, several were previously identified to have a neuronal-specific function, such as miR-132-3p which is known to enhance dendrite arborisation and spine formation of neurons (see *Section 1.15.4*). These same structural features are significantly altered during preclinical prion-induced neurodegeneration indicating that miRNAs upregulated at that time may play an important role in this process. However, most of the preclinically induced miRNAs have an uncharacterized function within neurons. Therefore, functional characterization of one of these miRNAs, miR-26a-5p, was performed to determine if it can modulate neuronal morphology. The rationale for this choice was because miR-26a-5p was predicted to target several structural genes that were downregulated during preclinical disease (see *Section 3.2.3*). Furthermore, its expression was induced in primary hippocampal neurons after stimulation of an activity-dependent neuroprotective program (see *Section 3.2.4*). Collectively, these data suggests that miR-26a-5p may also modulate neuronal morphology and thereby contribute to the pathology of prion disease. Therefore, miR-26a-5p was examined whether it can modulate anatomical features of primary mouse hippocampal neurons including the degree of arborisation and spine density (**Figure 3.40**).

3.3.1 Primary Mouse Hippocampal Cultures are Long-Lived and Consist Largely of Neurons

Embryonic day 18-20 (E18-20) CD-1 pups were used to prepare primary mouse hippocampal cultures. The hippocampal region was chosen for miRNA characterization studies

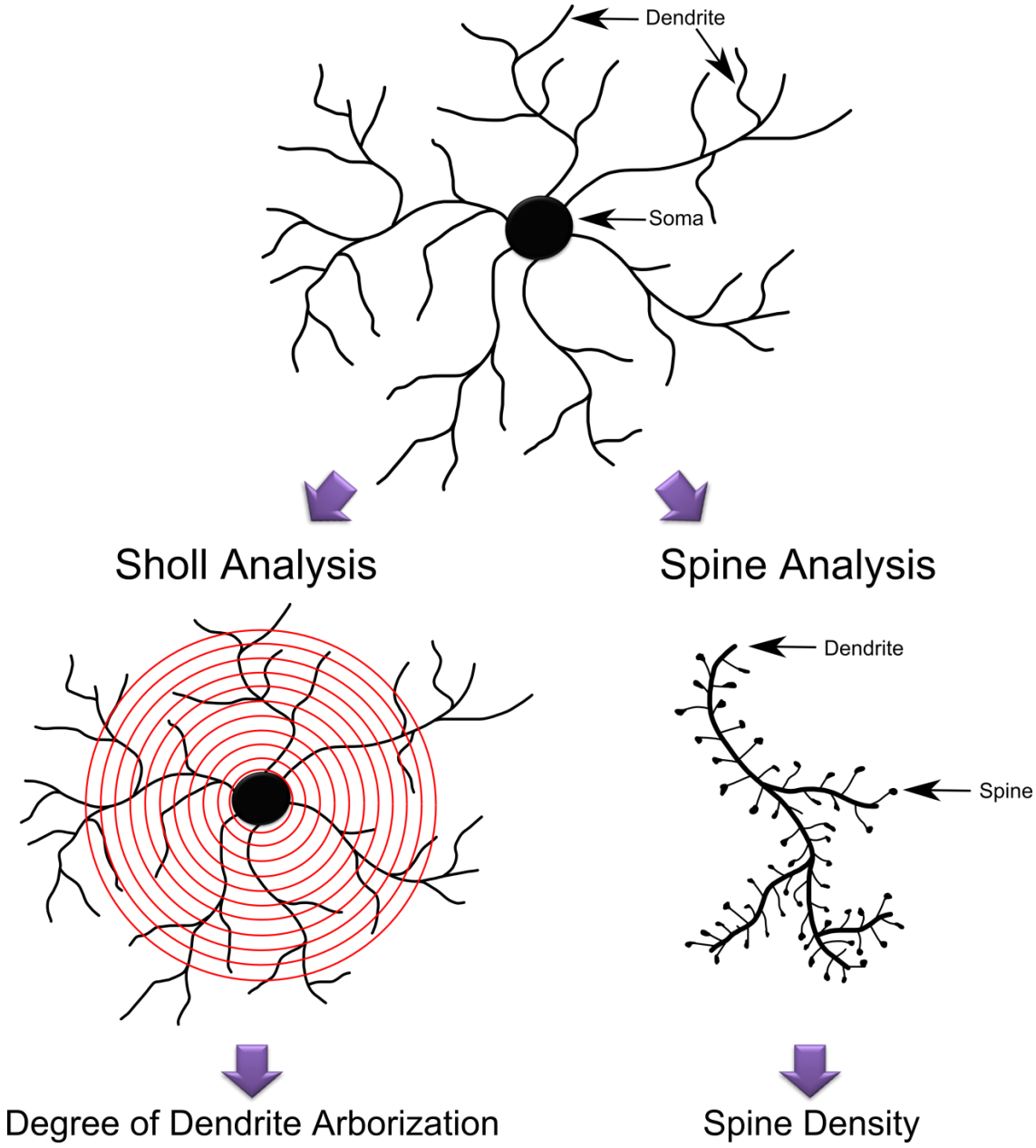

Figure 3.40. Schematic representation of the morphological analysis performed in this work after altering the concentration of miR-26a-5p within primary mouse hippocampal neurons. Neuronal structure can be assessed using Sholl analysis for degree of dendrite arborisation. In this analysis, concentric circles (red) originating from the soma of the neuron are places on top of the neuron. Intersections between the concentric circles and dendrites are counted. In addition, the numbers of spines detected on dendrites were also counted in the analysis.

for two main reasons. Firstly, hippocampal neurons were studied to identify which miRNAs were deregulated in a mouse model of prion disease. Secondly, miR-26a-5p is also expressed in astrocytes (Mor *et al.*, 2011) which, if present in large numbers, would confound the effects of miR-26a-5p on neuronal morphology. However, hippocampi are largely devoid of astrocytes and thus, provide an environment suitable to establish neuronal-specific function.

Primary mouse hippocampal cultures were assessed for neuronal enrichment, longevity and maturity of the neurons at every 2 DIV intervals using immunohistochemistry. An antibody against microtubule-associated protein 2 (MAP2) used to visualize neurons revealed that cells established an extensive network as they aged. This staining confirmed that the culture was primarily composed of long-lived, viable neurons (**Figure 3.41A**). To determine the proportion of astrocytes within the culture an antibody against GFAP was used in addition to MAP2 staining. Astrocytes were detected at relatively limited proportions throughout the lifespan of the cultures. In fact, astrocytes comprised ~10 % of the culture at 2 DIV with a modest increase to ~29.5 % by 20 DIV (**Figure 3.41B**). As expected for post-mitotic neuronal cultures, the number of neurons over the time of the culture progressively decreased. Compared to the number of neurons detected at 2 DIV (100 %), the number of neurons remained the same for the first 6 days in culture (~100 % at DIV 6) but decreased to ~50 % at DIV 16 and ~30 % at DIV 20 (**Figure 3.41C**). Conversely, astrocyte numbers in the culture remained the same for the first 6 days but gradually increased to ~150 % of the initial numbers at days 10-12. This was followed by a steady decline of astrocytes in the culture to approximately 70 % of the initial numbers by DIV 16. The number of astrocytes remained unchanged from DIV 16 up to and including DIV 20 (**Figure 3.41C**).

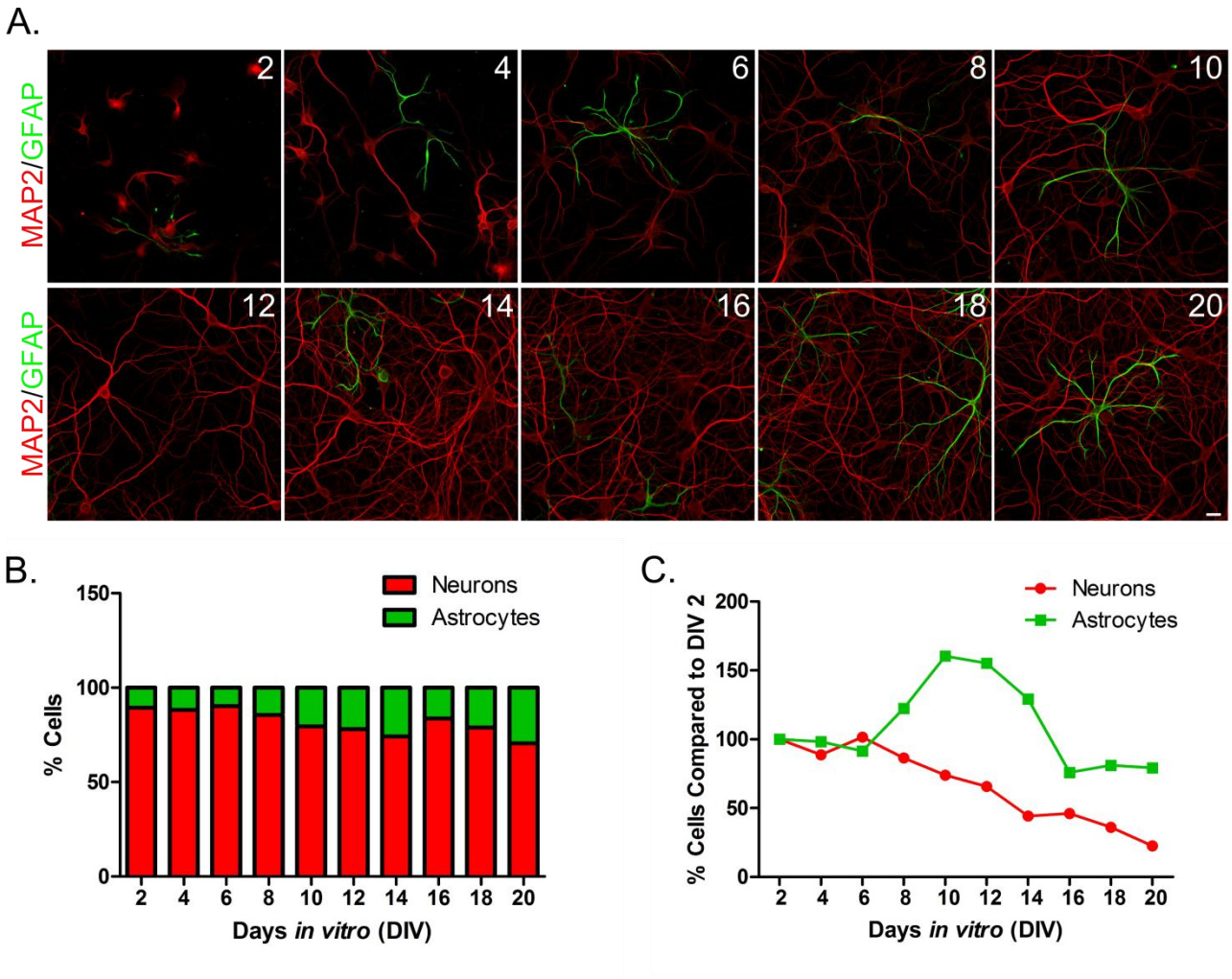

Figure 3.41. Primary hippocampal cultures are viable, long lived cultures largely composed of neurons. (**A**) Representative images of double immunofluorescence for MAP2 (a neuronal marker depicted in red) and GFAP (an astrocytic marker depicted in green). Cells were stained every two days starting from DIV 2 up to and including DIV 20. Scale bar = 20 µm. (**B**) Proportion of neurons and astrocytes represented throughout lifespan of the culture. Images were analyzed based on cell counts from a 3150 x 2150 µm area per time point. (**C**) Percent of neurons and astrocytes counted as compared to the number of cells detected at DIV 2 (n=2).

As the neuronal culture ages, the morphology of neurons changes from an "immature" to a "mature" phenotype. This is classically represented by the presence of extensive spine structures that emerge from dendrites (Lee *et al.*, 2012); these structures can be detected by various spine-specific markers such as the post-synaptic density 95 (PSD-95) protein. Therefore, to confirm the presence of spines and to establish the time at which these cultures were considered mature, immunohistochemistry using a PSD-95 antibody, counterstained with MAP2, was performed at every 4 DIV intervals. Punctate staining for PSD-95 was observed in association within neuronal structures at 12 DIV with progressively more pronounced staining as the culture aged (**Figure 3.42A**). These data confirmed that neurons clearly exhibited mature morphology by 16 DIV (**Figure 3.42B**).

3.3.2 MiRNA-26a-5p is Expressed under Basal Conditions in Primary Hippocampal Cultures

To determine the relative abundance of miR-26a-5p within primary mouse hippocampal neurons, the baseline expression profile of miR-26a-5p compared to miR-132-3p and miR-146a-5p was determined using qRT-PCR throughout the lifespan of the culture. MiR-132-3p is known to be upregulated during neuronal development (Pathania *et al.*, 2012) while miR-146a-5p is expressed at lower abundance within neurons (Jovicic *et al.*, 2013). These miRNAs therefore served to define a range where miR-132-3p represented highly abundant while miR-146a-5p represented low abundance miRNAs in neurons. In primary mouse hippocampal cultures, miR-26a-5p was expressed at relatively moderate levels having Ct values fall between the values determined for miR-132-3p and miR-146a-5p (**Figure 3.43A**). To identify whether the expression of miR-26a-5p varied over time, fold change was calculated by comparing each DIV

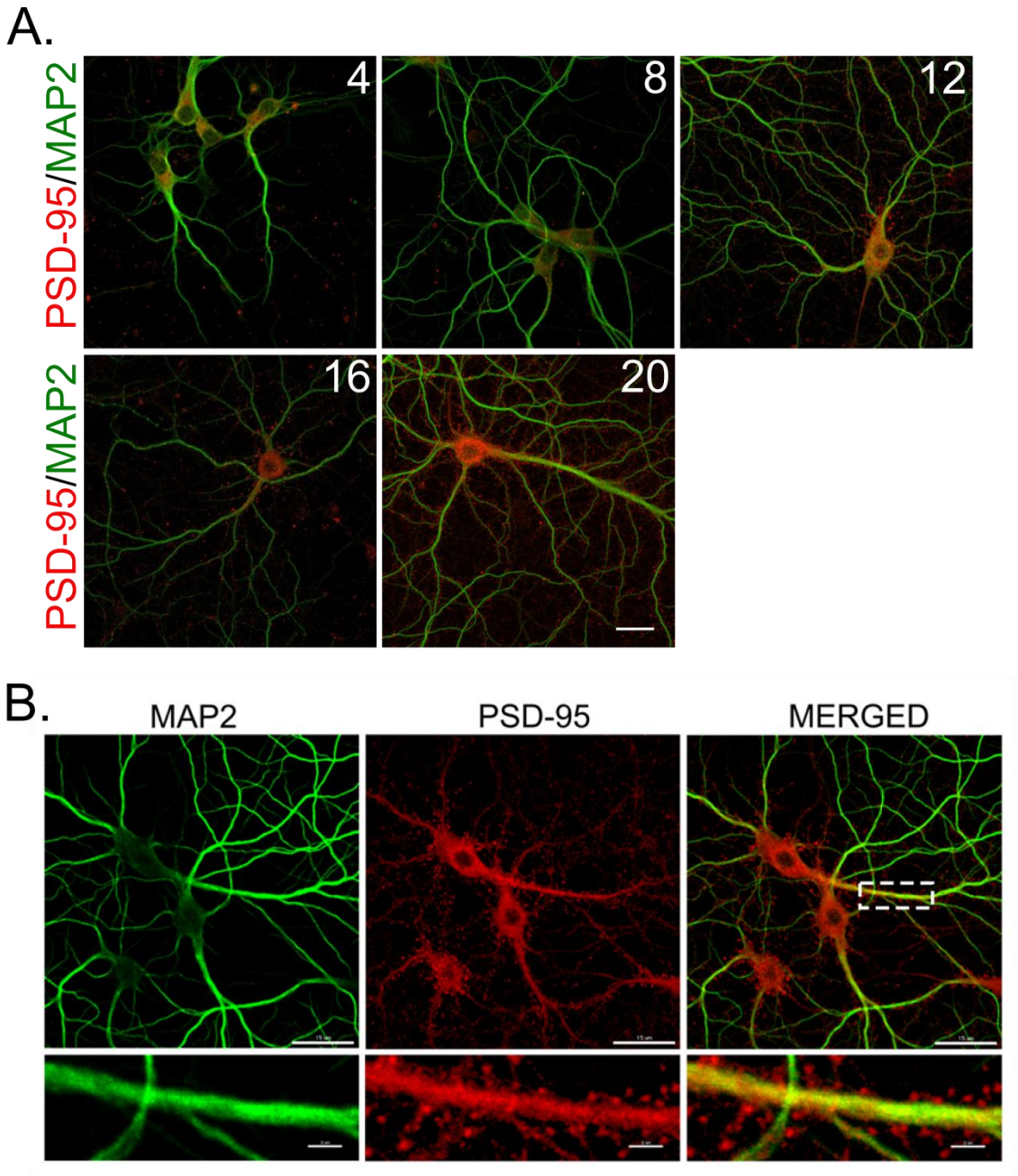

Figure 3.42. PSD-95 staining in primary mouse hippocampal cultures confirmed the presence of mature neurons. (**A**) Representative images of the PSD-95 (red) staining in primary mouse hippocampal cultures at every 4 days from 4-20 DIV. Neurons were counterstained with MAP2 (green). Scale bar = 20 µm. (**B**) A representative image of PSD-95 staining at 16 DIV where PSD-95 (red) is colocalized to neurons (green). Scale bar = 15 µm for large images and 2 µm for zoomed in panels.

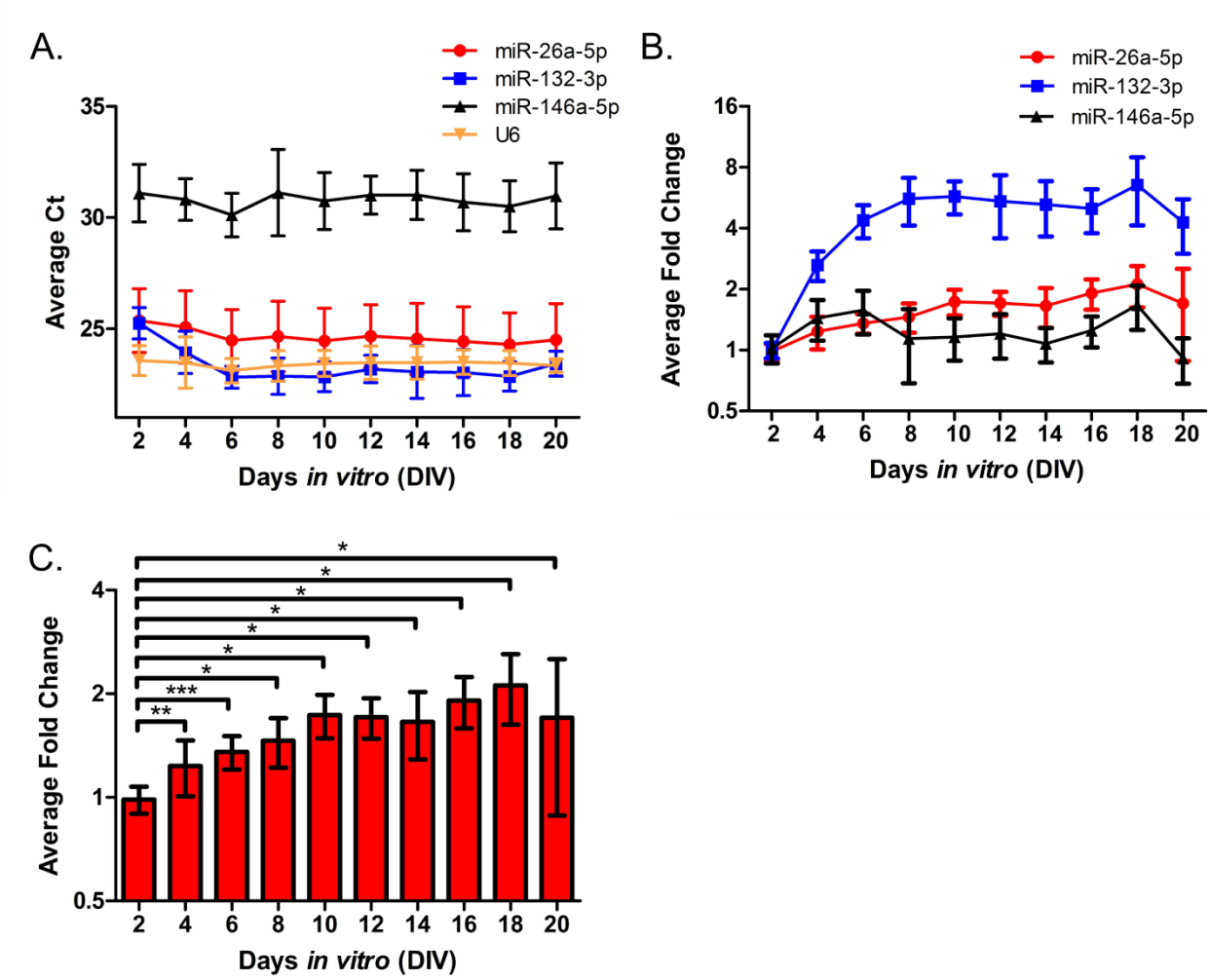

Figure 3.43. MiRNA-26a-5p is endogenously expressed within primary mouse hippocampal cultures. (**A**) The relative expression of miR-26a-5p, miR-132-3p and miR-146a-5p in primary mouse hippocampal cultures. Ct values represent relative abundance of each miRNA. (**B**) Average fold change of the expression levels of miR-26a-6p (red), miR-132-3p (blue) and miR-146a-5p (black) throughout the lifespan of the neuronal culture. (**C**) Average fold change of miR-26a-5p at each time point relative to DIV 2. Statistical significance was assessed by the student's t-test method where * represents a p-value ≤ 0.05, ** indicates a p-value ≤ 0.01 and *** refers to a p-value ≤ 0.001. The fold change was calculated by comparing each time point to the expression of that miRNA at DIV 2. For all graphs, the data is plotted as the mean and standard deviation from 6 biological replicates representing 3 independent culture preparations.

sampled to the earliest time point of the culture, 2 DIV. Expression of miR-26a-5p was significantly increased beginning at 4 DIV as compared to 2DIV, reached its peak of 2-fold induction at 10 DIV and persisted as the culture aged (**Figure 3.43C**). This increase in miR-26a-5p expression coincided with the time that primary mouse hippocampal neurons grow and reach maturity. The increase in miR-26a-5p expression was not as pronounced as measured for miR-132-3p, which reached approximately 6-fold higher levels by 6 DIV as compared to 2 DIV. In turn, expression of miR-146a-5p remained unchanged throughout the lifetime of the culture (**Figure 3.43B**).

3.3.3 Lentiviral Constructs Successfully Modified miRNA-26a-5p Expression in Primary Mouse Hippocampal Cultures

To determine whether miR-26a-5p had an effect on neuronal morphology, endogenous expression levels of miR-26a-5p in primary mouse hippocampal cultures were manipulated by using a lentiviral delivery system. This viral system was used because it efficiently delivers a user specified expression vector into hard-to-transfect cells, such as primary mouse hippocampal neurons. In addition, the vector also expresses a green fluorescent protein (GFP) for visualization of the transduced cell, allowing for single-cell analysis studies. The transduced GFP cells can be easily discriminated morphologically between excitatory pyramidal neurons (neurons chosen for analysis) from inhibitory neurons and astrocytes (Benson *et al.*, 1994).

For this work, the concentration of miR-26a-5p within the transduced cells was modified to obtain a gain-of-function phenotype. Viral particles were produced to increase (lenti-miR-26a) miR-26a-5p expression in transduced cultures as compared to controls (lenti-Scrambled). Viral

particles for each vector construct were prepared and viral titers were determined to be $6.8x10^6$ TU/mL for lenti-26a and $1.07x10^7$ TU/mL for lenti-Scrambled (**Figure 3.44**).

Several criteria had to be confirmed prior to performing single cell morphological analysis after transducing the primary mouse hippocampal cultures with these viral particles. The primary consideration was to confirm that the expression of miR-26a-5p was altered by lentiviral transduction as compared to basal levels. Also, incubation time post lentiviral transduction had to be established to determine the maximum induction of miR-26a-5p in the cultured neurons and to confirm adequate GFP expression for proper visualization of individual neurons. To address these considerations, primary mouse hippocampal cultures were first transduced with lenti-miR-26a (MOI≈1.36) and lenti-Scrambled (MOI≈2.14) at 8 DIV in order to determine whether miR-26a-5p was over-expressed in the transduced culture. Indeed, primary mouse hippocampal cultures transduced at these MOIs were producing miR-26a-5p at 3.75-fold higher levels after 72 hours while a 15-fold increase was observed after 96 hours post transduction as compared to lenti-Scrambled treated cultures (**Figure 3.45A**). Furthermore, distribution of GFP within the transduced neurons after 4 days allowed for precise definition of the total neuronal shape, highlighting both large structures such as dendrites and small structures such as spines. However, these structures were more pronounced when treating cultures with lentiviral particles at 12 DIV rather than at 8 DIV (**Figure 3.45B**).

Although the expression level of miR-26a-5p was significantly increased, lentiviral transduction at such a high MOI resulted in majority of cells to be GFP positive, inadvertently merging the signal from dendritic processes of neighboring cells for confocal microscopy. To obtain isolated GFP-positive neurons for single cell analysis, an MOI of approximately 0.2 [0.21 for lenti-Scrambled (20 % cells transduced) and 0.27 for lenti-miR-26a (24 % cells transduced)]

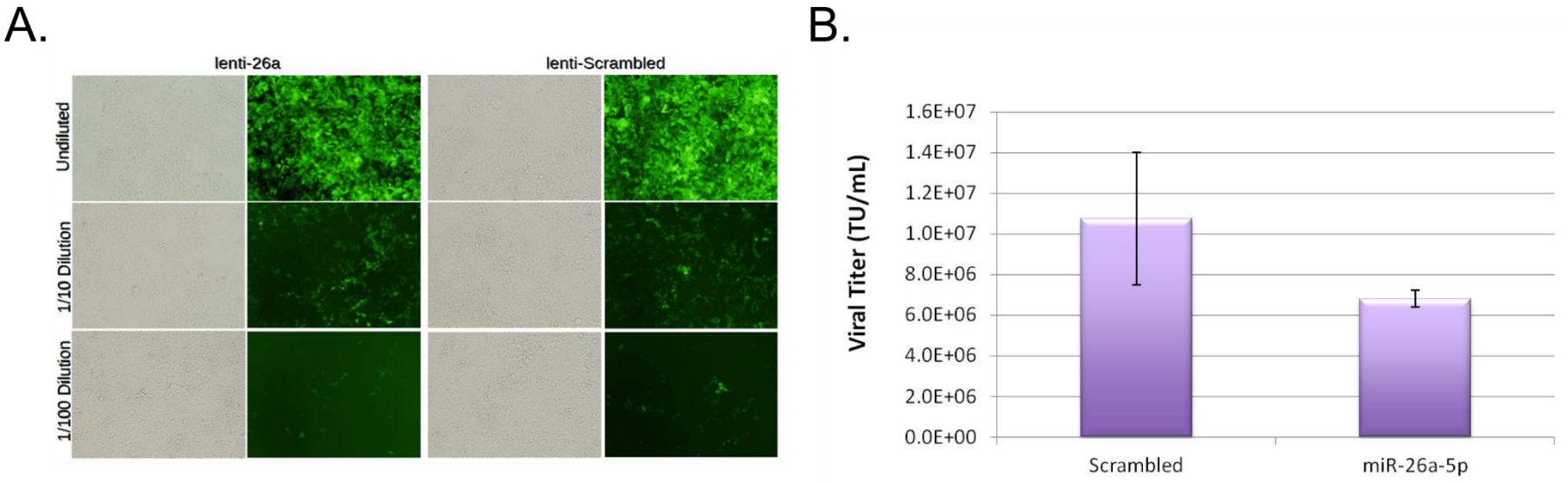

Figure 3.44. Titre determination of lentiviral constructs for miR-26a-5p overexpression (lenti-26a and lenti-scrambled) experiments. HeLa cells were transduced by adding 10 µL of the viral dilution per well. (**A**) Bright field and fluorescent images were taken for each representative dilution for the lentiviral constructs. (**B**) Viral titers were determined as described in the Material and Methods (*Section 2.16*). Data is represented as mean ± SD.

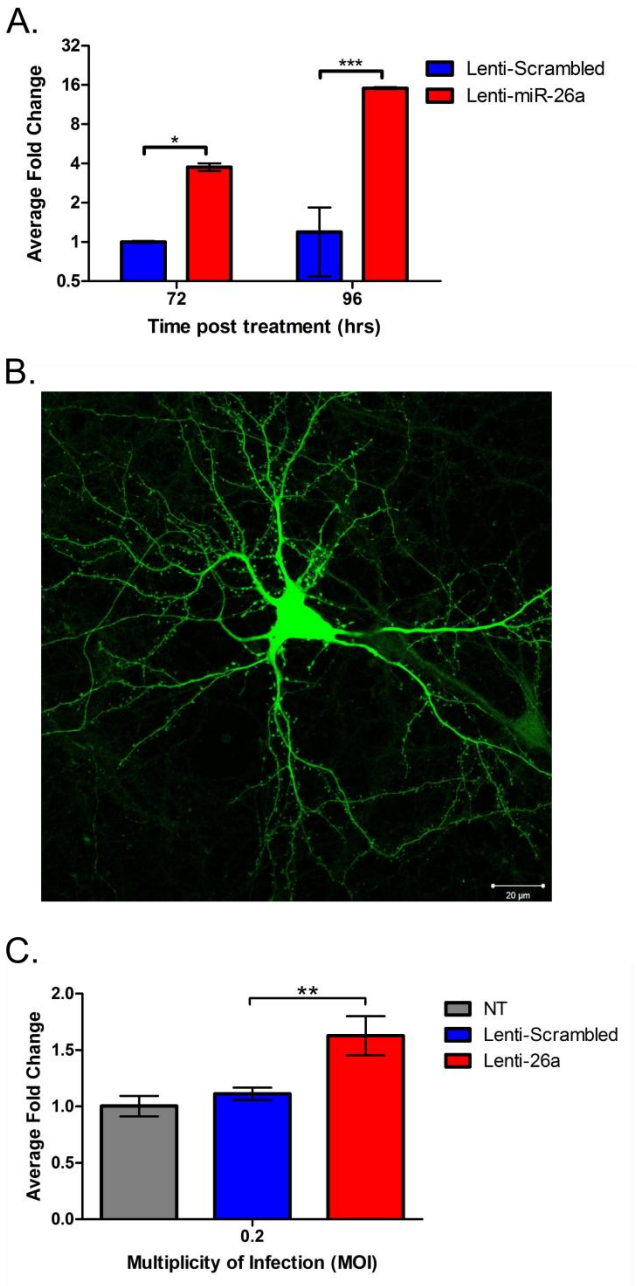

Figure 3.45. Confirmation of miR-26a-5p over-expression in lentivirus transduced primary mouse hippocampal neurons. (**A**) The expression levels of miR-26a-6p after transducing primary cultures with lenti-26a and lenti-Scrambled. (**B**) A GFP positive neuron suitable for single cell analysis of both dendrites and spines. Scale bar = 20 µm. (**C**) The expression levels of miR-26a-5p after transducing primary cultures with lenti-miR-26a and lenti-scrambled with 0.2 MOI viral particles as compared to no treatment (NT wells). All data is plotted as mean±SD (n=3) and student's t-test was used to assess significance where $p<0.05$ = *; $p<0.005$ = ** and $p<0.0005$ = ***.

was used. At this MOI, approximately 22 % of the culture was transduced, allowing for visualization of individual neurons within the culture. Furthermore, expression of miR-26a-5p was still significantly upregulated after 4 days post transduction resulting in a 1.6-fold induction (**Figure 3.45C**).

3.3.4 Lentiviral Constructs are Not Cytotoxic to Primary Mouse Hippocampal Cultures

Once the conditions of lentiviral transduction were optimized for effective over-expression of miR-26a-5p, the potential of these lentiviral constructs to evoke cytotoxicity in primary mouse hippocampal cultures was tested. One method readily used as a marker of relative cell death in primary neuronal cultures is the detection of lactate dehydrogenase (LDH) in culture medium. LDH is released from apoptotic cells and persists within the medium to allow for its measurement (Zhang and Wang, 2013). An LDH assay was therefore employed to measure the extent of cell death post lentiviral treatment.

The sensitivity of the LDH assay to detect cell death in primary mouse hippocampal cultures was initially evaluated. For this purpose, a range of cells (500-20000) was prepared from freshly collected primary mouse hippocampi. To calculate the relative cell death that can be detected by the assay, absorbance values from the prepared range of cells were each divided by the maximum number of cells present at a certain age of the culture. For the sensitivity analysis, the number of cells at DIV 16 was used to represent the maximum number of death possible. To discount any background reading from the culture medium, a negative control (well with no cells), was also assessed for the presence of LDH. Based on this analysis, the LDH assay is highly sensitive and can robustly distinguish the death of 5000 cells from background, medium only levels (**Figure 3.46A**). In fact, death of 5000 cells corresponds to approximately 6 % of cell

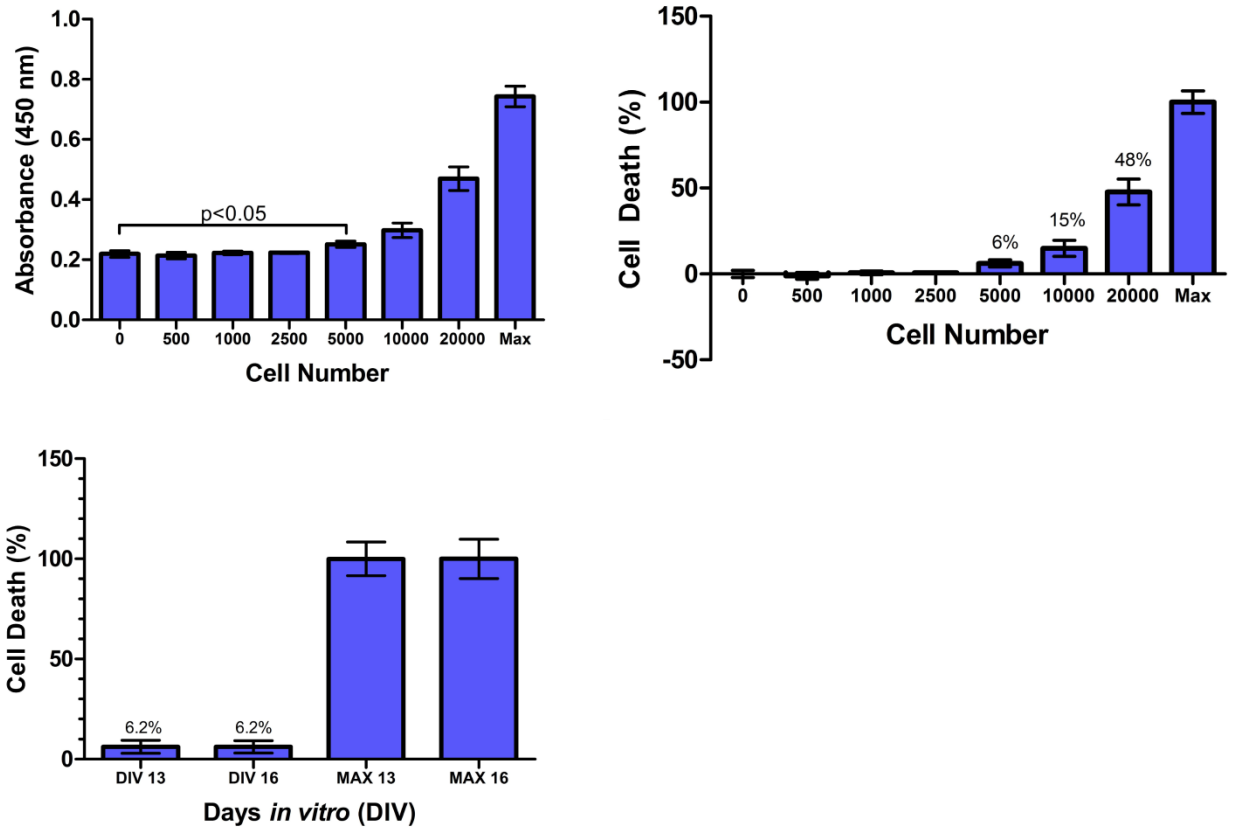

Figure 3.46. Basal level of cell death in primary mouse hippocampal cultures is detectable by the LDH assay. (**A**) The detection threshold for the assay indicating the number of cells required to apoptose in order to determine significant cell death over background, media only (or 0 cell number) levels. Student's *t*-test was used to calculate significance. (**B**) The percent of cell death determined for each cell number count as compared to the maximum, which is represented by the number of cells at DIV 16. (**C**) The basal level of cell death in primary mouse hippocampal cultures detected by the LDH assay.

death measured at DIV 16. Expectedly, as the number of lysed cells increased, the percentage of cell death as compared to the maximum was also increased (**Figure 3.46B**).

Based on the immunohistochemistry staining for MAP2 and GFAP, it was clear that neurons within the primary mouse hippocampal culture progressively died as the culture aged. Using the LDH assay, cultures at 13 and 16 DIV exhibited, on average, 6.2 % cell death as compared to the maximum cell death possible at each respective time point analysed (**Figure 3.46C**). Therefore, the LDH assay was sensitive enough to detect a basal level of cell death within the culture over time.

Primary mouse hippocampal cultures treated with the viral particles were assayed for LDH at 24 and 96 hours post transduction. These time points served to assess possible cell death due to the lentiviral treatment (24 hour time point) or due to the manipulation of the miRNA-26a-5p abundance within the cells (96 hour time points). Even at MOI > 1.0 the lenti-miR-26a and lenti-Scrambled did not stimulate cell death above the basal levels (6.2 %) at both 24 and 96 hours post transduction (**Figure 3.47**).

Overall, lentiviral transduction was non-toxic to primary hippocampal cultures. Specifically, LDH assay revealed that treatment of primary mouse hippocampal cultures with lentiviral particles did not stimulate cell death, even at MOIs above the levels used for single cell analysis. Similarly, manipulation of the endogenous miR-26a-5p levels within these cultures failed to trigger the induction of cell death.

3.3.5 MiRNA-26a-5p Over-Expression Enhances Dendrite Arborization and Spine Density of Primary Mouse Hippocampal Neurons

Single cell analysis was employed to measure two main morphological characteristics:

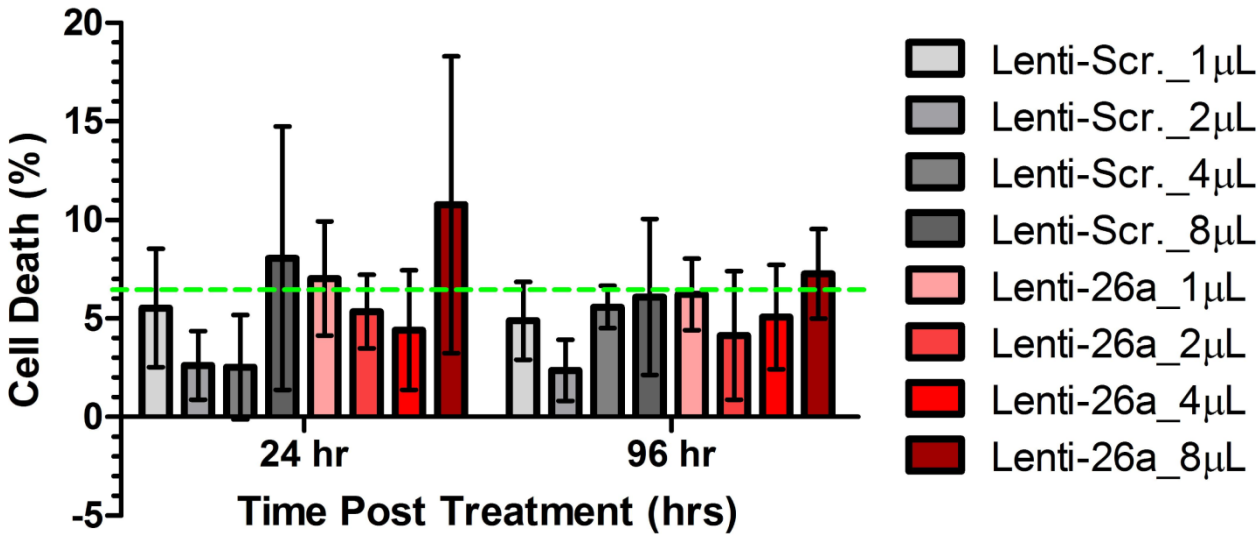

Figure 3.47. Manipulation of miR-26a-5p expression in primary mouse hippocampal cultures does not cause cell death. Over-expression of miR-26a-5p using lenti-26a as compared to lenti-Scrambled did not increase the cell death above basal levels when tested after 24 hours and 96 hours post transduction. Basal level at each time point analyzed is represented by the horizontal green dashed line. Data is represented as mean ± SD (n=6-8). MOI ~ 0.2 equates to 1 µL for Lenti-Scr and 2 µL for Lenti-26a while MOI ~ 1 equates to 4 µL for Lenti-Scr and 8 µL for Lenti-26a. Student's *t*-test was used to calculate significance.

the extent of dendrite arborization and the mean number of spines populating these processes. Fluorescence images of neurons from lenti-miR-26a and lenti-Scrambled treated cultures were analyzed using Imaris for Sholl analysis and ImageJ for spine counts. Neurons were traced in Imaris (**Figure 3.48**) and analysis of these tracings revealed that neurons over-expressing miR-26a-5p had a higher number of dendrites over the entire distance from soma (**Figure 3.49**). However, only at certain distances from the soma were these differences significant. Specifically, distances between 10 - 83 μm ($p < 0.05$), as well as 85 - 108 μm ($p < 0.05$) from the soma had significantly higher number of dendrites present than neurons transduced with the Scrambled sequence. Not surprisingly, comparing the total number of intersections between these two conditions revealed a significantly greater number of dendrites in neurons that were over-expressing miR-26a-5p (**Figure 3.50A**) and these neurons were also more arborized when comparing areas under the curve for the Sholl analysis (**Figure 3.50B**). Furthermore, miR-26a-5p over-expressing neurons also had a significantly higher mean spine density than neurons transduced with the scrambled lentivirus (**Figure 3.51**).

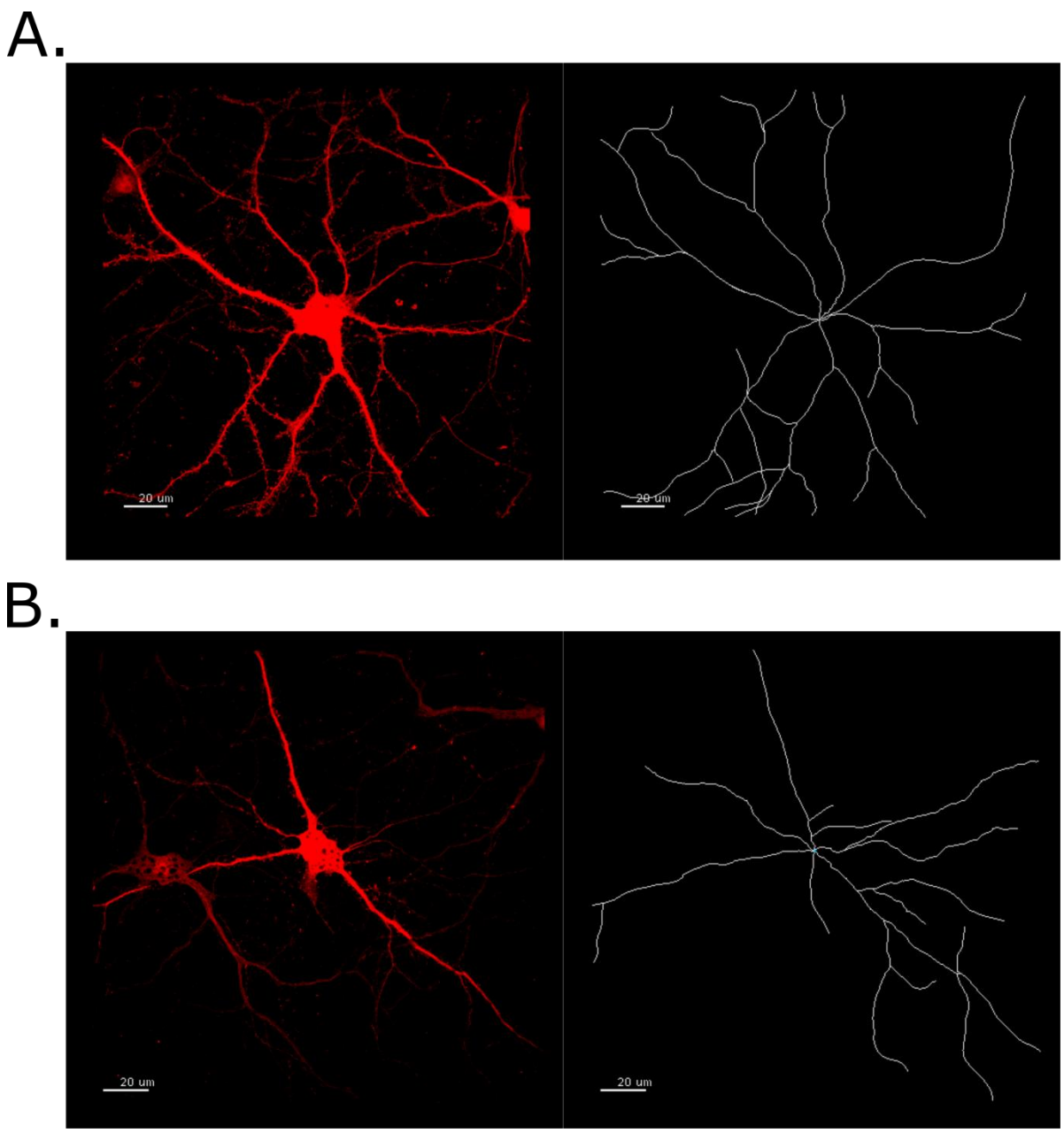

Figure 3.48. Representative images of primary hippocampal neurons used for Sholl analysis. Representative images of (**A**) miR-26a-5p and (**B**) Scrambled over-expression neurons that were transformed into dendrite tracings using Imaris for Sholl analysis (n=7). Scale bar = 20 μm.

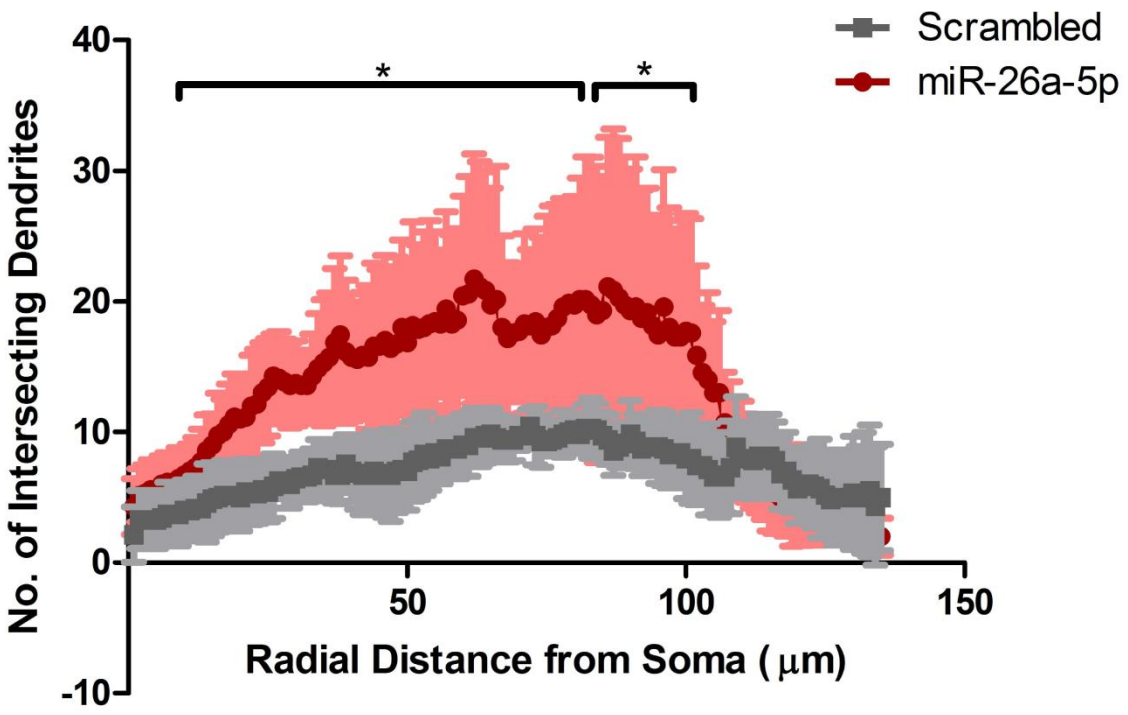

Figure 3.49. Increased miR-26a-5p expression enhances degree of arborization in primary mouse hippocampal neurons. The number of intersections for neurons treated with lentiviral constructs for miR-26a-5p or Scrambled sequences. Sholl analysis was used to count the number of dendrite intersections at 1μm intervals for a total radial distance of 135μm from the cell soma. Neurons from 2 individual primary neuronal preparations were counted for each treatment (n=7). Data is represented as mean ± SD. Student's t-test was used to determine significance at each interval where * represents a p-value < 0.05. Significant ranges between 10-82 and 85-107μm radial distances from soma.

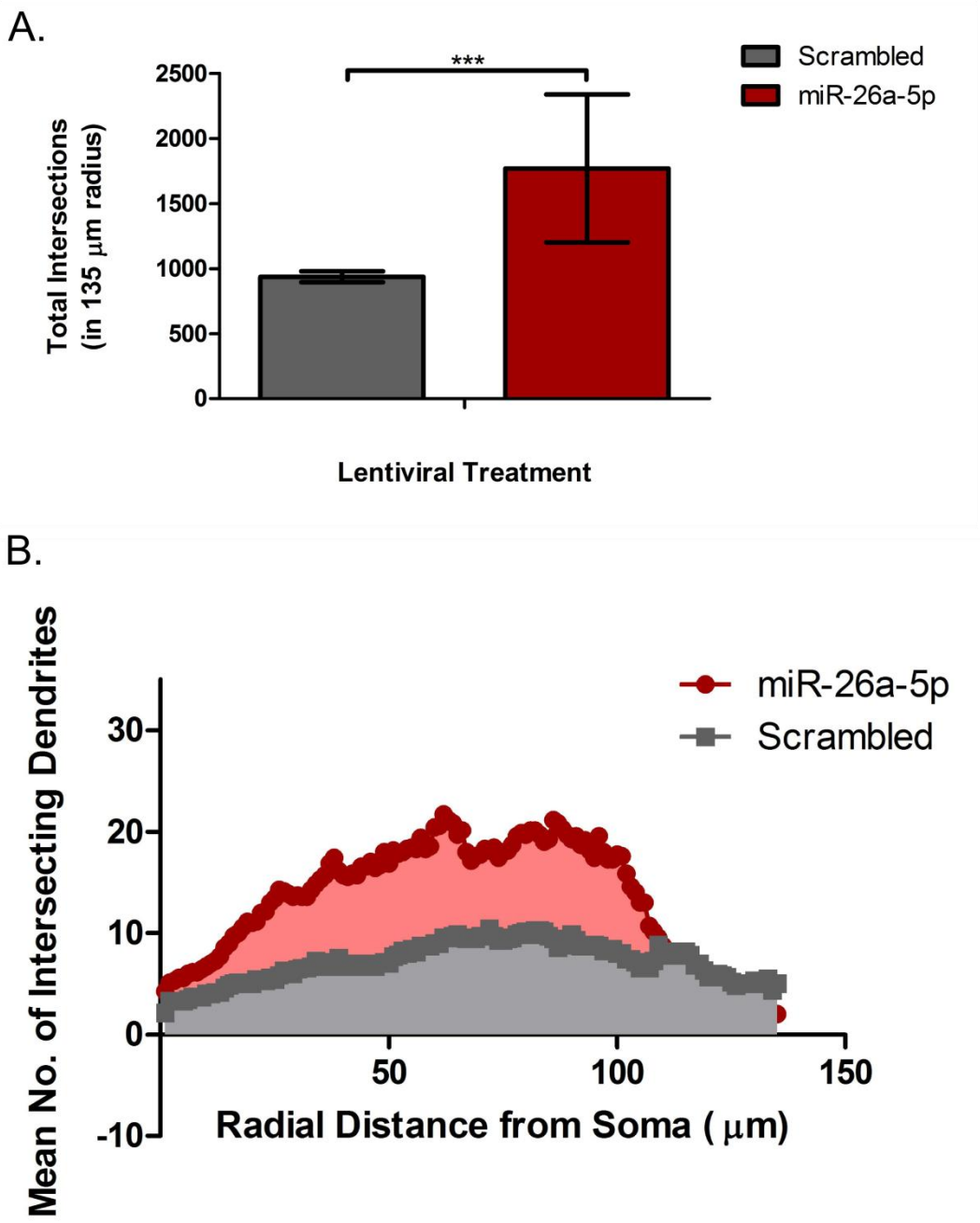

Figure 3.50. Over-expression of miR-26a-5p enhances degree of arborization in primary mouse hippocampal neurons. (**A**) Total number of intersections over a 135μm distance from soma was counted for each lentiviral treatment (n=7). Data is represented as mean ± SD. Student's t-test was used to determine significance where *** indicates a p-value < 0.005. (**B**) The total area under the curve was significantly larger for cells treated with miR-26a-5p expressing lentivirus than scrambled (n=7; p<0.0001).

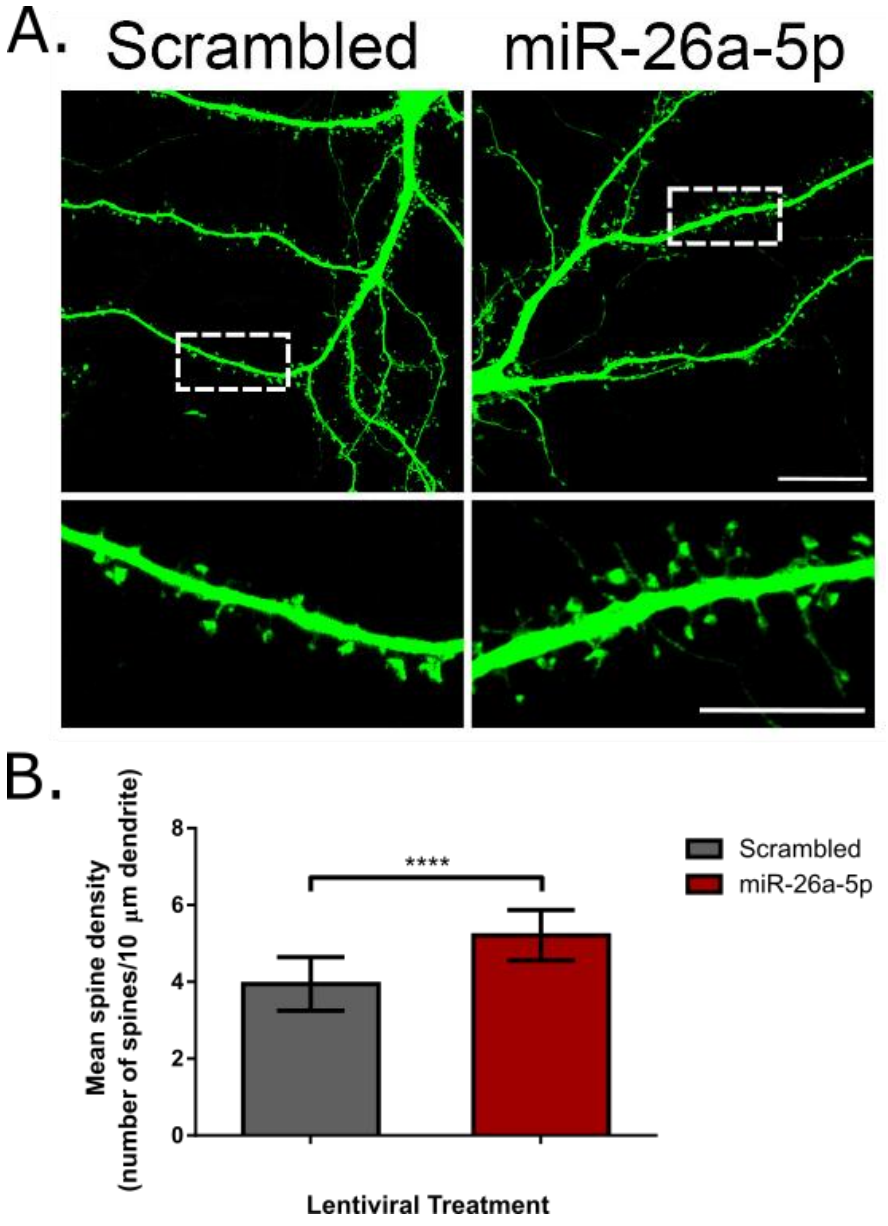

Figure 3.51. Increased miR-26a-5p expression enhances spine density in primary mouse hippocampal neurons. (**A**) Representative images of neurons taken for each lentiviral treatment for spine analysis. Scale bar = 20 µm and 10 µm for zoomed in panel. (**B**) Spine structures were manually counted using ImageJ for neurons from each treatment. Two independent primary neuronal preparations were used to collect images of miR-26a-5p over-expression (n=13) and scrambled (n=12) treated neurons. Data is represented as mean ± SD. Student's t-test was used to assess significance where **** represents a p-value < 0.0005.

4.0 DISCUSSION

Synopsis: It is well known that neuropathology such as synapse dysfunction and spine loss occurs well before clinical manifestation in most neurodegenerative diseases including Alzheimer's and prion disease (Ferrer *et al.*, 1981; Landis *et al.*, 1981; Heinonen *et al*., 1995; Masliah *et al*., 1995; Scheff *et al*., 2007). How this pathology shapes the molecular repertoire of disease-affected neurons remains largely elusive. To address this gap in knowledge, the primary research goal of this work was to identify molecular mechanisms that are altered within neurons during early prion disease. Specifically, the first objective was to describe how a neuronal-enriched sample was physically isolated from the surrounding brain tissue using microdissection. Consequently, molecular changes detected within these samples were primarily of neuronal-origin. During the preclinical stage of disease, microarray analysis of these samples revealed the induction of a distinct neuroprotective molecular program that had certain similarities to that mediated by activity-dependent calcium influx (*Section 4.1*). As the disease progresses however, this protective program was weakened and disappeared entirely by the time clinical disease was severe. In addition to the changes in gene expression, gene regulators called miRNAs were also significantly deregulated in neurons during prion disease. The expression profile of several miRNAs followed a similar induction pattern as to the activity-dependent neuroprotective gene signature detected within these neurons (*Section 4.2*). Of these miRNAs, a few are known to function in neurons to remodel spine structures, the very same structures known to be lost in prion disease. Based on this observation, it is possible that these miRNAs may be involved in the neurodegeneration process perhaps by delaying the loss of these morphological structures. However, the function for most of these miRNAs remained unknown within neurons. To determine whether these miRNAs could also induce a structural change within neurons upon overexpression, primary mouse hippocampal cultures were first established in the laboratory.

These cultures were subsequently validated to contain long-lived, viable neurons. Using this culture model, gain-of-function experiments for miR-26a-5p were performed to measure the effects of this miRNA on neuronal morphology. Neurons that over-expressed miR-26a-5p showed enhanced morphological complexity by increasing dendrite arborisation and spine density (*Section 4.3*). As this could potentially represent a neuroprotective mechanism that bypasses neurotoxicity induced by replicating PrP^{Sc}, it is possible that modulating miRNAs during prion disease could be a way to circumvent damage to neurons.

4.1 Gene Expression Profiling of CA1 Hippocampal Neurons

Neuronal enrichment of brain tissue is essential to detect changes in molecular processes that are specific to neurons during disease. This is because the brain is composed of a myriad of other cell types that dilute transcriptional signals of neurons. This is especially apparent when trying to detect changes during preclinical disease, a time when only a very small percentage of neurons are affected. To complicate matters further, progressive gliosis that begins very early during prion disease provides an extra layer of "transcriptional noise". To circumvent this challenge, cell bodies of CA1 hippocampal neurons using LCM microdissection were isolated from the rest of the brain tissue. As a result, robust neuronal-specific changes in transcriptional profiles were detectable even during preclinical disease.

4.1.1 Mouse Model of Prion Disease

The lack of a cell culture model for prion disease necessitates the use of animal models to study the process of prion-induced neurodegeneration. For the animal model used in these studies, intraperitoneal rather than intracranial inoculation was chosen because it stimulates a more natural route of infection that leads to neuroinvasion. Furthermore, the RML strain of scrapie (an archetype of TSEs) was used because it exhibits strong neuroinvasive properties that cause disease following peripheral exposure (Bett *et al.,* 2012) and is one of many prion strains that replicates within hippocampal neurons during preclinical disease (Bruce *et al.,* 1991).

All RML infected animals began to manifest classical symptoms of disease at approximately 140 DPI. Behavioural abnormalities including abnormal nest shedding activity, as well as weight loss and neurological signs such as ataxia were observed in prion-infected mice.

These observed phenotypes allowed a more adequate assessment of the stage of terminal disease. Animals were sacrificed due to symptom severity at 176.6 ± 11.5 DPI; a range well documented in the literature (Thackray *et al.,* 2003). Based on the time when severe symptoms were detected, it was observed that prion-infected animals experienced a lengthy preclinical stage of disease which lasted approximately 70 % of the disease process. This allowed ample time to study changes in gene expression before symptom onset.

4.1.2 Detection of PrP^{Sc} Deposits within Prion-Infected Brain

Primary PrP^{Sc} deposits were detected within several regions of the brain including the hypothalamus; where early detection of infectious prion particles typically occurs (Kimberlin and Walker, 1982). PrP^{Sc} was detected within the hippocampus beginning at 90 DPI and spotted among the cell bodies of pyramidal neurons at 110 DPI. In fact, PrP^{Sc} deposits were detected at 90 DPI in regions where neurites of these CA1 hippocampal neurons pass (*i.e. stratum lacunosum-moleculare*). This staining and therefore the amount of PrP^{Sc} deposits became more pronounced as disease progressed.

Comparing the temporal distribution of PrP^{Sc} to when transcripts were first deregulated in CA1 hippocampal neurons initially suggests that transcriptional changes occurred prior to direct association of PrP^{Sc} with these neurons. Interestingly, others also found adverse synaptic pathology ("synaptopathy") and synaptic loss prior to the detection of PrP^{Sc} within damaged regions (Gray *et al.,* 2009; Hilton *et al.,* 2013) suggesting that gene expression is altered in neurons before PrP^{Sc} deposits are readily detected and that cell bodies of CA1 hippocampal neurons may be responding to direct contact with replicating PrP^{Sc}. There are 3 plausible explanations for these observations. One explanation is that the most toxic oligomers of PrP^{Sc} are

too small to be detected by immunohistochemistry (Silveira *et al.,* 2005). Therefore, these small oligomers could be directly associating with cell bodies of CA1 hippocampal neurons even at 70 DPI, thereby stimulating a change in neuronal gene expression in response to PrP^{Sc} replication. A second explanation could be that PrP^{Sc} accumulated within regions far from the CA1 hippocampus, a region where distal processes of these neurons pass. In this case, PrP^{Sc} could be replicating far from the cell soma but still directly affecting the cell from those distal sites. Therefore, mapping the 3-dimensional neuronal structure within the brain (Koshy and Cabral, 2014) could help elucidate whether PrP^{Sc} does accumulate at distal sites of these neurons. A third explanation could be that PrP^{Sc} are able to spread to other cells through cell-to-cell contact and could also mitigate changes in gene expression without being detected by IHC.

4.1.3 Cell-Specific Gene Markers Mirror Pathological Findings

Gene expression profiling analysis revealed a total of 2,580 genes that were significantly deregulated at least at one time point during sampling. Prior to an in-depth analysis of the data, several cell-type specific gene markers were initially inspected and correlated with the classic neuropathological hallmarks of prion disease. This comparative analysis served 2 main purposes: 1) to assess the extent of glial encroachment in the pyramidal layer of the CA1 hippocampus as disease progressed and 2) to evaluate the relative proportion of neurons to glia within the region. These parameters served to better delineate the time in disease when glia contributed as "transcriptional noise" detected by the microarray.

4.1.3a Glial Encroachment

The microglia-specific gene marker, *Iba1*, was detected in all of the samples tested and its signal intensity significantly increased, beginning at 130 DPI and continuing to accumulate as disease progressed in prion-infected animals. Similarly, astrocyte cells were tracked using the astrocytic-gene marker *Gfap* and signal intensity was only detected at the terminal stage of disease in prion-infected samples. Pathological analysis of the same LCM region corroborated the microarray findings. Few microglia and astrocytes were detected among the densely packed neuronal cell bodies of pyramidal layer of uninfected as well as infected mice during majority of the disease progression. Only at clinical disease were glial cells detected at higher numbers among these neurons. Together, these data suggests that the gene expression of the pyramidal layer of CA1 hippocampal neurons would be primarily representative of neuronal transcripts. Beginning at 130 DPI however, the gene expression profile also included transcripts from infiltrating and/or activating glia, which by the terminal stage of disease, was extensive. This initial infiltration/activation of glia and progressive accumulation of these cells within the LCM-region is a characteristic pathology well documented in the literature to occur within the rest of the brain tissue (Tribouillard-Tanvier *et al.*, 2012; Carroll *et al.*, 2015). Therefore, these data also parallels the classic progressive gliosis observed in prion disease.

4.1.3b Degenerating Neurons

Expression of 3 neuronal-specific gene markers (*Nefl*, *Nefm* and *Snap25*) were also examined on the microarray to determine extent of neuronal degeneration and whether the proportion of neurons was reduced in the CA1 hippocampal region as disease progressed. These 3 genes were chosen to represent axonal and/or dendrite-related degeneration (neurofilaments

Nefl and *Nefm*) as well as pre-synaptic degeneration (*Snap25*). Signal intensity of *Snap25* in cell bodies of CA1 hippocampal neurons began to decrease at 130 followed by profound decrease of *Nefl* and *Nefm*. These data suggested that changes to synaptic structures detected at 130 DPI in pyramidal CA1 neurons preceded degeneration of neuronal filaments and therefore death of neurons. Indeed, degenerating neurons were detected only at terminal disease within the hippocampal region as visualized by Fluoro-Jade® C. Therefore, cell bodies of CA1 hippocampal neurons appeared relatively robust throughout majority of the time course while other neurons within the hippocampal formation were more vulnerable to degeneration. Only during symptomatic disease did transcriptional changes in neuronal structure genes coincide with the time when a small proportion of neurons were degenerating. These data mirrors other studies which showed that pre-synaptic alterations precede the process of neuronal loss (Jeffrey *et al.*, 2000; Siso *et al.*, 2002; Hilton *et al.*, 2013; Chiti *et al.*, 2006) and that cell death of hippocampal neurons occurs in the final stages of disease (Cunningham *et al.*, 2003; Russelakis-Carneiro *et al.*, 2004).

4.1.4 *Prnp* Expression in CA1 Hippocampal Neurons

The expression of *Prnp* was not significantly altered in the pyramidal layer of CA1 hippocampal neurons throughout prion disease. It is well known that PrP^{C} expression on the surface of neurons is critical for initiation of prion-related neuropathology and decreasing *Prnp* expression within neurons prevents onset of disease (Mallucci *et al.*, 2003). Interestingly, the expression of *Prnp* within CA1 hippocampal neurons showed a trend towards downregulation at 70 DPI in prion-infected samples. It would therefore be interesting to assess the expression of *Prnp* within these neurons at earlier time points of disease.

4.1.5 Temporally Deregulated Gene Expression Profiles

The most prominent finding identified by microarray data from the LCM region was that transcriptional alterations followed a biphasic temporal expression profile. Two main gene clusters were identified based on the pattern of gene expression. Genes in one cluster were induced during early stages of disease (70-110 DPI) of which expression either significantly decreased or remained at basal levels as disease progressed. Other genes that composed cluster two were either downregulated or unchanged at early stages of disease and were induced at either 130 DPI or EP. To obtain a more relevant appreciation of the deregulated genes, bioinformatic functional enrichment analysis of these genes was performed. This enrichment revealed that majority of the downregulated genes were involved in neuronal-specific function, regardless of the time point inspected. In turn, the largest proportion of upregulated genes was found at terminal disease and was involved in astrocytosis and microgliosis. More detailed discussion of these detected genes in terms of their functions, involvement and temporal environment in prion disease is described within the next several sections.

4.1.5a Induction of a Protective Mechanism in Neurons during Early Disease

Transcriptional signatures identified in CA1 hippocampal neurons during early prion disease were highly reminiscent of a molecular program that was induced after stimulation of synaptic NMDARs in primary hippocampal neurons (Zhang *et al.*, 2007; Zhang *et al.*, 2009). NMDAR signaling is well known to mediate a cellular survival or death response, depending on the location of this receptor on the synapse. If NMDARs are located intrasynaptically, stimulation of NMDAR results in a pro-survival transcriptional signature while stimulation of the

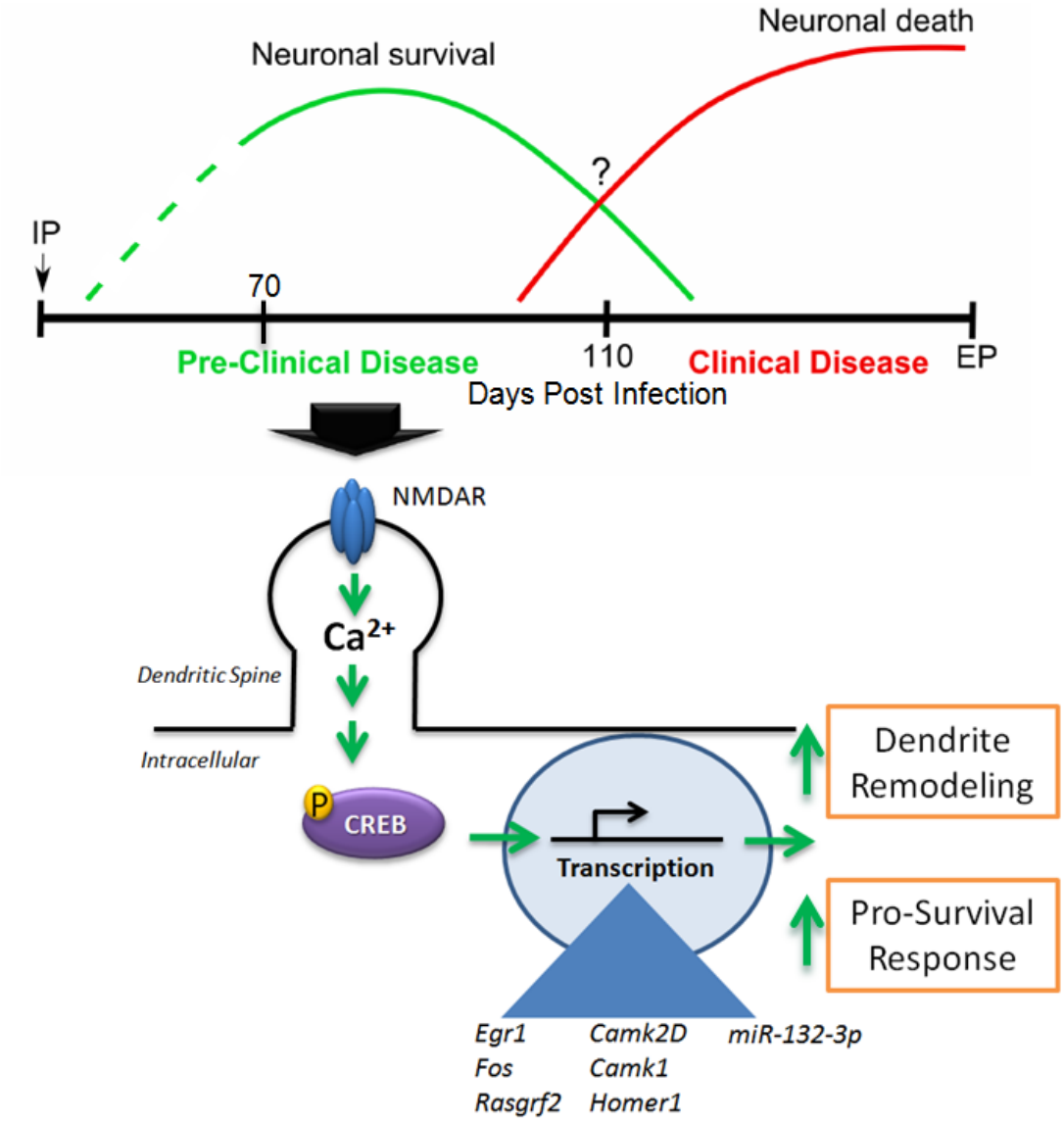

Figure 4.1. Schematic representation of transcriptional changes that occur in CA1 hippocampal neurons during preclinical prion disease. Selective enrichment of neuronal cell bodies revealed a transcriptional program highly reminiscent of the synaptic activity-induced neuroprotective response. During the preclinical stages of disease, stimulation of synaptically located NMDARs initiates calcium influx and subsequent signal transduction. As a result, CREB becomes phosphorylated, translocates into the nucleus and initiates transcription. Several genes as well as microRNAs are selectively transcribed that can modulate dendrite and spine structure and/or contribute to a pro-survival response. However, as disease progresses this protective response diminishes and is not detected at clinical disease. In turn, beginning at approximately 110 DPI, a different group of genes becomes induced and perpetuates into clinical stages of disease. Dashed line prior to 70 days post infection reflects time points not analyzed for changes in gene expression profiles.

same receptor located extrasynaptically results in the production of a cell death molecular response (Hardingham *et al.,* 2002; Zhang *et al.,* 2007). Not surprisingly, CREB is central to both of these pathways and its phosphorylation state dictates the switch between survival and death of neurons (Hardingham *et al.,* 2002). As such, pCREB induces a protective state in the neuron by activating a pro-survival transcriptional program. Within CA1 hippocampal neurons, pCREB levels were significantly increased during preclinical disease and likely responsible for stimulating the upregulation of activity-dependent neuroprotective genes. In fact, several genes known to be directly induced by pCREB, such as *Egr1*, *Fos*, and *Rasgrf2*, were upregulated during preclinical disease, further supporting the enhanced activation of CREB at that time in disease. The microarray data analysis in this study suggests, for the first time, that CA1 hippocampal neurons evoke a protective molecular response to early stages of prion disease (**Figure 4.1**).

Functional diversity of these receptors is also dictated by the distinct subunit composition (Sanz-Celemnte *et al.,* 2012). The ratio of NR2A (stimulates survival) and NR2B (stimulates excitotoxicity) subunits contributes to the balance between protective and pro-death pathways (Groc *et al.,* 2006; Tovar *et al.,* 2000). In addition, when the level of NR2B subunits decreases, NR2A increases in abundance at the synapse (Guillaud *et al.,* 2003). *Grin2b* encodes for NR2B and was detected by microarray and qRT-PCR to be significantly downregulated in CA1 hippocampal neurons during early prion disease. These data suggests that a greater number of NR2A-enriched NMDARs may be populating synapses during early stages of prion disease, further substantiating the NMDAR-mediated neuroprotective response. However, further experiments would need to be performed to validate this observation on a protein level.

Disruption of normal NMDAR signaling has been observed in prion disease and other neurodegenerative diseases. In fact, NMDAR was altered in PrP^C knockout mice which resulted in an impaired synaptic inhibition that was mediated by a weakened $GABA_A$ receptor-mediated fast inhibition (Collinge *et al.,* 1994). With a decrease in synaptic inhibition, neurons become more excitable which can lead to excitotoxicity. Indeed, prion-infected slice cultures were more easily excitable than cultures from wild-type mice (Maglio *et al.,* 2004). Furthermore, PrP^C knockout animals had enhanced NMDAR activity resulting in enhanced sensitivity to excitotoxicity (Khosravani *et al.,* 2008). NMDAR mediated excitotoxicity was previously observed in other neurodegenerative diseases including Alzheimer's and Huntington's diseases (reviewed in Parsons and Raymond, 2014) further suggesting that a similar molecular mechanism is driving these neurodegenerative conditions. Perhaps a molecular process such as the activity-stimulated neuroprotective program identified in CA1 hippocampal neurons could also precede excitotoxicity in AD and HD. It is therefore possible that the shift in gene expression patterns observed in CA1 hippocampal neurons at 110 and 130 DPI in prion disease represents a turning-point at which the overstimulation of NMDARs changes from protection to the induction of excitotoxicity-related cell death (discussed further in *Section 4.1.7*).

4.1.5b Unfolded Protein Binding Process

Transcriptional activation of the UPR system was detected in CA1 hippocampal neurons at 90 DPI and progressively diminished as disease progressed. Chaperones including the cytosolic chaperone protein 1 *Tcp1* (reviewed in Lund, 1995) and ER heat shock protein *Hspa9* (Wadhwa *et al.,* 2002) were upregulated in CA1 hippocampal neurons during this time. Their induction likely helps mediate proper protein folding implying that these neurons contained more

misfolded proteins. In support, previous transcriptional studies also reported an induction of several genes involved in oxidative and ER stress early in disease within hippocampi structures (Brown *et al.,* 2005) and whole brain tissue (Brown *et al.,* 2004; Sorensen *et al.,* 2008; Hwang *et al.,* 2009; Reimer *et al.,* 2004).

A growing body of evidence implicated the activation of UPR to greatly contribute to prion-induced neurodegeneration. Through phosphorylation of PERK, cell shuts-down global translation which inevitably inhibits the production of essential proteins for synaptic transmission and normal function of neurons (Moreno *et al.,* 2012). Interestingly, activation of UPR within CA1 hippocampal neurons was detected early but not late in the disease course while the negative regulator of the UPR, *Ppp1R15* was found to be significantly induced during preclinical stages of disease. This gene functions to dephosphorylate eIF2α-P during mammalian development (Harding *et al.,* 2009) and is known to be transcriptionally induced when eIF2α is phosphorylated (Ma and Hendershot, 2003). Although phosphorylation levels of eIF2α or PERK were not measured in the CA1 hippocampal neurons, the induction of *Ppp1R15* may signify a response by these cells to inhibit the phosphorylation of eIF-2α, and thereby prevent a persistent global shut-down of protein synthesis.

An alternative molecular mechanism that may lead to neuronal dysfunction but is not conducive to stimulate ER stress is the ER-overload response. This response represents accumulation of both well folded and misfolded proteins within the ER causing the swelling and malfunction of the organelle. Several genes involved in neurotransmission were deregulated in CA1 hippocampal neurons in accord with previous evidence suggesting that accumulating PrP^{Sc} within the ER interfere with secretory transport of PrP^{C} and/or other proteins that are involved in

neurotransmission (Quaglio *et al.*, 2011). This suggests that synaptic abnormalities observed in prion disease may be due to disruption of the secretory pathway.

4.1.6 Validation of Select Genes Support the Detection of Neuroprotective Processes

4.1.6a Ca^{2+}/Calmodulin-Related Gene Expression

NMDA receptors are highly permeable to calcium ions and disruption of Ca^{2+} homeostasis may be the major contributing factor leading to prion disease (see *Section 1.9.2*). However, signaling through NMDARs tends to be coupled to the activation of the Ras/Erk signaling cascade. One type of mediator of this signaling is the Ca^{2+}/calmodulin-regulated guanine-nucleotide exchange factor that activates the Ras GTPases (Feig, 2011). One of its family members, *Rasgrf2*, was induced during early stages of prion disease in hippocampal neurons. Although involvement of this gene was not previously reported in prion animal studies, ischemia-induced CREB activation is reduced in the brains of adult *Rasgrf* knockout mice resulting in enhanced neuronal damage (Tian *et al.*, 2004). This suggests that *Rasgrf* and activation of CREB are important mediators of preventing neuronal damage. Similarly, two Ca^{2+}/calmodulin-dependent protein kinases termed *Camk2d* and *Camk1* were induced during early stages of prion disease. Interestingly, these are known activators of CREB and provide additional transcriptional evidence to support the observation that Ca^{2+} signaling is altered in neurons during early disease which likely enhances activation of CREB.

In addition to inducing CREB expression, Ca^{2+}/calmodulin-dependent kinases have been described to remodel chromatin by inhibiting HDAC activity through phosphorylation events (Karamboulas *et al.*, 2006). Monitoring the expression level of *Hdac9* in CA1 hippocampal neurons revealed a progressive downregulation of the mRNA levels beginning at 90 DPI in prion

infected animals. Furthermore, a large proportion of deregulated genes identified during prion disease were involved in dendrite, axon and cytoskeleton development. These data suggests that Ca^{2+} related pathways are involved in mediating gene expression by regulating chromatin remodelling mechanisms. In fact, *Hdac9* has been previously implicated in modulating neuronal morphology where knockdown of HDAC9 promoted dendrite growth (Sugo *et al.,* 2010). Remodeling of chromatin structure via *Hdac9* deregulation may therefore contribute to altering the expression of several cytoskeletal genes.

Induction of several structural genes was also confirmed by qRT-PCR. One of these genes was *Dock1* which was found to be upregulated at 70 and 90 DPI, downregulated at 110 DPI and remained unchanged during clinical disease. Previous reports have shown that *Dock1* was involved in cytoskeletal reorganization (Hasegawa *et al.,* 1996) by mediating axon outgrowth, attraction (Li *et al.,* 2008) and pruning (Xu and Henkemeyer, 2009). Additionally, *Dock1* was found to promote spine morphogenesis in cultured hippocampal neurons (Kim *et al.,* 2011).

Other genes such as *Dab2* and *Wasf2* were upregulated at preclinical prion disease in CA1 hippocampal neurons and are known to negatively regulate neuronal morphology. *Dab2* was found to be a negative regulator of neurite outgrowth (Huang *et al.,* 2007) while *Wasf2* is known to regulate dendrite spine formation (Ito *et al.,* 2010). Another cytoskeletal gene found to be significantly induced during preclinical prion disease was *Homer1*. This gene belongs to a family of dendritic scaffold proteins that regulate group 1 metabotrophic glutamate receptor (mGluR) function and has roles in dendrite morphology (Gasperini *et al.,* 2009). By binding to mGluR1, HOMER1 is able to release intracellular calcium resulting in the activation of several cellular processes such as changes in neuronal excitability, increased release of

neurotransmitters, potentiation of NMDA or AMPA receptor activity and effects on dendrite spine density and morphology (Ango *et al.,* 2000; Ango *et al.,* 2002; Lu *et al.,* 2007; Ji *et al.,* 2010). Interestingly, upregulation of *Homer1* has also been noted in neurons during early Alzheimer's disease (Xiao *et al.,* 2000; Brakeman *et al.,* 1997; Williams *et al.,* 2009). Together, these data suggests that dendrite and spine morphology is dynamically altered within the CA1 hippocampal neurons at a higher rate in prion infected as compared to control animals. This process is mediated, at least in part, by altering Ca^{2+} homeostasis.

4.1.6b Synaptic Vesicle Transport and Synaptic Plasticity

Several genes involved in intracellular vesicle and organelle transport were found to be deregulated during early stages of prion disease. Involvement of these processes with respect to prion disease has been previously reported (Moore *et al.,* 2014), implicating these processes in the pathogenesis of prion disease. In terms of CA1 hippocampal neurons, an increase in expression of 2 myosin motor genes, *Myo5* and *Myo6* were found to be induced during early prion disease. Both of these genes are known to be involved in intracellular vesicle transport, exocytosis and endocytosis. Protein expressions of these genes has been localized to synaptic structures, particularly enriched at postsynaptic densities (Rudolf *et al.,* 2011; Osterweil *et al.,* 2005; Takamori *et al.,* 2006). MYO5 has been implicated to transport numerous neuronal-specific molecules as well as cellular organelles that mediate synaptic plasticity. Some of these include mRNA molecules for stabilizing actin which through MYO5 are transported to spine heads in a Ca^{2+}-dependent mechanism (Yoshimura *et al.,* 2006), leading to the reorganization of the synapse (Okamoto *et al.,* 2004). MYO5 is also pivotal for the extension of endoplasmic reticulum into the post-synaptic sites (Wagner *et al.,* 2011) thereby enlarging the post-synaptic

membrane and increasing the number of neurotransmitter receptors; both of which augment synaptic efficacy (reviewed in Rudolf *et al.,* 2011). Furthermore, MYO5 has been implicated in the recycling of neurotransmitter receptors, such as AMPARs and some subunits of GluRs (Lise *et al.,* 2006; Correia *et al.,* 2008; Wang *et al.,* 2008). Similarly, MYO6 has also been previously implicated in the recycling of cell surface glutamate receptors such as AMPARs in hippocampal neurons as well as modifying synaptic structures (Wu *et al.,* 2002; Osterweil *et al.,* 2005).

Collectively, inducing the expression of these motor genes within CA1 hippocampal neurons during early prion disease reflect a possible stimulation of synaptic plasticity events. In fact, monitoring synaptic processes in live animals revealed that neurons within the cortex of prion-diseased animals had formed a higher number of new spines prior to symptom manifestation as compared to control animals (Fuhrmann *et al.,* 2007). The number of spines on Purkinje cells was also increased during early stages of prion-infected organotropic slice cultures (Campeau *et al.,* 2013). These data suggest that neurons are able to respond to the progression of neurodegeneration by enhancing their structural remodeling capabilities of spines. The data presented in this thesis helps elucidate some of the molecular processes that are involved in mediating these changes.

4.1.7 Neuronal Death-Related Genes

It is possible that over-stimulation of NMDARs in CA1 hippocampal neurons changes the gene expression profile from a protective to an excitotoxic pathway. To test for this possibility, our gene expression profile was compared to the previously published excitotoxicity-related transcriptional signature (Zhang *et al.,* 2009). Although genes involved in excitotoxicity were expressed in the cell bodies of CA1 hippocampal neurons, deregulation of these genes was

not detected. Furthermore, an extrasynaptic pro-death pathway is typically mediated by dephosphorylation of CREB. However, no change in pCREB levels at terminal disease between prion-infected and control animals were observed in the CA1 hippocampal neurons. Of note, only 11 pro-death genes were detected by Zhang and colleagues, a much lower number than the 185 genes for the pro-survival pathway (Zhang *et al.,* 2009). This discrepancy in gene number suggests that novel transcription is not required to induce excitotoxic cell death and regulation of this process may occur via posttranslational mechanisms.

A recent kinase screen using the same animal model of prion disease as described herein revealed that activation of MST-1 and FOXO3 at 130 DPI results in the death of neurons (Shott *et al.,* 2014). This pathway was detected from a gross macrodissection of the brain implying that neurons outside the CA1 hippocampal region were undergoing this cell death response. CA1 hippocampal neurons are highly specialized and designed to survive for a very long time. Indeed, these neurons show signs of degeneration only at EP in prion disease. Therefore, the lack of a *bonafide* pro-death transcriptional pathway was not unexpected. Profiling other regions of the brain where neurons are more vulnerable to prion disease could reveal a more pronounced transcriptional mechanism of cell death.

At first glance, these findings are somewhat contradictory to reported studies which suggest that cell death mechanisms are either initiated or dysfunctional within neurons at early stages of disease that eventually contribute to the process of degeneration (Soto and Satani, 2011). However, several individual genes known to be involved in cell death were deregulated in CA1 hippocampal neurons. Only certain pro-apoptosis markers such as *Fadd* were upregulated at 130 DPI while the lysosomal activation marker *Lamp2* was upregulated at EP. Validation of *Bad* (pro-apoptotic marker) and *Pip5k3* (regulates endosomal and lysosomal degradation) by

qRT-PCR revealed both to be downregulated at preclinical and induced at clinical disease. A catalytic subunit of calcineurin, *Ppp3ca,* was downregulated early and induced at clinical disease in CA1 hippocampal neurons. A previous study in prion-infected mice showed that hyperactivation of calcineurin leads to neuronal dysfunction (Mukherjee *et al.,* 2010) and inhibition of this pathway limited extent of neurodegeneration and increased survival (Mukherjee *et al.,* 2010). In turn, several proteosomal genes *Psmc5* and *Psmd7* were induced at both early and late stages of disease suggesting that aspects of the proteosomal pathway were activated throughout the entire disease process. The activation of select molecules in endosome/lysosome pathway likely represents debris clearing by phagocytes. However, these processes could also be induced in neurons long after synaptic alterations become apparent in order to clear the accumulating PrP^{Sc}. However, mRNA levels of autophagy marker genes such as *Atg5, Atg7* and *Becn1* were unaffected throughout the entire study suggesting that CA1 hippocampal neurons do not initiate autophagy.

4.1.8 Immune Response Pathways and Related Genes

One of the clearest molecular signatures identified within the sampled LCM region during late stages of prion disease (130 DPI and EP) was the presence of a robust inflammatory response. The detection of an inflammatory molecular signature coincides well with the activation and infiltration of inflammatory cells (astrocytes and microglia) into the neuronal region, in accordance with published data (Sorensen *et al.,* 2008; Riemer *et al.,* 2004; Hwang *et al.,* 2009). Only several inflammatory-related genes were significantly deregulated during earlier stages of disease. Some of the genes involved in cell adhesion, cell proliferation and cell-cell signaling were sequentially upregulated beginning at 110 DPI and continued to increase in

expression as disease progressed. These genes could be induced in neurons or indicate early glial activation within the CA1 hippocampal region. For example, upregulated adhesion molecule *Icam1* has been found to be typically expressed from epithelial and immune cells such as astrocytes and microglia (Kyrkanides *et al.,* 1999). In fact, enhanced expression of *Icam1* in microglial populations was documented upon immunogenic activation of these cells (Shrikant *et al.,* 1995) suggesting that in CA1 hippocampal neurons, resident microglia may be activated in response to the presence of PrP^{Sc} deposits. These adhesion molecules may be involved in the activation of phagocytosis and prion-aggregate removal and may serve as indicators of very early cellular responses to damage.

4.2 MicroRNA Expression Profiling of CA1 Hippocampal Neurons during Prion Disease

MiRNAs are critical for the proper development and function of the central nervous system (see *Sections 1.15.2-1.15.3*). Therefore, comprehensive transcriptional profiling of neurons in disease was extended to include miRNAs. In fact, modulating the expression of only one miRNA in neurons, such as miR-132-3p, is enough to significantly alter their morphology and function (see *Section 1.15.4*). On a mechanistic level, phenotypic changes exemplified by a miRNA can help pinpoint gene(s) regulated by this miRNA and thereby reveal biological pathway(s) responsible for the change in phenotype. This is made possible because profiling miRNAs result in data that is inherently less complex than mRNA profiling or proteomic analyses. MiRNA profiling was therefore performed on the same RNA sample that was used for gene expression profiling (neuronal-enriched sample). From this screen, several miRNAs were deregulated during preclinical disease and their potential implications on disease progression are discussed below.

4.2.1 MiRNAs Deregulated During Early Prion Disease

The initial screen identified 17 miRNAs to be deregulated during preclinical stages of prion disease (70-110 DPI) of which 7 were tested and further validated by qRT-PCR. The expression of 4 was additionally confirmed using *in situ* hybridization. All of these 7 miRNAs (miR-16-5p, miR-26a-5p, miR-29a-3p, miR-124a-3p, miR-132-3p, miR-140-5p and miR-146a-5p) were upregulated at early stages of disease in prion as compared to control samples. Interestingly, the expression pattern of all these miRNAs paralleled the gene expression profile.

By association, these miRNAs likely participate as regulators of biological networks as the genes that were similarly co-induced.

Unlike genes, miRNAs expressed in different cell types typically infer a different biological function that is ultimately dependent on the expression of the target mRNA. It was therefore important to confirm that these simultaneously co-expressed miRNAs were in fact expressed in neurons under normal conditions. Analyzing qRT-PCR data from control animals revealed that all 7 miRNAs were expressed at basal levels and *in situ* hybridization further showed clear neuronal-specific staining within CA1 pyramidal layer of the hippocampus. In support, other studies also detected basal expression of these 7 miRNAs within neuronal tissue including cell bodies of rat hippocampal neurons (Kye *et al.,* 2007), mouse hippocampus tissue (Zovoilis *et al.,* 2011) and primary mouse hippocampal neurons (van Spronsen *et al.,* 2013). Even the 2 least abundant miRNAs, miR-140-5p and miR-146a-5p, were previously detected in hippocampal neurons by miRNA microarrays (Park and Tang, 2009) or *in situ* hybridization (Aronica *et al.,* 2010), respectively. Although different rodent species are compared across these studies, the miRNAs in question are highly conserved and likely exhibit similar cross-species expression.

A bioinformatics target prediction approach was employed to identify a possible function mediated by these deregulated miRNAs. A large proportion of neuronal-specific functions potentially regulated by these miRNAs included neurogenesis, postsynaptic density, neuronal differentiation and projection. Collectively, these processes are involved in remodeling of neuronal structure such as synapses, spines and/or dendrites; structures that deteriorate first in prion disease. The list of potential miRNA targets were further filtered to only include downregulated genes identified by the gene expression data. This was performed to narrow down

the list of potential miRNA targets to the ones most biologically relevant at early stages of prion disease. Even after filtering, several candidate miRNAs were still predicted to regulate genes involved in neurogenesis and post synaptic density. Although not all miRNAs were strictly involved in these specific processes, all miRNAs could potentially regulate genes that function within neuronal-specific compartments including spines and synapses.

Notably, the bioinformatics filtering approach that was used for miRNA target finding provides an advantage to identify biologically relevant processes because the genes deregulated during early stages of prion disease were identified from the same sample as the miRNAs. This stringent approach however discounts possible miRNA target genes of which the transcriptional levels remain unchanged while the protein levels are deregulated. Many reports have shown that miRNAs can sequester and/or inhibit the translation of target mRNAs rather than lead to outright degradation of the messenger RNA (Baek *et al.,* 2009; Chen and Shen, 2013). In these instances, miRNA regulation can only be measured at the protein level (Baek *et al.,* 2009; Chen and Shen, 2013). Therefore, additional miRNA target genes to the ones presented in this work cannot be discounted based on the lack of change in the gene expression. Future, proteomic analysis of the CA1 hippocampal region would greatly supplement the list of target genes potentially regulated by these 7 candidate miRNAs.

One technical aspect of the bioinformatic approach needs to be considered with respect to conclusions drawn from the presented data. The identification of the potential miRNA target genes was performed by using the TargetScan algorithm. This algorithm identifies miRNA binding sites based on several criteria (Grimson *et al.,* 2007) including the perfect binding between the miRNA seed sequence and the target sequence (Lewis *et al.,* 2005; Garcia *et al.,* 2011) as well as when the seed sequence binds imperfectly to the target sequence but is

compensated by a strong binding at the 3' compensatory site of the miRNA (Friedman *et al.*, 2009). Based on the current literature, the majority of the identified miRNA confer their function by binding to the 3' UTRs of the targeted mRNAs (Baek *et al.*, 2009; reviewed in Bartel, 2009). Therefore, additional miRNA binding sites that may be present within the 5'UTR and/or CDS sequences were not considered in this analysis. However, recent evidence has indicated that miRNAs may also regulate mRNAs by binding to either 5' UTRs (Kloosterman *et al.*, 2004; Lytle *et al.*, 2007) or open reading frames (ORFs) (Reczko *et al.*, 2012). For example, miRNA binding to the 5' UTR may lead to an enhanced protein translation and increased protein levels (Henke *et al.*, 2008; Tsai *et al.*, 2009: Orom *et al.*, 2008) or lead to the downregulation of the target transcript (Grey *et al.*, 2010; Zhou and Rigoutsos, 2014). It will be interesting to determine whether these 7 miRNAs may also regulate protein expression by binding to 5' UTR or CDS regions.

4.2.2 Contribution of Individual miRNAs During Early Prion Disease

A total of 7 candidate miRNAs were significantly induced during early stages of prion disease. Several miRNAs are known to play important roles in neuronal-specific functions. In particular, miR-29a-3p, miR-124a-3p, miR-132-3p and miR-146a-5p were shown to mediate neuronal synapse formation and plasticity. Some of these were also deregulated in other neurodegenerative diseases (discussed below). Interestingly, deregulation of miR-26a-5p and miR-140-5p were not previously reported in other neurodegenerative diseases, making this the first report where these miRNAs were implicated in neurodegenerative disease. Perhaps the expression of these two miRNAs may be unique to prion disease. In terms of miR-26a-5p and miR-140-5p, their deregulation in prion disease adds significance to a possible role in neurons

(for miR-26a-5p see *Sections 4.2.2f* and *4.3*) and future study of their function may further enhance our understating of their role in prion-induced pathobiology. The next several sections will discuss the known function of these 7 miRNAs in neurons and how that relates to prion disease and other neurodegenerative diseases (**Figure 4.2**).

4.2.2a miR-124a-3p

MiR-124a-3p is one of the most studied miRNAs in the nervous system and was identified to play a major role in differentiation and neurogenesis (reviewed in Meza-Sosa *et al.*, 2014). This miRNA mediates the differentiation between progenitor cells into mature neurons (Makeyev *et al.,* 2007; Krichevsky *et al.,* 2006) and promotes embryonic (Maiorano and Mallamaci, 2009; Visvanathan *et al.,* 2007) and adult neurogenesis *in vivo* (Cheng *et al.*, 2009). Several gene targets have been identified to illuminate parts of the molecular mechanisms responsible for mediating these processes. One miR-124a-3p gene target is Ephrin-B1 (Arvanitis *et al.,* 2010) which functions in regulating cytoskeletal dynamics (reviewed in Pasquale, 2008). Neurons over-expressing miR-124a-3p had increased neurite outgrowth (Maiorano and Mallamaci, 2009; Arvanitis *et al.*, 2010; Gu *et al.*, 2014) by mediating GTPase Rho kinases such as *Rock1* (Gu *et al.,* 2014) and other genes that may be directly involved in cytoskeletal reorganization (Yu *et al.*, 2008).

In addition to regulating neuronal morphology, miR-124a-3p was implicated in preventing neuronal apoptosis both during development and in trauma. By downregulating *Lhx2*, miR-124a-3p helped prevent apoptosis of hippocampal and retinal neurons during development and, in turn, stimulated neurogenesis (Sanuki *et al.,* 2011). Similarly, over-expression of miR-124a-3p decreased the damaged area and neuronal apoptosis induced by oxygen and glucose

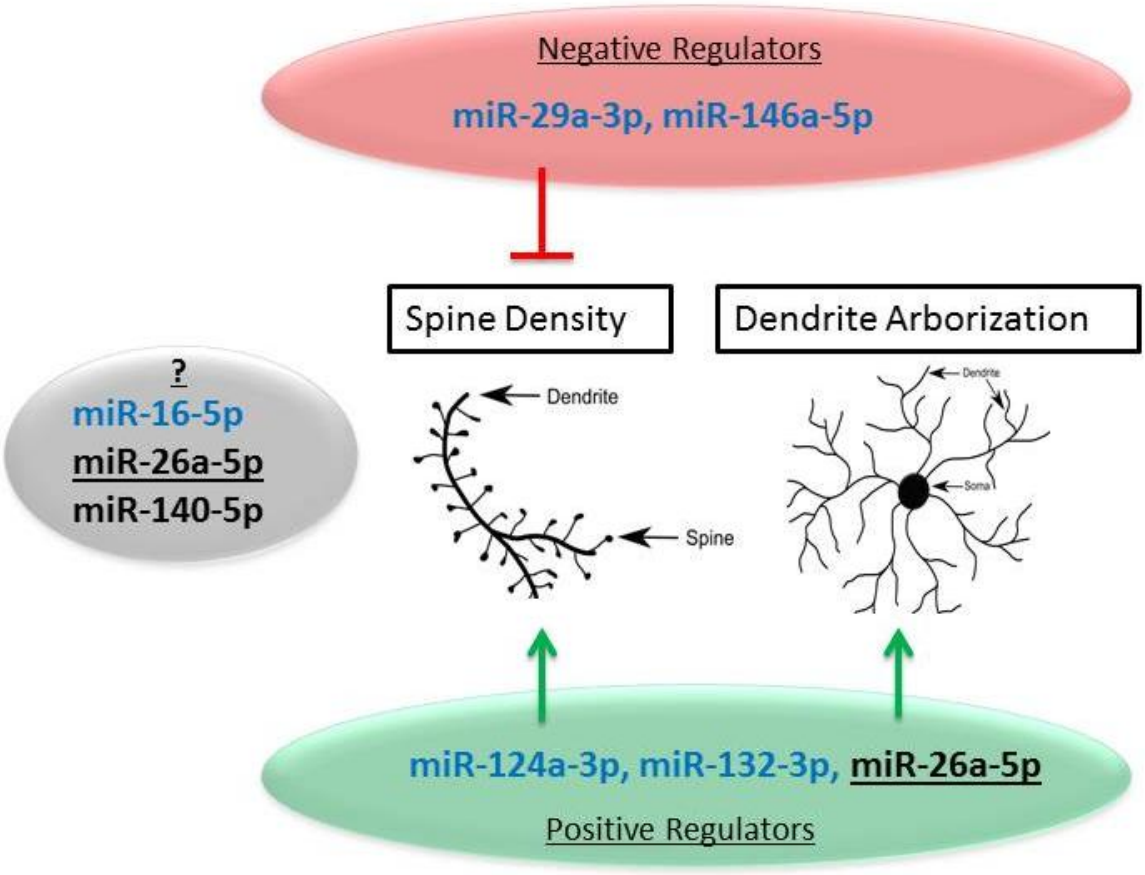

Figure 4.2. Schematic diagram showing involvement of preclinically deregulated miRNAs in neuronal function. From the 7 preclinically confirmed miRNAs, 4 were previously functionally characterized in neurons. MiR-29a-3p and miR-146a-5p were found to negatively regulate spine density while miR-124a-3p and miR-132-3p positively regulated both spine density and dendrite arborization. In turn, miR-16-5p, miR-26a-5p and miR-140-5p remained uncharacterized in neurons. Of these miRNAs, 5 are highlighted in blue to indicate their deregulation in other neurodegenerative diseases. MiRNAs highlighted in black are the first to be identified in neurodegenerative disease. MiR-26a-5p is underlined because it was tested hereine to have a positive regulatory effects on spine density and dendrite arborization.

deprivation in an animal model of ischemic stroke (Sun *et al.,* 2013; Doeppner *et al.,* 2013). Perhaps miR-124a-3p mediates a dual function in prion disease where it modulates cytoskeletal reorganization which may in turn help protect neurons.

Deregulation of miR-124a-3p has been observed in other neurodegenerative diseases including Alzheimer's disease (Smith *et al.,* 2011), Huntington's disease (Packer *et al.,* 2008; Morel *et al.,* 2013) and Amyotrophic lateral sclerosis (Marti *et al.,* 2010). The expression of miR-124a-3p was downregulated in these diseases at late stages, similar to its expression in CA1 hippocampal neurons. This suggests that a possible common molecular mechanism drives downregulation of numerous miRNAs including miR-124a-3p. By corollary, it is possible that miR-124a-3p is induced during preclinical stages in these other neurodegenerative diseases.

4.2.2b miR-132-3p

Activity-induced transcription of miR-132-3p is dependent on the activation of CREB (Vo *et al.,* 2005; Wayman *et al.,* 2008). Stimuli including neurotrophins (Vo *et al.,* 2005; Wayman *et al.,* 2008), contextual fear conditions and exposure to odorants also increased miR-132 expression (Nudelman *et al.,* 2010). In prion disease, activity-dependent neuroprotective programs mediated by pCREB were detected in CA1 hippocampal neurons during preclinical disease. It was therefore not surprising to detect the upregulation of miR-132-3p in the CA1 hippocampal region in prion-infected animals during early disease considering its CREB-dependent transcription.

MiR-132-3p is able to modulate dendrite and synaptic plasticity. By regulating several genes, including the Rho family GTPase-activating protein p250GAP which is involved in neuronal differentiation (Nakazawa *et al.,* 2003), miR-132-3p can modulate dendrite morphology

in vitro (Vo *et al.*, 2005; Wayman *et al.*, 2008) and *in vivo* (Magill *et al.*, 2010). Perhaps the induction of miR-132-3p during preclinical prion disease contributes to the observed increase in morphological alterations. Deletion of the miR-132 locus in mice leads to decreased spine density, dendrite length and arborisation of newborn hippocampal neurons (Magill *et al.*, 2010) suggesting that downregulation of miR-132-3p at clinical disease could also contribute to spine loss during prion disease. Conversely, when miR-132-3p is expressed within CA1 hippocampal neurons at early disease, the number of stubby and mushroom shaped spines exhibiting longer protrusion widths could be enhanced in CA1 hippocampal neurons, as observed in miR-132-3p over-expressing rat hippocampal neurons (Edbauer *et al.*, 2010). Since the shape of spines tend to dictate activity, neurons devoid of miR-132-3p showed reduced basal synaptic transmission and plasticity although spine number was the same as for wild-type (Remenyi *et al.*, 2013). In fact, knock-down of miR-132-3p expression using a miRNA sponge led to reduced spontaneous excitatory postsynaptic currents (Luikart *et al.*, 2011). Collectively, this evidence strongly suggests that miR-132-3p plays a key role in activity-dependent structural and functional plasticity. Understanding the mechanistic role of miR-132-3p in prion-induced neurodegeneration could help explain some of these neuropathological changes that occur during disease.

Recent evidence proposes that miR-132-3p has a neuroprotective role in Alzheimer's disease. By directly repressing key players of the FOXO3A death axis, including FOXO3A, miR-132-3p was able to abrogate apoptosis in neurons (Wong *et al.*, 2013). The authors found that miR-132/212 expression was decreased in AD patients while FOXO3A protein levels were increased at clinical stages of disease. The same mechanism may be occurring within hippocampal neurons of prion-infected animals. During early disease, miR-132-3p is

significantly induced in CA1 hippocampal neurons and begins to decrease at clinical disease. Only at clinical disease were FOXO3A protein levels significantly increased within prion-diseased hippocampi structures (Shott *et al.,* 2014). This miRNA-mediated protective mechanism may partially explain the observed robustness of CA1 hippocampal neurons considering that their degeneration was only detected during late stages of prion disease. If that is the case, enhancing the expression of miR-132-3p within these animals before clinical disease may help prolong disease onset.

MiR-132-3p was downregulated in patients with Alzheimer's disease (Cogswell *et al.,* 2008; Hebert *et al.,* 2008; Hebert *et al.,* 2013; Wong *et al.,* 2013: Lau *et al.,* 2013), Huntington's disease (Johnson and Buckley, 2009; Lee *et al.,* 2011) and also in animal models for Parkinsons' disease (Gillardon *et al.,* 2008). Collectively, deregulation of miR-132-3p in several neurodegenerative diseases suggests it is involved in a common process of neurodegeneration.

4.2.2c miR-146a-5p

The function of miR-146a-5p was first described in monocytes (Taganov *et al.,* 2006) and later in glia (Saba *et al.,* 2012) as a negative regulator of immune activation. However, miRNAs are known to evoke multifunctional properties in different cell-types of which miR-146a-5p is a great example. Recent studies in primary mouse hippocampal cultures revealed that miR-146a-5p modulates synaptic plasticity by repressing MAP1B protein synthesis (Chen and Shen, 2013). Contrary to the function of the other 2 miRNAs described above, miR-146a-5p promotes the impairment of long-term depression in neurons. MAP1B is involved in the formation and maturation of dendritic spines and when the protein expression is decreased, it results in the formation of immature filipodia-like protrusions rather than mature dendritic spines

(Tortosa *et al.,* 2011). In addition, deficiency of MAP1B alters synaptic plasticity by impairing long-term depression (LTD) as a result of failing to trigger AMPA receptor endocytosis and spine shrinkage during LTD (Benoist *et al.,* 2013). During prion disease, expression of *Map1b* remained unchanged in CA1 hippocampal neurons suggesting that miR-146a-5p does not regulate this mechanism. However, MAP1B protein levels should be tested to confirm this observation.

Deregulation of miR-146a-5p is well reported in other neurodegenerative diseases, especially Alzheimer's disease. However, these reports focus exclusively on sampling terminal stages of disease. Discussion of miR-146a-5p expression at terminal prion disease is addressed in a later section, *Section 4.2.3*.

4.2.2d miR-29a-5p

Similar to the function described for miR-146a-5p, miR-29a-5p was proposed to potentially function to counterbalance excessive positive cues to stimuli at the synapse (Lippi *et al.,* 2011). Specifically, miR-29a-5p binds to *Arpc3*, a component of the ARP2/3 actin nucleation complex (Goley and Welch, 2006). This complex regulates the morphology of dendritic spines (Lippi *et al.,* 2011) and when miR-29a-5p is over-expressed in hippocampal neurons, the number of mushroom-shaped spines is reduced while filipodia-like outgrowths became more frequent (Lippi *et al.,* 2011). This miRNA could therefore disrupt synapses that become over-stimulated, such as observed in neurodegenration.

Over-activation of synapses has been linked to prion disease (Collinge *et al.,* 1994; Maglio *et al.,* 2004; Khosravani *et al.,* 2008). It is possible that CA1 hippocampal neurons utilize miR-29a-5p to sever the connections between synapses that become over-stimulated in an

attempt to preserve the longevity of the neuron receiving the aberrant signal. In support of this possibility, knockdown of miR-29 in animal studies resulted in massive areas of cell death (Roshan *et al.,* 2014) while morphological analysis revealed that neuronal cells such as the Purkinje cells located within the cerebellum were smaller and less arborized than controls (Papadopoulou *et al.,* 2014).

Recent *in vitro* data suggests that miR-29a-5p is induced by glutamate receptor activation in mouse primary neurons and leads to enhanced degree of axonal branching by targeting and downregulating doublecortin in development of mouse cerebrum (Li *et al.,* 2014). In prion disease, glutamate receptor over-stimulation may also lead to the activation of miR-29a-5p expression which, in turn, modulates neuronal morphology. Another gene target identified for miR-29a-5p was the Huntingtin interacting protein 1 (HIP1) (Papadopoulou *et al.,* 2014) which is important for NMDAR function (Metzler *et al.,* 2007) and endocytosis of AMPAR s (Metzler *et al.,* 2003) within the hippocampus. Neurons deficient in HIP1 have shown partial protection against NMDA-dependent excitotoxicity (Metzler *et al.,* 2007), a toxicity that was implicated in prion disease (Khosravani *et al.,* 2008). Based on the microarray data, expression of *Hip1* was approximately 2-fold higher in prion infected hippocampal neurons as compared to controls at 90 DPI, a time when miR-29a-5p reached its maximum induction (~3-fold increase). It is possible that miR-29a-5p was induced in these neurons to control the expression levels of *Hip1*and thereby help protect neurons against toxicity. When a spine is over-stimulated, local miR-29a-5p expression may induce a structural change from a mushroom to a filipodia-like spine and thereby sever that toxic connection.

In terms of other neurodegenerative diseases, miR-29a-5p expression was downregulated in Alzheimer's (Hebert *et al.,* 2008; Geekiyanage and Chan, 2011; Wang *et al.,* 2011; Shioya *et*

al., 2010) and Huntington's diseases (Johnson *et al.,* 2008). Based on the potential protective function of miR-29a-5p in neurons, downregulation of this miRNA during disease progression may further contribute to the pathogenicity of neurodegenerative diseases.

4.2.2e miR-16-5p

Although a neuronal-specific function of miR-16-5p has not been well studied, this miRNA has been found to regulate a number of targets of which one is the amyloid protein precursor (APP) and other proteins involved in amyloid processing. In an animal model of early-onset Alzheimer's disease, APP was increased while the expression of miR-16-5p was decreased (Liu *et al.,* 2012). Short term infusion of miR-16-5p into the brain of diseased mice caused a decrease in APP accumulation suggesting that miR-16-5p has an inhibitory effect on APP protein formation (Liu *et al.,* 2012) and acts as a protective molecule in disease. Perhaps miR-16-5p may also play a similar neuroprotective role in prion-diseased mice.

Interestingly, miR-16-5p was upregulated in patients with early but downregulated in patients with late Alzheimer's disease (Muller et al. 2014). This observation is in parallel with the prion data studied in this dissertation. Deregulation of miR-16-5p was also observed in a genetic animal model of Parkinson's disease (Dorval *et al.,* 2014) further supporting the involvement of miR-16-5p in the neurodegenerative process.

4.2.2f miR-26a-5p

Only recently has there been evidence to suggest that miR-26a-5p directly modulates the morphology of neurons and could therefore impact progression of neurodegenerative disease. By targeting *Pten*, an inhibitor of cell growth, miR-26a-5p was able to markedly enhanced neurite

outgrowth in primary rat cortical neurons (Li and Sun, 2013). Interestingly, microarray data of the CA1 hippocamapal neurons showed that the expression of *Pten* was downregulated at preclinical prion disease, a time that coincides with an induction of miR-26a-5p expression. Perhaps under duress, neurons that become slightly impaired are able to induce the growth of neurites by over-expressing miR-26a-5p. In support of a positive effect of this miRNA on neuronal survival, *in vitro* experiments in chicken retina cells revealed that miR-26a-5p expression was activated by CREB (Shi *et al.,* 2009). Furthermore, upregulation of miR-26a-5p in mouse dorsal root ganglia neurons reduced apoptosis induced by bupivacaine and promoted neurite outgrowth by downregulating *Pten* expression (Cui *et al.,* 2015). It is conceivable that CREB also activates the expression of miR-26a-5p in the CA1 pyramidal layer of hippocampal neurons to reduce apoptosis signals. Aside from the detected deregulation in prion disease, there is currently no data implicating miR-26a-5p in other neurodegenerative diseases.

4.2.2g miR-140-5p

Although little is known about the function of miR-140-5p in neurons, evidence does point to its involvement within the central nervous system. MiR-140-5p has been identified to target *Egr2,* which allows it to modulate myelination in dorsal root ganglion and Schwann cell co-cultures (Viader *et al.,* 2011). There is no information currently available implicating the deregulation of miR-140-5p in other neurodegenerative diseases.

4.2.2h Convergent Function of 7 Candidate miRNAs in Early Prion Disease

Collectively, upregulation of these 7 miRNAs during preclinical prion disease implicates their role in prion-induced neuronal responses. Based on the literature, the majority of these

miRNAs (5 out of 7) are directly involved in regulating synaptic and dendrite morphology; which fits very well with the ontological assignments of the identified list of deregulated genes. Dendritic spines tend to be fairly dynamic throughout the lifetime of a healthy neuron (Chen *et al.,* 2014). However, spine remodelling is even more dynamic in prion disease where spines are gained and lost much faster in prion-infected as compared to control animals (Fuhrmann *et al.,* 2007). This remodeling occurs before the symptomatic phase which correlates with the increase in miRNA expression. As such, the co-expression of these 7 miRNAs in CA1 hippocampal neurons during early prion disease may further boost the structural remodelling capability of neurons. Even though the function of miR-16-5p, miR-26a-5p and miR-140-5p in neurons is fairly limited, these miRNAs may also contribute to this process.

One important consideration when analyzing these data is that the sample used for these experiments represent hundreds of neuronal cell bodies. It is possible that each of the 7 induced miRNAs is expressed in different CA1 hippocampal neurons. However, *in situ* hybridization revealed a profound and uniform staining pattern of these miRNAs in CA1 hippocampal neurons suggesting that the same neurons express all of these miRNAs during early disease.

Once expressed, it is likely that these miRNAs are then transported to different synaptic locations to mediate local synaptic plasticity. Although *de novo* synthesis of miRNAs that occurs in the nucleus was measured herein, it is possible that these miRNAs are then transported to distal spines to regulate synaptic plasticity. Several of these miRNAs may function to disrupt spine structures (miR-29a-3p and miR-146a-5p) while other miRNAs at different locations help mediate spine growth (miR-132-3p and miR-124a-3p). Previous data identified a large subset of these miRNAs within synaptoneurosomes (Ho *et al.,* 2014) supporting a possible functional role of these miRNAs at synaptic structures during prion disease. It would therefore be beneficial to

monitor the miRNA content within synaptoneurosomes from prion-infected animals to identify which miRNAs are deregulated and what is the potential local impact of these miRNAs on spine structure and function.

4.2.3 MiRNAs Deregulated at Clinical Prion Disease

Although several publications have reported a change in miRNA expression within prion infected brain tissue, none thus far have looked at miRNA deregulation in a neuronal-enriched sample. It was therefore interesting to determine which miRNAs were deregulated during late stages of prion disease, a time representing glial activation/invasion into the region profiled. Analogous to the gene expression data, it was not surprising to identify that a large proportion of deregulated miRNAs were implicated in immunogenic stimulation of glial cells. In fact, almost all miRNAs that were either significantly deregulated or only expressed in prion samples at clinical disease were also identified in activated astrocytes (Mor *et al.,* 2011). Interestingly, several of these miRNAs were also induced upon immunogenic stimulation of microglia (Saba *et al.,* 2012; Kong *et al.,* 2014), further indicating glial presence within the CA1 hippocampal region.

One miRNA in particular, miR-146a-5p, is a well-known immune regulatory miRNA that was induced at clinical stages of prion disease in CA1 hippocampal neurons. Increased expression of miR-146a-5p was previously detected in scrapie-infected whole mouse brain at terminal disease (Saba *et al.,* 2008), and in patients with sCJD or GSS (Lukiw *et al.,* 2011). Deregulation of miR-146a-5p was also observed in Alzheimer's disease patients (Muller *et al.,* 2014; reviewed in Alexandrov *et al.,* 2014) suggesting that this miRNA may in fact be a general

marker for neuroinflammation. By corollary, other miRNAs that were similarly expressed as miR-146a-5p at terminal disease may also hold similar neuroinflammatory roles.

In immune cells, miR-146a-5p is known to be a dominant, negative regulator of immune function by regulating the expression of genes such as *Traf*5 and *Irak1*, which effectively leads to the suppression of inflammatory responses (Taganov *et al.*, 2006). Specifically within microglia cells, miR-146a-5p was predicted to target genes involved in modifying microglial morphology and thereby altering activation states of these cells (Saba *et al.*, 2012). However, the significant downregulation of miR-146a-5p at 130 DPI in CA1 hippocampal neurons suggest that this miRNA is likely expressed from activated astrocytes rather than microglia. From the pathological analysis of the CA1 hippocampal region, microglia cells were detected within this region beginning at 130 DPI while astrocytes were only detected at EP. Furthermore, immunogenic stimulation of microglia failed to induce miR-146a-5p expression (Saba *et al.*, 2012).

An interesting observation attributed to miR-146a-5p expression levels was its biphasic induction during prion disease. This miRNA was upregulated in CA1 hippocampal neurons during preclinical prion disease (see *Section 4.2.2c*). Clearly, the versatility and multifunctionality of miR-146a-5p in the progression of prion disease with respect to the different cell-types involved in prion-induced pathology makes this miRNA a great candidate for further study. It will be interesting to determine whether miR-146a-5p plays a positive or negative role in the process of neuronal degeneration.

Of note, miR-494-3p was not detected while expression of miR-342-3p was not changed in the pyramidal layer of CA1 hippocampal neurons during prion disease. Both of these miRNAs were previously upregulated at terminal prion disease of scrapie-infected mice (Saba *et al.*, 2008)

and BSE-infected macaques, a model for CJD (Montag *et al.*, 2009). Although miR-342-3p was detected in the CA1 hippocampal region, the expression level was low when compared to other regions of the brain, such as the cerebellum (data not shown). Therefore, alteration in miR-342-3p and miR-494-3p expression likely originates from other regions of the brain besides CA1 neurons of the hippocampus.

4.2.4 MiRNAs Induced Upon Stimulation of Acquired Neuroprotection in Primary Mouse Hippocampal Neurons

The induction of 7 miRNAs during early prion disease mirrored the expression of the activity-dependent neuroprotective gene signature that was induced at this time in CA1 hippocampal neurons. By corollary, perhaps these 7 miRNAs are also involved in mediating this neuroprotective process. To test for this possibility, primary mouse hippocampal cultures were pharmacologically stimulated to induce this protective response and the expression of these miRNAs was tested. From the 7 candidate miRNAs, 4 (miR-16-5p, miR-26a-5p, miR-29a-3p and miR-132-3p) were significantly, albeit slightly upregulated after 16 hours post stimulation. Although it is possible that these miRNAs may be induced to suppress the expression of activity-dependent neuroprotective genes, it is more likely that these miRNAs are upregulated in order to stimulate a protective response. To corroborate the latter possibility, miR-132-3p is well known to be induced by pCREB and functions as a neuroprotective miRNA (discussed in more detail in *Section 4.2.2b*). Genes involved in the neuroprotective response, such as *Fos* and *Homer1*, were also induced upon stimulation of these cultures (data not shown). These data therefore suggests that 4 miRNAs that were induced in neuron during early prion disease may be involved in mediating an acquired neuroprotective response induced by synaptic activity. Interestingly, 3

(miR-26a-5p, miR-29a-3p and miR-132-3p) out of these 4 miRNAs are known to remodel synaptic and/or dendrite structures.

4.3 Functional Characterization of miR-26a-5p

This is the first study to implicate miR-26a-5p in prion disease and the process of neurodegeneration. However, no information was available as to its function in neurons. Therefore, this miRNA was chosen for further study to understand its functional role in neurons.

Data obtained from the previous aim implicated miR-26a-5p to be involved in regulating several neuronal-specific processes that were altered during prion-induced neurodegeration (see *Section 4.2.1*). Furthermore, this miRNA was induced upon activity-stimulated neuroprotective responses in primary neuronal cultures (see *Section 4.2.4*) suggesting its involvement in mediating this process. Previously, miR-26a-5p was found to be induced by CREB (Shi *et al.*, 2009) and may therefore function to enhance neuronal structural features in a similar manner to another CREB-induced miRNA, miR-132-3p. By determining whether miR-26a-5p can alter neuronal morphology, the potential targets that can mediate this process can be identified.

To perform these experiments, primary mouse hippocampal neurons were first established within the laboratory by me and Dr. Reuben Saba (post-doc in the laboratory). These cultures were characterized for several essential features to confirm the presence of long-lived, viable neurons. Subsequently, gain-of-function studies for miR-26a-5p were performed which showed that this miRNA not only increased dendrite arborisation but also spine density.

4.3.1 Primary Mouse Hippocampal Cultures

To obtain a better appreciation as to the function of a miRNA in terms of neuronal context, most neuroscientists use primary cultures for their work. The reason is that clonal cell lines do not form well-defined axons or dendrites and fail to form synapses, even when

stimulated with neurotrophins. In this study, primary mouse hippocampal cultures were established in the laboratory to characterize the function of miR-26a-5p in neurons.

The hippocampal region was specifically used as the basis of this culture because of several reasons. The population of nerve cells comprising the hippocampus is relatively simple when compared to most other regions of the CNS. In particular, excitatory pyramidal neurons account for the vast majority of the total neuronal population of the hippocampus with only approximately 6% of the population consisting of inhibitory interneurons which are morphologically distinct from excitatory pyramidal neurons (Benson *et al.*, 1994). Furthermore, cultured pyramidal neurons express many of the phenotypic features seen *in vivo* including well developed dendrites and spines, allowing neurons to make extensive and synaptically connected networks. Lastly, these cultures are typically prepared from late-embryonic brain tissue because at that time in development, the generation of pyramidal neurons is essentially complete while dentate granular neurons have not yet begun to form (Banker and Cowan, 1977). The hippocampus at this stage also contains comparatively few glial cells which tend to be the major source of contamination in these cultures. However, neurons used for this work were cultured in an environment that lacked the commonly used mitotic inhibitor, cytosine arabinoside (AraC), which allowed for the expansion of dividing cells such as astrocytes. The main advantage of not using a mitotic inhibitor in neuronal cultures is that at later stages of culture development, the presence of glia helps promote neuronal survival and enhance synapse formation and synaptic transmission (Haber *et al.*, 2006; Jones *et al.*, 2012).

For these reasons, primary mouse hippocampal cultures were first characterized to confirm the presence of the classic phenotypic features of primary neuronal cultures. Indeed, the culture consisted primarily of viable, long-lived neurons where less than 30 % of the culture was

made up of glia (*i.e.* astrocytes) at any given time over the 20 day culture period. This is comparable to the literature where primary rat hippocampal cultures that were not treated with AraC consisted of ~50 % astrocytes at 21 days *in vitro* (van Spronsen *et al.,* 2013). Subsequently, maturation of neurons was also measured. Neurons matured by 12 DIV when cultured in a nutrient enriched medium, similar to what was expected (Brewer *et al.,* 2008). Therefore, treatment of these cultures at 12 DIV allowed to monitor possible effects of miR-26a-5p on neuronal morphology because the measured structures were detected in these neurons by that time.

One important consideration when interpreting the data obtained from these cultures is the presence of astrocytes. The number of astrocytes between 8-14 days in culture was much higher than the steady number between 2-6 days in culture. However, even when these glia cells were propagating, they did not over-run the neurons at any time during the life-span of the culture. This suggests that astrocytes were responding to an environmental cue to replicate but their replication was controlled. It is likely that astrocytes were proliferating in order to provide adequate trophic support for maturing neurons. This is because when neurons mature, astrocytes are necessary for proper spine and synapse structure formation (Haber *et al.,* 2006; Jones *et al.,* 2012). In support, immunohistochemistry staining for post-synaptic structures using PSD-95 antibody revealed that neurons were beginning to form synaptic structures as early as 8-10 DIV. It is possible that astrocyte numbers were therefore required for proper structure formation and with the progressive death of neurons, the number of astrocytes diminished. On the other hand, progressive neuronal death could stimulate activation of astrocytes although this is less likely because a much larger proportion of astrocytes would have been expected by16- 20 DIV.

4.3.2 Endogenous Expression of miR-26a-5p

The basal expression of a miRNA within a culture provides clues as to the function of that miRNA within the biological system. MiR-26a-5p was expressed in primary mouse hippocampal neurons at comparable Ct values to miR-132-3p throughout the lifetime of the culture. In support, previous data found that miR-26a-5p is enriched in dendrites of primary rat hippocampal neurons at comparable levels to a neuronal-enriched miRNA, miR-132-3p (Kye *et al.*, 2007).

MiR-26a-5p was induced at a significant, albeit modest level when neurons were growing and reaching maturity. A similar temporal pattern of expression was observed for miR-132-3p although its induction was much more pronounced than for miR-26a-5p. Considering that miR-132-3p functions during neuronal differentiation and maturation (Pathania *et al.*, 2012), it was not surprising to confirm its expression during these stages of culture development. By corollary, the temporal expression pattern of miR-26a-5p within the culture also suggests possible involvement in neuronal maturation. In contrast, the expression of miR-146a-5p, although known to occur within neurons, was detected within the primary mouse hippocampal culture at relatively low levels when compared to miR-26a-5p. Furthermore, its expression remained unchanged throughout the lifetime of the culture indicating that miR-146a-5p is not required for neuronal maturation.

As a note, miR-26a-5p is also known to be expressed by astrocytes at basal and inducible conditions (Mor *et al.*, 2011). Addition experiments such as *in situ* hybridization may be performed to confirm neuronal specific expression of miR-26a-5p.

4.3.3 Lentiviral Delivery, miR-26a-5p Expression and Cell Death Analysis in Primary Mouse Hippocampal Cultures

Primary mouse hippocampal cultures that were transduced with lentiviruses at an MOI ≈ 0.2 resulted in GFP positive neurons that had well defined dendrites and spines after 4 days post transduction. This culture contained well-isolated GFP positive pyramidal cells for analysis. The induction of miR-26a-5p was less pronounced than when cells were transduced at MOI ≈ 2. This is expected because only a small population of cells within the culture would be over-expressing miR-26a-5p at the lower MOI. However, its expression level is reflective of the amount within those transduced neurons which undoubtedly contain much more copies of miR-26a-5p.

Lentiviral delivery does not typically induce cell death in primary neurons, however, over-expression of certain molecular elements including miRNAs have been shown to promote death in cells (Grimm *et al.*, 2006). Therefore, LDH assay was used to confirm that the lentivirus and miRNA expressed does not lead to death of neurons. LDH assay was able to detect basal cell death of these post-mitotic neurons which typically occurs as the culture ages, however, no change in cell death was observed after treatment with the lentivirus. Based on these data, lentiviral transduction and miRNA induction did not appear to be toxic to these neurons.

4.3.4 Over-expression of miR-26a-5p in Primary Mouse Hippocampal Cultures Enhances Dendrite Arborization and Spine Density

Single cell analysis using gain-of-function studies showed that over-expression of miR-26a-5p altered the structure of mature pyramidal neurons. In particular, hippocampal pyramidal neurons were more arborized and showed higher spine densities in miR-26a-5p over-expressing

cells as compared to the scrambled sequence. This suggests that the function of miR-26a-5p in neurons is to promote outgrowth of dendrites and spine formation.

During the course of this work, published data emerged on the potential role of miR-26a-5p on neuronal morphology which corroborated these findings. One publication reported that miR-26a-5p promoted neurite outgrowth in rat cortical cultures. The authors found that by decreasing the expression of PTEN, miR-26a-5p was able to promote the growth of neurites (Li and Sn, 2013). Another publication reported that the expression of miR-26a-5p in rat hippocampal cultures significantly increased the length of the axon (van Spronsen *et al.,* 2013) further supporting a role of this miRNA in promoting neuronal outgrowth. Recent data in mouse dorsal root ganglia revealed that miR-26a-5p not only promoted outgrowth of neurites but also ameliorated bupivacaine-stimulated apoptosis by suppressing *Pten* (Cui *et al.,* 2015). Collectively, these data suggests that miR-26a-5p may be involved in remodelling spine and dendrite structures which could potentially result in inhibiting apoptosis. Perhaps during prion disease, induction of this miRNA helps to prevent neuronal injury induced by the replicating PrP^{Sc}.

5.0 CONCLUSIONS

6.0 FUTURE DIRECTIONS

5.0 Conclusions

Prion diseases are fatal and currently incurable neurodegenerative diseases of the brain that share many common early pathological features to AD, HD and PD. One of the earliest is progressive loss of synapses and spines that occurs well before clinical manifestation. These earliest pathologies are therefore a measurable readout for when neurons begin to genetically respond to the disease process. As such, transcriptional profiling revealed clues to which cellular pathways are altered at the start of disease and thereby reveal possible targets for therapy development and/or identification of useful preclinical biomarker(s). Furthermore, these earliest pathologies hint at the perturbation of a common molecular mechanism that is at the center of these diseases and by identifying these pathways, a universal therapy to combat neurodegeneration becomes quite plausible. However, our current understanding of the molecular mechanisms mediating this early pathology is extremely limited and was therefore the focus of this thesis.

The prion mouse model was used to study neurodegeneration because it recapitulates almost all of the pathological hallmarks of prion disease in patients. A neuronal-enriched sample was physically isolated from the brain of these animals and was used to temporally delineate deregulation in the transcriptional profile. From this profile, a transcriptional signature reminiscent of an activity-dependent neuroprotective program was induced during preclinical disease which dissipated as disease progressed and was lost at clinical disease. This suggests that CA1 hippocampal neurons have the capability of mounting a neuroprotective transcriptional program that is driven by synaptic activity. The detection of this neuroprotective gene signature was further corroborated by a marked increase in phosphorylation of pCREB (neuroprotective

transcription factor) within these neurons during early disease and subsequent validation of numerous neuronal-specific genes by qRT-PCR, several of which are known to be induced by pCREB. Collectively, these data are the first to indicate that neurons are able to mount a protective response to the replicating PrP^{Sc}.

In conjunction with the gene expression profile, miRNA expression profiling of these neuronal-enriched samples also revealed the induction of numerous miRNAs during preclinical disease. Several preclinically induced miRNAs were further validated by qRT-PCR and *in situ* hybridization which paralleled the neuroprotective gene expression profile, implying their possible involvement in this cellular process. In fact, many of these miRNAs can modulate synaptic and spine structures, the very same structures first degraded during neurodegeneration. It is likely that these miRNAs are induced in response to the replicating PrP^{Sc} which may allow the affected neuron to remodel its spines and synapses at a much higher rate. One of these miRNAs, miR-132-3p, is especially well known for its remodeling capabilities of neuronal structures both *in vitro* and *in vivo*. In fact, this miRNA is induced by pCREB and is considered a neuroprotective miRNA that has recently been shown to abrogate apoptosis in neurons. Perhaps other miRNAs that were induced during early stages of prion disease also function in a similar manner which may help protect neurons from disease.

To determine if preclinically induced miRNAs for which neuronal function was not studied were able to remodel dendrites and spines, I performed a functional characterization on one of these miRNAs, miR-26a-5p. Primary mouse hippocampal neurons were established in the laboratory and long-lived, neuronal cultures were consistently prepared. Performing gain-of-function studies in these primary mouse hippocampal cultures revealed that over-expression of miR-26a-5p enhanced dendrite arborisation and spine density. This implies that miR-26a-5p was

induced in CA1 hippocampal neurons to further augment the structural remodeling capabilities of these cells during early disease.

Collectively, the work presented in this thesis contributed to the understanding of the neurodegenerative process in prion disease by several factors. The first chapter described the identification of an activity-dependent neuroprotective transcriptional program that was induced in CA1 hippocampal neurons during early prion disease. By identifying this transcriptional program, a temporal window for potential therapeutic intervention was identified. Furthermore, profiling miRNAs revealed that a number of these mirrored the neuroprotective signature which suggests that these regulatory RNAs may also play a role in mediating a protective state in these neurons. Lastly, gain-of-function studies for miR-26a-5p in primary hippocampal neurons were performed to determine its potential function during prion disease. Similar to other protective miRNAs induced preclinically in prion disease, miR-26a-5p was also able to modulate spine and dendrite structures, further contributing to enhancing the structural plasticity of these neurons. Better understanding of the intricate molecular mechanisms dictating the neuroprotective process and how miRNAs are involved may help elucidate suitable targets for therapy development.

6.0 Future Directions

Data presented in my thesis describe a temporal deregulation in both gene and microRNA expression within CA1 hippocampal neurons during prion-induced neurodegeneration. The identification of a protective molecular response induced during early stages of prion disease encourages the persuit of several aims to address in future studies.

One of the most feasible and immediate aims to persue is to characterize the potential function of miR-16-5p and miR-140-5p in primary mouse hippocampal neurons. From my research, this is the first instance in which these 2 miRNAs have been implicated in neurodegenerative diseases; however, their function in neurons remains unknown. To elucidate a functional role of these miRNAs on neuronal morphology, an analogous approach as the one described herein for miR-26a-5p can be used. As such, gain-of-function studies followed by single cell morphological analysis can be performed in primary mouse hippocampal neurons. Subsequent functional studies can be carried out on miR-16-5p, miR-140-5p as well as miR-26a-5p to identify the target(s) and therefore the molecular mechanism by which these miRNAs confer the observed morphological effects. Electrophysiological studies can be performed in tandem to delineate potential physiological effects when the expression of these miRNAs is modulated in neurons. Future study into the location of these miRNAs within neuronal cells could help reveal possible functional roles during prion disease.

Some of the miRNAs identified to be deregulated during the preclinical stages of disease are known to function in synapses. These neuronal structures are the first to be disrupted during prion-induced neurodegeneration and involvement of miRNAs during this dynamic process still is poorly characterized. In fact, many of the preclinically deregulated miRNAs are predicted to

target transcripts that are implicated in synaptic and spine remodeling. It would therefore be important to identify if the expression of any of the preclinically deregulated miRNAs are altered at synapses during prion disease. To test for this possibility, synaptic preparations called synaptoneurosomes can be isolated and subsequently profiled for changes in miRNA expression between prion-infected and mock brain tissue. Correlating the expression of miRNAs to these specialized structures will help futher elucidate the role of these miRNAs during prion disease.

To help elucidate possible cell death pathways that are deregulated during prion disease, transcriptional profiling would need to be performed on neurons found in other anatomical regions of the brain. Based on the gene expression and pathological analysis, CA1 hippocampal neurons were found to be highly robust during prion disease in this animal model. As a result, cell death mechanisms were not readily detected. To determine which molecular processes may govern pro-death pathways in degenerating neurons during prion disease, profiling should be performed in neurons that are more vulnerable to prion disease, such as neurons within the thalamus. Through the use of LCM, neurons from this brain region can be isolated to perform similar expression profiling studies described herein.

In this work, gene and miRNA deregulation was detected at 70 DPI. However, temporal changes prior to this time period remain uncharacterized. To gain a more comprehensive appreciation for the time when these neuroprotective processes are initiated, earlier time points such as 40 DPI would need to be assessed. It is possible that this neuroprotective program may be induced prior to 70 DPI and future studies would help to discern when CA1 hippocampal neurons begin to change their expression profiles during prion disease.

The ultimate goal of these studies is to identify a novel avenue for potential therapeutic intervention. This long-term future direction stems from the identification of a temporally

defined activity-dependent neuroprotective process that occurs during preclinical prion disease. Considering that the endogenous capabilities of CA1 hippocampal neurons are to mount a protective response early during prion disease, it may be possible to exploit this process to identify potential therapeutic targets. As such, several potential strategies can be utilized to determine whether targeting this process would be suitable to modulate disease progression. One potential approach would be to increase expression of neuroprotective genes at a time in disease when their expression diminishes. This could be achieved through viral-mediated systems such as by injecting of lentiviral expression vectors directly into brains of mice. As a result, this approach may help prolong a state of neuroprotection and delay the onset of clinical disease. However, further investigation to elucidate which neuroprotective gene(s) may be most effective as a neuroprotective agent still needs to be performed. To complement the gene expression data presented in this work and therefore help identify likely protective agents, proteomic analysis on these CA1 hippocampal neurons during prion disease could be studied using mass-spectrometry. This analysis would help identify changes within protein levels, which would further help reveal key players that are involved in this neuroprotective mechanism. This proof-of-concept study will then provide inroads to therapy development in a human prion disease context.

In addition to the gene expression profile, several miRNAs induced during preclinical disease are able to modulate neuronal morphology, such as dendrites and spines. The inherent regulatory potential of miRNAs makes them ideal candidates for regulating complex biological processes. Therefore, elucidating their functional roles during prion disease will undoubtedly help enhance our overall understanding of the neurodegenerative disease process. Several additional experiments however would need to be performed to better understand the contribution of microRNAs in neurodegenerative disease. One important experiment would be

to test whether supplementing either an individual miRNA or several of these preclinically induced miRNAs at a time when their expression is waning (~110 DPI) would be efficatious to delay the onset of clinical disease. For example, miR-132-3p was found to protect neurons from apoptosis and is known to enhance neuronal remodeling capabilities. This miRNA should therefore be tested to determine if inducing the expression of this miRNA at ~110-130 DPI would be sufficient to enhance this neuroprotective process in animal models of prion disease. As a proof-of-concept, lentiviral delivery vectors that over-express this miRNA can be used to supplement its expression in prion-infected animals. Subsequent analysis of the time taken by these animals to reach terminal disease followed by pathological examination of tissue damage can help elucidate possible protective effects of these exogenously supplemented miRNAs.

7.0 APPENDICES

Appendix 1: Reagents and solutions for primary mouse hippocampal cultures

Borate Buffer (Store at 4°C)
4.76g Boric Acid
2.54g Borax
1000mL of ddH_2O

Mix to dissolve and adjust pH to 8.4 with 5M NaOH. Filter sterilize using 0.22µm filter.

10x Dissection Medium (DM) (stored at -20°C)
450mL HBSS
100mM $MgCl_2$
10mM Kynureic-Acid (Sigma-Aldrich)
100mM HEPES

To HBSS add 10.15 g $MgCl_2$ X $6H_2O$ and 11.92 g HEPES. Dissolve and bring to ~ pH 7.0. Add 1, 182g Kynurenic Acid and heat to 65°C to get it into solution. Cool to room temperature and adjust pH to 7.2. Bring solution to 500 mL with HBSS and filter sterilize using 0.2µm filters.

Papain Solution (prepared fresh)

100µL	papain (carcia papaya latex; ~130 units) (Worthington)
5mL	1xDM
25µL	DNase (bovine pancreas; 250µg) (Sigma-Aldrich)

Reagents dissolved by placing at 37°C for up to 3 minutes and filter sterilized using a 0.2µm filter (Corning).

Trypsin Inhibitor Solution (prepared fresh)

0.15g	Trypsin Inhibitor (Sigma-Aldrich)
15mL	1xDM
75µL	DNase (bovine pancreas; 250µg)

Trypsin inhibitor was dissolved in 1xDM by placing the mixture at 37°C for up to 30 minutes. The pH was adjusted to 8.5, DNase added and filter sterilized using a 0.2µm filter.

4% Paraformaldehyde with 4% sucrose (4% PFA)

4g	sucrose (Thermo Fisher)
4g	PFA (paraformaldehyde) (Sigma-Aldrich)
100µL	10M NaOH
175mL	PBS (DEPC treated)

Heat solution to 60°C to help dissolve and cool to room temperature. Add 65µL of 12M HCL to adjust the pH and top up to 100 mL of PBS (DEPC treated). Store aliquots in -80°C.

Appendix 2: A total of 2,580 deregulated genes identified during prion-induced neurodegeneration.

	70		90		110		130		EP	
	Log Ratio	FDR	Log Ratio	FDR	Log Ratio	FDR	Log Ratio	FDR	Log Ratio	FDR
5430435G22Rik	-0.46	0.13	-0.07	12.52	-0.12	33.12	0.13	13.89	0.48	31.62
A2LD1	-0.14	3.16	-0.61	2.77	-0.18	12.58	0.14	41.83	0.45	0.21
AADAT	0.24	12.65	0.19	3.01	-0.13	6.93	-1.31	0.06	-0.15	24.40
ABCA3	0.12	49.54	-0.44	0.51	0.02	59.43	0.10	32.50	0.62	0.04
ABCA5	-0.38	0.51	0.26	0.60	-0.22	3.48	-0.64	11.24	0.25	24.40
ABCB10	-0.75	0.05	0.59	1.09	-0.37	4.05	-0.16	47.42	-0.49	8.00
Abcb1b	0.60	0.05	0.56	2.12	-0.41	2.66	-0.13	0.57	-0.27	6.00
ABCC1	-0.13	37.04	0.29	4.12	-0.16	22.90	-0.30	5.54	0.46	0.75
ABCC3	0.04	49.54	-0.20	3.01	0.06	49.13	-0.07	41.83	0.86	0.02
ABCC5	-0.17	15.28	0.81	0.60	0.06	49.13	0.24	3.87	0.64	0.02
ABHD16B	0.03	54.15	0.46	0.99	0.12	17.39	0.11	41.83	-0.25	0.31
ABI1	0.22	0.17	0.72	0.94	0.15	14.77	-0.10	19.97	-0.39	0.17
ABI3	0.17	37.04	-0.29	1.09	-0.10	36.89	0.15	32.50	0.61	0.02
ABL2	0.23	0.53	0.65	0.57	0.14	54.33	0.83	0.57	0.31	36.83
ABLIM2	-0.04	55.17	-0.28	5.83	0.27	2.06	0.22	8.99	0.51	0.07
ABLIM3	-0.09	29.67	-0.51	0.31	-0.14	20.03	0.20	3.87	0.20	2.89
ACAD10	0.20	0.78	0.35	6.70	0.02	58.93	0.91	0.06	0.12	43.18
Acan	-0.41	0.17	-0.24	2.86	-0.35	9.26	0.19	23.45	-0.15	33.88
ACAT2	-0.10	44.81	-0.48	5.83	0.20	8.12	-0.77	0.06	0.49	0.02
ACBD3	-1.23	0.05	0.07	7.54	-0.43	0.09	-0.89	0.06	-0.46	0.02
ACCS	0.19	5.93	-0.46	0.94	0.31	0.24	-0.11	49.36	0.34	24.40
ACER2	0.08	49.54	0.07	10.40	0.25	2.06	0.35	19.97	0.47	0.02
ACOT9	0.25	7.74	0.63	0.51	-0.19	2.31	0.05	50.49	-0.43	0.12
ACP1	-0.15	49.54	0.67	0.45	-0.30	26.12	0.53	0.29	-0.77	0.47
ACP2	-0.26	12.65	0.47	1.77	-0.16	33.12	-0.41	19.97	-0.66	0.02
ACSL1	-0.33	15.28	0.50	0.88	-0.35	1.56	-1.02	0.06	0.30	24.40
ACTG2	-0.26	0.17	0.39	0.60	0.57	4.73	-0.29	41.83	-0.27	24.40
ACTL6A	0.26	1.43	0.75	0.51	-0.04	56.82	-0.31	27.83	-0.14	31.62
ACTR3B	0.70	0.05	0.97	0.57	-0.16	2.66	-0.34	11.24	-0.41	6.00
ACVR2A	0.14	44.81	0.57	0.30	-0.54	2.31	0.49	16.94	-0.76	0.02
ADA	-0.17	1.43	-0.26	5.83	0.05	56.82	0.03	53.83	0.62	0.39
ADAM17	-0.24	5.93	0.28	7.54	-0.28	3.07	-0.91	1.21	-0.40	0.02
ADAM19	0.14	15.28	0.33	1.77	0.08	54.33	-0.77	1.62	-0.50	0.89
ADAM8	0.11	44.81	0.47	0.57	0.39	4.05	-0.44	32.50	0.15	31.62
ADAMTS1	-0.04	56.51	-0.17	11.78	-0.44	3.48	-0.72	0.91	0.12	44.20
ADAMTS2	-0.97	0.05	-0.91	0.99	0.14	41.10	0.51	1.21	0.78	0.05
ADAMTS20	0.30	0.67	0.42	0.30	0.17	26.12	0.16	13.89	0.12	43.01
ADAMTS7	-0.19	18.59	0.24	1.09	0.16	54.33	-0.19	32.50	1.17	0.02
ADAMTS9	-0.59	0.05	-0.90	2.86	0.13	29.33	-0.08	32.50	0.14	40.66
ADARB2	0.83	0.05	-0.52	2.86	0.56	0.09	-0.27	23.45	-0.34	0.39
ADAT1	0.13	44.81	-0.58	0.23	0.16	0.46	-0.56	0.11	0.31	24.40
ADCY1	-0.20	25.77	0.56	0.51	-0.07	56.82	-0.29	13.89	-0.43	0.99
ADCY4	-0.17	44.81	0.21	4.12	0.38	22.90	-0.19	32.50	0.94	0.02
ADCY7	-0.12	44.81	0.58	11.78	-0.33	10.69	0.81	0.51	1.13	0.08
ADCYAP1	0.10	44.81	-0.21	4.12	0.36	2.06	-0.55	0.34	-0.14	33.88
ADI1	-0.06	52.83	-0.60	0.11	0.10	20.03	-0.02	55.17	-0.25	0.17
ADM	0.28	0.05	-0.22	0.51			-0.48	0.25	-0.07	36.83

ADNP2	0.47	0.51	0.43	0.88	-0.18	3.48	0.10	11.24	-0.06	38.75
ADORA2A	-0.66	0.51	-0.27	3.01	0.13	54.33	0.20	19.97	0.13	14.82
ADRA2A	-0.15	3.16	-0.21	5.83	0.32	0.86	0.28	0.57	0.74	0.02
ADRB1	-0.14	10.00	0.68	0.51	0.10	54.33	0.25	0.12	-0.04	37.82
ADRBK1	0.22	0.53	0.48	1.03	0.72	1.82	0.20	23.45	0.58	0.02
AFAP1L1	-0.14	1.94	-0.48	0.78	0.37	3.07	-0.51	13.89	0.44	0.17
AFF3	0.19	21.80	0.53	0.51	-0.20	36.89	-0.17	27.83	-0.12	37.82
AFF4	-0.71	0.05	-0.58	2.77	-0.41	10.69	0.39	27.83	0.53	0.99
AFG3L1	-0.07	52.22	0.53	0.45	-0.21	9.26	0.38	1.33	0.38	11.00
AFP	-0.06	57.11	-0.77	1.09	-0.56	22.90	0.96	0.06	1.86	0.02
AFTPH	-0.14	49.54	0.25	6.70	-0.31	0.44	0.74	2.42	-0.71	0.02
AGA	0.45	0.67	0.51	0.99	-0.20	0.86	0.34	32.50	0.04	44.05
AGBL5	-0.42	0.40	-0.30	3.01	0.15	33.12	-0.06	41.83	0.63	0.04
AGPAT1	-0.10	49.54	-0.39	0.78	0.14	20.03	0.40	13.89	0.50	0.02
AGPAT2	-0.06	49.54	-0.10	9.63	-0.27	14.77	0.41	4.91	0.78	0.02
AGPAT9	0.17	1.43	0.54	0.11	0.20	2.31	1.01	0.06	-0.49	0.02
AGPS	-0.44	4.28	0.57	0.11	0.07	49.13	-0.45	13.89	-0.53	0.39
AGR2	-0.48	0.05	-0.29	0.99	-0.06	58.61	0.40	23.45	-0.20	14.82
AGT	-0.49	0.05	0.36	0.42	-0.71	0.09	0.53	0.29	0.82	0.06
AGTR1	0.46	29.67	-0.66	0.18	-0.29	29.33	-0.85	0.06	-0.66	0.02
AGXT2L1	-1.08	0.05	-0.27	0.60			1.06	0.95	1.15	0.21
AHCTF1	0.27	21.80	0.73	1.21	0.21	0.86	0.38	1.33	-0.27	31.62
AHCYL2	-0.51	0.67	0.28	2.30	-0.32	2.66	0.49	0.06	-0.71	0.02
AHDC1	-0.17	10.00	0.28	0.35	-0.21	29.33	0.16	32.50	0.78	0.02
AHNAK	-0.29	0.05	-0.30	0.78	0.66	0.09	-0.64	0.73	0.98	0.02
AIF1	-0.19	44.81	-0.09	0.26	-0.11	29.33	0.45	0.06	0.84	0.02
AIFM2	0.38	44.81	0.43	0.35			-0.22	0.95	0.22	24.40
AIM1	-0.51	0.05			-0.14	54.33	-0.17	52.66	0.52	11.00
AK2	-0.22	7.74	-0.30	2.12	0.21	49.13	-0.48	0.86	-0.85	0.07
AKAP10	0.32	0.13	0.59	0.60	0.39	2.66	0.15	23.45	-0.43	0.05
AKAP8	-0.04	55.56	0.32	3.01	-0.04	58.93	-0.57	0.51	0.23	24.40
AKAP9	0.07	44.81	0.22	2.77	0.13	20.03	-0.20	2.91	-0.57	0.02
AKR1B10	0.09	49.54	-0.38	2.12	-0.26	0.24	0.75	0.40	0.95	0.02
AKT3	0.11	37.04	0.27	5.83			0.62	0.06	-0.30	0.47
ALAS2	-0.19	4.28	-0.41	0.94	-0.16	22.90			0.63	0.12
ALDH16A1	-0.06	57.11	-0.65	0.51	0.75	0.09	-0.03	49.36	0.56	0.12
ALDH1A1	-0.15	55.87	-0.12	4.12	0.26	0.40	0.12	32.50	0.43	0.99
ALDH1A2	-0.64	0.05			-0.22	49.13			0.38	4.22
ALDH1B1	0.14	5.93	0.15	13.30			-0.18	13.89	-0.52	0.02
ALDH1L2	0.06	44.81	-0.38	0.86	0.12	33.12	-0.24	19.97	0.37	24.40
ALDH3B1	-0.17	37.04	-0.23	2.86	0.65	0.72	0.29	0.73	0.65	0.27
ALDOC	-0.04	49.54	-0.51	4.12	0.22	20.03	0.11	23.45	0.59	0.02
ALOX12B	0.07	54.15	-0.28	0.78	0.47	0.09	0.17	1.33	0.65	0.39
ALPK3	0.37	0.05	0.15	6.70	0.37	5.71	-0.51	27.83	-0.34	0.04
ALS2	0.27	0.17	-0.42	2.77	-0.16	14.77	-0.69	0.25	-0.34	0.12
AMHR2	0.60	0.13	0.30	5.83	0.52	3.07	-0.50	32.50	0.01	44.05
AMIGO2	-0.43	12.65	0.33	1.03	-1.05	0.72			-0.58	24.40
AMPH	-0.60	0.05			-0.37	0.09	0.06	47.42	0.09	44.05
AMZ1	-0.33	10.00	0.09	9.63	0.06	54.33	0.66	0.06	0.52	0.65
ANAPC16	0.02	56.13	0.23	5.83	0.03	58.07	-0.56	0.06	-0.45	0.47
ANGPTL4	0.09	44.81	-0.20	8.88	0.17	49.13	0.21	0.73	0.61	0.04
ANK1	0.44	0.17	0.25	4.12	-0.22	9.26	0.43	0.06	0.23	14.82

ANK2	-1.02	0.05	-0.47	6.70	-0.66	0.09	-1.73	0.06	-0.44	0.99
ANKRD11	-0.59	0.05	-0.35	2.77	-0.66	0.09	-0.37	11.24	0.43	0.65
ANKRD26	0.55	5.93	0.24	0.99	-0.64	0.09	-0.69	0.06	-1.11	0.02
ANKRD44	0.07	52.83	0.39	1.77	0.12	36.89			0.95	0.02
ANTXR1			0.56	0.99	0.10	33.12	-0.54	1.21	0.49	0.99
ANTXR2					-0.51	0.82	-0.08	41.83	-0.06	41.88
ANXA2	-0.08	29.67	0.28	8.88	0.29	1.31	-0.35	0.73	0.69	0.02
ANXA3	-0.33	12.65	0.40	1.77	0.40	0.44	0.18	41.83	1.00	0.02
ANXA4	-0.29	0.17	-0.24	4.12	0.12	36.89	-0.10	47.42	0.51	0.98
ANXA5	-0.23	5.93	0.33	1.21	0.15	17.39	-0.05	51.35	0.56	0.27
ANXA6	-0.54	0.05	0.44	2.12	-0.20	33.12	0.17	49.36	-0.43	0.99
ANXA7	0.15	15.28	0.46	5.83	-0.26	14.77	-0.24	0.18	-0.53	0.02
ANXA8/ANXA8L1	-0.19	0.67	-0.72	0.43	-0.06	49.13	0.06	51.35	0.20	24.40
AOC2	0.32	25.77	0.19	13.30	0.20	12.58			-0.68	0.02
AP1G1	-0.83	0.17	0.40	1.46	0.20	17.39	-0.16	1.33	-0.62	0.02
AP3M1	0.21	2.45	-0.40	2.12	-0.17	5.71	0.23	1.33	-0.53	0.07
AP3M2	-0.17	49.54	0.32	1.66	-0.24	36.89	-0.13	41.83	-0.58	0.02
AP3S1	0.14	44.81	0.65	0.42	-0.09	49.13	-0.05	51.35	-0.33	0.02
APBA1	-0.47	0.05	-0.60	0.51	0.45	0.09	0.17	49.36	0.18	24.40
APBB2	-0.56	0.05	-0.09	11.78	-0.44	1.82	-0.19	0.57	-0.53	0.21
APH1B	0.09	51.01	0.36	2.61	0.05	58.07	0.23	8.99	-0.40	0.99
APLF	0.30	0.67	0.35	1.53	0.12	49.13	0.66	0.06	0.32	11.00
APLN	-0.30	1.43	-0.33	3.21	0.04	49.13	-0.40	0.06	-1.11	0.02
APLNR	0.01	55.56	-0.24	2.86	0.39	0.09			-0.18	24.40
APOBEC1	-0.37	21.80	-0.33	6.70	-0.22	26.12	-0.06	53.27	0.84	0.07
APOC1			-0.24	4.12	0.08	49.13	-0.05	47.42	0.78	0.02
APOC2	0.09	44.81	-0.14	6.70	0.02	58.61			0.54	0.27
APOC3	-0.27	44.81	0.29	0.94	-0.25	2.06	0.98	0.13	0.87	0.02
APOD	-0.46	2.45	0.54	1.66	0.10	41.10			0.60	0.02
APOE			0.18	6.70	0.09	49.13	0.09	47.42	0.62	0.02
APOL2	0.13	12.65	-0.54	0.20	0.07	41.10	0.12	41.83	0.51	0.89
APP	-0.48	0.05	0.51	4.12	-0.40	3.48	0.37	19.97	-0.85	0.02
AQP4	-0.33	0.05	0.53	0.30	0.15	10.69	0.20	0.40	0.70	0.02
ARAP2	0.12	15.28	0.66	1.53			-0.13	19.97	-0.58	0.05
ARAP3	0.27	0.32	0.48	0.60	-0.02	60.51	0.18	8.99	0.44	0.12
ARC	0.58	0.05	0.31	0.57	0.27	1.10	-0.05	52.66	0.08	36.83
ARF3	0.15	37.04	0.71	0.26	0.02	59.43	-0.04	47.42	-0.38	0.05
ARFGEF2	0.26	1.43	0.58	1.03	-0.12	9.26	0.32	5.54	-0.32	0.02
ARHGAP24	-0.37	0.17	-0.90	2.61	-0.30	0.24	-0.27	27.83	-0.22	11.00
ARHGAP26	-0.28	44.81	0.41	0.11	0.18	22.90	-1.23	0.06	-0.50	24.40
ARHGAP4	-0.10	52.22	-0.57	0.77	0.28	20.03	-0.34	23.45	-0.07	38.75
ARHGAP42	-0.21	2.45	-0.52	0.11	-0.51	0.09	0.13	32.50	-0.65	0.02
ARHGAP44	0.07	44.81	0.07	8.25	-0.15	22.90	-0.14	8.99	-0.55	0.02
ARHGAP5	-0.10	44.81	0.73	0.51	0.04	59.79	0.77	0.25	-0.91	0.08
ARHGAP6	-0.56	0.05	0.20	2.61	0.27	8.12	-0.56	0.40	0.48	24.40
ARHGAP9	-0.08	52.83	-0.22	2.12	0.16	29.33	-0.03	53.27	0.52	0.02
ARHGDIB	0.13	49.54	0.13	2.61	0.02	59.79			0.73	0.08
ARHGEF2	0.50	0.93	0.37	7.54	0.21	1.56	0.31	5.54	0.18	37.82
ARHGEF3	0.58	7.74	0.69	0.42	0.04	56.82	0.09	41.83	-0.19	4.22
ARHGEF6	-0.62	0.05	0.65	1.29	-0.49	0.86	0.53	19.97	-0.46	0.75
ARID4A	0.36	4.28	0.56	0.94	-0.17	54.33	-0.39	0.40	-0.50	0.02
ARL1	0.07	49.54	0.71	0.35			-0.11	41.83	-0.33	0.04

ARL4C	0.06	44.81	0.16	2.77	0.06	54.33	0.40	0.29	0.44	0.89
ARL4D	0.38	0.53	0.44	0.51	0.15	8.12	0.08	32.50	-0.05	31.62
ARL6					-0.09	17.39	0.05	47.42	-0.51	0.02
ARMC9	0.14	21.80	0.41	0.67	0.25	33.12	0.37	0.34	0.22	33.88
ARPC1B	-0.08	44.81	-0.32	5.83	0.05	49.13	0.15	47.42	0.89	0.02
ARPP19	0.27	0.51	0.78	0.57	0.24	3.07	0.14	2.91	0.46	0.08
ARPP21	-0.26	44.81	-0.21	0.78	0.34	22.90	-0.15	5.54	-0.44	0.13
ARRB2	0.07	37.04	-0.38	0.78			0.30	2.42	0.40	0.02
ASAH2	-0.27	0.67	0.40	1.66	0.03	58.93	-0.42	0.35	-0.67	0.02
ASAP2	0.02	55.17	0.67	0.51	0.06	49.13	0.04	54.83	-0.15	1.98
ASB11	-0.22	0.93	0.28	1.77	-0.37	4.05	-0.08	52.12	-0.68	0.02
ASPA	-0.45	0.26	-0.64	2.86	-0.11	26.12	-0.13	52.12	-0.27	24.40
ASPG	-0.11	15.28	-0.23	1.53	0.34	0.09	0.29	11.24	1.21	0.02
ASPH	-0.34	0.53	0.56	2.86	-0.28	9.26	0.60	0.40	-0.41	0.12
ASXL2	0.14	44.81	0.42	3.21	-0.43	0.09	-0.99	1.33	-0.23	6.00
ATAD2	0.29	33.23	0.65	0.45	-0.13	55.77	0.13	11.24	0.25	0.75
ATAD5	-0.36	0.05	-0.20	0.51	-0.24	17.39	-0.10	41.83	-0.63	0.12
ATAT1	0.21	29.67	0.13	6.70	0.29	0.64	-0.45	13.89	0.47	0.02
ATE1	0.07	51.01	0.21	0.51	0.60	0.44	-0.45	4.91	-0.44	0.89
ATF1	0.21	33.23	0.68	0.51	0.11	49.13	-0.28	5.54	0.82	0.02
ATF2	-0.61	0.51	0.59	0.94	-0.40	8.12	0.45	0.06	-0.92	0.02
ATF5	0.02	54.70	0.39	1.77	-0.02	59.43	0.04	51.35	0.51	0.04
ATG10	-0.13	33.23	-0.29	5.83	-0.22	2.31	0.20	4.91	-0.52	0.02
ATIC	-0.23	51.01	-1.48	0.57	-0.52	0.24	-0.11	51.35	0.17	36.83
ATL2	0.20	2.45	0.42	0.46	0.40	3.07	0.30	4.91	0.08	39.47
ATM	0.39	0.51	-0.27	4.12	0.06	49.13	-0.18	27.83	-0.53	0.02
ATMIN	0.17	37.04	-0.36	2.30	0.09	26.12	0.13	41.83	0.71	0.02
ATN1	0.02	55.17	-0.39	5.83	0.13	49.13	0.18	41.83	0.59	0.02
ATOX1	0.04	49.54	-0.16	5.83	-0.20	1.82	-0.70	0.06	0.17	31.62
ATP13A3	-1.22	0.05	0.82	0.51	-0.10	54.33	0.07	52.66	0.43	24.40
ATP1A1	-0.08	49.54	0.13	11.78	0.29	4.05	0.14	47.42	0.53	0.65
ATP2A1	0.23	44.81	0.18	8.88	0.62	0.09	-0.79	0.06	0.71	0.99
ATP2B1	-0.14	10.00	0.69	1.29	0.17	12.58	-1.06	3.87	-0.73	0.05
ATP2C1	-0.46	0.17	0.23	4.12	-0.43	0.24	0.49	16.94	-0.62	0.02
ATP2C2			0.29	1.53	-0.26	41.10	0.77	0.29	-0.08	40.05
ATP4A	-0.05	56.87	0.09	12.52	0.66	4.73	-0.37	0.73	-0.40	0.75
ATP5F1	0.01	57.11	0.47	0.60	-0.14	3.07	0.08	47.42	0.38	33.88
ATP6V0A2	0.14	15.28	0.42	1.53	0.08	33.12	0.27	0.95	0.44	0.02
ATP8A1	-0.26	0.13	0.74	0.67	-0.58	0.52	-0.09	23.45	-0.54	0.99
ATRNL1	-0.52	0.05	0.54	0.27	-0.18	49.13	-0.34	1.21	0.40	0.99
AUH	0.46	0.05	-0.44	0.78	0.67	1.56	-0.84	0.95	0.55	0.02
AUTS2	0.09	37.04	-0.38	0.51	0.10	41.10	0.25	7.10	-0.39	0.65
B2M	-0.12	18.59	-0.44	3.21	0.12	49.13	-0.10	41.83	0.90	0.02
B3GALNT1	0.40	10.00	-0.41	0.57	0.04	55.77	-0.12	32.50	-0.15	24.40
B3GALT2	0.21	18.59	0.19	6.70	-0.20	1.82	0.49	0.91	0.26	33.88
B3GAT1	0.34	0.67	0.45	0.51	-0.07	55.77	-0.10	11.24	-0.16	24.40
B3GNT2	0.32	33.23	0.71	0.26	0.23	3.07	-0.04	50.49	-0.19	1.98
BACE2	0.80	0.32	0.07	8.88	-0.64	0.09	-0.87	0.40	0.62	0.02
BACH1	-0.35	0.78	-0.59	1.29	-0.41	5.71	0.23	32.50	-0.32	4.22
BACH2	-0.31	0.13			-0.15	14.77	-0.32	11.24	-0.56	0.02
BAD	-0.23	12.65	0.43	0.51	0.47	0.09	0.55	13.89	0.40	0.99
BAG4			0.69	0.88	0.09	29.33	0.14	47.42	-0.78	0.12

BAI3	0.21	10.00	0.69	0.51	0.21	5.71	-0.26	0.18	-0.62	0.05
BATF	-0.38	2.45	-0.19	2.30	-0.13	41.10	-0.71	1.88	0.70	0.02
BATF3			-0.13	0.78	0.20	36.89	0.22	32.50	0.44	0.60
BAZ2A	-0.12	49.54	-0.20	1.53	-0.10	58.41	-0.41	0.29	-0.06	33.88
BBC3	0.04	52.83	0.15	4.12	-0.23	12.58	0.17	32.50	0.58	0.02
BBIP1	0.06	44.81	0.39	5.83	-0.16	29.33	-0.06	47.42	-0.56	0.02
BBS1	0.66	0.05	0.59	0.60	-0.23	49.13	-1.18	0.06	-0.64	0.27
BBS5	0.03	54.70	0.65	0.60	-0.08	49.13	0.25	7.10	-0.36	0.99
BCKDHB	0.09	44.81	0.22	0.51					-0.41	0.02
BCL11A	-0.21	44.81	-0.38	3.01	-0.52	1.00	0.10	41.83	0.37	1.98
BCL2	0.16	44.81	0.53	0.93	0.22	6.93	0.34	11.24	0.40	0.21
BCL2A1	0.32	1.10	0.35	0.99	0.01	60.51			1.95	0.02
BCL2L2	-0.24	49.54	0.25	4.12	0.45	1.10	0.43	0.25	0.51	0.02
BCL3					-0.03	60.23	0.14	5.54	0.60	0.02
BCLAF1	-0.77	0.05	0.53	1.66	-0.40	10.69	-0.48	23.45	0.50	24.40
BDNF	0.18	0.78	0.87	0.67	0.23	2.06	-0.12	19.97	-0.94	0.02
BDP1	-0.20	0.67	-0.82	0.94	-0.10	54.33	-0.79	1.88	0.41	0.99
BECN1	0.19	12.65	0.54	1.09	0.03	58.07	0.10	47.42	-0.42	0.02
BEND3	-0.26	0.53	-0.43	3.21	0.06	54.33	0.43	0.13	0.09	39.47
BEND6	0.09	21.80	0.41	5.83	0.01	59.79	0.20	2.42	-1.18	0.02
BFSP2	-0.22	0.17	-0.29	8.25	0.34	3.07	0.18	19.97	0.93	0.02
BHLHE22	0.12	25.77	-0.14	4.12	0.35	1.31	0.39	4.91	0.60	0.02
BHLHE22	-0.40	0.93	1.11	1.03	-0.21	14.77	-0.14	41.83	-0.55	4.22
BICD2	-0.09	37.04	0.73	0.60	0.22	54.33	0.24	23.45	-0.37	0.12
BIN1	-0.51	0.05	0.50	2.86	-0.11	26.12	-0.49	32.50	-0.41	0.98
BIRC5	0.04	53.69	-0.13	8.88	0.30	0.66	-0.03	52.12	0.52	0.27
BIRC6	-0.25	0.67	-0.42	0.22	0.07	54.33			-0.03	39.47
BLCAP			-0.22	5.83	0.09	58.07	0.41	41.83	0.44	0.98
BLNK	-0.24	0.51	-0.16	6.70	-0.17	49.13	-0.20	23.45	0.49	0.89
BLVRB	0.21	5.93			0.09	33.12	0.06	49.36	0.56	0.12
BLZF1	0.09	51.01	-0.32	0.35	0.31	0.44	-0.31	0.95	-0.65	0.02
BMF	-0.08	33.23	-0.73	3.21	-0.05	56.82	-0.59	1.88	1.25	0.02
BMP2K	-0.51	0.05	-0.97	0.51	0.12	54.33	0.52	23.45	0.86	0.02
BMP6	-0.31	21.80	-0.12	0.78	0.46	0.09	-0.54	0.06	0.08	35.53
BMP7	-0.30	5.93			0.51	3.07	0.41	0.33	0.23	6.00
BMPER	0.13	44.81	-0.28	8.25	-0.39	41.10	0.37	47.42	-1.11	0.02
BMPR2	-0.66	0.05	0.38	1.66	-0.64	0.86	-0.28	0.11	-0.21	8.00
Bnip3	0.04	54.15	0.35	2.61	-0.14	22.90	-0.06	47.42	-0.59	0.02
BPNT1	0.09	49.54	0.40	0.60	0.13	49.13	0.07	49.36	0.21	24.40
BRCA1	0.45	0.32			0.19	41.10	-0.46	2.42	-0.14	33.88
BRDT	0.25	3.16	0.51	0.86	0.11	22.90	0.21	41.83	-0.09	33.88
BTAF1			0.62	4.12	0.09	20.03			-0.42	0.04
BTBD3	0.06	51.01	0.29	11.78	-0.21	26.12	-0.33	0.25	-1.07	0.02
BTBD9	0.19	33.23	0.22	1.66	0.11	17.39	0.43	1.88	-0.87	0.31
BTG2	-0.63	0.05	0.50	0.18	-0.36	26.12	0.56	13.89	0.21	36.83
BTK	-0.49	2.45	-0.50	0.60	-0.18	3.07	0.85	2.91	1.10	0.02
BUB3	-0.95	0.17	0.25	0.51	-0.41	49.13	-0.42	11.24	0.15	11.00
BYSL	0.26	2.45	-0.31	0.51	0.08	33.12	0.17	19.97	0.47	0.02
BZW1	0.29	4.28	0.57	0.78	-0.29	2.31	-0.21	2.91	-0.45	0.02
C10orf54	-0.19	44.81	0.15	3.01	-0.14	54.33	0.29	41.83	0.71	0.02
C10orf81	0.53	0.26	0.37	2.12	0.42	8.12	0.06	47.42	0.66	0.02
C12orf35	-0.20	0.67	0.37	0.78	-0.42	0.09	0.07	47.42	0.10	31.62

C12orf5	0.15	44.81	0.35	1.09	-0.30	2.31	0.49	0.06	-0.54	0.02
C12orf51	-0.60	0.26	-0.23	9.63	-0.61	0.09	0.25	1.21	0.60	0.05
C16orf45	-0.47	0.17	-0.12	4.12	-0.48	0.28	0.13	41.83	0.17	8.00
C16orf62	0.50	0.28	0.19	6.70	0.23	4.73	0.11	27.83	0.22	14.82
C16orf74	0.06	49.54			0.20	2.06	-0.09	47.42	0.42	0.19
C16orf88	0.69	0.05	0.28	1.03	0.07	57.40	0.60	0.34	0.21	14.82
C17orf59	0.26	0.26	0.21	8.25	0.27	17.39	0.53	19.97	-0.80	0.02
C17orf70	0.33	0.26	-0.13	2.86	0.05	54.33	-0.51	0.06	-0.62	0.02
C19orf12	0.03	54.70	0.13	0.51	0.09	41.10	0.09	41.83	0.48	0.08
C1GALT1	0.21	0.93	0.66	0.51	-0.06	49.13	-0.18	23.45	-0.42	0.12
C1orf159	0.06	54.15	0.48	1.77	0.08	41.10	0.20	41.83	-0.48	0.02
C1orf168	0.06	53.69	0.09	6.70	-0.35	33.12	-0.55	5.54	-0.72	0.65
C1orf190	0.31	0.13	0.42	1.66	0.06	54.33	0.51	0.06	0.46	0.12
C1orf38	0.06	49.54	-0.29	0.88	0.41	0.52	-0.14	13.89	1.12	0.02
C1QA	0.05	56.13			0.12	5.71	-0.07	27.83	1.07	0.02
C1QB			-0.34	2.86	0.06	49.13	0.09	32.50	0.87	0.02
C1QC	0.02	56.51			0.13	9.26	0.26	1.88	1.14	0.02
C1QTNF5	-0.30	0.53	-0.24	5.83	0.14	12.58	-0.18	1.62	0.46	0.13
C20orf194	0.58	0.78	0.50	2.61	0.39	8.12	-0.51	8.99	0.89	0.99
C20orf94	-0.05	52.83	0.25	2.12	0.11	49.13	-0.32	1.88	0.58	0.02
C21orf91	-0.30	52.22	-0.66	1.66	-0.22	9.26	0.91	0.06	-0.57	0.89
C3	-0.15	37.04	-0.13	5.83	-0.09	41.10	0.05	47.42	1.22	0.02
C3orf67	-0.44	0.40	-0.25	2.61	0.09	49.13	0.06	47.42	0.65	0.02
C4B	0.06	51.01	0.28	1.77	0.25	2.31	0.54	0.86	0.60	0.02
C4orf19	0.23	21.80	-0.40	0.99	-0.08	55.77	0.24	47.42	0.69	0.02
C4orf33	0.36	0.40	0.13	5.83	-0.33	3.48	0.44	0.18	0.40	0.05
C4orf43	0.28	25.77	0.53	0.30	0.04	54.33	0.15	19.97	-0.24	0.75
C6orf222	0.11	44.81	0.20	2.77	0.54	0.82	0.37	4.91	0.11	40.05
C6orf35	0.23	1.10	0.35	6.70	0.43	3.07	-0.32	32.50	-0.79	0.04
C7orf36	-0.55	0.17	0.80	1.21	-0.27	12.58	-1.58	0.06	-0.45	0.02
C7orf57	0.17	0.67	-0.13	4.12	-0.26	36.89	-0.55	0.12	0.21	33.88
C7orf60	0.07	49.54	0.76	0.51	0.07	36.89	-0.22	19.97	-0.50	0.39
C8orf34	-0.05	49.54	-0.20	0.78	-0.17	33.12	-0.45	0.06	-0.61	0.02
C8orf4	0.10	44.81	-0.38	3.21	-0.32	5.71	0.22	41.83	0.67	0.21
C9orf71	0.19	0.78	-0.23	3.21	0.20	17.39	0.16	47.42	0.72	0.02
CA13	0.57	0.17	0.87	0.11					-0.10	38.75
CA5B	-0.30	10.00			0.23	3.07	-0.37	4.91	0.50	0.39
CAB39	0.15	37.04	0.62	2.12	-0.13	36.89			-0.33	0.02
CACNA1B	0.08	49.54	0.58	0.99	0.16	3.07	0.32	0.13	-0.38	0.27
CACNA1C	0.17	5.93	0.33	0.99	-0.27	22.90	0.69	1.33	0.77	0.07
CACNA1E	-0.31	18.59	-0.32	5.83	0.12	14.77			-0.43	0.27
CACNA2D1	-0.55	0.40	0.40	5.83	-0.37	1.31	-0.83	0.11	-0.26	1.98
CACNG2	0.25	4.28	-0.48	0.51	0.36	3.48	-0.72	0.40	0.66	0.31
CACNG5	-0.71	0.05			-0.64	10.69			-0.48	24.40
CADPS2	-0.20	5.93	0.86	0.99	-0.12	33.12	0.38	11.24	0.42	0.47
CALB2	-0.37	0.17	-0.45	0.18	-0.51	0.28	0.47	0.12	0.40	0.39
CALCRL	-0.52	0.05	-0.23	4.12	-0.48	0.09	0.36	41.83	-0.26	24.40
Cald1	-0.17	21.80	-0.09	11.78	-0.34	3.07	-0.29	19.97	-0.38	0.75
Calm1	0.09	44.81	0.50	0.30	-0.14	33.12	-0.15	1.33	-0.49	0.08
CAMK1	0.09	12.65	0.49	0.83	0.28	0.72	-0.37	27.83	0.32	6.00
CAMK2D	-0.42	3.16	0.37	3.01	1.00	0.09	0.27	0.12	0.30	31.62
CAMK4	-0.20	44.81	0.27	0.45	-0.51	0.09	-0.59	0.35	-0.75	0.04

CAMKMT	-0.06	57.11	0.20	11.78	-0.28	3.07	-0.42	0.11	-0.16	37.82
CAMTA1	0.05	49.54	0.10	7.54	-0.07	58.07	-0.15	5.54	-0.44	0.89
CANT1	0.12	37.04	-0.51	0.22	0.16	6.93	0.15	47.42	0.41	24.40
CAP1	-0.29	0.17	-0.58	0.99	-0.25	22.90	-0.17	11.24	-0.49	0.02
CAPG	-0.08	57.37	-0.16	2.86	-0.11	33.12	0.61	0.06	0.86	0.02
CAPN3	0.32	21.80	0.44	0.66	0.04	58.07	-0.03	53.27	0.38	4.22
CAPSL	-0.31	0.51	0.33	0.17	0.13	58.41	0.27	47.42	-0.52	0.02
CARD6	-0.40	2.45			-0.17	54.33	0.61	0.06	-0.24	0.39
CARKD	-0.44	0.05	0.20	5.83	-0.29	4.73	-0.22	7.10	-0.29	0.65
CARTPT	-0.63	0.78	-0.15	4.12	0.19	12.58	-0.18	2.42	-0.33	24.40
CASP12	0.12	44.81	-0.15	4.12	0.11	49.13	-0.11	27.83	0.68	0.02
CASP8	0.12	51.01			-0.05	54.33	-0.29	19.97	0.43	0.90
CAV1	-0.18	4.28	-0.43	2.77	0.12	33.12	-0.15	23.45	0.47	0.31
CAV2	0.46	1.10	0.46	0.45	0.48	4.05	0.26	47.42	0.57	0.02
CBLN1	-0.35	0.40	-0.10	4.12	0.29	0.24	0.34	0.57	0.46	0.02
CBX3	-0.44	0.40	-0.58	2.12	-0.46	0.09	0.26	49.36	0.42	0.02
CBX8	0.17	12.65	-0.37	5.83	0.19	0.86	-0.32	47.42	0.69	0.05
CCBE1	-0.55	0.17	0.21	5.83	0.03	58.41	0.23	11.24	-1.50	0.02
CCBL1	0.11	37.04	-0.45	0.94	0.03	56.82	-0.04	49.36	0.12	37.82
CCDC102A			0.11	5.83	-0.40	0.86	-0.10	47.42	0.93	0.02
CCDC109B	0.04	54.15	0.45	0.12	0.11	36.89	0.07	41.83	0.52	31.62
CCDC19	-0.42	10.00	0.30	0.60	-0.14	9.26	0.37	2.91	-0.40	0.89
CCDC25	-0.54	0.05	0.70	1.46	-0.34	1.10	0.27	2.42	0.25	24.40
CCDC64	0.28	33.23	-0.10	3.21	0.05	54.33	-0.49	0.95	-0.25	1.19
CCDC80	-0.15	1.10	-0.10	10.40	0.32	0.66	-0.13	52.12	0.63	0.02
CCDC85A	-0.59	0.51	-0.88	1.09	-0.27	2.66	0.62	11.24	-0.37	0.99
CCDC88A	-0.48	0.05	-0.69	2.12	-0.38	6.93	-0.25	32.50	-0.56	0.02
CCHCR1	0.26	33.23			0.21	2.06	0.46	0.18	-0.19	31.62
CCKBR	-0.48	0.05	-0.13	12.52	0.37	0.66			-0.59	0.89
CCL13	-0.38	4.28	0.18	4.12	0.25	2.66	0.12	41.83	1.21	0.02
CCL2	-0.53	0.09	-0.36	2.77	-0.43	1.82	0.20	23.45	1.68	0.02
CCL3									1.62	0.02
CCL4	-0.28	37.04	-0.95	1.77	0.32	2.66	0.23	52.66	1.49	0.02
CCL5	-0.28	18.59	-0.13	5.83	-0.34	20.03	-0.08	47.42	0.60	0.02
Ccl6					-0.22	2.66	0.70	0.35	1.75	0.02
Ccl9	-0.17	37.04	-0.35	2.12	-0.32	0.44	0.12	41.83	1.32	0.02
CCNB1IP1	-0.26	52.22			0.27	6.93	0.20	47.42	0.61	0.02
CCND1	0.05	52.22	0.31	3.21	0.23	1.82	0.22	0.35	0.70	0.13
CCND2	0.41	0.05	0.45	1.46	-0.26	33.12			0.05	42.21
CCNG1	0.07	44.81	0.75	0.99	0.11	54.33	0.25	0.25	-0.31	2.89
CCNI	-0.43	0.05	0.26	0.51	-0.21	10.69	0.43	41.83	0.31	0.65
CCNJL	-0.15	29.67	0.34	3.01	-0.32	2.31	-0.24	8.99	-0.67	0.99
CCNL1	-0.54	0.05	0.65	2.61	-0.07	41.10	0.74	0.06	0.21	24.40
CCNL2	0.41	0.93	0.61	0.60	-0.09	41.10	-0.24	0.73	-0.36	0.12
CCR5	-0.08	44.81	0.41	0.45					-0.72	0.02
CCR6	0.15	1.94	-0.21	3.01			-0.47	0.06	0.11	31.62
CCR9	-0.06	44.81	-0.40	0.99	0.04	56.82			-0.19	24.40
CCRL2	-0.15	3.16	0.32	0.51	-0.25	3.07	1.12	0.06	1.14	0.02
CD14	0.16	21.80	-0.10	6.70			-0.49	0.06	1.17	0.02
CD1D	0.43	21.80	0.94	0.11	0.05	55.77	-0.23	51.35	0.54	0.98
CD248	0.07	52.22	-0.11	12.52	0.14	17.39	0.43	0.51	0.26	0.89
CD300A	0.24	1.10	-0.52	0.60	-0.37	1.56	0.85	0.95	1.24	0.02

CD37	-0.08	44.81	-0.59	0.51	0.21	17.39	0.11	49.36	0.74	0.02
CD44	-0.20	54.70	0.19	3.21	-0.43	0.09	-0.55	1.88	1.94	0.02
CD48	-0.11	57.29	0.07	13.30	0.42	0.86	-0.88	0.25	1.42	0.02
CD52	-0.09	49.54			0.19	49.13			1.20	0.02
CD59	0.60	0.17			0.40	0.86	-0.70	0.06	-0.95	0.02
CD5L	-0.09	44.81	-0.30	4.12	-0.06	54.33	-0.51	2.42	0.93	0.13
CD6	0.12	37.04	-0.22	3.21	0.49	0.44	-0.06	41.83	-0.16	24.40
CD63	-0.19	7.74	0.30	0.60	0.07	33.12	-0.08	49.36	0.69	0.02
CD68	-0.17	49.54	-0.10	7.54	0.31	2.06	0.13	8.99	1.21	0.02
CD74	-0.14	44.81	-0.36	0.57	0.18	2.31	0.03	55.17	0.88	0.02
CD79B			0.24	0.51					0.66	0.02
CD82	0.19	12.65			0.12	4.05	0.39	0.06	0.54	0.65
CD86			-0.13	8.88	0.41	0.64	0.25	19.97	1.01	0.02
CD9	-0.29	0.17	0.43	1.09	-0.12	49.13	0.43	11.24	1.07	0.02
Cd99	-0.17	1.10	-0.37	3.01	-0.13	54.33	0.21	11.24	0.44	0.02
CDAN1	-0.07	44.81	0.28	2.61	0.03	57.40	-0.08	19.97	0.78	0.02
CDC20	-0.31	2.45	-0.89	2.12	-0.09	49.13			0.61	0.99
CDC40	-0.92	0.05	0.47	0.60	-0.24	0.64	-0.92	0.06	-0.47	0.05
CDC42	0.08	44.81	0.64	0.51	-0.15	22.90	-0.17	19.97	-0.43	0.02
CDC42BPA	0.16	44.81	-0.29	2.77	0.17	12.58	-0.09	41.83	0.59	0.31
CDC42EP1	-0.15	37.04	-0.19	0.78	0.03	55.77	0.32	16.94	0.60	0.04
CDC42EP3	-0.74	0.09	0.36	4.12	-0.19	49.13	0.08	54.83	0.45	41.26
CDC42EP4	-0.27	37.04	-0.47	1.53	0.12	33.12	0.27	1.21	0.96	0.02
CDC42EP5	0.04	53.69			-0.27	5.71	0.36	2.42	0.44	0.89
CDC6	-0.09	56.13	0.51	0.48	0.56	5.71	0.55	2.42	-0.52	0.75
CDCA4	-0.04	52.22	0.22	9.63			-0.26	0.18	-0.35	0.99
Cdca7	0.11	44.81	0.24	6.70	-0.05	60.51	-0.54	0.06	-0.28	11.00
CDH11	-0.53	0.53	-1.00	1.03	-0.06	49.13	0.33	23.45	-0.44	0.02
CDH20	0.15	2.45	0.29	7.54	0.15	6.93	0.29	11.24	0.49	0.89
CDH7	-0.64	0.17	0.12	9.63	0.53	9.26	-0.40	7.10	-0.41	0.04
CDK11A/CDK11B	0.14	21.80	0.40	2.77	0.07	41.10	0.08	41.83	0.31	6.00
CDK12	-0.35	0.26	0.45	1.77	0.07	41.10	0.20	1.21	0.11	40.05
CDK18	-0.12	44.81	0.12	7.54	-0.09	58.07	0.32	0.06		
CDK6	-0.39	0.09	-0.17	5.83	-0.06	55.77	-0.14	27.83	-0.11	31.62
CDKL5	-0.31	0.53	-0.57	0.45	-0.55	0.09	0.12	47.42	0.07	42.37
CDKN1C	-0.62	0.53			0.14	54.33	-0.80	0.06	0.09	33.88
CDKN2AIP	0.27	0.51	-1.23	1.77	-0.45	5.71	-0.72	4.91	-0.40	0.99
CDS2	-0.16	44.81	0.55	1.29	0.11	54.33	0.46	0.06	-0.33	0.13
CEBPA			0.30	0.30	0.13	22.90	0.21	23.45	0.58	0.02
CEBPB	0.32	33.23	0.13	11.09	0.32	0.64	0.17	11.24	0.67	0.07
CECR6	0.53	0.05	0.38	0.51	0.37	0.40	0.22	19.97	-0.29	0.75
CELF2	-0.45	0.05	0.40	0.51	0.06	57.40	-0.34	0.86	-0.43	0.17
CELSR3	0.06	53.69	0.68	0.48	0.17	33.12	0.44	7.10	1.06	0.02
CENPA	0.10	49.54	-0.43	3.01	0.10	36.89	-0.09	49.36	0.75	0.02
CENPE	-0.09	49.54	-0.32	6.70	-0.85	0.09	0.38	47.42	-1.04	0.39
CENPM	-0.18	44.81	0.34	0.51	-0.05	54.33	0.81	0.06	-0.67	0.02
CENTG2	-0.13	15.28	0.26	1.77	-0.25	12.58	0.20	3.87	1.09	0.02
CEP120	0.14	33.23	-0.55	0.78	0.09	57.40	-0.18	8.99	-0.99	0.02
CEP152			-0.18	6.70	-0.10	54.33	-0.22	47.42	-0.79	0.02
CEP27	-0.56	0.78	0.37	0.57	-0.47	0.28	-0.40	2.42	-0.90	0.02
CEP55	-0.93	0.05	-0.15	4.12	0.83	0.09	0.18	27.83	-0.86	0.02
CES5A	-0.08	51.01	0.19	4.12	0.41	5.71			0.83	0.02

CES7	-0.32	7.74	-0.89	1.09	0.44	0.52	0.32	1.21	0.68	0.99
CFI	0.08	33.23	-0.22	5.83	0.08	49.13	0.20	1.88	0.89	0.02
CFLAR	-0.29	7.74	-0.58	1.29	0.29	0.64	0.36	13.89	0.53	0.27
CHAT	-0.12	3.16	-0.62	0.77	-0.04	56.82	0.04	52.66	0.14	31.62
CHCHD5	-0.14	44.81	-0.60	2.77	0.08	54.33	0.49	0.73	0.03	31.62
CHD1L	-0.12	49.54							1.28	0.02
CHD5	-0.41	0.17	0.46	0.51	0.20	4.73	0.24	27.83	0.12	31.62
CHFR	-0.55	0.05	0.63	0.60	0.04	55.77	-0.17	32.50	-0.11	31.62
CHI3L1	-0.06	56.51	-0.14	8.88	0.11	6.93	0.14	27.83	0.77	0.02
CHIC2	-0.10	33.23	0.55	0.18	0.05	58.07	0.03	52.66	-0.02	41.88
CHID1	0.26	7.74	0.51	0.43	0.09	41.10	-0.03	55.17	-0.03	40.05
CHKA	-0.23	0.26	0.61	2.77	-0.28	0.52	0.17	41.83	-0.44	0.75
CHL1	-0.34	29.67	-0.87	0.81	0.25	0.64	-0.15	13.89	0.23	24.40
CHMP1B	0.10	44.81	0.79	0.94	0.05	49.13			-0.44	0.02
CHMP6	0.41	0.05	-0.27	6.70	0.33	3.07			0.18	24.40
Chn1	0.23	0.53	0.52	4.12	-0.07	54.33	0.05	52.66	-0.35	0.27
CHPT1	-0.32	7.74	-0.32	2.86	-0.12	49.13	-0.58	0.06	0.19	14.82
CHRDL1	-0.49	10.00	0.40	1.77	0.90	1.31	0.28	3.87	1.08	0.12
CHRM1	0.17	3.16	0.29	5.83	0.03	58.07	0.45	0.73	-0.23	31.62
CHRM3	0.16	49.54	-0.80	1.53	-0.57	1.82	0.91	2.42	-0.27	6.00
CHRNA1	-0.64	0.13	0.50	0.26	0.16	54.33	-0.15	51.35	-0.20	24.40
CHRNA7	-0.65	0.65	-0.31	3.21	0.17	36.89	-0.19	32.50	0.05	43.97
CHST3	-0.49	0.32	-0.56	2.61	-0.10	36.89	0.07	51.35	0.26	0.98
CHTF8	0.17	18.59	-0.13	3.21	0.46	1.82	-0.30	23.45	-0.45	0.31
CIDEA	-0.30	7.74			-0.77	0.52	0.59	0.06	-0.18	37.82
CISH	-0.10	52.22	-0.14	4.12	0.03	59.79	0.09	51.35	0.45	0.99
CIT	-0.45	1.94	0.26	1.77	0.16	17.39	-0.37	0.51	0.27	33.88
CITED4	-0.09	37.04	-0.19	2.86	0.12	55.77	0.46	0.51	0.27	1.19
CKLF	0.18	29.67	-0.37	0.51	-0.19	8.12	0.21	41.83	0.43	0.47
CLDN11			0.16	0.78			-0.16	41.83	0.48	0.60
CLDN22	-0.36	15.28	0.20	5.83			-0.14	32.50	-0.56	0.99
CLDN23					-0.43	4.73			0.56	0.02
CLDND1	-0.28	21.80	0.41	0.51	0.29	14.77	-0.30	27.83	0.45	0.05
CLEC10A			0.54	0.17			0.38	47.42	0.53	0.89
CLEC1B									0.62	0.80
CLEC4A							0.29	41.83	0.56	0.02
Clec4b1	-0.05	54.70			0.05	54.33			0.72	0.05
CLEC5A	0.16	4.28	-0.17	13.30	-0.09	36.89	-0.41	7.10	0.96	0.02
CLEC7A	0.04	49.54	-0.15	5.83	-0.06	55.77			1.98	0.02
CLIC5	-0.18	5.93	-0.23	5.83	0.08	56.82	-0.76	0.81	0.60	0.99
CLIC6	-0.83	0.05	0.22	6.70	-0.31	4.05	-0.28	49.36	0.21	43.48
CLIP1	-0.15	44.81	-0.55	0.51	-0.26	1.82	0.05	47.42	-0.42	0.02
CLN8	0.38	1.94	0.46	0.11	0.60	0.09	-0.09	47.42	-0.67	8.00
CLOCK	0.36	0.17	0.55	1.77	-0.56	0.09	-0.27	1.88	-0.40	0.99
CLTC	0.17	29.67	0.66	0.78	-0.12	49.13	-0.44	3.87	-0.40	0.99
CLU	0.02	54.15			0.11	26.12	0.08	47.42	0.56	0.02
CLVS1	0.04	52.22	0.93	0.11	0.33	0.52	0.08	41.83	-0.58	0.02
CLYBL	0.34	0.05	0.53	2.30	0.13	33.12	-0.12	47.42	-0.52	0.02
CMAS	0.32	12.65	0.63	0.67	0.03	59.79	-0.11	16.94	-0.22	4.22
CMBL	-0.23	0.17	0.56	0.18	-0.14	20.03	0.06	41.83	-0.30	6.00
CMKLR1	-0.11	4.28	-0.42	0.78	-0.08	49.13	-0.05	55.17	-0.03	39.47
Cml5	0.17	44.81	0.47	0.78	0.15	33.12	-0.27	0.86	-0.42	0.99

CMTM7	0.27	29.67	0.38	1.03	0.08	54.33	0.09	11.24	0.68	0.02
CMTM8	-0.10	56.13	0.11	4.12	-0.53	0.09	0.50	0.51	-0.27	1.98
CNGB1	-0.73	0.32								
CNIH3	-0.11	49.54	0.80	0.67	-0.16	4.05	-0.14	49.36	0.45	0.02
CNKSR3	0.13	44.81	0.52	0.86	0.22	33.12	0.16	32.50	0.27	31.62
CNN3	0.07	44.81	-0.17	5.83	0.18	0.86	0.04	51.35	0.61	0.02
CNOT10	0.11	25.77	0.51	1.46	0.01	59.43	0.15	19.97	-0.74	0.02
CNOT3	-0.24	0.17	-0.50	0.94	0.22	4.05	0.29	47.42	0.74	0.89
CNOT6	0.04	56.51	-0.66	0.78	0.09	29.33	-0.10	13.89	-0.54	0.99
CNTLN	0.04	49.54	0.43	0.53	0.40	4.05	0.07	47.42	0.30	24.40
CNTN1	-0.04	52.83	0.14	4.12	-0.14	9.26	-0.17	23.45	-0.47	0.02
CNTN4	-0.12	3.16	0.39	5.83	-0.19	26.12	-0.55	1.33	-0.78	0.02
COBL	-0.50	0.05	-0.52	3.01	0.52	10.69	-0.45	3.87	0.05	43.48
COL16A1	0.07	52.22	0.53	0.48	0.07	49.13	0.65	0.13	0.95	0.02
COL18A1	-0.09	49.54	-0.17	3.21	0.47	0.56	0.55	5.54	0.27	11.00
COL1A1	-0.27	7.74	-0.32	6.70	-0.13	14.77	0.59	0.06	0.85	0.02
COL25A1	0.91	0.32	-0.50	0.51	-0.07	49.13	0.02	53.27	-0.03	40.05
COL4A1	0.06	49.54	0.37	1.09	0.03	54.33	-0.50	0.06	-0.38	0.05
COL4A2	0.27	4.28	0.29	4.12	0.08	49.13	-0.44	0.06	-0.66	0.02
COL5A1	-0.14	49.54	-0.22	4.12	0.17	55.77	0.42	27.83	0.92	0.02
COL5A3	0.08	52.83	-0.30	0.78	-0.26	2.06	0.94	0.06	0.98	0.02
COL6A3	-0.12	52.22	0.30	1.46	-0.50	0.09	0.22	7.10	0.08	33.88
COPZ2	0.09	44.81	0.45	4.12	0.48	0.64	0.45	1.62	0.60	0.02
COQ4	0.21	37.04	0.22	2.12	-0.14	29.33	-0.47	8.99	-0.60	0.02
COX6A2	-0.40	10.00	-0.35	4.12	0.33	0.09	0.12	41.83	0.57	0.99
CP	-0.27	29.67	-0.20	2.61	0.29	4.73	-0.35	0.12	0.34	4.22
CPE	0.24	1.43	0.67	0.45	-0.19	33.12	0.05	52.12	-0.48	0.08
CPLX2	-0.59	0.05	-0.25	8.25	0.35	26.12	0.28	19.97	-0.41	0.65
CPLX3	0.07	51.01	-0.52	0.86	0.60	3.48	-0.07	47.42	0.07	36.83
CPNE2	-0.22	0.78	-0.64	4.12	0.15	10.69	-0.15	41.83	0.52	0.02
CPNE4	-1.07	0.05	0.22	5.83	-1.03	0.09	0.86	1.62	-1.09	0.04
CPNE5	0.23	18.59	0.52	1.53	0.35	9.26	0.08	51.35	0.67	0.13
CPNE8	-0.04	54.70	0.73	0.42	0.06	41.10	0.21	16.94	0.40	0.99
CPNE9	-0.49	0.05	-0.23	6.70	0.47	3.07	-0.19	51.35	-0.57	14.82
CPSF2	-0.06	51.01	0.62	0.60	-0.36	12.58	0.70	0.51	0.25	0.65
CPSF3	0.30	0.93	0.45	0.99	0.20	17.39	0.07	47.42	-0.26	1.98
CPSF6	0.53	0.93	-0.30	2.86	0.01	59.79	0.37	23.45	-0.86	0.02
CPT2	0.06	49.54	-0.20	0.78	-0.28	0.24			0.48	0.89
CRABP1	0.63	0.17	0.34	0.35	0.41	4.73			0.32	11.00
CREB3L2	0.16	25.77	-0.26	0.60	0.48	0.09	-0.34	0.95	0.30	4.22
CREB5	0.30	7.74	0.45	0.51	-0.38	0.44	-0.32	41.83	0.87	0.99
CREBL2	-0.51	0.05	0.26	1.21	-0.18	49.13	0.30	0.13	0.66	0.21
CREG1	0.15	25.77	0.70	1.53	-0.12	26.12	0.09	52.12	-0.42	0.98
CRHR2	-0.19	33.23	-0.42	0.89	0.20	8.12	0.14	47.42	0.09	35.53
CRIM1	-0.76	0.09	0.28	5.83	-0.37	0.52	-0.39	23.45	-0.49	0.02
CRIP1	-0.07	49.54	0.45	0.60	0.25	0.44	-0.12	7.10	0.48	0.31
CRIP3			-0.44	0.99	0.22	0.86	0.06	47.42	-0.26	8.00
CRISPLD2	-0.15	10.00	-0.43	2.77	0.22	0.66	0.49	8.99	0.13	44.32
CRLF1	-0.30	21.80	-0.40	0.71	0.04	58.41	0.05	50.49	0.34	24.40
CRLS1	-0.13	44.81	0.69	1.29	-0.52	0.40	-0.10	13.89	0.37	31.62
CROT	-0.10	49.54	0.69	0.51	-0.10	22.90	0.28	1.62	-0.47	0.02
CRTAM	-0.08	49.54	-0.17	4.12	-0.21	20.03	-0.57	0.99	0.12	31.62

CRYAA	-0.67	0.05			-0.20	36.89	0.28	2.42	0.26	24.40
CRYBA4	-0.34	33.23			-0.21	54.33	0.31	27.83	0.91	0.02
CRYM	-0.09	52.22	0.12	8.25	-0.49	0.09	0.11	41.83	-0.42	0.04
CSE1L	0.09	37.04	0.49	3.21	-0.05	58.93	-0.22	0.29	-0.35	0.07
CSF1R	-0.07	57.37	-0.23	0.51	-0.10	26.12	0.23	2.42	0.63	0.02
CSF2RA			-0.44	2.77	0.10	41.10	-0.09	16.94	0.50	0.02
CSF2RB	-0.70	0.05	-0.23	4.12	-0.33	10.69	-0.38	27.83	0.68	0.02
CSNK1G1	-0.81	0.17	-0.64	2.77	-0.33	2.31	-0.70	1.88	-0.53	0.99
CSPG4	-0.24	3.16	-0.13	7.54	0.18	2.66	0.03	52.66	0.42	0.39
CSPP1	-0.06	55.17	0.09	10.40	-0.04	55.77	-0.38	0.06	-0.36	0.04
CSRP2	0.13	7.74	0.52	0.78	0.23	36.89	-0.60	0.51	0.15	14.82
CST7					-0.09	49.13			2.03	0.02
CSTF1	0.03	54.15	0.24	2.30	0.06	49.13	0.07	47.42	0.42	0.04
CTBP2	-0.32	0.17	-0.28	6.70	-0.22	36.89	0.05	47.42	-0.49	0.21
CTDSP1	-0.21	0.32	-0.11	7.54	0.03	57.40	0.18	2.42	0.45	0.27
CTF1	-0.26	10.00	0.14	7.54	0.09	41.10			0.71	0.02
CTGF	-0.43	1.94	0.39	0.48	0.18	49.13	-0.16	1.33	-0.10	33.88
CTH			0.69	0.30	0.04	58.07	-0.15	13.89	-1.10	0.02
CTNNA2	-0.30	0.05	0.44	0.60	-0.20	1.10	-1.06	0.06	-0.43	0.12
CTNNB1	-0.24	44.81	0.65	0.18	-0.11	33.12	-0.59	0.25	-0.95	0.02
CTNNBIP1	-0.07	37.04	-0.15	8.88	-0.05	56.82	0.08	47.42	0.47	0.65
CTNND1	0.23	1.94	-0.61	2.86	0.40	0.09	0.06	47.42	0.17	35.53
CTR9	0.08	44.81	-0.42	0.51	-0.09	26.12	0.08	27.83	-0.09	24.40
CTSC	0.14	44.81	0.46	2.30	-0.47	22.90	0.41	0.51	-0.12	36.83
CTSD	0.23	12.65	0.29	4.12	0.07	54.33			0.44	0.39
CTSE			-0.30	1.53			-0.04	50.49	0.46	0.40
CTSH	-0.02	57.29	-0.22	3.01	0.07	49.13	0.02	53.83	0.83	0.02
CTSS	-0.11	44.81	-0.16	4.12	-0.05	60.23			1.06	0.02
CTSZ	0.14	25.77	0.20	8.88			-0.05	51.35	0.64	0.02
CTTNBP2	0.29	21.80	0.46	0.99	-0.09	56.82	-0.29	16.94	-0.50	0.27
CUL2	0.08	52.22	0.51	2.86	0.03	58.61	0.12	41.83	0.83	0.02
CUL4B	0.07	52.22	0.51	0.99	-0.09	41.10	0.08	41.83	-0.29	1.19
CUL9	-0.11	29.67	0.39	2.77	0.05	54.33	-1.05	0.29	0.28	0.27
CUTC	-0.03	57.29	0.20	4.12	0.23	2.06	0.45	0.86	0.21	14.82
CUX2	0.09	29.67	0.21	2.77	0.27	12.58	0.21	1.88	0.57	0.65
CX3CR1	0.03	49.54	-0.39	0.51	0.34	33.12	-0.23	41.83	0.64	0.02
CXCL10									1.22	0.12
CXCL13					-0.09	54.33			1.17	0.02
CXCL14									1.01	0.02
CXCL16	-0.58	1.94	-0.34	0.51	-0.06	49.13	0.19	1.88	1.63	0.02
CYB5R4	0.10	33.23	0.52	1.53	0.30	17.39	0.54	11.24	-0.51	0.02
CYBA	-0.09	52.22			0.10	22.90	0.39	0.06	0.91	0.02
CYFIP2	-0.29	5.93	-0.45	0.60	-0.56	0.09	-0.14	47.42	-0.13	24.40
CYLD	0.42	0.17	0.29	1.46	-0.23	5.71	-0.11	32.50	-0.56	0.02
CYP1B1	-0.15	44.81	-0.23	11.78			-0.42	13.89	0.53	0.12
CYP26B1	-0.67	0.26	0.36	0.88	-0.61	1.31	-0.99	0.06	0.10	24.40
Cyp2c44	-0.15	49.54	-0.75	0.94	0.17	22.90			-0.31	4.22
CYP2D6	-0.59	0.05	0.31	0.78	0.04	55.77	-0.80	0.06	0.41	0.27
CYP2G1P	0.44	0.13	0.17	10.40	-0.15	3.48	0.40	4.91	0.54	0.02
CYP2J2	0.08	44.81	0.55	0.51	-0.07	49.13	0.33	2.42	-0.88	0.02
CYP46A1	-0.10	21.80	-0.57	0.61	0.01	60.51	0.02	55.17	0.12	31.62
CYP4F12	0.10	37.04	0.43	2.30	0.36	9.26	-0.32	0.11	0.47	0.99

CYP4X1	0.08	33.23	-0.44	1.03	-0.17	26.12	-0.04	49.36	-0.51	0.05
CYP51A1	0.22	0.17	0.65	1.21	0.32	3.48			-0.44	0.07
CYR61	0.04	52.22	0.13	1.53			-0.33	11.24	0.64	0.47
CYTH4	-0.09	33.23	0.10	12.52	0.06	49.13	0.63	0.29	0.94	0.02
D2HGDH	-0.35	1.10	0.34	0.78	-0.15	33.12	-0.52	0.06	0.35	31.62
D830050J10RIK	0.11	25.77	0.27	2.30	0.15	12.58	0.11	51.35	0.68	0.02
DAAM1	-0.31	1.43	0.44	1.03	-0.17	6.93	0.45	0.06	-0.34	0.02
DAB1	0.43	0.53	-0.53	5.83	0.28	1.31	-0.16	16.94	-0.23	0.17
DAB2	-0.09	44.81	0.42	0.12	0.02	56.82	-0.03	54.40	0.43	0.75
DACH1	0.17	12.65	-0.64	0.18	-0.30	6.93	0.23	0.73	0.04	43.01
DACT2	0.08	44.81	-0.39	4.12	0.27	6.93	0.41	1.62	0.55	0.07
DAG1	-0.09	51.01	0.56	0.78	0.22	10.69	-0.09	41.83	-0.43	0.02
DAGLA	0.23	1.43	-0.50	3.21	0.09	49.13	-0.30	8.99	0.62	0.17
DAP	0.08	53.69	0.25	3.21	0.51	0.09	0.16	41.83	0.24	11.00
DAPP1	0.48	0.40	-0.09	10.40	0.13	49.13	-0.61	2.42	0.10	44.05
DARS	0.38	12.65	0.72	1.46	-0.11	49.13	0.57	2.42	0.69	0.02
DBI	-0.03	55.56					0.13	16.94	0.54	0.07
DCAF10	0.17	18.59	0.51	0.51	0.10	17.39	0.37	0.12	-0.40	0.75
DCAF12	-0.32	37.04	0.63	0.20	0.07	49.13	0.18	0.86	0.40	0.12
DCC	0.02	54.70	0.28	0.51	-0.49	0.09	0.66	0.06	-0.39	0.39
DCK	0.20	2.45	0.23	4.12	0.09	54.33	-0.38	0.11	-0.53	0.12
DCLK1	-0.38	0.17	0.47	0.45	-0.58	0.09	-0.19	0.95	-0.54	0.02
DCLRE1A	0.21	21.80	-0.75	0.88	-0.26	17.39	-0.10	52.66	0.46	0.02
DCN	-0.27	37.04	0.18	8.25	0.59	5.71	0.11	8.99	0.50	0.80
DCTD	-0.28	33.23	0.58	3.01	0.62	0.09	0.19	47.42	-0.15	36.83
DCUN1D3	0.14	44.81	-0.35	2.86	0.11	49.13	-0.13	47.42	0.45	0.75
DCXR	0.20	5.93	-0.30	0.51	0.08	41.10	0.25	5.54	0.49	0.02
DDC	-0.48	1.43	0.19	11.78	-0.28	22.90	-0.94	0.06	0.34	24.40
DDHD2	0.07	44.81	0.31	2.30	0.02	58.61	0.25	23.45	0.43	0.27
DDIT4L	0.05	55.17	0.46	5.83	0.35	8.12	-0.12	49.36	-0.40	0.98
DDN	0.10	52.22	0.40	1.21	0.17	29.33	-0.31	0.11	-0.45	0.02
DDR1	-0.11	33.23			0.02	58.07	0.06	52.12	0.65	0.17
DDX1	-0.40	0.05	0.36	0.51	-0.25	2.31	-0.53	47.42	0.42	0.31
DDX17	-0.11	44.81	0.27	3.01	0.06	54.33	-0.14	3.87	-0.94	0.02
DDX31							-0.47	0.57	0.08	35.53
DDX46	-0.24	0.78	0.84	0.60	-0.36	0.09	-0.20	1.21	-0.23	1.98
DDX50	0.19	33.23	0.68	0.88	0.07	36.89	0.07	32.50	-0.42	0.07
DDX6	-0.50	1.43	0.08	11.09	-0.41	0.28	0.08	52.12	-0.26	0.47
DEAF1	0.17	29.67	-0.59	0.77	0.30	8.12	0.05	50.49	0.25	4.22
DEF6	0.44	0.05	0.15	0.78	0.52	0.09	0.69	0.29	-0.37	24.40
DENR	0.11	49.54	0.78	1.29	-0.09	54.33	0.16	23.45	-0.46	0.02
DEPTOR	0.13	49.54	-0.24	2.77	-0.61	4.05	-0.79	0.06	0.57	0.98
DFFA	0.38	0.05	0.44	0.51	0.41	9.26	0.08	49.36	-0.67	0.02
DFNB31	-0.51	0.05	0.08	12.52			0.13	13.89	0.50	0.02
DGKB	-0.10	33.23	0.52	1.29	0.26	4.05	0.41	7.10	-0.52	0.99
DGKH	-0.72	0.05	0.33	8.25	-0.33	20.03	0.32	2.91	-0.84	0.12
DHCR24	0.60	0.78	0.22	8.88	-0.08	56.82	-0.47	1.33	-0.52	0.99
DIDO1	-0.12	29.67	-0.53	0.99	-0.21	17.39	-0.50	27.83	-0.25	1.19
DIO2	-0.10	51.01	0.48	0.11	0.22	33.12	0.07	50.49	-0.15	14.82
DKKL1	-0.07	44.81	-0.30	3.01	0.52	0.52			-0.21	6.00
DLG1	-1.02	0.05	0.37	0.35	0.34	3.48	0.18	27.83	-1.17	0.02
DLG2	0.07	49.54	0.26	8.25	-0.68	0.09	0.43	2.42	-0.41	0.02

DLGAP2	-0.07	49.54	-0.18	4.12	-0.36	2.66	-0.19	41.83	0.97	0.02
DLL1	0.12	37.04	0.57	0.27	0.27	17.39	0.22	1.21	0.18	39.47
DMP1	0.19	0.93	-0.38	9.63	0.32	3.07	0.35	0.06	0.50	31.62
DMRT2					0.04	55.77	-0.78	0.06	0.25	35.53
DMXL2	-0.53	0.05	0.50	2.30	-0.39	0.64	0.35	13.89	-0.38	24.40
DNAH6	-0.03	56.87	0.44	4.12	0.33	0.64	0.51	0.73		
DNAJB4	-0.22	29.67	0.31	0.60	-0.24	4.73	-0.24	8.99	-0.88	0.02
DNAJB5	0.16	33.23	0.45	0.42	0.43	0.52	-0.37	0.13	-0.49	0.02
DNAJB9	-0.11	52.22	0.64	0.11	-0.14	12.58	0.38	7.10	-0.23	0.31
DNAJC1	-0.33	0.05	0.58	2.30	-0.38	1.00	-0.46	0.06	0.15	35.53
DNAJC13	0.95	0.40	0.34	4.12	0.10	26.12	0.03	52.12	-0.32	1.19
DNAJC18	-0.07	37.04	0.46	1.03	-0.35	8.12	0.58	23.45	0.41	0.75
DNAJC19	-0.34	0.13	-0.19	4.12	-0.10	49.13	-0.38	0.18	-0.28	11.00
DNAJC2	-0.14	49.54	-0.63	0.22	-0.29	0.40			0.16	33.88
DNAJC21	0.18	5.93	0.39	0.89	0.11	49.13	0.29	8.99	-0.34	4.22
DNAJC24	0.29	0.26	0.61	1.66	0.03	58.41	-0.09	41.83	-0.36	0.02
DNAJC28	-0.47	0.05	0.57	0.18	-0.87	0.09	0.68	0.06	0.73	0.47
DNAL1	-0.07	57.29	0.58	1.03	-0.16	41.10	-0.19	0.29	-0.45	0.39
DNALI1	-0.04	53.69	0.41	3.01	0.18	12.58	0.06	52.12	0.95	0.02
DNASE1L1	-0.26	52.22			-0.14	41.10	-0.26	49.36	0.51	0.02
DNM1L	-0.29	21.80	0.63	1.46	-0.52	0.09	0.03	51.35	-0.44	0.02
DNMT3A	-0.11	5.93	0.37	1.09	0.42	0.64	-0.81	0.86	-0.28	24.40
DOCK1	-0.31	0.53	-0.56	0.89	0.21	2.66	0.04	47.42	0.57	0.05
DOCK11	-0.71	0.78	0.47	0.67	-0.48	0.86	-0.69	5.54	-0.56	0.89
DOCK4	-0.34	0.32	0.55	1.21	-0.24	4.73	-1.07	0.25	-0.67	0.02
DOK1	0.35	1.10	0.29	0.30	0.21	0.64	0.15	19.97	0.76	0.02
DONSON	0.08	44.81	0.88	0.88	-0.08	33.12	0.08	41.83	-0.48	0.12
DPM1	-0.25	0.05	0.28	1.77	-0.28	0.64	-0.82	0.06	-0.59	0.02
DPPA2	-0.08	49.54	-0.51	0.51	-0.09	29.33	0.05	47.42	-0.10	24.40
DPYD	-0.32	25.77	0.24	5.83	-0.23	36.89	-0.23	47.42	-0.96	0.47
DPYSL4	0.04	52.22	-0.13	2.61	0.16	36.89	0.13	7.10	0.50	0.02
DR1	0.04	54.15	0.54	2.77	0.03	58.07	-0.27	0.51	-0.42	0.04
DRAM1	0.38	0.53	0.49	0.35	0.29	0.09	0.98	0.12	-0.18	14.82
DRAM2	0.01	56.77	-0.15	0.78					-0.37	0.89
DRD2	-0.59	0.53	-0.21	4.12	-0.22	8.12	-0.07	50.49	0.42	0.75
DRD4	-0.31	0.78	0.30	4.12	0.38	20.03	0.05	53.27	0.63	0.05
DRD5	-0.15	5.93	0.60	2.61	-0.08	54.33	-0.26	41.83	-0.23	0.47
DROSHA	0.13	12.65	0.45	2.61	0.17	1.10	0.14	47.42	-0.60	0.02
DRP2	0.26	3.16	0.32	7.54	-0.17	54.33	0.14	41.83	-0.56	0.07
DSG2	0.06	49.54	-0.20	5.83	-0.04	54.33			0.44	0.39
DSP	0.32	44.81	-0.55	0.61	-0.29	54.33	0.11	41.83	0.40	24.40
DSTN	0.14	44.81	0.67	0.51	-0.22	26.12	-0.07	47.42	-0.42	0.27
DTX4	-0.21	12.65	0.46	0.78	0.42	0.09	-0.27	1.33	0.58	0.02
DUSP1	-0.21	10.00			-0.21	41.10	-0.59	0.73	0.46	0.02
DUSP16	-0.45	0.05	0.76	0.35	0.05	49.13	0.54	0.13	0.63	0.99
DUSP2	0.02	56.77			0.13	49.13	0.54	0.06	0.21	0.75
DUSP26	-0.33	0.05	-0.33	2.86	0.25	17.39	0.49	0.06	0.34	4.22
DUSP4	0.21	0.93	0.19	1.66	0.19	3.48	0.11	41.83	-0.42	0.27
DUT	0.02	56.87	0.40	0.51	-0.03	57.40	0.16	13.89	0.25	4.22
DYNC1H1	-0.39	0.05	0.53	0.94	-0.18	58.93	-0.95	0.40	-0.18	11.00
DYNC2H1	-0.79	0.05	0.62	0.94	-0.76	0.44	-0.44	0.95	0.61	0.02
DYRK1A	-0.23	5.93	0.73	0.60	-0.21	10.69	-0.84	0.06	-0.40	0.27

DYRK1B	-0.05	51.01	-0.45	0.78	0.05	54.33	0.24	11.24	0.52	0.02
E2F1	0.27	1.10	0.21	0.51	0.41	2.06	0.28	41.83	0.82	0.12
E2F3	0.13	37.04	0.37	0.51	-0.37	0.72	0.53	0.12	-0.55	0.02
E2F5	-0.05	55.87	0.31	2.61	0.08	26.12	-0.42	0.06	-0.20	0.89
EARS2	0.11	44.81	0.42	4.12	-0.05	58.61	-0.78	0.06	-0.23	14.82
EBF3	0.28	44.81	-0.71	2.77	-0.42	0.28	0.99	0.06	0.41	39.47
EBI3	0.31	0.05	0.12	5.83	0.31	0.52	-0.36	11.24	0.40	0.98
ECHDC3	-0.09	54.70	0.25	1.53	0.18	56.82	-0.08	51.35	1.13	0.02
EDA	0.44	0.05	0.23	8.88	0.28	0.09	0.19	7.10	-0.61	0.02
EDNRB	-0.90	0.05	-0.41	0.18	-0.20	49.13	-0.15	41.83	0.75	0.02
EEA1	0.19	3.16	-0.90	0.67	-0.38	2.31	0.23	0.40	-0.27	0.08
EEF1D	-0.24	10.00	-0.39	0.67	0.74	0.09	-0.71	1.33	-0.93	0.02
EEPD1	0.26	0.53	0.11	5.83	-0.05	59.79	0.07	49.36	-0.49	0.04
EFCAB2	-0.28	33.23	0.71	1.03	-0.15	55.77	0.32	5.54	-0.68	0.02
EFEMP2	-0.24	0.17	0.06	11.78	0.02	60.23	0.10	49.36	0.55	0.98
EFHA1	-0.49	0.05	0.74	0.11	0.22	29.33	0.65	0.34	0.08	35.53
EFNA5	-0.15	44.81	-0.59	0.78	0.24	41.10	-0.66	0.06	0.11	24.40
EFNB2	-0.16	52.22	0.65	0.35	0.28	12.58	0.22	0.57	-0.21	0.89
EFR3A	0.20	44.81	0.71	2.12	-0.15	36.89	-0.46	0.34	-0.65	0.07
EFR3B	-0.15	49.54	0.61	0.57	-0.15	49.13	0.06	41.83	-0.50	0.99
EFS	-0.15	5.93	-0.54	2.86	-0.13	41.10	-0.10	51.35	0.52	0.02
EGF	-0.14	29.67	0.35	0.51	0.43	14.77	-0.72	0.06	-0.70	0.99
EGFR	-0.42	0.78	0.31	1.46	-0.30	0.28	0.77	3.87	0.45	0.12
EGR1	0.54	0.32	0.51	0.60	0.23	12.58	-0.22	1.88	-0.06	37.82
EGR2	1.35	0.05	0.60	0.27	0.59	0.66	-0.09	41.83	0.32	35.53
EGR4	0.65	0.05	0.11	11.09	0.21	3.48	0.11	47.42	0.35	1.19
EHD4	-0.28	0.17	-0.55	2.61	-0.03	60.51			0.53	0.12
EIF2AK1	-0.36	0.17	-0.25	3.21	0.21	1.56	0.52	0.06	-0.39	0.21
EIF2AK2			0.47	0.51	0.09	41.10	0.02	55.17	0.56	0.98
EIF2AK4	0.19	3.16	-0.56	2.77	-0.28	14.77	-0.15	13.89	-0.35	0.98
EIF2C1	0.27	3.16	-0.99	0.11	0.13	17.39	0.07	52.12	0.36	0.47
EIF2S3	-1.06	0.05	0.35	8.25	0.13	12.58	-0.68	0.35	-1.38	0.02
EIF3A	-0.18	33.23	0.72	1.66	-0.43	0.40	0.10	16.94	-0.44	0.04
EIF3D	0.14	49.54	0.20	11.78	-0.08	49.13	-1.04	0.51	-0.10	31.62
EIF3E	0.11	29.67	-0.38	0.77	-0.07	49.13	0.02	53.27	0.36	24.40
EIF3J	0.24	10.00	-0.13	5.83	0.08	49.13	0.30	32.50	0.60	0.02
EIF4A1	0.25	0.32	0.63	2.86	0.06	55.77	-0.15	3.87	0.62	0.12
Eif4e2	0.21	37.04	0.51	0.78	-0.12	49.13			-0.25	14.82
EIF4EBP1	-0.36	0.05	-0.79	2.61	0.27	2.31	0.02	53.27	0.52	0.02
EIF4G2	-0.32	0.17	0.71	2.30	-0.29	6.93	0.36	27.83	-0.51	0.02
EIF6	0.45	0.05	0.14	11.09	0.18	12.58	0.08	47.42	0.06	42.67
ELAVL2	-0.50	0.05	-0.66	0.18	-0.40	0.66	-0.39	23.45	-0.52	0.75
ELF1	-0.12	25.77	-0.89	2.77	-0.32	1.56	0.61	0.18	0.55	0.99
ELK3	-0.10	44.81	-0.24	0.51	0.06	49.13	-0.11	51.35	0.92	0.02
ELL2	-0.52	0.05	-0.77	1.29	0.22	2.66	-0.28	50.49	-0.42	0.65
ELMO1			0.16	5.83	0.04	54.33	-0.27	0.95	0.46	0.13
ELMO2	0.39	0.05	0.11	7.54	0.17	41.10	-0.06	47.42	0.48	0.65
ELMOD1	0.25	0.26	0.44	4.12	0.21	33.12	-0.54	0.06	-0.46	0.47
ELOVL1			-0.26	3.21	0.12	8.12	0.09	49.36	0.54	0.02
ELOVL7	0.04	55.87	0.61	2.30	0.02	59.43	-0.41	0.73	0.16	24.40
EMB	0.14	49.54	0.40	1.66	0.43	3.07	0.55	0.13	0.12	31.62
EMID1	-0.12	51.01	-0.04	13.30			-0.13	47.42	0.51	0.92

EML1	-0.41	7.74	-0.53	8.88	0.06	49.13	0.07	41.83	-0.52	0.13
EML5	0.01	56.51	0.31	4.12	0.03	58.93	-0.59	2.91	-0.80	0.02
EML6	0.24	1.43	0.61	0.21	0.12	36.89	0.85	7.10	0.14	33.88
EMP1	-0.31	0.93	0.17	12.52	0.15	49.13	-0.59	0.06	0.40	0.99
EMP3	-0.25	10.00	0.17	8.88	0.18	9.26	0.42	32.50	0.64	0.12
EMR1	0.01	57.11	-0.81	0.17	0.05	54.33	-0.07	51.35	0.84	0.02
EMX2	0.43	0.32	0.42	1.77			-0.19	41.83	-0.39	0.02
Enah	-0.36	0.13	-0.61	4.12	-0.12	26.12	-0.60	0.95	-0.76	0.02
ENC1	-0.76	0.17	-0.71	0.30	-0.57	0.44	-0.63	13.89	-0.27	11.00
ENO3	-0.25	7.74	-0.42	0.78	0.03	58.41	0.19	47.42	0.40	0.65
ENOX1	0.06	54.15	0.34	0.57	-0.10	33.12	0.02	53.27	-0.48	0.02
ENPP1	-0.30	25.77	-0.17	5.83			-0.28	49.36	0.46	0.13
ENTPD2	-0.14	3.16					-0.10	52.12	0.56	0.02
ENTPD3	-0.42	0.26	0.29	5.83	-0.53	0.09	-0.45	0.06	-0.59	0.99
ENTPD4	0.14	25.77	0.43	0.66	0.02	59.79	0.02	55.17	0.12	33.88
ENTPD7	0.38	1.43	-0.86	0.61	-0.05	54.33	-0.04	49.36	0.27	31.62
EPB41L2	-0.10	33.23	-0.12	5.83	0.47	0.09	0.06	41.83	0.61	0.02
EPC1	-0.49	7.74	-0.63	0.86	0.08	54.33	0.45	2.91	0.23	31.62
EPHA3	-0.38	0.51	0.78	0.18	-0.27	0.52	0.48	0.35	-0.51	0.17
EPHA5	0.30	25.77	0.62	0.78	-0.38	8.12	-0.13	41.83	-0.52	0.02
EPHB1	-0.15	12.65					-0.56	3.87	0.48	0.02
EPHB2			0.13	9.63	0.07	54.33	0.12	7.10	-0.43	0.02
ERAL1	-0.26	0.32	-0.57	0.23	-0.22	3.07	-0.28	2.42	0.29	24.40
ERBB2IP	-0.54	0.05	0.43	2.30	-0.14	6.93	0.67	8.99	0.29	31.62
ERBB3	0.09	37.04	0.40	0.67	0.24	14.77	0.45	1.62	0.51	0.27
ERC2	-0.17	18.59	0.56	1.21	-0.17	33.12	0.35	11.24	-0.44	0.31
ERCC6	-0.06	51.01	0.82	1.29	0.21	1.31	-0.09	41.83	-0.40	0.17
ERF	-0.06	44.81	0.09	7.54	0.16	20.03	0.19	2.42	0.41	0.12
ESCO1	0.42	3.16	0.55	0.42	-0.14	26.12	-0.33	3.87	-0.14	31.62
ETFDH	0.08	49.54	0.54	1.21	-0.11	36.89	-0.80	0.12	-1.06	0.02
ETV6	0.09	49.54	-0.44	1.09	0.20	2.31	-0.22	5.54	0.42	0.12
EVI5L	0.21	1.10	0.52	0.57	0.25	0.52	0.33	32.50	0.69	0.47
EVPL	-0.16	0.53	-0.47	0.51	0.32	9.26	0.30	3.87	0.47	0.02
EXD1	-0.71	0.05	0.35	0.48	-0.09	60.51	-0.35	50.49	0.70	0.75
EXOC2	0.40	0.17	0.28	0.60	-0.11	14.77	0.24	32.50	0.32	1.98
EXOC5	0.19	21.80	0.65	1.09	0.05	54.33	0.44	1.62	-0.56	0.07
EXOSC3	0.08	37.04	0.53	0.27	-0.48	2.31	0.27	0.13	-0.22	31.62
EZH2	0.04	52.22	0.47	0.67			-0.19	41.83	0.17	42.21
F11R	-0.39	18.59			0.06	36.89	-0.26	47.42	0.61	0.02
F2R	0.03	55.56	-0.12	12.52	-0.27	26.12	-0.17	1.88	-0.34	0.99
F3	0.01	56.13	0.57	0.99	0.01	59.79			0.29	44.32
FABP7	-0.47	0.26	0.51	0.88	0.23	12.58	0.29	0.18	0.38	24.40
FADD	-0.09	44.81	-0.42	0.51	0.10	41.10	0.56	0.25	0.17	2.89
FAIM			0.71	0.30			0.21	27.83	-0.13	14.82
FAM105A	0.30	29.67	0.44	0.60			0.20	50.49	0.13	41.88
FAM107B	0.08	52.22	0.22	0.51	0.10	36.89	-0.61	0.06	-0.12	24.40
FAM109A	-0.11	18.59	-0.15	2.86	-0.05	57.40			0.41	0.17
FAM114A1	0.46	0.05			0.75	1.56			0.29	2.89
FAM120B	0.10	44.81	0.30	0.78	0.05	49.13	0.03	49.36	-0.37	0.65
FAM123B	-0.48	0.05			-0.37	0.09	0.19	27.83	-0.32	31.62
FAM135A	-0.22	2.45	0.72	0.60	-0.09	36.89	-0.13	2.91	-0.59	0.02
FAM13B	0.09	44.81	0.67	1.09	0.07	41.10	-0.05	49.36	-0.69	0.04

FAM13C	0.03	56.77	0.81	0.67	-0.14	10.69	0.11	8.99	-0.53	0.02
FAM14A	-0.11	49.54	-0.17	4.12	0.01	59.43	1.15	0.34	1.62	0.02
FAM172A	-0.11	44.81	-0.68	0.89	-0.23	9.26	0.78	5.54	0.34	8.00
FAM176A	-0.35	0.51	0.62	0.60	-0.34	14.77	-0.48	11.24	-0.65	0.02
FAM184B	-0.87	0.05	0.19	0.60	-0.21	41.10	-0.14	32.50	-0.38	0.05
FAM185A	-0.13	15.28	0.10	12.52	0.03	55.77	0.07	49.36	-0.50	0.02
FAM188A	0.04	52.22	0.11	11.09	-0.17	41.10	0.08	51.35	-0.44	8.00
FAM198B	0.43	3.16	-0.07	11.09	-0.15	49.13	-0.09	52.12	-0.51	0.27
FAM19A1	0.26	1.10	0.40	1.29	0.06	54.33	0.17	27.83	-0.44	0.02
FAM19A2	-0.30	33.23	-0.06	13.30	-0.28	0.09	-0.05	47.42	-0.84	0.65
FAM203A/FAM203B	0.06	49.54	0.33	1.77	-0.09	54.33	-0.07	41.83	-0.44	0.02
FAM40B	0.03	54.70	0.17	2.61	-0.53	3.07	-0.27	0.51	-0.47	0.21
FAM46A	-0.33	0.09	-0.40	6.70	-0.36	6.93	-0.24	47.42	0.10	14.82
FAM49B	0.09	37.04	0.12	5.83	-0.17	8.12	-0.13	27.83	-0.46	0.02
FAM53B	0.31	5.93	0.36	5.83	0.45	0.28	-0.44	8.99	0.05	43.01
FAM59A	0.21	10.00	0.64	1.46	-0.12	22.90	0.11	47.42	-0.41	0.89
FAM5B	-0.07	55.87	0.47	2.77	-0.61	0.09	0.36	2.42	-0.28	6.00
FAM5C	0.21	44.81	0.62	0.35	0.18	49.13	0.37	0.25	-0.11	24.40
FAM65B	0.08	49.54	0.90	0.60	0.27	4.73	0.15	8.99	-0.23	4.22
FAM78B			-0.33	4.12	0.13	17.39	-0.12	11.24	-0.77	0.02
FAM81A	-0.13	49.54	-0.25	4.12	-0.12	49.13	-0.26	7.10	-0.38	0.89
FANCA	-0.80	0.05	-0.30	6.70	0.26	49.13			0.46	24.40
FANCB	0.26	12.65	0.58	0.51	-0.16	6.93	-0.55	0.40	-0.50	0.02
FANCD2	-0.59	0.53	0.34	2.77	0.35	5.71	0.45	4.91	-0.86	0.02
FAR1	0.11	52.22	0.45	1.21	-0.11	41.10	0.25	5.54	-0.54	0.31
FARP1	0.50	0.32	0.33	4.12	-0.22	29.33	-0.18	19.97	1.02	0.02
FAS	0.03	52.83	0.40	5.83	-0.18	8.12	0.29	0.18	0.57	0.02
FASLG	0.77	0.05	-0.27	6.70	0.36	0.72	0.09	41.83	0.14	33.88
FASTK	0.13	33.23	0.36	0.48	0.11	17.39	-0.48	0.06	0.20	44.05
FAT3	0.43	0.53	-0.40	4.12	-0.24	2.06	0.08	41.83	0.04	44.05
FAT4	0.10	25.77	0.77	0.60	0.03	55.77	-0.20	27.83	-0.63	0.02
FBLN2	-0.09	55.17			0.52	0.66	-0.11	53.83	0.29	0.21
FBLN5	-0.51	0.67	0.23	6.70	0.12	29.33	-0.29	11.24	0.93	0.02
FBN2	-0.10	37.04	0.30	2.77	0.24	0.86	-0.92	1.21	-0.09	41.26
FBRS	0.10	44.81	-0.30	3.01	0.09	49.13	0.18	13.89	0.62	0.05
FBXL18	-0.10	49.54	-0.27	6.70	-0.13	49.13	-0.30	32.50	0.48	0.02
FBXL7	0.10	44.81	-0.77	1.46	-0.43	5.71	1.27	0.12	0.69	0.98
FBXO21	0.26	12.65	0.27	0.51	-0.18	49.13	1.44	0.06	-0.83	0.02
FBXO22	0.31	0.17	0.67	0.78	0.10	49.13			-0.64	0.65
FBXO3	0.43	0.13	0.56	0.51	0.21	54.33	-0.36	0.06	-0.78	0.07
FBXO4	-0.09	33.23	-0.66	0.99	0.09	49.13	-0.15	4.91	0.05	40.66
FBXW8	0.09	49.54	0.37	5.83	0.11	33.12	0.61	0.06	-0.29	0.08
FCER1G	-0.13	49.54	-0.54	1.66	0.05	56.82	0.30	0.06	1.06	0.02
FCGR1A	0.31	0.67			0.02	58.41	0.17	5.54	1.45	0.02
FCGR2A	0.51	0.05	0.37	5.83	0.26	0.66	-0.28	2.91	0.71	0.02
FCGR2B	-0.63	0.05	-0.48	1.29	-0.32	2.66	0.29	0.35	-0.42	6.00
FCGR3A	0.04	51.01	-0.33	3.01	0.07	49.13	0.01	55.17	0.56	0.02
FCGRT	-0.09	52.22	0.23	4.12	0.07	54.33	0.23	2.91	0.44	0.07
FCHO2	0.34	0.40	0.41	1.09	0.06	41.10	-0.15	3.87	-0.55	0.02
FDX1	-0.14	7.74	0.67	0.26	0.08	49.13	0.23	2.42	0.18	1.98
FECH	-0.11	37.04	0.68	1.29	-0.18	14.77	-0.25	2.91	-0.40	0.12
FEM1C	-0.18	51.01	-0.36	3.21	-0.42	0.86	-0.71	5.54	-1.13	0.02

FES	-0.13	52.83	0.40	0.26	0.19	1.56	0.20	27.83	0.66	0.02
FGD2	0.16	10.00					0.56	0.06	0.67	0.02
FGD4	0.49	0.05	-0.56	1.66	0.08	41.10	-0.72	0.06	-0.07	38.75
FGD6			-0.71	0.57	0.35	33.12	-0.64	11.24	0.40	0.47
FGF10	0.18	18.59	0.78	0.23	0.08	33.12	-0.06	41.83	0.25	40.66
FGF11	0.13	49.54	0.39	0.31	0.19	3.48	0.03	50.49	0.12	41.26
FGF13	-0.16	4.28	0.67	0.57	0.07	49.13	-1.16	0.06	-0.67	0.02
FGF19	0.16	12.65	-0.29	3.01	0.29	3.07	-0.60	4.91	0.40	0.31
FGF5	-0.84	0.05	0.48	0.45	-0.70	1.56	-0.74	1.88	-0.67	0.99
FGF9	0.23	37.04	0.57	0.11	-0.11	20.03	-0.05	47.42	-0.56	0.27
FGFR2	-0.15	1.43	0.55	0.67	0.31	0.44	0.48	1.62	-0.11	24.40
FGFRL1							-0.09	47.42	0.44	0.42
FHDC1	0.47	0.17			-0.21	6.93	-0.38	1.62	0.17	33.88
FHOD1	0.09	49.54	0.22	2.30			0.86	0.95	0.52	0.04
FIGF	0.21	4.28	0.21	7.54	0.13	49.13	0.65	0.12	0.30	11.00
FKBP10					0.09	22.90	0.25	7.10	0.46	0.90
FKBP15	-0.39	0.05	-0.34	0.94	-0.36	1.56	0.38	1.88	-1.12	0.02
FKBP5	-0.49	7.74	0.30	5.83	0.24	55.77	0.82	8.99	0.59	0.80
FKTN	0.07	49.54	0.45	0.78	0.16	2.06	0.09	49.36	-0.37	0.12
FLNC	0.14	7.74	0.24	3.21	-0.10	41.10	0.13	49.36	1.31	0.02
FLRT3	-0.44	0.67	0.57	1.46	-0.28	36.89	-0.36	2.91	-0.39	8.00
FLT1	0.03	52.22	0.48	0.60	0.05	54.33	0.24	0.86	0.40	0.99
FLT3LG	0.02	56.51	-0.44	0.78	-0.25	1.82	-0.31	16.94	-0.19	11.00
FLVCR1	0.40	0.78	0.45	0.26	0.15	4.73				
Fmn1	-0.53	0.05	-0.24	4.12	0.21	49.13	-0.04	47.42	0.38	24.40
FMNL2	-0.43	0.05	-0.30	3.21			0.12	19.97	-0.23	11.00
FMNL3					0.06	54.33	0.14	23.45	0.62	0.88
FNTB	0.28	5.93	0.38	4.12	0.09	33.12	-0.49	0.34	0.24	24.40
FOS	0.97	0.05	0.68	0.11	0.19	0.64	0.26	0.51	-0.10	24.62
FOSB	0.20	37.04	0.19	11.09	0.48	0.09	0.20	1.33	0.00	44.32
FOSL2	0.41	3.16	0.98	0.11	0.56	0.09	0.18	27.83	-0.35	0.17
FOXC2	-0.92	0.05			0.15	33.12	-0.19	50.49	0.34	11.00
FOXF2	-0.08	57.29	0.82	0.99	0.17	20.03	-0.64	0.86	-0.57	0.02
FOXN3	-0.21	0.78	0.65	0.78	-0.50	0.52	0.64	13.89	0.53	0.05
FOXO1	-0.09	33.23	0.86	0.48	0.08	36.89	0.59	0.06	0.44	0.89
FOXP2	-0.35	1.10	-0.12	9.63	-0.63	0.86	0.24	1.21	-0.22	8.00
FPGS	-0.47	0.67	-0.18	0.78			0.15	41.83	0.30	11.00
FRAS1	-0.53	0.17	-0.48	1.46	0.01	60.23	-0.78	0.06	-0.64	0.99
FRMD5	0.13	29.67	0.36	5.83	0.10	49.13	-0.27	0.34	-0.44	0.47
FRRS1	-0.08	44.81	0.48	2.61	0.11	8.12	0.11	53.27	0.76	0.04
FRZB	-0.15	51.01	0.64	1.03	-0.18	4.73	0.43	0.51	-0.54	0.12
FSTL5	-0.64	0.26	-0.23	2.86	-0.34	10.69	-0.18	27.83	-0.71	0.13
FTO	0.36	18.59	0.42	0.35	-0.12	49.13	-0.24	32.50	-0.18	2.89
FUBP1	-0.31	3.16	0.44	1.09	0.52	9.26	0.31	51.35	-0.48	0.07
FUT8			0.49	5.83	0.14	5.71			-0.28	6.00
FXYD1	0.09	53.69	-0.33	2.86	0.25	1.31	-0.14	5.54	0.79	0.02
FXYD5	0.08	33.23					0.14	27.83	0.52	0.02
FXYD6			0.26	2.12	0.40	1.56	-0.04	53.83	0.65	0.47
FYB	-0.05	52.22	-0.27	3.21	0.03	58.07	0.31	1.62	0.45	0.02
FYCO1	-0.43	0.05	0.77	1.53	-0.35	9.26	-0.25	5.54	-0.11	0.13
FZD10	0.22	0.67	0.71	0.57	-0.04	59.79	0.03	53.27	0.24	33.88
FZD4	-0.23	1.43	-0.26	2.86	0.11	55.77	0.67	0.25	-0.21	0.65

FZD9	-0.21	29.67	-0.43	4.12	0.06	54.33	0.28	3.87	0.52	0.02
G2E3	0.23	37.04	0.35	0.20	0.32	1.82	-0.55	0.13	0.22	31.62
G3BP1	0.10	25.77	0.32	0.27	0.14	17.39	0.28	19.97	-0.51	0.31
G3BP2	-0.08	49.54	-0.15	8.25	-0.15	10.69	0.08	49.36	-0.48	0.02
GABBR1	0.09	44.81	-0.40	2.77	0.28	49.13	0.81	0.06	0.26	4.22
GABPA	0.20	7.74	0.62	0.51	0.04	54.33	-0.39	0.35	-0.49	0.05
GABRA1	-0.38	0.05	-1.10	0.11	-0.24	17.39	-0.84	0.73	-0.33	0.31
GABRA2	-0.38	0.05	-0.41	2.12	-0.14	41.10	-0.20	27.83	-0.44	0.31
GABRA3	0.03	54.70	-0.97	2.77	0.46	0.64	-0.38	3.87	-0.14	8.00
GABRA4	-0.05	54.15	-0.56	1.21	-0.24	10.69	-0.21	41.83	-0.39	0.02
GABRA5	0.09	44.81	0.43	2.12	-0.24	8.12	-0.11	16.94	-0.45	0.02
GABRG2	-0.19	33.23	0.40	5.83	-0.73	17.39	-0.51	27.83	-0.70	0.02
GABRG3	-0.04	53.69	-0.23	3.01	-0.45	0.09	-0.63	0.06	0.05	42.03
GABRR1	-0.05	54.70	-0.37	0.42	-0.02	60.51	-0.09	47.42	-0.06	31.62
GAD2	-0.23	0.53	0.39	0.78	-0.43	0.66	-0.44	1.33	-0.27	4.22
GADD45B	0.53	0.05	0.21	1.29	0.18	3.48	-0.11	41.83	0.53	0.99
GADD45G	0.17	3.23	0.49	0.99	0.08	36.89	0.05	47.42	0.08	31.62
GADD45GIP1	0.46	0.93	0.46	0.83	-0.04	57.40	0.14	13.89	0.20	11.00
GAL3ST1	-0.10	56.77	0.22	1.66	0.48	0.24			-0.10	36.83
GALC	0.85	0.09	-0.23	2.86	0.22	3.07	0.10	27.83	0.28	31.62
GALK2	0.53	0.05			0.06	57.40	-0.19	13.89	-0.09	36.83
GALNT1	-0.38	0.51	0.11	8.25	-0.23	1.82	0.26	47.42	-0.84	0.02
GALNT10	-0.46	0.67	0.22	1.53	-0.14	41.10	0.28	41.83	0.53	0.99
GALNT11	0.14	29.67	-0.50	4.12	-0.02	59.43	-0.23	1.21	-0.48	0.12
GALNT12	-0.43	1.43	-0.26	4.12	0.36	1.82	-0.63	0.06	0.74	0.02
GALNT13	-0.20	1.10	0.66	0.51	-0.14	49.13	-0.21	0.57	-0.38	0.99
GALNT14	0.42	0.43	-0.20	3.01	-0.12	29.33	-0.29	41.83	0.34	24.40
GALNT3	0.21	33.23	-0.77	1.09	-0.71	0.64	0.09	51.35	-0.34	24.40
GALNT6	0.48	0.05	0.22	0.51	0.23	49.13	0.27	41.83	0.29	24.40
GALNTL2	-0.46	0.13			-0.22	26.12	0.94	0.13	1.34	0.02
GALNTL4	-0.49	0.05	0.71	1.46	-0.51	0.09	-0.31	2.42	-0.88	0.02
GALT	-0.16	25.77	-0.50	0.60	0.02	60.51	0.03	53.27	-0.12	14.82
GARNL3	-0.18	1.94	-0.71	2.86	0.37	0.24	-0.53	16.94	0.43	0.39
GATA2	-0.28	4.28	0.69	0.60	0.44	10.69	-1.21	0.12	0.60	0.02
GATA6	-0.52	1.94	0.65	0.51	-0.11	22.90	-0.16	23.45	-0.18	31.62
GATM	-0.26	0.17	0.28	9.63	-0.15	12.58	-0.23	0.57	0.54	0.05
GBF1	-0.63	0.09	-0.43	0.48	-0.34	1.82	0.07	52.66	-0.03	38.75
GCC2	0.13	51.01	0.46	1.21	0.04	55.77	0.42	0.35	-0.48	0.02
GCN1L1	0.31	0.53	0.43	1.46	-0.69	0.09	-0.49	1.33	0.25	0.39
GCNT1	0.63	0.05	-0.21	3.21	0.35	9.26	-0.35	49.36	1.11	0.02
GCNT2	-0.78	0.05			0.12	29.33	-0.69	7.10	-0.26	24.40
GEN1	0.03	55.87	0.65	0.18	-0.13	36.89	0.63	0.06	0.08	33.88
GFAP									1.81	0.02
GFM1	0.17	25.77	0.78	0.27	0.11	26.12	-0.30	1.62	-0.46	0.02
GFRA1	-0.47	0.78	-0.17	0.51	-0.36	0.09	-0.66	0.06	-0.43	0.99
GGT5	-0.48	2.45	0.18	0.60			0.98	0.06	0.83	0.02
GGTA1P	-0.16	29.67	-0.15	4.12	0.36	22.90	0.47	0.35	0.74	0.89
GHR	-0.75	0.78	-0.23	1.66	0.35	0.66	-1.73	0.06	0.61	0.08
GIGYF1	0.13	44.81	-0.50	2.61	0.06	54.33	-0.55	0.06	0.14	24.40
GJA3			-0.49	0.42	-0.06	54.33	0.06	49.36	0.17	31.62
GJA5	0.26	7.74	-0.25	3.21	0.31	0.72	0.53	0.40	0.28	4.22
GJB2	0.03	55.17	0.93	0.18	-0.32	3.07	0.61	16.94	0.60	0.99

GJB6	-0.10	44.81	0.29	0.51	0.05	54.33	0.15	8.99	0.64	0.02
GLA	0.04	53.69	0.41	0.83	-0.09	49.13	-0.11	47.42	-0.11	33.88
GLI3	-0.15	37.04	-0.05	10.40	0.29	29.33	-0.08	50.49	0.82	0.02
GLIPR2	0.25	0.32	-0.08	12.52	-0.09	59.43	-0.20	0.25	0.93	0.02
GLMN	0.31	0.67			0.02	60.23			-0.50	0.05
GLRX2	0.25	0.53	0.48	0.11	-0.04	58.07	-0.08	41.83	0.28	8.00
GLS	-0.25	15.28	0.62	0.91	-0.45	1.31	-0.34	13.89	0.62	31.62
GMFB	0.40	0.51	0.58	0.17	-0.18	8.12	-0.17	0.95	-0.52	0.07
GMFG	-0.04	56.13	0.47	0.18	0.10	49.13	-0.37	0.13	0.65	0.02
GNAI1	-0.19	3.16	-0.48	0.11	-0.24	2.66	-0.08	49.36	0.14	24.40
GNAZ	0.34	21.80	0.59	0.27	0.14	36.89	-0.16	47.42	-0.39	0.12
GNB1	-0.09	54.70	0.46	0.51	0.16	41.10	-0.30	0.73	-0.28	0.27
GNG11	-0.19	18.59	-0.51	0.61	0.15	17.39	0.24	1.33	0.36	14.82
GNS	-0.07	55.87	-0.93	0.94	0.23	49.13	-0.27	49.36	0.27	24.40
GOLGA3	0.46	0.05	0.52	0.51	-0.07	41.10	0.22	1.21	-0.11	31.62
GOLGA5	0.32	15.28	0.25	5.83	-0.71	0.09	0.44	0.40	-0.14	24.40
GOLGA7	-0.09	55.56	0.53	0.35	0.12	49.13	0.05	49.36	-0.22	1.98
GOLGB1	-0.46	0.05	0.43	6.70	-0.54	0.28	0.59	0.13	-0.41	0.08
GOLPH3	0.13	44.81	0.71	0.11	0.25	9.26	-0.45	41.83	0.46	0.98
GOPC	0.18	44.81	-0.41	3.21	0.31	0.09	-0.68	4.91	-0.23	11.00
GORAB	0.18	2.45	-0.08	13.30	-0.23	3.48	-0.12	32.50	-0.50	0.02
GPAT2	0.11	18.59	-0.22	1.77	-0.11	49.13			0.47	0.17
GPC5	-0.36	1.43	0.79	0.09	-0.56	1.31	0.34	47.42	0.12	44.05
GPCPD1	-0.33	0.32	0.23	8.25	-0.13	55.77	0.08	47.42	-0.43	0.02
GPM6B	0.08	49.54	-0.36	0.51	-0.36	0.64	-0.11	13.89	-0.35	0.05
GPNMB	0.06	44.81	-0.29	0.51			0.14	16.94	1.23	0.13
GPR108	-0.06	54.15	-0.43	3.21	0.02	58.41	0.10	23.45	0.40	0.12
GPR124	-0.04	55.87	-0.42	4.12	0.40	0.64	0.04	53.27	0.17	33.88
GPR156	-0.19	0.32	-0.52	0.51	-0.07	41.10			0.27	11.00
GPR160	-0.79	0.05			-0.16	49.13	0.38	8.99	0.85	0.02
GPR17	0.11	49.54	-0.16	5.83	0.07	54.33	-0.04	51.35	0.56	0.02
GPR179	-0.46	0.05	-0.56	2.86	0.13	36.89	0.19	4.91	0.17	6.00
GPR26	-0.51	0.93	0.18	7.54	-0.41	5.71	-0.62	41.83	-0.25	14.82
GPR37	-0.07	49.54	-0.31	5.83	0.02	58.41	-0.47	0.06	-0.29	0.75
GPR37L1	-0.13	7.74	-0.08	5.83	0.04	49.13	0.16	27.83	0.48	0.75
GPR39	-0.09	44.81	-0.67	0.51			0.07	47.42	0.24	24.40
GPR4	-0.03	56.13	-0.47	2.86	-0.18	8.12	-0.52	0.06	0.09	37.82
GPR56			0.29	0.94			0.19	41.83	0.57	0.13
GPR6	-0.13	21.80	-0.21	0.78	0.04	54.33	0.42	0.13	-0.59	0.02
GPR64	0.07	37.04	0.57	0.99	0.07	54.33	0.30	41.83	-0.30	36.83
GPR84	-0.18	5.93	0.49	0.51					1.57	0.02
GPR85			0.63	0.67	-0.09	33.12	0.18	1.33	-0.53	0.02
GPR88	-1.33	0.05	-0.43	4.12					0.09	42.37
GPR98	0.07	37.04	-0.36	3.21	0.13	5.71	0.43	0.57	-0.07	31.62
GPRC5C	-0.14	2.45	-0.35	3.01	0.28	0.66	-0.29	32.50	0.67	0.02
GPSM3	0.62	0.05	0.18	5.83	0.14	9.26	-0.43	0.51	0.57	0.47
GPX3			0.24	5.83	-0.56	0.09	-0.32	0.25	0.49	0.04
GRAMD3	-0.10	33.23	-0.31	8.25	0.09	26.12	0.52	0.35	0.41	0.89
GRAP	0.05	52.22	-0.39	0.35	0.08	41.10			0.59	0.02
GRB7	-0.15	52.22	-0.20	3.21	-0.13	12.58	0.38	0.11	0.46	0.89
GREB1L			-0.52	0.60			-0.16	2.91	0.31	0.27
GREM1	-0.24	49.54	0.10	6.70	0.50	0.44	-0.64	7.10	0.61	31.62

GRIA2	0.25	2.45	0.59	0.42	-0.32	36.89	-0.23	27.83	-0.27	1.19
GRIA3	-0.47	0.05	0.45	1.66	-0.19	6.93	-0.20	0.73	-0.66	0.02
GRIA4	-0.56	0.05	0.40	4.12	-0.79	0.40	-0.60	8.99	-0.45	0.13
GRID1	-0.37	0.51	0.33	1.53	0.09	57.40	-0.92	0.06	-0.61	0.02
GRIK4	-0.65	0.05	0.31	0.94	-0.12	58.07	0.45	1.62	-0.65	0.75
GRIN1	-0.03	54.15	-0.16	4.12	0.12	22.90	-0.57	0.06	-0.17	24.40
GRIN2B	-0.08	44.81	-0.54	0.51	-0.13	1.31	-0.38	3.87	-0.42	0.99
GRIP1	-0.13	29.67	0.35	3.01	-0.23	2.06	-0.16	19.97	-0.53	0.12
GRK4	0.02	57.11	-0.40	0.31	0.02	58.41	0.11	41.83	0.31	0.98
GRK5	0.03	52.83	0.37	0.51	0.25	5.71	0.59	16.94	-0.63	0.12
GRK6	0.13	29.67	-0.42	0.60	-0.12	54.33	0.31	32.50	0.06	42.55
GRM5	-0.64	0.26	0.34	2.30	-0.58	6.93	-0.23	11.24	-0.16	24.40
GSDMA	0.14	2.45	-0.48	0.94	-0.22	26.12	0.05	47.42	0.33	31.62
GSDMD	0.21	2.45	-0.06	11.09	0.25	9.26	-0.41	0.35	0.84	0.02
GSG1L	0.08	49.54	0.46	0.18	0.23	36.89			0.00	44.32
GSK3A	0.31	3.16	0.31	5.83	0.03	57.40			0.42	0.39
GSN	0.23	4.28	0.12	9.63			-0.39	0.40	0.90	0.02
GSR	-0.05	49.54	0.34	2.30	0.03	58.61	0.46	0.40	0.11	40.66
GSTK1	-0.24	0.67	-0.63	1.66			0.25	3.87	0.27	24.40
Gstm3	-0.17	37.04	-0.16	4.12	0.16	36.89	0.09	27.83	0.58	0.02
GSTM5	-0.18	29.67	-0.18	3.21	0.16	20.03	0.10	41.83	0.56	0.02
GTDC1	-0.42	0.05	-0.22	5.83	0.19	6.93	0.17	8.99	-0.38	0.27
GTF2IRD1	-0.49	0.05	0.41	5.83	-0.62	9.26	-0.36	1.33	-0.13	24.40
GTF3C4	0.39	0.05	-0.58	3.21	0.13	6.93	0.06	50.49	0.13	33.88
GUCY1A3	-0.89	0.05	-0.40	3.01	0.51	1.31	0.29	41.83	-0.73	0.02
GUSB	0.04	54.15	-0.19	5.83	-0.09	58.07	0.13	27.83	0.63	0.02
GZMM			0.38	7.54	0.07	41.10	-0.21	19.97	-0.65	0.04
H1FX	1.14	0.17	-0.12	5.83	0.25	12.58	0.11	41.83	0.45	0.75
H6PD	-0.24	0.40	-0.36	0.83	-0.17	2.31	0.10	19.97	-0.06	33.88
HADH	-0.89	0.05	-0.49	3.01	0.12	10.69	0.81	0.06	0.97	0.02
HAO1	-0.49	0.51	0.41	0.11	0.19	4.05	-1.03	1.33	-0.87	0.02
HAPLN1	-0.48	0.17	0.92	0.30	0.12	41.10	1.36	0.06	-0.87	0.02
HAS1	-0.39	0.17	-0.18	4.12	-0.57	0.09	0.97	1.62	-0.43	0.89
HAS3	0.49	0.05	0.55	0.88	0.21	0.86	0.13	47.42	-0.48	0.02
HBEGF	0.12	12.65	0.25	5.83	0.17	3.48	-0.42	0.18	0.36	8.00
HCFC1	-0.75	0.05	-0.37	5.83	0.32	5.71	0.26	4.91	-0.12	24.40
HCFC2	0.13	37.04	0.52	2.77	-0.12	20.03	-0.21	0.25	0.49	0.99
HCK	0.54	0.17	-0.37	6.70	0.13	4.05			0.98	0.02
HCLS1	0.02	56.13	-0.28	2.86	0.08	29.33	0.11	47.42	0.57	0.07
HCN3	-0.36	15.28	-0.46	2.77	-0.69	0.09	0.94	0.13	-0.15	35.53
HCRTR2	-0.85	0.17	-0.43	4.12	-0.07	57.40	-0.72	1.62	-0.79	0.02
HCST	-0.05	57.37	-0.15	0.78	0.30	2.06	-0.48	0.06	1.24	0.02
HDAC7	-0.51	0.05	-0.29	3.01	0.16	20.03	-0.24	27.83	0.29	31.62
HDAC8	-0.16	3.16	0.29	8.88	0.14	49.13	-0.29	11.24	-0.75	0.02
HDAC9	-0.54	0.05	-0.26	0.78	-0.64	0.09	-0.60	0.25	-1.02	0.02
HDC	-1.37	0.05	0.76	0.30	0.49	12.58	-0.06	50.49	1.18	0.02
HDX	-0.25	54.70	-0.43	4.12	-0.39	0.40				
HEATR3	0.23	0.17	0.53	3.21	0.15	22.90	0.46	0.51	-0.93	0.02
HECTD2	0.06	44.81	0.28	1.66	-0.39	0.09	-0.65	0.95	-0.64	0.05
HECW1	-0.37	0.17	-1.11	2.61	0.12	49.13	0.05	51.35	0.28	24.40
HECW2	0.18	18.59	0.63	0.78	0.14	49.13	0.68	0.95	-0.54	0.13
HEG1	0.37	0.17	-0.32	3.21	-0.13	54.33	-0.75	0.06	0.26	0.98

HELB	0.24	4.28	-0.13	5.83	-0.27	8.12	0.17	41.83	-0.64	0.02
HELQ	0.23	37.04	-0.29	4.12	-0.44	2.31	-1.14	0.06	0.03	43.61
HERC1	0.35	1.94	0.35	3.21	-0.56	0.09	-0.68	0.06	-0.12	14.82
HEXB	0.06	44.81	0.15	1.66	-0.13	9.26	0.16	19.97	0.58	0.02
HFE	0.63	0.17	0.15	5.83	0.57	2.06	0.38	8.99	0.62	0.02
HGF	0.07	44.81	-0.45	0.12	0.47	0.44	0.03	53.83	-0.04	44.05
HHAT	0.11	25.77	-0.29	4.12	-0.09	36.89	-0.56	0.06	-0.07	40.05
HHEX									1.44	0.02
HIP1	0.20	37.04	0.28	3.01	0.07	41.10	-0.08	49.36	-0.62	0.02
HIVEP3	-0.77	0.13	-0.37	4.12	-0.25	3.07	-0.86	0.06	-0.38	0.08
HJURP	-0.79	0.13	-0.92	3.21	0.30	33.12	-0.64	23.45	-0.75	0.17
HK2	0.18	4.28	-0.41	5.83	0.03	56.82	0.08	52.12	0.84	0.02
HLA-B	1.14	0.17	0.31	2.12	0.25	12.58	0.11	41.83	0.50	0.02
HLA-C	0.11	44.81	-0.12	5.83	-0.18	20.03	-0.36	0.06	0.98	0.02
HLA-DMB	0.42	3.16	-0.35	0.27	0.71	0.40	0.55	23.45	0.89	0.02
HLA-DOA	-0.32	5.93			0.46	4.05	0.34	32.50	0.67	0.17
HLA-DQB1	0.32	44.81	0.24	6.70	0.28	0.64	-0.19	47.42	0.71	0.02
HLA-E	0.20	21.80	0.23	2.77	0.13	22.90			0.40	0.12
HLA-G	0.20	10.00	-0.19	4.12	-0.53	0.09	-0.22	4.91	0.58	0.02
HMCN1	-0.26	0.93			-0.57	0.44	0.05	52.66	0.53	0.07
HMGA2	-0.09	57.29	-0.53	0.26	-0.24	20.03	-0.24	13.89	-0.10	39.47
HMGCR	0.31	44.81	0.66	0.67	-0.38	0.09	0.33	47.42	-0.92	0.08
HMGXB4	0.25	0.17	0.78	0.57	0.56	0.09	0.13	41.83	-0.15	24.40
HMMR	0.11	49.54	-0.71	0.51			-0.47	32.50	-0.26	14.82
HN1L	-0.32	49.54	0.23	4.12	-0.45	0.09	0.40	1.21	0.79	0.39
HNRNPAB	-0.12	44.81	0.46	1.21	-0.12	26.12	-0.74	0.12	-0.76	0.02
HNRNPC	-0.21	18.59	0.64	1.66	-0.19	10.69	-0.18	0.40	-0.52	0.02
HNRNPR	-0.20	44.81	0.57	1.66	-0.24	2.31	-0.33	5.54	-0.36	0.17
HNRPDL	0.13	44.81	0.66	1.77	-0.06	57.40	-0.13	41.83	-0.34	0.04
HOMER1	0.31	0.93	0.63	0.99	-0.17	26.12	-0.40	0.57	-0.29	0.39
HOXA7	-0.07	49.54	-0.35	0.99	0.04	54.33	0.05	50.49	-0.01	24.40
HPS3	-0.89	0.05	0.61	0.18	-0.58	1.82	0.07	49.36	-0.69	0.02
HPS6	0.14	7.74	0.34	1.77	0.04	55.77	0.57	0.06	0.12	31.62
HS1BP3	0.17	5.93	-0.14	8.25	0.49	0.24	-0.43	7.10	0.88	0.02
HS2ST1	0.17	7.74	0.75	0.60	0.16	3.48	0.17	7.10	-0.37	6.00
HS3ST1	0.46	0.53	-0.40	4.12	-0.22	22.90			0.07	40.66
HS3ST3B1	-0.22	10.00	-0.12	11.78	-0.29	0.86	0.24	49.36	0.51	0.02
HSD3B7	-0.23	4.28	0.11	2.86	-0.08	54.33	-0.38	1.62	0.45	0.08
HSP90B1	0.09	37.04	-0.51	2.12	-0.48	0.09	0.13	47.42	-0.02	41.88
HSPA12A	0.27	0.05	-1.39	0.20	0.23	4.05	0.26	1.62	-0.30	0.17
HSPA2	-0.12	12.65	0.71	0.18	-0.16	14.77	0.15	3.87	-0.41	4.22
HSPA9	0.14	44.81	0.74	0.99	-0.09	54.33			-0.45	0.02
HSPB1			0.28	1.77	0.31	0.40	0.24	8.99	0.76	0.02
HSPB2	0.14	44.81	0.15	9.63	0.40	0.09	0.59	0.06	0.28	4.22
HSPB3	0.31	0.78	-0.47	1.46	0.15	29.33	0.41	16.94	0.48	0.04
HSPB6	0.27	1.10			0.22	17.39	0.06	49.36	0.97	0.02
HSPB8	-0.23	49.54	0.31	2.86	0.92	0.40	0.40	0.13	0.87	0.89
HTATIP2	0.48	0.78	0.41	1.53	0.16	1.82	0.20	16.94	0.07	42.67
HTR3A	0.29	18.59	0.39	2.77	0.05	56.82	0.17	7.10	-0.68	0.05
HTR5B	0.14	44.81	0.49	0.61	0.33	1.10	0.03	52.66	0.65	0.99
HTR6	-0.19	25.77	-0.56	0.78	-0.30	5.71	0.03	54.83	0.41	0.08
HUS1	-0.39	0.43	-0.17	6.70	-0.31	29.33			0.05	42.84

HUWE1	-0.18	3.16	-0.40	0.78	-0.72	0.64	-0.30	41.83	0.17	31.62
HYAL3	-0.43	10.00	-0.11	6.70	0.13	29.33	0.33	1.62	0.69	0.02
HYI	-0.30	0.26	-0.27	4.12			0.27	3.87	0.59	0.27
HYOU1	-0.10	49.54	-0.44	3.21	0.08	49.13	0.08	53.27	0.45	0.04
IARS2	0.09	44.81	0.55	0.66	-0.36	2.66	0.07	49.36	0.14	39.47
ICAM1	0.04	51.01	-0.23	3.21	0.35	2.06	0.53	0.34	1.18	0.02
ICAM2	0.04	49.54	0.25	7.54	0.30	0.64	-0.97	0.06	-0.02	44.32
ID1					0.22	22.90	0.09	32.50	0.99	0.02
ID2	0.03	55.17	0.42	5.83	0.44	0.72	0.18	41.83	0.17	24.40
ID3	-0.28	49.54	-0.14	4.12	0.08	33.12	0.45	0.13	0.74	0.02
IDH2	0.39	0.45	0.27	5.83	0.17	1.31	0.21	47.42	0.18	4.22
IDH3A	0.08	44.81	0.44	4.12	-0.09	41.10	-0.10	41.83	-0.43	0.02
IER2	0.50	0.05	0.42	0.51	0.29	1.56	0.46	11.24	-0.39	0.65
IER3	0.48	0.17	0.35	5.83	0.53	1.10	0.09	41.83	0.43	0.02
IFI27L2	0.06	44.81	-0.17	4.12	0.01	59.43	1.15	0.34	1.48	0.02
IFI30	0.18	15.28	0.07	8.88	0.28	3.07	-0.23	19.97	0.47	0.21
IFIH1	-0.18	44.81	0.22	8.25			0.71	0.06	0.67	0.02
IFIT3			0.63	0.99	-0.10	49.13	-0.30	0.06	0.90	0.21
IFITM2	0.03	52.22	-0.58	0.51	0.22	2.31	-0.16	8.99	0.66	0.02
IFITM3	-0.40	0.53	0.11	11.09			0.32	0.57	1.19	0.02
IFNGR1			-0.25	6.70	0.08	36.89			0.64	0.02
IFT140	-0.43	0.05	0.24	5.83	-0.06	49.13	0.07	41.83	0.26	31.62
IGF1	0.80	0.09	0.17	8.25	0.13	54.33	0.51	0.06	0.29	24.40
IGF1R	0.39	0.09	0.29	1.46	-0.47	41.10	0.05	50.49	-0.13	33.88
IGF2	-0.64	0.05	0.41	0.51	0.14	14.77	0.06	53.27	0.34	0.47
IGFBP2	-0.13	49.54	-0.10	8.88	0.19	26.12	0.16	3.87	0.58	0.02
IGFBP3	0.25	0.26	0.44	0.94	-0.56	0.09	0.14	19.97	-0.39	0.12
IGFBP5	-0.37	2.45	-0.28	3.21	0.16	12.58	0.40	0.95	1.29	0.02
IGFBP6	0.23	10.00			0.37	2.06	0.19	2.42	0.73	0.13
IGFBPL1	-0.06	44.81	-0.23	6.70	-0.05	49.13	0.36	1.21	0.45	0.80
IGHA1	-0.13	37.04	-0.94	0.66	-0.40	29.33	-0.27	2.91	0.42	11.00
IGHM	-0.07	44.81	-0.51	0.78	-0.21	0.86	0.21	0.73	0.44	0.08
IGSF3	-0.58	0.05	-0.51	0.45	-0.27	9.26	0.12	16.94	0.15	33.88
IGSF6	-0.31	7.74	-0.13	5.83	-0.19	54.33	-0.15	23.45	0.84	0.02
IL10RA	0.34	0.17	0.41	0.11	0.44	1.31	-0.37	32.50	0.62	0.02
IL10RB	0.26	10.00	0.46	2.12	0.11	8.12	0.37	0.06	0.59	0.02
IL11RA	-0.13	3.16	-0.36	3.21	0.24	9.26	-0.22	49.36	0.46	0.47
IL15RA	-0.06	33.23	-0.60	0.61	-0.05	54.33	-0.06	41.83	0.19	31.62
IL16	-0.47	0.05	-0.16	4.12	-0.62	2.31	0.43	13.89	-0.58	0.27
IL17F	0.46	0.16	-0.09	8.25	0.03	56.82	-0.14	32.50	0.01	44.05
IL18BP	-0.18	18.59	-0.28	3.21	0.16	22.90	-0.35	1.88	0.56	0.02
IL1RAP	-0.42	0.05	0.41	0.51	-0.51	0.09	-0.53	1.33	-0.48	0.99
IL20RA	-0.45	44.81	-0.39	6.70	0.72	0.09	0.22	54.83	-0.89	0.89
IL20RB	-0.71	0.09	0.46	0.35	0.47	0.09	-0.89	0.06	0.40	31.62
IL2RA	-0.48	0.05	0.33	5.83	0.02	59.43	-0.35	4.91	0.88	0.02
IL33	-0.16	3.16	-0.14	11.09	0.05	54.33	0.14	5.54	0.44	0.21
IL3RA	0.07	44.81	-0.12	9.63	-0.10	54.33	-0.14	27.83	0.39	0.17
IL4I1	-0.06	51.01	-0.08	11.09	0.04	54.33	0.28	4.91	0.68	0.02
IL4R	0.20	15.28			0.54	0.73	0.06	52.66	0.28	11.00
INADL	-0.37	1.10	-0.66	2.61	0.16	54.33	-0.71	0.57	0.65	0.02
INHA	-0.07	44.81	0.35	2.12	0.09	54.33	0.14	41.83	-0.91	0.02
INHBA	-0.23	21.80	0.29	5.83	0.46	0.09	0.07	19.97	0.38	14.82

INPP5D					-0.07	56.82	0.34	7.10	1.00	0.02
INPP5K	-0.38	2.45	-0.64	0.94	-0.08	54.33	0.08	47.42	0.18	36.83
INSIG1	-0.49	0.13	0.34	3.01	-0.38	5.71	-0.47	27.83	-0.66	0.02
INSM1	0.17	29.67	0.20	7.54	0.21	8.12	-0.15	16.94	-0.51	0.17
INTS3	-0.07	44.81	-0.54	3.21	0.05	58.07	0.12	27.83	0.51	0.47
IP6K1	-0.09	52.22	-0.10	10.40	0.08	49.13	0.58	0.06	-0.23	1.19
IPMK	0.21	33.23	0.61	0.11	0.15	12.58	-0.16	4.91	0.33	14.82
IPO5	0.26	12.65	0.82	0.88	-0.10	33.12	0.19	23.45	-0.40	0.02
IQGAP1	-0.50	0.05	-0.23	4.12	0.07	29.33	-0.13	54.40	-0.18	33.88
IQGAP3	-0.39	12.65	-0.21	0.78	0.64	0.09	0.88	8.99	0.93	0.65
IRAK1	0.03	55.87	0.42	1.77	-0.18	47.42	-0.12	6.93	-0.59	0.17
IRF1	-0.15	1.10	0.22	7.54	0.14	3.07	0.15	47.42	0.48	0.02
IRF5	-0.13	52.22	-0.36	2.86	0.29	41.10	0.28	23.45	0.83	0.02
IRF8	-0.42	18.59	0.19	8.25	-0.05	58.07	0.29	1.62	0.69	0.02
IRF9			0.55	2.61			-0.21	1.33	0.59	0.02
IRGM	0.27	0.26	0.60	0.60	0.08	26.12	0.27	4.91	0.47	0.47
Irgm2	0.03	56.87	0.29	0.30	0.33	2.66			0.76	0.02
ISG15	-0.14	44.81	0.28	1.09	0.34	0.28	0.10	53.27	0.49	0.13
ISL1	-0.94	0.53	-0.34	2.86	0.08	49.13	0.14	19.97	-0.15	24.40
ISLR	-0.53	0.67	-0.14	5.83	0.09	36.89	-0.15	52.12	0.40	0.99
ISOC1	-0.32	7.74	0.33	3.21	-0.09	41.10	-0.24	7.10	-0.51	0.12
ITGA3	0.41	5.93	-0.67	2.61	-0.22	2.31	0.08	53.83	-0.44	0.31
ITGA4	0.16	29.67	-0.99	0.11	-0.24	12.58	-0.78	1.88	0.38	0.02
ITGA7	0.67	0.05	-0.33	0.94	-0.35	20.03	0.29	47.42	-0.19	31.62
ITGA9	-0.29	44.81	-0.17	2.61	-0.13	22.90	-0.64	5.54	0.45	0.27
ITGAX	-0.08	37.04	-0.34	0.78	0.01	60.23	-0.03	54.40	1.22	0.02
ITGB1	0.29	0.78	0.60	0.18	0.08	36.89	0.26	4.91	0.12	24.40
ITGB2	-0.11	7.74	-0.28	0.78	0.01	59.43	-0.12	27.83	0.58	0.02
ITGB3	-0.23	5.93	-0.39	0.78	0.44	12.58	-1.06	0.06	0.67	0.02
ITGB4	-0.44	18.59	0.10	11.09			0.51	0.06	0.31	24.40
ITGB5	-0.07	54.70	-0.38	2.61	-0.03	58.41	-0.09	49.36	0.68	0.02
ITIH3	-0.23	10.00	0.30	3.01	-0.42	0.28	0.12	11.24	0.61	0.02
ITIH5	-0.13	25.77	-0.08	10.40	0.20	9.26	-0.09	27.83	0.49	0.75
ITPR3	-0.20	18.59	-0.84	1.77			0.12	47.42	0.65	0.02
JAK3	-0.36	21.80	0.22	5.83	0.23	0.64	0.37	1.21	0.62	0.02
JAKMIP2			-0.54	0.51	-0.39	1.82	0.07	41.83	-0.45	0.31
JHDM1D	0.43	0.05	0.39	2.30	0.34	2.66	-0.47	0.13	0.61	0.02
JMJD7-PLA2G4B	0.29	0.13	0.66	0.11	0.32	0.40	-0.11	47.42	-0.71	0.02
JMY	0.02	56.13	-0.41	3.21	-0.06	58.07	-0.40	7.10	-0.56	0.02
JTB	0.03	56.13	0.47	0.11	0.02	58.61	0.11	41.83	0.09	31.62
JUN	-0.36	0.40	0.32	0.60	0.31	0.52	0.08	41.83	1.01	0.02
JUND	0.15	33.23			0.11	41.10	0.32	19.97	0.50	0.04
KATNAL1	-0.10	37.04			0.15	49.13	0.23	47.42	-0.60	0.27
KATNAL2	-0.23	0.09	0.60	1.29	0.06	54.33	0.18	23.45	-1.15	0.02
KAZN	-0.38	0.43	0.23	2.30	0.19	4.05	0.14	49.36	0.46	0.31
KCNC1	0.19	49.54	-0.36	4.12	0.13	20.03	-0.11	27.83	-0.48	0.04
KCNF1	-0.57	0.17	0.69	0.26	0.50	49.13	0.06		-0.33	31.62
KCNG2	-0.08	55.17					-0.19	16.94	-0.52	0.99
KCNH1	-0.40	12.65	0.60	0.51	-0.18	12.58	-0.42	27.83	-0.84	0.02
KCNH3	0.06	53.69			0.03	58.07	-0.25	19.97	-0.38	0.27
KCNJ12	-0.47	7.74			0.38	1.31	-0.20	52.12	0.64	0.19
KCNJ16	-0.03	57.37							-0.57	0.99

KCNJ3	0.28	0.40	0.54	2.12	-0.13	41.10	0.13	47.42	-0.49	0.13
KCNK6	-0.40	0.05	0.18	0.51	0.05	54.33			0.87	0.02
KCNMA1	0.06	49.54	0.34	6.70	-0.11	54.33	-0.10	41.83	-0.40	0.31
KCNQ1OT1	-0.49	0.32	-0.10	3.21	-0.49	0.09	-0.43	7.10	-0.79	0.02
KCNT2	-0.25	2.45	0.22	4.12	0.08	49.13	0.16	47.42	-0.57	0.07
KCTD7	-0.06	52.22	0.57	0.94	-0.24	1.31	-0.38	2.42	0.31	31.62
KDM2A	-0.20	0.51	-0.34	4.12	-0.53	0.64	-0.22	5.54	-0.46	0.99
KDM2B	0.08	49.54	0.54	0.26	0.20	4.73	0.43	0.34	-0.26	2.89
KDM5B	-0.20	1.94	0.42	5.83	-0.18	14.77	-0.38	0.57	-0.35	0.13
KDM6B	-0.12	37.04			0.10	41.10	-0.77	0.06	-0.12	24.40
KDR	-0.29	0.09	-0.33	4.12	0.14	3.48	-0.10	54.40	-0.83	0.02
KHDRBS2	-0.23	7.74	0.11	11.09	0.40	4.05	0.11	23.45	-0.13	44.32
KIAA0090	-0.12	44.81	0.51	0.99	0.14	9.26	0.23	7.10	0.14	24.40
KIAA0101	-0.67	0.09	-0.93	1.03	-0.49	1.31	-0.61	0.35	0.55	0.02
KIAA0182	0.07	49.54	-0.35	3.21	0.13	10.69			0.58	0.12
KIAA0247	0.13	12.65	0.20	8.88	0.40	1.10	-0.49	0.06	0.10	33.88
KIAA0319	0.06	54.15	0.52	1.53	-0.30	0.09	0.05	47.42	-0.43	0.39
KIAA0368	-0.74	0.17	0.57	0.78	-0.19	49.13	0.29	1.62	-1.23	0.02
KIAA0913	-0.22	0.78	0.34	2.61	-0.06	54.33	-0.08	41.83	-0.61	0.05
KIAA0922	-1.33	0.05	0.40	5.83	-0.64	0.72	-0.48	49.36	-0.42	0.12
KIAA0947	0.02	55.56	0.52	3.01	0.04	54.33	-0.23	0.57	-0.41	0.02
KIAA1009	-0.51	0.05	-0.51	0.94	0.20	14.77	-0.73	0.86	0.76	0.02
KIAA1109	-0.16	12.65	-0.31	6.70	-0.29	2.06	-0.47	0.25	-0.54	0.02
KIAA1199	-0.43	0.05	0.66	0.26	0.26	2.06	-0.28	19.97	-0.93	0.99
KIAA1324	0.06	49.54	0.76	0.45	0.15	8.12	0.04	49.36	0.16	14.82
KIAA1377	0.49	0.17	0.52	2.12	-0.06	58.41	0.10	47.42	-0.29	1.98
KIAA1456	0.08	44.81	0.48	0.60			0.12	47.42	-0.19	1.98
KIAA1804	-0.17	4.28	0.38	4.12	-0.13	8.12	0.50	0.06	-0.13	8.00
KIAA1958	0.19	1.10	0.40	0.51	0.16	26.12	-0.13	41.83	0.42	0.07
KIF1B	-0.44	0.05	0.56	1.29	-0.31	4.05	-0.37	47.42	0.36	0.13
KIF1C	-0.19	21.80	-0.69	0.53	-0.13	26.12	0.24	11.24	0.22	24.40
KIF26B	-0.74	0.05	0.20	0.51			-0.95	0.25	-0.01	44.32
KIF2A	-0.26	0.17	0.67	0.30	-0.13	4.05	0.13	47.42	-0.20	4.22
KIF5C	-0.30	0.67	0.28	1.29	0.17	49.13	-0.58	7.10	-0.28	8.00
KIFAP3	-0.25	0.78	-0.51	1.66	-0.28	0.86	-0.23	1.88	-0.45	0.02
KIFC3	0.09	29.67			0.12	8.12	-0.51	0.35	0.34	0.08
KIT	-0.83	0.05	0.69	0.20	0.12	41.10	0.15	19.97	-0.76	0.02
KLC2	-0.04	52.83	-0.39	0.86	0.03	54.33	0.08	47.42	0.00	44.05
KLF13	-0.58	0.67	-1.20	0.94	0.12	36.89	0.09	47.42	0.23	31.62
KLF3	-0.16	44.81	0.54	1.29	-0.40	0.24	-0.18	47.42	0.77	0.05
KLF4	-0.15		-0.56	4.12	0.40	0.72	-0.13	49.36	0.00	44.05
KLHDC5	0.75	0.05	0.57	0.11	0.36	0.09	-0.69	0.06	-0.68	0.07
KLHL21	0.37	2.45	0.42	0.78	-0.09	17.39	0.32	0.40	-0.07	31.62
KLK6	-0.07	54.70	-0.58	2.61	-0.21	10.69	0.41	1.21	1.19	0.02
KLK7	0.32	0.26	-0.41	1.09	0.17	9.26	0.25	41.83	0.66	0.17
KLK9	0.08	44.81	-0.25	4.12	0.12	9.26	0.24	32.50	0.45	0.89
KPNA3	-0.09	54.70	-0.46	0.51	-0.08	41.10	0.04	53.83	-0.32	0.12
KPNA4	0.15	51.01	-0.40	2.86	-0.67	0.09	-0.11	7.10	0.41	0.99
KPNB1	0.07	49.54	-0.22	3.01	0.06	54.33	0.10	41.83	0.67	0.07
KRAS	-0.16	5.93	0.56	5.83	-0.11	17.39	-0.23	0.57	-0.63	0.02
KREMEN1	-0.77	0.40	0.30	2.12	0.29	1.56	-1.62	0.06	0.32	42.67
KRIT1	-0.57	0.40	0.42	4.12	-0.12	58.41	-0.31	1.88	-0.78	0.02

KRR1	-0.27	0.51	0.89	0.88	0.10	20.03	-0.45	1.62	-0.67	0.02
KRT2	-0.32	25.77	0.39	0.45	0.88	0.40	0.45	41.83	-0.35	31.62
KRT79	-0.18	52.22	0.39	0.67	0.88	0.52	0.43	0.06	-0.45	24.40
LAG3					0.47	3.48	0.04	52.12	1.21	0.02
LAIR1	-0.29	0.17	-0.82	0.78	0.36	1.56	-0.73	0.06	1.19	0.04
LAMA3	0.45	0.05	-0.20	3.21	0.46	0.09	0.28	1.88	0.20	31.62
LAMA5	-0.41	0.05	0.33	5.83	0.05	56.82	-0.38	19.97	0.23	44.20
LAMB2	0.06	49.54	0.52	1.77	0.35	1.31			0.42	0.02
LAMP2	-0.09	52.22	0.28	1.46	-0.15	6.93	-0.20	23.45	0.46	0.40
LANCL1	0.11	29.67	0.68	2.30			-0.29	0.06	-0.49	0.02
LANCL2	0.11	52.22	0.41	0.17	-0.10	36.89	0.60	1.88	1.14	0.02
LAPTM5	-0.13	3.16			-0.29	33.12			1.02	0.02
LARP4	0.16	18.59	0.72	0.51	-0.16	36.89	-0.15	27.83	-0.41	0.39
LARS	-0.77	0.05	0.64	0.94	-0.76	0.09	0.11	41.83	0.17	31.62
LASP1	0.21	18.59	-0.19	4.12	0.33	0.40	-0.27	0.34	0.48	0.12
LAT2	0.15	53.69	-0.24	1.66	0.32	0.09	-0.40	41.83	0.91	0.02
LCAT	-0.14	52.83	0.17	10.40	0.42	0.73	-0.13	8.99	0.28	24.40
LCn2									1.55	0.02
LCP1	-0.68	1.10	0.10	9.63	0.05	58.93	0.28	4.91	0.77	0.02
LDB2	-0.27	2.45	-0.16	5.83	0.39	0.72	-0.22	0.25	-0.18	33.88
LDLR	-0.05	53.69	-0.18	0.78	-0.45	0.09	-0.08	47.42	0.06	41.26
LDLRAP1	0.42	0.05	0.06	12.52	0.27	33.12	-0.37	27.83	0.60	0.02
LEFTY1			0.32	5.83	0.04	58.07			1.65	0.02
LEPREL4	0.02	57.11	0.23	0.60	-0.17	54.33	0.43	0.95	-0.11	24.40
LGALS1	-0.13	7.74	-0.33	3.21	0.17	36.89			0.79	0.02
LGALS3	-0.02	57.29	-0.23	4.12	-0.08	41.10	-0.08	32.50	0.95	0.02
LGALS3BP	0.02	56.77	-0.35	4.12	0.17	3.48	0.65	0.06	1.14	0.02
LGALS4	-0.69	0.40	1.06	0.11	0.27	0.72	0.43	11.24	0.39	0.75
LGI1	-0.24	0.40	0.53	2.77	-0.26	29.33	0.29	5.54	-0.67	0.47
LGI4	-0.11	44.81	0.13	4.12	-0.06	54.33	0.50	0.40	0.32	14.82
LGR5	0.93	0.26	-0.41	0.78	-0.54	4.73			-0.46	6.00
LHX9	-0.74	0.05	0.20	2.12	-0.90	0.09	-0.21	4.91	-1.21	0.02
LIG3	0.28	0.93	-0.65	0.51	0.06	54.33	0.11	41.83	0.16	35.53
Lilrb3	0.05	49.54	-0.72	0.51			0.05	50.49	1.26	0.02
LIMA1	-0.47	0.05	0.41	0.60	0.01	60.51	-0.32	32.50	0.85	0.02
LIMD1	0.14	25.77	0.18	2.61	0.08	36.89	0.45	0.06	0.31	2.89
LIME1	0.03	52.83	-0.50	0.21	0.05	55.77	0.13	32.50	0.19	11.00
LIMK1	-0.41	0.17	-0.49	3.01					0.09	33.88
LIMS2	0.11	49.54	-0.18	8.25	0.05	54.33	0.26	0.29	0.40	0.05
LIN28B			-0.39	0.78	-0.32	17.39	-0.54	32.50	-0.09	40.05
LIN7A	0.49	0.17	0.82	0.60	0.28	1.56	0.10	49.36	-0.62	0.27
LINGO2	-0.51	0.05	-0.36	0.20	0.27	41.10	0.20	2.42	-0.32	8.00
LIPE	0.10	44.81	-0.89	2.86	-0.13	22.90	0.39	0.34	0.32	24.40
LITAF	-0.34	0.09	0.22	0.51	0.05	57.40	-0.33	0.18	0.56	0.98
LMAN2	-0.06	44.81	0.47	0.51	-0.07	58.41	-0.13	23.45	-0.51	0.17
LMCD1	0.10	37.04	0.20	5.83	-0.07	56.82	0.74	0.06	-0.11	37.82
LMNB1	-0.23	0.26	0.29	5.83	-0.13	3.48	-0.85	0.12	-0.65	0.98
LMNB2	0.20	12.65	-0.40	4.12	0.66	0.09	-0.61	1.62	0.93	0.02
LMO3	0.16	12.65	0.51	0.51	-0.08	29.33	-0.10	32.50	-0.19	31.62
LMO4	-0.08	37.04	-0.14	5.83	-0.04	58.93	-0.28	41.83	-0.42	0.08
LMTK2	0.21	0.93	0.54	0.11	0.45	0.09	0.23	19.97	0.59	0.39
LOC100505793/SRSF10	-0.10	18.59	0.67	2.30	-0.14	58.07	-0.90	0.18	-0.26	4.22

LOC390760	-0.35	0.32	0.29	0.51	0.08	56.82	-0.56	1.21	-0.40	8.00
LPAR4			0.16	9.63	-0.48	0.09	0.13	7.10	-0.36	31.62
LPAR6	-0.56	0.05	-0.71	0.48	-0.30	10.69	-0.47	0.35	0.10	42.21
LPCAT2	-0.08	49.54	-0.11	5.83	-0.10	49.13	-0.22	23.45	0.55	0.05
LPGAT1	-0.21	0.17	0.05	10.40	-0.15	14.77	-0.08	49.36	-0.35	0.07
LPHN1	-0.19	0.51	-0.56	2.12	0.09	41.10	-0.08	27.83	-0.48	0.65
LPHN2	-0.10	52.83	0.19	3.21	0.42	0.86	-0.24	23.45	0.24	42.03
LPIN2	0.26	1.43	0.45	0.11	0.05	41.10	-0.45	3.87	-0.21	0.21
LPL	0.22	7.74	0.21	2.61	-0.17	4.73	-0.31	5.54	-0.52	0.02
LPP	0.52	5.93	0.66	0.11	-0.51	0.09	-1.40	0.06	-0.34	24.40
LPXN	-0.23	51.01	0.75	0.94	0.03	58.07	-0.31	50.49	1.39	0.02
LRCH1	-0.26	0.67	-0.14	10.40	-0.16	22.90	0.33	0.06	-0.44	0.02
LRIG2	0.56	0.09	0.18	5.83	-0.18	4.05	0.17	52.12	0.52	0.02
LRIG3	0.08	25.77	-0.28	9.63					-0.44	0.47
LRP2	0.11	15.28	-0.18	2.61	-0.97	0.86	0.35	16.94	-0.35	31.62
LRP8	-0.11	57.29	0.61	0.18	0.07	58.41	-0.78	11.24	0.28	33.88
LRRC15	0.04	49.54	-0.42	0.21	0.10	49.13	0.13	2.91	0.10	31.62
LRRC28	0.19	3.16	0.37	0.51	-0.28	1.56	-0.72	0.06	-0.58	0.08
LRRC46	-0.09	37.04	0.09	8.25	0.20	6.93	0.50	0.92	0.07	38.75
LRRC7	0.13	12.65	0.67	1.46	0.14	4.73	0.06	47.42	-0.40	0.47
LRRK2	-0.23	0.53	0.12	11.78	0.17	5.71	-0.52	0.06	-0.41	0.12
LRRN3	0.21	33.23	0.48	0.51	-0.16	4.73	0.29	1.21	-0.30	2.89
LRRN4	-0.24	49.54	0.53	2.12	-0.09	49.13	-0.91	0.06	-0.19	36.83
LRRTM3	-0.75	0.40	0.55	0.78	0.14	55.77	-0.95	2.42	-0.50	0.17
LSS	0.11	44.81	0.73	1.21	0.10	49.13	-0.43	11.24	-0.39	0.75
Lst1	-0.09	37.04	-0.39	3.21	0.33	0.72	-0.06	41.83	0.92	0.02
LTBP3	-0.11	12.65	-0.54	2.86	0.12	49.13	0.12	2.42	0.45	0.07
LTBR	0.04	49.54	0.48	0.60	-0.06	55.77	0.59	0.29	0.94	0.02
LTC4S	0.13	44.81	-0.10	8.88	0.20	0.86			0.63	0.02
LTK	0.08	52.83			0.29	1.82	-0.36	0.73	-0.22	14.82
LTN1	0.17	7.74	-0.42	0.51	0.05	54.33	0.11	19.97	-0.17	24.40
LUC7L	0.13	18.59	0.61	0.60	-0.16	14.77	-0.30	1.62	-0.26	31.62
LY6E	0.06	51.01			-0.12	49.13	0.04	51.35	-0.55	0.12
LY86	-0.57	0.17	-0.19	8.88	-0.06	58.07	0.13	5.54	1.36	0.02
LY96	-0.71	4.28	0.12	2.30	0.29	2.06	0.96	0.06	0.67	0.02
LYL1	0.09	37.04	-0.12	10.40	-0.10	58.93	0.44	2.91	0.74	0.02
LYN	0.35	0.05	0.67	0.67	0.23	0.66	0.11	7.10	0.51	0.99
LYVE1	-0.14	29.67	-0.83	1.66	0.31	20.03	-0.22	0.51	-0.52	0.31
Lyz1/Lyz2	0.11	49.54	-0.34	3.01	-0.31	0.28	0.25	0.18	1.48	0.02
LZTS1	-0.17	15.28	-0.75	0.60	0.21	33.12	-0.91	0.06	0.42	11.00
MAD2L1	0.29	0.51	0.35	2.86	0.16	17.39	0.29	7.10	-0.39	0.89
MADD	-0.21	1.10	-0.12	6.70	0.07	41.10	0.08	41.83	0.46	0.08
MAEL	-0.18	29.67			-0.53	2.06	-1.25	0.06	0.27	8.00
MAF	0.67	1.10	-0.44	2.86	0.27	9.26	-0.32	0.06	0.44	0.99
MAFB	0.12	49.54	-0.12	8.25	-0.07	58.93	0.13	32.50	0.62	0.02
MAFF	-0.45	18.59	0.59	0.20	0.51	0.09	-0.42	1.88	0.96	0.02
MAFG	0.28	0.17	0.40	0.45	0.28	4.73	-0.54	3.87	-0.06	35.53
MAGI2	0.03	52.83	-0.23	3.21	0.05	49.13	0.09	51.35	0.50	0.02
MAGT1	-0.06	44.81	0.41	2.12	0.08	55.77	0.40	16.94	0.80	0.08
MAL2	-0.05	55.87			0.51	0.52	-0.28	11.24	0.16	38.75
MALAT1	-0.79	0.17	0.45	5.83	-0.87	0.09	-1.33	0.06	0.51	0.02
MAMDC2	-0.11	44.81			-0.11	14.77			0.83	0.02

MAML1	0.47	0.94	0.17	5.83	-0.11	54.33	-0.06	54.40	0.21	2.89
MAN2A2	-0.31	2.45	0.36	2.30	0.32	3.07	-0.24	47.42	0.51	0.02
MAN2B1	-0.05	52.83	-0.23	2.30	-0.08	58.41	0.13	27.83	0.64	0.02
MAN2B2	-0.10	52.22			0.08	49.13	0.13	47.42	0.53	0.02
MAOB	-0.32	0.78	-0.56	0.89	-0.22	0.64	0.08	32.50	0.44	41.26
MAP1B	-0.10	44.81	-0.44	1.09	-0.41	0.24	0.05	53.83	0.12	31.62
MAP2	0.16	44.81	-0.60	4.12	-0.33	20.03	-1.07	0.06	-0.51	0.02
MAP2K1	0.01	56.13	0.49	1.66	0.05	55.77			-0.45	0.02
MAP2K6	-0.46	0.05	-0.44	1.46	0.05	57.40	0.40	47.42	0.04	42.67
MAP3K1	-0.43	0.17	0.25	5.83	-0.20	36.89	-0.26	0.35	0.61	0.07
MAP3K14	0.61	0.26	0.46	0.51	-0.07	41.10	-0.52	0.06	-0.19	31.62
MAP3K2	0.21	15.28	-0.27	4.12	-0.63	0.09	-0.27	41.83	0.33	24.40
MAP3K9	-0.35	4.28	-0.14	5.83	-0.14	9.26	0.13	50.49	0.84	0.02
MAP4K3	-0.27	0.67	0.54	1.46	-0.29	17.39	-0.34	0.73	-0.50	0.08
MAP4K5	-0.33	15.28	0.73	0.51	0.10	41.10	0.07	49.36	-0.50	0.89
MAP7	0.22	1.10	0.26	0.99	0.03	56.82	-0.76	0.06	0.59	0.31
MAPK1IP1L	-0.24	44.81	-0.19	1.77	-0.32	0.28	-0.86	0.06	-0.65	0.02
MAPK6	-0.13	25.77	-0.09	8.88	0.34	6.93	-0.20	0.86	-0.36	0.89
MAPK7	0.11	15.28	-0.44	0.78	-0.04	58.07	0.03	54.83	0.44	0.89
MAPK8	-0.35	0.13	-0.45	2.12	-0.24	36.89	-0.37	47.42	-0.51	0.05
MAPKAPK2	-0.35	25.77	0.27	0.48	0.16	33.12	-0.36	19.97	1.04	0.02
MARCH6	-0.15	49.54	0.62	0.11	-0.39	0.52	0.41	27.83	1.28	0.02
MARK1	0.07	44.81	0.10	11.78	0.09	49.13	0.10	41.83	-0.61	0.08
MAS1	0.26	0.17	0.20	7.54	0.15	36.89	-0.19	0.73	-0.48	0.99
MASP2	-0.60	0.05	-0.48	0.51	-0.25	55.77	0.39	3.87	0.16	24.40
MAST4	0.10	37.04	0.40	0.35	0.16	4.05	-0.09	8.99	-0.12	24.40
MAVS	-0.05	52.22	-0.27	3.21	0.11	20.03	0.02	54.83	0.41	0.42
MAZ	0.17	44.81	-0.54	2.86	0.19	0.86	-0.12	41.83	0.26	0.99
MB			-0.56	0.48			-0.23	41.83	-0.36	0.02
MB21D2	0.30	21.80	-0.45	0.51	0.12	49.13	0.16	41.83	0.67	0.12
MBD1	0.29	0.17	0.40	0.18	0.52	8.12	-0.72	0.51	-0.17	36.83
MBNL1	0.16	33.23	0.53	2.61	-0.11	33.12	-0.09	23.45	-0.38	0.02
MBOAT1	0.01	56.77	0.58	0.66	-0.04	58.93	-0.25	0.95	0.17	11.00
MBP	-0.12	15.28	0.34	0.78	0.25	14.77	-0.13	54.40	0.60	0.02
MCL1	0.36	0.13	0.56	1.46	-0.03	58.41	-0.08	32.50	0.25	1.98
MCM2	0.17	3.16	-0.51	2.86	-0.07	55.77	-0.15	49.36	0.50	0.02
MCM6	0.07	37.04	-0.46	1.29			0.47	0.51	0.18	8.00
MCM8	-0.04	52.22	-0.60	2.86	-0.05	58.61	0.20	13.89	-0.40	0.99
MCTP1	-0.42	0.32	0.24	2.61	-0.46	14.77	0.07	49.36	-1.26	0.02
MDGA2	0.19	44.81	0.57	1.29	-0.06	41.10	-0.44	0.95	-1.16	0.02
MDH1	-0.26	0.32	0.50	2.30	-0.16	17.39	-1.19	0.06	-0.41	0.02
MDM4	0.14	54.15	-0.47	0.89	0.32	22.90	-0.29	19.97	0.20	31.62
ME1	0.17	21.80	0.71	0.88	0.11	54.33	0.15	5.54	-0.44	0.02
MED13	0.65	0.17	0.40	1.77	0.12	33.12	-0.77	0.06	-0.62	0.12
MED13L	-0.24	0.67	0.54	2.61	-0.21	41.10	-0.14	50.49	-0.13	31.62
MED22	0.29	0.17	0.48	4.12	0.13	49.13	0.56	1.88	0.48	0.89
MED7	0.27	0.32	0.14	5.83	-0.21	6.93	0.51	0.12	1.09	0.02
MEF2B	-0.40	0.36	-0.13	5.83	0.13	6.93	0.17	16.94	-0.03	39.47
MEF2C	-0.34	15.28	-0.53	0.94	0.09	55.77			-0.06	38.75
MEGF6	0.21		0.48	0.51	0.73	0.09	0.19	47.42	0.36	40.66
MEGF9	-0.31	0.78	-0.45	2.86	-0.49	1.82	0.12	13.89	-0.30	2.89
MELK	-0.50	25.77	0.13	9.63			1.13	0.06	0.41	0.13

MET	-0.20	37.04	0.36	0.27	0.30	41.10	-0.61	0.40	0.35	31.62
METTL20	0.09	44.81	0.38	1.66	0.04	56.82			-0.67	0.02
METTL5	0.10	49.54	0.55	0.30	-0.09	33.12	0.14	7.10	-0.24	0.39
MFAP3	0.15	5.93	0.48	2.77	0.28	12.58	-0.51	0.06	-0.70	0.04
MFI2	-0.23	0.78	-0.30	0.48	0.04	55.77	0.34	27.83	0.72	0.02
MFN1	-0.07	51.01	0.89	0.42	0.06	49.13	-0.50	2.42	-0.18	24.40
MFSD8	0.07	44.81	0.76	0.60	0.10	20.03	0.49	5.54	-0.35	0.99
MGAT4A	0.66	0.17	0.62	0.20	0.02	57.40	0.15	51.35	-0.58	0.02
MGEA5	0.25	21.80	0.60	0.26	0.23	1.10	0.48	0.06	-0.12	14.82
MGP	-0.22	49.54	0.50	2.77	0.16	36.89	-0.26	41.83	0.05	24.40
MGST1	0.12	18.59	0.64	0.60	-0.17	20.03	0.24	23.45	0.67	0.02
MGST3	0.42	0.05	-0.53	2.86	-0.24	1.10	-0.13	41.83	-0.90	0.07
MIA	0.15	25.77	0.35	0.99	0.17	1.10	0.27	47.42	1.05	0.02
MIB1	-0.78	0.05	0.82	0.30	-0.44	5.71	0.52	19.97	-1.08	0.02
MICAL1	-0.09	29.67	-0.55	2.12	0.26	12.58	0.05	52.66	0.60	0.02
MICALL1	-0.06	49.54	-0.61	0.61	0.21	1.56	-0.15	41.83	0.60	0.99
MICALL2	-0.60	0.05	0.32	5.83	0.68	0.09	0.04	54.83	1.06	0.02
MID1	-0.12	5.93	-0.62	0.89	-0.18	8.12	0.04	52.66	0.25	0.89
MIER1	-0.31	0.09	-0.16	11.09	-0.41	0.09	1.18	0.40	-0.10	24.40
MITD1	0.52	15.28	0.58	0.18	0.12	4.73	0.23	47.42	-1.28	0.02
MITF	-1.15	0.05	0.26	0.35	-0.53	10.69	-1.54	0.06	0.48	31.62
MKL2	0.52	1.10	-0.39	2.61	0.23	2.06	0.33	8.99	-0.70	0.02
MLC1	-0.19	0.51	-0.18	0.51	0.06	54.33	0.09	27.83	0.52	0.39
MLLT4	0.31	29.67	0.71	1.09	0.13	41.10	0.19	19.97	-0.58	0.02
MLXIP	0.29	4.28	0.25	7.54	0.04	58.41	-0.61	0.51	-0.39	0.07
MLXIPL	-0.41	29.67	-0.20	4.12	0.20	41.10	0.43	7.10	0.88	0.02
MMD	-0.10	54.70	0.49	0.18	0.05	56.82	0.22	0.35	-0.21	11.00
MMP15	0.41	0.32	0.27	2.30					-0.18	35.53
MMP2	0.22	0.53	0.27	2.77	0.05	54.33	-0.46	1.21	0.79	0.02
MMP9	-0.22	10.00	0.26	5.83	-0.11	56.82	1.02	0.06	-1.07	0.02
MOBP	-0.31	44.81	-0.54	0.67	-0.35	0.86	-0.70	41.83	0.44	31.62
MOGAT1	-0.10	37.04	-1.31	0.35	0.05	54.33			-0.42	0.27
MORC3	0.13	37.04	0.75	1.46	0.02	58.93	-0.10	47.42	-0.48	0.02
MPDZ			-0.57	2.77	-0.11	12.58	-0.88	2.91	1.18	0.02
MPEG1	-0.49	0.05	-0.23	0.51	-0.28	41.10	0.29	11.24	0.75	0.02
MPHOSPH9	-0.15	12.65	0.73	0.11	-0.05	56.82	-0.47	0.13	-0.75	0.02
MPP1	-0.56	0.09	0.18	1.53	-0.35	4.73	-0.15	52.66	-0.40	0.05
MPP7	-0.28	25.77	-0.79	5.83	-0.03	59.43	-0.22	49.36	-0.87	0.08
MR1	-0.58	4.28	-0.27	1.09	-0.34	17.39	-0.11	41.83	0.83	0.02
MRC2	-0.22	49.54	-0.12	5.83			0.32	16.94	0.71	0.02
MRGPRF	-0.12	29.67	-0.53	2.30	0.21	4.05	0.08	50.49	0.99	0.02
MRI1	0.18	1.43	0.10	0.78	0.03	60.51	0.41	0.06	0.24	0.65
MRPL15	0.20	0.53	0.58	1.09	-0.26	6.93	0.54	0.29	-0.84	0.02
MRPS2	-0.16	7.74	-0.47	2.77	0.02	58.61	-0.20	5.54	-0.47	0.08
MSH3	-0.47	0.51	0.62	0.60	-0.19	20.03	0.69	16.94	-0.76	0.02
MSI2	-0.29	1.94	0.37	1.46	-0.43	0.09	-0.51	19.97	0.34	0.65
MSN	-0.29	0.67	0.38	1.66	0.23	1.31	0.13	41.83	0.86	0.02
MT1E					0.12	49.13			0.77	0.27
MT1F	0.27	0.17	0.26	5.83	0.26	0.40	-0.04	54.40	0.66	0.08
MTA1	0.43	0.32	0.32	0.60	0.08	49.13			0.09	37.82
MTA2	0.15	29.67	-0.39	0.43	-0.04	58.61	-0.11	41.83	0.17	24.40
MTDH	-0.16	49.54	0.51	0.60	-0.23	2.66	0.47	0.95	-0.08	31.62

MTHFSD	0.04	49.54	-0.59	2.77	0.03	58.07			-0.37	0.17
MTM1	-0.43	0.78	-0.31	0.78	0.29	33.12	-1.28	0.12	-0.48	24.40
MTMR10	-0.37	0.40	0.31	1.46	0.16	36.89	-0.53	16.94	0.33	35.53
MTMR11	0.03	52.83	0.41	0.51	-0.16	36.89	0.25	27.83	0.63	0.02
MTMR12	0.04	49.54	0.21	5.83	-0.06	55.77	-0.28	0.57	-0.62	0.02
MTPN	-0.15	29.67	-0.60	0.51	0.21	4.05	0.14	47.42	-0.39	0.12
MTRR	-0.34	3.16	-0.46	2.30	0.04	58.07	-0.69	13.89	0.84	0.12
MTSS1	-0.43	2.45	0.56	0.17	-0.45	0.09	-0.21	41.83	-0.83	0.27
MTSS1L	-0.31	1.43			0.16	14.77	-0.50	4.91	0.44	0.02
MTUS1	0.51	1.43	0.48	0.45	0.05	49.13	0.30	3.87	0.59	0.12
MUC1	-0.04	51.01	-0.47	0.01	0.02	59.43	0.06	41.83	0.02	44.05
MUTYH	0.23	1.10	-0.72	0.78	0.27	4.05	0.24	27.83	0.43	0.02
MX1	-0.38	0.53	0.14	11.09	0.18	54.33	-0.08	47.42	1.01	0.02
MXD3	-0.24	2.45	-0.17	4.12	-0.37	0.52	-0.62	0.51	-0.49	0.89
MXRA8	-0.14	52.83	0.37	0.26			1.02	0.06	0.32	11.00
MYB	0.06	44.81	-0.42	0.53	-0.31	49.13	-0.52	0.33	0.16	24.40
MYBPC3	0.28	0.32	0.52	0.60	0.05	55.77	-0.43	0.06	-0.08	31.62
MYCN	-0.14	51.01	0.88	1.53	0.21	9.26			-0.48	0.02
MYF6	-0.08	37.04	-0.21	5.83	0.06	41.10	0.45	0.92	0.01	44.32
MYH2	-0.40	0.05	-0.16	4.12	0.34	49.13	0.04	49.36	0.07	37.82
MYH3	0.35	0.05	0.81	0.26	0.29	0.72	-0.08	54.40	-0.28	33.88
MYH6	0.41	0.05	0.39	2.77	0.60	0.09	0.12	32.50	0.08	44.20
MYL12B	0.04	52.22	0.40	0.51	-0.04	58.61	0.03	51.35	0.44	0.31
MYL6B	-0.42	0.13	-0.31	5.83	-0.08	54.33	-0.17	41.83	-0.24	11.00
Myl9			0.26	2.30	0.27	4.73	0.14	2.42	0.58	0.02
MYO1B	-0.32	0.93	0.88	0.99	-0.37	0.44	-0.46	0.40	-1.22	0.02
MYO1F			-0.16	0.78	0.58	0.44			1.05	0.02
MYO3B	0.42	0.17	-0.27	5.83	-0.09	54.33	-0.57	11.24	-0.05	37.82
MYO5A	0.13	29.67	0.47	1.66	0.25	0.72	0.19	11.24	-0.72	0.02
MYO6	0.23	4.28	0.21	0.94	-0.22	6.93	0.48	0.40	0.28	0.47
MYO9A	0.33	4.28	0.50	0.89	0.04	54.33	0.15	47.42	-0.29	6.00
MYOD1	-0.20	0.67	-0.50	0.78	-0.11	41.10	-0.09	51.35	0.01	44.32
MYOM1	-0.64	0.05	0.17	0.51	0.44	0.64	1.13	0.25	-0.30	6.00
MYOM2	0.29		0.40	0.67	-0.33	29.33	0.62	0.99	-0.06	58.42
MYSM1	-0.83	0.05	0.40	0.94	-0.21	14.77	0.83	0.29	-0.91	0.02
NAA30	0.53	0.05	0.74	0.57	0.24	0.24	0.03	55.17	-0.22	0.89
NAB2	0.33	0.40	-0.34	7.54	0.09	54.33	-0.06	52.12	0.52	0.12
NANS	-0.39	25.77	-0.67	3.21	0.13	14.77	0.48	0.06	0.15	38.75
NAP1L3	-0.09	33.23	0.44	5.83	-0.06	55.77	-0.23	0.95	-0.52	0.02
NAPA	-0.06	51.01	-0.42	0.20	0.07	49.13	0.43	7.10	0.61	0.02
NAPG	0.17	18.59	0.48	1.03	0.17	12.58			-0.73	0.05
NAPRT1	-0.11	44.81	-0.33	2.86	0.11	17.39	-0.09	49.36	0.58	0.21
NAT	0.41	1.43	-0.25	2.12	-0.39	29.33	-1.01	0.06	-1.09	0.02
Nav2	-0.06	51.01	0.56	1.29	0.16	41.10	-0.15	27.83	-0.43	0.99
NAV3	-0.27	0.40	-0.37	0.51	-0.53	0.09	-1.09	0.73	-0.47	0.08
NBEAL1	-0.10	51.01	-0.80	0.35	-0.35	6.93	0.13	8.99	0.28	31.62
NCALD	-0.27	15.28	-0.49	3.01	-0.36	10.69	-0.09	54.40	-0.62	0.99
NCAM1	-0.20	5.93	0.77	1.09	-0.23	12.58	-0.43	0.35	-0.39	0.05
NCAPH2	0.20	5.93	0.41	0.67	-0.04	54.33	0.20	0.51	-0.50	0.99
NCF2	-0.19	5.93	0.39	0.88	0.08	49.13	0.23	0.86	1.23	0.02
NCF4	0.19	25.77	-0.12	5.83	0.15	6.93	0.16	1.62	1.24	0.02
NCK1	-0.24	37.04	0.51	0.51	0.05	58.41	0.09	32.50	-1.17	0.02

NCKAP1L	-0.22	44.81	-0.24	2.77	0.08	54.33	-0.15	41.83	0.91	0.02
Ncl	-0.18	1.94	0.59	1.46	-0.06	57.40	0.24	5.54	0.44	0.02
NCOA3	0.12	37.04	-0.46	3.01	0.21	41.10	0.48	0.06	0.06	39.47
NCOR1	-0.15	4.28	0.73	1.53	-0.26	2.66	0.24	19.97	-0.65	0.02
NDOR1	0.29	0.53	0.45	0.51	0.05	57.40	-0.22	16.94	-0.67	0.02
NDRG2			0.56	0.18			0.06	47.42	0.14	38.75
NDRG3	0.18	5.93	0.34	2.30	-0.18	22.90	-0.05	49.36	-0.56	0.12
NDST1	0.11	44.81	0.68	0.99	-0.24	49.13	0.27	4.91	-0.21	24.40
NDST3	-0.38	0.05	-0.05	11.09	-0.24	1.31	0.14	51.35	-0.03	40.66
NDUFAB1	-0.03	57.11	0.48	2.30	-0.11	36.89	-0.48	1.33	-0.40	0.99
NDUFAF4	0.06	44.81	0.48	0.67	0.03	57.40	0.24	0.57	0.04	43.75
NECAB2	-0.43	0.05	-0.08	10.40	-0.36	29.33	0.30	0.51	-0.28	31.62
NEDD4L	0.37	0.05	0.63	0.67	-0.15	36.89	0.21	7.10	-1.21	0.02
NEDD9	0.39	0.17	0.69	0.57	0.21	3.48	0.49	5.54	0.71	0.17
NEFL	0.05	51.01	0.14	13.30	-0.16	26.12	-0.09	19.97	-0.43	0.02
NEFM	0.26	33.23	0.63	11.78	-0.05	58.41	-0.02	47.42	-0.68	0.02
NEK1	-0.58	0.05	0.67	0.51	-0.90	0.09	0.34	23.45	-0.36	0.07
NEK4	-0.17	1.10	-0.73	0.11	-0.28	1.56	0.12	32.50	-0.09	33.88
NES	-0.18	0.32	-0.67	2.77	0.45	0.40	-0.15	32.50	0.33	11.00
NETO1	-0.37	0.05	-0.25	2.77	-0.42	3.48	-0.35	1.62	-0.23	1.19
NETO2	0.25	0.17	0.30	6.70	0.06	41.10	0.44	0.06	0.06	38.75
NEU2	-0.23	21.80	-0.30	4.12	0.35	9.26	-0.41	0.06	-0.07	31.62
NEUROD6	0.24	0.40	0.15	11.78	-0.16	26.12	0.05	47.42	-0.38	0.39
NFASC	0.16	44.81	-0.24	2.61	0.02	59.79	-0.46	0.06	0.06	42.55
NFATC2	0.15	37.04	-0.28	3.21	-0.49	49.13	0.11	23.45	-0.58	0.02
NFATC3	-0.51	0.32	0.47	0.11	-0.47	0.09	-0.33	0.11	-0.72	0.02
NFE2L2	-0.27	10.00	0.59	1.46	0.13	26.12	0.26	32.50	0.57	0.13
NFIA	-0.18	12.65	0.08	8.88	-0.18	2.31	0.06	52.12	0.44	0.75
NFIC	0.05	53.69	-0.18	4.12	0.17	49.13	0.12	11.24	0.47	0.02
NFIL3	0.20	37.04	0.39	1.09	0.52	0.64	-0.18	27.83	0.49	0.02
NFKB2	0.27	15.28	0.59	0.51	0.10	49.13	-0.42	19.97	-0.54	0.99
NFS1	0.71	0.05	0.58	0.51	0.27	49.13	0.33	0.95	-0.26	14.82
NFU1	0.27	1.94	0.62	0.78	-0.06	55.77	-0.13	16.94	-0.28	1.98
NHLH1	0.10	52.22	0.31	0.51	0.46	0.72	0.19	47.42	0.90	0.02
NIPA1	0.10	44.81	-0.44	2.86	-0.15	9.26	-0.18	16.94	-0.75	0.02
NKAIN2	-0.40	3.16	0.22	4.12	0.46	0.09	-0.72	5.54	-0.26	2.89
NKX6-2	0.02	54.15	0.19	6.70	-0.23	0.28			0.54	0.99
NLRP10	0.06	44.81	0.30	5.83	0.33	2.66	-0.83	0.06	-0.28	14.82
NME7	0.04	51.01	0.60	1.46	-0.07	54.33	0.30	8.99	-0.44	0.02
NMI	0.20	33.23	0.31	5.83	0.36	14.77	-0.13	53.83	-0.68	0.02
NNAT	-0.28	4.28	0.16	8.88	0.07	55.77	0.04	51.35	0.40	0.02
NOL6	-0.23	10.00	0.41	5.83	-0.22	3.48	-0.49	41.83	-0.53	0.02
NOP56	-0.20	4.28	0.30	5.83	-0.16	14.77	0.15	32.50	0.36	0.02
NOTCH3	0.09	44.81	-0.24	4.12	0.11	22.90	0.26	3.87	0.54	0.02
NOTCH4	0.01		0.47	1.66	0.48	0.09	0.78	0.86	0.48	0.06
NOV	-0.27	1.10	1.00	0.57	0.55	0.09	0.18	2.42	0.26	41.26
NOXO1	0.19	29.67			-0.12	41.10	-0.59	0.87	0.33	11.00
NPAS1	0.08	49.54	0.50	0.23	0.36	0.69	-0.03	52.66	0.31	11.00
NPAS4	0.09	49.54	0.40	0.99	0.34	14.77	0.08	50.49	-0.49	0.27
NPB	0.25	10.00	-0.65	0.51	0.24	0.44	0.19	2.91	0.84	0.07
NPC2	0.15	1.43	0.36	0.51			0.16	47.42	0.45	0.05
NPHP3	-0.48	0.26	0.60	1.46	0.30	33.12	0.71	0.40	0.69	0.07

NPPC	0.13	15.28			-0.22	10.69	-0.17	1.62	-0.60	0.75
NPR2	0.33	1.43	-0.32	4.12	0.15	20.03	-0.44	0.34	0.69	0.02
NPRL3	0.14	18.59	0.19	0.51	0.05	54.33	0.30	0.11	-0.44	0.47
NPY2R			1.00	0.35			-0.43	3.87	-0.30	11.00
NPY5R	0.10	44.81	0.69	2.61	0.09	36.89	0.26	13.89	-0.55	0.99
NR2C1	-0.09	52.22	0.50	2.30	0.48	0.40	-0.82	0.12	0.20	8.00
NR2E1	0.02	55.17	0.63	0.60	-0.05	59.79	0.08	52.66	0.51	0.02
NR2F2	-0.36	0.05	-0.34	3.01	0.09	41.10	0.11	32.50	0.33	14.82
NR4A1	0.59	0.17	0.42	3.21	0.05	55.77	-0.25	7.10	0.12	44.05
NR4A2	-0.06	55.56	-0.39	5.83	-0.07	57.40	-0.10	23.45	-0.46	0.39
NRARP	0.04	49.54	-0.44	0.45	-0.23	2.66	0.76	0.29	-0.64	0.89
NRAS	0.12	37.04	0.27	0.51	0.12	8.12	-0.37	0.13	-0.30	0.21
NRCAM	-0.73	0.17	0.85	0.60	-0.10	29.33	0.04	47.42	1.07	0.08
NRG1	-0.46	0.05	-0.25	3.21	0.58	0.52	0.10	41.83	0.35	8.00
NRIP1	-0.18	37.04	-0.54	0.78	-0.36	0.40	-0.29	23.45	0.64	24.40
NRP1	-0.48	0.17	0.50	2.30	-0.48	0.09	0.50	0.25	-0.50	0.02
NRXN1	-0.31	0.05	-0.50	0.11	0.60	2.66	0.27	41.83	-0.42	0.75
NRXN3	0.71	0.05	0.64	0.88	-0.30	0.40	-0.56	27.83	-0.63	0.47
NSBP1	0.20	49.54	0.64	1.46	-0.08	41.10	-0.12	50.49	-0.47	0.02
NSDHL	0.26	0.32	0.36	4.12	-0.10	41.10	0.19	47.42	-0.79	0.02
NSUN6	0.12	7.74	0.55	0.51	-0.06	54.33	-0.18	49.36	-0.44	0.12
NT5C2	-0.19	0.40	-0.53	2.30	0.18	2.06	-0.15	13.89	-0.20	8.00
NTF3	-0.39	1.10	-0.20	2.86	-0.45	33.12	0.31	32.50	-0.48	24.40
NTM	0.21	0.26	0.45	0.18	0.26	2.06	0.11	41.83	-0.09	33.88
NTNG1	-0.59	0.05	-0.63	0.78	-0.24	6.93	0.28	0.86	-0.38	0.47
NTRK2	-0.09	44.81	0.43	4.12	0.18	8.12	0.08	47.42	0.61	0.02
NTRK3	0.08	44.81	0.09	5.83	0.08	36.89	0.03	50.49	-0.41	0.04
NUAK1	-0.55	0.05	-0.12	6.70	-0.65	2.66	-0.27	0.06	0.01	44.05
NUAK2	-0.55	0.05	-0.12	6.70	-0.65	2.66	-0.27	0.06	0.21	31.62
NUCKS1	-0.07	49.54	0.44	0.57	-0.07	55.77	-0.04	51.35	-0.45	0.05
NUDCD1	0.47	0.17	0.35	5.83	0.05	54.33	0.27	27.83	-0.25	14.82
NUFIP2	-0.14	49.54	-0.62	0.51	-0.28	36.89	-0.27	0.57	-0.22	0.65
NUMB	0.19	21.80	0.48	0.51	0.30	2.66	-0.11	41.83	-0.82	0.02
NUP155	-0.47	0.05	-0.76	0.11	-0.15	10.69	-0.34	5.54	-0.61	0.21
NUP160	0.24	25.77	0.57	1.77	-0.33	0.66	0.10	54.83	-0.46	0.02
NUP205	-0.90	0.05	-0.52	4.12	0.45	0.86	0.20	1.62	0.13	33.88
NUPR1	0.18	49.54	0.64	0.30	0.41	3.07	-0.27	41.83	0.78	0.02
NVL	-0.53	0.05	0.37	5.83	-0.62	0.24	-0.34	32.50	1.13	0.02
NXN	0.13	37.04	0.18	1.66	0.33	0.44	-0.54	0.13	0.46	0.47
NXNL2	0.22	21.80	0.67	0.42	0.32	14.77			0.39	33.88
OAS1	0.48	0.05	0.09	12.52	0.61	0.09	0.68	2.42	0.72	0.02
Oas2			-0.09	11.09					1.14	0.02
OBFC2A	-0.14	4.28	0.22	2.30	-0.16	10.69	0.14	19.97	-0.42	0.12
OCRL	-0.14	55.17	0.48	0.11	-0.19	29.33	0.32	32.50	-0.77	0.12
ODF2L	0.16	10.00	0.75	0.78	-0.04	60.23	0.18	47.42	-0.22	24.40
ODZ3	0.43	15.28	-0.64	0.51	-0.38	2.66	-0.18	49.36	0.48	0.02
OGG1	0.21	25.77	-0.40	6.70	-0.09	54.33	0.40	8.99	0.55	0.02
OGN	-0.41	29.67	0.32	9.63	0.77	0.09	0.65	2.42	-0.41	24.40
OLFML2B	0.07	44.81	0.20	12.52	-0.16	56.82	-0.08	49.36	-0.52	0.39
OLFML3	0.07	37.04	-0.11	4.12	0.13	36.89	0.12	41.83	0.60	0.02
OPLAH	-0.56	0.05	0.23	8.88	0.20	9.26	0.61	1.62	0.43	31.62
OPN4			0.09	5.83					-0.47	0.89

OPRM1	0.02	52.83	-0.57	0.51	-0.11	54.33	-0.10	49.36	-0.23	8.00
ORC4	0.29	3.16	0.51	0.48	0.04	54.33	0.07	41.83	-0.36	0.39
OSBPL11	0.21	0.78	0.87	0.99	0.11	20.03	-0.05	47.42	-0.08	31.62
OSBPL3	0.35	4.28	0.31	5.83	0.27	4.05	-0.20	0.73	-0.95	0.02
OSMR	0.19	15.28			0.31	0.72	0.41	5.54	1.36	0.02
OTOF	-0.33	33.23	0.26	1.66	0.51	0.45	0.07	47.42	0.04	43.18
OTOR	-0.33	0.17	0.08	10.40	0.08	26.12	-0.12	41.83	-0.44	0.98
OTOS	-0.06	49.54	-0.24	2.61	-0.38	0.82	-0.10	13.89	0.11	43.01
OTUB1	-0.29	51.01	0.22	8.88	0.07	49.13	-0.43	0.06	-0.45	0.12
OXR1	0.19	33.23	0.47	0.11	-0.15	14.77	-0.26	11.24	-0.40	0.12
P2RX7	0.25	5.93			0.16	33.12	0.16	41.83	0.46	0.19
P2RY1	0.13	25.77	0.28	5.83	0.44	2.06	0.56	5.54	0.46	0.39
P2RY13	-0.14	25.77	0.21	9.63	0.06	33.12	0.44	2.42	0.66	0.02
P2RY2	-0.61	0.05	-0.71	0.48	-0.30	10.69	-0.47	0.35	0.10	42.21
P2RY6	0.31	0.05	0.25	0.78	-0.53	0.44	-0.17	53.83	0.41	0.99
PACSIN3	0.66	0.17	-0.77	1.77	0.16	10.69	0.04	54.83	0.45	0.39
PADI2	-0.25	4.28			0.17	3.07	0.20	0.86	0.84	0.02
PADI4	-0.41	3.16	-0.19	4.12	-0.17	56.82	-0.44	27.83	0.58	0.42
PAG1	0.03	56.87	-1.44	0.11	-0.29	1.10	-0.61	19.97	-0.52	24.40
PAK2	0.05	49.54	0.23	5.83	-0.07	41.10	-0.47	0.06	-0.43	0.02
PAK3	0.10	37.04	-0.71	0.20	-0.32	0.28	-0.13	47.42	-0.22	0.65
PAK4	0.05	44.81			0.10	36.89	-0.12	49.36	0.54	0.02
PAM	-0.31	0.17	-0.55	0.67	-0.24	12.58	-0.08	52.12	-0.48	0.07
PANK1	-0.07	49.54	0.40	2.30	0.23	2.31	-0.26	2.42	-0.62	0.39
PANK2	0.07	44.81	0.54	0.94	0.03	56.82	0.07	47.42	-0.39	0.02
PANK3	-0.14	51.01	0.70	3.21	-0.13	33.12	-0.16	41.83	-0.73	0.02
PAOX	0.05	44.81	-0.49	0.78	-0.11	36.89	0.24	8.99	0.49	0.27
PARD3	-0.10	44.81	0.57	0.60	0.23	0.86	-0.64	4.91	-0.17	24.40
PARD6G	0.28	15.28	0.56	1.46	0.24	1.82	0.03	52.66	-0.44	0.08
PARP14	0.24	18.59	0.23	8.25			0.44	5.54	1.41	0.02
PARP3	0.05	49.54	0.21	4.12	0.58	0.09	0.08	51.35	0.28	33.88
PARP9	-0.38	37.04			-0.14	5.71	0.33	32.50	0.49	0.02
PARVG	0.24	0.17	-0.16	4.12	0.36	10.69	-0.16	47.42	0.56	0.89
PAX6	-0.43	25.77	0.33	1.46	0.67	3.48	0.47	1.21	0.99	0.05
PBX1	-0.48	0.17	0.82	0.60	-0.41	2.66	-0.73	0.06	-0.46	0.65
PBX3	-0.13	49.54	0.38	1.09	0.31	4.05	0.17	3.87	-0.66	0.99
PBXIP1	-0.16	44.81	-0.35	0.78	0.16	29.33	-0.12	7.10	0.53	0.08
PCBP1	0.04	52.22	-0.58	2.77	0.06	56.82	-0.08	32.50	0.53	0.47
PCBP2	0.20	1.10	0.40	0.51	0.05	54.33	0.22	19.97	0.43	0.02
PCDH1	-0.06	51.01	-0.41	0.99			-0.05	50.49	0.01	44.32
PCDH17	-0.77	0.67	0.30	1.66	-0.75	0.09	-0.61	1.21	0.20	40.66
PCDH9	-0.61	0.05	0.55	5.83	-1.20	0.72	0.13	47.42	0.50	24.40
Pcdhb12	0.03	57.11	-0.87	2.86	-0.09	54.33	0.54	0.06	0.17	11.00
PCGF5	0.08	49.54	0.67	0.51	0.13	49.13	0.09	16.94	0.50	0.12
PCM1	-0.55	0.17	0.50	3.21	-0.47	0.40	-0.22	0.40	0.50	0.02
PCP4	-1.04	0.05	-0.21	0.51	-0.66	5.71	0.47	0.25	-0.32	33.88
PCSK1	0.73	52.22	0.91	2.61	0.18	3.48	0.70	32.50	0.77	0.98
PCYT1B	0.41	29.67	-0.46	4.12	-0.14	36.89	0.19	27.83	-0.51	0.05
PDCD1									1.20	0.02
PDCD11	0.47	0.05	0.46	2.77	0.57	0.09	0.63	32.50	0.53	1.19
PDE10A	-0.28	15.28	-0.56	1.09	0.23	41.10	-0.37	0.73	0.49	24.40
PDE12	0.40	0.17	0.59	0.51			-0.13	47.42	0.07	43.87

PDE1A	-0.12	37.04	0.46	4.12	-0.15	33.12	-0.11	13.89	-0.43	0.02
PDE2A	-0.09	49.54	-0.43	0.60	-0.23	0.52	-0.08	49.36	-0.07	36.83
PDE4A	0.09	49.54	0.35	0.51	-0.22	0.66	0.14	51.35	-0.50	0.12
PDE4DIP	-0.87	0.51	0.77	0.88	-0.20	20.03	-0.49	47.42	0.25	0.39
PDE6G	-0.08	21.80	-0.58	2.77			-0.06	41.83	0.47	0.89
PDE6H	0.08	55.56	-0.36	4.12	-0.69	0.09	-0.39	2.42	-0.06	31.62
PDEFD			-0.48	0.78					0.69	0.02
PDGFC	-0.70	0.05	0.70	1.03	0.31	4.05	0.71	0.25	-0.87	0.99
PDGFRA	0.09	44.81	0.64	0.60	0.09	36.89	-0.08	52.66	0.26	33.88
PDHA1	0.03	55.17	0.44	0.51	-0.26	0.64	-0.06	47.42	-0.52	0.02
PDIA5	0.15	2.45	0.40	0.18	0.05	54.33	-0.09	47.42	-0.23	31.62
PDlim1	-0.25	0.17	0.20	1.77	0.25	20.03	0.12	47.42	0.42	0.02
PDLIM2	0.16	0.93	0.29	0.99	-0.06	54.33	-0.08	52.66	0.62	0.89
PDLIM4	-0.11	25.77	-0.38	3.21	0.19	41.10	0.40	0.13	1.22	0.02
PDP1	0.14	37.04	0.36	2.30	0.28	0.28	0.29	5.54	-0.54	0.65
PDSS1	0.25	7.74	0.36	7.54			0.34	1.21	-0.86	0.02
PDXK	-0.43	3.16	-0.95	0.11	-0.68	0.09	0.29	41.83	0.45	0.07
PDYN	-0.18	44.81	-0.22	7.54	0.37	5.71	0.11	41.83	0.50	0.02
PDZD2	-0.95	0.05	0.34	1.77	0.90	0.09	-0.64	5.54	-0.22	6.00
PDZD3	0.18	1.43	0.23	2.12	0.21	41.10	-0.31	19.97	-0.92	0.02
PEBP1	1.00	0.05	0.18	8.25	-0.06	54.33	-0.43	41.83	0.23	37.82
PELI1	0.37	0.53	-0.37	2.77	-0.47	0.40	-1.05	0.06	-0.44	0.12
PELI2	0.43	0.05	0.85	0.57	-0.31	9.26	0.31	19.97	0.70	0.02
PELP1	0.09	49.54	0.49	0.11	0.80	0.09	-0.87	0.73	0.20	1.19
PEMT	0.27	44.81			0.21	14.77	-0.93	0.06	0.55	0.02
PENK	-0.40	0.26	0.61	0.18	0.55	0.52	-0.20	51.35	0.67	0.65
PER1	0.33	0.32	0.19	7.54	0.17	1.31	-0.42	0.06	-0.27	11.00
PER2	0.19	3.16	0.81	0.57	0.01	60.51	-0.10	11.24	-0.22	31.62
PERP	-0.14	5.93	0.47	1.09	-0.06	56.82	0.53	0.13	0.25	11.00
PES1	-0.17	25.77			-0.10	58.07	0.47	32.50	1.06	0.02
PEX1	-0.80	0.17	0.83	0.88	0.15	49.13	0.65	0.06	-0.61	14.82
PEX13	0.31	12.65	0.67	0.60	0.14	33.12	-0.11	52.66	-0.56	0.08
PEX14	0.21	21.80	-0.51	2.86	0.09	49.13	0.06	47.42	0.63	0.27
PEX5L	0.05	49.54	-0.41	0.94	0.07	49.13	0.08	32.50	0.14	38.75
PFDN2	-0.08	53.69	0.54	0.26	0.05	54.33	0.08	47.42	0.08	36.83
PFKFB3	0.02	56.87	-0.48	0.78	0.31	0.09	0.03	50.49	0.26	0.27
PFKFB4	-0.09	44.81	-0.14	2.61	0.03	57.40	-0.10	50.49	0.50	0.02
PGCP	-0.48	10.00	0.56	0.51	-0.14	41.10	0.14	41.83	0.49	0.89
PGD	0.11	44.81	0.32	0.60	-0.07	49.13	0.46	0.06	-0.21	24.40
PGDS									0.79	0.05
PGM2L1	-0.20	1.43	0.44	5.83	0.44	0.09	-0.69	19.97	-1.28	0.02
PGM3	0.07	37.04	-0.18	0.51	0.05	49.13	-0.43	0.06	0.45	0.21
PGM5	0.03	51.01	-0.27	3.21	0.33	1.82	0.25	19.97	0.54	0.07
PGM5	-0.32	1.94	-0.27	3.21	0.33	1.82	0.25	19.97	0.54	0.07
PGRMC2	0.27	0.17	0.50	0.11	0.05	54.33	0.18	7.10	-0.20	1.19
PHACTR1	0.18	37.04	0.40	0.20	-0.21	49.13	0.75	0.06	-0.51	0.99
PHC3	-0.13	33.23	0.36	5.83	0.05	49.13	-0.08	52.12	-0.46	0.02
PHF14	0.33	15.28	0.58	0.78	0.07	41.10	0.06	53.27	-0.42	0.08
PHF20L1	0.28	25.77	0.54	0.51	-0.15	54.33	-0.12	32.50	-0.63	0.02
PHF21A	-0.05	56.77	0.53	5.83	-0.19	54.33	-0.11	52.66	-0.41	0.05
PHKA1	0.18	33.23	0.08	10.40			0.92	0.57	0.51	0.99
PHKA2	-0.21	0.67	-0.55	0.30	-0.13	49.13	-0.39	41.83	0.62	0.47

PHTF2	0.01	56.77	-0.21	4.12	0.06	54.33	0.12	32.50	0.64	0.47
PHYHD1			-0.24	2.30	0.03	58.41	0.13	47.42	0.84	0.02
PIAS1	0.16	18.59	0.54	1.29	0.12	54.33	-0.32	0.86	-0.44	0.31
PIGG	-0.31	0.26	-0.65	0.78	0.19	14.77	-0.28	47.42	0.46	0.27
PIGh	-0.18	1.94	0.26	8.88	-0.27	20.03	-0.26	1.21	-0.80	0.02
PIK3C2G	-0.15	10.00	-0.67	2.77	0.38	14.77	-0.44	23.45	-0.40	0.21
PIK3CD	0.05	44.81	-0.62	3.01	0.13	9.26	0.16	41.83	0.45	0.02
PIK3IP1	0.14	49.54	0.42	0.51	0.22	9.26	0.16	49.36	0.44	0.02
PIK3R1	-0.16	10.00	0.55	1.09	0.48	22.90	-0.69	0.06	0.53	0.65
PIKFYVE			0.47	0.94	0.03	58.61	0.28	0.57	-0.31	11.00
PIN1	0.12	44.81	0.16	9.63	0.15	4.05	-0.15	16.94	-0.45	0.47
PIP5K3	0.03	49.54	-0.44	0.45	-0.23	0.40	0.04	55.77	0.10	33.88
PITPNC1	-0.34	0.05	0.37	2.86	-0.24	29.33	-0.49	5.54	-0.52	0.02
PKD2L2	0.09	44.81	-0.25	6.70	-0.05	54.33	0.07	47.42	0.48	0.65
PKIB	-0.30	0.93	0.52	0.78	-0.46	1.10	0.33	2.91	-0.78	0.12
PKM2	-0.18	55.87	0.14	4.12	-0.61	0.09	-1.37	0.06	0.19	14.82
PKN2	-0.16	3.16	0.60	1.77	-0.19	10.69	-0.49	7.10	0.68	0.02
PKP3	0.04	52.83	-0.07	10.40	0.17	54.33	0.06	49.36	0.54	0.02
PLA2G16	-0.07	56.87	-0.14	8.25	0.49	0.24	0.17	13.89	0.88	0.02
PLA2G2F	0.01	56.51	-0.48	0.83					-0.07	33.88
PLA2G4C	0.09		-0.38	0.67	0.05	49.13	0.07	41.83	0.23	14.82
PLA2G5	-0.16	54.70	0.24	5.83	0.50	0.24	-0.19	47.42	0.51	0.04
PLAA	0.45	0.32	0.36	0.78	0.07	55.77	-0.20	0.95	-0.10	24.40
PLAGL1	-0.36	0.05	-0.52	4.12	0.20	8.12	0.19	16.94	0.31	33.88
PLAUR			-0.10	9.63	0.33	1.31	0.39	0.11	0.65	0.02
PLCB1	0.35	0.53	0.41	2.77	-0.53	0.09	-0.24	41.83	-0.63	0.02
PLCb2	0.14	1.94	0.17	9.63	-0.31	20.03	-0.09	41.83	0.99	0.02
PLCE1	0.54	0.78	-0.13	5.83	0.13	12.58	0.76	0.06	1.02	0.02
PLCG1	0.08	53.69	-0.42	0.86	0.61	2.66	0.14	13.89	0.09	33.88
PLCG2	0.17	4.28	-0.28	4.12			0.09	49.36	0.66	0.47
PLCZ1	-0.52	0.05	0.31	5.83	0.35	4.73	0.66	0.06	0.32	24.40
PLD4	0.21	1.94	-0.12	5.83	0.06	54.33	0.17	19.97	0.53	0.13
PLEC	-0.85	0.13	0.54	0.11	0.19	4.05	-1.48	0.06	-0.91	0.07
PLEKHA3	0.01	57.11	-0.06	11.09	0.16	29.33	-0.19	0.35	-0.37	0.08
PLEKHA5	-0.45	0.05	0.49	0.51	0.02	58.41	-0.04	47.42	-0.06	35.53
PLEKHA6	-0.40	0.93	-0.37	0.78	0.47	1.31	-0.17	52.12	-0.14	4.22
PLEKHG3	-0.36	0.26	0.41	0.60	-0.83	0.09	0.43	0.06	0.54	0.17
PLIN1	0.09	44.81	-0.12	6.70	-0.37	33.12	0.11	27.83	-0.48	0.98
PLIN2	-0.16	37.04	0.19	4.12			0.33	1.88	0.68	0.05
PLK3	0.44	0.09	0.10	4.12	0.10	10.69	-0.08	41.83	0.07	40.66
PLOD1	0.06	52.83	-0.25	2.86	-0.17	54.33	0.13	47.42	-0.51	0.17
PLP1	-0.17	1.94	-0.17	4.12	0.12	12.58	-0.19	41.83	0.61	0.02
PLSCR1	-0.89	0.17	0.12	11.78	0.05	59.43	0.24	8.99	0.60	0.02
PLSCR2	-0.94	0.05	0.28	6.70	0.27	0.24			1.10	0.02
PLXDC1	-0.07	55.87	-0.17	2.86	0.13	49.13	0.25	1.62	0.57	0.17
PLXDC2	-0.07	54.15	-0.59	3.21	-0.16	3.48	0.02	55.17	0.66	0.02
PLXNA2	0.11	51.01	-0.09	8.25	0.03	56.82	-0.14	32.50	-0.43	0.06
PLXNB1	0.09	49.54	0.40	0.94	0.21	1.31	-0.23	0.86	0.17	31.62
Pmaip1	-0.38	3.16	-0.41	4.12	0.15	33.12	-0.58	27.83	0.58	0.12
PMCH			-0.38	7.54	-0.23	8.12	0.18	47.42	0.68	0.02
PMS2	-0.26	44.81	0.26	2.12	-0.20	54.33	0.55	0.73	-0.23	11.00
PNMT	0.05	44.81	-0.13	6.70	0.03	55.77	0.45	0.57	-0.09	31.62

PNN			0.39	0.17	-0.13	26.12			-0.37	0.02
PNOC	0.31	1.43	-0.18	8.88	0.04	55.77	-0.54	0.06	0.10	43.01
PNPLA2	0.09	49.54	-0.36	4.12	-0.09	36.89	0.21	4.91	0.67	0.02
POFUT1	0.17	3.16	-0.26	4.12	-0.23	0.66	-0.85	0.06	0.15	42.84
POLE	-0.39	3.16	0.41	0.43	-0.11	49.13	0.64	23.45	0.42	0.99
POLG2	0.31	29.67	0.32	0.60	-0.02	60.51	0.46	0.06	0.34	0.75
POLH	0.04	54.70	-0.65	0.51	0.40	3.48	0.21	13.89	-0.18	2.89
POLI	0.22	3.16	-0.15	4.12	-0.18	17.39	0.51	0.06	0.28	1.98
POLK	0.02	56.87	0.46	4.12	-0.15	17.39	-0.44	0.06	-0.40	0.65
POLL	0.16	15.28	-0.45	2.77	0.18	4.73	-0.22	27.83	-0.42	0.75
POLM	-0.14	3.16	-0.59	0.78	-0.27	0.40	0.13	27.83	0.13	14.82
POLR1E	0.47	0.05	0.48	0.51	0.02	58.41			-0.19	8.00
POLR2A	-0.09	25.77	-0.41	0.89	-0.40	5.71	-0.04	52.66	0.06	40.66
POLR2I	-0.06	54.70	-0.41	0.78	0.18	6.93	0.13	19.97	0.44	0.39
POLR3A	-1.01	0.40	-0.83	0.30	-0.26	2.31	-0.25	0.13	-0.35	14.82
POLR3E	-0.40	0.17	0.40	1.53	0.07	49.13	0.35	41.83	-0.62	0.02
POLR3F	-0.44	0.51	0.56	0.51	0.26	12.58	-0.47	0.18	-0.27	11.00
POLR3H	0.09	33.23	0.26	3.21	0.16	49.13	0.16	47.42	-0.74	0.04
POLR3K	-0.16	44.81	0.57	1.09	0.25	8.12	0.43	41.83	-1.14	0.02
POLRMT			-0.09	11.78	0.05	49.13	0.33	3.87	0.47	0.13
POM121/POM121C	0.15	1.43	0.34	2.12	-0.22	49.13	-0.95	0.11	-0.79	0.02
PON3	0.09	44.81	-0.32	0.51	0.51	0.09	0.54	0.34	0.84	0.02
POPDC2	0.25	1.94	0.17	6.70	-0.25	3.48	-0.25	0.12	-0.54	0.02
PPAPDC1A	-0.31	3.16	-0.39	0.30	-0.30	1.56	-0.09	53.27	-0.11	31.62
PPARG	-0.14	1.43	-0.40	0.81	0.11	29.33	0.10	32.50	0.33	11.00
PPARGC1B	-0.27	37.04	0.49	1.09	-0.50	0.09	0.03	52.66	0.43	0.02
PPFIBP2	0.14	25.77	0.76	0.67	0.59	0.09	-0.46	32.50	0.35	0.17
PPHLN1	-0.28	44.81	0.60	1.21	-0.10	49.13	-0.06	47.42	-0.65	0.02
PPIC	0.01	56.51	0.87	2.30	-0.13	33.12	-0.12	47.42	-0.36	0.02
PPM1D	0.29	0.53	0.21	3.01	-0.13	41.10	-0.30	0.51	-0.39	0.21
PPM1H	0.07	44.81	-0.37	0.27	0.34	4.73	-0.26	4.91	-0.91	0.02
PPM1L	-0.44	0.13			-0.17	17.39	-0.22	41.83	-0.34	0.89
PPP1R12B	0.12	44.81	0.56	0.60	-0.10	55.77	0.12	41.83	-0.18	33.88
PPP1R14A	0.05	52.22	0.28	5.83	0.08	41.10	-0.05	47.42	0.43	0.60
PPP1R15	0.28	29.67	0.38	0.88	0.37	0.09	0.13	54.40	-0.45	0.08
PPP1R3C	0.11	7.74	0.44	0.51	0.11	54.33	0.02	53.27	0.52	0.39
PPP2R1B	0.10	49.54	-0.67	0.18	-0.20	49.13	-0.12	13.89	0.49	0.99
PPP2R2B	-0.24	1.43	0.20	5.83	-0.14	20.03	-0.32	19.97	-0.56	0.02
PPP2R3A	0.07	49.54	-0.50	0.45	-0.70	0.09	-0.42	0.06	-0.06	39.47
PPP3R1	-0.08	44.81	0.76	0.78	-0.07	55.77	-0.28	0.18	0.69	0.12
PPP5C	0.29	10.00	0.55	4.12	0.21	20.03	0.14	47.42	-0.55	0.13
PPP6R1	-0.45	0.13	-0.15	5.83	0.02	55.77	-0.32	47.42	-0.41	0.08
PPTC7	-0.07	51.01	0.22	0.26	-0.12	9.26	0.14	41.83	0.55	0.08
PRCP	0.34	0.78	-0.60	0.83	-0.37	4.05	0.17	19.97	0.60	11.00
PRDM2	0.59	0.17	0.51	0.88	-0.32	10.69	-0.61	41.83	-0.65	0.07
PRDX6	-0.47	1.94	0.53	1.09	-0.14	56.82	-0.12	32.50	0.56	0.13
Prdx6b	0.13	37.04	0.25	4.12	0.03	54.33	0.10	16.94	0.57	0.02
PRELP	-0.28	0.51	-0.38	4.12	0.21	0.64	0.18	11.24	0.56	0.02
PRICKLE1	-0.61	0.05	0.28	1.09	-0.26	14.77	-0.03	52.66	0.54	24.40
PRIM1	0.44	0.05	-0.21	8.25	-0.05	59.43	0.31	1.62	-0.04	39.47
PRIM2	-0.37	44.81	-0.46	0.82	-0.71	9.26	-0.09	13.89	0.26	4.22
PRKAA2	-0.15	1.43			0.15	36.89	0.05	53.83	-0.77	0.02

PRKACB	-0.44	29.67	0.38	3.21	0.17	17.39	-1.25	0.34	-0.37	0.75
PRKAR2A	0.19	5.93	0.17	8.25	0.07	54.33	-0.10	41.83	-0.84	0.02
PRKAR2B	-0.26	2.45	-0.43	0.78	0.31	4.73	0.04	53.27	0.04	43.48
PRKCA	0.13	10.00	0.66	1.77	-0.14	49.13	-0.12	47.42	-0.43	0.04
PRKCD	0.11	49.54	-0.16	5.83	-0.31	49.13	0.61	0.06	0.74	0.21
PRKCDBP	-0.18	44.81	-0.53	0.88	0.03	59.79	0.21	0.57	0.58	0.02
PRKCE	-0.14	52.83	0.64	0.94	-0.20	36.89	-0.36	0.51	-0.39	0.02
PRKCQ	-0.45	12.65	-0.22	3.01	-0.17	2.31	-0.77	0.54	0.33	24.40
PRKD3	-0.22	3.16	-0.43	5.83	0.11	9.26	-0.62	0.06	0.59	0.65
PRKG1	-0.60	0.05	0.56	0.51	0.48	0.09	0.21	1.33	-0.37	1.98
Prl3b1	-0.11	7.74	-0.48	0.67			-0.05	49.36	0.01	44.32
PRMT3	0.14	33.23	0.46	0.51	0.18	3.48	-0.40	0.06	-0.45	0.39
PROCR					0.29	49.13			1.29	0.02
PROP1	-0.05	49.54	-0.40	0.67	0.03	55.77			0.22	44.32
PROS1	-0.39	0.05	-0.38	1.09	-0.15	6.93	0.42	16.94	0.57	0.04
PROSC	0.49	3.16	-0.59	2.61	-0.87	17.39	0.57	0.06	0.80	0.39
PRPF40A	0.21	21.80	0.61	0.48	-0.16	5.71	0.23	7.10	-0.43	0.31
PRPF4B	0.13	49.54	0.66	1.03	0.16	26.12	0.59	0.57	0.58	0.02
PRR13	-0.12	49.54	0.59	0.11	0.12	33.12	-0.03	52.66	0.10	44.05
PRR15L	0.10	33.23	-0.41	0.78			-0.06	50.49	0.09	44.32
PRR16	-0.66	0.53			0.05	58.93	-0.53	0.06	-0.98	0.13
PRR5L	-0.75	0.09	0.21	1.09	-0.07	36.89	-0.21	47.42	0.25	36.83
PRRC2C	0.28	0.40	0.34	0.30	0.14	17.39	0.15	52.12	0.72	0.12
PRRX1	-0.45	0.78	-0.67	2.86	-0.68	0.09	-0.55	1.88	0.62	0.65
PRRX2	-0.27	33.23	0.23	0.30	0.06	58.07	0.82	0.06	1.26	0.02
PRTG	-0.19	4.28	0.32	0.53	0.48	0.09	0.26	47.42	0.23	1.98
PSCD4	-0.10	57.29	-0.40	3.01	0.06	49.13	0.63	0.29	0.94	0.02
PSD3	-0.28	7.74	-0.50	0.78	-0.20	17.39	-0.54	1.21	-0.51	0.99
PSMA6	0.10	51.01	0.64	0.18	-0.08	29.33	0.06	50.49	-0.17	6.00
PSMA8	-0.08	37.04			0.76	0.09	0.35	13.89	-0.13	36.83
PSMB11	0.11	15.28			-0.26	10.69	0.23	47.42	-0.49	0.05
PSMB8	0.05	52.22	0.61	1.66	0.11	54.33			0.62	0.02
PSMB9	0.30	0.51	0.29	2.77			-0.15	13.89	0.45	0.12
PSMC3IP	0.20	7.74	0.77	0.46	-0.09	36.89	-0.33	0.86	0.23	36.83
PSMC5	0.12	5.93	0.68	1.03	0.12	22.90	0.31	0.11	0.47	0.21
PSMD7	0.10	37.04	0.65	0.60	-0.09	26.12	0.31	0.40	0.48	0.02
PSME4	0.19	1.10	0.38	0.51	0.09	49.13	-0.08	27.83	-0.36	0.99
PSMF1	0.27	0.17	0.66	0.51	0.13	41.10	-0.35	2.42	1.32	0.02
PSPC1	-0.03	56.51	0.57	1.53	0.08	26.12	-0.07	49.36	-0.53	0.02
PTBP1	-0.06	51.01	0.12	9.63			0.07	47.42	0.49	0.12
PTCHD1	-0.55	0.05	0.08	5.83	0.32	49.13	0.15	50.49	0.14	40.05
PTDSS2	-0.13	25.77	-0.42	0.78	0.10	49.13	-0.07	51.35	-0.36	0.98
PTGDS	-0.54	0.93	-0.09	7.54	0.33		-0.07	55.17	-0.24	44.20
PTGES	0.33	0.93	0.18	0.67	0.14	49.13	0.22	27.83	0.50	0.02
PTGR1	0.11	33.23	0.49	0.45	0.11	22.90	0.08	52.66	0.35	0.02
PTGS2	1.08	0.05	0.48	2.30	0.23	3.07	0.86	0.06	-0.94	0.02
PTH1R	-0.62	0.26	0.20	1.77	0.11	12.58			0.50	0.98
PTHLH	-0.05	57.29	-0.53	1.53	0.15	33.12	-0.26	0.73	-0.42	0.89
PTPLAD2	-0.46	1.43	-0.15	4.12	0.48	3.07	-0.36	16.94	0.90	0.02
PTPN21	-0.70	1.43	0.46	0.20	0.02	60.23			0.20	40.05
PTPN5	0.03	54.15			-0.15	49.13	-0.07	27.83	-0.58	0.13
PTPN6	-0.04	52.22	0.48	3.21	0.28	12.58	0.39	41.83	1.39	0.02

PTPRC	-0.11	52.22	0.19	6.70	0.11	54.33	-0.43	23.45	1.00	0.02
Ptprd	0.24	5.93	0.10	11.09					1.13	0.02
PTPRR	0.08	52.22	0.45	1.53	-0.28	0.09	-0.20	0.73	-0.30	0.17
PUS10	0.12	33.23	0.36	1.09	0.19	0.66	0.06	49.36	-0.38	0.17
PUS3	0.15	7.74	0.46	0.78	-0.14	10.69	0.41	0.51	0.54	0.05
PVRL3	-0.10	56.51	0.61	0.60	-0.11	26.12	-0.83	0.86	-0.73	0.31
PVT1	-0.25	0.17	-0.89	0.23					0.28	24.40
PWP1	-0.06	54.15	-0.40	0.48	0.02	58.41	-0.04	51.35	-0.09	24.40
PXDN	-0.41	0.05	0.30	6.70	0.07	54.33	-0.20	1.88	-0.24	2.89
PYCARD	-0.10	52.22	-0.24	4.12	0.11	49.13	-0.08	53.27	1.01	0.02
QRFPR			-0.48	3.01	0.20	49.13			-0.33	2.89
QRICH1	-0.03	55.56	0.45	1.53	-0.12	49.13	-0.40	19.97	-1.12	0.02
R3HDM1	-0.45	0.26	0.53	5.83	-0.23	2.06	-0.24	41.83	-0.43	0.12
RAB11FIP4	0.39	0.26	0.48	2.30	0.11	12.58	-0.19	1.62	-0.35	0.99
RAB1A	0.19	29.67	0.55	1.77	-0.28	20.03	-0.33	0.29	-0.51	0.02
RAB22A	-1.03	0.05	0.24	0.67	0.34	41.10	-0.30	0.95	0.42	0.02
RAB23	0.13	37.04	-0.47	2.61	-0.12	33.12	-0.50	0.12	0.46	0.65
RAB27A	-0.43	0.05	0.45	2.61	0.33	2.66	1.02	0.06	-0.87	0.02
RAB28	0.15	25.77	0.54	0.99	-0.10	33.12	-0.65	0.06	-0.39	0.47
RAB32	-0.26	44.81	0.11	7.54	0.29	20.03	-0.26	1.21	0.94	0.13
RAB3C	0.34	0.13	0.66	1.53	0.08	49.13	-0.12	49.36	-0.55	0.05
RAB3D	-0.41	0.67	-0.62	2.61	0.07	36.89	-0.08	27.83	0.31	24.40
RAB40B	0.22	4.28	0.75	1.77	0.04	49.13	0.15	47.42	-0.25	0.99
RAB7L1	0.04	55.17	-0.28	4.12	-0.14	14.77	0.34	0.11	0.66	0.02
RABIF	0.17	10.00	0.66	1.53	0.05	54.33			-0.35	0.39
RAC1	0.22	0.17	0.45	0.88	0.02	60.51	-0.13	13.89	0.35	0.02
RAC2	-0.08	51.01	-0.46	1.66	0.02	60.51	0.45	0.86	0.90	0.02
RALGAPA1	-0.13	1.10	0.37	1.29	0.04	54.33	0.50	0.29	-0.27	0.75
RALGPS1	0.12	10.00	0.19	0.51	-0.16	1.82	-0.42	11.24	-0.48	0.21
RALY	-0.25	0.67	-0.70	0.66	0.07	41.10	0.03	55.17	0.23	31.62
RANBP17	-0.09	51.01	-0.17	0.51	0.50	0.86	-0.20	41.83	0.57	0.39
RANBP3	0.11	37.04	0.10	11.78	-0.19	12.58	-0.66	0.06	-0.58	0.99
RAP1GAP2	0.12	18.59	-0.15	6.70	0.13	49.13	-0.40	7.10	0.66	0.13
RAP2B	0.13	44.81	0.48	0.20	-0.14	3.07	0.03	51.35	-0.55	0.04
RAPGEF3	0.04	49.54	0.18	2.86			0.09	49.36	0.51	0.89
RAPGEF6	-0.17	44.81	0.49	0.17	-0.47	0.09	-0.16	47.42	-1.09	0.02
RARB	-0.50	0.40	0.50	0.30	-0.10	17.39	-0.14	47.42	-0.20	0.31
RARRES1			-0.22	9.63	-0.30	36.89	-0.76	0.06	0.37	31.62
RARRES2	-0.11	49.54	-0.24	3.21	0.08	54.33	0.11	27.83	0.81	0.02
RASA2	0.27	2.45	-0.89	1.66	-0.11	29.33	-0.14	47.42	-0.63	0.98
RASA4/RASA4B	0.03	51.01	-0.37	3.21	-0.04	56.82	0.44	0.06	0.42	0.08
RASD2	0.55	7.74	0.08	10.40	0.07	36.89	-0.23	41.83	0.50	0.98
RASGEF1B	-0.38	1.10	0.66	0.60	0.52	0.28	0.17	1.62	0.40	0.31
RASGRF2	-0.13	52.22	0.38	0.88	0.31	0.44	-0.22	3.87	-0.76	0.02
RASGRP3	0.01	56.77	0.40	0.99	-0.07	57.40	-0.18	41.83	0.60	0.04
RASIP1	0.20	15.28	0.11	8.25	0.06	49.13	-0.56	0.57	0.18	11.00
RASL12	-0.27	25.77	-0.08	6.70	-0.15	36.89	-0.53	0.91	0.08	42.55
RASSF2	0.21	3.16	-0.48	2.86	-0.31	0.40	-0.30	7.10	0.51	0.98
RB1CC1	-0.35	0.78	0.19	8.25	-0.28	0.52	-0.26	13.89	-0.48	0.39
RBBP4	0.16	44.81	0.55	1.53	-0.20	1.56	-0.23	19.97	0.51	0.75
RBFOX2	-0.20	0.51			0.01	58.93	0.28	32.50	0.50	0.02
RBM8A	-0.15	2.45	0.50	0.99	0.09	54.33	-0.72	0.06	0.44	11.00

RBMS3	0.05	52.83	0.46	0.42	-0.58	0.09	0.32	0.25	0.26	24.40
RBMX	0.15	18.59	0.61	1.77	-0.13	20.03	-0.35	0.11	0.63	0.13
RBP1	-0.32	21.80	0.48	0.51	0.06	56.82	-0.11	16.94	1.15	0.02
RBP4	-0.29	7.74	-0.27	5.83	0.66	0.09	-0.20	32.50	0.39	0.99
RCAN1	0.03	53.69	-0.48	1.21	-0.38	1.31	-0.53	0.18	-0.14	31.62
RCOR1	0.09	44.81	-0.56	0.60	0.26	0.66	0.54	0.06	-0.27	24.40
RCSD1	-0.29	44.81	0.12	10.40			-0.64	1.21	0.71	0.02
RDH10	0.38	0.13	0.68	1.66	0.27	0.40	-0.28	11.24	-0.41	8.00
RDH5	-0.15	49.54	-0.21	6.70	0.16	10.69	-0.16	47.42	0.63	0.39
RECQL	0.10	29.67	0.73	0.78			0.64	0.73	-0.23	1.19
RELN	-0.16	3.16	0.57	0.83	0.35	2.31	0.15	13.89	0.17	40.66
REN	0.41	0.17	-0.22	3.21	0.46	26.12	-0.56	4.91	-0.19	31.62
RENBP	0.17	1.94			0.23	0.64	0.16	27.83	0.84	0.02
REST	-0.15	29.67	0.34	0.78	0.47	0.66	0.34	0.73	0.18	33.88
RETSAT	0.20	25.77	0.30	0.78	-0.06	58.61	-0.43	0.06	0.71	0.02
REV3L	-0.43	0.17	-0.28	0.51	-0.08	26.12	-0.57	7.10	-0.46	0.17
RFFL	0.14	37.04	0.64	0.20	1.19	0.09	0.44	27.83	0.42	0.27
RFX3	-0.74	0.05	0.44	5.83	-0.43	0.09	-0.54	23.45	-1.07	0.02
RGMA	-0.13	49.54	-0.36	2.77	-0.33	0.86	0.51	0.86	0.78	0.02
RGMB	0.32	0.05	0.67	0.11	-0.13	17.39	-0.29	0.95	0.60	0.04
RGS14	-0.11	49.54	0.24	5.83	-0.30	22.90			-0.58	0.47
RGS3	-0.13	25.77	-0.48	2.86	0.08	55.77	-0.60	0.06	-0.21	24.40
RGS6	-0.54	0.32	-0.22	0.78			0.06	47.42	0.76	0.02
RGS9	0.25	1.10	0.74	0.60	0.37	6.93	-0.25	41.83	-0.38	0.02
RHOBTB1	0.41	0.05	-0.41	5.83	-0.07	55.77	-0.14	32.50	-0.16	33.88
RHOC	-0.28	15.28	0.16	2.77	0.14	14.77	0.05	52.12	0.71	0.02
RHOD	0.16	21.80	0.21	1.66	0.81	0.09	-0.06	54.40	1.11	0.02
RHOG	-0.22	1.94	-0.22	1.53	0.07	49.13	0.03	54.40	0.55	0.02
RHOH	0.54	0.05	-0.38	1.66	-0.35	0.52	-0.23	13.89	1.22	0.04
RHOJ	-0.38	0.05	0.23	1.09	-0.27	26.12	1.56	0.06	1.11	0.02
RHOT1	0.16	1.43	0.39	1.09	0.13	9.26	0.36	0.57	-0.32	0.02
RHPN2	0.37	0.78	0.55	0.99	0.36	20.03	-0.90	5.54	-0.02	41.88
RIF1	-0.41	0.09	0.61	1.53	-0.42	2.06	-1.01	0.06	0.42	31.62
RIMS2	0.15	15.28	0.57	5.83	0.06	49.13	-0.23	0.29	-0.66	0.02
RIN2	0.13	18.59	0.47	0.94	-0.09	29.33	0.14	41.83	0.29	24.40
RINT1	0.13	33.23	0.39	4.12	-0.15	4.73	-0.35	49.36	-0.19	31.62
RLBP1	-0.25	7.74	0.28	1.29	0.14	26.12	0.03	53.83	0.78	0.02
RLBP1	-0.25	7.74	0.28	1.29	0.14	26.12	0.03	53.83	0.78	0.02
RLN1/RLN2	-0.33	37.04			0.03	59.79	1.13	0.73	-0.23	11.00
RMND1	0.02	55.17	0.82	0.18	0.20	3.07	0.25	32.50	-0.18	0.89
RNASEN	-0.13	29.67	-0.71	0.57	0.27	5.71	-0.64	0.06	-0.21	31.62
RND1	0.04	54.70	-0.25	4.12	0.07	54.33	-0.15	23.45	-0.46	0.12
RND3	-0.32	0.17	0.53	5.83	0.05	54.33	0.15	47.42	-0.12	24.40
RNF111	-0.59	0.05	0.26	2.30	-0.34	4.05	-0.41	41.83	-0.17	2.89
RNF121	-0.84	0.05	0.39	0.88	0.07	49.13	0.15	41.83	-0.68	0.02
RNF122	-0.05	53.69	-0.11	9.63	-0.05	55.77	-0.08	47.42	0.54	0.02
RNF128	-0.22	4.28	0.83	0.88			-0.21	2.91	-0.71	0.02
RNF130	-0.17	7.74	-0.34	3.01	0.09	14.77	-0.03	54.83	0.45	0.13
RNF135	-0.11	49.54	0.06	10.40	0.17	9.26	0.47	5.54	0.39	0.89
RNF141	0.22	0.53	0.68	0.94	0.20	4.05	-0.93	0.06	-0.45	0.27
RNF144B	0.47	1.10	0.22	0.48	0.32	49.13	0.80	0.73	-0.32	31.62
RNF185	0.16	7.74	0.45	1.66	0.01	60.51	0.83	0.06	0.22	42.37

RNF2	0.07	33.23	0.39	2.12	0.12	49.13	-0.08	47.42	0.43	0.39
RNF213	0.08	44.81	-0.42	3.01	0.05	56.82	0.28	0.25	1.02	0.02
RNF38	0.06	52.83	0.26	4.12	0.39	0.44			-0.12	36.83
RNF4	-0.14	29.67	0.45	3.21	0.40	0.64	-0.80	8.99	-0.23	0.47
RNF41	0.05	49.54	-0.21	5.83	0.06	58.61	-0.85	0.34	0.05	41.88
RNLS	-0.17	5.93	0.20	3.21	0.01	58.93	-1.03	0.95	-0.25	14.82
ROBO1	-0.30	0.67	0.65	0.42	-0.24	20.03	0.35	41.83	-0.48	0.02
ROBO3	0.22	29.67	-0.46	2.12	0.24	10.69	0.18	16.94	0.71	0.02
RP2	-0.20	25.77	-0.75	0.89	-0.23	14.77	-0.21	32.50	0.36	6.00
RPH3A	0.03	56.51	-0.14	4.12	0.25	22.90	-0.37	0.06	-0.23	4.22
RPL37	0.15	10.00	0.33	5.83	0.59	0.09	-0.63	3.87	-0.42	0.99
RPL39L	-0.62	12.65	-0.75	0.51			-0.37	49.36	1.40	0.02
RPL7A	0.15	37.04	-0.37	1.77	0.07	49.13	0.16	3.87	0.54	0.13
RPRM	-0.97	0.51	0.71	0.11	0.53	0.24	-0.25	41.83	0.88	0.02
RPS21	-0.07	55.87	-0.44	0.51	0.08	54.33	0.16	41.83	0.84	0.02
Rps24	0.48	0.09	0.61	0.51	-0.22	33.12	-1.14	0.11	-0.66	0.02
RPS6KB1	-0.55	0.05	0.55	1.77	-0.43	36.89	0.19	1.21	-0.35	0.12
RPS6KC1	-0.20	2.45	0.29	1.66	0.39	0.40	0.17	23.45	0.62	0.02
RRAD	-0.33	1.94	0.27	0.51	0.41	9.26	0.37	0.73	0.49	0.02
RRAS2	-0.13	15.28	0.53	1.29	-0.16	29.33	0.13	41.83	-0.41	0.99
RRBP1	-0.54	4.28	-0.21	13.30	-0.31	0.52	-0.56	11.24	-0.96	0.02
RRN3	-0.46	0.05	-0.12	7.54	-0.14	8.12	-0.32	47.42	-0.60	0.02
RRP1B	-0.20	15.28	-0.98	0.45	-0.16	33.12	-0.63	2.91	-0.34	14.82
RRP8	-0.16	0.93	0.25	0.42	0.04	56.82	-0.53	0.34	-0.16	24.40
RSPO1	-0.67	0.09	-0.46	4.12	0.58	22.90	0.66	0.06	1.51	0.02
RSPO2	-0.93	7.74	0.77	0.42			-0.19	23.45	-0.83	0.02
RSRC2	0.20	37.04	0.39	1.03	-0.09	41.10	0.12	41.83	-0.36	0.17
RTN4	-0.51	0.05	0.76	1.77	-0.20	20.03	0.26	16.94	-0.40	0.02
RTN4R	0.18	29.67	-0.40	3.21	0.12	41.10	0.18	11.24	0.56	0.12
RTP4	-0.31	3.16	0.19	7.54	0.72	0.09	0.31	23.45	0.55	0.12
RUNX2	0.13	44.81	-0.24	8.25	0.07	55.77	0.54	3.87	-0.90	0.02
RXRA	0.08	44.81	-0.13	8.88	-0.20	9.26	0.29	0.29	0.46	0.04
RXRG	-0.71	4.28	-0.26	1.46	-0.06	49.13	0.91	0.29	1.02	0.02
S100A1	-0.12	51.01			0.03	59.79	0.11	23.45	0.68	0.02
S100A10	0.17	2.45	0.16	0.51	0.38	1.31	0.13	23.45	1.01	0.02
S100A11	-0.28	49.54	0.14	6.70	0.28	29.33	-0.06	50.49	1.10	0.02
S100A13	-0.09	18.59	0.35	0.11	0.15	41.10	0.12	4.91	0.60	0.02
S100A16	0.05	49.54	0.40	2.30	0.09	33.12	-0.12	5.54	0.40	0.04
S100A3	0.05	44.81	-0.22	3.01	0.30	0.64			0.42	0.99
S100A4	-0.13	44.81	-0.09	14.77	0.21	9.63	0.35	0.35	1.43	0.02
S100A6	-0.20	44.81	0.05	11.09	0.47	12.58	0.03	54.40	1.35	0.02
S100B	-0.13	51.01	-0.21	5.83	-0.05	57.40	0.14	47.42	0.55	0.10
S1PR3	-0.11	49.54	-0.18	3.21	-0.09	54.33	0.07	41.83	0.62	0.12
SAG	-0.08	49.54	0.53	0.99	-0.18	58.07	0.50	0.06	-1.04	0.08
SAMD4A	-0.54	0.05	-0.13	5.83	0.30	14.77	-0.31	0.34	-0.32	14.82
SAMSN1	-0.16	49.54	-0.20	5.83	-0.37	17.39	-0.29	1.62	1.50	0.02
SAP130	-0.20	25.77	-0.10	5.83	-0.20	4.73	-0.60	0.73	-0.97	0.07
SAP18	-0.20	0.93	0.65	1.21	-0.08	22.90	-0.64	0.06	-0.41	0.08
SATB1	0.34	21.80	0.32	4.12	-0.43	0.09	-0.57	23.45	-0.57	0.02
SATB2	0.15	33.23	0.75	0.99	0.51	1.31	0.08	52.12	-0.40	8.00
SAV1	0.18	4.28	0.13	7.54	-0.05	54.33	0.12	47.42	-0.53	0.75
SBNO2	-0.03	57.11	-0.46	0.51	0.10	8.12	-0.14	2.91	-0.27	0.17

SCAMP1	-0.79	0.13	0.40	0.99			0.52	23.45	-0.46	0.12
SCAMP5	0.06	54.70			0.40	0.09	-0.12	41.83	-0.27	0.27
SCAPER	-0.21	21.80	0.42	4.12	-0.43	0.09	0.31	32.50	-0.25	14.82
SCARA3	0.22	33.23	0.27	0.51	0.14	36.89	0.05	53.83	0.47	0.02
SCGB3A1	-0.45	0.32	-0.36	0.51	0.37	17.39	-0.12	41.83	1.13	0.02
SCIN	-0.58	0.51	0.50	0.18	0.04	54.33	0.74	0.51	-0.24	14.82
SCN1A	0.27	37.04	0.23	11.78	0.02	60.23	-0.04	49.36	-0.41	0.02
SCPEP1	0.11	44.81	-0.45	4.12	0.03	56.82	0.38	16.94	0.40	0.98
SCRG1	-0.27	29.67	-0.33	2.61			0.10	32.50	0.62	0.02
SDC4	-0.30	7.74	0.74	0.51	-0.18	4.73	0.22	32.50	0.77	0.02
SDF4	-0.07	37.04	0.31	2.61	0.06	54.33	0.11	47.42	-0.43	0.47
SDPR	0.07	37.04	-0.40	0.60			-0.48	0.13	0.23	4.22
SDSL	-0.04	56.77	0.27	5.83	-0.07	36.89	0.09	51.35	0.48	0.27
SEC23IP	-0.24	0.93	0.63	0.78	0.17	3.48	-0.08	41.83	-0.36	0.13
SEC63	0.19	25.77	0.95	0.48	-0.09	41.10	0.14	4.91	-0.50	0.02
SECISBP2	0.05	44.81	0.70	0.18	0.03	58.93	0.55	0.06	-0.56	8.00
SEL1L	-0.33	0.05	-0.41	0.42	-0.28	10.69	0.37	19.97	-0.84	0.12
SELENBP1	0.09	37.04	-0.35	3.01	-0.09	55.77	0.13	41.83	0.46	0.89
SELPLG	-0.07	55.87	-0.43	2.77	0.12	5.71	0.10	47.42	0.56	0.02
SELT	0.39	15.28	0.38	1.29	0.10	54.33	0.45	1.88	-0.94	0.02
SEMA3C	-0.11	49.54	0.30	0.51	0.41	2.06	0.04	50.49	0.82	0.19
SEMA3G	-0.03	55.17	0.14	6.70	0.47	0.09	-0.16	52.66	-0.46	0.65
SEMA5A	0.04	52.83			-0.06	55.77	-0.14	41.83	-0.33	0.99
SEPP1	-0.17	12.65	-0.30	2.77	-0.07	54.33	0.14	27.83	0.52	0.02
SEPT11	-0.06	52.83	0.46	0.51	0.18	33.12	0.15	47.42	-0.62	0.02
SEPT6	0.23	0.51	0.64	0.57	0.26	4.05	0.35	0.06	0.44	0.08
SEPT7	0.09	49.54	0.24	2.77	-0.13	17.39	-0.11	32.50	-0.46	0.02
SEPT8	-0.20	44.81	-0.36	0.51	0.13	22.90	0.12	19.97	0.64	0.17
SERBP1	-0.04	57.11	0.66	0.27	0.11	10.69	-0.16	0.95	-0.19	4.22
SERPINA1	-0.09	37.04	-0.23	3.21	0.04	57.40	0.28	41.83	0.43	0.02
SERPINA9	0.15	15.28	-0.20	5.83	0.02	58.07	0.03	52.12	-0.46	0.07
SERPINF1	-0.17	44.81	-0.14	5.83	0.13	49.13	0.46	41.83	0.84	0.02
SERPINF2	0.30	0.05	-0.08	5.83			-0.22	41.83	0.98	0.02
SERPING1	-0.19	12.65	0.45	4.12	-0.04	58.61	0.36	1.33	0.59	0.31
SERPINH1	-0.31	21.80	0.08	7.54	0.13	9.26			0.71	0.02
SERTAD1	0.47	0.67	0.39	1.09	0.40	0.09	-0.02	53.27	0.44	0.65
SERTAD4	0.13	18.59	0.59	0.67	0.08	41.10	0.45	0.06	-0.04	41.26
SESN3	-0.15	49.54	0.66	0.35	0.06	49.13	-0.23	0.51	0.58	0.02
SESTD1	0.07	49.54	-0.08	12.52	-0.04	56.82	-0.16	13.89	-0.53	0.02
SET	-0.12	21.80	-0.39	4.12	-0.03	60.23	-0.10	41.83	-0.48	0.31
SETBP1	0.15	4.28	-0.33	2.86	0.14	49.13	-0.04	47.42	0.56	0.17
SETD3	-0.05	54.15	0.73	0.67	0.16	17.39	0.50	27.83	-0.79	0.02
SETD5	-0.38	3.16	0.40	7.54	-0.46	9.26	0.59	13.89	-0.98	0.02
SETD8	0.14	44.81	0.19	6.70	0.15	6.93	-0.39	0.51	-0.49	0.12
SF3B3	0.11	52.22	0.44	0.51	-0.20	12.58	0.14	41.83	-0.44	0.02
SFMBT1	-0.14	7.74	0.45	0.51	0.10	17.39	0.19	0.95	0.35	24.40
SFRP4	0.19	3.16			-0.42	0.72	0.23	49.36	-0.14	38.75
SFSWAP	-0.16	1.43	-0.55	3.01	0.07	49.13	0.25	8.99	0.49	0.21
SFT2D2	0.05	51.01	0.59	1.03	0.59	0.09	0.04	51.35	0.46	0.02
SFTPC	-1.25	0.05	0.25	0.60	-0.24	12.58	-0.74	3.87	-1.20	0.02
SFXN1	-0.10	52.83	-0.27	4.12	-0.19	2.66	-0.30	7.10	-0.49	0.02
SGCZ	-0.61	0.67	-0.42	3.01					0.03	31.62

SGPL1	-0.12	53.69	-0.15	5.83	0.28	1.31			0.44	0.13
SGSH	0.46	0.78	0.54	1.09	0.45	1.31	0.55	0.12	0.30	24.40
SGTB			0.53	1.77	0.19	2.66	-0.10	50.49	-0.45	0.39
SH3BGRL	0.04	49.54	0.37	5.83	-0.22	26.12	-0.30	11.24	-0.43	0.12
SH3BP1	0.13	33.23	-0.54	4.12	0.07	41.10	0.04	52.66	0.45	0.04
SH3D19	-0.42	0.17	0.49	2.86	-0.42	22.90	-0.40	4.91	-0.52	0.75
SH3GL2	-0.16	25.77	-0.28	3.21	-0.15	41.10	-0.17	0.73	0.77	0.02
SH3GL3	-0.41	0.51	-0.25	0.51	0.21	17.39	0.09	41.83	0.09	38.75
SH3KBP1	-0.51	0.17	0.75	0.67	-0.27	0.09	0.17	2.42	-0.01	41.26
SH3PXD2B	-0.09	44.81	0.26	8.25	0.34	4.73	0.19	41.83	0.49	0.19
SH3RF1	0.20	44.81	0.46	0.78	-0.36	36.89	-0.74	0.06	0.39	0.99
SH3TC1	-0.03	56.77	-0.19	8.88	0.26	14.77	-0.41	0.51	1.07	0.02
SHANK2	0.08	29.67	0.19	0.51	-0.17	8.12	0.34	0.35	0.59	0.02
SHCBP1	-0.28	0.94	-0.52	0.81	0.16	12.58	0.06	52.12	0.23	31.62
SHMT1	0.08	52.22	-0.33	3.01	-0.23	49.13	-0.69	0.06	-0.22	0.27
SHROOM2	-0.08	37.04	-0.15	10.40	0.10	29.33	-0.53	0.29	0.17	4.22
SIK1	0.19	37.04	0.54	0.11	0.41	0.72	-0.95	0.86	-0.54	0.02
SIPA1L1	0.20	37.04	-0.40	0.67	0.01	59.79	-0.14	27.83	-0.19	4.22
SIPA1L3	0.32	15.28	0.64	0.60	-0.09	49.13	0.02	55.17	0.07	40.66
SIRT1	0.14	29.67	0.89	1.03	-0.52	0.40	-0.25	27.83	0.46	0.02
SIVA1	0.02	55.17	-0.27	5.83			0.09	47.42	0.53	0.02
SKAP1	-0.17	52.22	0.18	7.54	0.40	0.64	0.47	1.21	-0.10	24.40
SKI	-0.49	0.93	0.16	0.94	-0.34	0.44	-0.34	23.45	-0.27	4.22
SLA	0.72	0.13	-0.34	3.21	-0.30	0.44	-0.29	27.83	0.56	0.02
SLAMF9	0.14	1.43	-0.29	3.21	-0.20	1.56	0.27	0.73	0.76	0.02
SLC11A1	0.05	52.83			0.02	57.40	-0.10	54.83	1.25	0.02
SLC11A2	0.16	10.00	0.52	1.09	-0.07	49.13	0.13	49.36	0.46	0.31
SLC12A4	-0.05	49.54	0.49	0.60	0.21	0.52	0.07	52.12	0.62	0.47
SLC12A7	0.08	49.54	0.30	0.94	-0.30	1.31	-0.14	47.42	0.42	0.39
SLC14A1	0.25	10.00	0.45	0.51	-0.20	3.48	0.23	0.34	0.77	0.02
SLC15A2	0.35	0.26	0.71	0.45	0.64	1.82	0.17	32.50	-0.26	4.22
SLC16A1	0.15	3.16	-0.17	5.83	-0.43	4.73	0.47	0.11	0.98	0.02
SLC16A9	0.01	57.29	0.16	5.83			0.52	0.06	0.10	36.83
SLC17A2	-0.15	0.53	-0.63	2.86	0.02	58.41	0.02	55.17	0.12	24.40
SLC17A5	0.31	0.17	0.43	5.83	-0.07	55.77	-0.48	0.35	-0.25	0.39
SLC18A2	-1.09	0.09	-0.20	0.78	-0.72	0.09	-1.01	0.25	-0.07	31.62
SLC1A2	0.27	0.40	-0.85	0.11	0.25	1.10	0.28	1.62	-0.82	0.02
SLC1A4	-0.10	44.81	-0.37	0.78	-0.13	22.90	-0.13	2.91	-0.13	31.62
SLC22A1	-0.36	7.74	-0.39	0.78	-0.15	10.69	-0.15	41.83	-0.28	11.00
SLC22A15	0.15	18.59	-0.42	4.12	0.05	55.77	0.21	41.83	0.53	0.07
SLC22A2	0.05	51.01	-0.64	0.30	-0.25	55.77			0.29	40.05
SLC22A4	0.04	53.69	0.34	0.51			-0.24	0.86	1.31	0.02
SLC25A17	0.17	18.59	0.35	0.20	-0.22	10.69	-0.46	0.06	-0.47	0.12
SLC26A3			-0.74	2.86	0.03	55.77	-0.04	49.36	-0.42	0.99
SLC27A2	-0.29	0.09	0.35	1.53	-0.52	1.82	-0.16	50.49	-1.74	0.02
SLC27A3	-0.04	56.77	0.48	2.77	0.26	0.52	-0.43	4.91	-0.24	6.00
SLC27A5	0.11	44.81	0.34	0.18	0.33	0.09	-0.73	0.62	-0.40	14.82
SLC2A4	-0.17	51.01	0.17	0.51	-0.34	4.73	-0.58	1.88	1.43	0.02
SLC2A5	-0.07	29.67	0.32	6.70	-0.09	41.10	0.48	0.06	0.32	11.00
SLC31A2	0.25	3.16	0.54	0.45	-0.23	41.10	-0.15	0.86	0.08	38.75
SLC35D1	-0.22	44.81	0.22	7.54	0.02	60.23			0.54	0.60
SLC35D3	0.16	37.04	-0.55	0.26	0.11	20.03	0.12	27.83	-0.10	39.47

SLC35F3	-0.13	3.16	-0.31	6.70	-0.11	8.12	-0.19	13.89	0.41	0.12
SLC38A1	-0.26	29.67	0.95	0.88	-0.21	12.58	-0.34	0.06	-0.70	0.02
SLC39A12	-0.64	7.74	0.31	8.88	-0.08	49.13	-0.16	32.50	0.41	0.02
SLC39A14	1.00	0.05	0.34	4.12	0.05	54.33	-0.07	32.50	0.17	8.00
SLC46A1	-0.18	44.81	-0.46	0.23	-0.11	26.12	0.14	32.50	0.28	1.98
SLC47A1	-0.36	0.17	-0.53	0.11	-0.33	10.69	0.59	16.94	0.31	37.82
SLC4A10	-0.34	0.05	-0.53	2.86	-0.28	0.64	0.24	41.83	0.71	0.02
SLC6A13	0.91	0.05	0.13	9.63	0.71	0.66	0.84	0.95	0.65	0.21
SLC6A15	-0.79	0.05	0.68	2.30	-1.07	0.09	0.51	41.83	-1.43	0.02
SLC6A9	-0.12	12.65	-0.26	6.70	0.07	41.10	0.30	2.42	0.46	0.99
SLC7A1	-0.13	1.43	-0.64	2.77	-0.05	49.13	-0.20	0.29	-0.47	0.08
SLC7A3	-0.17	7.74	0.29	4.12	0.03	57.40	0.53	0.51	0.55	0.12
SLC7A7	-0.24	44.81	-0.32	0.78	0.17	29.33	0.44	11.24	0.67	0.04
SLC8A3	-0.19	1.94	-0.42	0.66	0.05	55.77	0.07	50.49	-0.13	11.00
SLCO1A2	-0.16	0.32	-0.69	2.61	-0.04	57.40	0.07	49.36	0.22	24.40
Slco1a5	-0.11	25.77	-0.69	0.61	-0.04	57.40	0.07	49.36	0.22	24.40
SLCO2A1	-0.36	25.77	-0.40	0.78			0.47	3.87	-0.27	0.65
SLCO2B1	0.04	52.83	0.46	1.77	0.10	41.10	0.18	7.10	0.84	0.02
SLCO3A1	-0.06	51.01	0.07	8.25	-0.29	4.05	0.11	41.83	-0.50	0.02
SLCO4A1	-0.35	0.17	0.46	0.60	-0.56	0.09	0.55	16.94	0.77	0.02
SLFN2	-0.64	0.17	0.18	9.63	0.23	10.69	0.33	32.50	0.99	0.02
SLIT2	-0.46	0.05	-0.25	4.12	-0.10	54.33	-0.58	27.83	0.09	44.05
SLMAP	-0.36	33.23	-0.46	1.77	-0.41	0.66	-0.11	8.99	-0.45	0.04
SLPI	-0.20	2.45	-0.37	2.86	0.52	0.09			0.39	24.40
SMAD3	0.18	4.28	0.47	0.46	0.32	22.90	0.19	52.66	0.32	31.62
SMARCA5	0.07	51.01	0.80	0.60	0.06	54.33	0.14	50.49	-0.47	0.08
SMC6	-0.21	44.81	0.61	0.23	0.17	12.58	0.44	0.95	-0.23	0.13
SMEK1	-0.20	10.00	0.69	0.78	-0.40	4.73	-0.54	27.83	-0.90	0.02
SMG6	-0.56	0.05	0.60	0.51	-0.35	0.24	-0.57	8.99	0.60	0.12
SMG7	0.28	0.17	0.28	1.66	0.20	22.90	-0.93	0.06	0.40	0.02
SMNDC1	0.02	54.70	0.59	0.89	0.05	54.33	0.10	41.83	-0.28	6.00
SMOC2	-0.66	0.05	-0.37	0.18	-0.36	4.73	0.23	3.87	-0.22	24.40
SMPD2	-0.15	10.00	0.33	3.21	0.09	49.13	-1.04	0.06	0.18	33.88
SMPD3	-0.88	0.05	-0.49	0.27	-0.20	33.12	0.07	47.42	0.15	38.75
SMS	-0.27	33.23	0.52	0.11	-0.24	17.39	0.05	47.42	-0.95	0.02
SMTNL2	0.37	0.17	0.21	8.88			-0.64	0.06	-0.56	0.02
SMUG1	0.06	44.81	0.58	0.67	0.29	49.13	0.12	23.45	-0.44	0.99
SMURF1	0.26	0.32	0.30	0.30	0.25	0.66	0.09	23.45	0.51	0.12
SNAP25	0.01	56.51	0.23	10.40	0.21	54.33	-0.21	0.13	-0.48	0.12
SNCA	-0.13	51.01	0.26	5.83	-0.10	58.07			-0.43	0.75
SNF1LK	1.00	0.05	0.54	0.11	0.41	0.72	-0.95	0.86	1.41	0.02
SNTG2	-0.79	0.17	0.51	1.29	-0.17	54.33	-0.47	0.95	-0.95	0.75
SNX16	0.20	44.81	0.51	0.42	-0.15	20.03	-0.13	16.94	-0.49	0.07
SNX33	-0.09	49.54	0.21	0.51	0.20	9.26			0.41	0.02
snx4	0.06	49.54	0.48	1.29	0.12	55.77	-0.19	23.45	0.53	0.02
SNX7	-0.15	1.43	0.25	7.54	-0.06	59.43	-0.15	13.89	-0.45	0.02
SNX8	-0.07	52.22	-0.15	5.83	0.10	49.13	-0.43	0.06	0.07	39.47
SOAT1	-0.69	0.05	-0.45	4.12	0.29	22.90	-1.28	0.06	-0.50	0.99
SOCS2	-0.61	0.05	0.41	1.66	-0.40	0.09	-0.47	27.83	-1.77	0.02
SOCS3			-0.33	2.86	0.28	17.39	-0.31	0.13	0.81	0.02
SOCS4	0.20	44.81	0.71	0.67	0.12	29.33			-0.47	0.12
SOCS6	-0.06	55.17	0.54	0.11	0.02	58.41	0.50	1.33	-0.36	31.62

SORCS2	-0.05	54.15	-0.12	7.54	-0.23	49.13			-0.40	8.00
SOS1	0.58	0.93	1.40	0.11	0.18	14.77	0.35	0.40	-0.53	0.02
SOSTDC1			0.17	4.12	-1.04	8.12	0.54	1.21	-0.90	0.98
SOX10	-0.16	3.16	-0.56	0.78			0.11	41.83	0.48	0.17
SOX11	-0.55	0.26	0.63	0.94	0.11	49.13	1.13	0.06	1.25	0.02
SOX14	-0.16	0.93	-0.63	0.83	-0.04	54.33	0.04	53.27	0.16	11.00
SOX15	-0.46	0.93	-0.76	2.77			0.03	53.83	0.27	24.40
Sox17	0.04	51.01	0.69	0.51	0.25	1.56	-0.29	1.88	-0.46	0.02
SOX21	-0.41	0.17	-0.41	3.01	0.15	22.90	-0.62	0.06	-0.31	0.75
SOX9	0.18	15.28	0.59	0.35	-0.27	0.72	-0.34	0.25	0.84	0.02
SP110	0.41	3.16	0.29	8.88	-0.09	54.33	0.24	41.83	1.00	0.02
SP4	-0.41	0.09	-0.62	0.11	-0.42	1.56	0.28	0.35	0.35	0.47
SPARC	-0.28	0.17	-0.49	2.77	-0.18	5.71	0.08	47.42	0.84	0.02
SPATA5	0.11	44.81	-0.57	2.12	-0.08	49.13	0.38	13.89	-0.10	24.40
SPINT2			0.13	6.70	0.14	29.33	0.43	1.88	0.81	0.47
SPOCK1	0.21	0.32	0.17	6.70	-0.53	3.48	-0.43	11.24	-0.76	0.99
SPOCK3	0.06	51.01	-0.10	10.40	-0.42	1.56			-0.71	0.08
SPON1	0.05	52.83	0.38	4.12	0.33	3.07	0.49	0.95	0.27	24.40
SPP1	-0.40	0.32	0.89	0.11	-0.21	12.58	-0.67	0.86	1.52	0.02
SPPL2A	-0.26	0.53	0.53	0.21	-0.37	12.58	0.10	52.12	0.21	36.83
SPRED1	-0.30	0.26			0.19	41.10	0.11	41.83	0.55	0.47
Sprr1a	-0.04	49.54	-0.16	5.83			0.02	55.17	0.43	0.12
SPRY4	0.45	18.59	-0.40	0.78	0.17	29.33	-0.23	11.24	0.82	0.02
SPSB2	0.15	25.77			0.01	60.51	0.08	49.36	-0.52	0.99
SPTBN1	0.30	0.53	0.72	0.51	-0.63	0.72	0.29	41.83	0.53	0.99
SPTLC2	0.22	7.74	-0.56	1.09	-0.18	1.10	-0.51	0.18	-0.06	40.05
SQRDL	-0.18	0.67	0.38	0.42	0.27	41.10	-0.08	41.83	0.55	0.02
SRCAP	-0.49	0.05	0.18	0.99	-0.23	3.48	-0.27	0.13	0.22	4.22
SRD5A1	0.05	55.17	0.50	0.18	-0.13	29.33	-0.33	11.24	-0.44	0.13
SREBF1	-0.15	44.81			-0.05	55.77	-0.12	41.83	0.58	0.04
SREK1	-0.08	44.81	0.54	1.46	-0.26	1.31	-0.05	41.83	-0.42	0.02
SRGAP1	0.71	0.05	0.41	1.29	-0.38	6.93	-0.99	0.06	-0.55	0.02
SRGN	-0.43	0.17	-0.53	3.01	0.04	58.07	0.14	41.83	0.80	0.02
SRL					-0.26	29.33	0.09	50.49	-0.50	0.89
SRPK3	0.31	44.81	0.56	1.66	0.14	22.90	0.72	0.06	-0.44	0.07
SRPR	-0.36	0.67	0.58	1.46	0.17	5.71	0.28	19.97	-0.37	0.99
SSBP1	-0.15	5.93	0.80	0.99	0.22	12.58	-0.58	2.91	-0.39	0.17
SSTR2	-0.26	12.65	-0.17	0.51	-0.39	3.48	-0.21	16.94	-0.63	0.39
SSX2IP	0.26	44.81	0.23	8.88	0.15	41.10	-0.56	0.86	-0.25	4.22
ST14	-0.11	44.81	-0.56	2.86	-0.06	54.33	0.08	27.83	0.42	0.75
ST18	-0.30	44.81	0.27	8.25	0.04	58.93	-0.89	0.25	-0.31	24.40
St3gal3	-0.84	0.05	-0.30	6.70	0.34	33.12	0.83	0.13	0.57	0.99
ST5	-0.12	49.54			0.40	3.48	-0.14	41.83	-0.53	0.31
ST6GALNAC2	-0.10	52.22	-0.39	0.78	0.42	0.40	0.51	0.12	0.05	44.32
ST8SIA6	-0.48	0.09	0.54	2.30	-0.65	6.93	-0.63	2.42	-0.49	0.99
STAM	0.28	10.00	0.65	1.21	0.38	4.73	-0.06	47.42	-0.49	0.02
STAP2	0.14	49.54	-0.25	2.12	-0.19	20.03	-0.27	16.94	-0.84	0.04
STAR	0.25	5.93	0.77	0.60	0.32	3.07	-0.35	50.49	-0.59	0.02
STARD8	-0.19	2.45	0.18	7.54	0.57	0.52	-0.39	1.62	0.89	0.17
STAT1	-0.31	0.32	0.53	0.26	-0.21	0.64	-0.60	0.25	-0.63	0.02
STAT3	-0.25	1.43	0.41	0.67	0.10	54.33	-0.29	13.89	0.28	31.62
STAT5B	-0.64	0.67	-0.15	7.54	0.35	1.31	-0.20	11.24	0.59	0.05

STBD1	0.82	0.05	0.57	0.57	-0.46	10.69	1.11	11.24	-0.24	31.62
STC1	-0.35	0.05	0.31	1.77	-0.35	4.73	-0.30	41.83	-1.50	0.02
STEAP3	-0.53	0.26	-0.25	4.12	-0.62	0.24	-0.39	47.42	-1.05	0.02
STK35	-0.41	15.28	-0.45	0.78	0.29	49.13	-0.29	19.97	-0.52	0.02
STRADA	0.02	56.87	-0.18	2.61	-0.20	36.89	0.09	47.42	-0.74	0.02
STRBP	-0.04	57.11	0.88	1.21	0.09	14.77	0.09	27.83	-0.27	0.12
STRN	0.41	0.93	0.82	0.35	-0.06	54.33	0.40	0.11	-0.16	4.22
STT3B	-0.27	21.80	0.42	0.51	0.07	49.13	-0.40	19.97	-0.72	0.27
STX16	-0.46	10.00	0.25	0.94	0.28	0.52	-0.32	1.62	-0.55	0.27
STX3	0.20	52.22	0.89	0.11	0.60	4.73	-1.21	0.25	0.57	0.89
STX5	-0.07	49.54	0.29	4.12	0.07	41.10	0.32	0.06	-0.49	0.02
SULF1	-0.68	0.05			0.09	55.77	0.14	47.42	1.35	0.02
SULT1A1	0.30	25.77	0.29	5.83	-0.35	3.48	0.18	50.49	0.57	0.12
SULT6B1	0.18	49.54	-0.69	0.78	-0.39	3.07	-0.31	47.42	-0.23	24.40
SUPT3H	0.03	52.83	0.58	0.51			0.15	50.49	-0.38	0.17
SUSD3	-0.23	1.10	-0.21	5.83			-0.10	49.36	0.40	0.05
SUV39H2	0.33	18.59	0.61	0.30	-0.35	17.39	0.67	4.91	-1.12	0.02
SUV420H1	0.43	15.28	0.57	0.17	-0.73	0.09	-0.33	27.83	0.05	41.26
SV2B	-0.08	29.67	0.55	2.77	-0.11	49.13	-0.05	49.36	-0.56	0.27
SYCE2	-0.07	55.56	-0.33	0.88	-0.53	5.71	0.28	0.11	-0.15	38.75
SYK	0.06	44.81			0.07	58.41	-0.77	0.13	0.39	0.39
SYNCRIP	-0.23	49.54	0.75	2.30	-0.79	0.28	0.26	7.10	-0.56	0.02
SYNE1	-0.23	5.93	0.63	2.12	-0.09	56.82	-0.22	2.42	-0.75	0.31
SYNE2	-0.34	0.05	-0.40	4.12	0.10	41.10	-0.92	0.06	0.58	11.00
SYNGR1	0.33	1.94	-0.61	1.66	0.14	26.12	-0.22	1.88	0.90	0.02
SYNGR2	-0.29	3.16	-0.09	8.25	0.17	0.86	0.30	7.10	0.47	0.47
SYNJ2	0.50	0.17	0.21	5.83	0.27	0.44	0.17	7.10	0.95	0.02
SYNPO	0.20	21.80	-0.26	4.12	0.39	6.93	-0.25	47.42	0.71	0.47
SYP	0.42	0.67	0.15	2.30			-0.10	5.54	-0.20	0.65
SYPL1	-0.26	0.17	0.54	4.12	0.17	1.31	0.53	0.06	-0.44	0.98
SYT10	0.49	0.05	-0.09	8.25	-0.07	54.33			-0.09	31.62
SYT17	-0.11	55.56	0.25	6.70	0.45	0.09	0.08	51.35	-0.52	4.22
SYT4	0.09	29.67	0.78	1.46	-0.17	12.58	-0.30	19.97	-0.51	0.27
TAC1	-0.44	12.65	0.52	0.45	0.17	2.31	-0.16	13.89	-0.91	0.27
TAC10	0.29	0.05	0.54	0.51	0.33	0.09	0.13	16.94	-0.41	0.02
TAF9B	0.11	49.54	0.78	0.67	0.05	54.33			-0.62	0.99
TAGLN	0.52	0.53	0.47	0.51	0.57	0.09	-0.63	0.11	1.10	0.02
TANC1	-0.03	57.37	0.67	0.11	0.13	49.13	0.23	16.94	0.23	0.39
TARDBP	-0.27	0.53	0.72	1.09	-0.14	4.05	0.35	23.45	-0.40	0.05
TAS1R1	0.07	44.81	-0.22	2.30	0.14	26.12	0.39	0.40	0.22	33.88
TASP1	0.22	21.80	0.60	0.30	0.30	8.12	-0.37	3.87	-0.29	1.19
TBC1D2	-0.18	0.51	-0.71	2.77	0.06	55.77	0.21	32.50	0.67	0.02
TBC1D4	-0.19	5.93	-0.18	4.12	-0.15	49.13	0.72	0.25	0.78	0.02
TBPL1	-0.27	1.43	0.85	0.57	0.26	6.93	-0.18	47.42	-0.36	0.99
TBX1			0.35	8.88	0.98	0.64	0.52	2.91	0.32	8.00
TBXAS1	-0.23	33.23	0.47	0.99	0.24	49.13	0.11	47.42	1.22	0.02
TCF12	0.36	1.94	0.43	0.88	-0.05	55.77	-1.12	0.40	-0.44	24.40
TCF7L2	-0.29	5.93	0.40	0.51	-0.34	1.82	-0.57	0.11	0.77	0.02
TCP1	0.15	44.81	0.89	0.42	-0.09	41.10	-0.22	4.91	-0.17	6.00
TDG	0.29	1.94	0.77	0.94	0.23	0.28	0.29	0.86	0.50	0.07
Tdg	-0.46	0.05	-0.63	2.61	-0.48	0.09	-0.17	1.62	-0.21	24.40
TDP2	-0.09	56.13	0.56	0.21	-0.22	0.82	-0.28	0.57	0.08	41.26

TDRD5	0.05	53.69	0.18	4.12	-0.25	26.12	-0.30	27.83	0.58	0.60
TEK	-0.54	0.05	-0.31	2.77	0.34	0.66	-0.20	23.45	-0.56	0.13
TF	-0.34	21.80	-0.48	0.78	0.79	3.07	0.30	27.83	1.21	0.02
TFAP4	-0.28	1.10	-0.68	2.86	0.15	22.90	0.30	23.45	0.52	0.21
TFDP2	-0.32	21.80	0.58	0.20	-0.18	26.12	0.50	0.73	0.59	1.19
TFRC	0.32	0.93	0.87	0.99	-0.09	36.89	0.26	2.91	-0.43	0.21
TGFB1	0.27	7.74	0.19	5.83	0.47	1.56	0.49	1.21	0.88	0.02
TGFBR1	0.11	25.77	0.11	8.88	-0.50	0.24	-0.09	32.50	0.37	0.17
TGFBR2	-0.06	54.15	0.46	3.21	-0.14	36.89	-0.46	0.57	0.60	0.02
TGFBRAP1	0.27	10.00	0.61	0.51	-0.12	54.33	-1.29	0.06	-0.44	0.02
TGIF2	-0.19	37.04	-0.19	9.63	0.23	17.39	0.29	8.99	0.69	0.02
TGM1	0.49	0.17			0.56	0.09	-0.46	7.10	1.35	0.02
TGM2	-0.57	0.05	-0.55	0.78	0.24	1.31	0.38	2.91	0.48	0.31
Tgtp1	-0.21	55.87	0.78	0.11	-0.71	0.28	0.19	41.83	0.54	0.02
TH	-0.11	33.23	-0.38	0.35	-0.50	9.26	0.16	23.45	0.62	0.75
THAP2	-0.21	29.67	0.78	0.60	-0.14	10.69	0.22	3.87	0.53	0.02
THBD	-0.08	51.01	-0.54	0.31	0.33	12.58	-0.06	47.42	0.22	31.62
THBS2	-0.27	1.43	-1.04	0.77					0.29	24.40
THBS4	-0.15	29.67	-0.20	2.86	0.42	0.82	0.16	41.83	0.23	31.62
THOC2	-0.19	1.10	0.22	4.12	-0.31	0.86	-0.40	0.86	0.45	0.99
THPO	-0.20	37.04	-0.65	3.21	0.28	4.73	-0.09	47.42	0.46	0.02
THRAP3	-0.15	49.54	0.59	0.45	-0.50	0.09	-0.87	1.33	-0.22	14.82
THRB	-0.14	44.81	-0.32	4.12	-0.15	17.39	-0.59	0.12	-0.90	0.12
THSD7B	0.06	52.22	0.91	0.94	-0.17	4.05	0.11	47.42	-0.40	0.89
TIA1	-0.11	51.01	0.71	0.60	-0.22	1.82	-0.29	0.11	-0.40	0.27
TIAM1	-0.16	33.23	0.06	8.88	0.12	49.13	-0.13	19.97	-0.52	0.27
TIAM2	-0.68	0.05	0.27	0.78	0.09	54.33	0.13	41.83	-0.90	0.99
TICAM1	0.02	56.51	0.14	2.61	0.29	0.40	0.23	16.94	0.52	0.02
TIFA	0.14	44.81	-0.38	5.83	-0.04	54.33	-0.06	41.83	0.51	0.65
TIMM17B	-0.13	5.93	0.30	5.83	0.33	36.89	0.17	27.83	-0.58	0.02
TIMP1	-0.32	12.65	-0.30	3.01	0.35	0.72	-0.36	8.99	1.33	0.02
TIMP2	-0.66	0.09	0.09	10.40	0.24	20.03	0.26	41.83	0.19	24.40
TIMP4	-0.37	0.40	-0.38	0.57	-0.18	8.12	0.20	2.42	0.04	43.18
TIRAP	0.17	33.23	-0.57	0.60	0.41	0.44	-0.95	0.06	-0.09	36.83
TLE3	0.17	5.93	-0.57	0.86	0.19	2.06	0.14	32.50	0.33	0.47
TLE6	0.04	49.54			0.38	26.12	-0.12	49.36	-0.43	0.89
TLN1	0.14	7.74	-0.16	0.78	0.23	2.31	0.11	41.83	0.59	0.02
TLR1	0.29	0.17	0.62	0.11	0.17	55.77	-0.27	49.36	0.96	0.02
TLR2	-0.52	1.43	0.19	6.70	0.43	2.31	0.68	11.24	1.57	0.02
TLR7	-0.15	56.87	0.21	8.88	0.37	3.07	0.15	41.83	0.72	0.02
TM4SF1	-0.17	5.93	0.12	11.78	0.19	12.58	0.11	23.45	0.65	0.02
TM4SF5	0.35	0.17	0.16	5.83	-0.04	57.40	0.95	0.06	-0.34	14.82
TM6SF1	0.13	37.04	0.75	0.88	0.02	60.23	-0.37	1.33	-0.59	0.02
TMBIM4	0.35	2.45	0.30	0.51	0.07	29.33	-0.23	41.83	0.57	0.02
TMC6	0.07	51.01	-0.29	0.78	0.58	0.09	-0.06	41.83	0.69	0.02
TMCC3	-0.33	0.05	0.06	11.78	0.33	0.64	-0.27	1.33	0.72	0.02
TMEM132D	-0.28	37.04	-0.56	0.46					0.18	35.53
TMEM158	0.10	44.81	0.10	8.88	-0.06	55.77	0.16	16.94	0.57	0.12
TMEM163	-0.21	18.59	0.51	1.46	0.19	29.33	-0.07	49.36	0.89	0.02
TMEM173	-0.23	0.53	-0.43	2.86	0.05	49.13	0.17	13.89	0.64	0.02
TMEM176B	-0.16	49.54	0.39	2.61	0.16	8.12	0.13	13.89	0.78	0.02
TMEM189					0.34	2.31	-0.37	23.45	0.70	0.02

TMEM47	-0.24	0.67	-0.83	0.77	-0.06	54.33	0.04	53.83	0.27	24.40
TMEM51	-0.06	53.69	0.26	0.60	0.53	1.82	-0.22	54.40	0.70	0.02
TMEM57	0.04	52.83	0.22	0.51	0.05	56.82	0.46	0.11	0.22	14.82
TMEM63A	0.17	5.93	-0.56	3.21	0.08	26.12	0.25	0.18	-0.35	0.99
TMEM86A	-0.35	0.13	-0.07	11.78			0.25	0.40	0.49	0.02
tmf1	0.18	44.81	0.65	1.03	0.07	49.13	-0.15	4.91	-0.42	0.08
TMLHE	0.21	18.59	-0.39	5.83	0.18	26.12	0.13	41.83	-0.39	0.08
tmod1	0.40	0.17	0.44	0.45	0.16	33.12	-0.29	1.62	-0.58	0.02
TMOD2	-0.57	0.51	0.49	0.51	-0.50	0.72	0.15	16.94	-0.34	0.12
TMPRSS6	0.28	21.80	-0.17	3.21	0.36	0.66			0.80	0.02
TMSB10/TMSB4X	0.18	33.23	0.31	1.66	0.25	29.33	-0.23	0.95	0.78	0.27
TMTC1	-0.21	0.51	0.76	1.46	0.19	10.69	-0.29	4.91	-0.50	0.02
TMTC2	0.22	0.67	0.20	0.94	0.04	56.82	0.10	49.36	-0.53	0.65
TMX1	-0.14	1.10	0.77	1.03	0.02	58.41			-0.47	0.02
TMX4	-0.11	44.81	0.68	1.77	0.16	49.13	0.07	52.12	-0.75	0.02
TNFAIP2	-0.06	44.81	-0.62	1.77	-0.04	58.41	-0.03	54.83	0.41	0.02
TNFAIP8L2	-0.16	29.67	0.19	2.77	0.54	0.40	-0.37	0.51	0.36	0.02
TNFRSF21	0.23	0.40	0.53	0.88	0.04	56.82	0.08	47.42	-0.61	0.65
TNFRSF9									0.69	0.02
TNIK	-0.21	25.77	0.76	1.29	-0.25	36.89	-0.41	32.50	-0.38	0.31
TNKS	-0.26	37.04	0.61	1.66	-0.35	0.64	0.14	23.45	-0.36	0.31
TNNI2	-0.16	33.23	-0.29	2.61	0.37	1.31	0.08	50.49	0.61	0.04
TNS1	-0.37	0.05	-0.35	3.21	0.42	0.72	-0.97	0.35	0.65	0.07
TNS3	0.23	15.28	0.68	0.20	0.13	49.13	0.22	16.94	0.34	6.00
TNXB	0.22	37.04	0.46	0.99	0.95	0.09	-0.23	47.42	0.64	0.65
TOM1L2	-0.35	0.26	0.43	0.45	0.63	0.09	-0.29	0.29	-0.49	0.21
TOMM34	0.27	1.94	0.25	7.54	0.10	54.33	0.12	50.49	-0.48	0.02
TOMM70A	-0.20	7.74	0.34	0.60	-0.10	49.13	0.05	47.42	-0.38	0.17
TOR3A	-0.13	52.83	0.56	0.27	-0.12	26.12	0.27	41.83	0.61	0.02
TP73	0.62	0.17	0.65	0.60	-0.46	26.12	0.64	0.35	0.27	1.98
TPD52L2	0.26	0.67	0.72	0.88	0.13	22.90	0.14	19.97	-0.37	1.98
TPM1			0.24	1.21	0.55	0.09	-0.27	16.94	-0.13	24.40
TPMT	-0.13	25.77	0.47	0.11	-0.35	3.07	-0.51	0.95	0.42	0.99
TPP2	0.35	0.05	0.44	0.18	-0.04	56.82	0.04	47.42	-0.12	11.00
TPPP	-0.07	44.81	0.24	5.83	-0.14	8.12	-0.16	8.99	-0.47	0.02
TPPP3			0.28	5.83	0.04	57.40	0.06	53.27	0.59	0.12
TRA2A	-0.23	18.59	0.58	1.46	0.26	3.07	-0.16	13.89	-0.57	0.02
TRAF3IP3	0.09	37.04	0.65	0.60	0.16	36.89	0.11	41.83	-0.56	0.02
TRAF4	-0.32	29.67	0.36	0.51	-0.13	54.33	-0.77	0.34	1.23	0.02
TRAF5	0.27	33.23	0.68	1.03	0.69	0.09	-0.45	1.33	0.46	0.47
TRAPPC8	0.30	0.26	-0.14	3.21	0.12	41.10	0.16	41.83	-0.37	0.04
TRDMT1	-0.12	37.04	0.20	12.52	-0.13	14.77	0.46	0.25		
TREM2	0.19	3.16	-0.68	0.57	0.04	56.82	0.12	47.42	1.28	0.02
TREML1	0.06	44.81			0.22	0.66	-0.86	0.06	-0.33	11.00
TRERF1	-0.33	0.05			0.17	49.13	0.52	0.06	0.62	0.07
TRHDE	0.21	18.59	0.55	2.77	-0.24	0.86	-0.18	4.91	-0.47	0.02
TRIB1	1.02	0.05	0.90	0.35	0.61	0.09	-0.05	55.17	-0.35	44.20
TRIM25	0.07	49.54	0.65	0.78	-0.18	9.26	-0.06	47.42	-0.47	0.12
Trim30a/Trim30d			-0.25	2.61	-0.66	0.09	0.46	19.97	0.67	0.65
TRIM37	-0.94	0.05	0.43	2.12	-0.65	0.09	-0.11	23.45	-0.30	0.12
TRIM68	-0.06	51.01	-0.15	8.25	-0.16	4.05	0.56	0.06	-0.79	0.02
TRIM7	0.13	15.28	0.13	5.83	0.27	8.12	0.06	52.12	0.46	0.47

TRIP13	0.20	5.93	0.45	1.53	-0.16	55.77	0.15	47.42	-0.67	0.02
TRIP4	0.10	51.01	-0.35	0.57	0.20	49.13	0.77	0.86	-0.78	0.02
TRIP6	0.03	55.17	0.27	1.46	0.23	0.64	0.78	0.06	0.44	0.02
TRMT12	-0.72	0.17	-0.77	2.77	-0.49	0.44	-0.35	41.83	-0.41	0.13
TRMT1L	0.13	18.59	0.66	0.51	0.08	54.33			-0.40	0.21
TRMT6	-0.53	0.05	0.27	11.09	-0.51	0.09	0.15	23.45	0.89	0.99
TROVE2	0.15	1.94	-0.59	1.46	-0.22	10.69	-0.38	0.57	-0.23	1.19
TRPC2	-0.32	3.16	0.76	0.51	0.67	1.31	1.17	0.06	-0.38	0.65
TRPC4	-0.27	0.78	-0.12	8.88	0.31	10.69	1.25	0.51	-0.24	0.65
TRPM3	0.02	57.29	0.22	1.53	-0.29	1.10	-0.65	0.06	-0.85	0.12
TRPS1	-0.74	0.05	0.41	0.26	-0.28	4.05	0.21	1.88	-0.77	0.02
TSC1	-0.49	0.05	0.58	1.53	0.43	10.69	-0.28	13.89	-0.63	0.02
TSC22D4	-0.45	0.05	0.49	0.67	0.27	26.12	0.72	0.06	0.64	0.99
TSHZ3	0.12	44.81	-0.63	3.01	-0.29	3.48	-0.80	0.06	-0.22	0.65
TSN	-0.36	0.17	0.46	0.42	-0.61	0.44	-0.40	0.06	-0.56	24.40
TSPAN15			0.57	0.57	0.28	1.82	-0.19	19.97	0.61	0.21
TSPAN18	0.05	49.54	0.09	8.25	-0.16	49.13	0.79	0.06	0.99	0.02
TSPAN2	-0.03	55.87	-0.35	4.12			0.37	0.06	0.64	0.31
TSPAN4					-0.08	49.13			0.52	0.39
TSPAN9	0.22	0.67	-0.14	6.70	0.33	0.40	0.05	53.27	0.49	0.13
TSPEAR	0.10	29.67	-0.81	0.31	0.28	0.86			0.31	0.31
TSPO	-0.45	18.59	-0.35	5.83	0.23	0.52	0.54	0.73	0.94	0.02
TTBK2	0.17	15.28	0.19	5.83	-0.19	1.56	-0.67	0.06	-0.51	0.02
TTC30B	0.22	5.93	0.51	1.53	0.08	36.89	0.11	49.36	-0.38	0.02
TTC38	-0.19	51.01	0.16	8.88	0.13	41.10	0.94	0.06	-0.38	31.62
TTC7A	-0.13	44.81	-0.36	3.01			0.19	0.57	0.54	0.02
TTC9C	0.30	0.51	0.69	1.77	-0.17	10.69	0.15	11.24	-0.48	0.27
TTF1	0.44	10.00	0.31	2.77	-0.37	0.66	-0.08	47.42	0.22	31.62
TTF2	-0.24	37.04	-0.31	0.78	-0.21	33.12	-1.23	0.06	0.33	6.00
TTLL7	0.03	56.13	0.37	2.30	0.29	2.31	0.17	55.17	-1.01	0.02
TUBA1C	-0.63	0.17	0.30	0.48	0.10	26.12	0.45	0.06	1.10	0.02
TUBB2B	-0.11	33.23	-0.29	5.83	0.06	49.13	-0.07	41.83	0.43	0.02
TUBB6	0.35	0.09	-0.29	4.12	0.27	33.12	0.57	0.40	0.74	0.13
TUBGCP4	0.13	7.74	0.79	1.03	0.10	36.89	-0.46	5.54	-0.70	0.02
TULP1	0.14	15.28	-0.67	0.94			0.05	52.66	0.13	31.62
TUSC3	0.08	44.81	0.63	1.29	-0.08	49.13			-0.43	0.17
TWF1	-0.56	2.45	0.52	2.61	-0.56	0.09	0.41	0.35	-0.62	0.31
TWIST2	-0.23	3.16	-0.14	5.83	-0.81	3.07	0.58	0.06	-0.61	0.95
TXNDC9	-0.46	0.78	-0.37	4.12	0.33	1.56	0.12	27.83	0.05	43.75
TXNRD2	-0.08	49.54	0.10	6.70	0.06	49.13	-0.48	0.11	0.05	40.66
TYMS	-0.22	0.51	0.45	0.51	-0.48	4.73	0.22	41.83	0.14	42.37
TYRO3	0.29	18.59	0.30	5.83	0.42	0.09	-0.18	13.89	0.06	43.18
TYROBP	-0.21	44.81			0.09	54.33	0.11	23.45	0.93	0.02
U2AF1	0.20	33.23	-0.62	0.66	0.13	3.07	0.18	27.83	-0.15	11.00
U2af2	0.07	54.70	-0.16	10.40	0.26	2.31	-1.26	0.06	-0.37	0.99
UBA5	0.34	33.23	0.50	0.51	-0.55	0.28	-0.75	0.11	-0.18	2.89
UBAP2L	-0.64	0.05	0.61	0.11	-0.75	0.09	-0.48	2.91	-1.19	0.02
UBE2D1	0.42	0.51	0.47	2.12	0.22	0.72	-0.25	5.54	-0.32	0.75
UBE2D2	0.06	49.54	0.70	0.60	-0.09	36.89	0.14	47.42	-0.48	0.31
UBE2E1	0.12	44.81	0.65	0.60	-0.18	8.12	-0.05	49.36	-0.46	0.02
UBE2E2	-0.04	57.37	-0.39	3.21	0.15	36.89	0.13	4.91	0.51	0.04
UBE2I	-0.37	0.78	0.32	4.12	0.11	41.10	-0.25	8.99	-0.49	0.99

UBE2J2	0.16	21.80	0.61	0.51	0.03	56.82	0.10	41.83	-0.18	2.89
UBE2N	0.16	21.80	0.55	0.18	-0.09	41.10	-0.46	0.13	-0.90	0.02
UBE2T	0.27	1.10	-0.29	3.01	-0.15	17.39	0.55	0.06	-0.06	35.53
UBE2V2	0.18	37.04	-0.41	0.60	-0.11	29.33	-0.15	2.91	-0.38	0.02
UBE2W	0.22	49.54	0.58	0.60	-0.11	22.90	0.26	47.42	-0.53	0.02
UBE3A	-0.20	25.77	0.93	1.03	-0.20	26.12	0.14	1.62	-0.45	0.02
UBR2	0.16	18.59	0.25	0.51	-0.20	0.72	0.45	0.06	0.23	38.75
UBR3	-0.48	0.05	-0.21	0.78	-0.72	0.40	0.11	41.83	0.21	24.40
UCHL3	0.13	44.81	0.61	0.26	-0.09	41.10			-0.06	38.75
UCP2	0.10	49.54	-0.27	0.60	0.02	58.41	-0.35	5.54	0.84	0.02
UGT2B10	-0.43	0.05	0.16	8.25	-0.60	2.66	0.98	0.11	1.54	0.02
UMPS	0.18	0.53	0.53	0.60	0.08	41.10	0.18	23.45	-0.17	24.40
UNC45B	0.04	51.01	-0.40	4.12	0.49	0.52	-0.23	13.89	-0.36	24.40
UNC93B1	-0.07	56.77	-0.31	3.21	0.08	41.10	-0.17	49.36	0.79	0.02
UPF2	0.54	29.67	-1.10	2.61	-0.40	0.09	-0.03	53.27	-0.33	14.82
UPF3B	-0.13	18.59	0.79	0.60	-0.21	1.56	0.47	0.51	-0.31	0.89
UQCRQ	-0.37	0.17	0.24	4.12	-0.17	5.71			0.22	39.47
USH1C	0.03	51.01	-0.40	0.21	0.01	60.23	0.09	41.83	0.20	8.00
USO1	-0.08	51.01	0.48	1.09	-0.05	57.40	0.26	32.50	-0.37	0.17
USP13	0.25	4.28	0.39	3.21	0.23	6.93	-0.04	47.42	-0.37	0.02
USP15	-0.90	0.05	0.55	1.66	-0.57	0.09	-1.16	0.06	0.80	0.99
USP25	0.18	33.23	0.65	0.60	0.12	6.93	-0.27	3.87	-0.18	0.75
USP32	-0.13	1.94	-0.36	4.12	0.06	49.13	-0.05	47.42	-0.46	0.02
USP33	0.11	44.81	0.53	1.46	-0.09	33.12	0.08	51.35	-0.44	0.02
USP36	-0.47	0.05	0.13	7.54	-0.41	0.09	0.64	19.97	-0.38	0.99
USP39	-0.11	52.22	0.81	0.60	-0.11	29.33	0.26	32.50	-0.38	0.02
USP45	-0.11	44.81			-0.13	49.13	-0.17	47.42	-0.49	0.65
USP46	-0.32	29.67	0.47	0.78	0.22	8.12	0.17	41.83	-0.54	0.02
USP47	-1.08	0.05	0.26	5.83	-0.53	1.31	0.70	0.40	-0.41	0.17
USP53	-0.98	1.10	0.56	0.18	0.08	41.10	0.11	41.83	0.42	0.31
UST	-0.05	52.22	-0.43	3.21	-0.21	8.12	-0.39	0.29	0.09	37.82
UTP18	0.21	29.67	-0.36	4.12	0.29	14.77	-0.57	0.25	0.13	33.88
UTP23	-0.21	7.74	0.82	0.11	-0.22	26.12	0.38	41.83	-0.87	0.02
VAMP7	0.02	54.70			-0.29	3.48	-0.29	0.57	-0.39	0.47
VAMP8	0.23	0.32	0.32	1.77	-0.08	55.77	-0.12	8.99	0.52	0.05
VANGL1	-0.58	0.26	-0.13	3.21	0.31	5.71	-0.17	11.24	0.40	0.99
VANGL2	-0.72	0.78	-1.04	1.03	0.37	0.28	-0.56	19.97	0.49	0.75
VAPB	-0.49	0.05	0.41	0.17	0.07	49.13	0.34	8.99	0.24	8.00
VARS2	0.10	33.23	0.25	0.99	-0.04	60.23	0.48	0.06	0.07	40.66
VAT1L	-0.24	33.23	0.25	5.83	0.32	0.09	-0.05	52.12	0.53	0.02
VAV1	0.49	2.45	-0.53	2.30	0.37	22.90	0.53	41.83	1.27	0.02
VCAM1	-0.18	1.43	-0.33	4.12	0.26	1.31	0.41	0.95	0.43	0.21
VCL	0.16	25.77	0.54	0.83	0.21	0.72	-0.17	0.57	0.35	0.99
VEGFA	0.23	0.26	-0.19	7.54	0.67	0.09	-0.77	5.54	-0.68	0.08
VEGFB	-0.06	53.69	-0.44	0.16	0.12	6.93	0.19	3.87	0.29	1.98
VIM	-0.39	0.05	0.64	0.45	0.20	0.86	0.30	1.33	1.57	0.02
VPS13A	0.16	0.93	0.52	0.60	-0.08	54.33	0.25	2.91	-0.53	0.07
VPS24	0.13	25.77	0.60	0.51	0.13	49.13	0.18	47.42	-0.11	37.82
VPS35	-0.42	0.17	0.23	2.61	-0.43	4.73	0.08	49.36	-0.35	0.02
VPS36	-0.44	44.81	0.61	0.18	-0.07	56.82	-0.47	0.25	-0.03	39.47
VSNL1	0.16	44.81	0.54	0.17	-0.08	41.10	-0.07	23.45	-0.55	0.05
VSX2	-0.30	33.23	0.20	8.25	0.07	58.41	-0.17	41.83	0.48	0.98

VTA1	0.03	55.17	-0.36	3.21	0.08	55.77	0.06	41.83	0.75	0.13
VTI1A	0.46	0.09	0.62	0.67	0.30	1.56	-0.36	49.36	-0.55	0.75
VWA3B	-0.10	49.54	-0.14	9.63	0.23	8.12	0.52	11.24	0.56	0.02
VWF	-0.83	0.05	0.83	0.30	0.18	10.69	-0.26	23.45	0.56	0.02
WAPAL	0.22	0.67	0.64	2.30	-0.08	41.10	0.13	41.83	-0.66	0.02
WARS2	-0.56	0.26	0.62	0.67	0.37	1.56	0.76	1.88	0.44	24.40
WASF2	0.08	51.01	0.30	0.44	0.30	8.88	0.18	19.97	0.64	0.02
WASF3	-0.13	55.56	-0.42	0.67	-0.04	58.61	-0.05	49.36	-0.19	4.22
WBP4	0.02	55.87	0.98	0.26	0.04	54.33	0.08	41.83	-0.58	0.02
WBSCR17	-0.13	49.54	0.48	0.99	0.49	2.06	-0.85	0.95	0.48	0.99
WDFY3	-0.50	15.28	-0.11	6.70	0.86	0.09	-0.17	1.62	0.55	0.02
WDR11	-0.86	0.05	0.41	5.83	-0.45	0.09	-0.30	47.42	-0.54	0.02
WDR12	-0.20	25.77	0.65	0.51	-0.81	0.09	-0.54	0.95	-0.38	4.22
WDR20	0.28	4.28	0.95	0.27	-0.22	2.66	-0.14	11.24	-0.43	0.02
WDR33	0.20	44.81	0.53	0.51	-0.11	41.10	0.23	27.83	-0.31	11.00
WDR37	0.13	44.81	1.09	0.99	0.17	41.10	-0.75	7.10	-0.62	0.02
WDR59	0.45	0.05	0.42	0.67	0.05	54.33	0.27	0.13	-0.71	0.08
WDR70	-0.11	18.59	-0.14	10.40	-0.18	4.73	-0.23	27.83	-0.48	0.89
WDR77	0.39	0.17	0.63	1.66	0.23	4.05	-0.52	0.06	-0.58	0.89
WFDC5	-0.14	51.01			-0.48	8.12	0.52	0.57	0.45	0.89
WHSC1	0.28	0.17	0.58	0.67	0.15	2.06	0.25	2.91	0.56	1.19
WHSC1L1	0.38	0.51	0.27	1.09	0.30	0.24	-0.58	0.06	-0.66	0.02
WIF1	-0.78	0.05	-0.17	6.70	-0.29	9.26	0.48	0.86	-0.08	38.75
WISP1	-0.30	4.28	0.13	13.30	0.29	29.33	-0.75	0.06	-0.68	24.40
WISP2	-0.25	5.93	-0.11	3.21	0.29	0.28	0.23	2.42	1.00	0.02
WNK1	0.13	44.81	-0.49	0.99	-0.32	1.10		50.00	-0.96	0.02
WNT3A	0.50	18.59	0.84	0.11	0.24	26.12	0.33	0.51	-0.06	37.82
WNT4	0.06	55.17	0.35	5.83	0.28	2.06	0.46	0.95	-0.26	24.62
WRN	0.52	0.51	0.38	0.57	-0.25	4.73	0.74	27.83	0.46	0.02
WSCD2	0.10	33.23	0.05	8.88	0.02	58.61	0.13	41.83	0.62	0.60
WWOX	-0.45	0.05	0.38	0.60	0.21	3.07	0.20	13.89	-0.55	0.31
WWP1	0.27	15.28	0.56	1.66	0.16	4.73	-0.68	1.88	0.73	0.02
XDH	-0.57	0.26	-0.57	1.03	-0.22	26.12	-0.18	47.42	0.39	36.83
XRCC2	0.23	0.40	-0.57	0.94			-0.84	0.95	0.12	31.62
XRN1	0.15	25.77	0.21	0.51	-0.03	60.23	0.26	41.83	-0.38	0.99
YARS2	0.13	33.23	0.73	0.60	-0.06	57.40	-0.58	0.06	-0.50	0.02
YEATS2	-0.05	44.81	-0.05	13.30	0.08	41.10	0.23	7.10	0.42	0.39
YLPM1	-0.20	18.59	0.54	0.42	-0.96	0.09	-0.72	1.88	-0.56	0.17
YTHDC2	0.04	54.70	0.79	0.88	0.02	59.79	0.27	0.57	-0.30	6.00
YWHAG	0.07	49.54	0.90	0.27			-0.05	50.49	-0.43	0.02
Ywhaq	-0.38	0.05	0.64	0.51	-0.36	0.86	0.07	47.42	-0.22	2.89
YY1	0.33	37.04	0.80	1.53	-0.12	6.93	-0.50	8.99	0.43	0.65
ZAP70	-0.10	33.23	0.46	0.17	0.13	36.89	-0.22	1.88	0.44	0.89
ZBTB10	0.50	0.51	0.62	0.51	0.37	0.72	0.94	0.06	0.30	1.98
ZBTB12	-0.29	0.13	-0.37	0.51	-0.38	0.66	-0.29	0.73	0.93	0.02
ZBTB20	-0.13	44.81	0.45	1.77	-0.54	0.09	-0.23	4.91	-0.39	0.39
ZBTB43	0.11	15.28	0.44	0.11	0.08	54.33	0.17	11.24	0.10	38.75
ZBTB5	-0.09	44.81	-0.25	2.12	-0.30	0.64	-0.67	0.57	-0.62	0.02
ZBTB7A	0.24	12.65	0.13	10.40	0.23	20.03	0.25	3.87	0.62	0.02
ZC3H12C	0.53	0.05	-0.11	6.70	0.42	5.71	-0.60	1.88	1.03	0.02
ZCCHC11	-0.51	0.05	-0.36	4.12	-0.21	9.26	-0.24	23.45	-1.00	0.02
ZCCHC7	-0.42	0.09	0.70	2.30	-0.35	0.09	0.15	41.83	0.30	14.82

ZCCHC8	0.02	54.15	-0.35	0.78	0.06	58.41	-1.13	0.06	0.22	0.47
ZDHHC21	0.09	44.81	0.68	1.46	-0.21	1.10	-0.43	8.99	-0.70	0.12
ZEB2	-0.30	0.26	0.45	0.29	-0.37	29.33	-0.60	0.06	0.18	36.83
ZFC3H1	0.18	49.54	0.36	2.30	-0.09	41.10	0.67	0.18	0.17	8.00
ZFHX3	-0.92	0.17	0.77	0.17	-0.23	29.33			1.03	0.02
Zfp386	0.44	0.78	0.97	0.11	-0.43	0.44	-0.54	1.33	-1.63	0.02
ZFP91	-0.75	0.09	0.71	1.21	-0.33	4.73	-0.68	0.13	1.05	0.02
ZFPM1	0.18	2.45			0.25	8.12	0.07	49.36	0.60	0.27
ZFR	0.32	1.10	0.50	0.30	-0.35	0.72	-0.58	0.35	-0.27	24.40
ZFYVE26	-0.38	0.05	-0.61	0.78	-0.43	0.28	1.17	0.06	0.29	0.39
ZIC1	-1.54	0.05	0.39	2.77	-0.57	0.09	-0.34	32.50	0.40	31.62
ZKSCAN1	-0.43	0.05	0.73	0.60	0.04	56.82	0.27	2.91	0.07	40.66
ZKSCAN2	-0.08	33.23	-0.91	0.43	-0.06	49.13			0.42	0.98
ZKSCAN5	0.08	49.54	0.45	2.30	0.10	41.10	-0.37	0.95	-0.33	0.27
ZMAT1	-0.46	0.05	0.32	8.25	-0.40	0.09	0.22	1.62	-0.48	0.02
ZMYM2	0.19	7.74	0.57	0.48	-0.16	3.48	-0.21	13.89	0.35	0.89
ZNF169	-0.68	0.05			-0.24	6.93			-0.74	0.21
ZNF175	0.51	0.05	0.49	2.12	0.11	55.77	-0.74	1.88	-0.74	0.02
ZNF202	0.25	0.17	-0.28	4.12	0.17	2.06	-0.38	0.95	-0.26	11.00
ZNF205	0.14	44.81	0.66	0.89	0.09	29.33	-0.16	23.45	-0.22	8.00
ZNF276	0.25	0.51	-0.32	4.12	-0.12	54.33	-0.56	0.34	-0.30	6.00
ZNF317	-0.06	55.56	0.67	0.51	-0.15	6.93	0.64	0.06	-0.36	0.75
ZNF385B	0.42	12.65	-0.13	13.30	0.43	4.73	-0.12	32.50	1.18	0.21
ZNF440/ZNF808	0.53	5.93	0.17	5.83	0.64	0.09	0.46	19.97	-0.15	24.40
ZNF451	-0.21	0.53	0.71	0.51	0.49	3.07	0.40	0.34	-0.39	0.04
ZNF469	-0.28	0.05	-0.70	0.94	-0.11	29.33	0.35	8.99	0.14	31.62
ZNF536	0.39	0.05	-0.58	1.53	-0.16	9.26	0.12	47.42	0.44	0.31
ZNF593	-0.16	15.28	-0.31	4.12	0.10	49.13	-0.62	0.06	0.23	1.19
ZNF642	-0.15	33.23	0.59	0.78			0.22	2.91	0.82	0.02
ZNF652	0.11	21.80	0.40	0.16	0.22	9.26	-0.71	16.94	-0.04	40.66
ZNF667	0.03	53.69	0.59	1.21	-0.04	58.93	-0.14	19.97	-0.49	0.07
ZNF668	-0.78	0.05	-0.42	0.88	-0.87	0.64	-1.21	0.06	0.64	0.02
ZNFX1	0.36	0.78	-0.38	2.86	-0.15	26.12	0.40	27.83	-0.48	0.39
ZNHIT6	-0.10	51.01	0.53	0.78	0.09	41.10	0.34	11.24	-0.39	0.04
ZNRF3	0.31	5.93	0.42	0.18	0.28	9.26			-0.12	33.88
ZWILCH	0.12	44.81	-0.49	1.66	-0.32	2.66	-0.50	0.34	-0.12	31.62
ZWINT	0.19	4.28	0.50	0.17			0.33	23.45	0.28	0.21

Appendix 3: A list of deregulated miRNAs during prion disease.

	70	70	90	90	110	110	130	130	EP	EP
let-7b-5p	0.68	0.81	1.09	0.79			0.18	0.18	0.52	0.33
let-7c-5p	1.02	1.39	0.64	0.86	1.65	2.26	0.98	0.52	0.84	0.84
let-7d-5p	0.39	0.56	1.36	2.56	0.60	1.37	1.20	0.25	1.19	0.90
let-7e-5p	0.37	0.51	5.29	3.21	0.06	0.22	5.40	0.90	0.72	0.49
let-7g-5p					0.95	8.07	7.41	7.03	0.39	0.21
miR-100-5p	1.19	3.07	0.37	0.42	0.75	2.20	3.77	0.77	0.59	0.75
miR-101a-3p	1.49	0.29	0.54	0.84	1.21	0.77	4.01	1.84	0.59	0.35
miR-124a-3p	5.13	0.40	0.45	1.53			3.25	0.39	1.37	0.89
miR-125a-5p	1.40	2.65	0.67	2.02	3.79	10.21	4.53	2.40	1.52	0.82
miR-125b-5p	2.64	2.24	0.47	0.59	2.99	1.39	2.76	1.14	1.52	1.89
miR-126-3p	0.72	1.41	0.92	1.65	1.49	5.45	2.67	0.83	1.14	1.47
miR-126-5p	0.03	0.07	0.92	2.23					4.56	4.26
miR-127-3p	0.93	0.92	1.05	1.19	1.58	1.41	2.97	1.28	1.43	1.44
miR-128a-3p	0.39	0.80	0.32	0.30	0.86	0.94	1.16	0.41	1.02	0.91
miR-129-3p	1.06	0.93	0.96	0.86	0.68	1.85	1.36	0.60	0.80	0.82
miR-132-3p	2.45	6.44	0.72	0.85	3.25	8.00	7.63	1.63	1.24	2.63
miR-133a-3p	1.23	2.69	0.60	0.44	0.79	3.24	0.32	0.22	2.51	1.30
miR-134-5p	0.25	0.61			0.34	3.65			3.79	1.56
miR-136-5p	1.27	1.54	0.32	0.55	1.49	10.91	1.16	0.46	1.30	1.04
miR-137-3p	1.52	2.12	0.14	0.59	1.48	1.22	1.01	0.84	1.32	1.15
miR-138-5p	1.41	1.76	0.91	1.69	1.11	1.89	1.32	0.54	0.79	0.91
miR-139-5p	0.88	1.41	0.46	0.97	1.56	2.65	3.82	1.22	1.24	1.17
miR-140-5p	1.92	2.33			0.36	2.17	1.40	0.47	2.66	1.42
miR-145a-5p	3.38	1.60	0.66	1.01	1.05	4.13	1.70	1.95	1.57	2.10
miR-146a-5p	3.10	1.71	2.87	1.70	1.73	8.63	1.00	0.14	11.57	6.02
miR-146b-5p	1.40	2.03	1.57	1.67	1.51	5.30	2.62	0.85	1.80	3.38
miR-150-5p	1.82	2.43	0.44	0.85	2.27	7.67	1.34	0.76	2.76	2.03
miR-16-5p	2.88	2.94	1.36	1.67			2.80	0.71	1.18	0.88
miR-181a-5p	1.40	0.73	0.46	1.35			2.53	0.48	1.64	1.17
miR-186-5p	1.19	2.37	0.93	1.21	1.25	7.92	4.03	0.67		
miR-188-5p	2.45	1.83	4.83	1.76	1.75	0.95	0.21	0.40	1.13	1.12
miR-191-5p	1.28	2.30	0.64	1.03	2.33	3.81	4.05	1.29	1.06	1.00
miR-192-5p	0.16	0.34	0.66	3.74	2.70	1.02				
miR-193b-3p	2.02	4.50	0.70	0.85	0.83	2.95	2.85	1.37	1.35	1.09
miR-195-5p	1.40	0.51	1.98	1.20	2.04	2.87	2.31	0.80	2.12	0.58
miR-19b-3p	1.44	1.09	0.46	0.57	1.34	2.02	1.15	0.78	1.35	1.36
miR-204-5p	2.64	0.52	1.40	1.23	0.15	3.04	1.00	0.45	1.30	0.67
miR-218-5p	1.50	1.69	0.68	1.20	1.73	2.56	2.53	0.85	1.68	1.62
miR-222-3p	1.20	1.91	1.06	2.43	3.06	4.07	2.02	0.52	1.41	2.06

miR-24-3p	1.43	1.17	1.31	1.90	2.40	5.49	1.07	0.50	1.27	1.08
miR-26a-5p	1.45	1.48	1.06	1.22	1.62	1.60	2.09	0.87	1.25	1.09
miR-29a-3p	1.51	1.55	1.44	2.30	1.54	2.76	2.43	0.56	1.25	1.18
miR-29b-3p	3.89	0.63	0.33	0.28	0.65	3.09			0.84	6.21
miR-29c-3p	1.50	0.95	0.89	1.17	1.29	2.06	1.00	1.21	1.18	1.03
miR-301a-3p	4.50	1.83	0.68	0.59	3.45	3.34	14.00	1.91	1.22	0.58
miR-301b-3p	2.01	1.65	2.01	3.44	0.84	3.84	2.56	0.94	3.03	1.05
miR-30a-5p	1.20	0.72	0.24	0.56	1.24	2.02	3.24	0.84	1.37	1.15
miR-30b-5p	1.32	1.72	0.70	0.86	1.13	1.99	2.56	1.30	1.18	1.08
miR-30c-5p	1.53	1.87	1.31	1.71	1.30	2.32	4.19	1.10	1.20	1.41
miR-30d-5p	0.89	0.88	0.50	0.58	1.11	3.56	2.55	0.71	1.47	2.40
miR-30e-5p	0.61	0.34	0.93	2.13	1.15	2.55	0.90	0.46	0.95	0.77
miR-31-5p	0.81	1.88	1.14	1.21	1.84	3.93	0.89	0.41	1.64	0.72
miR-320-3p	2.47	1.08	0.64	1.91	1.82	5.88	0.37	0.11	1.69	0.22
miR-324-5p			0.08	0.99	3.25	2.00	9.05	0.46	2.58	1.10
miR-328-3p	1.39	1.63	0.55	1.19	1.62	1.46	1.31	0.52	1.62	1.08
miR-331-3p	1.84	1.59	1.14	2.40	1.85	2.22	1.60	0.41	1.18	1.13
miR-335-5p	1.06	1.44					0.63	0.95	0.43	0.26
miR-337-3p					1.79	0.49	0.40	0.37	0.84	0.53
miR-342-3p	7.01	9.80	2.26	3.38	4.83	15.92	6.51	1.87	3.30	3.23
miR-365-3p	2.89	4.66	0.32	0.43	1.17	1.38	3.36	0.40		
miR-376a-3p	1.18	1.02	1.66	2.40			2.71	0.85	0.66	0.89
miR-376b-3p	0.25	0.11	2.82	0.85			0.36	0.39	1.15	0.49
miR-376c-3p	1.12	1.90	1.16	1.19	1.75	1.11	3.52	1.50	0.28	0.65
miR-379-5p	1.18	2.86	0.85	0.41	1.15	1.55	18.43	1.54	1.10	0.18
miR-384-3p	0.76	1.42	0.25	0.60	1.62	2.70	4.67	1.40	1.85	1.51
miR-409-3p	2.25	2.34			1.51	3.87	0.62	1.09	0.33	2.03
miR-410-3p	0.68	0.59	0.47	0.84	1.55	4.50	7.28	3.86	1.16	1.50
miR-411-5p	1.34	2.03	0.97	0.84	2.23	6.31	3.00	0.96	0.95	2.36
miR-433-3p			0.64	6.16	2.15	14.18	3.26	4.84		
miR-434-3p	3.48	3.24	0.93	1.20	2.51	4.38	2.17	0.63	1.06	2.20
miR-434-5p	0.53	3.54	0.92	2.16	1.87	3.60	0.56	0.35	0.69	0.43
miR-484	1.47	1.82	0.54	1.20	1.99	7.26	1.67	0.61	2.22	1.15
miR-491-5p	0.16	0.13	0.00	0.00					0.34	0.70
miR-495-3p	0.63	1.03	0.98	1.22	0.27	0.46	6.64	1.21	1.05	0.29
miR-532-3p	1.71	0.60	0.18	0.60			0.51	0.48		
miR-544-3p			3.60	6.58	1.03	0.60			1.35	0.85
miR-574-3p			5.21	26.33	0.74	18.30			0.62	1.25
miR-667-3p	0.78	1.32	0.64	1.74	1.24	2.72	1.29	0.39	0.91	1.04
miR-668-3p	4.60	1.17					3.54	2.99	0.46	0.29
miR-708-5p	0.48	0.19	0.31	0.85	1.94	1.36			0.81	1.00
miR-744-5p	0.94	0.85	0.66	7.62	1.56	2.98	0.68	0.07	1.85	0.29

miR-7b-5p	1.51	3.66	0.43	0.20	11.27	1.95				
miR-9-5p	1.50	2.17	0.48	0.65	2.52	4.57	1.99	2.03	0.96	0.84
miR-92a-3p	1.22	0.17	1.37	0.42	1.17	2.00	1.85	1.67	1.99	1.00
miR-99a-5p			0.32	0.66	1.63	2.56	1.36	0.80	0.31	0.35
miR-99b-5p	1.97	1.91	0.43	0.84	0.82	0.84	2.19	0.90	0.65	0.55

8.0 REFERENCES

Abid K, Soto C. 2006. The intriguing prion disorders. Cell Mol Life Sci. 63:2342-2351.

Adlard PA, Tran BA, Finkelstein DI, Desmond PM, Johnston LA, Bush AI, Egan GF. 2014. A review of beta-amyloid neuroimaging in Alzheimer's disease. Front Neurosci. 8:327.

Aguib Y, Heiseke A, Gilch S, Riemer C, Baier M, Schatzl HM, Ertmer A. 2009. Autophagy induction by trehalose counteracts cellular prion infection. Autophagy. 5:361-369.

Aguzzi A, Weissmann C. 1996. Spongiform encephalopathies: a suspicious signature. Nature. 383:666-667.

Aguzzi A, Nuvolone M, Zhu C. 2013. The immunobiology of prion diseases. Nat Rev Immunol. 13:888-902.

Akhtar MW, Kim MS, Adachi M, Morris MJ, Qi X, Richardson JA, Bassel-Duby R, Olson EN, Kavalali ET, Monteggia LM. 2012. In vivo analysis of MEF2 transcription factors in synapse regulation and neuronal survival. PLoS One. 7:e34863.

Alais S, Simoes S, Baas D, Lehmann S, Raposo G, Darlix JL, Leblanc P. 2008. Mouse neuroblastoma cells release prion infectivity associated with exosomal vesicles. Biol Cell. 100:603-615.

Alexandrov PN, Dua P, Lukiw WJ. 2014. Up-Regulation of miRNA-146a in Progressive, Age-Related Inflammatory Neurodegenerative Disorders of the Human CNS. Front Neurol. 5:181.

Alper T, Cramp WA, Haig DA, Clarke MC. 1967. Does the agent of scrapie replicate without nucleic acid? Nature. 214:764-766.

Anderson KA, Kane CD. 1998. Ca2+/calmodulin-dependent protein kinase IV and calcium signaling. Biometals. 11:331-343.

Ango F, Pin JP, Tu JC, Xiao B, Worley PF, Bockaert J, Fagni L. 2000. Dendritic and axonal targeting of type 5 metabotropic glutamate receptor is regulated by homer1 proteins and neuronal excitation. J Neurosci. 20:8710-8716.

Ango F, Robbe D, Tu JC, Xiao B, Worley PF, Pin JP, Bockaert J, Fagni L. 2002. Homer-dependent cell surface expression of metabotropic glutamate receptor type 5 in neurons. Mol Cell Neurosci. 20:323-329.

Antoni FA. 2000. Molecular diversity of cyclic AMP signalling. Front Neuroendocrinol. 21:103-132.

Antoni FA, Sosunov AA, Haunso A, Paterson JM, Simpson J. 2003. Short-term plasticity of cyclic adenosine 3',5'-monophosphate signaling in anterior pituitary corticotrope cells: the role of adenylyl cyclase isotypes. Mol Endocrinol. 17:692-703.

Arnold FJ, Hofmann F, Bengtson CP, Wittmann M, Vanhoutte P, Bading H. 2005. Microelectrode array recordings of cultured hippocampal networks reveal a simple model for transcription and protein synthesis-dependent plasticity. J Physiol. 564:3-19.

Aronica E, Fluiter K, Iyer A, Zurolo E, Vreijling J, van Vliet EA, Baayen JC, Gorter JA. 2010. Expression pattern of miR-146a, an inflammation-associated microRNA, in experimental and human temporal lobe epilepsy. Eur J Neurosci. 31:1100-1107.

Arvanitis DN, Jungas T, Behar A, Davy A. 2010. Ephrin-B1 reverse signaling controls a posttranscriptional feedback mechanism via miR-124. Mol Cell Biol. 30:2508-2517.

Atarashi R, Sano K, Satoh K, Nishida N. 2011. Real-time quaking-induced conversion: a highly sensitive assay for prion detection. Prion. 5:150-153.

Baccarini A, Chauhan H, Gardner TJ, Jayaprakash AD, Sachidanandam R, Brown BD. 2011. Kinetic analysis reveals the fate of a microRNA following target regulation in mammalian cells. Curr Biol. 21:369-376.

Bahl JM, Heegaard NH, Falkenhorst G, Laursen H, Hogenhaven H, Molbak K, Jespersgaard C, Hougs L, Waldemar G, Johannsen P et al. . 2009. The diagnostic efficiency of biomarkers in sporadic Creutzfeldt-Jakob disease compared to Alzheimer's disease. Neurobiol Aging. 30:1834-1841.

Bailly Y, Haeberle AM, Blanquet-Grossard F, Chasserot-Golaz S, Grant N, Schulze T, Bombarde G, Grassi J, Cesbron JY, Lemaire-Vieille C. 2004. Prion protein (PrPc) immunocytochemistry and expression of the green fluorescent protein reporter gene under control of the bovine PrP gene promoter in the mouse brain. J Comp Neurol. 473:244-269.

Banker GA, Cowan WM. 1977. Rat hippocampal neurons in dispersed cell culture. Brain Res. 126:397-342.

Banks WA, Niehoff ML, Adessi C, Soto C. 2004. Passage of murine scrapie prion protein across the mouse vascular blood-brain barrier. Biochem Biophys Res Commun. 318:125-130.

Barmada SJ, Harris DA. 2005. Visualization of prion infection in transgenic mice expressing green fluorescent protein-tagged prion protein. J Neurosci. 25:5824-5832.

Barrow PA, Holmgren CD, Tapper AJ, Jefferys JG. 1999. Intrinsic physiological and morphological properties of principal cells of the hippocampus and neocortex in hamsters infected with scrapie. Neurobiol Dis. 6:406-423.

Bartel DP. 2009. MicroRNAs: target recognition and regulatory functions. Cell. 136:215-233.

Bartz JC, Kincaid AE, Bessen RA. 2002. Retrograde transport of transmissible mink encephalopathy within descending motor tracts. J Virol. 76:5759-5768.

Basler K, Oesch B, Scott M, Westaway D, Walchli M, Groth DF, McKinley MP, Prusiner SB, Weissmann C. 1986. Scrapie and cellular PrP isoforms are encoded by the same chromosomal gene. Cell. 46:417-428.

Belichenko PV, Brown D, Jeffrey M, Fraser JR. 2000. Dendritic and synaptic alterations of hippocampal pyramidal neurones in scrapie-infected mice. Neuropathol Appl Neurobiol. 26:143-149.

Bennett MJ, Schlunegger MP, Eisenberg D. 1995. 3D domain swapping: a mechanism for oligomer assembly. Protein Sci. 4:2455-2468.

Benoist M, Palenzuela R, Rozas C, Rojas P, Tortosa E, Morales B, Gonzalez-Billault C, Avila J, Esteban JA. 2013. MAP1B-dependent Rac activation is required for AMPA receptor endocytosis during long-term depression. Embo j. 32:2287-2299.

Benson DL, Watkins FH, Steward O, Banker G. 1994. Characterization of GABAergic neurons in hippocampal cell cultures. J Neurocytol. 23:279-295.

Berman HM, Kleywegt GJ, Nakamura H, Markley JL, Burley SK. 2010. Safeguarding the integrity of protein archive. Nature. 463:425.

Bernoulli C, Siegfried J, Baumgartner G, Regli F, Rabinowicz T, Gajdusek DC, Gibbs CJ,Jr. 1977. Danger of accidental person-to-person transmission of Creutzfeldt-Jakob disease by surgery. Lancet. 1:478-479.

Bernstein E, Kim SY, Carmell MA, Murchison EP, Alcorn H, Li MZ, Mills AA, Elledge SJ, Anderson KV, Hannon GJ. 2003. Dicer is essential for mouse development. Nat Genet. 35:215-217.

Bessen RA, Marsh RF. 1994. Distinct PrP properties suggest the molecular basis of strain variation in transmissible mink encephalopathy. J Virol. 68:7859-7868.

Bett C, Joshi-Barr S, Lucero M, Trejo M, Liberski P, Kelly JW, Masliah E, Sigurdson CJ. 2012. Biochemical properties of highly neuroinvasive prion strains. PLoS Pathog. 8:e1002522.

Bhattacharyya SN, Habermacher R, Martine U, Closs EI, Filipowicz W. 2006. Relief of microRNA-mediated translational repression in human cells subjected to stress. Cell. 125:1111-1124.

Biasini E, Massignan T, Fioriti L, Rossi V, Dossena S, Salmona M, Forloni G, Bonetto V, Chiesa R. 2006. Analysis of the cerebellar proteome in a transgenic mouse model of inherited prion disease reveals preclinical alteration of calcineurin activity. Proteomics. 6:2823-2834.

Bicker S, Khudayberdiev S, Weiss K, Zocher K, Baumeister S, Schratt G. 2013. The DEAH-box helicase DHX36 mediates dendritic localization of the neuronal precursor-microRNA-134. Genes Dev. 27:991-996.

Black SA, Stys PK, Zamponi GW, Tsutsui S. 2014. Cellular prion protein and NMDA receptor modulation: protecting against excitotoxicity. Front Cell Dev Biol. 2:45.

Blennow K, Johansson A, Zetterberg H. 2005. Diagnostic value of 14-3-3beta immunoblot and T-tau/P-tau ratio in clinically suspected Creutzfeldt-Jakob disease. Int J Mol Med. 16:1147-1149.

Bolton DC, McKinley MP, Prusiner SB. 1984. Molecular characteristics of the major scrapie prion protein. Biochemistry. 23:5898-5906.

Bonni A, Ginty DD, Dudek H, Greenberg ME. 1995. Serine 133-phosphorylated CREB induces transcription via a cooperative mechanism that may confer specificity to neurotrophin signals. Mol Cell Neurosci. 6:168-183.

Booth S, Bowman C, Baumgartner R, Sorensen G, Robertson C, Coulthart M, Phillipson C, Somorjai RL. 2004. Identification of central nervous system genes involved in the host response to the scrapie agent during preclinical and clinical infection. J Gen Virol. 85:3459-3471.

Borden LA, Smith KE, Vaysse PJ, Gustafson EL, Weinshank RL, Branchek TA. 1995. Re-evaluation of GABA transport in neuronal and glial cell cultures: correlation of pharmacology and mRNA localization. Receptors Channels. 3:129-146.

Bounhar Y, Zhang Y, Goodyer CG, LeBlanc A. 2001. Prion protein protects human neurons against Bax-mediated apoptosis. J Biol Chem. 276:39145-39149.

Bourne JN, Harris KM. 2008. Balancing structure and function at hippocampal dendritic spines. Annu Rev Neurosci. 31:47-67.

Brakeman PR, Lanahan AA, O'Brien R, Roche K, Barnes CA, Huganir RL, Worley PF. 1997. Homer: a protein that selectively binds metabotropic glutamate receptors. Nature. 386:284-288.

Brandner S, Isenmann S, Raeber A, Fischer M, Sailer A, Kobayashi Y, Marino S, Weissmann C, Aguzzi A. 1996. Normal host prion protein necessary for scrapie-induced neurotoxicity. Nature. 379:339-343.

Brengues M, Teixeira D, Parker R. 2005. Movement of eukaryotic mRNAs between polysomes and cytoplasmic processing bodies. Science. 310:486-489.

Brewer GJ, Boehler MD, Jones TT, Wheeler BC. 2008. NbActiv4 medium improvement to Neurobasal/B27 increases neuron synapse densities and network spike rates on multielectrode arrays. J Neurosci Methods. 170:181-187.

Brown AR, Rebus S, McKimmie CS, Robertson K, Williams A, Fazakerley JK. 2005. Gene expression profiling of the preclinical scrapie-infected hippocampus. Biochem Biophys Res Commun. 334:86-95.

Brown DR, Nicholas RS, Canevari L. 2002. Lack of prion protein expression results in a neuronal phenotype sensitive to stress. J Neurosci Res. 67:211-224.

Brown DR, Schulz-Schaeffer WJ, Schmidt B, Kretzschmar HA. 1997. Prion protein-deficient cells show altered response to oxidative stress due to decreased SOD-1 activity. Exp Neurol. 146:104-112.

Brown DR, Qin K, Herms JW, Madlung A, Manson J, Strome R, Fraser PE, Kruck T, von Bohlen A, Schulz-Schaeffer W et al. . 1997. The cellular prion protein binds copper in vivo. Nature. 390:684-687.

Bruce ME, Will RG, Ironside JW, McConnell I, Drummond D, Suttie A, McCardle L, Chree A, Hope J, Birkett C et al. . 1997. Transmissions to mice indicate that 'new variant' CJD is caused by the BSE agent. Nature. 389:498-501.

Bruce ME, McConnell I, Fraser H, Dickinson AG. 1991. The disease characteristics of different strains of scrapie in Sinc congenic mouse lines: implications for the nature of the agent and host control of pathogenesis. J Gen Virol. 72 (Pt 3):595-603.

BSEinfo, 2015. <http://www.bseinfo.org/prionsanddisease.aspx>. Accessed August 22, 2015.

Bueler H, Fischer M, Lang Y, Bluethmann H, Lipp HP, DeArmond SJ, Prusiner SB, Aguet M, Weissmann C. 1992. Normal development and behaviour of mice lacking the neuronal cell-surface PrP protein. Nature. 356:577-582.

Calella AM, Nerlov C, Lopez RG, Sciarretta C, von Bohlen und Halbach O, Bereshchenko O, Minichiello L. 2007. Neurotrophin/Trk receptor signaling mediates C/EBPalpha, -beta and NeuroD recruitment to immediate-early gene promoters in neuronal cells and requires C/EBPs to induce immediate-early gene transcription. Neural Dev. 2:4.

Campeau JL, Wu G, Bell JR, Rasmussen J, Sim VL. 2013. Early increase and late decrease of purkinje cell dendritic spine density in prion-infected organotypic mouse cerebellar cultures. PLoS One. 8:e81776.

Carafoli E, Santella L, Branca D, Brini M. 2001. Generation, control, and processing of cellular calcium signals. Crit Rev Biochem Mol Biol. 36:107-260.

Carp RI. 1982. Transmission of scrapie by oral route: effect of gingival scarification. Lancet. 1:170-171.

Carroll JA, Striebel JF, Race B, Phillips K, Chesebro B. 2015. Prion infection of mouse brain reveals multiple new upregulated genes involved in neuroinflammation or signal transduction. J Virol. 89:2388-2404.

Castilla J, Gonzalez-Romero D, Saa P, Morales R, De Castro J, Soto C. 2008. Crossing the species barrier by PrP(Sc) replication in vitro generates unique infectious prions. Cell. 134:757-768.

Caughey B, Lansbury PT. 2003. Protofibrils, pores, fibrils, and neurodegeneration: separating the responsible protein aggregates from the innocent bystanders. Annu Rev Neurosci. 26:267-298.

Caughey BW, Dong A, Bhat KS, Ernst D, Hayes SF, Caughey WS. 1991. Secondary structure analysis of the scrapie-associated protein PrP 27-30 in water by infrared spectroscopy. Biochemistry. 30:7672-7680.

Centers for Disease Control and Prevention (CDC). 2008. Update: Creutzfeldt-Jakob disease associated with cadaveric dura mater grafts--Japan, 1978-2008. MMWR Morb Mortal Wkly Rep. 57:1152-1154.

Chandrasekar V, Dreyer JL. 2009. microRNAs miR-124, let-7d and miR-181a regulate cocaine-induced plasticity. Mol Cell Neurosci. 42:350-362.

Chattopadhyay M, Walter ED, Newell DJ, Jackson PJ, Aronoff-Spencer E, Peisach J, Gerfen GJ, Bennett B, Antholine WE, Millhauser GL. 2005. The octarepeat domain of the prion protein binds Cu(II) with three distinct coordination modes at pH 7.4. J Am Chem Soc. 127:12647-12656.

Chen CC, Lu J, Zuo Y. 2014. Spatiotemporal dynamics of dendritic spines in the living brain. Front Neuroanat. 8:28.

Chen J, Bardes EE, Aronow BJ, Jegga AG. 2009. ToppGene Suite for gene list enrichment analysis and candidate gene prioritization. Nucleic Acids Res. 37:W305-11.

Chen YL, Shen CK. 2013. Modulation of mGluR-dependent MAP1B translation and AMPA receptor endocytosis by microRNA miR-146a-5p. J Neurosci. 33:9013-9020.

Cheng LC, Pastrana E, Tavazoie M, Doetsch F. 2009. miR-124 regulates adult neurogenesis in the subventricular zone stem cell niche. Nat Neurosci. 12:399-408.

Chesebro B, Race R, Kercher L. 2005. Scrapie pathogenesis in brain and retina: effects of prion protein expression in neurons and astrocytes. J Neurovirol. 11:476-480.

Chiarini LB, Freitas AR, Zanata SM, Brentani RR, Martins VR, Linden R. 2002. Cellular prion protein transduces neuroprotective signals. Embo j. 21:3317-3326.

Chiti Z, Knutsen OM, Betmouni S, Greene JR. 2006. An integrated, temporal study of the behavioural, electrophysiological and neuropathological consequences of murine prion disease. Neurobiol Dis. 22:363-373.

Choi CJ, Kanthasamy A, Anantharam V, Kanthasamy AG. 2006. Interaction of metals with prion protein: possible role of divalent cations in the pathogenesis of prion diseases. Neurotoxicology. 27:777-787.

Choi CJ, Anantharam V, Saetveit NJ, Houk RS, Kanthasamy A, Kanthasamy AG. 2007. Normal cellular prion protein protects against manganese-induced oxidative stress and apoptotic cell death. Toxicol Sci. 98:495-509.

Chong ZZ, Li F, Maiese K. 2005. Oxidative stress in the brain: novel cellular targets that govern survival during neurodegenerative disease. Prog Neurobiol. 75:207-246.

Clarke MC, Kimberlin RH. 1984. Pathogenesis of mouse scrapie: distribution of agent in the pulp and stroma of infected spleens. Vet Microbiol. 9:215-225.

Cline MS, Smoot M, Cerami E, Kuchinsky A, Landys N, Workman C, Christmas R, Avila-Campilo I, Creech M, Gross B et al. . 2007. Integration of biological networks and gene expression data using Cytoscape. Nat Protoc. 2:2366-2382.

Cogswell JP, Ward J, Taylor IA, Waters M, Shi Y, Cannon B, Kelnar K, Kemppainen J, Brown D, Chen C et al. . 2008. Identification of miRNA changes in Alzheimer's disease brain and CSF yields putative biomarkers and insights into disease pathways. J Alzheimers Dis. 14:27-41.

Cohen FE, Prusiner SB. 1998. Pathologic conformations of prion proteins. Annu Rev Biochem. 67:793-819.

Colby DW, Prusiner SB. 2011. Prions. Cold Spring Harb Perspect Biol. 3:a006833.

Cole S, Kimberlin RH. 1985. Pathogenesis of mouse scrapie: dynamics of vacuolation in brain and spinal cord after intraperitoneal infection. Neuropathol Appl Neurobiol. 11:213-227.

Colling SB, Collinge J, Jefferys JG. 1996. Hippocampal slices from prion protein null mice: disrupted Ca(2+)-activated K+ currents. Neurosci Lett. 209:49-52.

Collinge J. 2010. Medicine. Prion strain mutation and selection. Science. 328:1111-1112.

Collinge J, Sidle KC, Meads J, Ironside J, Hill AF. 1996. Molecular analysis of prion strain variation and the aetiology of 'new variant' CJD. Nature. 383:685-690.

Collinge J, Whitfield J, McKintosh E, Beck J, Mead S, Thomas DJ, Alpers MP. 2006. Kuru in the 21st century--an acquired human prion disease with very long incubation periods. Lancet. 367:2068-2074.

Collinge J, Whittington MA, Sidle KC, Smith CJ, Palmer MS, Clarke AR, Jefferys JG. 1994. Prion protein is necessary for normal synaptic function. Nature. 370:295-297.

Correia SS, Bassani S, Brown TC, Lise MF, Backos DS, El-Husseini A, Passafaro M, Esteban JA. 2008. Motor protein-dependent transport of AMPA receptors into spines during long-term potentiation. Nat Neurosci. 11:457-466.

Criado JR, Sanchez-Alavez M, Conti B, Giacchino JL, Wills DN, Henriksen SJ, Race R, Manson JC, Chesebro B, Oldstone MB. 2005. Mice devoid of prion protein have cognitive deficits that are rescued by reconstitution of PrP in neurons. Neurobiol Dis. 19:255-265.

Cui C, Xu G, Qiu J, Fan X. 2015. Upregulation of miR-26a promotes neurite outgrowth and ameliorates apoptosis by inhibiting PTEN in bupivacaine injured mouse dorsal root ganglia. Cell Biol Int. .

Cunningham C, Deacon R, Wells H, Boche D, Waters S, Diniz CP, Scott H, Rawlins JN, Perry VH. 2003. Synaptic changes characterize early behavioural signs in the ME7 model of murine prion disease. Eur J Neurosci. 17:2147-2155.

Dartigues JF. 2009. Alzheimer's disease: a global challenge for the 21st century. Lancet Neurol. 8:1082-1083.

Daude N, Marella M, Chabry J. 2003. Specific inhibition of pathological prion protein accumulation by small interfering RNAs. J Cell Sci. 116:2775-2779.

Davis TH, Cuellar TL, Koch SM, Barker AJ, Harfe BD, McManus MT, Ullian EM. 2008. Conditional loss of Dicer disrupts cellular and tissue morphogenesis in the cortex and hippocampus. J Neurosci. 28:4322-4330.

Dawson TM, Ko HS, Dawson VL. 2010. Genetic animal models of Parkinson's disease. Neuron. 66:646-661.

De Pietri Tonelli D, Pulvers JN, Haffner C, Murchison EP, Hannon GJ, Huttner WB. 2008. miRNAs are essential for survival and differentiation of newborn neurons but not for expansion of neural progenitors during early neurogenesis in the mouse embryonic neocortex. Development. 135:3911-3921.

DebBurman SK, Raymond GJ, Caughey B, Lindquist S. 1997. Chaperone-supervised conversion of prion protein to its protease-resistant form. Proc Natl Acad Sci U S A. 94:13938-13943.

Degterev A, Boyce M, Yuan J. 2003. A decade of caspases. Oncogene. 22:8543-8567.

Deleault NR, Walsh DJ, Piro JR, Wang F, Wang X, Ma J, Rees JR, Supattapone S. 2012. Cofactor molecules maintain infectious conformation and restrict strain properties in purified prions. Proc Natl Acad Sci U S A. 109:E1938-46.

Denkers ND, Hayes-Klug J, Anderson KR, Seelig DM, Haley NJ, Dahmes SJ, Osborn DA, Miller KV, Warren RJ, Mathiason CK et al. . 2013. Aerosol transmission of chronic wasting disease in white-tailed deer. J Virol. 87:1890-1892.

Diaz-Espinoza R, Soto C. 2010. Generation of prions in vitro and the protein-only hypothesis. Prion. 4:53-59.

Dickinson AG, Meikle VM. 1969. A comparison of some biological characteristics of the mouse-passaged scrapie agents, 22A and ME7. Genet Res. 13:213-225.

Doeppner TR, Doehring M, Bretschneider E, Zechariah A, Kaltwasser B, Muller B, Koch JC, Bahr M, Hermann DM, Michel U. 2013. MicroRNA-124 protects against focal cerebral ischemia via mechanisms involving Usp14-dependent REST degradation. Acta Neuropathol. 126:251-265.

Donaldson DS, Kobayashi A, Ohno H, Yagita H, Williams IR, Mabbott NA. 2012. M cell-depletion blocks oral prion disease pathogenesis. Mucosal Immunol. 5:216-225.

Dong XX, Wang Y, Qin ZH. 2009. Molecular mechanisms of excitotoxicity and their relevance to pathogenesis of neurodegenerative diseases. Acta Pharmacol Sin. 30:379-387.

Dorval V, Mandemakers W, Jolivette F, Coudert L, Mazroui R, De Strooper B, Hebert SS. 2014. Gene and MicroRNA transcriptome analysis of Parkinson's related LRRK2 mouse models. PLoS One. 9:e85510.

Duffy P, Wolf J, Collins G, DeVoe AG, Streeten B, Cowen D. 1974. Letter: Possible person-to-person transmission of Creutzfeldt-Jakob disease. N Engl J Med. 290:692-693.

Edbauer D, Neilson JR, Foster KA, Wang CF, Seeburg DP, Batterton MN, Tada T, Dolan BM, Sharp PA, Sheng M. 2010. Regulation of synaptic structure and function by FMRP-associated microRNAs miR-125b and miR-132. Neuron. 65:373-384.

Emerman AB, Zhang ZR, Chakrabarti O, Hegde RS. 2010. Compartment-restricted biotinylation reveals novel features of prion protein metabolism in vivo. Mol Biol Cell. 21:4325-4337.

Enari M, Flechsig E, Weissmann C. 2001. Scrapie prion protein accumulation by scrapie-infected neuroblastoma cells abrogated by exposure to a prion protein antibody. Proc Natl Acad Sci U S A. 98:9295-9299.

Ettaiche M, Pichot R, Vincent JP, Chabry J. 2000. In vivo cytotoxicity of the prion protein fragment 106-126. J Biol Chem. 275:36487-36490.

Farlow MR, Yee RD, Dlouhy SR, Conneally PM, Azzarelli B, Ghetti B. 1989. Gerstmann-Straussler-Scheinker disease. I. Extending the clinical spectrum. Neurology. 39:1446-1452.

Feig LA. 2011. Regulation of Neuronal Function by Ras-GRF Exchange Factors. Genes Cancer. 2:306-319.

Ferrer I, Costa F, Grau Veciana JM. 1981. Creutzfeldt-Jacob disease: a golgi study. Neuropathol Appl Neurobiol. 7:237-242.

Fevrier B, Vilette D, Archer F, Loew D, Faigle W, Vidal M, Laude H, Raposo G. 2004. Cells release prions in association with exosomes. Proc Natl Acad Sci U S A. 101:9683-9688.

Fimia GM, Piacentini M. 2010. Regulation of autophagy in mammals and its interplay with apoptosis. Cell Mol Life Sci. 67:1581-1588.

Finkbeiner S. 2000. CREB couples neurotrophin signals to survival messages. Neuron. 25:11-14.

Fjorback AW, Muller HK, Wiborg O. 2009. Membrane glycoprotein M6B interacts with the human serotonin transporter. J Mol Neurosci. 37:191-200.

Florio T, Thellung S, Amico C, Robello M, Salmona M, Bugiani O, Tagliavini F, Forloni G, Schettini G. 1998. Prion protein fragment 106-126 induces apoptotic cell death and impairment of L-type voltage-sensitive calcium channel activity in the GH3 cell line. J Neurosci Res. 54:341-352.

Ford MJ, Burton LJ, Li H, Graham CH, Frobert Y, Grassi J, Hall SM, Morris RJ. 2002. A marked disparity between the expression of prion protein and its message by neurones of the CNS. Neuroscience. 111:533-551.

Francis PT, Palmer AM, Snape M, Wilcock GK. 1999. The cholinergic hypothesis of Alzheimer's disease: a review of progress. J Neurol Neurosurg Psychiatry. 66:137-147.

Fraser H, Dickinson AG. 1973. Scrapie in mice. Agent-strain differences in the distribution and intensity of grey matter vacuolation. J Comp Pathol. 83:29-40.

Friedman RC, Farh KK, Burge CB, Bartel DP. 2009. Most mammalian mRNAs are conserved targets of microRNAs. Genome Res. 19:92-105.

Fuhrmann M, Mitteregger G, Kretzschmar H, Herms J. 2007. Dendritic pathology in prion disease starts at the synaptic spine. J Neurosci. 27:6224-6233.

Fuhrmann M, Bittner T, Mitteregger G, Haider N, Moosmang S, Kretzschmar H, Herms J. 2006. Loss of the cellular prion protein affects the Ca2+ homeostasis in hippocampal CA1 neurons. J Neurochem. 98:1876-1885.

Gadotti VM, Bonfield SP, Zamponi GW. 2012. Depressive-like behaviour of mice lacking cellular prion protein. Behav Brain Res. 227:319-323.

Gains MJ, Roth KA, LeBlanc AC. 2006. Prion protein protects against ethanol-induced Bax-mediated cell death in vivo. Neuroreport. 17:903-906.

GAJDUSEK DC, REID LH. 1961. Studies on kuru. IV. The kuru pattern in Moke, a representative Fore village. Am J Trop Med Hyg. 10:628-638.

GAJDUSEK DC, ZIGAS V. 1957. Degenerative disease of the central nervous system in New Guinea; the endemic occurrence of kuru in the native population. N Engl J Med. 257:974-978.

Garcia DM, Baek D, Shin C, Bell GW, Grimson A, Bartel DP. 2011. Weak seed-pairing stability and high target-site abundance decrease the proficiency of lsy-6 and other microRNAs. Nat Struct Mol Biol. 18:1139-1146.

Gasperini R, Choi-Lundberg D, Thompson MJ, Mitchell CB, Foa L. 2009. Homer regulates calcium signalling in growth cone turning. Neural Dev. 4:29-8104-4-29.

Geekiyanage H, Chan C. 2011. MicroRNA-137/181c regulates serine palmitoyltransferase and in turn amyloid beta, novel targets in sporadic Alzheimer's disease. J Neurosci. 31:14820-14830.

Geschwind MD, Kuo AL, Wong KS, Haman A, Devereux G, Raudabaugh BJ, Johnson DY, Torres-Chae CC, Finley R, Garcia P et al. . 2013. Quinacrine treatment trial for sporadic Creutzfeldt-Jakob disease. Neurology. 81:2015-2023.

Ghaemmaghami S, Colby DW, Nguyen HO, Hayashi S, Oehler A, DeArmond SJ, Prusiner SB. 2013. Convergent replication of mouse synthetic prion strains. Am J Pathol. 182:866-874.

Ghani AC, Donnelly CA, Ferguson NM, Anderson RM. 2002. The transmission dynamics of BSE and vCJD. C R Biol. 325:37-47.

Gibbings D, Leblanc P, Jay F, Pontier D, Michel F, Schwab Y, Alais S, Lagrange T, Voinnet O. 2012. Human prion protein binds Argonaute and promotes accumulation of microRNA effector complexes. Nat Struct Mol Biol. 19:517-24, S1.

Giese A, Brown DR, Groschup MH, Feldmann C, Haist I, Kretzschmar HA. 1998. Role of microglia in neuronal cell death in prion disease. Brain Pathol. 8:449-457.

Gilch S, Wopfner F, Renner-Muller I, Kremmer E, Bauer C, Wolf E, Brem G, Groschup MH, Schatzl HM. 2003. Polyclonal anti-PrP auto-antibodies induced with dimeric PrP interfere efficiently with PrPSc propagation in prion-infected cells. J Biol Chem. 278:18524-18531.

Giles K, Glidden DV, Patel S, Korth C, Groth D, Lemus A, DeArmond SJ, Prusiner SB. 2010. Human prion strain selection in transgenic mice. Ann Neurol. 68:151-161.

Gillardon F, Mack M, Rist W, Schnack C, Lenter M, Hildebrandt T, Hengerer B. 2008. MicroRNA and proteome expression profiling in early-symptomatic alpha-synuclein(A30P)-transgenic mice. Proteomics Clin Appl. 2:697-705.

Giraldez AJ, Cinalli RM, Glasner ME, Enright AJ, Thomson JM, Baskerville S, Hammond SM, Bartel DP, Schier AF. 2005. MicroRNAs regulate brain morphogenesis in zebrafish. Science. 308:833-838.

Glatzel M, Abela E, Maissen M, Aguzzi A. 2003. Extraneural pathologic prion protein in sporadic Creutzfeldt-Jakob disease. N Engl J Med. 349:1812-1820.

Glaysher BR, Mabbott NA. 2007. Role of the draining lymph node in scrapie agent transmission from the skin. Immunol Lett. 109:64-71.

Goldgaber D, Goldfarb LG, Brown P, Asher DM, Brown WT, Lin S, Teener JW, Feinstone SM, Rubenstein R, Kascsak RJ. 1989. Mutations in familial Creutzfeldt-Jakob disease and Gerstmann-Straussler-Scheinker's syndrome. Exp Neurol. 106:204-206.

Goley ED, Welch MD. 2006. The ARP2/3 complex: an actin nucleator comes of age. Nat Rev Mol Cell Biol. 7:713-726.

Goold R, McKinnon C, Rabbanian S, Collinge J, Schiavo G, Tabrizi SJ. 2013. Alternative fates of newly formed PrPSc upon prion conversion on the plasma membrane. J Cell Sci. 126:3552-3562.

Govaerts C, Wille H, Prusiner SB, Cohen FE. 2004. Evidence for assembly of prions with left-handed beta-helices into trimers. Proc Natl Acad Sci U S A. 101:8342-8347.

Graveland GA, Williams RS, DiFiglia M. 1985. Evidence for degenerative and regenerative changes in neostriatal spiny neurons in Huntington's disease. Science. 227:770-773.

Gray BC, Siskova Z, Perry VH, O'Connor V. 2009. Selective presynaptic degeneration in the synaptopathy associated with ME7-induced hippocampal pathology. Neurobiol Dis. 35:63-74.

Grabrucker AM, Schmeisser MJ, Udvardi PT, Arons M, Schoen M, Woodling NS, Andreasson KI, Hof PR, Buxbaum JD, Garner CC et al. . 2011. Amyloid beta protein-induced zinc sequestration leads to synaptic loss via dysregulation of the ProSAP2/Shank3 scaffold. Mol Neurodegener. 6:65-1326-6-65.

Graner E, Mercadante AF, Zanata SM, Forlenza OV, Cabral AL, Veiga SS, Juliano MA, Roesler R, Walz R, Minetti A et al. . 2000. Cellular prion protein binds laminin and mediates neuritogenesis. Brain Res Mol Brain Res. 76:85-92.

Grey F, Tirabassi R, Meyers H, Wu G, McWeeney S, Hook L, Nelson JA. 2010. A viral microRNA down-regulates multiple cell cycle genes through mRNA 5'UTRs. PLoS Pathog. 6:e1000967.

Griffith JS. 1967. Self-replication and scrapie. Nature. 215:1043-1044.

Grimm D, Streetz KL, Jopling CL, Storm TA, Pandey K, Davis CR, Marion P, Salazar F, Kay MA. 2006. Fatality in mice due to oversaturation of cellular microRNA/short hairpin RNA pathways. Nature. 441:537-541.

Grimson A, Farh KK, Johnston WK, Garrett-Engele P, Lim LP, Bartel DP. 2007. MicroRNA targeting specificity in mammals: determinants beyond seed pairing. Mol Cell. 27:91-105.

Groc L, Heine M, Cousins SL, Stephenson FA, Lounis B, Cognet L, Choquet D. 2006. NMDA receptor surface mobility depends on NR2A-2B subunits. Proc Natl Acad Sci U S A. 103:18769-18774.

Gu X, Meng S, Liu S, Jia C, Fang Y, Li S, Fu C, Song Q, Lin L, Wang X. 2014. miR-124 represses ROCK1 expression to promote neurite elongation through activation of the PI3K/Akt signal pathway. J Mol Neurosci. 52:156-165.

Guillaud L, Setou M, Hirokawa N. 2003. KIF17 dynamics and regulation of NR2B trafficking in hippocampal neurons. J Neurosci. 23:131-140.

Guo H, Ingolia NT, Weissman JS, Bartel DP. 2010. Mammalian microRNAs predominantly act to decrease target mRNA levels. Nature. 466:835-840.

Haber M, Zhou L, Murai KK. 2006. Cooperative astrocyte and dendritic spine dynamics at hippocampal excitatory synapses. J Neurosci. 26:8881-8891.

Hagiwara K, Hara H, Hanada K. 2013. Species-barrier phenomenon in prion transmissibility from a viewpoint of protein science. J Biochem. 153:139-145.

Haik S, Faucheux BA, Sazdovitch V, Privat N, Kemeny JL, Perret-Liaudet A, Hauw JJ. 2003. The sympathetic nervous system is involved in variant Creutzfeldt-Jakob disease. Nat Med. 9:1121-1123.

Halperin L, Jung J, Michalak M. 2014. The many functions of the endoplasmic reticulum chaperones and folding enzymes. IUBMB Life. 66:318-326.

Hansen MR, Bok J, Devaiah AK, Zha XM, Green SH. 2003. Ca2+/calmodulin-dependent protein kinases II and IV both promote survival but differ in their effects on axon growth in spiral ganglion neurons. J Neurosci Res. 72:169-184.

Harding HP, Zhang Y, Scheuner D, Chen JJ, Kaufman RJ, Ron D. 2009. Ppp1r15 gene knockout reveals an essential role for translation initiation factor 2 alpha (eIF2alpha) dephosphorylation in mammalian development. Proc Natl Acad Sci U S A. 106:1832-1837.

Hardingham GE, Bading H. 2010. Synaptic versus extrasynaptic NMDA receptor signalling: implications for neurodegenerative disorders. Nat Rev Neurosci. 11:682-696.

Hardingham GE, Fukunaga Y, Bading H. 2002. Extrasynaptic NMDARs oppose synaptic NMDARs by triggering CREB shut-off and cell death pathways. Nat Neurosci. 5:405-414.

Hardingham GE, Arnold FJ, Bading H. 2001. Nuclear calcium signaling controls CREB-mediated gene expression triggered by synaptic activity. Nat Neurosci. 4:261-267.

Harrington MG, Merril CR, Asher DM, Gajdusek DC. 1986. Abnormal proteins in the cerebrospinal fluid of patients with Creutzfeldt-Jakob disease. N Engl J Med. 315:279-283.

Harris DA, True HL. 2006. New insights into prion structure and toxicity. Neuron. 50:353-357.

Harris DA, Lele P, Snider WD. 1993. Localization of the mRNA for a chicken prion protein by in situ hybridization. Proc Natl Acad Sci U S A. 90:4309-4313.

Hasegawa H, Kiyokawa E, Tanaka S, Nagashima K, Gotoh N, Shibuya M, Kurata T, Matsuda M. 1996. DOCK180, a major CRK-binding protein, alters cell morphology upon translocation to the cell membrane. Mol Cell Biol. 16:1770-1776.

Haybaeck J, Heikenwalder M, Klevenz B, Schwarz P, Margalith I, Bridel C, Mertz K, Zirdum E, Petsch B, Fuchs TJ et al. . 2011. Aerosols transmit prions to immunocompetent and immunodeficient mice. PLoS Pathog. 7:e1001257.

Hebert SS, Wang WX, Zhu Q, Nelson PT. 2013. A study of small RNAs from cerebral neocortex of pathology-verified Alzheimer's disease, dementia with lewy bodies, hippocampal sclerosis, frontotemporal lobar dementia, and non-demented human controls. J Alzheimers Dis. 35:335-348.

Hebert SS, Horre K, Nicolai L, Papadopoulou AS, Mandemakers W, Silahtaroglu AN, Kauppinen S, Delacourte A, De Strooper B. 2008. Loss of microRNA cluster miR-29a/b-1 in sporadic Alzheimer's disease correlates with increased BACE1/beta-secretase expression. Proc Natl Acad Sci U S A. 105:6415-6420.

Heckmann JG, Lang CJ, Petruch F, Druschky A, Erb C, Brown P, Neundorfer B. 1997. Transmission of Creutzfeldt-Jakob disease via a corneal transplant. J Neurol Neurosurg Psychiatry. 63:388-390.

Hegde RS, Tremblay P, Groth D, DeArmond SJ, Prusiner SB, Lingappa VR. 1999. Transmissible and genetic prion diseases share a common pathway of neurodegeneration. Nature. 402:822-826.

Heggebo R, Gonzalez L, Press CM, Gunnes G, Espenes A, Jeffrey M. 2003. Disease-associated PrP in the enteric nervous system of scrapie-affected Suffolk sheep. J Gen Virol. 84:1327-1338.

Heinonen O, Soininen H, Sorvari H, Kosunen O, Paljarvi L, Koivisto E, Riekkinen PJ S. 1995. Loss of synaptophysin-like immunoreactivity in the hippocampal formation is an early phenomenon in Alzheimer's disease. Neuroscience. 64:375-384.

Heiseke A, Aguib Y, Riemer C, Baier M, Schatzl HM. 2009. Lithium induces clearance of protease resistant prion protein in prion-infected cells by induction of autophagy. J Neurochem. 109:25-34.

Hengst U, Cox LJ, Macosko EZ, Jaffrey SR. 2006. Functional and selective RNA interference in developing axons and growth cones. J Neurosci. 26:5727-5732.

Henke JI, Goergen D, Zheng J, Song Y, Schuttler CG, Fehr C, Junemann C, Niepmann M. 2008. microRNA-122 stimulates translation of hepatitis C virus RNA. Embo j. 27:3300-3310.

Heppner FL, Christ AD, Klein MA, Prinz M, Fried M, Kraehenbuhl JP, Aguzzi A. 2001. Transepithelial prion transport by M cells. Nat Med. 7:976-977.

Herms JW, Tings T, Dunker S, Kretzschmar HA. 2001. Prion protein affects Ca2+-activated K+ currents in cerebellar purkinje cells. Neurobiol Dis. 8:324-330.

Herms JW, Korte S, Gall S, Schneider I, Dunker S, Kretzschmar HA. 2000. Altered intracellular calcium homeostasis in cerebellar granule cells of prion protein-deficient mice. J Neurochem. 75:1487-1492.

Herms JW, Kretzchmar HA, Titz S, Keller BU. 1995. Patch-clamp analysis of synaptic transmission to cerebellar purkinje cells of prion protein knockout mice. Eur J Neurosci. 7:2508-2512.

Hetz C, Russelakis-Carneiro M, Maundrell K, Castilla J, Soto C. 2003. Caspase-12 and endoplasmic reticulum stress mediate neurotoxicity of pathological prion protein. Embo j. 22:5435-5445.

Hill AF, Collinge J. 2004. Prion strains and species barriers. Contrib Microbiol. 11:33-49.

Hill AF, Joiner S, Linehan J, Desbruslais M, Lantos PL, Collinge J. 2000. Species-barrier-independent prion replication in apparently resistant species. Proc Natl Acad Sci U S A. 97:10248-10253.

Hill AF, Desbruslais M, Joiner S, Sidle KC, Gowland I, Collinge J, Doey LJ, Lantos P. 1997. The same prion strain causes vCJD and BSE. Nature. 389:448-50, 526.

Hill AF, Zeidler M, Ironside J, Collinge J. 1997. Diagnosis of new variant Creutzfeldt-Jakob disease by tonsil biopsy. Lancet. 349:99-100.

Hilton KJ, Cunningham C, Reynolds RA, Perry VH. 2013. Early Hippocampal Synaptic Loss Precedes Neuronal Loss and Associates with Early Behavioural Deficits in Three Distinct Strains of Prion Disease. PLoS One. 8:e68062.

Ho VM, Dallalzadeh LO, Karathanasis N, Keles MF, Vangala S, Grogan T, Poirazi P, Martin KC. 2014. GluA2 mRNA distribution and regulation by miR-124 in hippocampal neurons. Mol Cell Neurosci. 61:1-12.

Hogan RN, Baringer JR, Prusiner SB. 1987. Scrapie infection diminishes spines and increases varicosities of dendrites in hamsters: a quantitative Golgi analysis. J Neuropathol Exp Neurol. 46:461-473.

Hu Z, Yu D, Gu QH, Yang Y, Tu K, Zhu J, Li Z. 2014. miR-191 and miR-135 are required for long-lasting spine remodelling associated with synaptic long-term depression. Nat Commun. 5:3263.

Huang CH, Cheng JC, Chen JC, Tseng CP. 2007. Evaluation of the role of Disabled-2 in nerve growth factor-mediated neurite outgrowth and cellular signalling. Cell Signal. 19:1339-1347.

Huntzinger E, Izaurralde E. 2011. Gene silencing by microRNAs: contributions of translational repression and mRNA decay. Nat Rev Genet. 12:99-110.

Hwang D, Lee IY, Yoo H, Gehlenborg N, Cho JH, Petritis B, Baxter D, Pitstick R, Young R, Spicer D et al. . 2009. A systems approach to prion disease. Mol Syst Biol. 5:252.

Imajo M, Nishida E. 2010. Human Tribbles homolog 1 functions as a negative regulator of retinoic acid receptor. Genes Cells. 15:1089-1097.

Impey S, Davare M, Lesiak A, Fortin D, Ando H, Varlamova O, Obrietan K, Soderling TR, Goodman RH, Wayman GA. 2010. An activity-induced microRNA controls dendritic spine formation by regulating Rac1-PAK signaling. Mol Cell Neurosci. 43:146-156.

Impey S, McCorkle SR, Cha-Molstad H, Dwyer JM, Yochum GS, Boss JM, McWeeney S, Dunn JJ, Mandel G, Goodman RH. 2004. Defining the CREB regulon: a genome-wide analysis of transcription factor regulatory regions. Cell. 119:1041-1054.

Imran M, Mahmood S. 2011. An overview of human prion diseases. Virol J. 8:559-422X-8-559.

Isaacs JD, Jackson GS, Altmann DM. 2006. The role of the cellular prion protein in the immune system. Clin Exp Immunol. 146:1-8.

Ito H, Morishita R, Shinoda T, Iwamoto I, Sudo K, Okamoto K, Nagata K. 2010. Dysbindin-1, WAVE2 and Abi-1 form a complex that regulates dendritic spine formation. Mol Psychiatry. 15:976-986.

Jackson GS, Murray I, Hosszu LL, Gibbs N, Waltho JP, Clarke AR, Collinge J. 2001. Location and properties of metal-binding sites on the human prion protein. Proc Natl Acad Sci U S A. 98:8531-8535.

Janka J, Maldarelli F. 2004. Prion Diseases: Update on Mad Cow Disease, Variant Creutzfeldt-Jakob Disease, and the Transmissible Spongiform Encephalopathies. Curr Infect Dis Rep. 6:305-315.

Jeffrey M, Martin S, Barr J, Chong A, Fraser JR. 2001. Onset of accumulation of PrPres in murine ME7 scrapie in relation to pathological and PrP immunohistochemical changes. J Comp Pathol. 124:20-28.

Jeffrey M, Halliday WG, Bell J, Johnston AR, MacLeod NK, Ingham C, Sayers AR, Brown DA, Fraser JR. 2000. Synapse loss associated with abnormal PrP precedes neuronal degeneration in the scrapie-infected murine hippocampus. Neuropathol Appl Neurobiol. 26:41-54.

Ji Y, Lu Y, Yang F, Shen W, Tang TT, Feng L, Duan S, Lu B. 2010. Acute and gradual increases in BDNF concentration elicit distinct signaling and functions in neurons. Nat Neurosci. 13:302-309.

Johnson R, Buckley NJ. 2009. Gene dysregulation in Huntington's disease: REST, microRNAs and beyond. Neuromolecular Med. 11:183-199.

Johnson R, Zuccato C, Belyaev ND, Guest DJ, Cattaneo E, Buckley NJ. 2008. A microRNA-based gene dysregulation pathway in Huntington's disease. Neurobiol Dis. 29:438-445.

Johnston AR, Black C, Fraser J, MacLeod N. 1997. Scrapie infection alters the membrane and synaptic properties of mouse hippocampal CA1 pyramidal neurones. J Physiol. 500 (Pt 1):1-15.

Joilin G, Guevremont D, Ryan B, Claudianos C, Cristino AS, Abraham WC, Williams JM. 2014. Rapid regulation of microRNA following induction of long-term potentiation in vivo. Front Mol Neurosci. 7:98.

Jones EV, Cook D, Murai KK. 2012. A neuron-astrocyte co-culture system to investigate astrocyte-secreted factors in mouse neuronal development. Methods Mol Biol. 814:341-352.

Jovicic A, Roshan R, Moisoi N, Pradervand S, Moser R, Pillai B, Luthi-Carter R. 2013. Comprehensive expression analyses of neural cell-type-specific miRNAs identify new

determinants of the specification and maintenance of neuronal phenotypes. J Neurosci. 33:5127-5137.

Kaimal V, Bardes EE, Tabar SC, Jegga AG, Aronow BJ. 2010. ToppCluster: a multiple gene list feature analyzer for comparative enrichment clustering and network-based dissection of biological systems. Nucleic Acids Res. 38:W96-102.

Kaneko M, Sugiyama N, Sasayama D, Yamaoka K, Miyakawa T, Arima K, Tsuchiya K, Hasegawa K, Washizuka S, Hanihara T et al. . 2008. Prion disease causes less severe lesions in human hippocampus than other parts of brain. Psychiatry Clin Neurosci. 62:264-270.

Kaneko M, Arai K, Hattori T, Imai T. 1999. Parahippocampal pathology in Creutzfeldt-Jakob disease. Clin Neuropathol. 18:9-16.

Karamboulas C, Swedani A, Ward C, Al-Madhoun AS, Wilton S, Boisvenue S, Ridgeway AG, Skerjanc IS. 2006. HDAC activity regulates entry of mesoderm cells into the cardiac muscle lineage. J Cell Sci. 119:4305-4314.

Karapetyan YE, Sferrazza GF, Zhou M, Ottenberg G, Spicer T, Chase P, Fallahi M, Hodder P, Weissmann C, Lasmezas CI. 2013. Unique drug screening approach for prion diseases identifies tacrolimus and astemizole as antiprion agents. Proc Natl Acad Sci U S A. 110:7044-7049.

Kasahara K, Sanai Y. 1999. Possible roles of glycosphingolipids in lipid rafts. Biophys Chem. 82:121-127.

Kawase-Koga Y, Otaegi G, Sun T. 2009. Different timings of Dicer deletion affect neurogenesis and gliogenesis in the developing mouse central nervous system. Dev Dyn. 238:2800-2812.

Kawase-Koga Y, Low R, Otaegi G, Pollock A, Deng H, Eisenhaber F, Maurer-Stroh S, Sun T. 2010. RNAase-III enzyme Dicer maintains signaling pathways for differentiation and survival in mouse cortical neural stem cells. J Cell Sci. 123:586-594.

Khosravani H, Zhang Y, Tsutsui S, Hameed S, Altier C, Hamid J, Chen L, Villemaire M, Ali Z, Jirik FR et al. . 2008. Prion protein attenuates excitotoxicity by inhibiting NMDA receptors. J Cell Biol. 181:551-565.

Kim JY, Oh MH, Bernard LP, Macara IG, Zhang H. 2011. The RhoG/ELMO1/Dock180 signaling module is required for spine morphogenesis in hippocampal neurons. J Biol Chem. 286:37615-37624.

Kim HO, Snyder GP, Blazey TM, Race RE, Chesebro B, Skinner PJ. 2008. Prion disease induced alterations in gene expression in spleen and brain prior to clinical symptoms. Adv Appl Bioinform Chem. 1:29-50.

Kim J, Inoue K, Ishii J, Vanti WB, Voronov SV, Murchison E, Hannon G, Abeliovich A. 2007. A MicroRNA feedback circuit in midbrain dopamine neurons. Science. 317:1220-1224.

Kimberlin RH, Walker CA. 1989. The role of the spleen in the neuroinvasion of scrapie in mice. Virus Res. 12:201-211.

Kimberlin RH, Walker CA. 1982. Pathogenesis of mouse scrapie: patterns of agent replication in different parts of the CNS following intraperitoneal infection. J R Soc Med. 75:618-624.

Kincaid AE, Hudson KF, Richey MW, Bartz JC. 2012. Rapid transepithelial transport of prions following inhalation. J Virol. 86:12731-12740.

Kiss-Toth E. 2011. Tribbles: 'puzzling' regulators of cell signalling. Biochem Soc Trans. 39:684-687.

Kiss-Toth E, Bagstaff SM, Sung HY, Jozsa V, Dempsey C, Caunt JC, Oxley KM, Wyllie DH, Polgar T, Harte M et al. . 2004. Human tribbles, a protein family controlling mitogen-activated protein kinase cascades. J Biol Chem. 279:42703-42708.

Kitamoto T, Shin RW, Doh-ura K, Tomokane N, Miyazono M, Muramoto T, Tateishi J. 1992. Abnormal isoform of prion proteins accumulates in the synaptic structures of the central nervous system in patients with Creutzfeldt-Jakob disease. Am J Pathol. 140:1285-1294.

Klamt F, Dal-Pizzol F, Conte da Frota ML,Jr, Walz R, Andrades ME, da Silva EG, Brentani RR, Izquierdo I, Fonseca Moreira JC. 2001. Imbalance of antioxidant defense in mice lacking cellular prion protein. Free Radic Biol Med. 30:1137-1144.

Klein ME, Lioy DT, Ma L, Impey S, Mandel G, Goodman RH. 2007. Homeostatic regulation of MeCP2 expression by a CREB-induced microRNA. Nat Neurosci. 10:1513-1514.

Kloosterman WP, Wienholds E, Ketting RF, Plasterk RH. 2004. Substrate requirements for let-7 function in the developing zebrafish embryo. Nucleic Acids Res. 32:6284-6291.

Kolonics A, Apati A, Janossy J, Brozik A, Gati R, Schaefer A, Magocsi M. 2001. Activation of Raf/ERK1/2 MAP kinase pathway is involved in GM-CSF-induced proliferation and survival but not in erythropoietin-induced differentiation of TF-1 cells. Cell Signal. 13:743-754.

Kong H, Omran A, Ashhab MU, Gan N, Peng J, He F, Wu L, Deng X, Yin F. 2014. Changes in microglial inflammation-related and brain-enriched MicroRNAs expressions in response to in vitro oxygen-glucose deprivation. Neurochem Res. 39:233-243.

Korth C, May BC, Cohen FE, Prusiner SB. 2001. Acridine and phenothiazine derivatives as pharmacotherapeutics for prion disease. Proc Natl Acad Sci U S A. 98:9836-9841.

Koshy AA, Cabral CM. 2014. 3-D imaging and analysis of neurons infected in vivo with Toxoplasma gondii. J Vis Exp. (94). doi:10.3791/52237.

Kostylev MA, Kaufman AC, Nygaard HB, Patel P, Haas LT, Gunther EC, Vortmeyer A, Strittmatter SM. 2015. Prion-Protein-interacting Amyloid-beta Oligomers of High Molecular Weight Are Tightly Correlated with Memory Impairment in Multiple Alzheimer Mouse Models. J Biol Chem. 290:17415-17438.

Kramer ML, Kratzin HD, Schmidt B, Romer A, Windl O, Liemann S, Hornemann S, Kretzschmar H. 2001. Prion protein binds copper within the physiological concentration range. J Biol Chem. 276:16711-16719.

Krebs J, Agellon LB, Michalak M. 2015. Ca2+ homeostasis and endoplasmic reticulum (ER) stress: An integrated view of calcium signaling. Biochem Biophys Res Commun. 460:114-121.

Krichevsky AM, Sonntag KC, Isacson O, Kosik KS. 2006. Specific microRNAs modulate embryonic stem cell-derived neurogenesis. Stem Cells. 24:857-864.

Kujala P, Raymond CR, Romeijn M, Godsave SF, van Kasteren SI, Wille H, Prusiner SB, Mabbott NA, Peters PJ. 2011. Prion uptake in the gut: identification of the first uptake and replication sites. PLoS Pathog. 7:e1002449.

Kye MJ, Liu T, Levy SF, Xu NL, Groves BB, Bonneau R, Lao K, Kosik KS. 2007. Somatodendritic microRNAs identified by laser capture and multiplex RT-PCR. Rna. 13:1224-1234.

Kyrkanides S, Olschowka JA, Williams JP, Hansen JT, O'Banion MK. 1999. TNF alpha and IL-1beta mediate intercellular adhesion molecule-1 induction via microglia-astrocyte interaction in CNS radiation injury. J Neuroimmunol. 95:95-106.

Ladogana A, Sanchez-Juan P, Mitrova E, Green A, Cuadrado-Corrales N, Sanchez-Valle R, Koscova S, Aguzzi A, Sklaviadis T, Kulczycki J et al. . 2009. Cerebrospinal fluid biomarkers in human genetic transmissible spongiform encephalopathies. J Neurol. 256:1620-1628.

Ladogana A, Puopolo M, Croes EA, Budka H, Jarius C, Collins S, Klug GM, Sutcliffe T, Giulivi A, Alperovitch A et al. . 2005. Mortality from Creutzfeldt-Jakob disease and related disorders in Europe, Australia, and Canada. Neurology. 64:1586-1591.

Lagos D, Pollara G, Henderson S, Gratrix F, Fabani M, Milne RS, Gotch F, Boshoff C. 2010. miR-132 regulates antiviral innate immunity through suppression of the p300 transcriptional co-activator. Nat Cell Biol. 12:513-519.

Landis DM, Williams RS, Masters CL. 1981. Golgi and electronmicroscopic studies of spongiform encephalopathy. Neurology. 31:538-549.

Laroche-Pierre S, Jodoin J, LeBlanc AC. 2009. Helix 3 is necessary and sufficient for prion protein's anti-Bax function. J Neurochem. 108:1019-1031.

Lasmezas CI, Deslys JP, Robain O, Jaegly A, Beringue V, Peyrin JM, Fournier JG, Hauw JJ, Rossier J, Dormont D. 1997. Transmission of the BSE agent to mice in the absence of detectable abnormal prion protein. Science. 275:402-405.

Lau P, Bossers K, Janky R, Salta E, Frigerio CS, Barbash S, Rothman R, Sierksma AS, Thathiah A, Greenberg D et al. . 2013. Alteration of the microRNA network during the progression of Alzheimer's disease. EMBO Mol Med. 5:1613-1634.

Lauren J, Gimbel DA, Nygaard HB, Gilbert JW, Strittmatter SM. 2009. Cellular prion protein mediates impairment of synaptic plasticity by amyloid-beta oligomers. Nature. 457:1128-1132.

Lazzari C, Peggion C, Stella R, Massimino ML, Lim D, Bertoli A, Sorgato MC. 2011. Cellular prion protein is implicated in the regulation of local Ca2+ movements in cerebellar granule neurons. J Neurochem. 116:881-890.

Lee KF, Soares C, Beique JC. 2012. Examining form and function of dendritic spines. Neural Plast. 2012:704103.

Lee KS, Linden R, Prado MA, BrentaniRR, Martins VR. 2003a. Towards cellular receptors for prions. Rev. Med. Virol. 13:399-408.

Lee Y, Ahn C, Han J, Choi H, Kim J, Yim J, Lee J, Provost P, Radmark O, Kim S et al. . 2003b. The nuclear RNase III Drosha initiates microRNA processing. Nature. 425:415-419.

Lee Y, Dawson VL, Dawson TM. 2012. Animal models of Parkinson's disease: vertebrate genetics. Cold Spring Harb Perspect Med. 2:10.1101/cshperspect.a009324.

Lee IY, Westaway D, Smit AF, Wang K, Seto J, Chen L, Acharya C, Ankener M, Baskin D, Cooper C et al. . 1998. Complete genomic sequence and analysis of the prion protein gene region from three mammalian species. Genome Res. 8:1022-1037.

Lee JA. 2009. Autophagy in neurodegeneration: two sides of the same coin. BMB Rep. 42:324-330.

Lee RC, Feinbaum RL, Ambros V. 1993. The C. elegans heterochronic gene lin-4 encodes small RNAs with antisense complementarity to lin-14. Cell. 75:843-854.

Lee ST, Chu K, Im WS, Yoon HJ, Im JY, Park JE, Park KH, Jung KH, Lee SK, Kim M et al. . 2011. Altered microRNA regulation in Huntington's disease models. Exp Neurol. 227:172-179.

Leone DP, Srinivasan K, Brakebusch C, McConnell SK. 2010. The rho GTPase Rac1 is required for proliferation and survival of progenitors in the developing forebrain. Dev Neurobiol. 70:659-678.

Lewis BP, Burge CB, Bartel DP. 2005. Conserved seed pairing, often flanked by adenosines, indicates that thousands of human genes are microRNA targets. Cell. 120:15-20.

Li B, Sun H. 2013. MiR-26a promotes neurite outgrowth by repressing PTEN expression. Mol Med Rep. 8:676-680.

Li H, Zhong X, Chau KF, Williams EC, Chang Q. 2011. Loss of activity-induced phosphorylation of MeCP2 enhances synaptogenesis, LTP and spatial memory. Nat Neurosci. 14:1001-1008.

Li H, Mao S, Wang H, Zen K, Zhang C, Li L. 2014. MicroRNA-29a modulates axon branching by targeting doublecortin in primary neurons. Protein Cell. 5:160-169.

Li J, Browning S, Mahal SP, Oelschlegel AM, Weissmann C. 2010. Darwinian evolution of prions in cell culture. Science. 327:869-872.

Li X, Gao X, Liu G, Xiong W, Wu J, Rao Y. 2008. Netrin signal transduction and the guanine nucleotide exchange factor DOCK180 in attractive signaling. Nat Neurosci. 11:28-35.

Liberski PP, Brown DR, Sikorska B, Caughey B, Brown P. 2008. Cell death and autophagy in prion diseases (transmissible spongiform encephalopathies). Folia Neuropathol. 46:1-25.

Liberski PP, Sikorska B, Bratosiewicz-Wasik J, Gajdusek DC, Brown P. 2004. Neuronal cell death in transmissible spongiform encephalopathies (prion diseases) revisited: from apoptosis to autophagy. Int J Biochem Cell Biol. 36:2473-2490.

Lin DT, Jodoin J, Baril M, Goodyer CG, Leblanc AC. 2008. Cytosolic prion protein is the predominant anti-Bax prion protein form: exclusion of transmembrane and secreted prion protein forms in the anti-Bax function. Biochim Biophys Acta. 1783:2001-2012.

Linden R, Martins VR, Prado MA, Cammarota M, Izquierdo I, Brentani RR. 2008. Physiology of the prion protein. Physiol Rev. 88:673-728.

Linseman DA, Loucks FA. 2008. Diverse roles of Rho family GTPases in neuronal development, survival, and death. Front Biosci. 13:657-676.

Lippi G, Steinert JR, Marczylo EL, D'Oro S, Fiore R, Forsythe ID, Schratt G, Zoli M, Nicotera P, Young KW. 2011. Targeting of the Arpc3 actin nucleation factor by miR-29a/b regulates dendritic spine morphology. J Cell Biol. 194:889-904.

Lise MF, Wong TP, Trinh A, Hines RM, Liu L, Kang R, Hines DJ, Lu J, Goldenring JR, Wang YT et al. . 2006. Involvement of myosin Vb in glutamate receptor trafficking. J Biol Chem. 281:3669-3678.

Liu W, Liu C, Zhu J, Shu P, Yin B, Gong Y, Qiang B, Yuan J, Peng X. 2012. MicroRNA-16 targets amyloid precursor protein to potentially modulate Alzheimer's-associated pathogenesis in SAMP8 mice. Neurobiol Aging. 33:522-534.

Livak KJ, Schmittgen TD. 2001. Analysis of relative gene expression data using real-time quantitative PCR and the 2(-Delta Delta C(T)) Method. Methods. 25:402-408.

Lonze BE, Ginty DD. 2002. Function and regulation of CREB family transcription factors in the nervous system. Neuron. 35:605-623.

Lu J, Nozumi M, Takeuchi K, Abe H, Igarashi M. 2011. Expression and function of neuronal growth-associated proteins (nGAPs) in PC12 cells. Neurosci Res. 70:85-90.

Lu J, Helton TD, Blanpied TA, Racz B, Newpher TM, Weinberg RJ, Ehlers MD. 2007. Postsynaptic positioning of endocytic zones and AMPA receptor cycling by physical coupling of dynamin-3 to Homer. Neuron. 55:874-889.

Lugli G, Torvik VI, Larson J, Smalheiser NR. 2008. Expression of microRNAs and their precursors in synaptic fractions of adult mouse forebrain. J Neurochem. 106:650-661.

Luhr KM, Nordstrom EK, Low P, Ljunggren HG, Taraboulos A, Kristensson K. 2004. Scrapie protein degradation by cysteine proteases in CD11c+ dendritic cells and GT1-1 neuronal cells. J Virol. 78:4776-4782.

Luikart BW, Bensen AL, Washburn EK, Perederiy JV, Su KG, Li Y, Kernie SG, Parada LF, Westbrook GL. 2011. miR-132 mediates the integration of newborn neurons into the adult dentate gyrus. PLoS One. 6:e19077.

Lukiw WJ, Dua P, Pogue AI, Eicken C, Hill JM. 2011. Upregulation of micro RNA-146a (miRNA-146a), a marker for inflammatory neurodegeneration, in sporadic Creutzfeldt-Jakob disease (sCJD) and Gerstmann-Straussler-Scheinker (GSS) syndrome. J Toxicol Environ Health A. 74:1460-1468.

Lund PA. 1995. The roles of molecular chaperones in vivo. Essays Biochem. 29:113-123.

Lytle JR, Yario TA, Steitz JA. 2007. Target mRNAs are repressed as efficiently by microRNA-binding sites in the 5' UTR as in the 3' UTR. Proc Natl Acad Sci U S A. 104:9667-9672.

Ma Y, Hendershot LM. 2003. Delineation of a negative feedback regulatory loop that controls protein translation during endoplasmic reticulum stress. J Biol Chem. 278:34864-34873.

Maattanen P, Taschuk R, Ross L, Marciniuk K, Bertram L, Potter A, Cashman NR, Napper S. 2013. PrP(Sc)-specific antibodies do not induce prion disease or misfolding of PrP(C) in highly susceptible Tga20 mice. Prion. 7:434-439.

Magill ST, Cambronne XA, Luikart BW, Lioy DT, Leighton BH, Westbrook GL, Mandel G, Goodman RH. 2010. microRNA-132 regulates dendritic growth and arborization of newborn neurons in the adult hippocampus. Proc Natl Acad Sci U S A. 107:20382-20387.

Maglio LE, Perez MF, Martins VR, Brentani RR, Ramirez OA. 2004. Hippocampal synaptic plasticity in mice devoid of cellular prion protein. Brain Res Mol Brain Res. 131:58-64.

Maiorano NA, Mallamaci A. 2009. Promotion of embryonic cortico-cerebral neuronogenesis by miR-124. Neural Dev. 4:40-8104-4-40.

Majer A, Booth SA. 2014. Microdissection and transcriptional profiling: a window into the pathobiology of preclinical prion disease. Prion. 8:67-74.

Majer A, Medina SJ, Niu Y, Abrenica B, Manguiat KJ, Frost KL, Philipson CS, Sorensen DL, Booth SA. 2012. Early mechanisms of pathobiology are revealed by transcriptional temporal dynamics in hippocampal CA1 neurons of prion infected mice. PLoS Pathog. 8:e1003002.

Makarava N, Kovacs GG, Bocharova O, Savtchenko R, Alexeeva I, Budka H, Rohwer RG, Baskakov IV. 2010. Recombinant prion protein induces a new transmissible prion disease in wild-type animals. Acta Neuropathol. 119:177-187.

Makeyev EV, Zhang J, Carrasco MA, Maniatis T. 2007. The MicroRNA miR-124 promotes neuronal differentiation by triggering brain-specific alternative pre-mRNA splicing. Mol Cell. 27:435-448.

Mallucci G, Collinge J. 2005. Rational targeting for prion therapeutics. Nat Rev Neurosci. 6:23-34.

Mallucci G, Dickinson A, Linehan J, Klohn PC, Brandner S, Collinge J. 2003. Depleting neuronal PrP in prion infection prevents disease and reverses spongiosis. Science. 302:871-874.

Mallucci GR, Ratte S, Asante EA, Linehan J, Gowland I, Jefferys JG, Collinge J. 2002. Post-natal knockout of prion protein alters hippocampal CA1 properties, but does not result in neurodegeneration. Embo j. 21:202-210.

Manson J, West JD, Thomson V, McBride P, Kaufman MH, Hope J. 1992. The prion protein gene: a role in mouse embryogenesis? Development. 115:117-122.

Manson JC, Clarke AR, Hooper ML, Aitchison L, McConnell I, Hope J. 1994. 129/Ola mice carrying a null mutation in PrP that abolishes mRNA production are developmentally normal. Mol Neurobiol. 8:121-127.

Martel MA, Wyllie DJ, Hardingham GE. 2009. In developing hippocampal neurons, NR2B-containing N-methyl-D-aspartate receptors (NMDARs) can mediate signaling to neuronal survival and synaptic potentiation, as well as neuronal death. Neuroscience. 158:334-343.

Marti E, Pantano L, Banez-Coronel M, Llorens F, Minones-Moyano E, Porta S, Sumoy L, Ferrer I, Estivill X. 2010. A myriad of miRNA variants in control and Huntington's disease brain regions detected by massively parallel sequencing. Nucleic Acids Res. 38:7219-7235.

Martin HC, Wani S, Steptoe AL, Krishnan K, Nones K, Nourbakhsh E, Vlassov A, Grimmond SM, Cloonan N. 2014. Imperfect centered miRNA binding sites are common and can mediate repression of target mRNAs. Genome Biol. 15:R51-2014-15-3-r51.

Martin JB. 1999. Molecular basis of the neurodegenerative disorders. N. Eng. J. Med. 340: 1970-1980.

Masliah E, Mallory M, Ge N, Alford M, Veinbergs I, Roses AD. 1995. Neurodegeneration in the central nervous system of apoE-deficient mice. Exp Neurol. 136:107-122.

Matsui Y, Satoh K, Mutsukura K, Watanabe T, Nishida N, Matsuda H, Sugino M, Shirabe S, Eguchi K, Kataoka Y. 2010. Development of an ultra-rapid diagnostic method based on heart-type fatty acid binding protein levels in the CSF of CJD patients. Cell Mol Neurobiol. 30:991-999.

Matsuzaki M, Honkura N, Ellis-Davies GC, Kasai H. 2004. Structural basis of long-term potentiation in single dendritic spines. Nature. 429:761-766.

McBride PA, Beekes M. 1999. Pathological PrP is abundant in sympathetic and sensory ganglia of hamsters fed with scrapie. Neurosci Lett. 265:135-138.

McGuire LI, Peden AH, Orru CD, Wilham JM, Appleford NE, Mallinson G, Andrews M, Head MW, Caughey B, Will RG et al. . 2012. Real time quaking-induced conversion analysis of cerebrospinal fluid in sporadic Creutzfeldt-Jakob disease. Ann Neurol. 72:278-285.

McKinley MP, Braunfeld MB, Bellinger CG, Prusiner SB. 1986. Molecular characteristics of prion rods purified from scrapie-infected hamster brains. J Infect Dis. 154:110-120.

McKinley MP, Meyer RK, Kenaga L, Rahbar F, Cotter R, Serban A, Prusiner SB. 1991. Scrapie prion rod formation in vitro requires both detergent extraction and limited proteolysis. J Virol. 65:1340-1351.

McLennan NF, Rennison KA, Bell JE, Ironside JW. 2001. In situ hybridization analysis of PrP mRNA in human CNS tissues. Neuropathol Appl Neurobiol. 27:373-383.

McNeill E, Van Vactor D. 2012. MicroRNAs shape the neuronal landscape. Neuron. 75:363-379.

Medori R, Montagna P, Tritschler HJ, LeBlanc A, Cortelli P, Tinuper P, Lugaresi E, Gambetti P. 1992. Fatal familial insomnia: a second kindred with mutation of prion protein gene at codon 178. Neurology. 42:669-670.

Metzler M, Gan L, Wong TP, Liu L, Helm J, Liu L, Georgiou J, Wang Y, Bissada N, Cheng K et al. . 2007. NMDA receptor function and NMDA receptor-dependent phosphorylation of huntingtin is altered by the endocytic protein HIP1. J Neurosci. 27:2298-2308.

Metzler M, Li B, Gan L, Georgiou J, Gutekunst CA, Wang Y, Torre E, Devon RS, Oh R, Legendre-Guillemin V et al. . 2003. Disruption of the endocytic protein HIP1 results in neurological deficits and decreased AMPA receptor trafficking. Embo j. 22:3254-3266.

Meza-Sosa KF, Pedraza-Alva G, Perez-Martinez L. 2014. microRNAs: key triggers of neuronal cell fate. Front Cell Neurosci. 8:175.

Miele G, Alejo Blanco AR, Baybutt H, Horvat S, Manson J, Clinton M. 2003. Embryonic activation and developmental expression of the murine prion protein gene. Gene Expr. 11:1-12.

Mizushima N. 2009. Physiological functions of autophagy. Curr Top Microbiol Immunol. 335:71-84.

Mohan J, Brown KL, Farquhar CF, Bruce ME, Mabbott NA. 2004. Scrapie transmission following exposure through the skin is dependent on follicular dendritic cells in lymphoid tissues. J Dermatol Sci. 35:101-111.

Mohri S, Handa S, Tateishi J. 1987. Lack of effect of thymus and spleen on the incubation period of Creutzfeldt-Jakob disease in mice. J Gen Virol. 68 (Pt 4):1187-1189.

Montag J, Hitt R, Opitz L, Schulz-Schaeffer WJ, Hunsmann G, Motzkus D. 2009. Upregulation of miRNA hsa-miR-342-3p in experimental and idiopathic prion disease. Mol Neurodegener. 4:36-1326-4-36.

Moore RA, Sturdevant DE, Chesebro B, Priola SA. 2014. Proteomics analysis of amyloid and nonamyloid prion disease phenotypes reveals both common and divergent mechanisms of neuropathogenesis. J Proteome Res. 13:4620-4634.

Moosmang S, Haider N, Klugbauer N, Adelsberger H, Langwieser N, Muller J, Stiess M, Marais E, Schulla V, Lacinova L et al. . 2005. Role of hippocampal Cav1.2 Ca2+ channels in NMDA receptor-independent synaptic plasticity and spatial memory. J Neurosci. 25:9883-9892.

Mor E, Cabilly Y, Goldshmit Y, Zalts H, Modai S, Edry L, Elroy-Stein O, Shomron N. 2011. Species-specific microRNA roles elucidated following astrocyte activation. Nucleic Acids Res. 39:3710-3723.

Morales R, Abid K, Soto C. 2007. The prion strain phenomenon: molecular basis and unprecedented features. Biochim Biophys Acta. 1772:681-691.

Morel L, Regan M, Higashimori H, Ng SK, Esau C, Vidensky S, Rothstein J, Yang Y. 2013. Neuronal exosomal miRNA-dependent translational regulation of astroglial glutamate transporter GLT1. J Biol Chem. 288:7105-7116.

Moreno JA, Halliday M, Molloy C, Radford H, Verity N, Axten JM, Ortori CA, Willis AE, Fischer PM, Barrett DA et al. . 2013. Oral treatment targeting the unfolded protein response prevents neurodegeneration and clinical disease in prion-infected mice. Sci Transl Med. 5:206ra138.

Moreno JA, Radford H, Peretti D, Steinert JR, Verity N, Martin MG, Halliday M, Morgan J, Dinsdale D, Ortori CA et al. . 2012. Sustained translational repression by eIF2alpha-P mediates prion neurodegeneration. Nature. 485:507-511.

Mori M, Burgess DL, Gefrides LA, Foreman PJ, Opferman JT, Korsmeyer SJ, Cavalheiro EA, Naffah-Mazzacoratti MG, Noebels JL. 2004. Expression of apoptosis inhibitor protein Mcl1 linked to neuroprotection in CNS neurons. Cell Death Differ. 11:1223-1233.

Moriguchi S, Oomura Y, Shioda N, Han F, Hori N, Aou S, Fukunaga K. 2011. Ca2+/calmodulin-dependent protein kinase II and protein kinase C activities mediate extracellular glucose-regulated hippocampal synaptic efficacy. Mol Cell Neurosci. 46:101-107.

Morrissette DA, Parachikova A, Green KN, LaFerla FM. 2009. Relevance of transgenic mouse models to human Alzheimer disease. J Biol Chem. 284:6033-6037.

Mukherjee A, Morales-Scheihing D, Gonzalez-Romero D, Green K, Taglialatela G, Soto C. 2010. Calcineurin inhibition at the clinical phase of prion disease reduces neurodegeneration, improves behavioral alterations and increases animal survival. PLoS Pathog. 6:e1001138.

Muller M, Kuiperij HB, Claassen JA, Kusters B, Verbeek MM. 2014. MicroRNAs in Alzheimer's disease: differential expression in hippocampus and cell-free cerebrospinal fluid. Neurobiol Aging. 35:152-158.

Murashov AK, Chintalgattu V, Islamov RR, Lever TE, Pak ES, Sierpinski PL, Katwa LC, Van Scott MR. 2007. RNAi pathway is functional in peripheral nerve axons. Faseb j. 21:656-670.

Nagerl UV, Eberhorn N, Cambridge SB, Bonhoeffer T. 2004. Bidirectional activity-dependent morphological plasticity in hippocampal neurons. Neuron. 44:759-767.

Nakanishi H. 2003. Neuronal and microglial cathepsins in aging and age-related diseases. Ageing Res Rev. 2:367-381.

Nakazawa T, Watabe AM, Tezuka T, Yoshida Y, Yokoyama K, Umemori H, Inoue A, Okabe S, Manabe T, Yamamoto T. 2003. p250GAP, a novel brain-enriched GTPase-activating protein for Rho family GTPases, is involved in the N-methyl-d-aspartate receptor signaling. Mol Biol Cell. 14:2921-2934.

Nelson R, Sawaya MR, Balbirnie M, Madsen AO, Riekel C, Grothe R, Eisenberg D. 2005. Structure of the cross-beta spine of amyloid-like fibrils. Nature. 435:773-778.

Neuendorf E, Weber A, Saalmueller A, Schatzl H, Reifenberg K, Pfaff E, Groschup MH. 2004. Glycosylation deficiency at either one of the two glycan attachment sites of cellular prion protein preserves susceptibility to bovine spongiform encephalopathy and scrapie infections. J Biol Chem. 279:53306-53316.

NEVIN S, McMENEMEY WH, BEHRMAN S, JONES DP. 1960. Subacute spongiform encephalopathy--a subacute form of encephalopathy attributable to vascular dysfunction (spongiform cerebral atrophy). Brain. 83:519-564.

Nichols TA, Spraker TR, Rigg TD, Meyerett-Reid C, Hoover C, Michel B, Bian J, Hoover E, Gidlewski T, Balachandran A et al. . 2013. Intranasal inoculation of white-tailed deer (Odocoileus virginianus) with lyophilized chronic wasting disease prion particulate complexed to montmorillonite clay. PLoS One. 8:e62455.

Nudelman AS, DiRocco DP, Lambert TJ, Garelick MG, Le J, Nathanson NM, Storm DR. 2010. Neuronal activity rapidly induces transcription of the CREB-regulated microRNA-132, in vivo. Hippocampus. 20:492-498.

Nuvolone M, Sorce S, Schwarz P, Aguzzi A. 2015. Prion pathogenesis in the absence of NLRP3/ASC inflammasomes. PLoS One. 10:e0117208.

Oh JM, Choi EK, Carp RI, Kim YS. 2012. Oxidative stress impairs autophagic flux in prion protein-deficient hippocampal cells. Autophagy. 8:1448-1461.

Okamoto K, Nagai T, Miyawaki A, Hayashi Y. 2004. Rapid and persistent modulation of actin dynamics regulates postsynaptic reorganization underlying bidirectional plasticity. Nat Neurosci. 7:1104-1112.

Orom UA, Nielsen FC, Lund AH. 2008. MicroRNA-10a binds the 5'UTR of ribosomal protein mRNAs and enhances their translation. Mol Cell. 30:460-471.

Orsi A, Fioriti L, Chiesa R, Sitia R. 2006. Conditions of endoplasmic reticulum stress favor the accumulation of cytosolic prion protein. J Biol Chem. 281:30431-30438.

Osterweil E, Wells DG, Mooseker MS. 2005. A role for myosin VI in postsynaptic structure and glutamate receptor endocytosis. J Cell Biol. 168:329-338.

Owen F, Poulter M, Lofthouse R, Collinge J, Crow TJ, Risby D, Baker HF, Ridley RM, Hsiao K, Prusiner SB. 1989. Insertion in prion protein gene in familial Creutzfeldt-Jakob disease. Lancet. 1:51-52.

Packer AN, Xing Y, Harper SQ, Jones L, Davidson BL. 2008. The bifunctional microRNA miR-9/miR-9* regulates REST and CoREST and is downregulated in Huntington's disease. J Neurosci. 28:14341-14346.

Pai B, Siripornmongcolchai T, Berentsen B, Pakzad A, Vieuille C, Pallesen S, Pajak M, Simpson TI, Armstrong JD, Wibrand K et al. . 2014. NMDA receptor-dependent regulation of miRNA expression and association with Argonaute during LTP in vivo. Front Cell Neurosci. 7:285.

Palmer MS, Dryden AJ, Hughes JT, Collinge J. 1991. Homozygous prion protein genotype predisposes to sporadic Creutzfeldt-Jakob disease. Nature. 352:340-342.

Pan KM, Baldwin M, Nguyen J, Gasset M, Serban A, Groth D, Mehlhorn I, Huang Z, Fletterick RJ, Cohen FE. 1993. Conversion of alpha-helices into beta-sheets features in the formation of the scrapie prion proteins. Proc Natl Acad Sci U S A. 90:10962-10966.

Papadopoulou AS, Serneels L, Achsel T, Mandemakers W, Callaerts-Vegh Z, Dooley J, Lau P, Ayoubi T, Radaelli E, Spinazzi M et al. . 2014. Deficiency of the miR-29a/b-1 cluster leads to ataxic features and cerebellar alterations in mice. Neurobiol Dis. 73C:275-288.

Paquet S, Langevin C, Chapuis J, Jackson GS, Laude H, Vilette D. 2007. Efficient dissemination of prions through preferential transmission to nearby cells. J Gen Virol. 88:706-713.

Parchi P, Strammiello R, Giese A, Kretzschmar H. 2011. Phenotypic variability of sporadic human prion disease and its molecular basis: past, present, and future. Acta Neuropathol. 121:91-112.

Parchi P, de Boni L, Saverioni D, Cohen ML, Ferrer I, Gambetti P, Gelpi E, Giaccone G, Hauw JJ, Hoftberger R et al. . 2012. Consensus classification of human prion disease histotypes allows reliable identification of molecular subtypes: an inter-rater study among surveillance centres in Europe and USA. Acta Neuropathol. 124:517-529.

Park CS, Tang SJ. 2009. Regulation of microRNA expression by induction of bidirectional synaptic plasticity. J Mol Neurosci. 38:50-56.

Parsons MP, Raymond LA. 2014. Extrasynaptic NMDA receptor involvement in central nervous system disorders. Neuron. 82:279-293.

Pastore A, Zagari A. 2007. A structural overview of the vertebrate prion proteins. Prion. 1:185-197.

Pasquale EB. 2008. Eph-ephrin bidirectional signaling in physiology and disease. Cell. 133:38-52.

Pathania M, Torres-Reveron J, Yan L, Kimura T, Lin TV, Gordon V, Teng ZQ, Zhao X, Fulga TA, Van Vactor D et al. . 2012. miR-132 enhances dendritic morphogenesis, spine density, synaptic integration, and survival of newborn olfactory bulb neurons. PLoS One. 7:e38174.

Pauly PC, Harris DA. 1998. Copper stimulates endocytosis of the prion protein. J Biol Chem. 273:33107-33110.

Peretz D, Scott MR, Groth D, Williamson RA, Burton DR, Cohen FE, Prusiner SB. 2001. Strain-specified relative conformational stability of the scrapie prion protein. Protein Sci. 10:854-863.

Peretz D, Williamson RA, Kaneko K, Vergara J, Leclerc E, Schmitt-Ulms G, Mehlhorn IR, Legname G, Wormald MR, Rudd PM et al. . 2001. Antibodies inhibit prion propagation and clear cell cultures of prion infectivity. Nature. 412:739-743.

Piccardo P, Manson JC, King D, Ghetti B, Barron RM. 2007. Accumulation of prion protein in the brain that is not associated with transmissible disease. Proc Natl Acad Sci U S A. 104:4712-4717.

Pichardo-Casas I, Goff LA, Swerdel MR, Athie A, Davila J, Ramos-Brossier M, Lapid-Volosin M, Friedman WJ, Hart RP, Vaca L. 2012. Expression profiling of synaptic microRNAs from the adult rat brain identifies regional differences and seizure-induced dynamic modulation. Brain Res. 1436:20-33.

Powell AD, Toescu EC, Collinge J, Jefferys JG. 2008. Alterations in Ca2+-buffering in prion-null mice: association with reduced afterhyperpolarizations in CA1 hippocampal neurons. J Neurosci. 28:3877-3886.

Prinz M, Huber G, Macpherson AJ, Heppner FL, Glatzel M, Eugster HP, Wagner N, Aguzzi A. 2003. Oral prion infection requires normal numbers of Peyer's patches but not of enteric lymphocytes. Am J Pathol. 162:1103-1111.

Prusiner SB. 1982. Novel proteinaceous infectious particles cause scrapie. Science. 216:136-144.

Puckett C, Concannon P, Casey C, Hood L. 1991. Genomic structure of the human prion protein gene. Am J Hum Genet. 49:320-329.

Puoti G, Bizzi A, Forloni G, Safar JG, Tagliavini F, Gambetti P. 2012. Sporadic human prion diseases: molecular insights and diagnosis. Lancet Neurol. 11:618-628.

Quaglio E, Restelli E, Garofoli A, Dossena S, De Luigi A, Tagliavacca L, Imperiale D, Migheli A, Salmona M, Sitia R et al. . 2011. Expression of mutant or cytosolic PrP in transgenic mice

and cells is not associated with endoplasmic reticulum stress or proteasome dysfunction. PLoS One. 6:e19339.

Rane NS, Kang SW, Chakrabarti O, Feigenbaum L, Hegde RS. 2008. Reduced translocation of nascent prion protein during ER stress contributes to neurodegeneration. Dev Cell. 15:359-370.

Rangel A, Burgaya F, Gavin R, Soriano E, Aguzzi A, Del Rio JA. 2007. Enhanced susceptibility of Prnp-deficient mice to kainate-induced seizures, neuronal apoptosis, and death: Role of AMPA/kainate receptors. J Neurosci Res. 85:2741-2755.

Raymond CR, Aucouturier P, Mabbott NA. 2007. In vivo depletion of CD11c+ cells impairs scrapie agent neuroinvasion from the intestine. J Immunol. 179:7758-7766.

Reczko M, Maragkakis M, Alexiou P, Grosse I, Hatzigeorgiou AG. 2012. Functional microRNA targets in protein coding sequences. Bioinformatics. 28:771-776.

Reder AT, Mednick AS, Brown P, Spire JP, Van Cauter E, Wollmann RL, Cervenakova L, Goldfarb LG, Garay A, Ovsiew F. 1995. Clinical and genetic studies of fatal familial insomnia. Neurology. 45:1068-1075.

Remenyi J, van den Bosch MW, Palygin O, Mistry RB, McKenzie C, Macdonald A, Hutvagner G, Arthur JS, Frenguelli BG, Pankratov Y. 2013. miR-132/212 knockout mice reveal roles for these miRNAs in regulating cortical synaptic transmission and plasticity. PLoS One. 8:e62509.

Riccio A, Ahn S, Davenport CM, Blendy JA, Ginty DD. 1999. Mediation by a CREB family transcription factor of NGF-dependent survival of sympathetic neurons. Science. 286:2358-2361.

Richfield EK, Thiruchelvam MJ, Cory-Slechta DA, Wuertzer C, Gainetdinov RR, Caron MG, Di Monte DA, Federoff HJ. 2002. Behavioral and neurochemical effects of wild-type and mutated human alpha-synuclein in transgenic mice. Exp Neurol. 175:35-48.

Richt JA, Kasinathan P, Hamir AN, Castilla J, Sathiyaseelan T, Vargas F, Sathiyaseelan J, Wu H, Matsushita H, Koster J et al. . 2007. Production of cattle lacking prion protein. Nat Biotechnol. 25:132-138.

Riemer C, Burwinkel M, Schwarz A, Gultner S, Mok SW, Heise I, Holtkamp N, Baier M. 2008. Evaluation of drugs for treatment of prion infections of the central nervous system. J Gen Virol. 89:594-597.

Riemer C, Neidhold S, Burwinkel M, Schwarz A, Schultz J, Kratzschmar J, Monning U, Baier M. 2004. Gene expression profiling of scrapie-infected brain tissue. Biochem Biophys Res Commun. 323:556-564.

Roshan R, Shridhar S, Sarangdhar MA, Banik A, Chawla M, Garg M, Singh VP, Pillai B. 2014. Brain-specific knockdown of miR-29 results in neuronal cell death and ataxia in mice. Rna. 20:1287-1297.

Roucou X, Guo Q, Zhang Y, Goodyer CG, LeBlanc AC. 2003. Cytosolic prion protein is not toxic and protects against Bax-mediated cell death in human primary neurons. J Biol Chem. 278:40877-40881.

Rudolf R, Bittins CM, Gerdes HH. 2011. The role of myosin V in exocytosis and synaptic plasticity. J Neurochem. 116:177-191.

Russelakis-Carneiro M, Hetz C, Maundrell K, Soto C. 2004. Prion replication alters the distribution of synaptophysin and caveolin 1 in neuronal lipid rafts. Am J Pathol. 165:1839-1848.

Saba R, Goodman CD, Huzarewich RL, Robertson C, Booth SA. 2008. A miRNA signature of prion induced neurodegeneration. PLoS One. 3:e3652.

Saba R, Gushue S, Huzarewich RL, Manguiat K, Medina S, Robertson C, Booth SA. 2012. MicroRNA 146a (miR-146a) is over-expressed during prion disease and modulates the innate immune response and the microglial activation state. PLoS One. 7:e30832.

Sanuki R, Onishi A, Koike C, Muramatsu R, Watanabe S, Muranishi Y, Irie S, Uneo S, Koyasu T, Matsui R et al. . 2011. miR-124a is required for hippocampal axogenesis and retinal cone survival through Lhx2 suppression. Nat Neurosci. 14:1125-1134.

Sanz-Clemente A, Nicoll RA, Roche KW. 2013. Diversity in NMDA receptor composition: many regulators, many consequences. Neuroscientist. 19:62-75.

Saumet A, Lecellier CH. 2006. Anti-viral RNA silencing: do we look like plants? Retrovirology. 3:3.

Schaefer A, O'Carroll D, Tan CL, Hillman D, Sugimori M, Llinas R, Greengard P. 2007. Cerebellar neurodegeneration in the absence of microRNAs. J Exp Med. 204:1553-1558.

Scheff SW, Price DA, Schmitt FA, DeKosky ST, Mufson EJ. 2007. Synaptic alterations in CA1 in mild Alzheimer disease and mild cognitive impairment. Neurology. 68:1501-1508.

Schmued LC, Stowers CC, Scallet AC, Xu L. 2005. Fluoro-Jade C results in ultra high resolution and contrast labeling of degenerating neurons. Brain Res. 1035:24-31.

Schneider CA, Rasband WS, Eliceiri KW. 2012. NIH Image to ImageJ: 25 years of image analysis. Nat Methods. 9:671-675.

Schratt GM, Tuebing F, Nigh EA, Kane CG, Sabatini ME, Kiebler M, Greenberg ME. 2006. A brain-specific microRNA regulates dendritic spine development. Nature. 439:283-289.

Scott JR, Fraser H. 1984. Degenerative hippocampal pathology in mice infected with scrapie. Acta Neuropathol. 65:62-68.

Sebastiao AM, Colino-Oliveira M, Assaife-Lopes N, Dias RB, Ribeiro JA. 2013. Lipid rafts, synaptic transmission and plasticity: impact in age-related neurodegenerative diseases. Neuropharmacology. 64:97-107.

Sgambato V, Pages C, Rogard M, Besson MJ, Caboche J. 1998. Extracellular signal-regulated kinase (ERK) controls immediate early gene induction on corticostriatal stimulation. J Neurosci. 18:8814-8825.

Shi L, Ko ML, Ko GY. 2009. Rhythmic expression of microRNA-26a regulates the L-type voltage-gated calcium channel alpha1C subunit in chicken cone photoreceptors. J Biol Chem. 284:25791-25803.

Shin D, Shin JY, McManus MT, Ptacek LJ, Fu YH. 2009. Dicer ablation in oligodendrocytes provokes neuronal impairment in mice. Ann Neurol. 66:843-857.

Shioya M, Obayashi S, Tabunoki H, Arima K, Saito Y, Ishida T, Satoh J. 2010. Aberrant microRNA expression in the brains of neurodegenerative diseases: miR-29a decreased in Alzheimer disease brains targets neurone navigator 3. Neuropathol Appl Neurobiol. 36:320-330.

Shott RH, Majer A, Frost KL, Booth SA, Schang LM. 2014. Activation of pro-survival CaMK4beta/CREB and pro-death MST1 signaling at early and late times during a mouse model of prion disease. Virol J. 11:160-422X-11-160.

Shrikant P, Weber E, Jilling T, Benveniste EN. 1995. Intercellular adhesion molecule-1 gene expression by glial cells. Differential mechanisms of inhibition by IL-10 and IL-6. J Immunol. 155:1489-1501.

Shyng SL, Heuser JE, Harris DA. 1994. A glycolipid-anchored prion protein is endocytosed via clathrin-coated pits. J Cell Biol. 125:1239-1250.

Shyng SL, Huber MT, Harris DA. 1993. A prion protein cycles between the cell surface and an endocytic compartment in cultured neuroblastoma cells. J Biol Chem. 268:15922-15928.

Shyng SL, Moulder KL, Lesko A, Harris DA. 1995. The N-terminal domain of a glycolipid-anchored prion protein is essential for its endocytosis via clathrin-coated pits. J Biol Chem. 270:14793-14800.

Sikorska B, Liberski PP, Giraud P, Kopp N, Brown P. 2004. Autophagy is a part of ultrastructural synaptic pathology in Creutzfeldt-Jakob disease: a brain biopsy study. Int J Biochem Cell Biol. 36:2563-2573.

Silveira JR, Raymond GJ, Hughson AG, Race RE, Sim VL, Hayes SF, Caughey B. 2005. The most infectious prion protein particles. Nature. 437:257-261.

Sim VL, Caughey B. 2009. Recent advances in prion chemotherapeutics. Infect Disord Drug Targets. 9:81-91.

Simoneau S, Rezaei H, Sales N, Kaiser-Schulz G, Lefebvre-Roque M, Vidal C, Fournier JG, Comte J, Wopfner F, Grosclaude J et al. . 2007. In vitro and in vivo neurotoxicity of prion protein oligomers. PLoS Pathog. 3:e125.

Singh A, Mohan ML, Isaac AO, Luo X, Petrak J, Vyoral D, Singh N. 2009. Prion protein modulates cellular iron uptake: a novel function with implications for prion disease pathogenesis. PLoS One. 4:e4468.

Siso S, Puig B, Varea R, Vidal E, Acin C, Prinz M, Montrasio F, Badiola J, Aguzzi A, Pumarola M et al. . 2002. Abnormal synaptic protein expression and cell death in murine scrapie. Acta Neuropathol. 103:615-626.

Sitia R, Braakman I. 2003. Quality control in the endoplasmic reticulum protein factory. Nature. 426:891-894.

Skinner PJ, Abbassi H, Chesebro B, Race RE, Reilly C, Haase AT. 2006. Gene expression alterations in brains of mice infected with three strains of scrapie. BMC Genomics. 7:114.

Smith P, Al Hashimi A, Girard J, Delay C, Hebert SS. 2011. In vivo regulation of amyloid precursor protein neuronal splicing by microRNAs. J Neurochem. 116:240-247.

Smoot M, Ono K, Ideker T, Maere S. 2011. PiNGO: a Cytoscape plugin to find candidate genes in biological networks. Bioinformatics. 27:1030-1031.

Smoot ME, Ono K, Ruscheinski J, Wang PL, Ideker T. 2011. Cytoscape 2.8: new features for data integration and network visualization. Bioinformatics. 27:431-432.

Solforosi L, Criado JR, McGavern DB, Wirz S, Sanchez-Alavez M, Sugama S, DeGiorgio LA, Volpe BT, Wiseman E, Abalos G et al. . 2004. Cross-linking cellular prion protein triggers neuronal apoptosis in vivo. Science. 303:1514-1516.

Solforosi L, Milani M, Mancini N, Clementi M, Burioni R. 2013. A closer look at prion strains: characterization and important implications. Prion. 7:99-108.

Soto C, Satani N. 2011. The intricate mechanisms of neurodegeneration in prion diseases. Trends Mol Med. 17:14-24.

Sorensen G, Medina S, Parchaliuk D, Phillipson C, Robertson C, Booth SA. 2008. Comprehensive transcriptional profiling of prion infection in mouse models reveals networks of responsive genes. BMC Genomics. 9:114-2164-9-114.

Sparkes RS, Simon M, Cohn VH, Fournier RE, Lem J, Klisak I, Heinzmann C, Blatt C, Lucero M, Mohandas T. 1986. Assignment of the human and mouse prion protein genes to homologous chromosomes. Proc Natl Acad Sci U S A. 83:7358-7362.

Spires-Jones TL, Kay K, Matsouka R, Rozkalne A, Betensky RA, Hyman BT. 2011. Calcineurin inhibition with systemic FK506 treatment increases dendritic branching and dendritic spine density in healthy adult mouse brain. Neurosci Lett. 487:260-263.

Spudich A, Frigg R, Kilic E, Kilic U, Oesch B, Raeber A, Bassetti CL, Hermann DM. 2005. Aggravation of ischemic brain injury by prion protein deficiency: role of ERK-1/-2 and STAT-1. Neurobiol Dis. 20:442-449.

Stahl N, Borchelt DR, Hsiao K, Prusiner SB. 1987. Scrapie prion protein contains a phosphatidylinositol glycolipid. Cell. 51:229-240.

Stahl N, Baldwin MA, Teplow DB, Hood L, Gibson BW, Burlingame AL, Prusiner SB. 1993. Structural studies of the scrapie prion protein using mass spectrometry and amino acid sequencing. Biochemistry. 32:1991-2002.

Standaert DG. 2005. Applications of laser capture microdissection in the study of neurodegenerative disease. Arch Neurol. 62:203-205.

Steele AD, Lindquist S, Aguzzi A. 2007. The prion protein knockout mouse: a phenotype under challenge. Prion. 1:83-93.

Steinhoff BJ, Racker S, Herrendorf G, Poser S, Grosche S, Zerr I, Kretzschmar H, Weber T. 1996. Accuracy and reliability of periodic sharp wave complexes in Creutzfeldt-Jakob disease. Arch Neurol. 53:162-166.

Sugo N, Oshiro H, Takemura M, Kobayashi T, Kohno Y, Uesaka N, Song WJ, Yamamoto N. 2010. Nucleocytoplasmic translocation of HDAC9 regulates gene expression and dendritic growth in developing cortical neurons. Eur J Neurosci. 31:1521-1532.

Sulzer D, Surmeier DJ. 2013. Neuronal vulnerability, pathogenesis, and Parkinson's disease. Mov Disord. 28:715-724.

Sun Y, Gui H, Li Q, Luo ZM, Zheng MJ, Duan JL, Liu X. 2013. MicroRNA-124 protects neurons against apoptosis in cerebral ischemic stroke. CNS Neurosci Ther. 19:813-819.

Sun X, Wu Y, Chen B, Zhang Z, Zhou W, Tong Y, Yuan J, Xia K, Gronemeyer H, Flavell RA et al. . 2011. Regulator of calcineurin 1 (RCAN1) facilitates neuronal apoptosis through caspase-3 activation. J Biol Chem. 286:9049-9062.

Taganov KD, Boldin MP, Chang KJ, Baltimore D. 2006. NF-kappaB-dependent induction of microRNA miR-146, an inhibitor targeted to signaling proteins of innate immune responses. Proc Natl Acad Sci U S A. 103:12481-12486.

Takamori N, Shimomura A, Senda T. 2006. Microtubule-bundling activity of APC is stimulated by interaction with PSD-95. Neurosci Lett. 403:68-72.

Tanaka M, Hara H, Nishina H, Hanada K, Hagiwara K, Maehama T. 2010. An improved method for cell-to-cell transmission of infectious prion. Biochem Biophys Res Commun. 397:505-508.

Telling GC, Parchi P, DeArmond SJ, Cortelli P, Montagna P, Gabizon R, Mastrianni J, Lugaresi E, Gambetti P, Prusiner SB. 1996. Evidence for the conformation of the pathologic isoform of the prion protein enciphering and propagating prion diversity. Science. 274:2079-2082.

Thackray AM, Klein MA, Bujdoso R. 2003. Subclinical prion disease induced by oral inoculation. J Virol. 77:7991-7998.

Thackray AM, Knight R, Haswell SJ, Bujdoso R, Brown DR. 2002. Metal imbalance and compromised antioxidant function are early changes in prion disease. Biochem J. 362:253-258.

Tian X, Gotoh T, Tsuji K, Lo EH, Huang S, Feig LA. 2004. Developmentally regulated role for Ras-GRFs in coupling NMDA glutamate receptors to Ras, Erk and CREB. Embo j. 23:1567-1575.

Tichopad A, Pfaffl MW, Didier A. 2003. Tissue-specific expression pattern of bovine prion gene: quantification using real-time RT-PCR. Mol Cell Probes. 17:5-10.

Tilly G, Chapuis J, Vilette D, Laude H, Vilotte JL. 2003. Efficient and specific down-regulation of prion protein expression by RNAi. Biochem Biophys Res Commun. 305:548-551.

Tobler I, Gaus SE, Deboer T, Achermann P, Fischer M, Rulicke T, Moser M, Oesch B, McBride PA, Manson JC. 1996. Altered circadian activity rhythms and sleep in mice devoid of prion protein. Nature. 380:639-642.

Tortosa E, Montenegro-Venegas C, Benoist M, Hartel S, Gonzalez-Billault C, Esteban JA, Avila J. 2011. Microtubule-associated protein 1B (MAP1B) is required for dendritic spine development and synaptic maturation. J Biol Chem. 286:40638-40648.

Torres M, Castillo K, Armisen R, Stutzin A, Soto C, Hetz C. 2010. Prion protein misfolding affects calcium homeostasis and sensitizes cells to endoplasmic reticulum stress. PLoS One. 5:e15658.

Tovar KR, Sprouffske K, Westbrook GL. 2000. Fast NMDA receptor-mediated synaptic currents in neurons from mice lacking the epsilon2 (NR2B) subunit. J Neurophysiol. 83:616-620.

Tribouillard-Tanvier D, Race B, Striebel JF, Carroll JA, Phillips K, Chesebro B. 2012. Early cytokine elevation, PrPres deposition, and gliosis in mouse scrapie: no effect on disease by deletion of cytokine genes IL-12p40 and IL-12p35. J Virol. 86:10377-10383.

Tsai NP, Lin YL, Wei LN. 2009. MicroRNA mir-346 targets the 5'-untranslated region of receptor-interacting protein 140 (RIP140) mRNA and up-regulates its protein expression. Biochem J. 424:411-418.

Tschampa HJ, Neumann M, Zerr I, Henkel K, Schroter A, Schulz-Schaeffer WJ, Steinhoff BJ, Kretzschmar HA, Poser S. 2001. Patients with Alzheimer's disease and dementia with Lewy bodies mistaken for Creutzfeldt-Jakob disease. J Neurol Neurosurg Psychiatry. 71:33-39.

Tsuruta F, Green EM, Rousset M, Dolmetsch RE. 2009. PIKfyve regulates CaV1.2 degradation and prevents excitotoxic cell death. J Cell Biol. 187:279-294.

Tuzi NL, Cancellotti E, Baybutt H, Blackford L, Bradford B, Plinston C, Coghill A, Hart P, Piccardo P, Barron RM et al. . 2008. Host PrP glycosylation: a major factor determining the outcome of prion infection. PLoS Biol. 6:e100.

Uchiyama K, Miyata H, Sakaguchi S. 2013. Disturbed vesicular trafficking of membrane proteins in prion disease. Prion. 7:447-451.

Valleron AJ, Boelle PY, Will R, Cesbron JY. 2001. Estimation of epidemic size and incubation time based on age characteristics of vCJD in the United Kingdom. Science. 294:1726-1728.

van Spronsen M, van Battum EY, Kuijpers M, Vangoor VR, Rietman ML, Pothof J, Gumy LF, van Ijcken WF, Akhmanova A, Pasterkamp RJ et al. . 2013. Developmental and activity-dependent miRNA expression profiling in primary hippocampal neuron cultures. PLoS One. 8:e74907.

Veith NM, Plattner H, Stuermer CA, Schulz-Schaeffer WJ, Burkle A. 2009. Immunolocalisation of PrPSc in scrapie-infected N2a mouse neuroblastoma cells by light and electron microscopy. Eur J Cell Biol. 88:45-63.

Viader A, Chang LW, Fahrner T, Nagarajan R, Milbrandt J. 2011. MicroRNAs modulate Schwann cell response to nerve injury by reinforcing transcriptional silencing of dedifferentiation-related genes. J Neurosci. 31:17358-17369.

Visvanathan J, Lee S, Lee B, Lee JW, Lee SK. 2007. The microRNA miR-124 antagonizes the anti-neural REST/SCP1 pathway during embryonic CNS development. Genes Dev. 21:744-749.

Vo N, Klein ME, Varlamova O, Keller DM, Yamamoto T, Goodman RH, Impey S. 2005. A cAMP-response element binding protein-induced microRNA regulates neuronal morphogenesis. Proc Natl Acad Sci U S A. 102:16426-16431.

von Engelhardt J, Coserea I, Pawlak V, Fuchs EC, Kohr G, Seeburg PH, Monyer H. 2007. Excitotoxicity in vitro by NR2A- and NR2B-containing NMDA receptors. Neuropharmacology. 53:10-17.

Wadhwa R, Taira K, Kaul SC. 2002. An Hsp70 family chaperone, mortalin/mthsp70/PBP74/Grp75: what, when, and where? Cell Stress Chaperones. 7:309-316.

Wagner W, Brenowitz SD, Hammer JA,3rd. 2011. Myosin-Va transports the endoplasmic reticulum into the dendritic spines of Purkinje neurons. Nat Cell Biol. 13:40-48.

Walz R, Amaral OB, Rockenbach IC, Roesler R, Izquierdo I, Cavalheiro EA, Martins VR, Brentani RR. 1999. Increased sensitivity to seizures in mice lacking cellular prion protein. Epilepsia. 40:1679-1682.

Wang LL, Zhang Z, Li Q, Yang R, Pei X, Xu Y, Wang J, Zhou SF, Li Y. 2009. Ethanol exposure induces differential microRNA and target gene expression and teratogenic effects which can be suppressed by folic acid supplementation. Hum Reprod. 24:562-579.

Wang WX, Huang Q, Hu Y, Stromberg AJ, Nelson PT. 2011. Patterns of microRNA expression in normal and early Alzheimer's disease human temporal cortex: white matter versus gray matter. Acta Neuropathol. 121:193-205.

Wang X, McGovern G, Zhang Y, Wang F, Zha L, Jeffrey M, Ma J. 2015. Intraperitoneal Infection of Wild-Type Mice with Synthetically Generated Mammalian Prion. PLoS Pathog. 11:e1004958.

Wang Z, Edwards JG, Riley N, Provance DW,Jr, Karcher R, Li XD, Davison IG, Ikebe M, Mercer JA, Kauer JA et al. . 2008. Myosin Vb mobilizes recycling endosomes and AMPA receptors for postsynaptic plasticity. Cell. 135:535-548.

Wayman GA, Davare M, Ando H, Fortin D, Varlamova O, Cheng HY, Marks D, Obrietan K, Soderling TR, Goodman RH et al. . 2008. An activity-regulated microRNA controls dendritic plasticity by down-regulating p250GAP. Proc Natl Acad Sci U S A. 105:9093-9098.

Wayman GA, Kaech S, Grant WF, Davare M, Impey S, Tokumitsu H, Nozaki N, Banker G, Soderling TR. 2004. Regulation of axonal extension and growth cone motility by calmodulin-dependent protein kinase I. J Neurosci. 24:3786-3794.

Wendholt D, Spilker C, Schmitt A, Dolnik A, Smalla KH, Proepper C, Bockmann J, Sobue K, Gundelfinger ED, Kreutz MR et al. . 2006. ProSAP-interacting protein 1 (ProSAPiP1), a novel

protein of the postsynaptic density that links the spine-associated Rap-Gap (SPAR) to the scaffolding protein ProSAP2/Shank3. J Biol Chem. 281:13805-13816.

White AR, Collins SJ, Maher F, Jobling MF, Stewart LR, Thyer JM, Beyreuther K, Masters CL, Cappai R. 1999. Prion protein-deficient neurons reveal lower glutathione reductase activity and increased susceptibility to hydrogen peroxide toxicity. Am J Pathol. 155:1723-1730.

White MD, Farmer M, Mirabile I, Brandner S, Collinge J, Mallucci GR. 2008. Single treatment with RNAi against prion protein rescues early neuronal dysfunction and prolongs survival in mice with prion disease. Proc Natl Acad Sci U S A. 105:10238-10243.

Will RG. 2003. Acquired prion disease: iatrogenic CJD, variant CJD, kuru. Br Med Bull. 66:255-265.

Will RG, Zeidler M, Stewart GE, Macleod MA, Ironside JW, Cousens SN, Mackenzie J, Estibeiro K, Green AJ, Knight RS. 2000. Diagnosis of new variant Creutzfeldt-Jakob disease. Ann Neurol. 47:575-582.

Will RG, Ironside JW, Zeidler M, Cousens SN, Estibeiro K, Alperovitch A, Poser S, Pocchiari M, Hofman A, Smith PG. 1996. A new variant of Creutzfeldt-Jakob disease in the UK. Lancet. 347:921-925.

Wille H, Michelitsch MD, Guenebaut V, Supattapone S, Serban A, Cohen FE, Agard DA, Prusiner SB. 2002. Structural studies of the scrapie prion protein by electron crystallography. Proc Natl Acad Sci U S A. 99:3563-3568.

Williams C, Mehrian Shai R, Wu Y, Hsu YH, Sitzer T, Spann B, McCleary C, Mo Y, Miller CA. 2009. Transcriptome analysis of synaptoneurosomes identifies neuroplasticity genes overexpressed in incipient Alzheimer's disease. PLoS One. 4:e4936.

Wong HK, Veremeyko T, Patel N, Lemere CA, Walsh DM, Esau C, Vanderburg C, Krichevsky AM. 2013. De-repression of FOXO3a death axis by microRNA-132 and -212 causes neuronal apoptosis in Alzheimer's disease. Hum Mol Genet. 22:3077-3092.

Wong K, Qiu Y, Hyun W, Nixon R, VanCleff J, Sanchez-Salazar J, Prusiner SB, DeArmond SJ. 1996. Decreased receptor-mediated calcium response in prion-infected cells correlates with decreased membrane fluidity and IP3 release. Neurology. 47:741-750.

Wopfner F, Weidenhofer G, Schneider R, von Brunn A, Gilch S, Schwarz TF, Werner T, Schatzl HM. 1999. Analysis of 27 mammalian and 9 avian PrPs reveals high conservation of flexible regions of the prion protein. J Mol Biol. 289:1163-1178.

Wu HY, Hudry E, Hashimoto T, Kuchibhotla K, Rozkalne A, Fan Z, Spires-Jones T, Xie H, Arbel-Ornath M, Grosskreutz CL et al. . 2010. Amyloid beta induces the morphological

neurodegenerative triad of spine loss, dendritic simplification, and neuritic dystrophies through calcineurin activation. J Neurosci. 30:2636-2649.

Wu H, Nash JE, Zamorano P, Garner CC. 2002. Interaction of SAP97 with minus-end-directed actin motor myosin VI. Implications for AMPA receptor trafficking. J Biol Chem. 277:30928-30934.

Xiang W, Windl O, Wunsch G, Dugas M, Kohlmann A, Dierkes N, Westner IM, Kretzschmar HA. 2004. Identification of differentially expressed genes in scrapie-infected mouse brains by using global gene expression technology. J Virol. 78:11051-11060.

Xiao B, Tu JC, Worley PF. 2000. Homer: a link between neural activity and glutamate receptor function. Curr Opin Neurobiol. 10:370-374.

Xu NJ, Henkemeyer M. 2009. Ephrin-B3 reverse signaling through Grb4 and cytoskeletal regulators mediates axon pruning. Nat Neurosci. 12:268-276.

Yano H, Ninan I, Zhang H, Milner TA, Arancio O, Chao MV. 2006. BDNF-mediated neurotransmission relies upon a myosin VI motor complex. Nat Neurosci. 9:1009-1018.

Yoshimura A, Fujii R, Watanabe Y, Okabe S, Fukui K, Takumi T. 2006. Myosin-Va facilitates the accumulation of mRNA/protein complex in dendritic spines. Curr Biol. 16:2345-2351.

Yu G, Chen J, Xu Y, Zhu C, Yu H, Liu S, Sha H, Chen J, Xu X, Wu Y et al. . 2009. Generation of goats lacking prion protein. Mol Reprod Dev. 76:3.

Yu JY, Chung KH, Deo M, Thompson RC, Turner DL. 2008. MicroRNA miR-124 regulates neurite outgrowth during neuronal differentiation. Exp Cell Res. 314:2618-2633.

Zahn R, Liu A, Luhrs T, Riek R, von Schroetter C, Lopez Garcia F, Billeter M, Calzolai L, Wider G, Wuthrich K. 2000. NMR solution structure of the human prion protein. Proc Natl Acad Sci U S A. 97:145-150.

Zerr I, Kallenberg K, Summers DM, Romero C, Taratuto A, Heinemann U, Breithaupt M, Varges D, Meissner B, Ladogana A et al. . 2009. Updated clinical diagnostic criteria for sporadic Creutzfeldt-Jakob disease. Brain. 132:2659-2668.

Zhang CC, Steele AD, Lindquist S, Lodish HF. 2006. Prion protein is expressed on long-term repopulating hematopoietic stem cells and is important for their self-renewal. Proc Natl Acad Sci U S A. 103:2184-2189.

Zhang, S. and Wang, Y. T. 2013. NMDA-induced Excitotoxicity and Lactate Dehydrogenase Assay in Primary Cultured Neurons. *Bio-protocol* 3(21): e965. http://www.bio-protocol.org/e965

Zhang SJ, Zou M, Lu L, Lau D, Ditzel DA, Delucinge-Vivier C, Aso Y, Descombes P, Bading H. 2009. Nuclear calcium signaling controls expression of a large gene pool: identification of a gene program for acquired neuroprotection induced by synaptic activity. PLoS Genet. 5:e1000604.

Zhang SJ, Steijaert MN, Lau D, Schutz G, Delucinge-Vivier C, Descombes P, Bading H. 2007. Decoding NMDA receptor signaling: identification of genomic programs specifying neuronal survival and death. Neuron. 53:549-562.

Zhang Z, Zhang Y, Wang F, Wang X, Xu Y, Yang H, Yu G, Yuan C, Ma J. 2013. De novo generation of infectious prions with bacterially expressed recombinant prion protein. Faseb j. 27:4768-4775.

Zhou H, Rigoutsos I. 2014. MiR-103a-3p targets the 5' UTR of GPRC5A in pancreatic cells. Rna. 20:1431-1439.

Zito K, Knott G, Shepherd GM, Shenolikar S, Svoboda K. 2004. Induction of spine growth and synapse formation by regulation of the spine actin cytoskeleton. Neuron. 44:321-334.

Zhu C, Li B, Yu G, Chen J, Yu H, Chen J, Xu X, Wu Y, Zhang A, Cheng G. 2009. Production of Prnp-/- goats by gene targeting in adult fibroblasts. Transgenic Res. 18:163-171.

Zovoilis A, Agbemenyah HY, Agis-Balboa RC, Stilling RM, Edbauer D, Rao P, Farinelli L, Delalle I, Schmitt A, Falkai P et al. . 2011. microRNA-34c is a novel target to treat dementias. Embo j. 30:4299-4308.